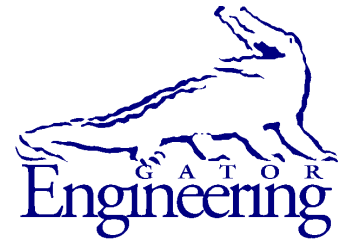




University of Florida
Civil and Coastal Engineering

Geotechnical Research
Report 2022/0215606



University of Florida
Civil and Coastal Engineering

Final Report

Deliverable 7, January 2023

Geo-statistical Deep Foundation Software

Principal investigator:

Michael T. Davidson

Co-Principal investigators:

Michael B. Rodgers, Gary R. Consolazio

Project Consultant:

Michael A. Faraone

Bridge Software Institute
Engineering School of Sustainable Infrastructure & Environment
College of Engineering
University of Florida
P.O. Box 116580
Gainesville, Florida 32611

Sponsor:

Florida Department of Transportation (FDOT)

Project Manager:

Rodrigo Herrera

Contract:

FDOT BDV31-977-143
UF Project No. 0215606

DISCLAIMER

The opinions, findings, and conclusions expressed in this publication are those of the authors and not necessarily those of the State of Florida Department of Transportation.

UNIT CONVERSION

APPROXIMATE CONVERSIONS TO SI UNITS

SYMBOL	WHEN YOU KNOW	MULTIPLY BY	TO FIND	SYMBOL
LENGTH				
in	inches	25.4	millimeters	mm
ft	feet	0.305	meters	m
yd	yards	0.914	meters	m
mi	miles	1.61	kilometers	km

SYMBOL	WHEN YOU KNOW	MULTIPLY BY	TO FIND	SYMBOL
AREA				
in²	square inches	645.2	square millimeters	mm ²
ft²	square feet	0.093	square meters	m ²
yd²	square yard	0.836	square meters	m ²
mi²	square miles	2.59	square kilometers	km ²

SYMBOL	WHEN YOU KNOW	MULTIPLY BY	TO FIND	SYMBOL
VOLUME				
fl oz	fluid ounces	29.57	milliliters	mL
ft³	cubic feet	0.028	cubic meters	m ³
yd³	cubic yards	0.765	cubic meters	m ³

NOTE: volumes greater than 1,000 L shall be shown in m³

SYMBOL	WHEN YOU KNOW	MULTIPLY BY	TO FIND	SYMBOL
MASS				
oz	ounces	28.35	grams	g
lb	pounds	0.454	kilograms	kg
T	short tons (2,000 lb)	0.907	megagrams (or "metric ton")	Mg (or "t")

SYMBOL	WHEN YOU KNOW	MULTIPLY BY	TO FIND	SYMBOL
TEMPERATURE (exact degrees)				
°F	Fahrenheit	5 (F-32)/9 or (F-32)/1.8	Celsius	°C

SYMBOL	WHEN YOU KNOW	MULTIPLY BY	TO FIND	SYMBOL
ILLUMINATION				
fc	foot-candles	10.76	lux	lx
fl	foot-Lamberts	3.426	candela/m ²	cd/m ²

SYMBOL	WHEN YOU KNOW	MULTIPLY BY	TO FIND	SYMBOL
FORCE and PRESSURE or STRESS				
lbf	pound force	4.45	newtons	N
kips	kips	4,448.22	newtons	N
lbf/in²	pound force per square inch	6.89	kilopascals	kPa
ksi	kips per square inch	6,894.76	kilopascals	kPa
tsf	tons (short) per square foot	95.67	kilopascals	kPa
pcf	pound force per cubic foot	156.967	newtons per cubic meter	N/m ³

APPROXIMATE CONVERSIONS TO ENGLISH UNITS

SYMBOL	WHEN YOU KNOW	MULTIPLY BY	TO FIND	SYMBOL
LENGTH				
mm	millimeters	0.039	inches	in
m	meters	3.28	feet	ft
m	meters	1.09	yards	yd
km	kilometers	0.621	miles	mi

SYMBOL	WHEN YOU KNOW	MULTIPLY BY	TO FIND	SYMBOL
AREA				
mm ²	square millimeters	0.0016	square inches	in ²
m ²	square meters	10.764	square feet	ft ²
m ²	square meters	1.195	square yards	yd ²
ha	hectares	2.47	acres	ac
km ²	square kilometers	0.386	square miles	mi ²

SYMBOL	WHEN YOU KNOW	MULTIPLY BY	TO FIND	SYMBOL
VOLUME				
mL	milliliters	0.034	fluid ounces	fl oz
L	liters	0.264	gallons	gal
m ³	cubic meters	35.314	cubic feet	ft ³
m ³	cubic meters	1.307	cubic yards	yd ³

SYMBOL	WHEN YOU KNOW	MULTIPLY BY	TO FIND	SYMBOL
MASS				
g	grams	0.035	ounces	oz
kg	kilograms	2.202	pounds	lb
Mg (or "t")	megagrams (or "metric ton")	1.103	short tons (2,000 lb)	T

SYMBOL	WHEN YOU KNOW	MULTIPLY BY	TO FIND	SYMBOL
TEMPERATURE (exact degrees)				
°C	Celsius	1.8C+32	Fahrenheit	°F

SYMBOL	WHEN YOU KNOW	MULTIPLY BY	TO FIND	SYMBOL
ILLUMINATION				
lx	lux	0.0929	foot-candles	fc
cd/m ²	candela/m ²	0.2919	foot-Lamberts	fl

SYMBOL	WHEN YOU KNOW	MULTIPLY BY	TO FIND	SYMBOL
FORCE and PRESSURE or STRESS				
N	newtons	0.225	pound force	lbf
N	newtons	0.000224809	kips	kips
kPa	kilopascals	0.145	pound force per square inch	lbf/in ²
kPa	kilopascals	0.000145	kips per square inch	ksi
kPa	kilopascals	0.000145038	kips per square inch	ksi
N/m ³	newtons per cubic meter	0.0104526	pound force per cubic foot	pcf

*SI is the symbol for International System of Units. Appropriate rounding should be made to comply with Section 4 of ASTM E380. (Revised March 2003).

TECHNICAL REPORT DOCUMENTATION PAGE

1. Report No.	2. Government Accession No.	3. Recipient's Catalog No.	
4. Title and Subtitle Geo-statistical Deep Foundation Software		5. Report Date January 2023	
		6. Performing Organization Code	
7. Author(s) Davidson, M. T., Rodgers, M. B., Consolazio, G. R., and Faraone, M. A.		8. Performing Organization Report No.	
9. Performing Organization Name and Address Bridge Software Institute University of Florida 1949 Stadium Rd. Room 365 P.O. Box 116580 Gainesville, FL 32611		10. Work Unit No. (TR AIS)	
		11. Contract or Grant No. BDV31-977-143	
12. Sponsoring Agency Name and Address Florida Department of Transportation 605 Suwannee Street, MS 30 Tallahassee, FL 32399		13. Type of Report and Period Covered Final Report 07/15/2021 - 01/15/2023	
		14. Sponsoring Agency Code	
15. Supplementary Notes			
<p>16. Abstract</p> <p>When performing geotechnical design of bridge foundations, two sources of uncertainty that arise are spatial variability of soil (and rock) properties and bias intrinsic to empirical correlations (method error) that relate geotechnical site measurements to predictions of foundation member resistance. In current practice, spatial variability and method error are either largely neglected or considered indirectly using simplified assumptions. As a result, foundation members such as driven piles may be designed with non-uniform levels of conservatism. Further, foundation design and construction costs can be significant relative to those allocated for other bridge components. Adoption of design methodologies that directly account for spatial variability and method error phenomena can lead to increased uniformity in levels of conservatism associated with bridge foundation members. In turn, more appropriate costs may be allocated across various stages of the bridge design process. Previous FDOT research focused on analytical techniques for characterizing spatial correlations, regression expressions derived from load-test data versus resistance predictions, and development of a prototype Geo-statistical tool. Subsequently, the prototype tool was transitioned to a design-oriented software package. The current project was undertaken to enhance the design-oriented Geo-statistical analysis software, including (1) addition of analysis features for Cone Penetration Testing (CPT) data; (2) addition of analysis features for Measuring While Drilling (MWD) data; (3) quality assurance testing; (4) investigation of a technique to estimate radii of geological zones within a site; and, (5) development of technology transfer materials.</p>			
17. Key Words Deep foundation design; Geostatistics; Spatial variability; Method error; Axial capacity		18. Distribution Statement No restrictions.	
19. Security Classif. (of this report) Unclassified	20. Security Classif. (of this page) Unclassified	21. No. of Pages 397	22. Price

ACKNOWLEDGEMENTS

The authors would like to thank the Florida Department of Transportation (FDOT) for providing the funding that made this project possible.

EXECUTIVE SUMMARY

Spatial variability of soil and rock, and biases (method error) in empirical correlations that relate geotechnical site measurements to foundation member resistance constitute two sources of uncertainty in geotechnical design of bridge foundations. Owing in part to these phenomena, foundation design and construction costs can be significant relative to those allocated for other bridge components. In current practice, the phenomena of spatial variability and method error are either largely neglected or considered indirectly using simplified and more conservative assumptions. As a result, foundation members such as driven piles may be designed with non-uniform levels of conservatism.

Adoption of design methodologies that directly account for spatial variability and method error can lead to increased uniformity in levels of conservatism associated with bridge foundation members. In turn, more appropriate costs may be allocated across various stages of the bridge design process. For example, assessments of whether sufficient geotechnical site data have been gathered can be made more objective. Additionally—owing to adoption of a site-specific, reliability-based design approach—increased knowledge of uncertainty and risk reduction can be achieved regarding how representative foundation resistance predictions are relative to respective, built conditions.

In previous FDOT-funded research (BDK77-977-23), analytical techniques for characterizing spatial correlations and regression expressions derived from pile-axial load-test data versus resistance predictions were packaged into a prototype Geo-statistical tool. Subsequently, in BDV31-977-108, the prototype tool was transitioned to a design-oriented software package, referred to as GeoStat (Bridge Software Institute (BSI), University of Florida, Gainesville, FL), intended for use by practicing engineers. The GeoStat guides engineers through the processes of incorporating spatial variability and method error into design-level predictions of pile and shaft axial capacities. Accompanying the resistance predictions is the uncertainty associated with use of a given set (or subset) of geotechnical site data (e.g., Standard Penetration Testing, SPT-N, values; unconfined compression strength of rock, q_u). In this way, an increasingly site-specific approach to foundation design can be integrated into bridge design applications.

Enhancements to the GeoStat software were focused upon in the present implementation project. Specific enhancements include adding the ability to perform Geo-statistical analysis by operating on Cone Penetration Testing (CPT) data and, separately, Measuring While Drilling (MWD) data. Quality assurance testing and sponsor review of a beta software package (including documentation of the newly added feature sets in the GeoStat software manuals) were undertaken as part of the overall project efforts. Investigation of a technique to estimate radii of geological zones within a site was also considered. To better facilitate proliferation of Geo-statistical tools in design practice, development of technology transfer materials was also included among the project activities. Documented in the following report are efforts, methodologies, and outcomes pertaining to each implementation item.

TABLE OF CONTENTS

DISCLAIMER	ii
UNIT CONVERSION	iii
TECHNICAL REPORT DOCUMENTATION PAGE	v
ACKNOWLEDGEMENTS	vi
EXECUTIVE SUMMARY	vii
LIST OF FIGURES	xi
LIST OF TABLES	xiv
1. INTRODUCTION	1
1.1 Introduction.....	1
1.2 Motivation.....	2
1.3 Objective and Supporting Tasks	2
1.3.1 Task 1 – Incorporate Analysis of CPT Data	3
1.3.2 Task 2 – Incorporate Analysis of MWD Data	3
1.3.3 Task 3 – Conduct Quality Assurance Testing.....	4
1.3.4 Task 4 – Investigate Methodology for Effective Radius	4
1.3.5 Task 5 – Technology Transfer	5
1.4 Scope.....	5
2. GEO-STATISTICAL APPROACH FOR USING CPT DATA TO PREDICT PILE AXIAL CAPACITIES	7
2.1 Overview.....	7
2.2 CPT Parameters for Use in Geo-statistical Simulation.....	7
2.2.1 Cone Resistance	7
2.2.2 Sleeve Friction	8
2.2.3 Friction Ratio	8
2.3 CPT Analysis Methods	8
2.3.1 Schmertmann Method.....	8
2.3.2 UF Method	9
2.3.3 LCPC Method	9
2.4 Variogram Generation	9
2.4.1 Selection of Variogram Variable	10
2.4.2 Procedure	10
2.5 Geo-statistical Simulation of Pile Axial Capacity Using CPT Data.....	10
2.5.1 Overview.....	10
2.5.2 Simulation of Cone Resistance Values	12

2.5.3 Co-simulation of Sleeve Friction Values	12
2.5.4 Computing Pile Axial Capacity	14
2.6 Method Error.....	15
2.6.1 Overview.....	15
2.6.2 Approach.....	15
2.6.3 Catalog of Measured and Predicted Pile Axial Capacities	17
2.6.4 Method Error Parameters.....	18
3. GEO-STATISTICAL APPROACH FOR USING MWD DATA TO PREDICT SHAFT AXIAL RESISTANCE IN LIMESTONE LAYERS	21
3.1 Overview.....	21
3.2 MWD Parameters for Use in Geo-statistical Simulation.....	21
3.2.1 Specific Energy.....	21
3.2.2 Unconfined Compressive Strength and Tensile Strength	22
3.3 Variogram Generation	22
3.3.1 Selection of Variogram Variable	23
3.3.2 Procedure	23
3.4 Geo-statistical Simulation of Shaft Axial Resistance in Limestone with MWD Data	23
3.4.1 Overview.....	23
3.4.2 Simulation of Unconfined Compressive Strength Values	25
3.4.3 Calculation of Tensile Strength Values	25
3.4.4 Estimation of Rock Recovery and RQD.....	26
3.4.5 Considerations for Additional Parameters.....	28
3.4.6 Computing Shaft Axial Resistance in Limestone	28
3.5 Method Error.....	29
3.5.1 Overview.....	29
3.5.2 Approach and Parameters	29
4. VERIFICATION OF SPATIAL CORRELATION CALCULATIONS AND GEO- STATISTICAL SIMULATION	31
4.1 Verification of Spatial Correlation Calculations using CPT and MWD Data	31
4.1.1 Overview.....	31
4.1.2 Variograms Generated Using CPT Cone Resistance.....	31
4.1.3 Variograms Generated Using MWD Estimates of Unconfined Compressive Strength.....	34
4.2 Verification of Geo-Statistical Simulation.....	38
4.2.1 Overview.....	38
4.2.2 CPT-based Simulation for Driven Pile	38
4.2.3 MWD-based Simulation for Drilled Shafts in Limestone	42
5. GEO-STATISTICAL APPROACH FOR ESTIMATING ZONAL RADII	47
5.1 Overview.....	47
5.2 Conceptual Approach.....	47

5.2.1	Detection of Zonal Anisotropy Using Variograms	47
5.2.2	Key Steps of the Procedure.....	49
5.3	Illustration Case	51
5.3.1	Scope.....	52
5.3.2	Formation of Variograms Using Site-wide Boring Data	52
5.3.3	Region of Interest for Illustration Case.....	54
5.3.4	Formation of Variograms Using Progressively Larger Subsets of Borings	55
5.3.5	Observations	61
6.	SUMMARY AND CONCLUSIONS	64
6.1	Summary of Work Completed.....	64
6.1.1	Summary of Task 1 Work Completed	64
6.1.2	Summary of Task 2 Work Completed	65
6.1.3	Summary of Task 3 Work Completed	65
6.1.4	Summary of Task 4 Work Completed	66
6.1.5	Summary of Task 5 Work Completed	66
6.2	Recommendations.....	66
6.2.1	Recommendations for Design.....	67
6.2.2	Recommendations for Potential Future Research.....	67
APPENDIX A:	GeoStat Help Manual.....	71
APPENDIX B:	GeoStat Technical Manual	200

LIST OF FIGURES

<u>Figure</u>	<u>Page</u>
Figure 1. Preparatory steps for performing stochastic simulation of pile axial capacity with use of CPT data.....	11
Figure 2. Co-simulation of sleeve friction, f_{s_CPT}	13
Figure 3. Method error procedure for CPT-based analysis of pile axial capacity	16
Figure 4. Scatterplots of (filtered) measured versus CPT-based predictions of pile axial capacity: (a) Schmertmann; (b) UF; (c) LCPC	19
Figure 5. Preparatory steps for performing stochastic simulation of shaft axial resistances within limestone layers with use of MWD data.....	24
Figure 6. Estimation of rock recovery for use in MWD-based stochastic simulation (REC_{MWD}) .	27
Figure 7. Estimation of RQD for use in MWD-based stochastic simulation (RQD_{MWD})	27
Figure 8. Illustrative set of CPT cone resistance (q_{t_CPT}) values: (a) Plan view and through-depth scatterplot; (b) Histogram of values in layer 3.....	32
Figure 9. Comparison of horizontal variograms generated using values of q_{t_CPT} in layer 3: (a) Variogram ordinates; (b) Variogram pairs.....	33
Figure 10. Comparison of vertical variograms generated using values of q_{t_CPT} in layer 3: (a) Variogram ordinates; (b) Variogram pairs.....	34
Figure 11. Illustrative set of MWD-estimated values of unconfined compressive strength (q_{u_MWD}): (a) Plan view and through-depth scatterplot; (b) Histogram of values in layer 4	35
Figure 12. Comparison of horizontal variograms generated using values of q_{u_MWD} in layer 4: (a) Variogram ordinates; (b) Variogram pairs.....	36
Figure 13. Comparison of vertical variograms generated using values of q_{u_MWD} in layer 4: (a) Variogram ordinates; (b) Variogram pairs.....	37
Figure 14. Illustrative set of bridge site data for producing benchmark results: (a) Plan view of boring locations; (b) Sitewide scatterplot of SPT blow count values versus elevation	39
Figure 15. Verification of CPT-based stochastic simulation results for driven piles: (a) Mean side shear resistance; (b) Coefficient of variation; (c) Resistance factor	41

Figure 16. Illustrative set of specific energy values (e) for use in verification of MWD-based stochastic simulation: (a) Plan view of boring locations; (b) Scatterplot versus elevation	43
Figure 17. Illustrative set of bridge site data for producing benchmark results: (a) Unconfined compressive strength (q_u); (b) Tensile strength (q_t); (c) Rock recovery (REC)	44
Figure 18. Verification of MWD-based stochastic simulation results for drilled shafts in limestone: (a) Mean resistance; (b) Coefficient of variation; (c) Resistance factor	45
Figure 19. Illustrative characteristics of variograms: (a) Geometric anisotropy; (b) Geometric and zonal anisotropy	48
Figure 20. Procedure for estimation of zonal radii	50
Figure 21. Overview of site data for illustration case: (a) Plan view of 51 boring locations; (b) Measured values of specific energy, e	51
Figure 22. Scatterplots of site-wide geotechnical data versus elevation (51 borings) and estimated layer bottom elevations (solid blue lines): (a) Specific energy, e ; (b) MWD estimate of q_u	53
Figure 23. Selected variograms obtained using site-wide data (51 borings): (a) Layer 1 horizontal; (b) Layer 1 vertical; (c) Layer 2 horizontal; (d) Layer 2 vertical	54
Figure 24. Region of interest for illustration case: (a) Relative to overall site; (b) Inset of 17 boring locations and test shaft location.....	55
Figure 25. Scatterplots of geotechnical data versus elevation from region of interest (17 borings) and estimated layer bottom elevations (solid blue lines): (a) MWD estimate of q_u ; (b) MWD estimate of rock recovery	56
Figure 26. Selected variograms for 4-boring subset: (a) Plan view of boring locations; (b) Layer 1 horizontal; (c) Layer 1 vertical; (d) Layer 4 horizontal; (e) Layer 4 vertical	57
Figure 27. Selected variograms for 7-boring subset: (a) Plan view of boring locations; (b) Layer 1 horizontal; (c) Layer 1 vertical; (d) Layer 4 horizontal; (e) Layer 4 vertical	58
Figure 28. Selected variograms for 14-boring subset: (a) Plan view of boring locations; (b) Layer 1 horizontal; (c) Layer 1 vertical; (d) Layer 4 horizontal; (e) Layer 4 vertical	59
Figure 29. Selected variograms for 17-boring subset: (a) Plan view of boring locations; (b) Layer 1 horizontal; (c) Layer 1 vertical; (d) Layer 4 horizontal; (e) Layer 4 vertical	60
Figure 30. Illustrative depiction of estimated zone for 17-boring subset	61
Figure 31. Comparison of variograms for progressively larger subsets of borings: (a) Layer 1 horizontal; (b) Layer 1 vertical; (c) Layer 4 horizontal; (d) Layer 4 vertical	61

Figure 32. Selected variograms for 18-boring subset: (a) Plan view of boring locations; (b) Layer 4 horizontal; (c) Layer 4 vertical62

Figure 33. Comparison of variograms between 17-boring and 18-boring subsets: (a) Layer 4 horizontal; (b) Layer 4 vertical63

Figure 34. Comparison of computed LRFD resistance factor (ϕ) values63

LIST OF TABLES

<u>Table</u>	<u>Page</u>
Table 1. Applicable pile types for the empirical methods of CPT analysis.....	14
Table 2. Measured versus CPT-based predictions of Davisson capacity for driven piles in Florida (Bloomquist et al. 2007)	18
Table 3. Descriptive statistics of measured versus predicted pile axial capacity for filter usage..	18
Table 4. Load tests excluded by filter	18
Table 5. Method error parameters for CPT-based total uncertainty calculations	20
Table 6. Limestone parameters for MWD-based stochastic simulation of drilled shaft axial resistance.....	28
Table 7. Method error parameters for MWD-based total uncertainty calculations	30
Table 8. Descriptive statistics for values of q_{t_CPT} (tsf) in layer 3	32
Table 9. Descriptive statistics for values of q_{u_MWD} (tsf) in layer 4.....	36
Table 10. Descriptive statistics for SPT blow count (blows/ft) values per layer.....	39
Table 11. Descriptive statistics for unconfined compressive strength (tsf) values per layer.....	44
Table 12. Selected layer bottom elevations and variogram data based on site-wide collection of 51 borings.....	53
Table 13. Layer bottom elevations and variogram data for 17 borings in the region of interest....	55

CHAPTER 1

INTRODUCTION

1.1 Introduction

Considerations for two sources of uncertainty that are encountered in deep foundation design are focused upon in the current project. The first source of uncertainty is that of spatial variability: within a given soil (or rock) volume, horizontal and vertical variations are present in the material properties, and such spatial variations carry over into geotechnical site measurements. The second source of uncertainty is referred to as “method error.” As context, a routine component of deep foundation member design for bridges structures with respect to axial resistance is to correlate geotechnical site measurements to unit resistances along the lengths of piles and shafts. The unit resistance values (e.g., skin friction, end bearing) are then integrated to estimate nominal member (axial) capacities. In turn, the nominal capacities are factored to produce design-level axial capacities. When correlating geotechnical site measurements to unit resistance quantities, empirical relationships of predicted versus measured resistance under (presumably) comparable conditions are drawn upon. However, the empirical relationships inherently contain biases, which are carried into calculations of nominal and design-level axial capacities.

In current practice, uncertainties associated with spatial variability and method error phenomena are either accounted for indirectly (e.g., via prescriptive use of non-site-specific resistance factors) or are greatly simplified when designing deep foundation members such as piles and drilled shafts. Necessarily then, additional—and potentially non-uniform—conservatism is introduced into the member configurations. Such levels of conservatism can be made more uniform by adopting design-oriented methodologies that directly address spatial variability and method error (i.e., on a site-specific or even zone-specific level). Furthermore, use of Geo-statistical analysis tools can address commonly encountered issues in deep foundation member design (e.g., assessment of whether sufficient site data have been gathered). Still further, use of Geo-statistical tools can improve foundation cost-effectiveness (Rivers, 2018).

Techniques for quantitatively characterizing spatial variability were developed as part of previously funded research by the Florida Department of Transportation (FDOT). Past efforts such as BDK75-977-23 (McVay et al. 2012) included characterizations for standard penetration test blow counts (SPT-N) and rock coring measurements (e.g., unconfined compressive strength of rock, q_u) across cohesive, cohesionless, and limestone materials. Efforts in BDK75-977-23 (McVay et al. 2012) also included synthesis of data pertaining to (and correlations between) measured and predicted foundation-member axial resistance quantities, as pertaining to method error. Furthermore, in McVay et al. (2012), both spatial variability and method error analysis methods were packaged into a prototype research tool, in turn, that facilitated (Geo-statistical) axial capacity calculations of deep foundation members. In Faraone et al. (2021), combined use of the spatial variability characterizations and method error formulations were demonstrated to be capable of bringing about site-specific estimates of axial resistances for deep foundation members (piles, shafts) across a variety of embedded media (sand, clay, limestone).

Outcomes from McVay et al. (2012) were leveraged in BDV31-977-108 (Davidson et al. 2020) to create a design-oriented Geo-statistical analysis tool, intended for use by practicing

engineers. The computational tool, referred to as GeoStat, operates on collections of geotechnical site data and facilitates assignment of representative soil/rock layers. In addition, the software can be used to form horizontal and vertical spatial correlation structures for each defined layer (i.e., to quantitatively characterize the spatial variability of the site data). Stochastic simulation can then be conducted to predict profiles of elevation versus axial resistance (and descriptive statistics) for piles and drilled shafts. Furthermore, method error calculations can be carried out and incorporated into the computed resistance profiles. Afterward, profile plots of design resistance, including site-specific LRFD resistance factors (ϕ), can be produced (e.g., for making comparisons to prescriptive factors provided in design provisions such as AASHTO 2020 and FDOT 2022). Tools such as GeoStat can be used to bring about more representative (more uniformly conservative) foundation designs in comparison to relatively more simplified approaches typical of current practice.

1.2 Motivation

Included among the sources of uncertainty that should be considered when estimating design resistances of deep foundation members are spatial variability and method error. Incorporation of geostatistics into design calculations facilitates characterization of both spatial variability and method error, particularly when estimating axial capacities of deep foundation members such as piles and drilled shafts. In addition, use of software tools possessing Geo-statistical analysis capabilities can facilitate (1) identification of geological zones across bridge sites; (2) assessment of the adequacy of collected site data; (3) increased uniformity in design practice; and, (4) the potential for improved cost-effectiveness of bridge foundation designs.

The present study is motivated by the need to implement and provide practicing geotechnical engineers with design-oriented software tools that directly account for spatial variability and method error phenomena. Building upon previous FDOT-funded research, including development of software capable of analyzing certain types of geotechnical site data (e.g., SPT-N blow count values), the present study is also motivated by the need to increase the types of geotechnical site data that can be utilized as part of Geo-statistical analysis. Accordingly, two site investigation methods have been identified: Cone Penetration Testing (CPT) and Measuring While Drilling MWD. Feature sets for analysis using both CPT and MWD data are included among the implementation efforts. In addition, the potential benefits associated with technology transfer of Geo-statistical analysis procedures to practicing engineers constitute a motivating factor for the present study.

1.3 Objective and Supporting Tasks

The objective of the present implementation project is to enhance the GeoStat software, and thereby increase both the means and ease with which practicing engineers can incorporate Geo-statistical phenomena into bridge foundation designs. Implementation efforts of the present project include (1) use of CPT data in Geo-statistical analysis; (2) use of MWD (Rodgers et al. 2018b) data in Geo-statistical analysis of drilled shafts in limestone; (3) quality assurance testing of the CPT and MWD features, along with submission of a beta software package for sponsor review (including updated software manuals); (4) investigation of a methodology for effective

plan-view radii as estimation of geological zones throughout sites; and, (5) development and delivery of technology transfer materials that facilitate proliferation of Geo-statistical analysis software in practice. The remainder of the current report documents methodologies, feature sets, verification activities, and outcomes associated with the implementation items listed above. In addition, two updated software manuals are included in the present report. Specifically, the updated GeoStat Help Manual is presented in Appendix A, while the Technical Manual is provided in Appendix B.

1.3.1 Task 1 – Incorporate Analysis of CPT Data

Task 1 focused upon item (1) above: implementation of Cone Penetration Testing (CPT) analysis within the Geo-statistical software, GeoStat. The implementation was carried out to broaden the types of geotechnical site data that can be utilized in Geo-statistical analysis of driven piles. Accordingly, the implementation complemented existing program capabilities such as those pertaining to SPT-based analysis of driven piles. Newly added features included reading, writing, and employing elevation-based profiles of two types of CPT measurements (cone resistance, sleeve friction). Cone resistance was selected as the variable for use in generation of variogram points within a given soil layer. In addition, three CPT-specific empirical methods were identified and made available for use as part of the stochastic simulation feature set. Accompanying implementation of the three empirical methods were development of default method error parameters (one set of parameter values for each empirical method).

Outcomes from the Task 1 efforts included updates to the GeoStat Help Manual (see Appendix A). Help manual updates included listings of new entries within the standardized format of GeoStat input files such as the selected empirical method for stochastic simulation. Also, documentation of newly added user interface (UI) controls (input boxes, table columns) was added to the Help manual. Newly implemented algorithms pertaining to stochastic simulation (e.g., co-simulation of sleeve friction) and method error (e.g., default regression parameter values for method error calculations) were documented in the GeoStat Technical manual (see Appendix B).

1.3.2 Task 2 – Incorporate Analysis of MWD Data

Task 2 focused upon item (2) above: implementation of Geo-statistical analysis features that make use of site data obtained from Measuring While Drilling (MWD) operations. The resulting feature set requires only specification of elevation profiles of (physically measured) specific energy and unit weight throughout a given site. The Task 2 efforts therefore necessitated reading, writing, and processing of elevation profiles of measured specific energy values (whereas such capabilities already existed for unit weight data). All other parameters necessary for generation of variograms and conducting stochastic simulation are then automatically interpreted as part of the overall MWD implementation. Empirical correlations were adopted from the literature for producing all interpreted values. For example, values of unconfined compressive strength are produced based on a correlation to measured values of specific energy. Further, unconfined compressive (interpreted from specific energy measurements) was selected as a key variable for generation of variograms and for driving co-simulation of other interpreted parameter values (e.g., tensile strength) during stochastic simulation. A method error formulation that is

amenable to input of site-specific regression parameters was adopted as part of the Task 2 implementation efforts.

As an outcome from the Task 2 efforts, existing program features for Geo-statistical analysis of drilled shafts in limestone were significantly expanded upon. Outcomes also included corresponding updates to the GeoStat Help Manual (see Appendix A). These updates pertaining to Geo-statistical analysis of MWD data entailed the addition of new entries within the standardized format of GeoStat input files (e.g., a threshold value of specific energy for use in producing interpreted parameter values of limestone). Also, newly implemented dialogs and UI controls (e.g., a column for specific energy input within tabulated boring data dialogs) were added to the Help manual documentation. Algorithms pertaining to stochastic simulation with use of MWD data sets, and the adopted method error formulation, were also documented in the GeoStat Technical manual (see Appendix B).

1.3.3 Task 3 – Conduct Quality Assurance Testing

Task 3 focused upon item (3) above: conducting quality assurance while focusing on those enhancements made during Task 1 (for CPT-based analysis) and Task 2 (for MWD-based analysis). Quality assurance efforts were divided into three distinct stages. First, dialogs and UI controls specific to the CPT and MWD implementations were subjected to data validation testing (e.g., ensuring that GeoStat detects, remains stable, and appropriately responds to input of conspicuous data such as negative strength quantities). Next, verification of engineering routines was carried out in association with generation of experimental variogram points within a given soil (or limestone) layer. Third, benchmark results sets were produced and utilized in verifying stochastic simulation results that were obtained from CPT-based (and separately, MWD-based) analyses.

Outcomes from Task 3 included documentation of the quality assurance efforts. Also, the Task 3 efforts led to confirmation that both the CPT-based and MWD-based implementations produced verifiable simulation output. In addition, a beta version of the GeoStat software that contained the newly implemented CPT and MWD analysis features was submitted for FDOT review. Based on the review, several feature suggestions were implemented, including implementation of an option that allows for selection of the desired resistance factor formulation. For each feature added as a result of the beta software review, corresponding updates were added to the Help manual (Appendix A) and Technical manual (Appendix B).

1.3.4 Task 4 – Investigate Methodology for Effective Radius

Task 4 focused upon item (4) above: investigation of a methodology for engineers to make use of when estimating zonal radii. In this context, ‘zonal radii’ corresponds to the plan-view extents of distinct geological zones that may (or may not) be distributed across a bridge site. An anticipated application of the methodology is for making estimates of a suggested radius away from a candidate (i.e., not yet performed) shaft load-test location, within which the applicability of LRFD resistance factors may remain applicable. Such a methodology was investigated and documented as part of Task 4. Delineation of major steps in the methodology were then

exemplified via an illustrative set of site data. Furthermore, visualization of the estimated radius was added as a new feature among the existing plan-view plot features of the GeoStat software.

As an outcome from Task 4, engineers can leverage GeoStat capabilities to assess and visualize circular plan-view bounds of distinct geological zones. Also, a potential avenue for Owner assessment of the sufficiency of site data was identified (i.e., if all site data are taken into consideration, but horizontal and vertical variograms cannot be produced, then additional site data may need to be gathered). Zonal assignment and visualization features implemented as part of the Task 4 efforts were included in the GeoStat Help manual.

1.3.5 Task 5 – Technology Transfer

Task 5 focused upon item (5) above: developing technology transfer materials for dissemination to FDOT engineers. Also included among the Task 5 efforts was a hosted half-day web-based technology transfer event, exclusive to FDOT engineers. Supporting materials that were developed for the half-day (4-hour) web-based technology transfer event (e.g., slides, illustrative models) were provided to the FDOT as an information resource. The technology transfer event included presentation of materials that covered the theoretical basis of key algorithms implemented in GeoStat. Also, live demonstrations were given from within the GeoStat software, encompassing Geo-statistical analyses of both (illustrative) driven pile and drilled shaft configurations.

A key outcome from the Task 5 efforts consisted of establishing comprehensive materials that can be used to facilitate proliferation of Geo-statistical analysis tools in geotechnical design applications. Technology transfer content was also included for the newly added CPT-based and MWD-based Geo-statistical analysis features.

1.4 Scope

Organization of the report is as follows:

- In Chapter 2, a Geo-statistical approach is documented for predicting pile axial capacities with use of CPT data.
- In Chapter 3, a Geo-statistical approach is documented for using MWD data to predict axial resistances of drilled shaft portions located within limestone layers.
- In Chapter 4, documentation is provided for verifying computation of spatial correlation structures (variograms) when performing CPT-based analysis, and separately, MWD-based analyses. Also, stochastic simulation results are verified against respective results data when such simulation results are produced under CPT-based analysis, and separately, MWD-based analysis.

- In Chapter 5, an approach by which engineers can potentially estimate zonal radii is documented along with an illustrative case study.
- In Chapter 6, a summary is given of the project efforts for Tasks 1 through 5. In addition, recommendations for practice and potential future research are provided.
- Presented in Appendix A is the GeoStat Help Manual.
- Presented in Appendix B is the GeoStat Technical Manual

CHAPTER 2

GEO-STATISTICAL APPROACH FOR USING CPT DATA TO PREDICT PILE AXIAL CAPACITIES

2.1 Overview

Documented in Ch. 2 is an approach for conducting Geo-statistical analysis to predict axial capacities (and associated levels of uncertainty) of driven piles, with use of CPT measurements. In Sec. 2.2, key parameters are identified in relation to use of CPT site measurements in Geo-statistical analysis. Commonly used empirical methods for correlating CPT measurements to unit side and end bearing resistances of piles are summarized in Sec. 2.3. The adopted approach for characterizing spatial correlation structures, expressed as variograms, is discussed in Sec. 2.4. Stochastic simulation of pile axial resistance, based on CPT data, is focused upon in Sec. 2.5. A means of modifying simulated pile axial resistances to reflect CPT-specific method error is documented in Sec. 2.6.

2.2 CPT Parameters for Use in Geo-statistical Simulation

Collection of site measurements using CPT equipment was originally developed in Delft, the Netherlands; following the establishment of procedures and guidelines by Schmertmann (1978), this form of site investigation has become globally pervasive. As a high-level overview, CPT investigations involve pushing a cone with distinct tip and sleeve components into subsurface stratigraphy at a desired location within a site, and at a controlled rate of penetration. Instrumentation fitted along the cone permits measurements of the resistance that are attributable to the cone, and separately, the sleeve friction, and that must be overcome for the equipment to continue undergoing downward motion. Given a profile of CPT tip and sleeve measurements (typically assigned units of stress), unit resistances of foundation members such as driven piles are then calculated via empirical correlations. Given the prominent roles held by measurements of cone resistance (as related to tip) and sleeve friction (as related to side friction) as part of CPT data collection, these two parameters are focused upon in developing a Geo-statistical simulation approach.

2.2.1 Cone Resistance

During penetration of cones into soil media as part of CPT investigations, magnitudes of resistance measured by instrumentation dedicated to the cone are typically larger than respective measurements of sleeve friction. For example, even in soft fine-grained soils, cone resistance is generally measured to vary between (approximately) 1 tsf to 10 tsf, while respective measurements of sleeve friction range from approximately 0.01 tsf to 0.5 tsf (Robertson, 2013). Additionally, measurements of cone resistance are considered more accurate and repeatable than those of sleeve friction (Robertson, 2013). As indicated later in Ch. 2, the relatively greater accuracy and repeatability associated with cone resistance measurements (versus sleeve friction) holds implications when it is necessary to select a single parameter for use in procedures such as characterization of spatial correlation structures within a soil layer. Furthermore, note that cone

resistance is a required input parameter when performing CPT axial-capacity analysis for driven piles in software packages such as FB-Deep (Bridge Software Institute (BSI), University of Florida, Gainesville, FL).

2.2.2 Sleeve Friction

As aforementioned, the accuracy and repeatability of sleeve friction measurements as part of CPT is considered less than that associated with cone resistance. In an absolute sense though, sleeve friction measurements are widely utilized and remain indispensable for making CPT-based predictions of skin friction resistance of driven piles. For example, sleeve friction is included among the required inputs for pile axial capacity analysis in software such as FB-Deep when CPT data are being considered.

2.2.3 Friction Ratio

The ratio of sleeve friction to cone resistance, referred to as the friction ratio, is also taken into consideration in the present study. Variations in friction ratios along a given range of elevations proves useful in activities such as identification of soil type. For example, cohesionless soils typically exhibit friction ratios on the order of 1% or less (Rogers, 2014). Similarly, through-depth changes in friction ratio can also aid in estimation of layer top and bottom elevations (here, “through-depth” denotes from the top elevation to the bottom elevation for a vertically oriented profile of measured site data).

2.3 CPT Analysis Methods

Three analysis methods are identified for the purpose of empirically relating profiles of CPT measurements to unit end bearing and side friction quantities when calculating driven pile axial capacity. As discussed later in Sec. 2.5, these three methods are carried forward into an approach for conducting CPT-based Geo-statistical analysis. To aid in contextualizing the geostatistics approach discussed in Sec. 2.5, brief summaries of each empirical method are provided immediately below.

2.3.1 Schmertmann Method

The Schmertmann method of CPT analysis for predicting pile axial capacity was originally proposed in Schmertmann (1978). Unit end bearing resistance is calculated via the minimum path rule and is limited to 150 tsf. Unit side friction is limited to 1.2 tsf and is computed as the product of sleeve friction and an empirical scale factor. In turn, the empirical scale factor varies with respect to soil type, pile material, and measured values of sleeve friction. Additional details, including the various forms of the empirical expressions, are listed in Sec. 2.2.1 of the FB-Deep Help manual. Note that the Schmertmann method is applicable only to square and pipe piles.

2.3.2 UF Method

Previous FDOT-funded research (BD545, RPWO #43; Bloomquist et al. 2007) was undertaken, in part, to update the FDOT design procedures pertaining to CPT. Therein, a CPT analysis method was developed for use in Florida, and which is referred to as the UF method. Consistent with the Schmertmann method for CPT analysis, the UF method limits empirical calculations of pile (unit) end bearing resistance and side friction to 150 tsf and 1.2 tsf, respectively. However, the UF method only makes direct use of cone resistance for calculations of pile unit end bearing and side friction resistances. For example, depending on the soil type assigned to a given layer, the UF method specifies values of tip coefficients for empirically relating cone resistance to pile unit end bearing. Furthermore, skin friction resistance calculations make use of averaged cone resistance measurements along specified distances relative to the pile tip elevation of interest, as well as soil-specific side coefficients. Delineations of the empirical expressions, and averaging lengths specific to use of the UF method are listed in Sec. 2.2.2 of the FB-Deep Help manual. Note that the UF method is applicable only to square and round piles.

2.3.3 LCPC Method

Previous research funded by the French Highway Department led to the development of the LCPC method of CPT analysis for predicting pile axial capacity (Bustamante and Giamante, 1982). Unit end bearing resistance is calculated by taking the product of filtered, length-averaged cone resistance measurements at a given tip elevation and a soil-dependent empirical bearing factor. Unit side friction is calculated by selecting from families of pre-formed empirical curves that, in turn, relate values of cone resistance to unit side friction. Selection of an individual pre-formed empirical curve is based on the type of pile and soil being considered. The end bearing resistance expression; tabulated look-up procedure for selecting a pre-formed curve; and, families of pre-formed empirical curves are found in Sec. 2.2.3 of the FB-Deep Help manual. The LCPC method is applicable to square, round, cylinder, H-section, and pipe piles.

2.4 Variogram Generation

In the context of Geo-statistical applications, variograms graphically express the correlation structure of a given soil (or rock) property with respect to a spatial dimension (e.g., horizontal, vertical). That is, for a type of geotechnical site measurement (such as CPT cone resistance), the strength of correlation with respect to physical separation distance is encapsulated within a single variogram curve. See Ch. 2 of the GeoStat Technical Manual for a detailed treatment of variograms, and further, the role of variograms in Geo-statistical simulation. Discussed immediately below are those aspects of variogram generation that are pertinent to implementation of CPT analysis into the GeoStat software.

2.4.1 Selection of Variogram Variable

Variograms relate correlation strength to separation distance for a single variable. Given that cone resistance constitutes the more accurate and reliable measurement (versus sleeve friction), cone resistance is selected as the variable for use in generating layer-specific (horizontal, vertical) variograms. As discussed in Sec. 2.5, cone resistance is therefore treated as a ‘primary’ variable for both the CPT-based characterization of spatial correlation structure as well as for stochastic simulation.

2.4.2 Procedure

The algorithm for generating variograms implemented in GeoStat is robust to the variable of interest. That is, the algorithm can generate spatial correlation structures for any of SPT-N blow counts, unconfined compression strength (e.g., for drilled shaft portions in limestone layers), and CPT cone resistance. Therefore, the horizontal and vertical variogram generation algorithm detailed in Sec. 2.5.3 of the GeoStat Technical Manual is adopted as part of the implementation efforts for CPT analysis.

2.5 Geo-statistical Simulation of Pile Axial Capacity Using CPT Data

2.5.1 Overview

Considerations made for identifying key variables (Sec. 2.2), empirical pile resistance calculation methods (Sec. 2.3), and variogram generation (Sec. 2.4) are now combined as preparatory steps for the purpose of conducting Geo-statistical simulation using CPT data (Fig. 1). In particular, the preparatory steps are initiated by gathering a collection of at least two vertical profiles of CPT cone resistance and sleeve friction measurements. Here, each profile possesses an associated plan-view location (e.g., northing, easting) and each measurement along a vertical profile possesses an associated elevation.

Next, the empirical method to be used during stochastic simulation is selected from that of the Schmertmann, UF, or LCPC methods. Subsequently (Fig. 1, center), layers are defined for the collection of CPT data. GeoStat facilitates visual inspection of through-depth profiles for several types of geotechnical site measurements. More specifically, all profiles for a type of measurement are collapsed down to a single plot of a measurement versus elevation (regardless of northing, easting). In this way, indications of the number of layers can potentially be inferred from (for example) sudden changes along the vertical profiles of CPT cone resistance and sleeve friction. Profile plots of the friction ratio may serve as a particularly effective means of identifying both layer top and bottom elevations as well as soil type. As documented in Sec. 2.3.2, if the UF method is selected as the empirical calculation method for CPT analysis, then the side coefficient and tip coefficient must also be given for each layer.

As the final preparatory step preceding stochastic simulation (Fig. 1, bottom), variograms are formed (horizontal, vertical) using available pairs of cone resistance measurements. The

GeoStat tool automatically searches for pairs of measurements, per layer, given a specified range of separation (lag) distances and search tolerances. Guidance for selecting variogram lag distance intervals and search tolerance parameters is given Ch. 2, 4, and 5 of the GeoStat Technical Manual.

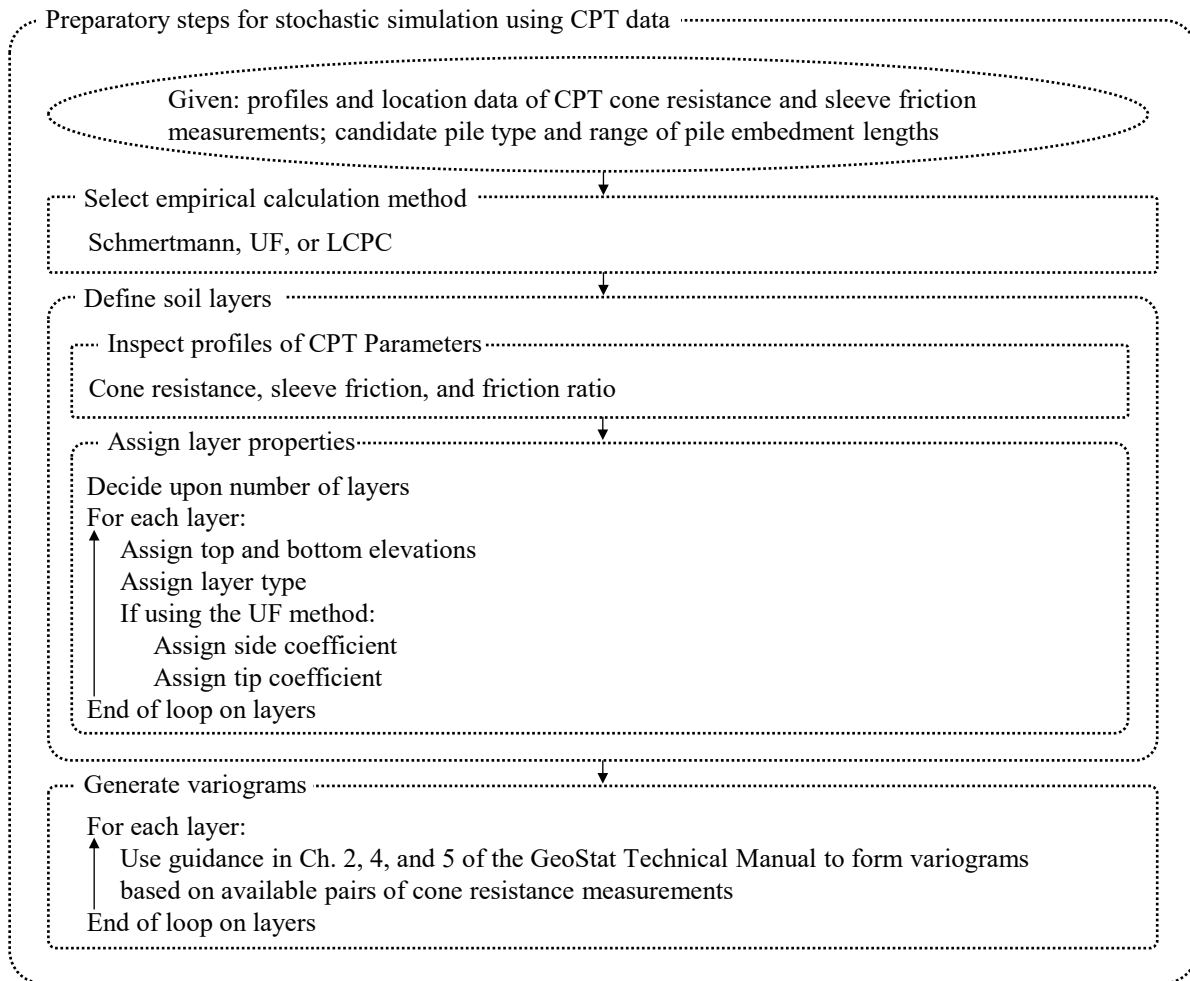


Figure 1. Preparatory steps for performing stochastic simulation of pile axial capacity with use of CPT data

Focus for the remainder of Sec. 2.5 is given to documenting the procedure for generating realizations of CPT data and quantifying pile axial capacity (and uncertainty), as facilitated by carrying out the preparatory steps discussed above. In particular, key aspects of the CPT-based stochastic simulation procedure include: 1) producing through-depth realizations of cone resistance values (as discussed in Sec. 2.5.2); 2) co-simulation of sleeve friction values (Sec. 2.5.3); 3) performing axial capacity analysis for each realization (Sec. 2.5.4); and, 4) generation of profile plots of mean pile (axial) capacity along with profile plots of descriptive statistics.

2.5.2 Simulation of Cone Resistance Values

Recall that cone resistance measurements are utilized when forming layer variograms for CPT analysis, and further, cone resistance is designated as the ‘primary’ variable for use in CPT analysis within GeoStat. The algorithms implemented in GeoStat for the purposes of producing realizations of the ‘primary’ variable are robust to the type of geotechnical data being processed. Therefore, the existing algorithm portions of unconditional and conditional simulation—that involve generation of ‘primary’ variable values—are utilized for producing through-depth realizations of cone resistance when conducting CPT analysis. The unconditional and conditional simulation algorithms are presented, respectively, in Sec 2.6.1 and Sec. 2.6.2 of the GeoStat Technical Manual (Appendix B).

2.5.3 Co-simulation of Sleeve Friction Values

Consistent with other forms of analysis available within GeoStat, CPT-based stochastic simulation is conducted such that through-depth values of cone resistance are produced prior to generation of other types of CPT data. Then, other geotechnical parameter values required for axial capacity calculations (e.g., sleeve friction) are generated via the process of co-simulation. The procedure for simulating values of sleeve friction is presented in Fig. 2. For the sake of brevity, the following two definitions are introduced, where cone resistance is denoted to as q_{c_CPT} and sleeve friction is denoted to as f_{s_CPT} .

The co-simulation approach allows for incorporation of the strength of correlation between physically measured values of q_{c_CPT} and f_{s_CPT} on a site-specific (or zone-specific) basis. Two major steps are included in the co-simulation procedure: preparation of simulation parameters (Fig. 2, top); and, performing stochastic simulation to produce counterpart realizations of f_{s_CPT} values (Fig. 2, bottom). The preparatory step begins by iterating through all profiles ($n_{borings}$) of physically measured CPT data to identify pairs of q_{c_CPT} and f_{s_CPT} . Having cataloged the set of physically measured values and the respective elevations within the profile, a nearest-neighbor search is then conducted. Namely, for every value of q_{c_CPT} within $\{q_{c_CPT}\}$, the nearest vertically positioned value of f_{s_CPT} (within $\{f_{s_CPT}\}$) is assigned as a paired value. The paired values of q_{c_CPT} and f_{s_CPT} are then stored, respectively in $\{q_{c_nearest}\}$ and $\{f_{s_nearest}\}$. Note that all profiles of physical measurements contribute to the $\{q_{c_nearest}\}$ and $\{f_{s_nearest}\}$ quantities (i.e., these quantities are site-specific or zone-specific, but not profile-specific).

As the next preparatory step in co-simulation of f_{s_CPT} values, data transformations are carried out (Fig. 2, middle). Specifically, for the total number of pairs (n_{pairs}) across all profiles of measured values, the computed natural log is computed for values within $\{q_{c_nearest}\}$ and then stored in $\{q_{c_ln}\}$. Likewise, computed natural log values of $\{f_{s_nearest}\}$ are computed and stored in $\{f_{s_ln}\}$. Next, a regression expression is formed where entries within $\{f_{s_ln}\}$ are designated as the dependent variable:

$$\{f_{s_ln}\} = b \cdot \{q_{c_ln}\} + a \quad (1)$$

Where b is the slope of the regression expression and a is the intercept. Note that a correlation coefficient, R , is also produced as part of the regression expression formation.

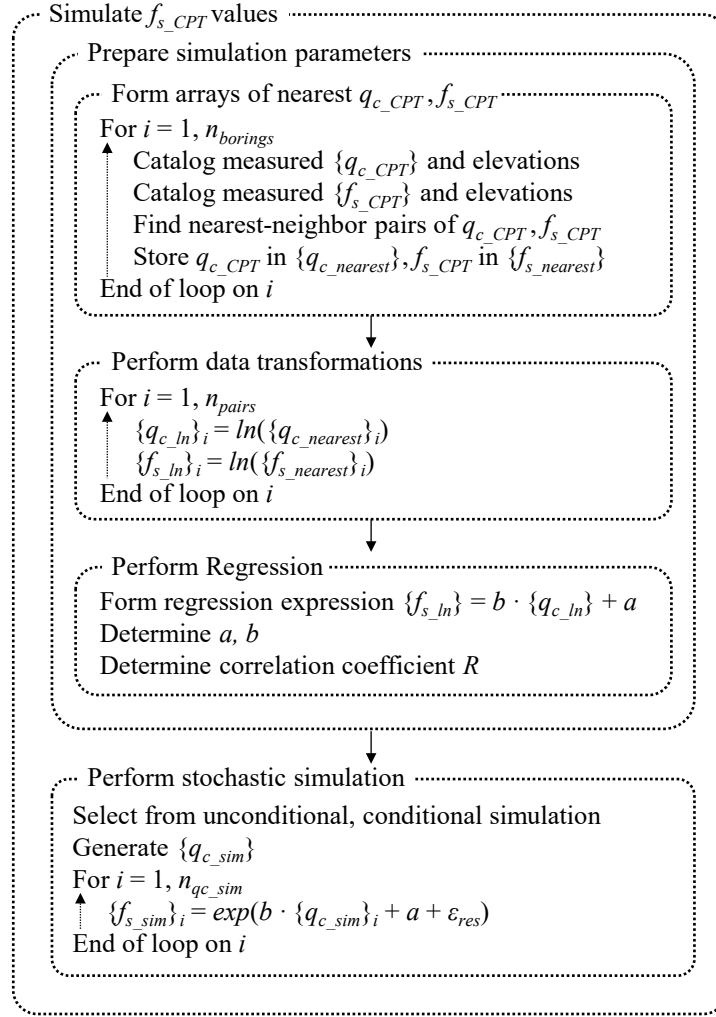


Figure 2. Co-simulation of sleeve friction, f_{s_CPT}

Subsequent to preparation of the simulation parameters, stochastic simulation is carried out as co-simulation of values for sleeve friction (Fig. 2, bottom). Here, a selection is made regarding unconditional or conditional simulation, and the algorithms documented in Ch. 2 of the GeoStat Technical Manual are utilized to produce the desired number of simulated profiles of cone resistance, $\{q_{c_sim}\}$. For the number of entries (n_{qc_sim}) comprising a given profile of $\{q_{c_sim}\}$ values, the exponential of the regression expression from Eq. 1 is utilized:

$$\{f_{s_sim}\}_i = \exp(b \cdot \{q_{c_sim}\}_i + a + \varepsilon_{res}) \quad (2)$$

where the i^{th} entry in $\{f_{s_sim}\}$ contains a simulated value of sleeve friction. Note that a residual error term, ε_{res} , is introduced when populating entries within $\{f_{s_sim}\}$. For each time Eq. 2 is

evaluated, the residual error (ϵ_{res}) is sampled from normal distribution with zero-valued mean and variance, σ_{res}^2 , of:

$$\sigma_{res}^2 = \sigma_{f_{s_ln}}^2 \cdot (1 - R^2)^2 \quad (3)$$

where $\sigma_{f_{s_ln}}^2$ is the variance of the entries contained within $\{f_{s_ln}\}$.

2.5.4 Computing Pile Axial Capacity

As the next major step in the overall stochastic simulation procedure, pile axial capacity is calculated throughout a range of desired elevations. That is, one profile at a time is analyzed by relating the associated cone resistance and sleeve friction values to unit resistances and then integrating the unit resistances. As indicated in McVay et al. (2012) and Faraone et al. (2021), 2000 realizations is generally considered to constitute a sufficient sample size. Regardless of the sample size (i.e., number of profiles simulated), the approach adopted herein is to make default use of the axial capacity calculation software FB-Deep to compute resistance quantities.

For pile axial capacity analysis with use of CPT data, the FB-Deep software requires as input: the pile type and size; range of candidate embedment lengths; soil layer top and bottom elevations; the empirical calculation method; and, profiles of cone resistance and sleeve friction. Additionally required inputs include the friction ratio (f_{s_CPT} / q_{c_CPT} , expressed as a percentage), and specific to use of the UF method, the layer-specific side friction (F_s) and tip (k_b) coefficients. Guidance on selection of F_s and k_b values per layer is given Sec. 2.2.2 of the FB-Deep Help Manual, along with default values that are utilized if no custom values are specified. Recalling the method summaries provided in Sec. 2.3, only those pile types indicated in Table 1 may be carried forward into the axial capacity calculations, given a selected empirical method.

Table 1. Applicable pile types for the empirical methods of CPT analysis

Empirical method for CPT analysis	Square	Round	Cylinder	Pipe	H-section
Schmertmann	✓			✓	
UF	✓	✓			
LCPC	✓	✓	✓	✓	✓

As part of the overall CPT-based stochastic simulation procedure, the GeoStat software (by default) makes use of the FB-Deep engine to compute axial capacities along the range of specified embedment lengths, and for each profile of simulated values of cone resistance and sleeve friction. Profile plots of the pile mean side, end bearing, and total resistance are then formed within GeoStat, using the collected set of analysis results obtained from repeated use of the FB-Deep engine. Also, profile plots of variability (e.g., variance; coefficient of variation, CV) are formed and made available for visual inspection within the GeoStat UI.

2.6 Method Error

2.6.1 Overview

Stochastically simulated pile axial resistance quantities (side, tip, and total), obtained from the CPT-based procedure discussed in Sec. 2.5, are modified to reflect bias intrinsic to the underlying, empirical axial capacity calculation methods. In this way, profiles of design-relevant resistance quantities and associated uncertainties (e.g., expressed as LRFD resistance factors, ϕ) are formed. The approach for incorporating method error into CPT analysis (discussed in Sec. 2.6.2) is adopted from Faraone et al. (2021). To ensure that the method error approach adopted herein is representative of deep foundation member design for bridges located in Florida, a catalog containing load-test data and empirical pile capacity predictions is first identified, as documented in Sec. 2.6.3. Then, the methodology described in Faraone et al. (2021) is applied to the catalog of data (one empirical method at a time) to establish method error parameters for use in CPT-based analysis within GeoStat (Sec. 2.6.4).

2.6.2 Approach

As noted above, the approach for incorporating method error into Geo-statistical analysis with use of CPT data is adopted from the relatively more general approach proposed in Faraone et al. (2021). Key steps of the method approach are presented in Fig. 3. As emphasis, this approach is robust to the resistance variable being considered. However, the procedure (as delineated) requires the ratios of measured versus predicted resistance to be lognormally distributed.

The overall process begins with collection of load-test data across pertinent sites (Fig. 3, top), including pile properties, soil conditions, and measured resistance (the latter stored in $\{q_{meas}\}$). An empirical method for calculating predictions of axial capacity is then selected. Next, for each of the number of load tests identified (n_{lt}), the selected empirical method is utilized to calculate respective predictions of axial capacity, stored in $\{q_{pred}\}$. Further, for each load test, the ratio of measured and predicted resistance is determined, $\{R_{mp}\}$.

A filtering step is then undertaken (Fig. 3), which involves calculation of the mean of the ratios of measured versus predicted resistance, R_{mean_mp} . The standard deviation, σ_{mp} , of the entries within $\{R_{mp}\}$ is also determined. A filter is then applied, where any entries in $\{R_{mp}\}$ that lie outside of ± 2 standard deviations (σ_{mp}) from the mean resistance ratio, R_{mean_mp} , are removed. The associated load tests are excluded from further consideration, and n_{lt} is accordingly decremented. In other words, only those load tests that remain after application of the filter are carried further forward into the method error procedure.

Assessment of lognormality is carried out upon the remaining data set (Fig. 3, middle). The assessment begins with selection of an acceptable significance level, p_s , where 5% ($p_s = 0.05$) is typical, and is adopted herein. Then, for each of the (post-filtering) load tests, the $\{R_{mp_ln}\}$ is formed as the entry-wise natural log of $\{R_{mp}\}$. In turn, Lilliefors (1967) statistical test is conducted using $\{R_{mp_ln}\}$ and p_s . Here, because the entries in $\{R_{mp_ln}\}$ have been transformed using the natural log function, the null hypothesis being tested can (effectively) be stated as: the data come from a

lognormally distributed population. If the Lilliefors test leads to rejection of the null hypothesis, then the method error procedure is halted and cannot be utilized. Otherwise, if the null hypothesis cannot be rejected, then the method error procedure is applicable and can be continued.

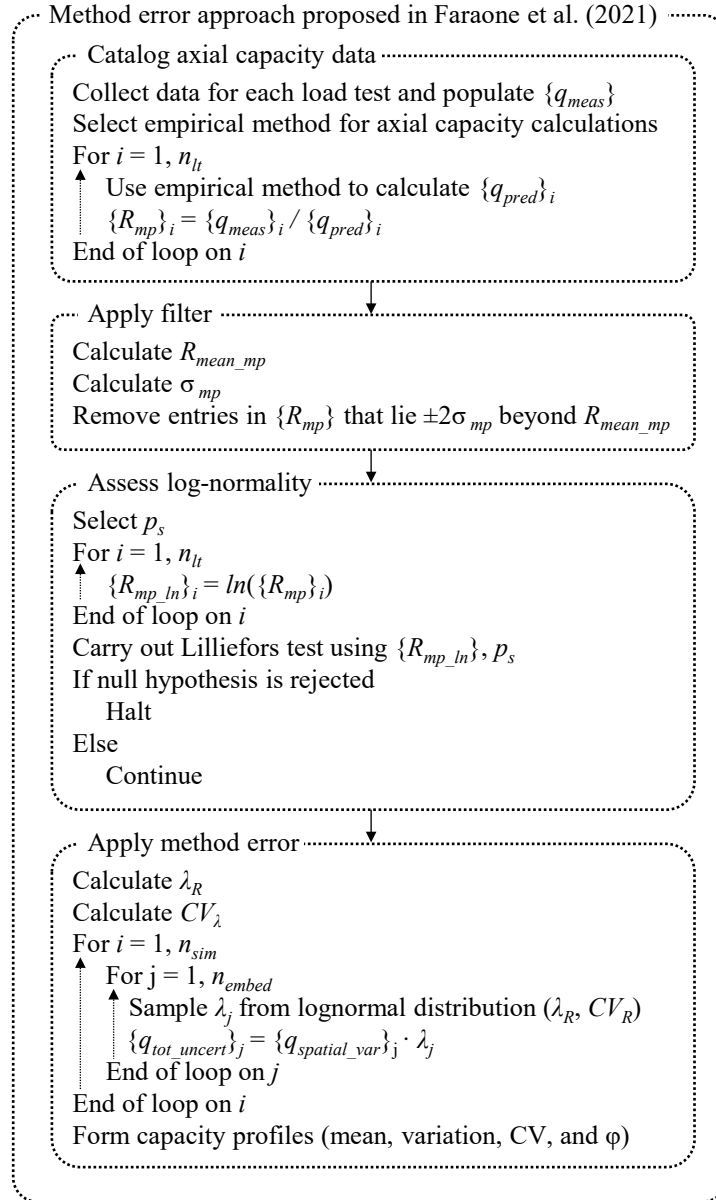


Figure 3. Method error procedure for CPT-based analysis of pile axial capacity

Having collected load test data, formed empirical predictions of axial capacity, applied data filtering, and assessed lognormality, the method error procedure from Faraone et al. (2021) culminates in sampling and applying resistance ratios to resistance quantities obtained from stochastic simulation. In this way, predictions of (for example) axial capacity are produced that reflect both spatial variability and method error phenomena (i.e., total uncertainty). As delineated

in Fig. 3, bottom, application of the method error corrections begins with calculation of the mean (again, post-filtering) resistance ratio, λ_R :

$$\lambda_R = \frac{1}{n_{lt}} \sum \lambda_i \quad (4)$$

where λ_i is the ratio of the i^{th} entry in $\{q_{meas}\}$ and, respectively, in $\{q_{pred}\}$ after the filtering step has been completed. Note that the summation is carried out on i from 1 to n_{lt} . A coefficient of variation, CV_λ , is also calculated with use of Bessel's correction:

$$CV_\lambda = \frac{\left(\frac{1}{n_{lt} - 1} \sum (\lambda_i - \lambda_R)^2\right)^{0.5}}{\lambda_R} \quad (5)$$

Then, the method error is applied for each of the number of realizations (n_{sim}) produced from stochastic simulation (and which reflect spatial variability phenomena), and in turn, profiles of resistance values, $\{q_{spatial_var}\}$, associated with the number of candidate member embedment lengths considered (n_{embed}). Namely, for the i^{th} profile realization and j^{th} entry of simulated resistance within $\{q_{spatial_var}\}$, a ratio of measured versus predicted resistance, λ_j , is sampled from a lognormal distribution. Note that the lognormal distribution being sampled from satisfies the parameters λ_R and CV_λ . A simulated value of resistance that reflects total uncertainty is then calculated as the product of λ_j and $\{q_{spatial_var}\}_j$, denoted as $\{q_{tot_uncert}\}_j$. Subsequently, profiles of mean capacity can be formed, along with profiles of variance, coefficient of variation (CV), and LRFD- ϕ .

2.6.3 Catalog of Measured and Predicted Pile Axial Capacities

To ensure that the method error approach described in Sec. 2.6.2 is implemented in a manner that is representative of CPT analysis of Florida bridges, a catalog of measured and CPT-based predictions of pile axial capacities throughout Florida bridge sites is identified and utilized. More specifically, previous FDOT research (BD545, RPWO #43; Bloomquist et al. 2007) is drawn upon. Listed in Table 2 are measured and predicted pile axial capacities as obtained from 21 configurations and more than 10 Florida bridge sites (Bloomquist et al. 2007). For each configuration, the Davisson capacity associated with the load-test measurement is given along with respective predictions obtained from use of the Schmertmann, UF, and LCPC (empirical) methods.

In accordance with the filtering process detailed above (recall Fig. 3), the mean of the ratios (R_{mean_mp}) and corresponding standard deviation (σ_{mp}) associated with each of the Schmertmann, UF, and LCPC methods are listed in Table 3. The respective lower and upper bound thresholds associated with the filtering process are also given. Applying these filters to the 21 candidate configurations listed in Table 2 results in exclusion of load test 18 for all three empirical methods, and additionally, exclusion of load test 21 when considering the LCPC method (Table 4).

Subsequent to application of the filtering process, all remaining terms are transformed using the natural log function, and Lillieforth testing for lognormality is conducted (again, recall

Fig. 3). For each of the (filtered) data sets, one set pertaining to each empirical method, the null hypothesis of lognormality cannot be rejected at a significance level of 5% (i.e., $p_s = 0.05$). Therefore, each of the empirical methods (with associated, filtered data sets) are judged to be applicable for use in computing CPT-based pile axial capacities in a manner that accounts for total uncertainty.

Table 2. Measured versus CPT-based predictions of Davisson capacity for driven piles in Florida (Bloomquist et al. 2007)

Load test	Measured (tons)	Schmertmann (tons)	UF (tons)	LCPC (tons)
1	140	112	152	184
2	165	224	170	264
3	103	217	143	228
4	250	223	266	374
5	266	166	225	273
6	213	205	245	305
7	194	155	192	255
8	283	242	358	434
9	185	275	272	286
10	479	311	375	604
11	479	405	380	545
12	249	174	236	273
13	480	229	303	387
14	250	216	262	337
15	393	283	329	378
16	438	304	411	501
17	425	468	693	792
18	735	187	432	502
19	332	281	221	336
20	250	271	221	317
21	425	310	344	304

Table 3. Descriptive statistics of measured versus predicted pile axial capacity for filter usage

Empirical method	Ratio mean, $R_{mean\ mp}$	Ratio standard deviation, σ_{mp}	Filter lower bound, $R_{mean\ mp} - 2\sigma_{mp}$	Filter upper bound, $R_{mean\ mp} + 2\sigma_{mp}$
Schmertmann	1.32	0.69	0.00	2.71
UF	1.08	0.29	0.50	1.65
LCPC	0.85	0.26	0.33	1.38

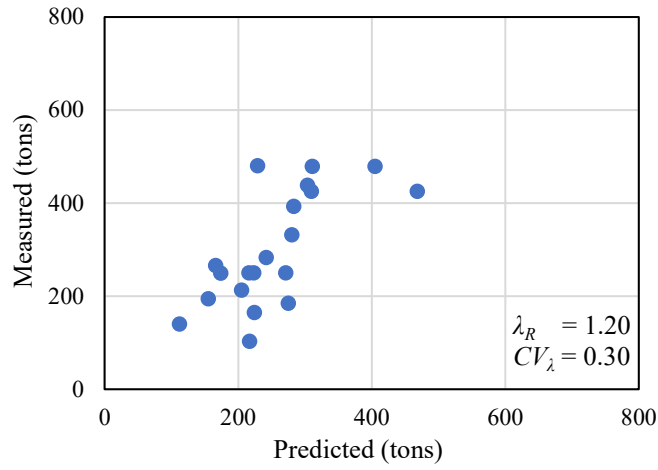
Table 4. Load tests excluded by filter

Empirical method	Load test(s) excluded
Schmertmann	18
UF	18
LCPC	18, 21

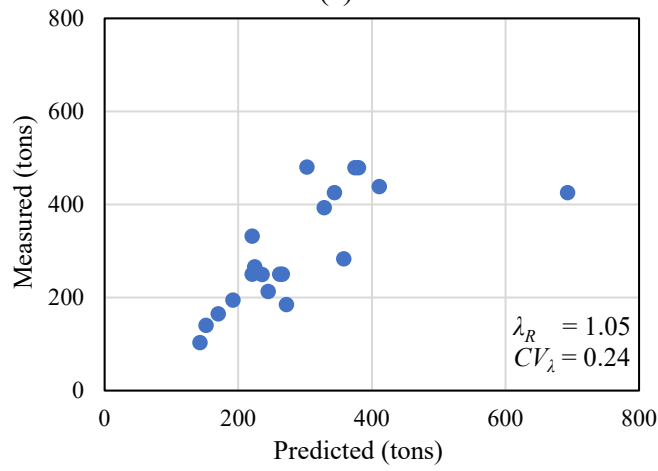
2.6.4 Method Error Parameters

Mean ratios, λ_R (Eq. 4), and coefficients of variation, CV_λ (Eq. 5), for use in method error calculations are annotated along with scatterplots of (post-filtering) measured versus predicted resistance in Fig. 5. Parameter values are additionally listed in Table 5. For the three CPT-based

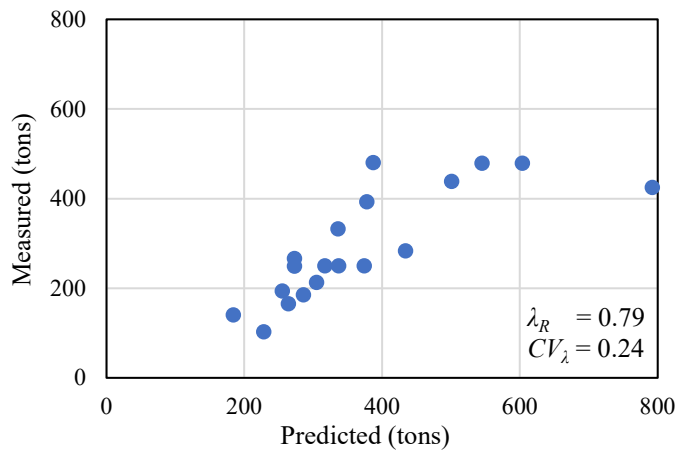
methods implemented in GeoStat, these parameter values (Table 5) are recommended for use when calculating total uncertainty of driven pile axial capacities.



(a)



(b)



(c)

Figure 4. Scatterplots of (filtered) measured versus CPT-based predictions of pile axial capacity: (a) Schmertmann; (b) UF; (c) LCPC

Table 5. Method error parameters for CPT-based total uncertainty calculations

Empirical method	λ_R	CV_λ
Schmertmann	1.20	0.30
UF	1.05	0.24
LCPC	0.79	0.24

CHAPTER 3

GEO-STATISTICAL APPROACH FOR USING MWD DATA TO PREDICT SHAFT AXIAL RESISTANCE IN LIMESTONE LAYERS

3.1 Overview

Documented in Ch. 3 is an MWD-based approach for conducting Geo-statistical analysis to predict axial resistances and associated levels of uncertainty of portions along drilled shafts that are embedded in limestone. Geo-statistical analysis for drilled shaft portions in non-limestone layers is conducted in the same manner as that developed in BDV31-977-108 (Davidson et al. 2020, where SPT-N blow count values are utilized). In Sec. 3.2, key parameters are identified in relation to use of MWD site measurements in Geo-statistical analysis. An approach for characterizing spatial correlation structures, expressed as variograms, is discussed in Sec. 3.3. Stochastic simulation of shaft axial resistance, based on MWD data, is focused upon in Sec. 3.4. Modification of simulated shaft axial resistances to reflect MWD-specific method error is documented in Sec. 3.5.

3.2 MWD Parameters for Use in Geo-statistical Simulation

The assessment of rock strength properties during construction of drilled shafts has been identified as an area of interest within geotechnical engineering (ISO 2016; FDOT MWD Test Method FM 5-625). Motivated in part by this identified area of interest, FDOT-funded research was previously undertaken to establish drilled shaft construction technologies that facilitate real-time assessment of rock strengths (namely, Florida limestone), leading to improved assessments of subsurface variability for geotechnical design. More specifically, MWD has been investigated across multiple studies, where MWD consists of the application of monitoring and recording of drilling data during the drilling process (McVay and Rodgers, 2020). In BDV31-977-20 (McVay and Rodgers, 2016), the potential for using drilling parameters to predict strengths of Florida limestone was assessed. After investigating the influences of drilling parameters such as crowd, torque, penetration rate, rotational speed, and bit diameter, McVay and Rodgers (2016) found that it was viable to use drilling parameters to estimate rock strengths (and in turn, side shear resistances associated with drilled shafts in limestone). Accordingly, drilling parameters are focused upon in developing a Geo-statistical simulation approach in the following.

3.2.1 Specific Energy

In previous studies, the influences of drilling parameters on rock strengths (and side shear of drilled shafts) were assessed individually and in combination. However, as reported in BDV31-977-91 (McVay and Rodgers, 2020), combining the drilling parameters for use in geotechnical assessments is particularly effective. One such combination is found in that of specific energy (e), as defined in McVay and Rodgers (2020):

$$e = \frac{F}{A} + \frac{2\pi NT}{Au} \quad (6)$$

where F is the average crowd (downward force); A is the cross-sectional area of the excavation, defined by the bit diameter; N is the rotational speed; T is the torque; and, u is the penetration rate.

Based on field testing and laboratory experiments (McVay and Rodgers 2020), specific energy has been shown to be an excellent parameter for estimating the side shear resistance of drilled shafts and auger cast piles socketed into limestone. For example, field testing was carried out to measure specific energy and to evaluate nominal side shear for load tested drilled shafts and auger cast piles at multiple Florida bridge sites spread across the state. From all of the locations tested, a total of 36 data points were collected that directly compared specific energy and mobilized unit side shear. Specific energy was found to correlate with the mobilized unit side shear to the extent that the coefficient of determination (R^2) was determined to be 0.99, when the relationships developed by the University of Florida were used. It should be noted that ongoing research is in progress to continue collecting data and update the correlation coefficients for different areas of the State. Based on the successful results obtained in previous research efforts, specific energy is selected for use as part of the MWD implementation in the present study.

3.2.2 Unconfined Compressive Strength and Tensile Strength

Two parameters that are commonly used in estimating axial resistances of drilled shafts in limestone are unconfined compressive strength, q_u , and tensile strength, q_t . That is, given values of q_u and q_t , many formulations exist for estimating quantities such as unit side shear (e.g., the formulation given in McVay et al. 1992). In Rodgers et al. (2018b), a correlation was developed between specific energy (e) and unconfined compressive strength (q_u) of Florida limestone. Further, in McVay and Rodgers (2020), a derivation was given that allows for specific energy (e) to be correlated to unconfined compressive strength (q_u , per Rodgers et al. 2018b), and in turn, for unconfined compressive strength (q_u) to then be used in estimating tensile strength (q_t). Pertinent expressions from these previous studies are utilized in the present study (where the expressions are presented later in Sec. 3.4) as part of developing a Geo-statistical analysis methodology with use of MWD site data.

3.3 Variogram Generation

In Geo-statistical analysis, variograms are used to graphically (and quantitatively) express correlation structures of soil/rock properties with respect to horizontal and vertical spatial dimensions. Stated alternatively, for a collection of geotechnical site data (such as unconfined compressive strength values), the strength of correlation with respect to physical separation distance between pairs of values is contained in the respective ordinate of the variogram curve. See Ch. 2 of the GeoStat Technical Manual for a detailed treatment of variograms, and further, for discussion of the role of variograms in Geo-statistical simulation. Discussed in Sec. 3.3 of the current report are aspects of variogram generation that are pertinent to implementation of MWD analysis in the GeoStat software.

3.3.1 Selection of Variogram Variable

Unconfined compressive strength (q_u) plays a prominent role in the determination of unit resistances of drilled shafts in limestone. Given such prominence—and the derivations from Rodgers et al. (2018b), McVay and Rodgers (2020)—unconfined compressive strength (q_u) is selected as the variable for use in generating layer-specific (horizontal, vertical) variograms. In other words, unconfined compressive strength (q_u) is treated as a “primary” variable for both the MWD-based characterization of spatial correlation structure as well as for stochastic simulation.

3.3.2 Procedure

The algorithm for generating variograms implemented in GeoStat is robust to the variable of interest. That is, the algorithm can generate spatial correlation structures for any of SPT-N blow count, unconfined compression strength (e.g., for drilled shaft portions in limestone layers), and CPT cone resistance. Therefore, the horizontal and vertical variogram generation algorithm detailed in Sec. 2.5.3 of the GeoStat Technical Manual is adopted as part of the implementation efforts for MWD analysis.

3.4 Geo-statistical Simulation of Shaft Axial Resistance in Limestone with MWD Data

3.4.1 Overview

Considerations made for identifying key variables (Sec. 3.2) and variogram generation (Sec. 3.3) are now combined as preparatory steps for the purpose of conducting Geo-statistical simulation using MWD data (Fig. 5). In particular, the preparatory steps are initiated by gathering (Fig. 5, top) a collection of at least two vertical profiles of specific energy (e) measurements. Here, each profile possesses an associated plan-view location (e.g., northing, easting) and each measurement along a vertical profile possesses an associated elevation. In addition, for the drilled shaft of interest, the geometric properties (e.g., diameter, range of embedment lengths) must be known.

Upon moving forward with use of an MWD empirical calculation method (Fig. 5, center), layers are defined for the collection of MWD data, where GeoStat facilitates visual inspection of through-depth profiles for several types of geotechnical site measurements. More specifically, all profiles for a type of measurement are collapsed down to a single plot of a measurement versus elevation (regardless of northing, easting). In this way, indications of the number of layers can potentially be inferred from (for example) sudden changes along the vertical profiles of specific energy values. In addition, values of unconfined compressive strength (q_u), as calculated from measurements of specific energy (per Rodgers et al. (2018b), see Sec. 2.4.2) can be viewed to aid in identifying both layer top and bottom elevations.

As the final preparatory step preceding stochastic simulation (Fig. 5, bottom), variograms are formed (horizontal, vertical) using available pairs of unconfined compressive strength (q_u) values. The GeoStat tool automatically searches for pairs of measurements, per layer, given a

specified range of separation (lag) distances and search tolerances. Guidance for selecting variogram lag distance intervals and search tolerance parameters is given Ch. 2, 4, and 5 of the GeoStat Technical Manual.

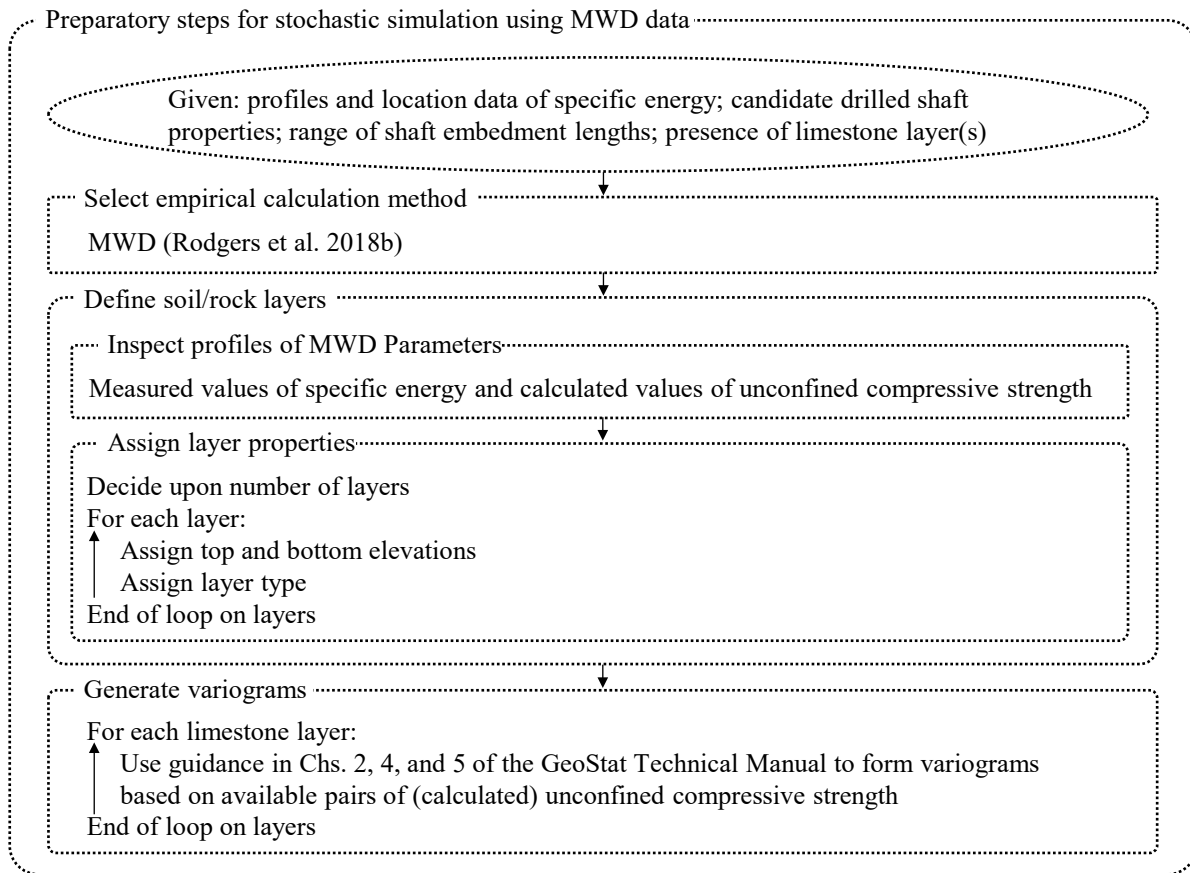


Figure 5. Preparatory steps for performing stochastic simulation of shaft axial resistances within limestone layers with use of MWD data

Focus for the remainder of Sec. 3.4 is given to documenting the procedure for generating realizations of MWD data and quantifying shaft axial capacity (and uncertainty), as facilitated by carrying out the preparatory steps discussed above. In particular, key aspects of the MWD-based stochastic simulation procedure include: 1) producing through-depth realizations of unconfined compressive strength values (as discussed in Sec. 3.4.2); 2) calculation of tensile strength values (Sec. 3.4.3) and other supporting parameters (Sec. 3.4.4, Sec. 3.4.5); 3) performing axial shaft resistance analysis for each realization (Sec. 3.4.6); and, 4) generation of profile plots of mean shaft (axial) resistance along with profile plots of descriptive statistics.

3.4.2 Simulation of Unconfined Compressive Strength Values

As aforementioned, the expression given in Rodgers et al. (2018b) that relates values of q_u and e is adopted as part of the MWD implementation in the present study. More specifically, the expression given in Rodgers et al. (2018b) is:

$$e = 0.0066 \cdot q_u^2 + 13.68 \cdot q_u \quad (7)$$

where units for all variables are in psi. Note that in Eq. 7, unconfined compressive strength (q_u) serves as the independent variable. However, for the MWD-based implementation in GeoStat as part of the present project, measurements of specific energy (e) are taken as the independent variable and used to calculate values of the “primary” variable (unconfined compressive strength, q_u). Therefore, an inverted expression of Eq. 7 is utilized, and is given as:

$$q_u = \frac{-13.7 + (13.7^2 - 4 \cdot 0.0066 \cdot (-e))^{0.5}}{2 \cdot 0.0066} \quad (8)$$

where units for all variables are in psi (adapted from the SI expression in Rodgers et al. 2018a).

Having developed a means of producing values of the “primary” variable for MWD analysis (q_u), the algorithms available within GeoStat can be leveraged without the need for further modification. In other words, the algorithms implemented in GeoStat for the purposes of producing realizations of the “primary” variable are robust to the type of geotechnical data being processed. Therefore, the existing algorithm portions of unconditional and conditional simulation—that involve generation of “primary” variable values—are utilized for producing through-depth realizations of unconfined compressive strength (q_u) when conducting MWD analysis. The unconditional and conditional simulation algorithms are presented, respectively, in Sec 3.6.1 and Sec. 3.6.2 of the GeoStat Technical Manual.

3.4.3 Calculation of Tensile Strength Values

When computing axial capacities of drilled shafts in limestone, it is typically necessary to consider additional data types beyond that of unconfined compressive strength (q_u). In particular, values of tensile strength (q_t) are also commonly needed for estimation of unit side shear resistance. Accordingly, as part of producing MWD-based realizations of limestone properties during Geostatistical simulation in GeoStat, values of tensile strength (q_t) are estimated based on simulated values of q_u . More specifically, the derivation given in McVay and Rodgers (2020) is drawn upon, which makes use of the Florida geomaterials equation:

$$q_t = 0.436 \cdot q_u^{0.825} \quad (9)$$

where units for all variables are in psi. In this way, for every simulated value of unconfined compressive strength (q_u) that is produced, a corresponding value of tensile strength (q_t) is directly calculated using Eq. 9.

3.4.4 Estimation of Rock Recovery and RQD

Rock recovery and RQD are generally determined by inspecting cores obtained from rock coring operations. Rock recovery is defined as the borehole core recovery percentage and is calculated as the total length of the recovered core sample divided by the length of the core run. In contrast, RQD signifies the degree of jointing or fracture in a rock mass, measured as a percentage. Values of RQD are calculated by summing the lengths of all sound rock pieces that are a minimum of 4 in. long and dividing the sum by the total length of the core run. When MWD is applied in bored pile applications (e.g., drilled shafts, auger cast piles), core samples are not extracted within the footprint of the foundation during the drilling process. Therefore, rock recovery and RQD are not physically measured. However, these quantities can be simulated for MWD bored pile applications to allow for settlement and side shear adjustments to be made using only the collected MWD data.

The procedure for estimating rock recovery values for use in MWD-based stochastic simulation (REC_{MWD}) is summarized in Fig. 6. First, a given profile of measured values of specific energy (e) versus elevation (z) is divided into n_{int} intervals of 5 ft, starting at the ground surface elevation. A length of 5 ft is adopted to mimic rock coring operations that typically occur over 5-ft intervals (i.e., the typical total length of a core run). [Note that the bottommost interval may be less than 5 ft.] For the i^{th} interval, and in turn, for each measured value of specific energy, e , within the interval, a comparison is made with respect to a threshold value. Here, a specific energy threshold is adopted such that $e_{threshold} = 2,000$ psi. The specific energy threshold is used to eliminate any data points that fall below the defined threshold, and thereby, to exclude soil and IGM materials from counting toward the assessment of rock strength. Accordingly, the number of values of specific energy, e , (within the interval) that are equal to or greater than the threshold value, $e_{threshold}$, are accumulated via incrementation of n_{accept} . The REC_{MWD} value for the interval is then calculated as the number of data points (again, per interval) possessing specific energy values greater than $e_{threshold}$, divided by the total number of data points within the interval (i.e., the ratio of n_{accept} and the pre-excluded data points, n_e). Note that the total number of data points within the interval (n_e) is dependent upon the MWD sampling resolution. Furthermore, note that one unique value of rock recovery (REC_{MWD}) is assigned throughout each interval. During MWD-based stochastic simulation, when the process is carried out to pair simulated q_u values with values of rock recovery, the recovery values are selected from the set of interval-specific values from across all currently enabled boring locations.

Estimation of RQD values in association with MWD-based stochastic simulation is summarized in Fig. 7, where the estimated values are referred to herein as RQD_{MWD} . Note that the same overall process as that utilized for rock recovery (REC_{MWD}) is employed (e.g., one value of RQD_{MWD} is estimated per interval). However, for estimating values of RQD_{MWD} , differences in elevation (z) associated with consecutive (i.e., sub-interval) data points are summed (L_{sub} in Fig. 7) and checked against the RQD length threshold ($L_{threshold}$) of 4 in. Each consecutive length identified as being equal to or greater than $L_{threshold}$ is then accumulated within L_{RQD} . After all data points within the interval have been assessed, the accumulation of sub-interval lengths exceeding $L_{threshold}$ (i.e., the accumulated length assigned to L_{RQD}) is divided by the total length of the interval (L_{int}), thus allowing RQD to be estimated (as RQD_{MWD}) within each interval.

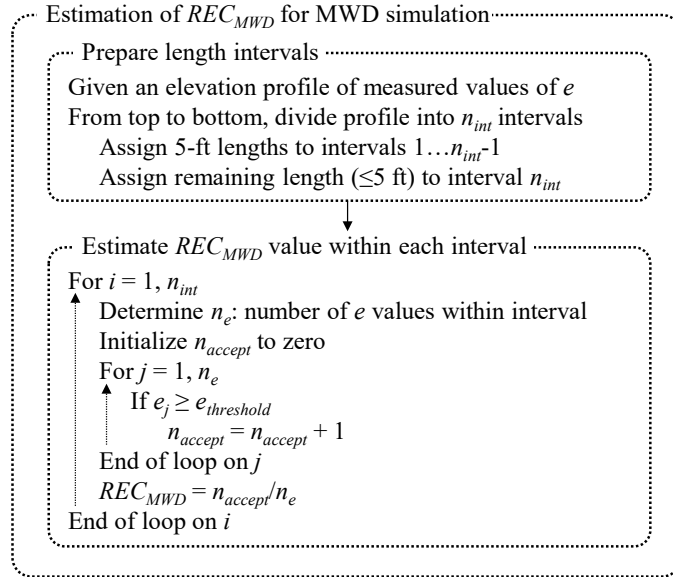


Figure 6. Estimation of rock recovery for use in MWD-based stochastic simulation (REC_{MWD})

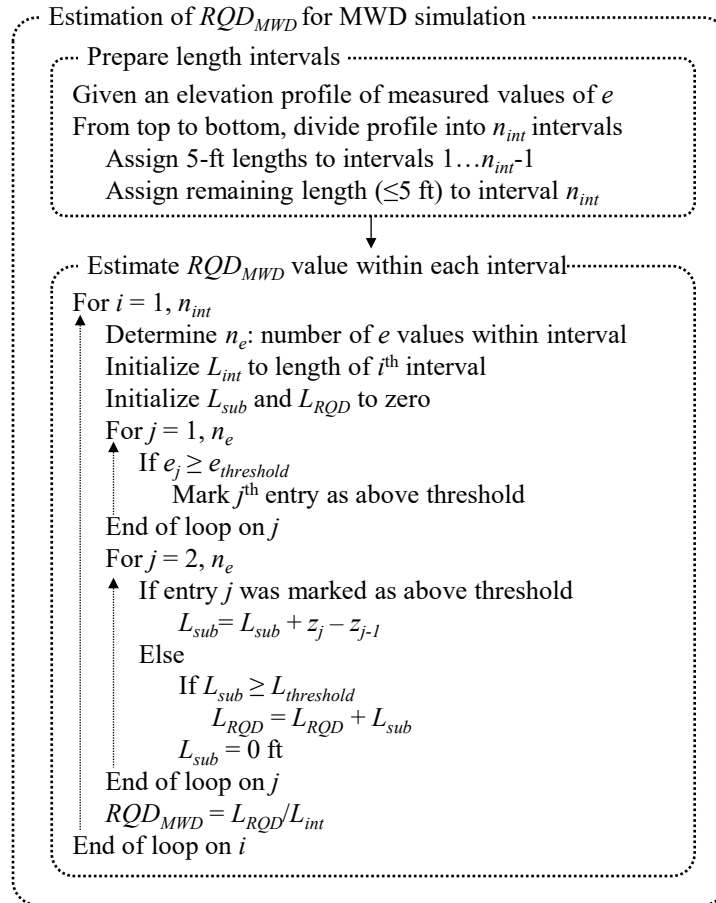


Figure 7. Estimation of RQD for use in MWD-based stochastic simulation (RQD_{MWD})

3.4.5 Considerations for Additional Parameters

As part of the MWD-based implementation, additional parameters beyond q_u and q_t are taken into consideration. These include unit weight (γ), mass modulus (E_m), rock quality designation (RQD), and recovery (REC). For every realization of through-depth limestone properties (as part of stochastic simulation), values for γ and E_m are determined in the same manner as that detailed in Sec. 2.7 of the GeoStat Technical Manual. That is, the existing algorithms in GeoStat are robust to simulating profiles of values for these additional parameters without further modification.

A summary listing of the limestone parameters pertinent to stochastic simulation of axial resistances of drilled shafts is given in Table 6. Also listed in Table 6 are the units and determination method for each parameter. Note that, for the MWD approach, measurements of specific energy (e), unit weight (γ) are utilized. In contrast, values of q_u , q_t , rock recovery (REC , for side friction), and RQD (for settlement) are estimated based on values of specific energy, e .

Table 6. Limestone parameters for MWD-based stochastic simulation of drilled shaft axial resistance

Parameter	Units	Determination method
e	psi (kPa)	Site measurement
q_u	tsf (kPa)	Eq. 8
q_t	tsf (kPa)	Eq. 9
REC_{MWD}	N/A	Fig. 6
RQD_{MWD}	N/A	Fig. 7
γ	pcf (kN/m ³)	GeoStat v1.1.0 Technical Manual Sec. 2.7.4
E_m	ksi (MPa)	GeoStat v1.1.0 Technical Manual Sec. 2.7.4.2

3.4.6 Computing Shaft Axial Resistance in Limestone

As the next major step in the overall stochastic simulation procedure, shaft axial resistance is calculated across a range of candidate embedment lengths. That is, one profile at a time is analyzed by relating the associated limestone parameter values to unit resistances and then integrating the unit resistances. As indicated in McVay et al. (2012) and Faraone et al. (2021), 2000 realizations is generally considered to constitute a sufficient sample size. Regardless of the sample size (i.e., number of profiles simulated), the approach adopted herein is to make default use of the axial capacity calculation software FB-Deep to compute resistance quantities. For example, for computing side shear resistance the expression developed in McVay et al. (1992) is utilized:

$$f_s = 0.5 \cdot (q_u \cdot q_t)^{0.5} \quad (10)$$

where f_s is unit side shear. Note that values of f_s calculated using Eq. 10 are further scaled by the associated rock recovery, REC , (where the domain of rock recovery values lies between 0.0 and 1.0).

3.5 Method Error

3.5.1 Overview

Stochastically simulated shaft axial resistance quantities, obtained from the MWD-based procedure discussed in Sec. 3.4, can be modified to reflect bias intrinsic to the underlying, empirical axial capacity calculation methods. In this way, profiles of design-relevant resistance quantities and associated uncertainties (e.g., expressed as LRFD resistance factors, ϕ) are formed. The approach for incorporating method error into MWD analysis, and selections for default method error parameters, are discussed in Sec. 3.5.2.

3.5.2 Approach and Parameters

The most fundamental variable of the MWD-based implementation in GeoStat is specific energy (e). For example, the “primary” variable (q_u) used in generation of variograms and stochastic simulation, in association with the MWD formulation, is calculated based on measurements of specific energy (e). As noted in Sec. 3.2, previous research has demonstrated that specific energy is correlated to unit side shear of drilled shafts in limestone at a strength (i.e., R^2) of 0.99, even with respect to field testing (McVay and Rodgers, 2020).

Given that the strength of correlation observed between specific energy and unit side shear is near to unity, an approach is adopted in the GeoStat implementation for MWD such that method error has no effect on the simulation results when the proposed shaft/pile will have MWD conducted in the footprint at full-scale because spatial uncertainty and upscaling effects are removed. Even so, the need is anticipated to be able to account for levels of method error specific to a site or zone when MWD will not be conducted in the footprint of the proposed shaft/pile at full scale. Therefore, the following expression is also made available as part of the implementation to allow for custom (site-specific) method error calculations:

$$q_{comp_meas} = a + b \cdot q_{pred} \quad (11)$$

where q_{comp_meas} is the computed value of resistance that reflects total uncertainty (i.e., takes into account both spatial variability and method error); a (intercept) and b (slope) are regression expression coefficients; and q_{pred} is the predicted value of resistance that incorporates spatial variability.

Adoption of a linear form for the method error expression (Eq. 11) is consistent with previous implementations of Geo-statistical analysis for drilled shafts in limestone (e.g., McVay et al. 2012; Davidson et al. 2020). For the MWD-based methodology implemented in GeoStat as part of the present project, default parameter values are listed in Table 7. As emphasis, note that values for the regression expression coefficients are selected such that method error has no effect on simulated results ($a = 0$, $b = 1$). Furthermore, the default value of the regression error variance (σ_e^2) is selected as zero. However, values of the regression error variance (σ_e^2) that are non-zero

can also be supplied when performing custom method error calculations, where the role of σ_e^2 is discussed in Sec. 3.6 of the GeoStat Technical Manual.

Table 7. Method error parameters for MWD-based total uncertainty calculations

Parameter	Value
a	0.00
b	1.00
σ_e^2	0.00

CHAPTER 4

VERIFICATION OF SPATIAL CORRELATION CALCULATIONS AND GEO-STATISTICAL SIMULATION

4.1 Verification of Spatial Correlation Calculations Using CPT and MWD Data

4.1.1 Overview

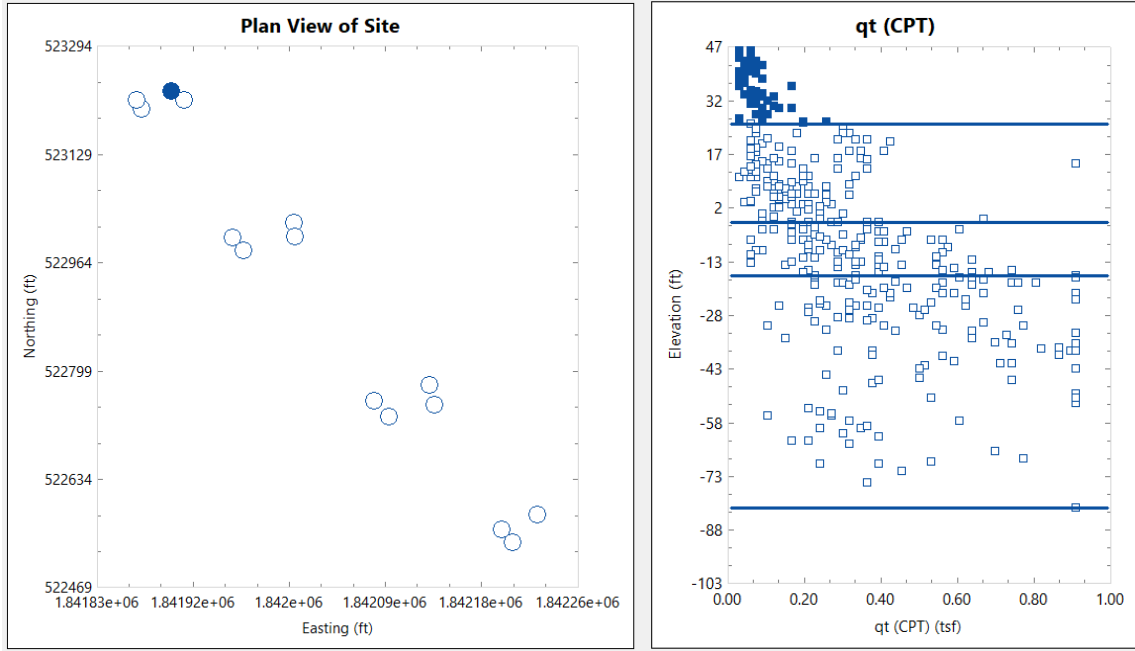
Spatial correlation structures in GeoStat are packaged into layer-specific variograms (horizontal and vertical). In turn, these graphical constructs, which characterize how covariance within a given layer changes with respect to distance between data points, are drawn upon in forming multitudes of soil parameter profiles during statistical simulation. Presented in Sec. 4.1 are verification efforts pertaining to generation of variograms in association with CPT-based, and separately, MWD-based analyses. Reported in Sec. 4.1.2 are comparisons between manually calculated variogram data and variogram data generated within GeoStat using CPT cone resistance (q_{t_CPT}) data. In Sec. 4.1.3, focus is given to verification of variogram calculations in GeoStat for MWD-based analysis by again comparing against manual calculations.

4.1.2 Variograms Generated Using CPT Cone Resistance

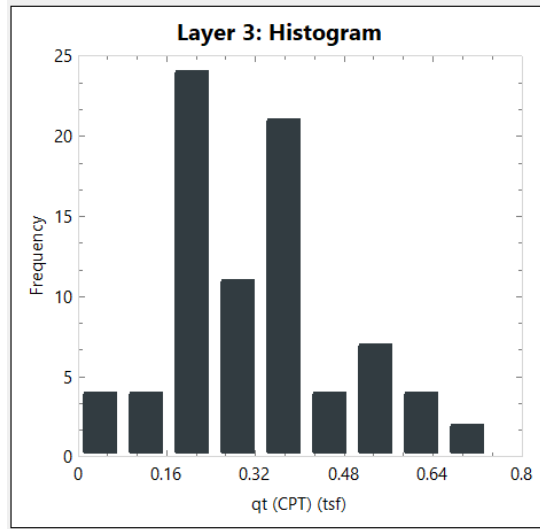
Documented in Sec. 4.1.2 is verification of variograms generated within GeoStat using values of CPT cone resistance (q_{t_CPT}), where comparisons are made to manual calculations. Shown in Fig. 8a are the plan view of 15 boring locations and a through-depth scatterplot of 380 q_{t_CPT} values. Also plotted in Fig. 8a are estimates of layer bottom elevations. Note that the collection of q_{t_CPT} values is synthetic and is utilized purely for verification purposes.

Recall that variograms are generated (horizontal, vertical) on a per-layer basis. As verification of the variogram generation procedure specific to CPT-based analysis, focus is given in the following to horizontal and vertical variograms associated with one of the layers belonging to the profile shown in Fig. 8a. Namely, variogram data associated with layer 3 are utilized for verification purposes. Plotted in Fig. 8b is the histogram for the q_{t_CPT} values located within layer 3. In addition, manually determined and program-generated descriptive statistics for the q_{t_CPT} values in layer 3 are compared in Table 8. Exact agreement is found across the listings of statistical quantities.

Comparative plots of horizontal variograms (manual vs. program-generated) are presented for the layer 3 data set in Fig. 9. Vertical variograms associated with the cone resistance values are plotted in Fig. 10. Manual versus computed (using GeoStat) variogram ordinates indicate practically identical agreement across all lag distances considered (Fig. 9a, Fig. 10a). Likewise, the intensities associated with each variogram ordinate (i.e., the number of data pairs found at each lag distance) show excellent agreement (Fig. 9b, Fig. 10b). The collective comparisons between manual and program-generated statistical quantities serve to verify the generation of variograms, when operating on values of CPT cone resistance, using GeoStat.



(a)

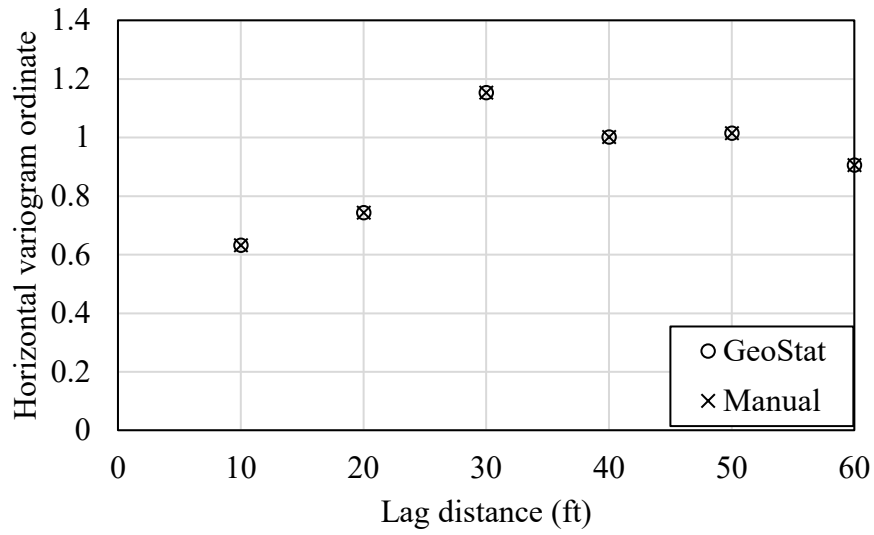


(b)

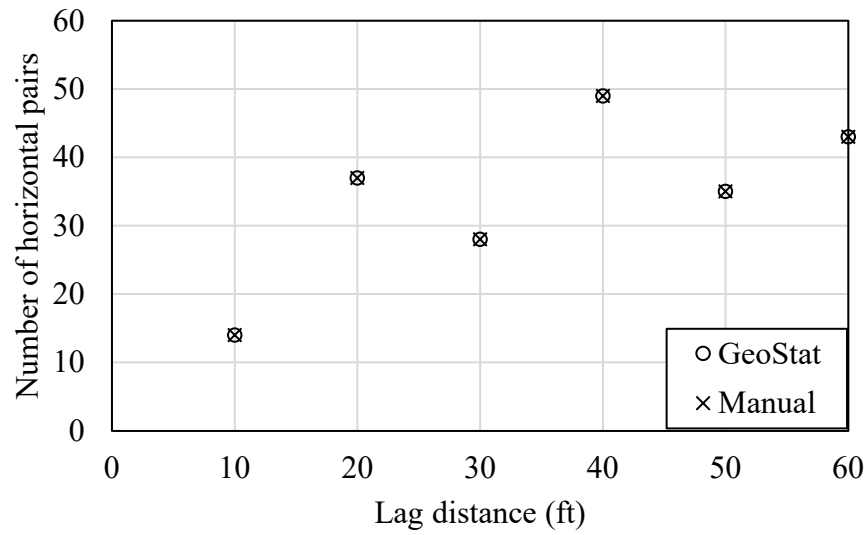
Figure 8. Illustrative set of CPT cone resistance (q_{t_CPT}) values: (a) Plan view and through-depth scatterplot; (b) Histogram of values in layer 3

Table 8. Descriptive statistics for values of q_{t_CPT} (tsf) in layer 3

Statistical measure	Manual	GeoStat
Sample size	81	81
Mean	0.32	0.32
Variance	0.02	0.02
COV	0.47	0.47

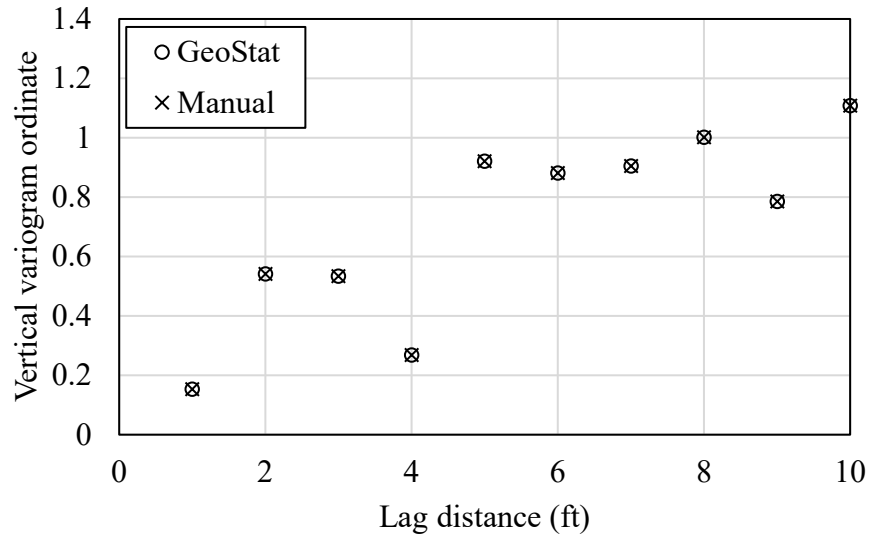


(a)

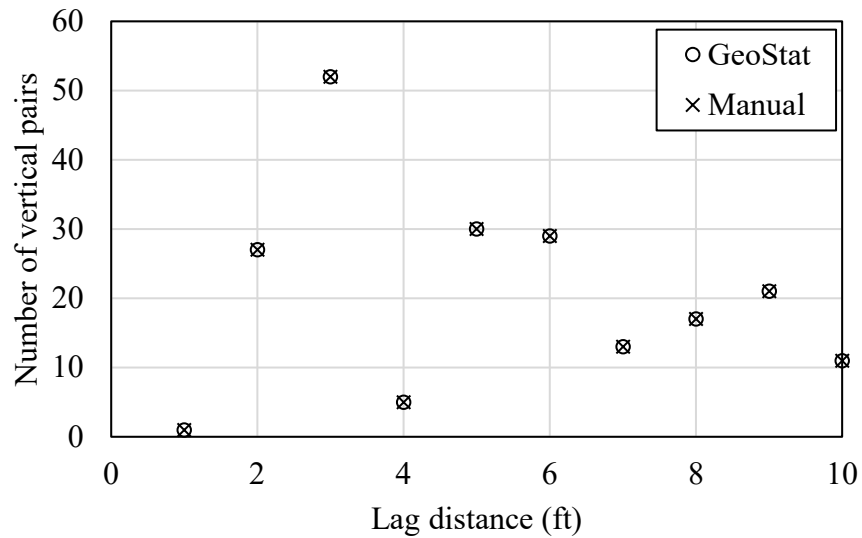


(b)

Figure 9. Comparison of horizontal variograms generated using values of q_{L_CPT} in layer 3: (a) Variogram ordinates; (b) Variogram pairs



(a)



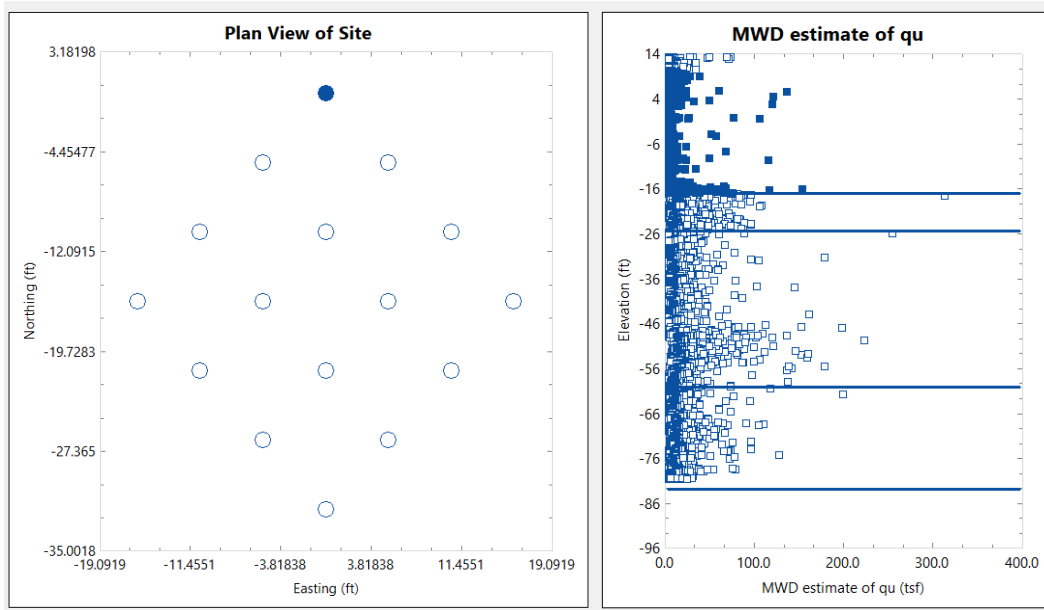
(b)

Figure 10. Comparison of vertical variograms generated using values of q_{t_CPT} in layer 3: (a) Variogram ordinates; (b) Variogram pairs

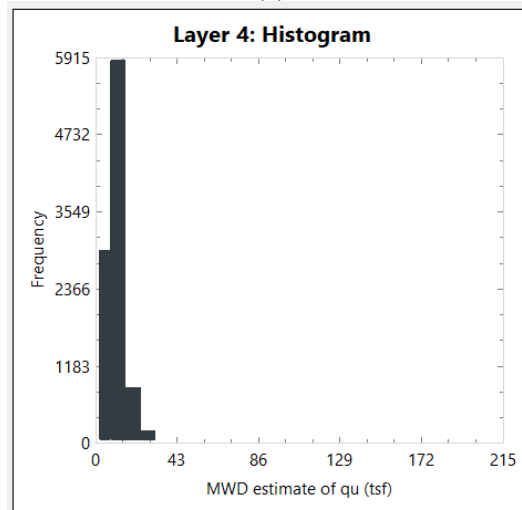
4.1.3 Variograms Generated Using MWD Estimate of Unconfined Compressive Strength

Verification of variograms generated within GeoStat—using values of unconfined compressive strength q_{u_MWD} that are estimated from specific energy—is documented in Sec. 4.1.3. Here, comparisons are again made with respect to manual calculations. The data set utilized for verification purposes is presented in Fig. 11, including the plan view of 16 boring locations and a

through-depth scatterplot of 45,860 q_{u_MWD} values. Also plotted in Fig. 11a are estimates of layer bottom elevations. The collection of q_{u_MWD} values is utilized purely for verification purposes.



(a)



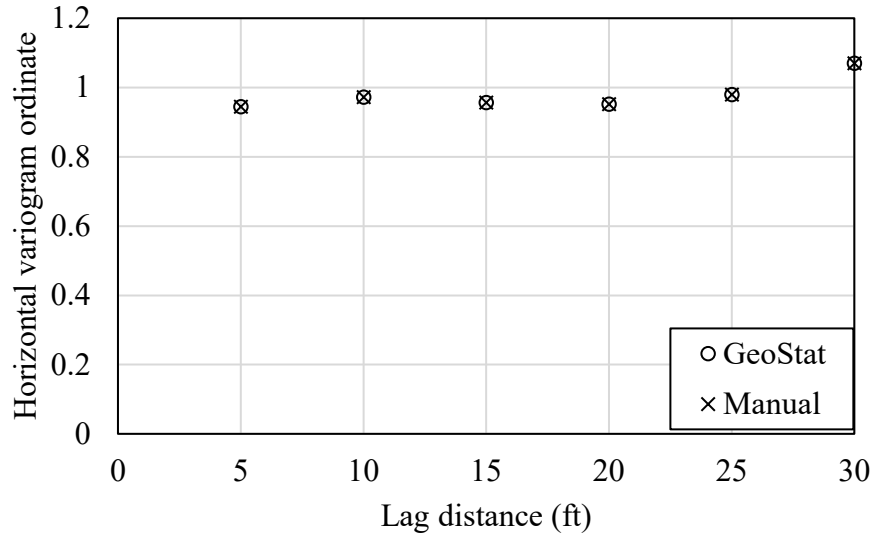
(b)

Figure 11. Illustrative set of MWD-estimated values of unconfined compressive strength (q_{u_MWD}): (a) Plan view and through-depth scatterplot; (b) Histogram of values in layer 4

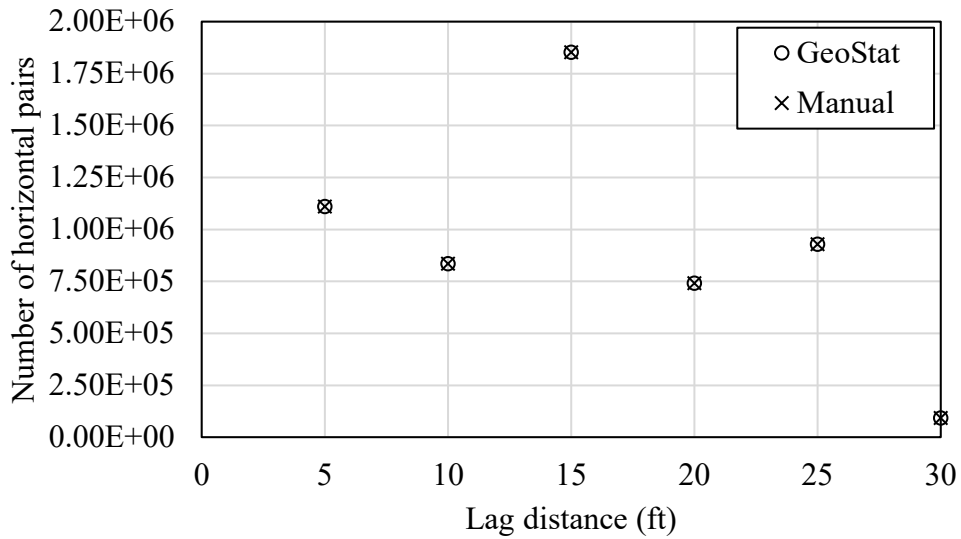
Regarding verification of the variogram generation procedure specific to MWD-based analysis, focus is given to values of q_{u_MWD} located within layer 4 (see the histogram in 11b). Manually determined and program-generated descriptive statistics for the q_{u_MWD} values in layer 4 (Table 9) show excellent agreement. Comparative plots of horizontal and vertical variograms are presented for the layer 4 data set in Fig. 12 and Fig. 13, respectively.

Table 9. Descriptive statistics for values of q_{u_MWD} (tsf) in layer 4

Statistical measure	Manual	GeoStat
Sample size	10030	10030
Mean	11.25	11.25
Variance	47.21	47.21
COV	0.61	0.61



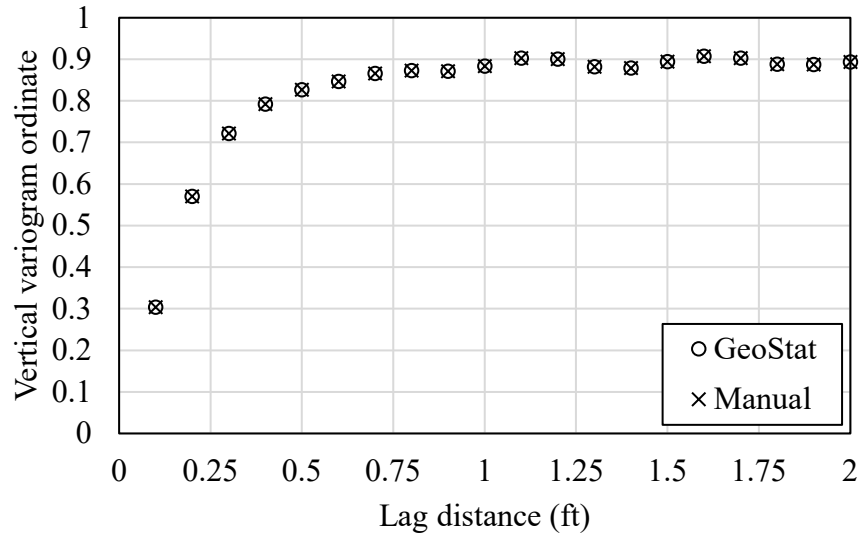
(a)



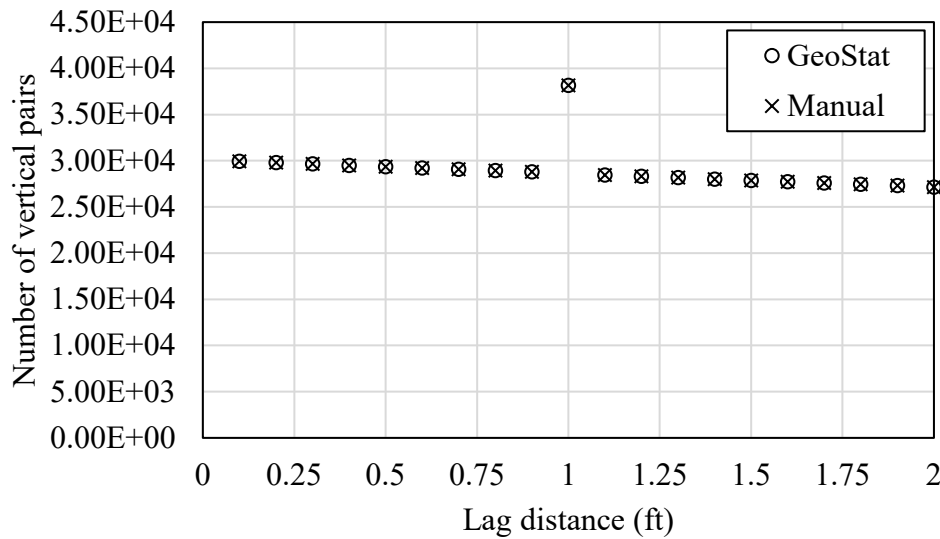
(b)

Figure 12. Comparison of horizontal variograms generated using values of q_{u_MWD} in layer 4: (a) Variogram ordinates; (b) Variogram pairs

Manual versus computed variogram ordinates indicate excellent agreement across all lag distances considered. In addition, excellent agreement is observed with regard to the intensities associated with each variogram ordinate (i.e., the number of data pairs). The collective comparisons between manual and program-generated statistical quantities serve to verify MWD-based generation of variograms.



(a)



(b)

Figure 13. Comparison of vertical variograms generated using values of q_{u_MWD} in layer 4: (a) Variogram ordinates; (b) Variogram pairs

4.2 Verification of Geo-Statistical Simulation

4.2.1 Overview

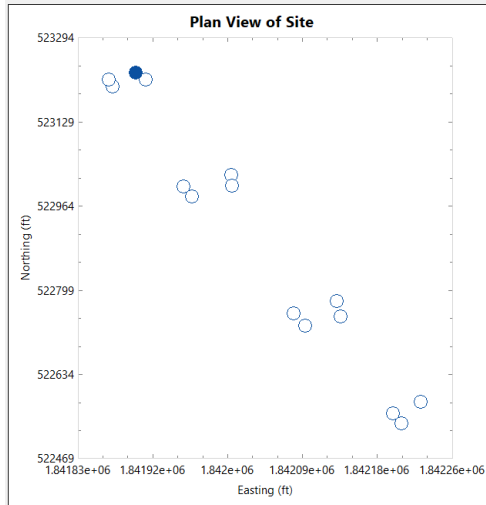
Documented in Sec. 4.2 are verification efforts pertaining to Geo-statistical simulation of axial resistances for foundation members modeled in GeoStat. In Sec. 4.2.2, focus is given to verification of the CPT-based approach for analysis of driven piles, which was implemented in Task 1. Verification of an MWD-based approach for drilled shafts in limestone (implemented during Task 2) is documented in Sec. 4.2.3. For each of the CPT and MWD simulation methodologies, benchmark data sets are first identified. Respective, synthetic data sets are then created purely for verification purposes. For each verification case, two stochastic simulations are then performed with the expectation that good agreement is observed between the sets of results, thereby constituting verification of the CPT, and separately, MWD stochastic simulation processes implemented in GeoStat.

4.2.2 CPT-based Simulation for Driven Piles

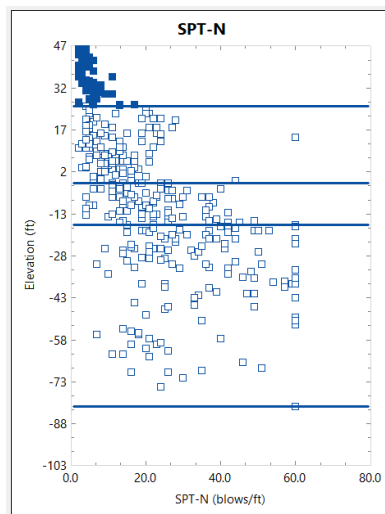
For verification of stochastic stimulation with use of CPT-related site data, a benchmark data set is first identified. Here, the benchmark data set consists of a collection of boring locations and associated profiles of SPT blow count values. Given a layered profile and assigned soil types, empirical equations that relate SPT blow count values to unit quantities of axial resistance are also identified, along with empirical equations that relate CPT cone resistance values to unit resistance (for the same soil types). Then, using the SPT blow count values and the as-identified empirical equations, a synthetic set of CPT cone resistance values is produced (purely for verification purposes). In this way, equal values of unit resistance are obtained when empirically evaluating the CPT cone resistance values as those that are obtained when evaluating respective values of SPT blow counts. Further, this verification strategy creates the expectation that stochastic simulation results obtained from use of the SPT site data exhibit agreement with results obtained from simulation of the (synthetic, and for verification purposes only) CPT site data. Note that stochastic simulation with use of SPT blow count values in GeoStat was verified in Davidson et al. (2020).

4.2.2.1 Benchmark Data Set

Presented in Fig. 14 are 15 boring locations (Fig. 14a) and 380 SPT blow count values (Fig. 14b), which are distributed across an example bridge site. Results obtained from simulations that utilize this data set serve as benchmarks for verification of CPT-based stochastic simulation of a 32-in. square pile, with embedment lengths ranging from 80 ft to 110 ft. Four sand layers are defined (with bottom elevations indicated as blue lines in Fig. 14b). Descriptive statistics of the SPT blow counts (blows/ft) are listed for layer 1 through layer 4 in Table 10.



(a)



(b)

Figure 14. Illustrative set of bridge site data for producing benchmark results: (a) Plan view of boring locations; (b) Sitewide scatterplot of SPT blow count values versus elevation

Table 10. Descriptive statistics for SPT blow count (blows/ft) values per layer

Statistical measure	Layer 1	Layer 2	Layer 3	Layer 4
Sample size	62	117	81	120
Mean	4.9	11.4	21.3	33.1
COV	0.52	0.76	0.49	0.47

Solely to enable comparisons between stochastic simulation results obtained from use of the SPT data set and those obtained from CPT-based simulation, the SPT blow count values are mapped to values of CPT cone resistance. More specifically, such a mapping is undertaken for calculating unit side shear resistance in association with SPT analysis as well as the UF method of CPT analysis. As excerpted from the FB-Deep Help Manual, the empirical expression for relating

SPT blow counts to unit side shear resistance of square precast concrete piles embedded in sand layers is given as:

$$f_s = 0.019 \cdot N \quad (12)$$

where f_s is unit side shear resistance, and N is the SPT-N blow count value (blows/ft). In addition, when the UF method is utilized for CPT analysis, unit side shear resistance (f_s) is expressed in the FB-Deep Help Manual in relation to CPT cone resistance (q_{t_CPT}) as:

$$f_s = q_{t_CPT} \cdot 1.25/F_s \quad (13)$$

where F_s is a friction factor. For the purposes of the CPT-based verification, a friction factor value of 1.0 is utilized.

Combining Eq. 12 and Eq. 13, and solely for verification purposes, synthetic values of q_{t_CPT} are estimated as:

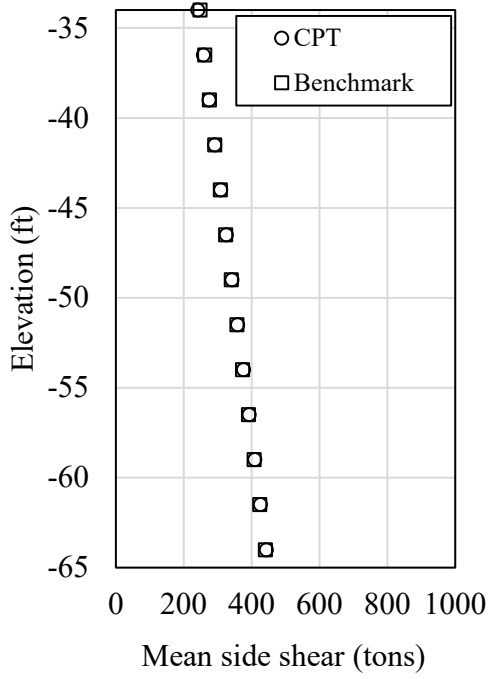
$$q_{t_CPT} \approx N \cdot 0.0152 \quad (14)$$

where the collection of synthetic q_{t_CPT} values was presented in Sec. 3.2 (recall Fig. 8).

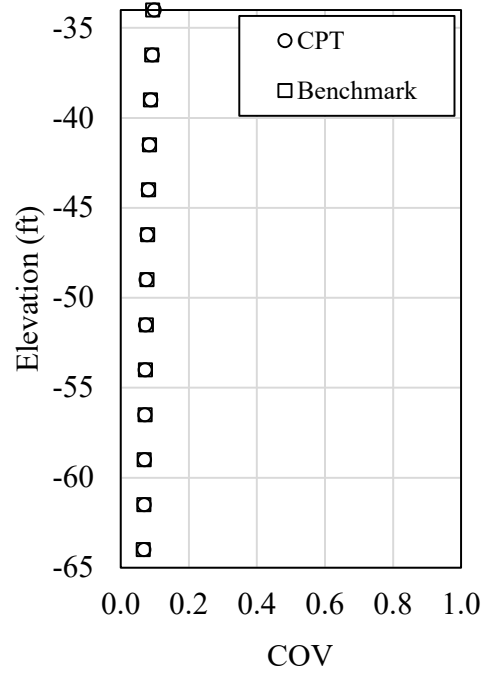
4.2.2.2 Comparison of Stochastic Simulation Results

Plotted in Fig. 15 are comparisons of through-depth results quantities pertaining to driven pile axial capacity. One set of results was obtained from stochastic simulation with use of the CPT based approach and the other set was obtained through use of the benchmark data set (consisting of SPT blow count values). Recall that the site data associated with the CPT based simulation was presented in Sec. 4.1.2, while the corresponding benchmark data were presented in Sec. 4.2.2.1. Recall also that, in each case, stochastic simulation was conducted on a 32-in. square pile over the range of candidate embedment lengths of 80 ft to 110 ft (in sand).

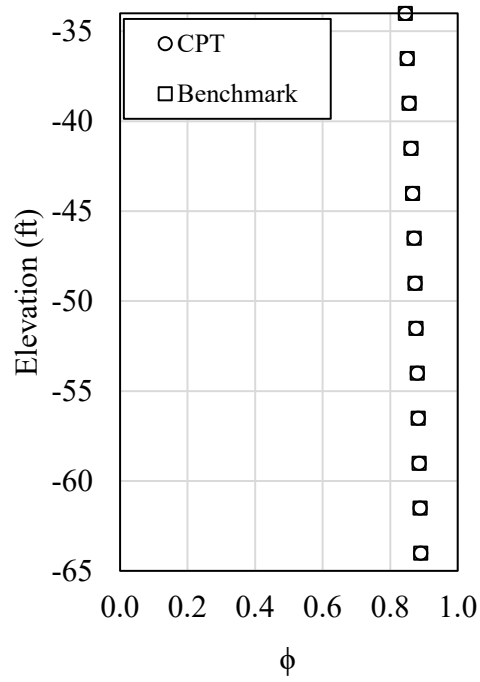
Excellent agreement is maintained along the profile of mean-valued side shear resistance (Fig. 15a), where the two sets of results produce resistance values that differ by less than 1%. As plotted in Fig. 15b, agreement to within 1% is also present among the computed values of coefficient of variation, COV, which indicates that variability manifests in a consistent manner between the two sets of computed results. Both the mean-valued resistances and COV values influence calculations of LRFD resistance factors (ϕ , from Styler 2006 for these results), as plotted in Fig. 15c. Again, excellent agreement (with differences of less than 1%) is maintained across the range of embedment lengths considered. Note that, solely to facilitate meaningful result comparisons, resistance factor (ϕ) values up to 1.0 were permitted to be computed (the default upper bound value of ϕ is equal to 0.6 in GeoStat).



(a)



(b)



(c)

Figure 15. Verification of CPT-based stochastic simulation results for driven piles: (a) Mean side shear resistance; (b) Coefficient of variation; (c) Resistance factor

4.2.3 MWD-based Simulation for Drilled Shafts in Limestone

Verification of stochastic simulation results pertaining to the MWD implementation in GeoStat is based on comparisons to benchmark results, where the benchmark results are generated by operating on rock coring data. In particular, benchmark simulation results are produced by making use of a collection of values of unconfined compressive strength (q_u), tensile strength (q_t), and rock recovery (REC). In turn, values of these three quantities are used to compute unit resistances of a drilled shaft embedded in limestone. The unit resistances are then integrated to produce profiles of axial resistance, as well as profiles of descriptive statistics and resistance factors.

To establish the (benchmark) collection of q_u , q_t , and REC values, empirical expressions from the literature and a pre-existing collection of specific energy values from an illustrative bridge site are utilized. That is, values of specific energy are processed through selected empirical expressions to generate corresponding values of q_u , q_t , and REC. In this way, the two data sets are intentionally configured so that a given value of specific energy should produce an equal value of unit side shear resistance relative to what is obtained if corresponding (benchmark) values of q_u , q_t , and REC are utilized. Furthermore, an expectation is created such that stochastic simulation results obtained from use of the MWD site data (i.e., values of specific energy) exhibit agreement with results obtained from simulation of the benchmark set of q_u , q_t , and REC values. Note that stochastic simulation of drilled shafts in limestone with use of q_u , q_t , and REC values was verified for drilled shafts in limestone in Davidson et al. (2020).

4.2.3.1 Benchmark Data Set

Plotted in Fig. 16 are 16 boring locations distributed across an example bridge site (Fig. 16a) and a scatterplot of 44,250 specific energy values versus elevation (Fig. 14b). The collection of specific energy values is utilized, along with empirical expressions from the literature, to produce a benchmark data set of q_u , q_t , and REC values. Verification of the MWD feature set corresponds to stochastic simulations of a 30-in. diameter drilled shaft. Additionally, drilled shaft embedment lengths between 50 ft and 80 ft are considered along with a layered limestone profile (layer bottom elevations are depicted as blue lines in Fig. 16b).

The first step in building up benchmark values of site data for the MWD-based verification consists of relating specific energy (e) to unconfined compressive strength (q_u). Accordingly, the inverse of the expression given in Rodgers et al. (2018b) is employed:

$$q_u = \frac{-13.7 + (13.7^2 - 4 \cdot 0.0066 \cdot (-e))^{0.5}}{2 \cdot 0.0066} \quad (15)$$

where units for all variables in Eq. 15 are psi. The resulting q_u values are plotted in Fig. 17a. Note that for this verification case, no upper bound limit was enforced for mapping from measured values of specific energy to estimates of q_u . Given the prominent role of the q_u variable in stochastic

simulations that involve rock coring data, descriptive statistics are listed for the q_u values (per layer) in Table 11.

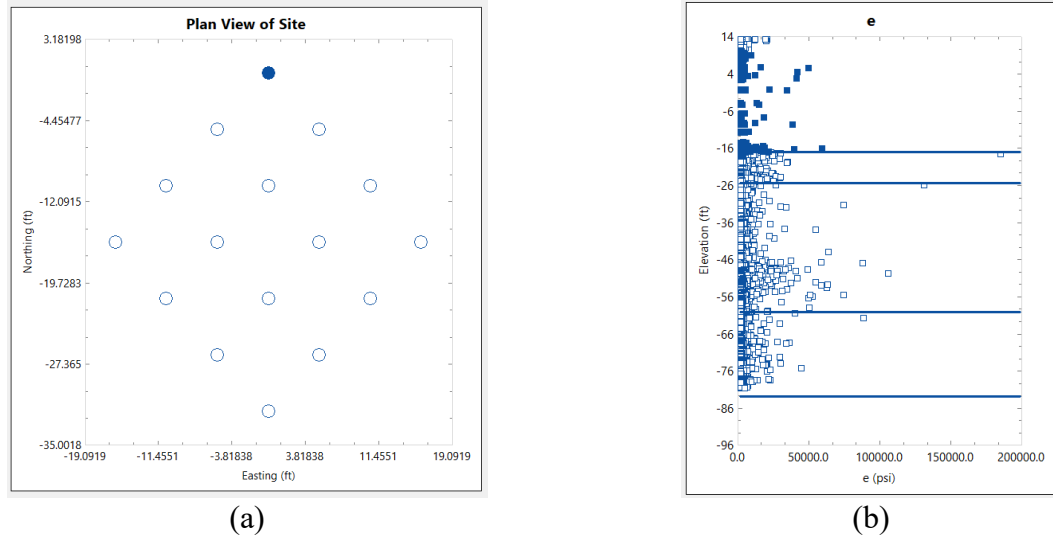


Figure 16. Illustrative set of specific energy values (e) for use in verification of MWD-based stochastic simulation: (a) Plan view of boring locations; (b) Scatterplot versus elevation

Having produced values of unconfined compressive strength (solely for verification purposes), corresponding values of tensile strength (q_t) are next calculated using the Florida geomaterials equation:

$$q_t = 0.436 \cdot q_u^{0.825} \quad (16)$$

where units for all variables in Eq. 16 are psi. The resulting q_t values are plotted in Fig. 17b.

For verification purposes only, the benchmark set of rock recovery (REC) values are estimated from the collection of specific energy values (recall Fig. 16b). Note that the algorithm developed in Task 2—which can be used to examine through-depth values of specific energy and estimate rock recovery over 5-ft intervals based on a sitewide threshold value of specific energy—is utilized for this purpose. Here, a specific energy threshold value of 2000 psi is adopted for estimating the values of REC, which are plotted in Fig. 17c.

For stochastic simulation results obtained using collections of benchmark values for q_u , q_t , and REC (Fig. 17), the expression for computing unit side shear resistance is adopted from McVay et al. (1992):

$$f_s = 0.5 \cdot (q_u \cdot q_t)^{0.5} \quad (17)$$

Likewise, Eq. 17 is employed in when conducting MWD-based stochastic simulation in GeoStat. Note that values of f_s calculated using Eq. 17 are further scaled by the associated value of rock recovery, REC.

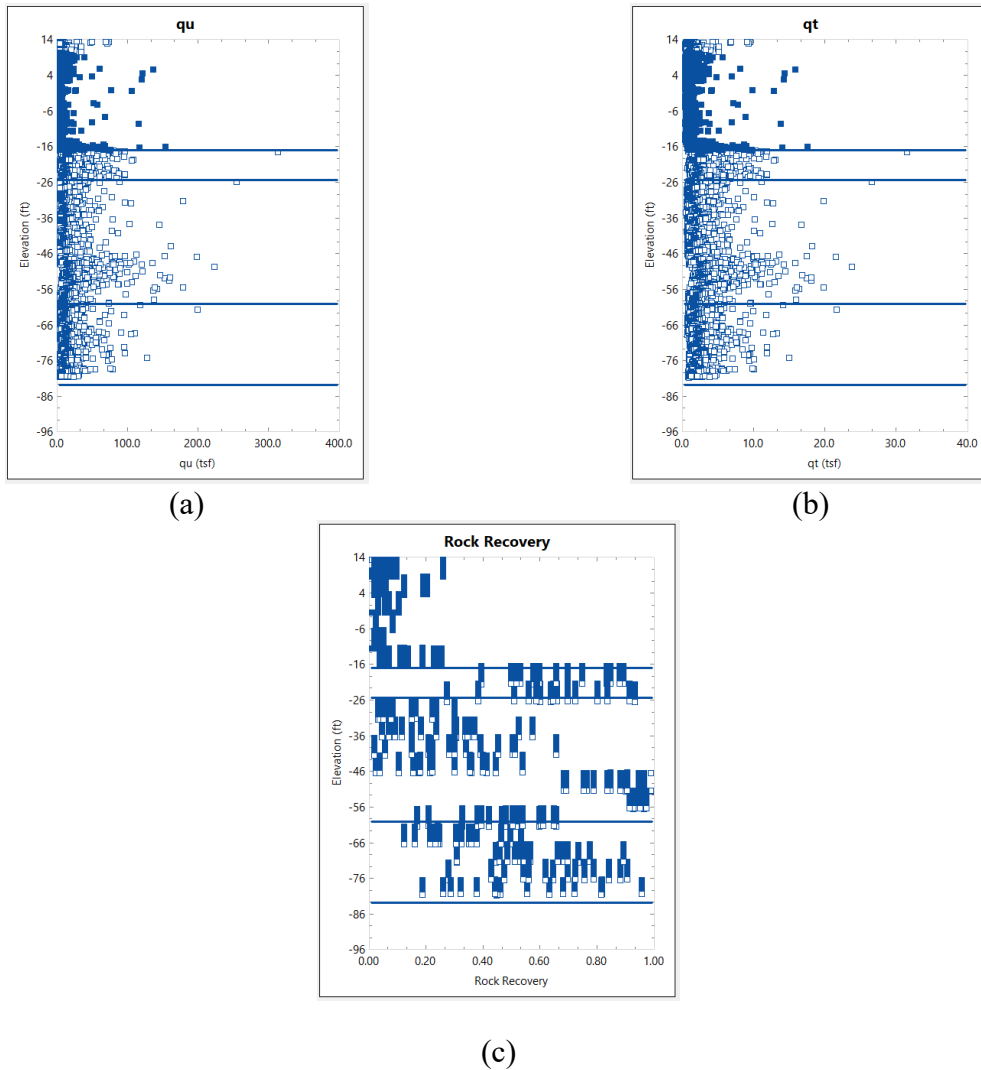


Figure 17. Illustrative set of bridge site data for producing benchmark results: (a) Unconfined compressive strength (q_u); (b) Tensile strength (q_t); (c) Rock recovery (REC)

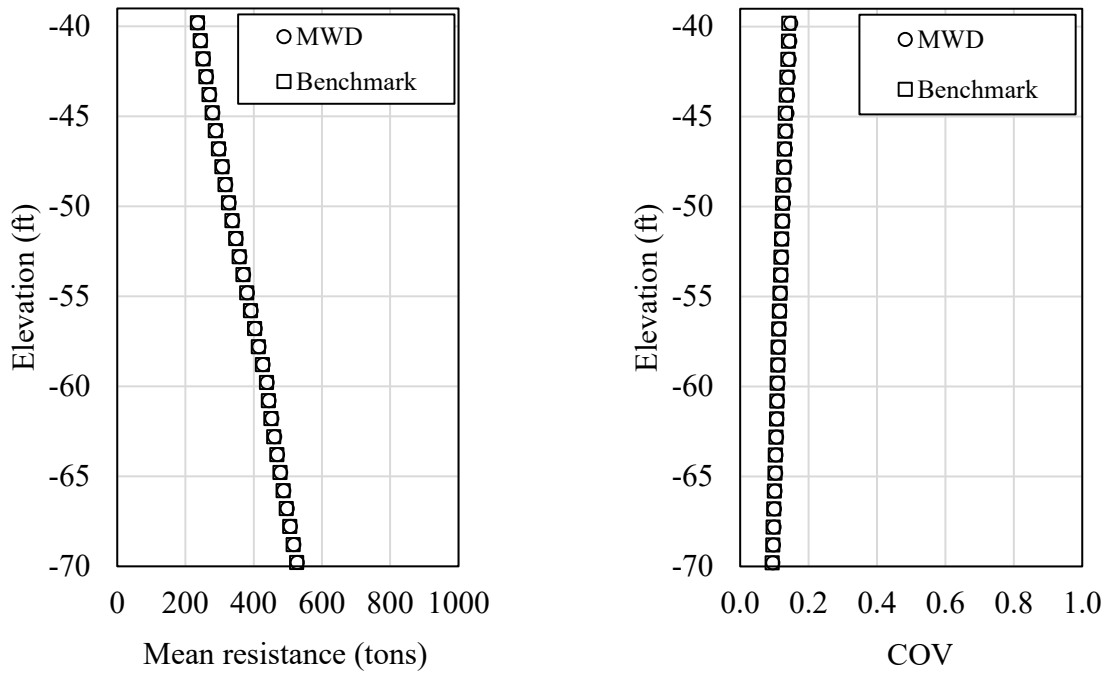
Table 11. Descriptive statistics for unconfined compressive strength (tsf) values per layer

Statistical measure	Layer 1	Layer 2	Layer 3	Layer 4
Sample size	13,304	3,979	16,937	10,030
Mean	4.9	14.9	11.6	11.3
COV	1.00	0.78	0.82	0.61

4.2.3.2 Comparison of Stochastic Simulation Results

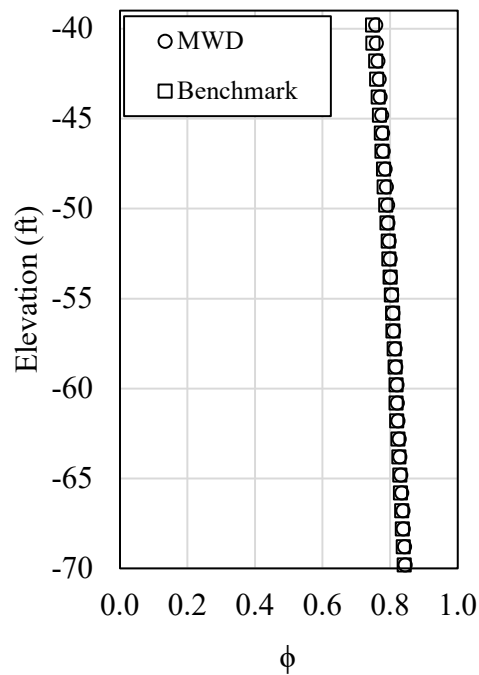
Plotted in Fig. 18 are comparisons of through-depth quantities pertaining to drilled shaft axial capacity. Results are obtained from stochastic simulation with use of the MWD-based approach documented in Task 2 and site data displayed in Fig. 16. Benchmark results are obtained

using the benchmark data set (Fig. 17) and the feature set for using rock coring data to perform Geo-statistical analysis of drilled shafts in limestone (implemented as part of Davidson et al. 2020).



(a)

(b)



(c)

Figure 18. Verification of MWD-based stochastic simulation results for drilled shafts in limestone: (a) Mean resistance; (b) Coefficient of variation; (c) Resistance factor

Excellent agreement is maintained along the profile of mean-valued resistance (Fig. 18a), where the two sets of stochastic simulation results produce resistance values that differ by less than 1%. In addition, comparable levels of agreement are maintained across the profile plots of COV (Fig. 18b) and resistance factor (Fig. 18c). Solely to facilitate meaningful result comparisons, resistance factor (ϕ) values up to 1.0 were permitted to be computed for this verification case. Note also that the resistance factor formulation from Styler (2006) was employed.

CHAPTER 5 GEO-STATISTICAL APPROACH FOR ESTIMATING ZONAL RADII

5.1 Overview

Documented in Ch. 5 is a Geo-statistical approach for estimating zonal radii. In this context, a zone refers to a distinct, spatial subdomain located below the ground surface of a bridge site. Within each spatial subdomain, consistent geological properties can be inferred through Geo-statistical analysis and then utilized in geotechnical design applications. Radii are taken, in this context, with respect to a plan-view perspective of the bridge site. Identification of geological zones throughout bridge sites is necessary prior to performing design calculations, where consideration should be given to one zone at a time. Otherwise, simultaneous use of geotechnical site data, as drawn from multiple geological zones, could lead to non-representative predictions of design quantities such as the axial capacities of deep foundation members.

Provided in Sec. 5.2 is discussion of a conceptual approach for detection of geological zones and key steps of a detection procedure leading to estimation of zonal radii. An illustrative case study is detailed in Sec. 5.3, with emphasis on estimation of an effective radius relative to a given test shaft location. Observations and additional considerations associated with the case study are also documented in Sec. 5.3.

5.2 Conceptual Approach

Variograms serve to compactly represent changes in correlation of geotechnical site data with respect to separation distance between physically measured data points. The Geo-statistical approach presented herein for estimating zonal radii is contingent upon formation and inspection of layer-specific variograms in the horizontal and vertical directions. Relevant variogram phenomena that are queried as part of such inspections are discussed in Sec. 5.2.1. Subsequently, in Sec. 5.2.2, key steps are delineated for a procedure that can be used to estimate zonal radii.

5.2.1 Detection of Zonal Anisotropy Using Variograms

Plotted in Fig. 19 are idealized variograms, such as those pertaining to a given soil (or rock) layer. Both horizontal and vertical variograms are shown. For relatively small values of lag distance (e.g., spatial separation between any two measurements of geotechnical site data), the variogram ordinates exhibit relatively steep ascents. Increasing ordinate values in variograms correspond to decreasing correlation between measured data points (e.g., two values of unconfined compressive strength, q_u). With increasing lag distance, the variograms exhibit increasingly asymptotic behavior. The variogram ordinate associated with the asymptote is referred to as the sill; the corresponding lag distance is referred to as the range. It is generally desirable for the sill values of variograms to converge upon a value equal to the variance of the full, underlying data set.

In Geo-statistical analysis, comparisons of the range and sill values across direction-specific variograms allow for inferences to be made regarding the characteristics of the underlying

data (including geotechnical site data). For example, when horizontal and vertical variograms are identical, then the underlying data set can be categorized as isotropic (i.e., spatial variability of the underlying data is not direction dependent). As an additional example, consider the variograms plotted in Fig. 19a. The sills of the horizontal and vertical variograms converge upon the same variogram ordinate, while the range value of the horizontal variogram is greater than the range value of the vertical variogram. This condition is referred to as geometric anisotropy and indicates that changes in correlation (with respect to separation, or lag, distance) of the underlying data differ in the horizontal versus vertical directions. Collections of variograms that exhibit isotropy or (separately) geometric anisotropy can be acceptably carried forward into Geo-statistical processes such as stochastic simulation (e.g., for predicting foundation member axial capacities).

Shown in Fig. 19b are horizontal and vertical variograms that not only exhibit geometric anisotropy, but also, zonal anisotropy. Stated alternatively, differences occur in both the ranges and the sills of the variograms shown in Fig. 19b. Of particular significance is that the values of the the horizontal sill and vertical sill do not reach the same variogram ordinate, thus constituting zonal anisotropy. For geotechnical design of foundation members involving Geo-statistical analysis, it is not generally acceptable to employ variograms that exhibit zonal anisotropy (e.g., Fig. 19b). This is because the presence of zonal anisotropy indicates that the constituent site data pertain to multiple geological zones (and therefore predictions of foundation resistance may not be representative of physical conditions).

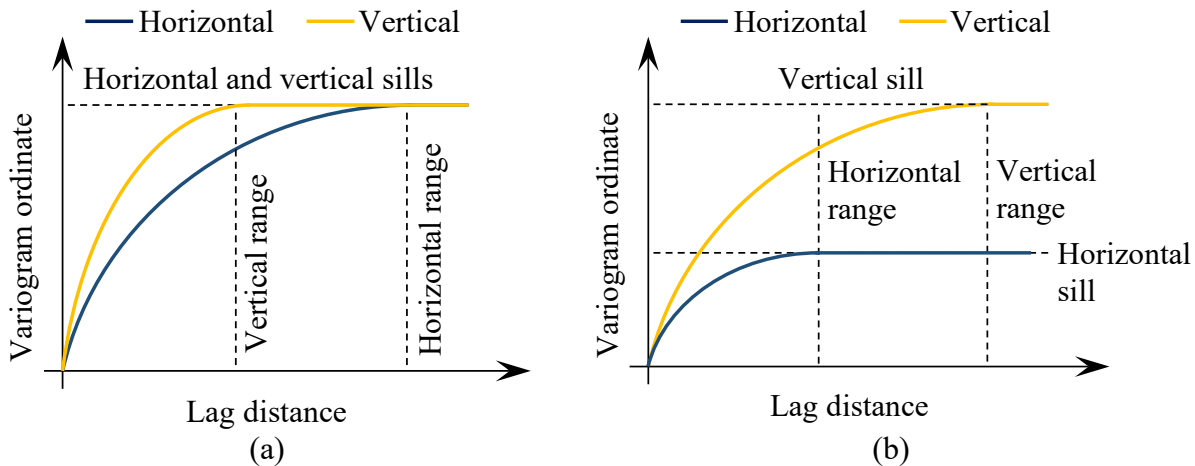


Figure 19. Illustrative characteristics of variograms: (a) Geometric anisotropy; (b) Geometric and zonal anisotropy

Zonal anisotropy is not a desirable characteristic given a collection of horizontal and vertical variograms. Even so, inspection of variograms for the purpose of detecting zonal anisotropy can be leveraged to identify the presence, and approximate extents, of geological zones. A procedure is presented below that centers around repeated generation and inspection of variograms (with respect to zonal anisotropy) to facilitate identification and associated plan-view extents of geological zones throughout bridge sites.

5.2.2 Key Steps of the Procedure

When conducting Geo-statistical analysis of geotechnical site data, characterization of spatial correlation structures (variograms) among the site data is necessary prior to performing stochastic simulation (which in turn, leads to predictions of foundation member resistance). Geotechnical site data are typically packaged into elevation profiles (boring or coring data), with distinct plan-view coordinates. For analysis, collections of borings are selected and profiles of site data are collapsed down to a single profile for identifying soil layers. Horizontal and vertical variograms are then formed for each layer, based on the relative spatial positions and magnitudes of site measurements making up the collection (or subset) of selected borings. This overall progression is upheld in the procedure for estimating zonal radii, shown in Fig. 20.

The procedure operates on boring locations and respective elevation-profiles of geotechnical site data and consists of two major steps: (1) assessment of variograms using all available site data; and, (2) identification of collections (subsets) of borings that belong to distinct geological zones. Outcomes from the first major step serve to indicate whether sufficient site data have been gathered for the purpose of estimating zonal radii, and also, whether multiple geological zones are indeed present across the site. For scenarios where sufficient site data have been gathered and multiple geological zones are present, then the second major step is subsequently undertaken to identify the subsets of borings belonging to each zone. As an outcome from the second major step, the smallest plan-view circular subdomains that encompass each subset of borings are defined, constituting the estimates of zonal radii.

The first major step begins with visual assessment of elevation profiles of site data from all borings, collapsed down to a single elevation profile (per type of site measurement). The visual assessment leads to determination of the number the soil (or rock) layers. For each layer, the top and bottom elevations are also defined. Next, both horizontal and vertical variograms are formed per layer. If both horizontal and vertical variograms cannot be formed within a given layer, then the procedure is halted due to insufficient site data. Otherwise, after all layer-specific horizontal and vertical variograms have been formed, the sills of the variograms are inspected for the purpose of detecting zonal anisotropy (recall Fig. 19b).

The implementation in GeoStat is such that variograms are normalized by the variance of the underlying (layer-specific) data set. Therefore, inspection of variogram sills consists of confirming that the sills approach unity (Fig. 20). If all variogram sills approach unity, then only a single zonal radius is estimated to be applicable across the site-wide data set, where the zonal radius is the smallest circle that encompasses all boring locations from a plan-view perspective. Otherwise, more than one geological zone is present across the site, and the site data must be divided into subsets of borings that are associated with each, distinct geological zone.

The second major step in the estimation of zonal radii begins with selection of unique subsets of borings. Engineering judgement is required in selecting a given subset of borings. For example, borings that are clustered together (e.g., within the intended footprint of a pier) may be more amenable to zone assessment as opposed to borings that are positioned hundreds or thousands of feet apart. For each subset, the number of layers is decided upon, and the layer top and bottom elevations are assigned. Also, horizontal and vertical variograms are formed for each defined layer.

For any layer, if both horizontal and vertical variograms cannot be formed, then additional borings should be incorporated into the subset.

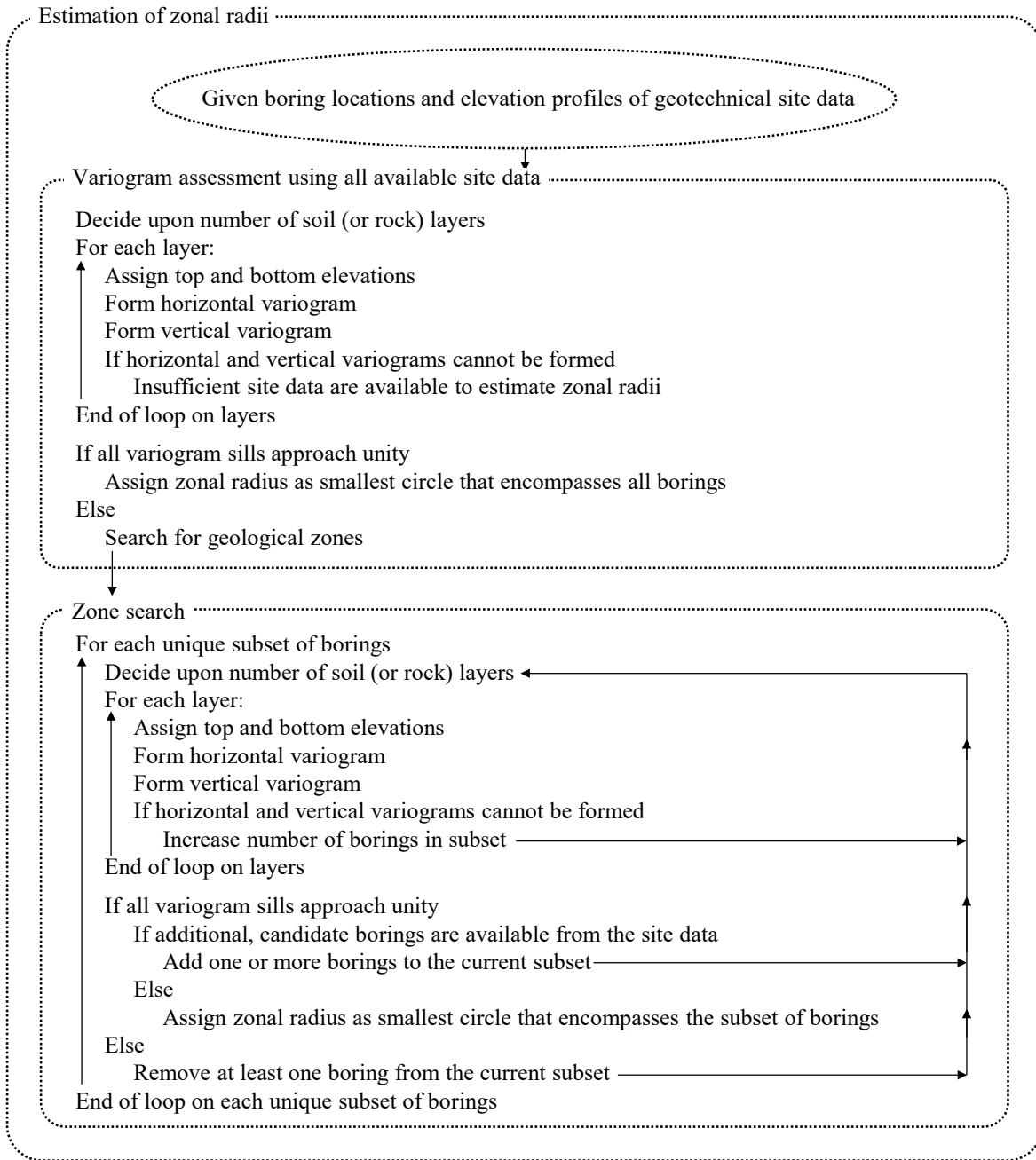


Figure 20. Procedure for estimation of zonal radii

After forming all variograms for layers associated with the subset, then the variogram sills are inspected. If all variogram sills approach unity, then additional borings can be incorporated into the subset. When adding borings to the subset, engineering judgment is again required (e.g., borings nearest, in plan view, to those of the existing subset may potentially be selected as candidates). For any instances where one or more borings are added to a subset, then the processes of defining layers and forming variograms (per layer) are repeated for the newly modified subset.

If all variogram sills for the current subset of borings approach unity and no additional, candidate borings are available from the site data, then the subset is designated as belonging to a distinct geological zone. A zonal radius is then estimated as the radius of the smallest circle that encompasses the plan-view positions of the subset of borings. In contrast, if one or more variogram sills do not approach unity, then one or more borings should be removed from the current subset. When removing one more borings from a given subset, the processes of defining layers and forming variograms are repeated.

5.3 Illustration Case

An illustration case is presented in the following to elucidate various steps within the procedure for estimating zonal radii (recall Fig. 20). Shown in Fig. 21 are site data for the illustration case. The 51 total boring locations are distributed, as shown in Fig. 21a, into four prominent clusters across a site spanning approximately 4000 ft (with respect to easting values) and approximately 1750 ft (with respect to northing values). Across the 51 borings, the below-surface medium predominantly consists of Florida limestone. Note that of the (approximately) 177,000 measured values of specific energy plotted in Fig. 21b, 99% of the measured values are less than or equal to (again, approximately) 15,000 psi.

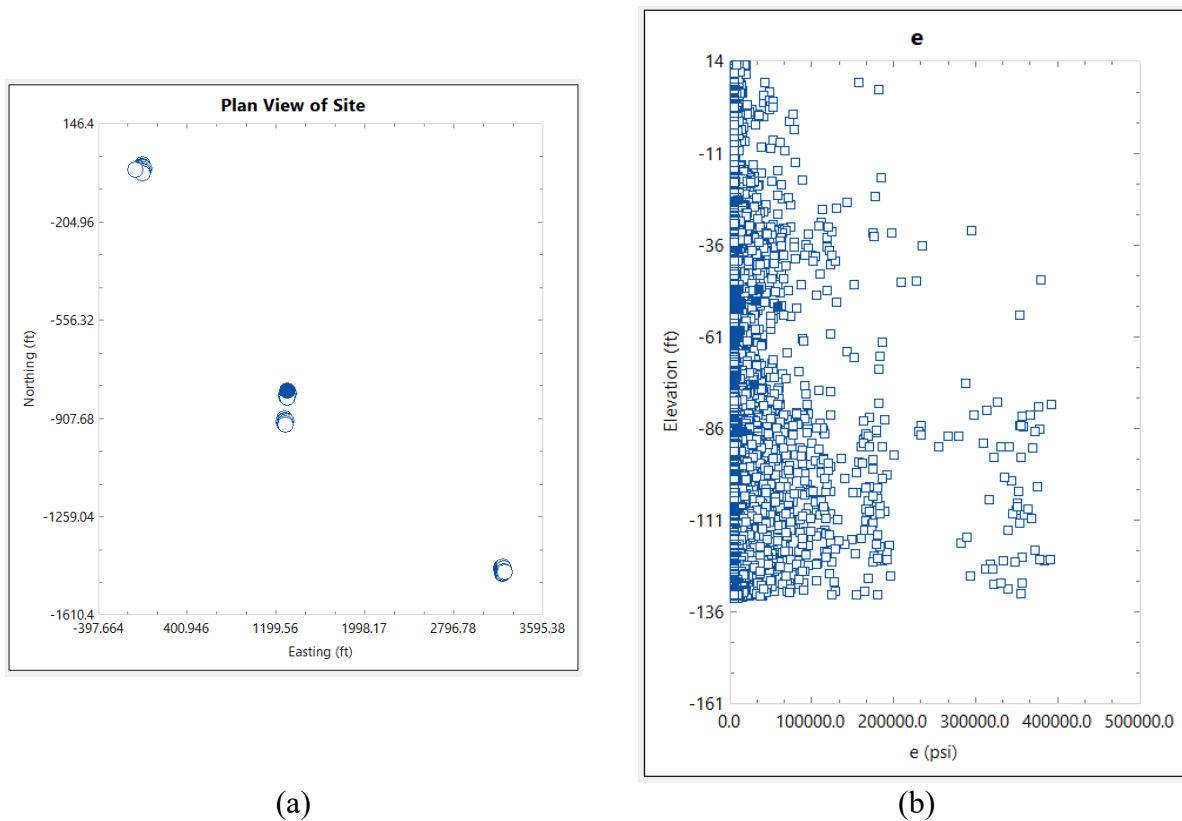


Figure 21. Overview of site data for illustration case: (a) Plan view of 51 boring locations; (b) Measured values of specific energy, e

Approximately 177,000 measured values of specific energy (e) are distributed across the 51 boring locations. A scatterplot of all measured values of e versus elevation is shown in Fig. 21b. Values of specific energy were measured from elevations of 14 ft down to approximately -135 ft.

5.3.1 Scope

The scope of the illustration case is to proceed through an instance for each of the two major steps of the procedure for estimating zonal radii (Fig. 20). First, all available site-wide measurements of specific energy (e), as compiled from the 51 total boring locations, are utilized along with interpreted geotechnical data to create layer definitions. For each layer, it is then confirmed that sufficient data are available to form both horizontal and vertical variograms (i.e., horizontal and vertical variograms are formed per layer). The sills of the variograms are then inspected, revealing that multiple geological zones are present within the site.

An instance of the second major step from Fig. 20 is then undertaken, wherein a plan-view region of interest within the site, containing a test-shaft location, is focused upon. Borings positioned within said region—and the process of accumulating progressively larger subsets of borings—is demonstrated, leading up to assessment of a 17-boring subset. As a result, a zonal radius is estimated for the subset of 17 borings positioned within the plan-view region of interest.

5.3.2 Formation of Variograms Using Site-wide Boring Data

Scatterplots of site-wide boring data are plotted in Fig. 22. Measured values of specific energy (e) are given in Fig. 22a; interpreted values of unconfined compressive strength, q_u , are shown in Fig. 22b. Note that for this verification case, no upper bound limit was enforced for mapping from measured values of specific energy to estimates of q_u . In accordance with the procedure for estimating zonal radii (Fig. 20), the first major step is undertaken by utilizing the site-wide data set to define layers. Accordingly, layer bottom elevations are superimposed on each plot as solid blue lines and are based on distinct shifts in the compiled values of e and q_u throughout the through-depth scatterplots.

Having defined the layering, variograms are subsequently formed. Recalling the procedure from Fig. 20, formation of variograms with use of the full 51-boring data set serves (in part) to indicate whether sufficient data are available to form both horizontal and vertical variograms. Listed in Table 12 are selected layer data, including data pertaining to layers 1 and 2. Guidance provided in the GeoStat Technical Manual is followed for selection of the layer-specific variogram parameters. Values of lag (i.e., the interval of separation distance) and the number of lags (i.e., the number of intervals at which pairs of measurements are searched for) are iterated upon. For a trial value of lag, horizontal tolerance is set equal to one-half of the lag distance. Values of horizontal bandwidth are limited to 2 ft. Vertical tolerance values are likewise set equal to one-half of the vertical lag, while vertical values of bandwidth are limited to 0 ft. Note that, for a given separation distance, values of tolerance and bandwidth incorporate bidirectional tolerances into the search for pairs of site measurements. Values of lag and the number of lags are iterated upon (within each layer, for both horizontal and vertical directions) until a sufficient number of experimental

variogram points are produced so as to, at minimum, permit qualitative (e.g., visual) assessment of the overall variogram shape.

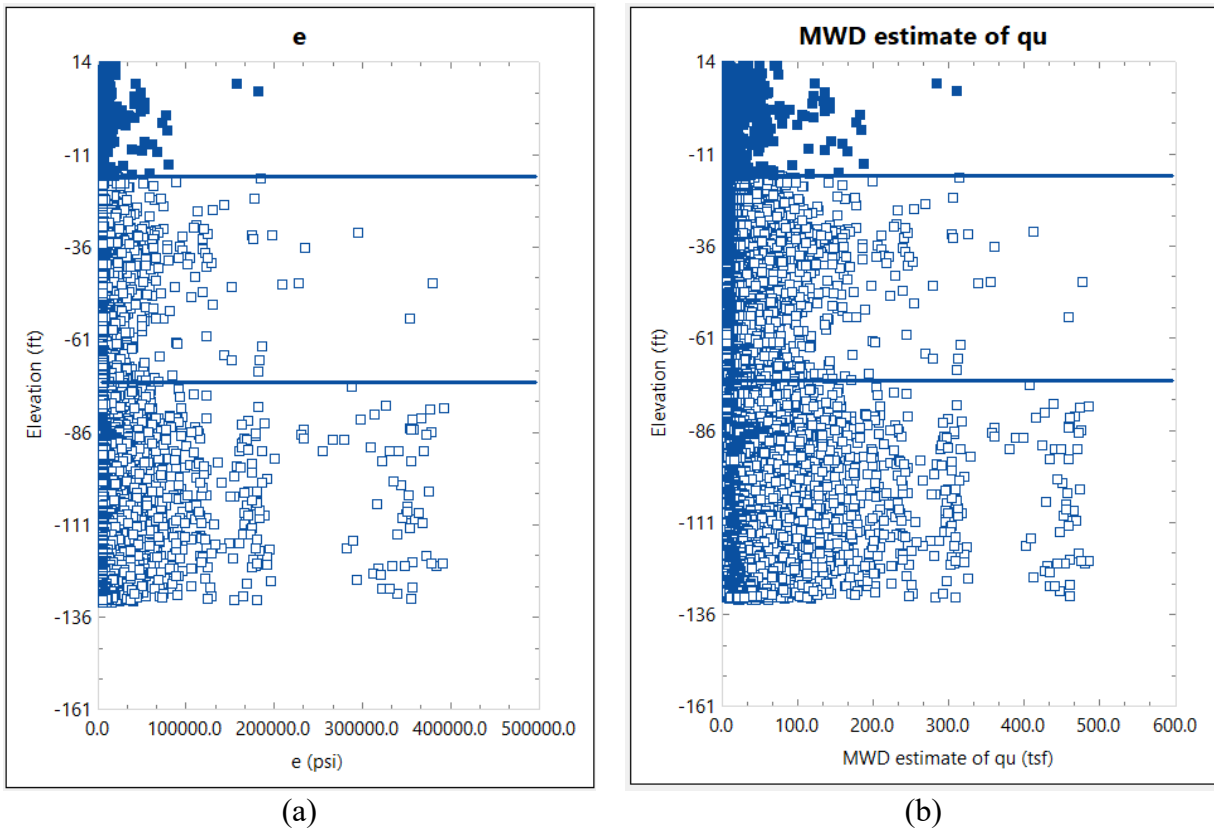


Figure 22. Scatterplots of site-wide geotechnical data versus elevation (51 borings) and estimated layer bottom elevations (solid blue lines): (a) Specific energy, e ; (b) MWD estimate of q_u

Table 12. Selected layer bottom elevations and variogram data based on site-wide collection of 51 borings

Layer	Bottom elevation (ft)	Horizontal				Vertical			
		Lag (ft)	No. lags	Tolerance (ft)	Bandwidth (ft)	Lag (ft)	No. lags	Tolerance (ft)	Bandwidth (ft)
1	-17	5	12	2.5	2	2	10	1	0
2	-72	4	20	2	2	1	12	0.5	0

Selected variogram data for layers 1 and 2, as obtained from the site-wide (51-boring) data set, are plotted in Fig. 23. More specifically, experimental variogram points are shown for layer 1 (Fig. 23b-c) and layer 2 (Fig. 23d-e). With regard to the vertical variograms (Fig. 23c, Fig. 23e), the experimental variogram points exhibit well-formed characteristics. The initial portions of the variograms exhibit relatively steep ascents, while for increasing lag distances, the variogram points indicate reductions in slope, converging on values near to unity. In contrast, the horizontal variograms (Fig. 23b, Fig. 23d) exhibit asymptotic characteristics at (normalized) variogram ordinate values less than unity (e.g., the horizontal variogram points for layer 2, Fig. 23b, converge to a variogram ordinate of approximately 0.6). Outcomes from performing the first major step in

the procedure for estimating zonal radii (Fig. 20) indicate that: (1) sufficient data are available for forming horizontal and vertical variograms; and, (2) that multiple geological zones are present across the site.

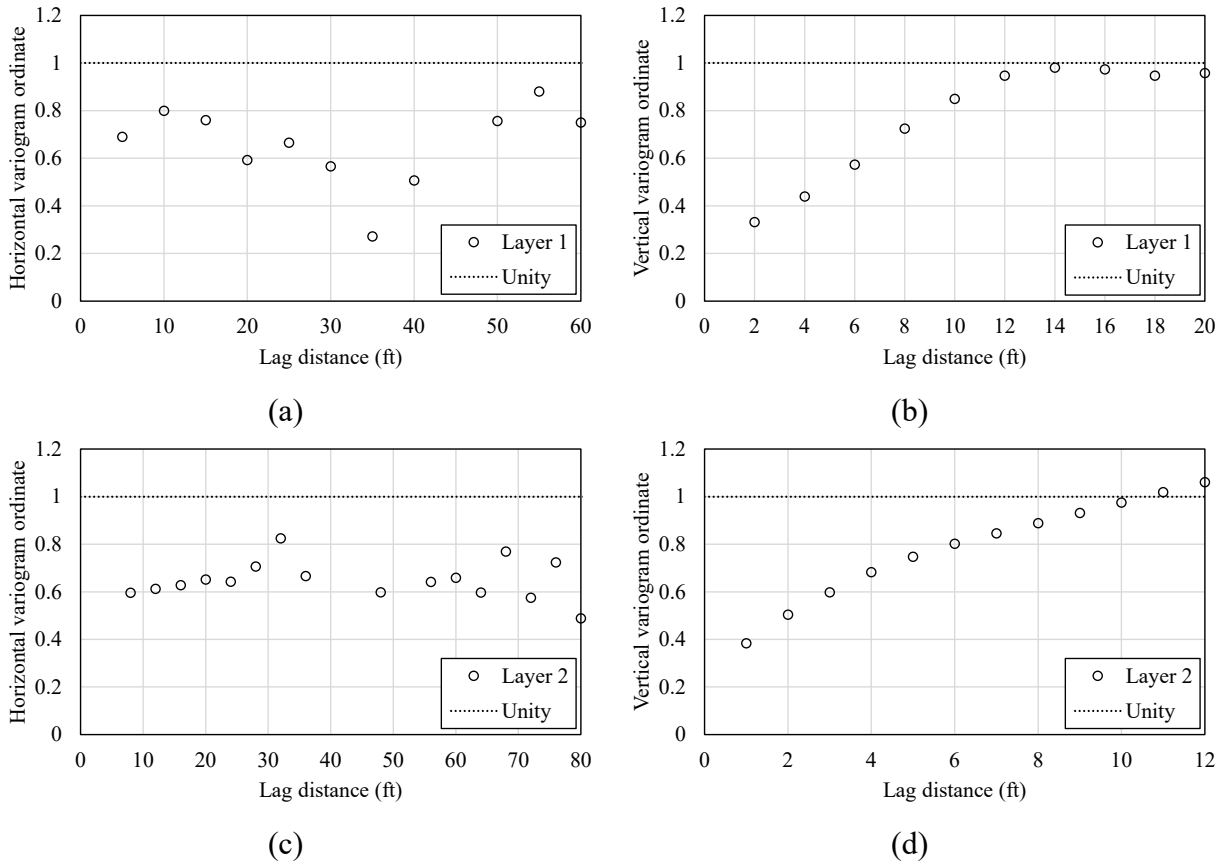


Figure 23. Selected variograms obtained using site-wide data (51 borings): (a) Layer 1 horizontal; (b) Layer 1 vertical; (c) Layer 2 horizontal; (d) Layer 2 vertical

5.3.3 Region of Interest for Illustration Case

For the remainder of the illustration case, focus is given to investigation of geological zones for a region of interest within the site. In particular, one instance of utilizing the second major step of the procedure for estimating zonal radii (recall Fig. 20) is documented. Note that only the boring data associated with a given subset of borings is utilized (on a per layer basis) to form experimental variogram points.

As situated in the northwest portion of the site, the region of interest is denoted in Fig. 24a. A plan-view inset of the region is depicted in Fig. 24b. The region contains one boring at a test shaft location and 16 additional borings (for a total of 17 borings). Permutations of the 17-boring data set are investigated in the following to demonstrate the manner by which geological zones can be identified, including characterization of zonal extents.

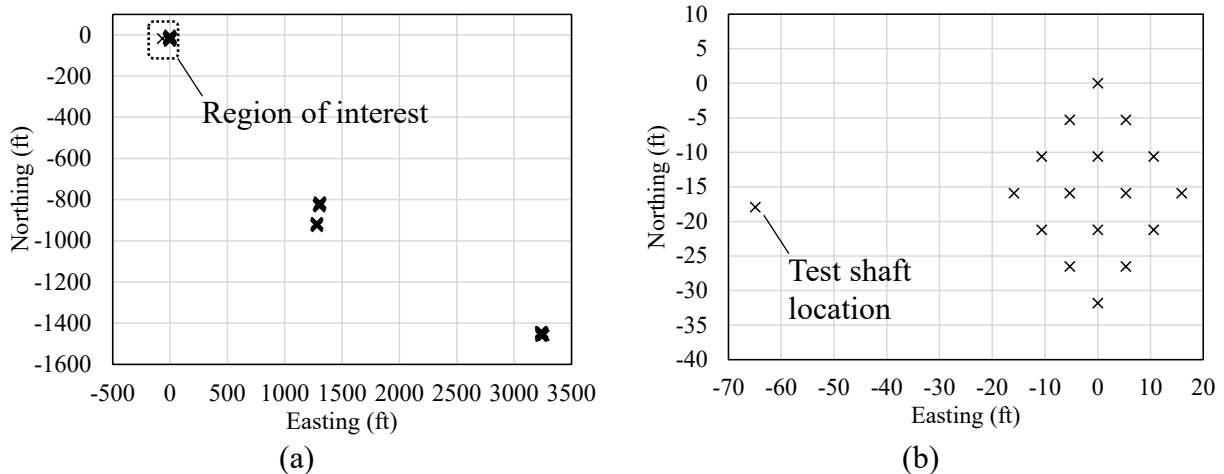


Figure 24. Region of interest for illustration case: (a) Relative to overall site; (b) Inset of 17 boring locations and test shaft location

5.3.4 Formation of Variograms Using Progressively Larger Subsets of Borings

Interpreted values of unconfined compressive strength (q_u) and rock recovery—as estimated from measured values specific energy, e , and compiled from all 17 borings within the region of interest—are plotted versus elevation in Fig. 25. Superimposed atop the scatterplots are layer bottom elevations (as solid blue lines). Here, interpreted values of rock recovery exhibit prominent shifts in values with respect to depth, and therefore, are of particular use in assigning layer elevations. Listed in Table 13 are selected layer bottom elevations and variogram parameter values for layers 1 through 4, again, as obtained from examination of the 17-boring data set.

Presented in Fig. 26 through Fig. 29 are selected horizontal and vertical variograms, as produced from Geo-statistical analysis of progressively larger subsets of borings within the region of interest. For brevity, variogram results are presented for selected layers (layer 1, layer 4) across four increasingly large subset selections. For each subset investigated, constituent geotechnical data (interpreted values of q_u , rock recovery) are examined for the purposes of defining layers and assigning variogram parameter values. For all permutations of boring subsets within the region of interest, the layer bottom elevations and variogram parameter values listed in Table 13 are judged to remain acceptably representative. Note that this approach also enables insights to be made regarding the evolution of generated variogram points with respect to increasingly larger subsets.

Table 13. Layer bottom elevations and variogram data for 17 borings in the region of interest

Layer	Bottom elevation (ft)	Horizontal				Vertical			
		Lag (ft)	No. lags	Tolerance (ft)	Bandwidth (ft)	Lag (ft)	No. lags	Tolerance (ft)	Bandwidth (ft)
1	-17	5	12	2.5	2	2	10	1	0
2	-28	4	10	2	2	2	10	1	0
3	-45	5	12	2.5	2	2	10	1	0
4	-57	4	20	2	2	1	12	0.5	0

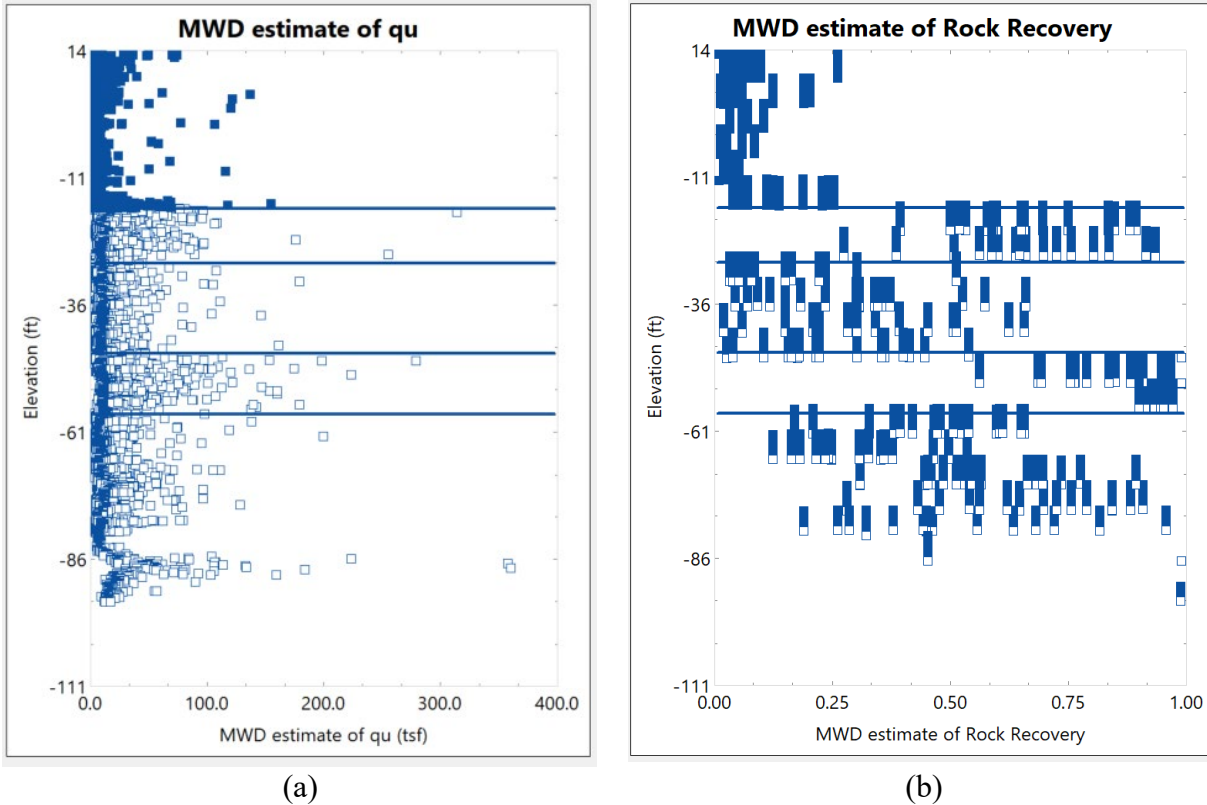


Figure 25. Scatterplots of geotechnical data versus elevation from region of interest (17 borings) and estimated layer bottom elevations (solid blue lines): (a) MWD estimate of q_u ; (b) MWD estimate of rock recovery

Recalling the procedure from Fig. 20, the zone search within the region of interest begins with selection of a subset of borings. Given the emphasis placed on estimation of zonal radii with respect to test shaft locations, the boring associated with the test shaft location and the three nearest borings are initially selected for investigation (Fig. 26a). The layer definitions are examined and the variogram parameters are assigned (as aforementioned, the tabulations given in Table 13 are found to be representative). Examination of the vertical variograms for layer 1 (Fig. 26c) and layer 4 (Fig. 26e) reveals variogram sills that approximately approach unity. Relatively fewer experimental variogram points are able to be generated for the horizontal variograms (Fig. 26b, Fig. 26d). However, the four experimental variogram points in each graph are judged to approach sills (approximately) near unity for increasing lag distances. Note that engineering judgement is required for determining an acceptable number of variogram points, and further, an acceptable deviation in the perceived asymptote of the variogram ordinates relative to unity. Also note that selection of a smaller subset of borings (e.g., fewer than four) may prohibitively limit the number of variogram points that can be generated. Given that all variogram sills approximately approach unity, and further, that additional, candidate borings are available, additional borings are added to the 4-boring subset.

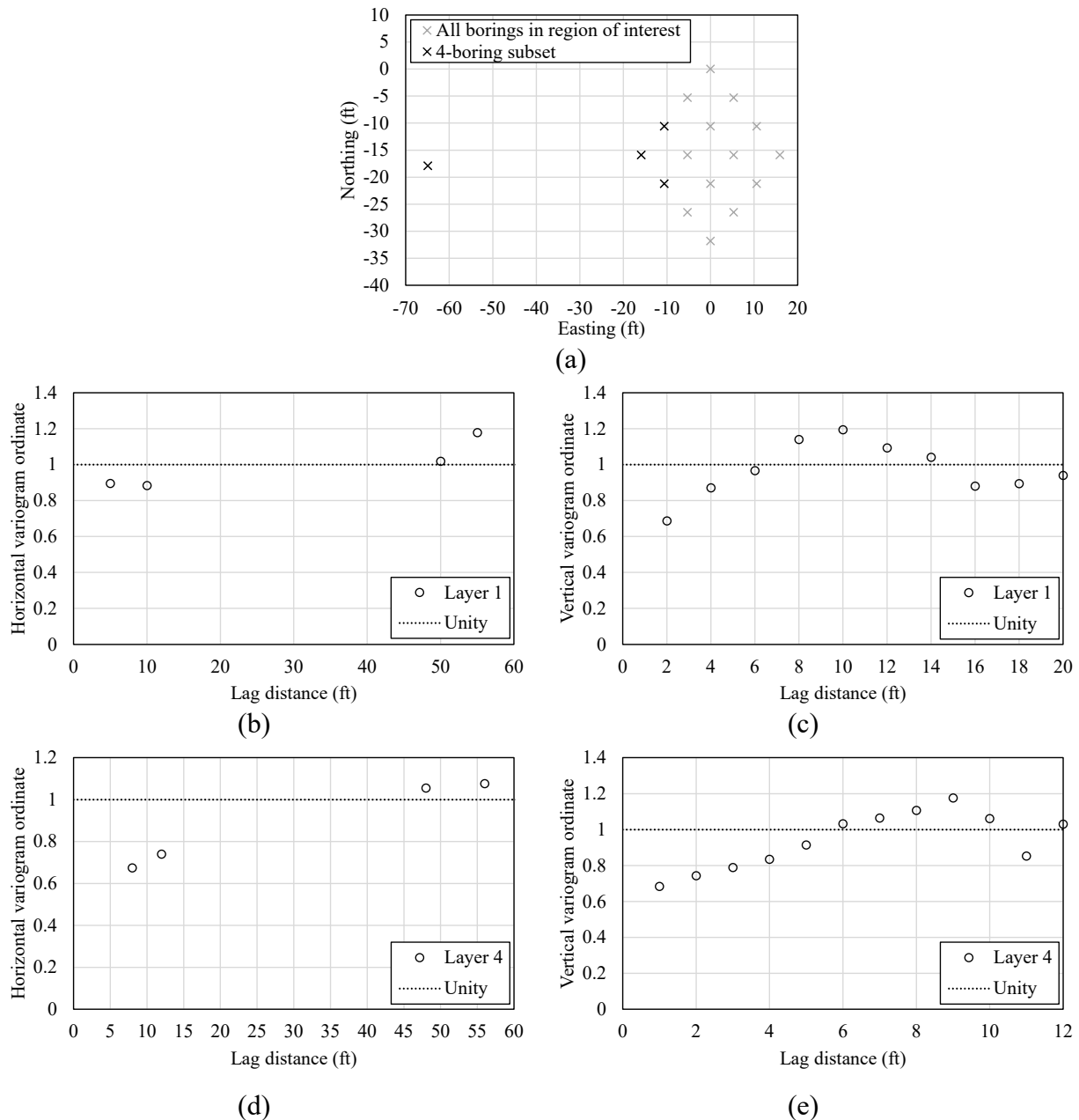


Figure 26. Selected variograms for 4-boring subset: (a) Plan view of boring locations; (b) Layer 1 horizontal; (c) Layer 1 vertical; (d) Layer 4 horizontal; (e) Layer 4 vertical

Three additional borings are incorporated into the subset, totaling 7 borings (Fig. 27a). Namely, the next three borings nearest to the test shaft location are added to the subset. The layer definitions are again examined and the variogram parameters are assigned using the tabulations given in Table 13. Cyclicity (i.e., undulations with respect to lag) is present among the variograms (e.g., Fig. 27e), which could potentially be reduced through further refinement of the layer definitions. However, the intensity of the cyclicity is judged to be acceptably mild. Further, the variograms collectively exhibit sills that (approximately) approach unity with increasing lag distance. Additional, candidate borings are therefore considered for investigation.

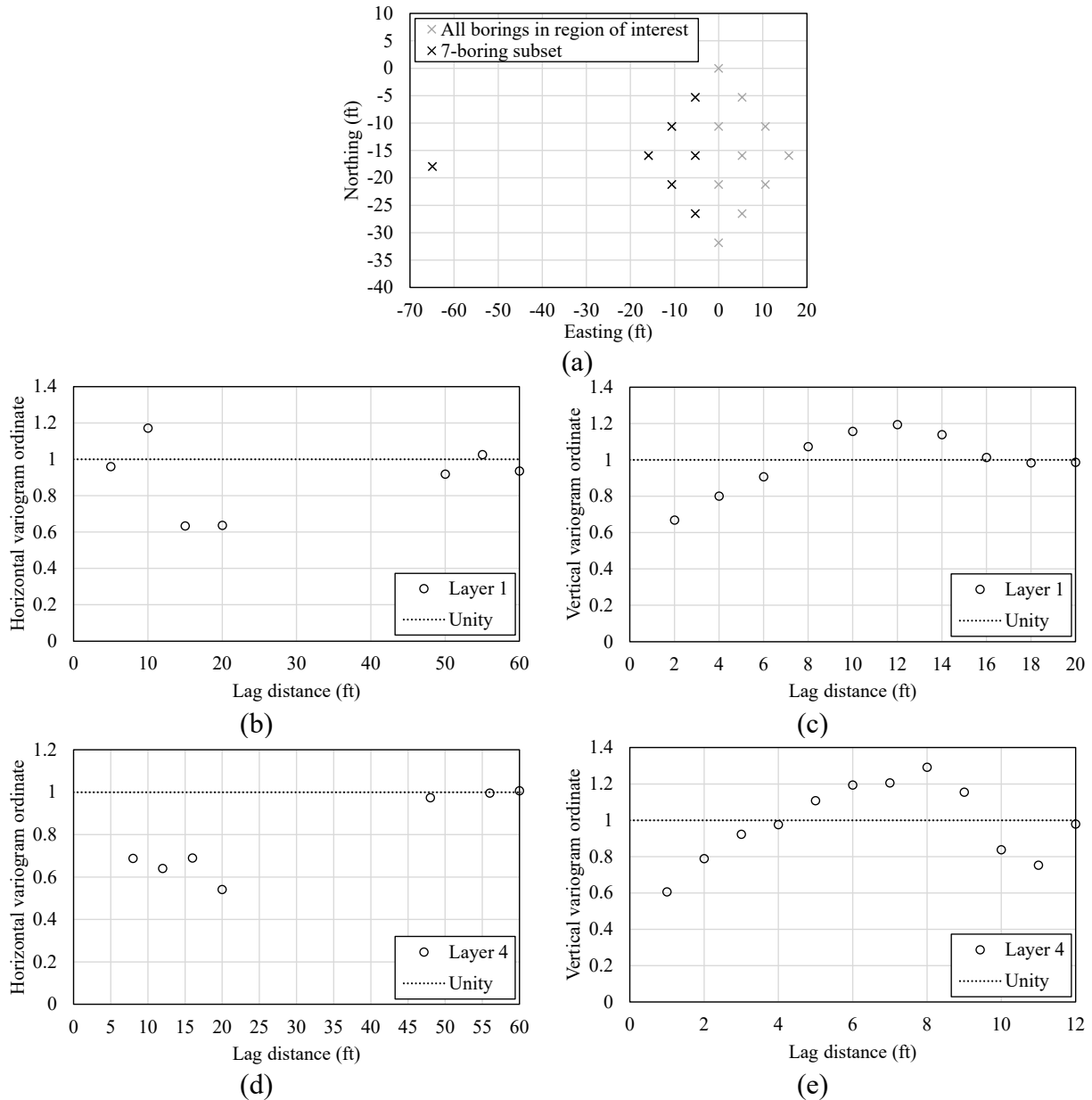


Figure 27. Selected variograms for 7-boring subset: (a) Plan view of boring locations; (b) Layer 1 horizontal; (c) Layer 1 vertical; (d) Layer 4 horizontal; (e) Layer 4 vertical

Shown in Fig. 28 is a subset that includes the boring at the test shaft location and the 13 nearest borings within the region of interest. Also plotted in Fig. 28 are selected variograms (for layer 1, layer 4). The layer definitions and variogram parameters from Table 13 are utilized for this 14-boring subset. Cyclicity is again exhibited by the variograms (e.g., Fig. 28b). Cyclicity in the horizontal variogram of layer 1 may be attributable to the relatively low values of (interpreted) rock recovery, which suggests the presence of gaps in the available data. Even so, the intensity of the cyclicity is judged to be acceptably mild. Furthermore, the variograms continue to exhibit sills that (approximately) approach unity with increasing lag distance, and further, exhibit decreasing changes as the subset grows larger.

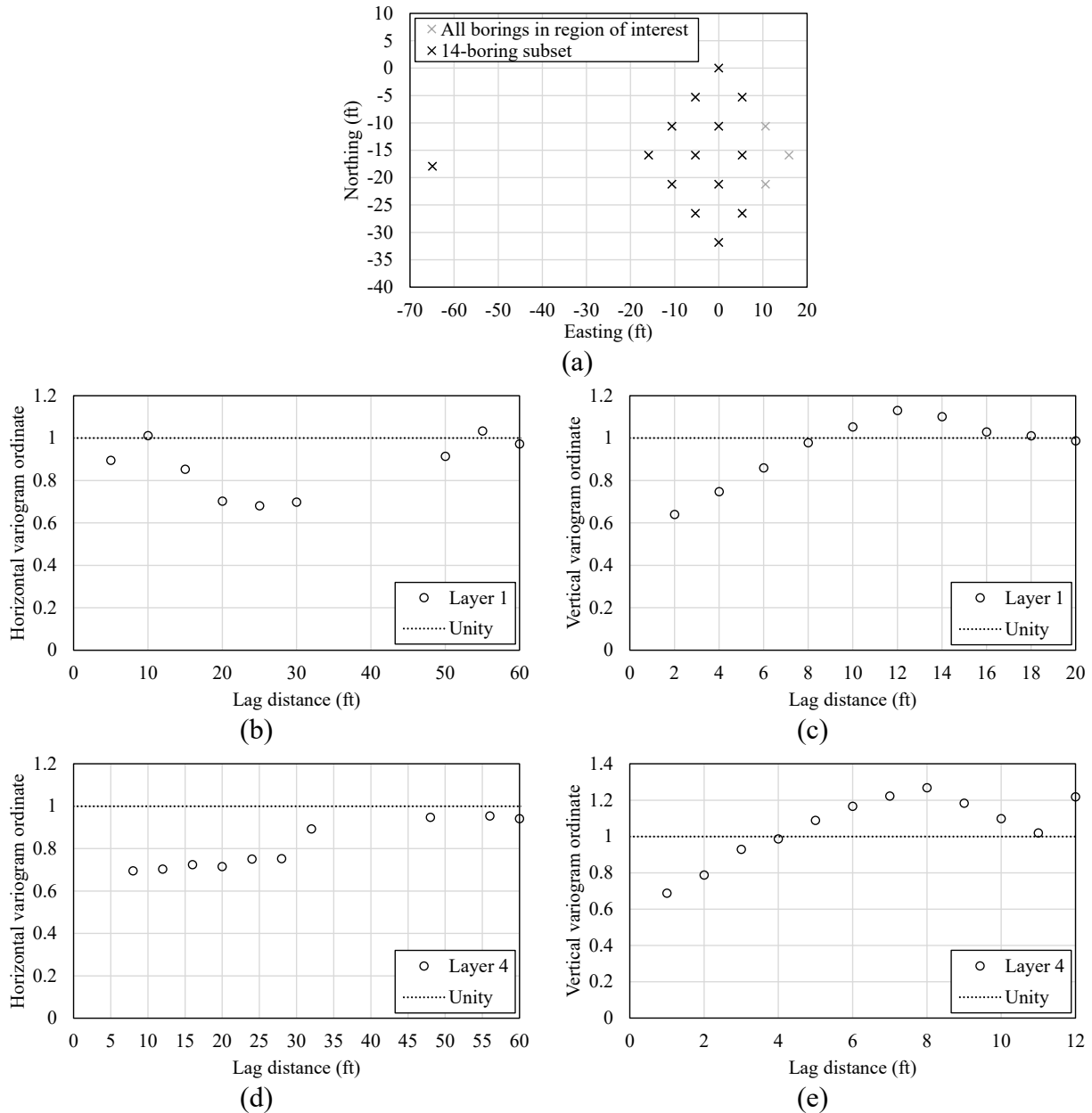


Figure 28. Selected variograms for 14-boring subset: (a) Plan view of boring locations; (b) Layer 1 horizontal; (c) Layer 1 vertical; (d) Layer 4 horizontal; (e) Layer 4 vertical

All 17 borings within the region of interest are included in the subset shown in Fig. 29, where this subset is associated with the layer definitions and variogram parameters from Table 13. All layer-specific variograms (e.g., those shown in Fig. 29b-e) exhibit sill values that are approximately near to unity. Furthermore, a visual comparison of variograms produced from the 14-boring (Fig. 28), and 17-boring (Fig. 29) subsets reveals increasing stability of the variograms.

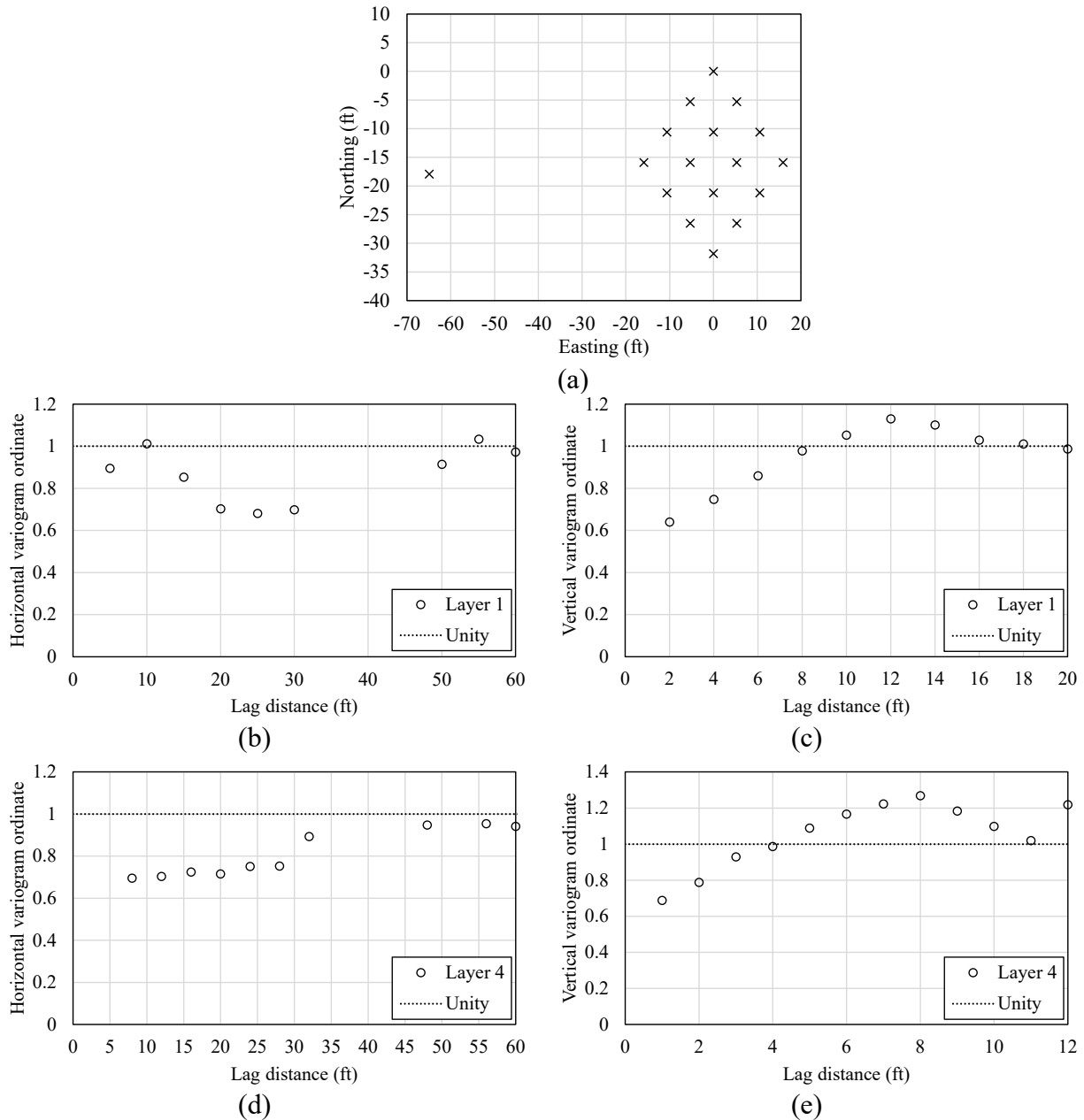


Figure 29. Selected variograms for 17-boring subset: (a) Plan view of boring locations; (b) Layer 1 horizontal; (c) Layer 1 vertical; (d) Layer 4 horizontal; (e) Layer 4 vertical

Recalling the plan view of the site-wide data set (Fig. 24a), the region of interest is situated in the northwest portion of the site, while the 51 total borings are distributed into four clusters across the site. The next adjacent cluster of borings relative to the region of interest is situated more than 1000 ft away in plan view. No additional, candidate borings are therefore considered for incorporation with the 17 borings that are positioned within the region of interest. Continuing onward with the procedure for estimating zonal radii (Fig. 20), the 17-boring subset (Fig. 29) is then designated as a distinct geological zone. The zonal radius is subsequently estimated as the smallest circle that encompasses the boring at the test shaft location and the 16 other borings within the region of interest. An illustrative depiction of the estimated zone is provided in Fig. 30.

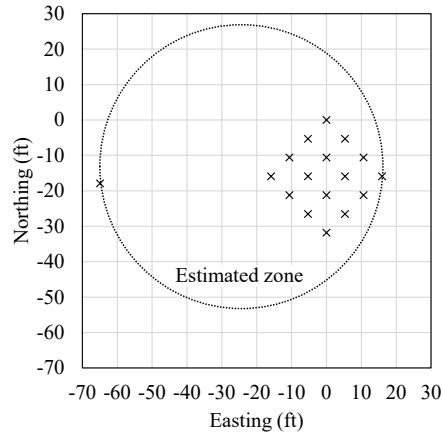


Figure 30. Illustrative depiction of estimated zone for 17-boring subset

5.3.5 Observations

Plotted in Fig. 31 are selected horizontal and vertical variogram points, with respect to increasingly larger subsets of borings within the region of interest. At a given lag distance, the normalized variogram ordinates vary over ranges of approximately 0.2 to 0.35 as the size of the boring subset increases from 4 borings to 17 borings.

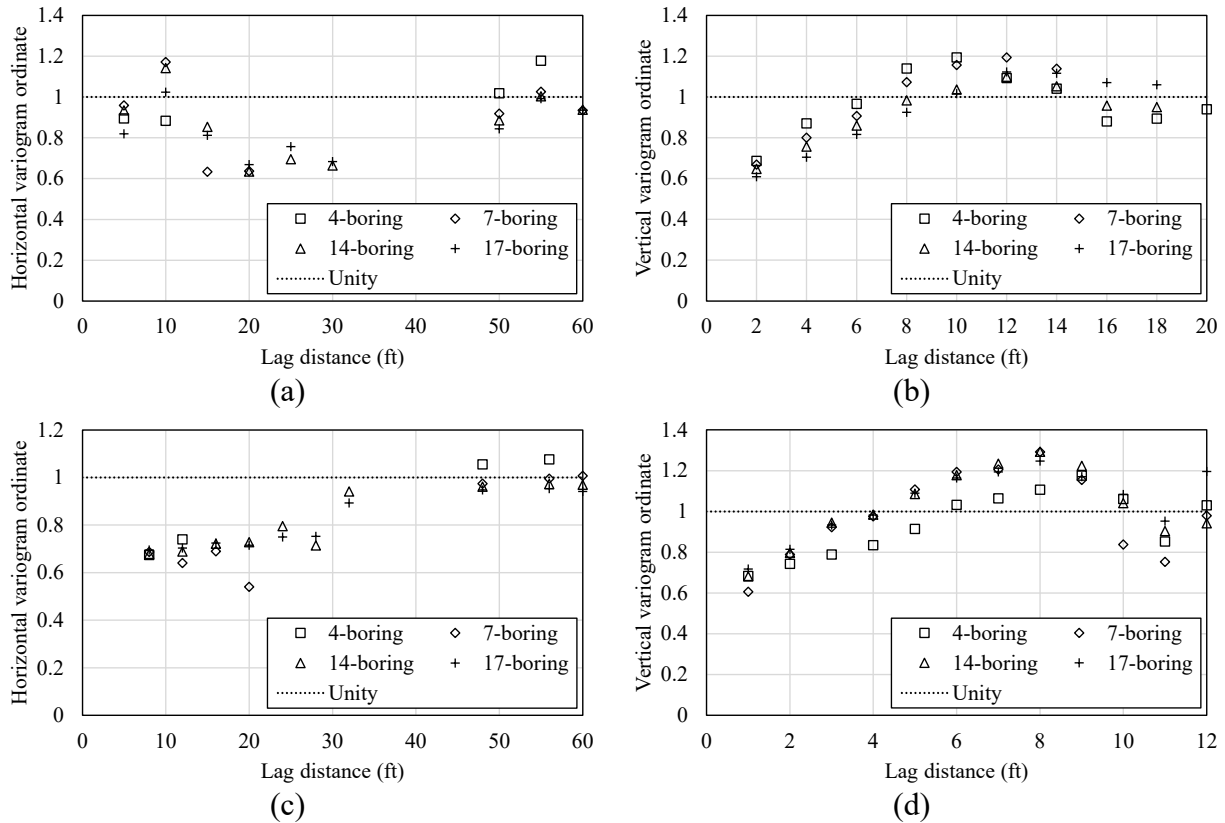


Figure 31. Comparison of variograms for progressively larger subsets of borings: (a) Layer 1 horizontal; (b) Layer 1 vertical; (c) Layer 4 horizontal; (d) Layer 4 vertical

Even so, the qualitative shapes exhibited by the variogram points exhibit consistency across the four subset sizes. As examples, all variograms generally exhibit increasing values over the same intervals of lag distance, and all variograms (approximately) converge to unity with increasing lag distance. Overall, the evolution and trends (e.g., sills) of the variograms support the designation of the 17-boring subset as being contained within a single geological zone.

To demonstrate the effect that a single boring can have on generated variogram values, when said boring pertains to a disparate geological zone, consider the scenario depicted in Fig. 32. For this latter scenario, 17 borings within the region of interest and one boring from the nearest cluster of borings are combined into a subset (Fig. 32a). The layer definitions and variogram parameter values given previously in Table 13 are again utilized (i.e., are found to remain acceptably representative). Horizontal and vertical variogram points—pertaining to layer 4 of the 18-boring subset—are plotted in Fig. 32b and Fig. 32c, respectively.

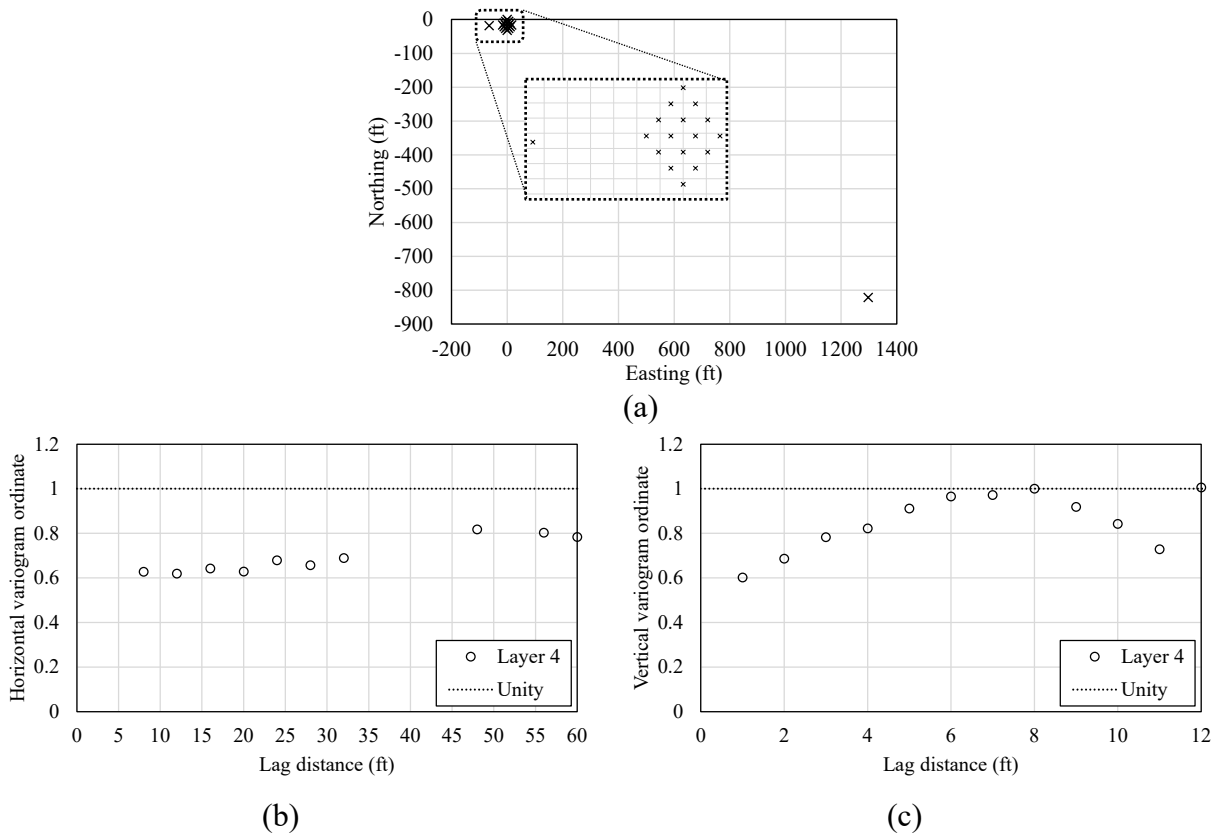


Figure 32. Selected variograms for 18-boring subset: (a) Plan view of boring locations; (b) Layer 4 horizontal; (c) Layer 4 vertical

Consider the comparative plots of experimental variogram points for layer 4, as shown in Fig. 33, and as obtained from the 17-boring subset (Fig. 29) and the 18-boring subset (Fig. 32). Every ordinate produced using the 18-boring subset, across both the horizontal and vertical variograms, is reduced relative to the counterpart value obtained from use of the 17-boring subset. The introduction of one boring from the adjacent cluster increases the variance of the 18-boring data set (relative to that of the 17-boring data set) by 10-20%.

Reductions in all variogram ordinate values, as a result of incorporating one additional boring, are not consistent with evolutions in the variograms produced using previously investigated subsets (compare the changes in variograms from the 14-boring subset, 28, to the 17-boring subset, Fig. 29). In addition, the sill of the horizontal variogram obtained for the 18-boring subset (Fig. 33a) does not approach unity. Therefore, the 18-boring data set should not be assumed to pertain to a single geological zone. For such instances (per the procedure from Fig. 20), the offending boring would be removed from the subset. Furthermore, if the two datasets were carried forward into stochastic simulation, then the effect of adding the single (18th) boring is demonstrated to lead to reductions in computed LRFD resistance factor values (Fig. 34). Note that, to facilitate comparisons, the computed resistance factor values were permitted to reach up to 1.0.

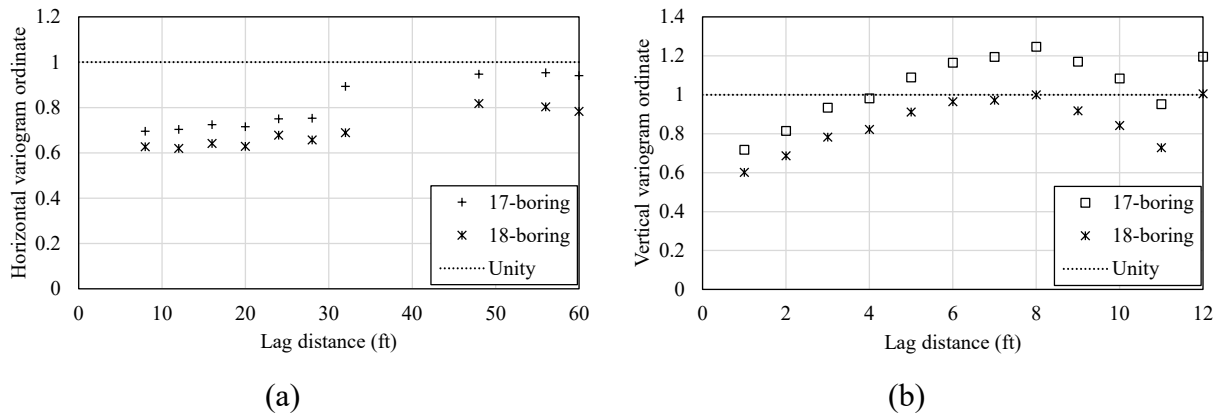


Figure 33. Comparison of variograms between 17-boring and 18-boring subsets: (a) Layer 4 horizontal; (b) Layer 4 vertical

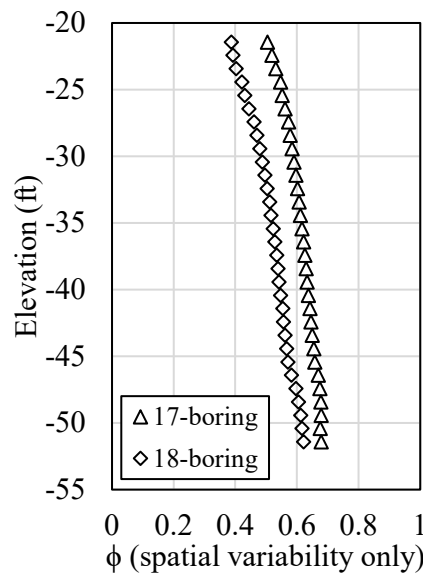


Figure 34. Comparison of computed LRFD resistance factor (ϕ) values

CHAPTER 6 SUMMARY AND CONCLUSIONS

6.1 Summary of Work Completed

The current implementation project was undertaken to enhance the design-oriented Geo-statistical analysis software, GeoStat. In this way, engineers are provided with increasingly feasible means of incorporating Geo-statistical phenomena into bridge foundation design applications. Updates and enhancements that were implemented included (1) read-in, storage, processing, and usage of CPT data (cone tip resistance, sleeve friction) for Geo-statistical analysis of driven piles; (2) read-in, storage, processing, and usage of MWD data (specific energy) for Geo-statistical analysis of drilled shafts in limestone; (3) quality assurance testing for both the CPT and MWD feature sets (including verification of variogram generation and stochastic simulation results), as well as submission of a beta software package to the FDOT for sponsor review; (4) investigation, documentation, and demonstration of an approach for estimating effective plan-view radii of geological zones throughout bridge sites; and, (5) development and delivery of technology transfer materials to promote use of Geo-statistical analysis software in practice. The GeoStat software manuals were also updated as part of the project efforts. Summaries of the efforts and outcomes for each of items (1) through (5) are documented below.

6.1.1 Summary of Task 1 Work Completed

The primary objective of Task 1 was to implement Cone Penetration Testing (CPT) analysis within the Geo-statistical software, GeoStat. Features added for CPT analysis complemented existing program capabilities (e.g., those associated with SPT-based analysis; analysis of drilled shafts in limestone layers). In addition, the new program features increased the range of foundation design applications that can more directly incorporate spatial variability and method error phenomena into calculations of pile axial capacity.

Geo-statistical analysis with use of CPT data within GeoStat necessitated the addition of reading, writing, and processing of profiles of CPT measurements (e.g., cone resistance, sleeve friction). Three empirical methods commonly used for CPT analysis were also identified, where any one of which can be selected as part of the overall Geo-statistical analysis using CPT data. Measurements of cone resistance were identified as a ‘primary’ variable for use in generation of layer-specific variograms. Correspondingly, CPT-based stochastic simulation processes were developed as part of Task 1, entailing realizations of cone resistance followed by co-simulation of sleeve friction.

Program capabilities were also added for writing CPT analysis files (one per realization) and reading results obtained from respective pile axial calculations. Further, a method error technique was identified from the literature and adapted for use in CPT analyses as part of total uncertainty calculations. Additionally, respective portions of the software manuals were updated.

6.1.2 Summary of Task 2 Work Completed

The primary objective of Task 2 was to implement Measuring While Drilling (MWD) analysis within the Geo-statistical software, GeoStat. Features added in relation to MWD analysis significantly expanded existing program capabilities. In particular, the newly implemented MWD features further increased the range of foundation design applications that can more directly incorporate spatial variability and method error phenomena into calculations of shaft axial capacity for drilled shafts embedded in limestone.

Geo-statistical analysis with use of MWD data within GeoStat necessitated the addition of reading, writing, and processing of profiles of MWD measurements (namely, specific energy). An empirical method that was previously developed for MWD analysis was also identified and included among the MWD implementation. Calculated (i.e., interpreted) values of unconfined compressive strength, as obtained from measurements of specific energy, were identified as a “primary” variable for use in generation of layer-specific variograms. Correspondingly, MWD-based stochastic simulation processes were developed as part of Task 2, entailing realizations of unconfined compressive strength, followed by calculation of values for tensile strength and other pertinent limestone variables.

Program capabilities were also added for writing MWD analysis files (one analysis file per through-depth realization of limestone parameters) and reading results obtained from respective shaft axial resistance calculations. Further, a method error technique was adopted for use in GeoStat MWD analyses as part of total uncertainty calculations. Also, respective portions of the software manuals were updated to reflect new user interface (UI) controls and underlying algorithms for data read-in, storage, processing, and analysis.

6.1.3 Summary of Task 3 Work Completed

The primary objective of Task 3 was to conduct quality assurance on the GeoStat software, with focus given to those enhancements made during Task 1 (CPT implementation) and Task 2 (MWD implementation). Additionally, the quality assurance efforts constituted an integral step toward forming a beta version of the program. Work completed for Task 3 included documentation of the quality assurance efforts (submitted as part of Task 3.1) and submission of a beta software package containing the newly implemented CPT and MWD analysis features (i.e., a beta version of the GeoStat software, submitted as part of Task 3.2).

The manner in which quality assurance was carried out for GeoStat was divided into three thrusts: (1) data validation of user interface controls that were added in association with the CPT and MWD feature sets; (2) verification of engineering routines associated with calculation of spatial correlation structures (variograms); and, (3) verification of stochastic simulation results produced from CPT-based, and separately, MWD-based analyses.

Outcomes from Task 3 included confirmation that the CPT-based and MWD-based implementations produced expected results when compared to (quantitative) benchmark result sets. In addition, several feature suggestions were implemented as part of the FDOT review of the

GeoStat beta package (e.g., implementation of an option that allows the engineer to select from among two resistance factor formulations).

6.1.4 Summary of Task 4 Work Completed

The primary objective of Task 4 was to assess the potential for engineers to make use of the updated GeoStat software for estimating zonal radii (i.e., the plan-view extents of geological zones distributed across a bridge site). Although the methodology presented was intended for use in identifying geological zones (and associated extents) across a wide range of scenarios, particular focus was given to estimation of zonal radii associated with candidate test-shaft locations. Key steps of the methodology were developed and documented as part of Task 4.

As an outcome from Task 4, engineers can potentially leverage feature sets within GeoStat to identify and, in an approximate manner, assign circular plan-view bounds to geological zones. A case study was utilized to illustrate the major steps of the approach. Furthermore, software features were added to the existing plan-view plot features in the GeoStat software to aid in visualizing zonal radii, as assigned by the engineer. Corresponding updates were also made to the software manuals.

6.1.5 Summary of Task 5 Work Completed

The primary objectives of Task 5 consisted of developing technology transfer materials for dissemination to FDOT engineers as well as consultants, and also, hosting a half-day web-based technology transfer event exclusive to FDOT engineers. Materials developed for the half-day (4-hour) web-based technology transfer event were divided up into two 2-hour sessions. The first 2-hour session included presentation of materials concerning the theoretical basis of analysis, and also, live usage of the GeoStat software for an illustrative driven pile project. Focus in the second 2-hour session was placed on presentation of contextual materials and live usage of the GeoStat software for an illustrative drilled shaft project.

Additionally included in the technology transfer materials was content pertaining to the newly implemented feature sets for CPT-based and MWD-based Geo-statistical analyses. For each of the 2-hour sessions, previously documented driven pile and drilled shaft cases found in BDV31-97-108 were leveraged. Outcomes from Task 5 included establishment of technology transfer materials that facilitate proliferation of Geo-statistical analysis tools in bridge foundation design.

6.2 Recommendations

Recommendations spanning two distinct categories were cultivated over the course of the implementation project. In particular, recommendations aimed toward improvements to workflows in design practice were identified, and are presented in Sec. 6.2.1. Furthermore, recommendations that may inform future research directions were accumulated, as listed in Sec. 6.2.2.

6.2.1 Recommendations for Design

GeoStat has been enhanced to further facilitate computation of resistance quantities, and associated statistical quantities, for deep foundation members such as driven piles and drilled shafts. The software enhancements expanded upon previously implemented capabilities for directly incorporating both spatial variability and uncertainty due to method error into axial capacity calculations. Stated alternatively, the implemented enhancements entailed expanding the available types of site geotechnical data and uncertainties that routinely accompany geotechnical design processes, with considerations for both relatively more mature site investigation methods (e.g., CPT) as well as burgeoning methods such as MWD.

The potential effectiveness of GeoStat in design is robust to a wide range of scenarios, spanning sites that are associated with relatively dense collections of geotechnical site data as well as sites where only limited site data are available. Use of GeoStat in practice can lead to more uniformly conservative foundation designs as compared to deterministic design methodologies. Also, methodologies developed as part of the current implementation project can serve to equip Owners with quantitative indicators of whether sufficient site data have been collected.

Accordingly, improvements to bridge design procedures that pertain to axial capacities of deep foundation members may potentially be achieved based on the following recommendations:

- For predicting axial capacities of deep foundation members (piles, drilled shafts), Geo-statistical analysis techniques (e.g., variogram formation, stochastic simulation) should be utilized in place of deterministic analysis methods;
- The GeoStat software contains features encompassing numerous types of site investigation methods (and corresponding types of geotechnical site data). It is therefore recommended that GeoStat be utilized for predicting axial capacities of driven pile and drilled shaft foundations. This recommendation spans across deep foundation members embedded in clay, silty sand, sand, and limestone media; and,
- Consistent with recommendations from previous FDOT research, site-specific resistance factors (ϕ) that are computed based on Geo-statistical analysis should only be utilized in design when Owner approval is granted.

6.2.2 Recommendations for Potential Future Research

Over the course of the current implementation project, several (potential) future enhancement items were identified for the GeoStat software. The as-identified items are anticipated to hold potential for further streamlining the means by which practicing engineers may incorporate spatial variability and uncertainty due to method error into design-level predictions of pile and shaft axial capacities. The list of enhancements are recommended to be undertaken, in part or in whole, as part of potential future research efforts.

- Complementary to ongoing, FDOT-funded research pertaining to MWD technology and methodologies, it is recommended that—when additional empirical relationships become available—said relationships are implemented for mapping from measured values of specific energy to interpreted values of various soil parameters (e.g., those required for Geo-statistical analysis of foundation members embedded in clay and/or sand media). In this way, MWD site data can be more broadly leveraged beyond shaft member portions embedded in limestone for predicting foundation member capacities.
- There is potential for automating portions of the methodology developed for estimating zonal radii. It is recommended that the extent to which automation is feasible be investigated and then implemented in the GeoStat software.
- It is recognized that for current practice in Florida, when designing drilled shafts in limestone, skin friction is predominantly of interest (as opposed to both skin friction and end bearing resistance). However, to facilitate automation of Geo-statistical calculations of end bearing resistance for drilled shafts in limestone, it is recommended that options are implemented for site-specific correlations of parameters such as mass modulus.
- For Geo-statistical analysis involving drilled shafts, the average value of unit weight and corresponding COV must be supplied for the media comprising each defined layer. It is recommended that a feature be added to automatically calculate the mean and COV of unit weight per layer when physically measured data are available.
- As an added convenience to engineers utilizing GeoStat, it is recommended that an option is added for performing nonlinear regression of experimental variogram points and populating corresponding (best-fit) parameter values of theoretical variogram curves.

REFERENCES

- AASHTO. (2020). *LRFD bridge design specifications, 9th Ed.* Washington D.C.
- Bloomquist, D., McVay, M. C., Hu, Z. (2007). Updating Florida Department of Transportation's (FDOT) Pile/Shaft Design Procedures Based on CPT & DTP Data, FDOT Research Report BD545, RPWO # 43, Tallahassee, FL.
- Davidson, M. T., McVay, M. C., Consolazio, G. R., Monari, C. J., Patil, A. P., Faraone, M. A. (2020). *Geo-statistical Deep Foundation Design Software*, FDOT Research Report BDV31-977-108, Tallahassee, FL.
- Faraone, M. A., Klammlar, H., McVay, M., Davidson, M., Herrera, R., Horhota, D. (2021). Design methodology for site-specific resistance factors based on foundation location and size, *Computers and Geotechnics*, 138, 104328.
- FDOT. (2022). *Structures Design Guidelines, Structures Manual, Vol. 1*, Tallahassee, FL.
- ISO. (2016). "Geotechnical investigation and testing—field testing—part 15: Measure while drilling", *ISO 22476-15:2016(en)*, Geneva, Switzerland.
- McVay, M. C., Klammlar, H., Faraone, M. A., Krishmarao, D., Jenneisch, C. (2012). *Development of Variable LRFD ϕ Factors for Deep Foundation Design Due to Site Variability*, FDOT Research Report BDK75 977-23, Tallahassee, FL.
- McVay, M. C., Rodgers, M. (2016). *Drilled Shaft Resistance Based on Diameter, Torque and Crowd (Drilling Resistance vs. Rock Strength) Phase II (FLMWDS)*, FDOT Research Report BDV31-977-91, Tallahassee, FL.
- McVay, M. C., Rodgers, M. (2020). *Implementation of Measuring While Drilling Shafts in Florida (FLMWDS)*, FDOT Research Report BDV31-977-91, Tallahassee, FL.
- McVay, M. C., Townsend, F. C., Williams, R. C. (1992). "Design of Socketed Drilled Shafts in Limestone", *ASCE Journal of Geotechnical Engineering*, 118(10): 1626-1637.
- Rivers, B. (2018). Advanced Geotechnical Methods in Exploration (The A-GaME), *49th Annual Southeastern Transportation Geotechnical Engineering Conference (STGEC)*, Louisville, KY, Oct. 8-11.
- Robertson, P. K. (2013). Cone Penetration Test (CPT) Quality Control (QC), Webinar #10, Gregg Drilling & Testing, Inc.
- Rodgers, M., McVay, Horhota, D., Hernando, J. (2018a). "Assessment of rock strength from measuring while drilling shafts in Florida limestone", *Canadian Geotechnical Journal*, 55:1154-1167.

- Rodgers, M., McVay, M. C., Ferraro, C., Horhota, D. (2018b). “Measuring Rock Strength While Drilling Shafts Socketed in Florida Limestone”, *ASCE Journal of Geotechnical and Geoenvironmental Engineering*, 144(3).
- Rogers, J. D. (2014). Fundamentals of Cone Penetrometer Test (CPT) Soundings, Missouri S&T GE 6441, Rolla, MO.
- Styler, M. (2006). Development and Implementation of the DIGGS Format to Perform LRFD Resistance Factor Calibration of Driven Concrete Piles in Florida. *Master's thesis*, University of Florida, Gainesville, FL.

APPENDIX A GEOSTAT HELP MANUAL

Presented below is the Help Manual for the GeoStat software, which is included as a standalone document, and is accessible from within the GeoStat UI. The Help Manual integrates work carried out during project Task 1 through Task 4 and contains documentation of program installation and licensing; input file formatting; and, all UI controls. A companion manual, which focuses on geotechnical engineering concepts, selection of modeling parameters, and underlying engineering calculations that are carried out when using the GeoStat software, is provided in Appendix B.



GeoStat



Help Manual

DISCLAIMER

No warranty, expressed or implied, is made by the Florida Department of Transportation or the University of Florida as to the accuracy and functioning of any programs or the results they produce, nor shall the fact of distribution constitute any such warranty, and no responsibility is assumed by the Florida Department of Transportation or the University of Florida in any connection therewith.

TABLE OF CONTENTS

DISCLAIMER	i
1. INTRODUCTION	1
1.1 Introduction	1
1.2 Software Description	1
1.3 Help Manual Scope	2
2. PROGRAM INSTALLATION AND LICENSING	3
2.1 Installation	3
2.2 Licensing	9
3. INPUT FILE FORMAT	28
3.1 Overview	28
3.2 Input Format for Data Pertaining to Member Configuration and Conditions	28
3.3 Input Format for Geotechnical Investigation Site Data	47
4. USER INTERFACE CONTROLS	57
4.1 Overview	57
4.2 File Menu and Toolbar	57
4.3 Project Information Tab	61
4.4 Profile Tab	70
4.5 Geostatistics Tab	76
4.6 Simulation Tab	88
4.7 Spatial Variability Tab	97
4.8 Method Error Tab	106
4.9 LRFD- ϕ Tab	110
5. GENERATION AND BATCH PROCESSING OF MODEL ANALYSIS FILES	118
5.1 Overview	118
5.2 Generating Model Analysis Files	118
5.3 Running Batch Mode Analysis	119
5.4 Parsing Output for Driven Piles with Analysis of SPT Datasets	120
5.5 Parsing Output for Driven Piles with Analysis of CPT Datasets	120
5.6 Parsing Output for Analysis of Drilled Shafts	121
6. REFERENCES	125

CHAPTER 1 INTRODUCTION

1.1 Introduction

Due in part to intrinsic variability of soil and rock materials, design and construction of deep foundations typically comprise significant costs for bridges. Measured soil properties exhibit spatial variability across a given site (both with respect to depth and horizontal position), while empirical methods by which measured soil properties are correlated to design-relevant soil or rock resistances introduce a separate form of uncertainty into the design process. These sources of uncertainty present challenges in determining layering and distinct zones as well as if sufficient site data have been gathered as part of required geotechnical investigations, which can result in non-representative (i.e., overly conservative or unconservative) estimates of Load and Resistance Factor Design (LRFD) resistances (ϕ) of deep foundation members. Quantifying these distinct sources of uncertainty (spatial variability, method error) allows for better determination of whether or not sufficient geotechnical site data have been gathered and also makes clear the level of uncertainty that can be attributed to predicted resistance of deep foundation members.

The GeoStat software allows engineers to characterize these forms of uncertainty, more efficiently carry out design efforts, and potentially arrive at more economical allocation of construction materials for bridge substructure configurations. GeoStat can be used to compute pile or shaft (axial) soil resistance, the associated uncertainty of those estimates, and LRFD resistance (ϕ) factors over a selected range of member embedment lengths, for given site data and engineer-selected layering and zones. The program accepts a collection of borings/corings pertinent to a site of interest, the engineer divides the site into zones, and for each zone, determines the layering. GeoStat is then used to perform both spatial-variability analysis and method error estimation on a pile/shaft, resulting in generation of through-depth resistance profiles and associated resistance (ϕ) factors.

1.2 Software Description

The GeoStat user interface (UI), which is a tabbed interface, guides engineers through the process of: (1) cataloging site data (borings, corings); (2) permitting zone definitions (i.e., subsets of the collected site data, i.e., zones); (3) permitting definitions of soil or rock layering; (4) forming spatial correlation structures given the subset of site data and soil or rock layering; (5) simulating numerous realizations of through-depth soil strength parameters; (6) computing through-depth axial resistance for each realization; (7) adjusting axial capacities using appropriate method error correlations; and, (8) reporting descriptive statistics (e.g., mean, variance, and COV) of resistance throughout the site and location-specific LRFD resistance (ϕ) factors.

Foundation design data generated in this manner overcome significant simplifications typical of current practice, where phenomena such as rock layering, area zones (i.e., spatial variability) are either ignored or indirectly accounted for via significantly more conservative (and more costly) configurations. By incorporating GeoStat into the design process, quantitative indicators of scope and sufficiency can be made available for budgeting, and conducting, geotechnical investigations. Also, the ability to quantify variability in foundation resistance quantities (e.g., the effect of pile/shaft lengths on LRFD resistance ϕ factors) can enable practicing engineers to achieve more optimized (and cost-effective) foundation designs.

1.3 Help Manual Scope

Program documentation for the GeoStat software is divided into two components: (1) a Help Manual; and, (2) a Technical Manual. Accordingly, the GeoStat Help Manual is a standalone document that details the program installation and licensing procedures, input file layout, and all user interface (UI) controls. In contrast, as a separate document, the GeoStat Technical Manual focuses on underlying engineering calculations (originally developed in McVay et al. 2012; Faraone, 2014; and, Faraone et al. 2021), and utilizes representative anonymized data from bridge sites to provide guidance and recommendations for establishing GeoStat model files (and interpreting results).

The present document, the GeoStat Help Manual, provides engineers with a centralized resource to aid in navigating through all input file contents and UI controls while making use of the GeoStat software for bridge foundation design. Organization of remaining chapters of the GeoStat Help Manual is as follows:

- In Chapter 2, step-by-step guides are provided for program installation and licensing.
- In Chapter 3, all input parameters (and formatting) making up GeoStat input files are identified and described.
- In Chapter 4, listings and descriptions are provided for all controls that comprise the GeoStat UI.
- In Chapter 5, the means by which analysis model files are created (for analysis) and parsed (for results viewing) are documented.

CHAPTER 2 PROGRAM INSTALLATION AND LICENSING

2.1 Installation

Documented in Section 2.1 are the GeoStat installation package contents and the procedure for installing the software.

2.1.1 Installation Package Overview

Sec. 2.1.2 delineates the various program executable, support, license, and settings files that collectively make up the GeoStat software package. A step-by-step guide for installing GeoStat is provided in Sec. 2.1.3.

2.1.2 Installation Package Contents

The GeoStat installation package, created using InstallShield (Flexera, Itasca, IL), streamlines the creation and placement of all required program components on a target machine. For the GeoStat program (a Microsoft Windows desktop application) to work properly, appropriate components need to be installed in "Program Files (x86)" and "Users" directories. As part of the software installation operations, all necessary ActiveX Controls are also registered. In addition, program shortcuts are created in the Windows Start Menu and Desktop.

The installation package (GeoStat_ins.exe) contents consist of three major parts: program prerequisites, program execution files, and program settings files. In particular, the installation procedure ensures that a prerequisite "Microsoft Visual C++ 2017 Redistributable Package (x86)" is present on the target machine. This prerequisite redistributable contains runtime libraries that, in turn, are required for the GeoStat program to function properly. If not found, then the installation package installs the redistributable package prior to carrying out remaining stages in the installation procedure.

After prerequisite files have been placed on (or confirmed to preexist on) a target machine, program files are created. Shown in Fig. 1 are the files that are placed within the "Program Files (x86)" directory during installation. These files are needed to carry out the functioning and display of the UI, as well as for performing engineering calculations.

This screenshot shows the Windows File Explorer window for the directory 'C:\Program Files (x86)\BSI\GeoStat'. The window displays a list of files and folders with their respective types.

Name	Type
HelpFiles	File folder
Images	File folder
eoul.exe	Application
GeoStat.exe	Application
libxl.dll	Application extension
NTGraphGS.ocx	ActiveX control
PDFSpooler.dll	Application extension

Figure 1. Program files included in the GeoStat installation package

By default, program files are installed in "C:\Program Files (x86)\BSI\GeoStat". However, as shown later, a custom installation location can be specified. Program files include: program documentation (Help and Technical manuals); user interface (UI) graphical resources (images); a support executable (eoul.exe); the executable UI (GeoStat.exe); a support library (libxl.dll); and, ActiveX control (NTGraphGS.ocx). The ActiveX control is registered during the installation process.

Shown in Fig. 2 are program settings files generated by the GeoStat software during the first program session after the installation package is run. These files are located in "C:\Users\Public\Documents\BSI\GeoStat", and consist of wider software settings (GeoStat.ini) and within-UI settings (ProgramSettings.ini). Also included here is a folder containing illustrative program example files (one for driven piles and one for drilled shafts). As discussed later, for GeoStat deployments with machine-locked (standalone) licensing, the software license file also resides here.

This screenshot shows the Windows File Explorer window for the directory 'C:\Users\Public\Documents\BSI\GeoStat'. The window displays a list of files and folders with their names, dates modified, and types.

Name	Date modified	Type
ExampleFiles	6/15/2020 3:40 PM	File folder
GeoStat.INI	6/5/2020 10:58 AM	Configuration settings
ProgramSettings.INI	5/4/2020 7:20 PM	Configuration settings

Figure 2. Program settings files generated during the first GeoStat session

2.1.3 Step-by-Step Installation Guide

Installation of the GeoStat software can be carried out by following the nine steps listed below, where many of the steps are guided by an Installation Wizard tool:

1. Download the installation package executable (GeoStat_ins.exe) from the BSI website.

2. Double-click the installer executable, and click "Yes", when asked for permission to install the program (Fig. 3).
3. If prerequisite program files are not present on the machine, then the necessary files will be installed prior to proceeding any further with the GeoStat installation.
4. The Installation Wizard will appear (Fig. 4). Click "Next" to proceed.
5. The software End User License Agreement (EULA) will be displayed for review (Fig. 5), where example language contained within the EULA is given in Appendix A. Click "Next" to accept the terms of the EULA and proceed with the GeoStat installation.
6. As shown in (Fig. 6), the program installation directory can be selected. The default location is "C:\Program Files (x86)\BSI\GeoStat". If it is desired to modify the default location, click the "Change..." button and provide the new destination folder location. Click "Next" to proceed.
7. If any settings were not assigned as intended, then click "Back" (Fig. 7). Otherwise, click "Install" to proceed with the GeoStat installation.
8. The installation progress is updated in real-time on the progress page (Fig. 8). After all files have been created, and all supporting libraries (or controls) registered, the Completed page will appear (Fig. 9). Click "Finish" to complete the installation.
9. A desktop shortcut for the GeoStat software will be located on the Desktop. Double-click the newly created GeoStat shortcut to run the program.



Figure 3. User Account Control message box for initiating program installation

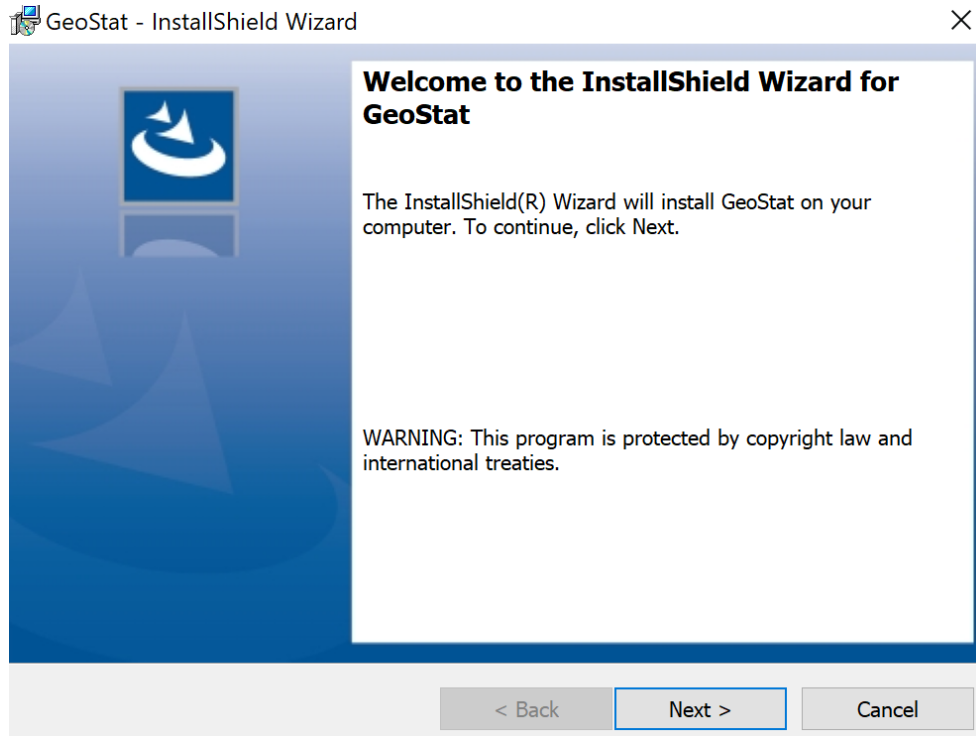


Figure 4. Welcome page in the Installation Wizard

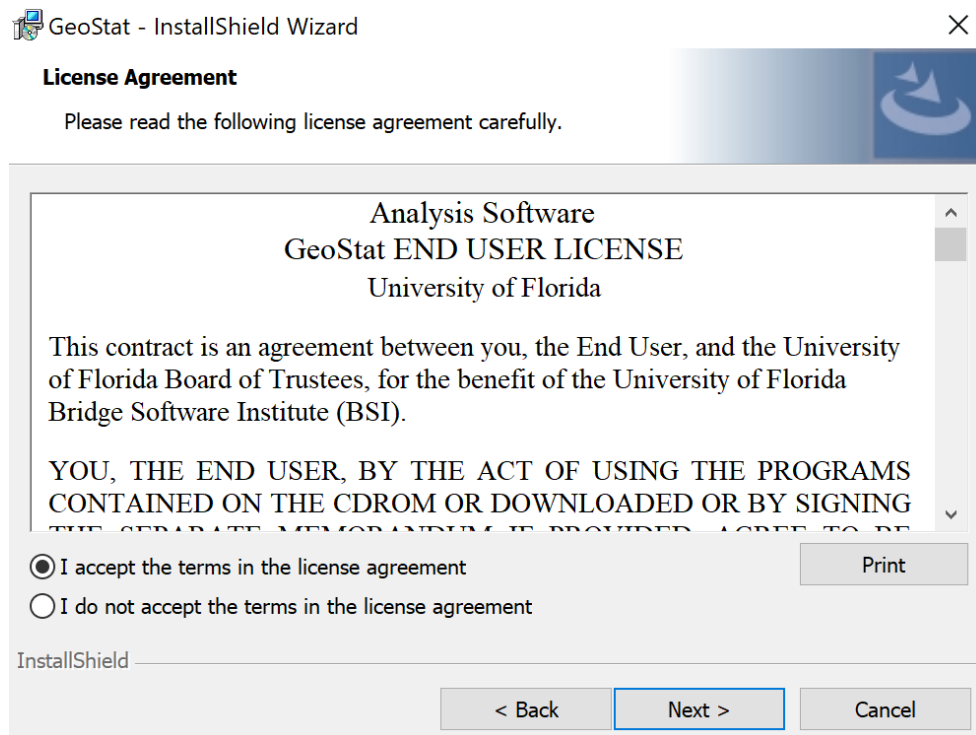


Figure 5. End User License Agreement (EULA) page in the Installation Wizard

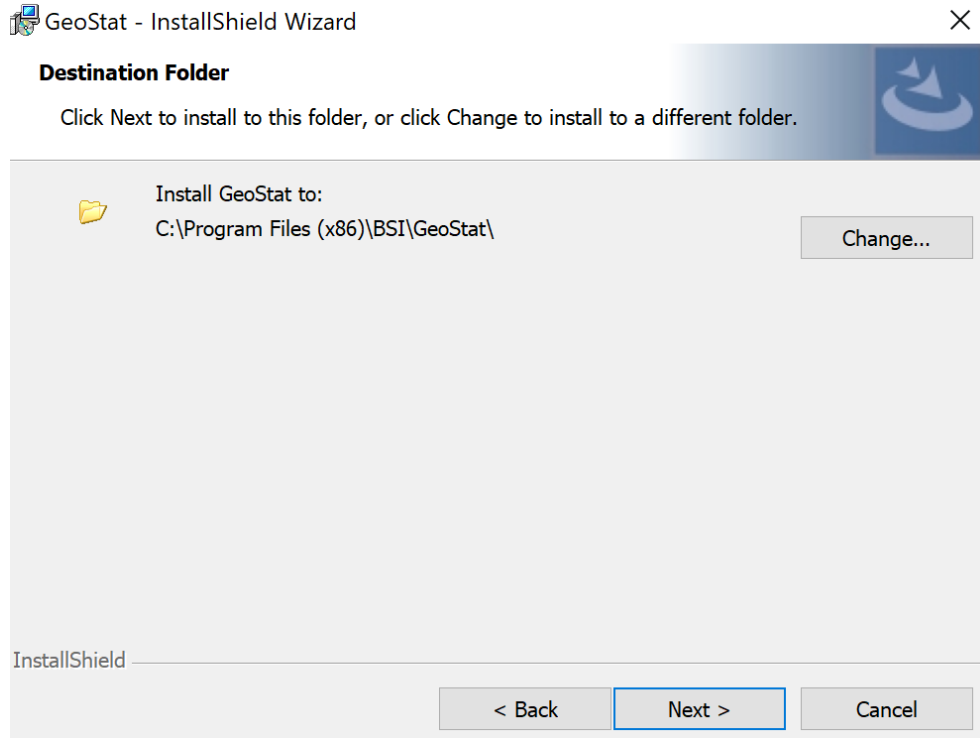


Figure 6. Destination Folder page in the Installation Wizard

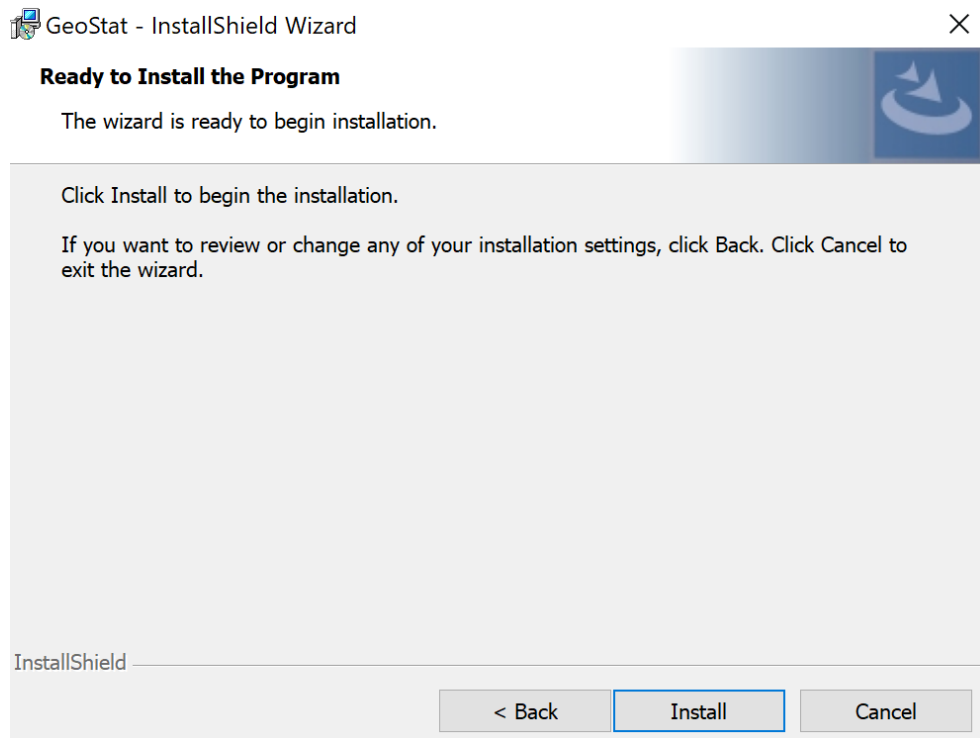


Figure 7. User Account Control page in the Installation Wizard

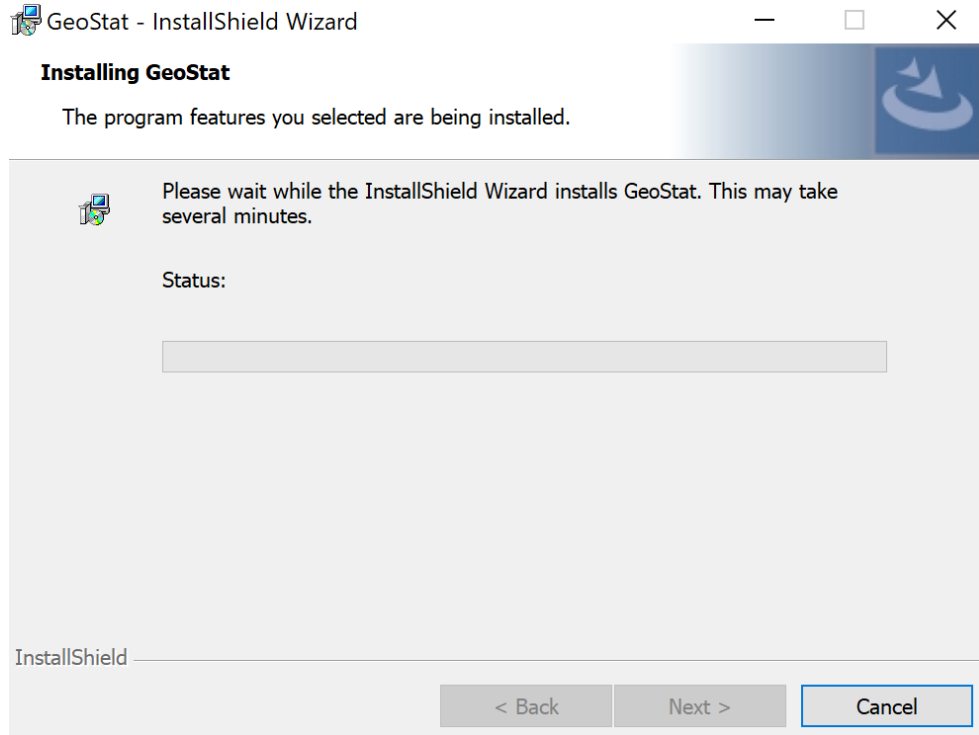


Figure 8. Installing GeoStat progress page in the Installation Wizard

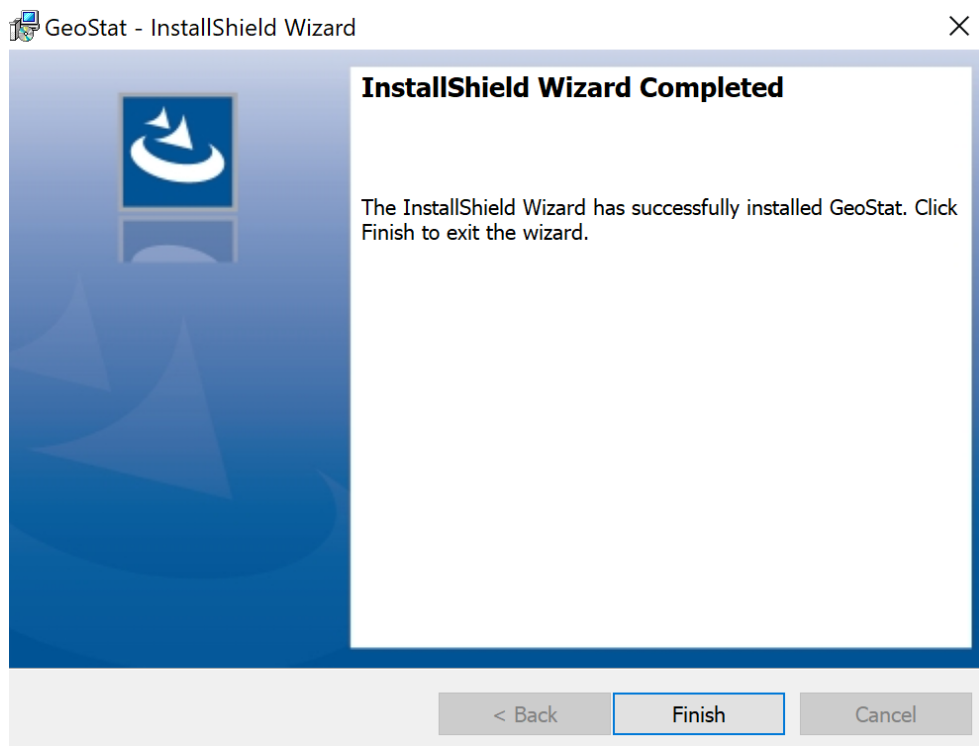


Figure 9. Completed page in the Installation Wizard

2.2 Licensing

Presented in Sec. 2.2 is documentation concerning licensing of the GeoStat software.

2.2.1 Licensing Overview

In Sec. 2.2.2, step-by-step guides are provided for accessing a program License Wizard. Also, guides are provided for program deployments under machine-locked (standalone, Sec. 2.2.2.1) and networked (Sec. 2.2.2.2) license scenarios. Guides for making various modifications to the licensing file (custom path, transfer to another machine) are provided in Sec. 2.2.3 through Sec. 2.2.5.

2.2.2 Step-by-Step Licensing Guide

A licensing system has been implemented in the GeoStat software, as a means of restricting program access, such that only authorized users can access the program. Central to this licensing system is the license file (GeoStat.lfx). The license file is inspected during each GeoStat session to ensure the user has permission to operate the software. Examples of the types of license file authentication performed include ensuring that the computer or network is authorized to run GeoStat.

Upon initial installation of GeoStat on a target machine, and by design, a license file will not exist. During the first program session, however, GeoStat will create a license with a 30-day duration. This license will allow GeoStat to run in Demo mode, which greatly limits program functionality. To convert the Demo license to a Standard (full) license, a license update must be performed. Performing a license update requires action to be taken on the part of the end user. To facilitate this process, a License Wizard can be utilized. Through use of the License Wizard and initial contact with BSI, licensed use of the program can be achieved.

2.2.2.1 Accessing the License Wizard

The License Wizard is accessible directly from within the GeoStat UI. To access the License Wizard, click the Help menu item (Fig. 10). Then, select the Update Software License sub-item (Fig. 11).

The License Wizard provides a centralized set of pages for performing various license operations, as accessed from the Select Type of License Update page (Fig. 12). There are five license modification modes: Update Standalone License; Update Network License; Set License File Path for Standalone License; Set License File Path for Network License; and, Transfer License to Different Computer. Guides for operating within each mode are given below.

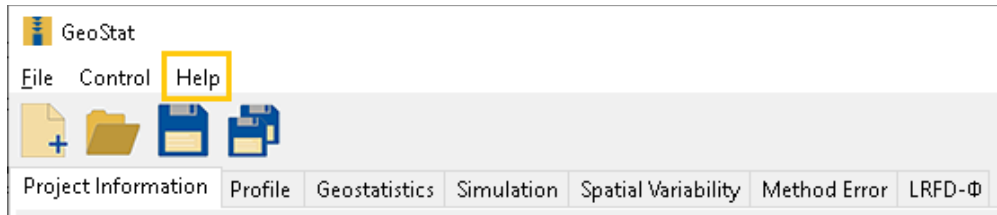


Figure 10. Help file menu item in the GeoStat UI

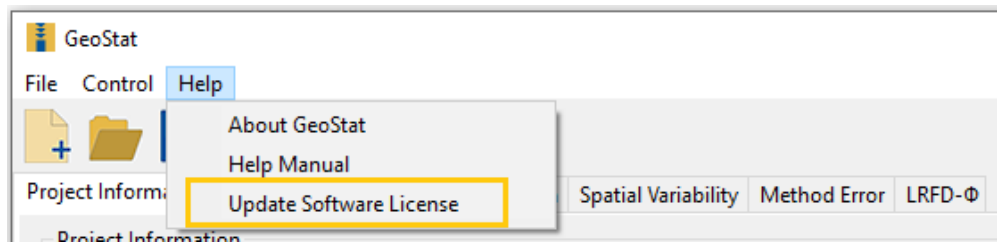


Figure 11. Update Software License file menu sub-item in the GeoStat UI

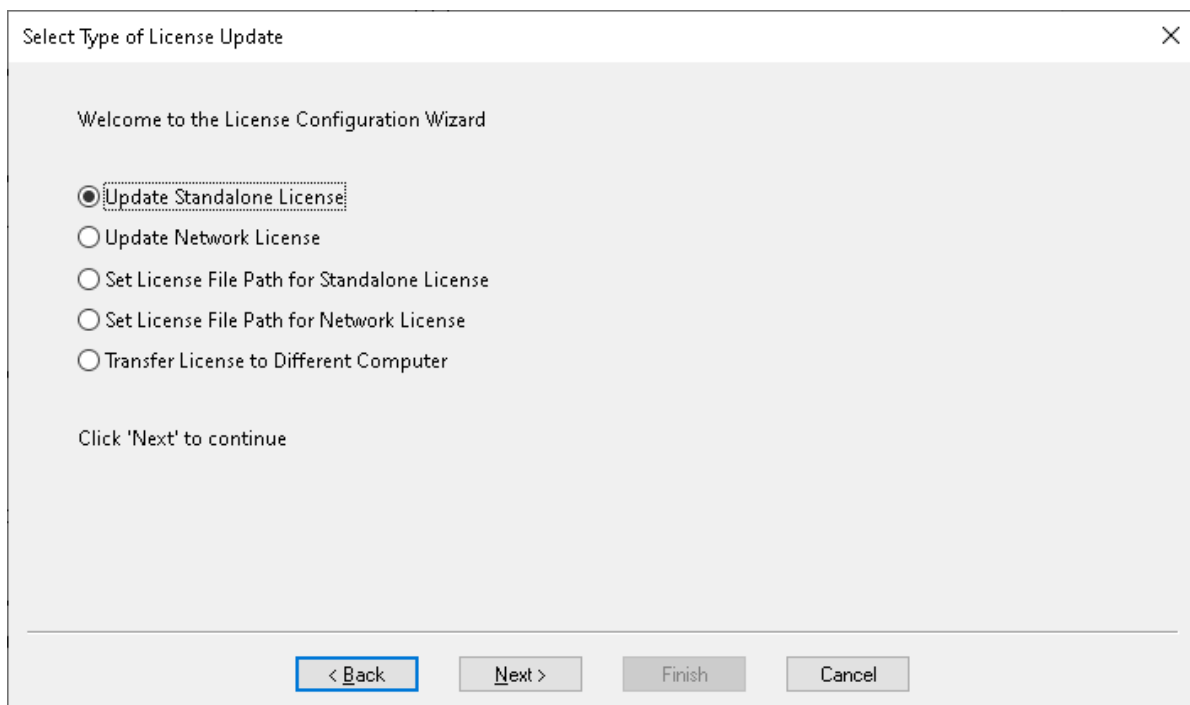


Figure 12. Select Type of License Update page in License Wizard

2.2.2.2 Configuring a Standalone License

The Update Standalone License option is used to update a license file when both the license file and GeoStat program files are located on the same machine. The Update Standalone

License option is used to put additional time on the license file, for example to extend the license expiration by one year. To use this option, select the Update Standalone License radio button (Fig. 13), and click the "Next" button (Fig. 14). The License Codes page displays the Session Code and Machine ID (Fig. 15). At this juncture, contact with BSI must be made to continue the license update, where the Session Code and Machine ID are emailed to bsi@ce.ufl.edu. For convenience and accuracy in copying these codes into an email, the Copy Codes to Clipboard button can be clicked (Fig. 16) to transfer the Session Code and Machine ID to the clipboard.

Upon receiving the codes, BSI will email back seven required unlocking codes. These seven codes will need to be selected, copied, and then pasted into the seven text boxes on the License Codes page (Fig. 17). Similar to using the Copy Codes to Clipboard button, the Paste Codes from Clipboard button can be used to transfer all seven codes into the License Wizard at one time. Copy the seven unlocking codes from the email (sent from BSI) to the clipboard. Then, paste all seven codes into the License Update page (at once) by clicking the Paste Codes from Clipboard button (Fig. 18). After the codes are copied into the License Codes page, click the "Finish" button to complete the license update (Fig. 19). The GeoStat program will then automatically close. Upon reopening the program, the updated license file will be utilized.

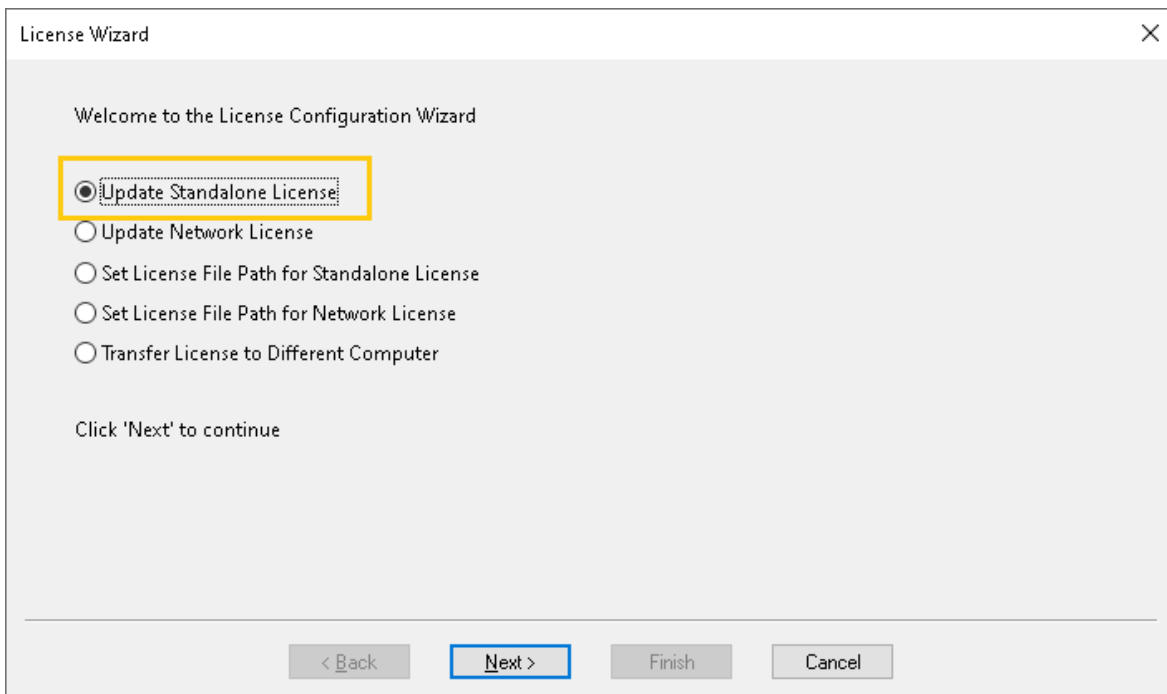


Figure 13. Update Standalone License radio button

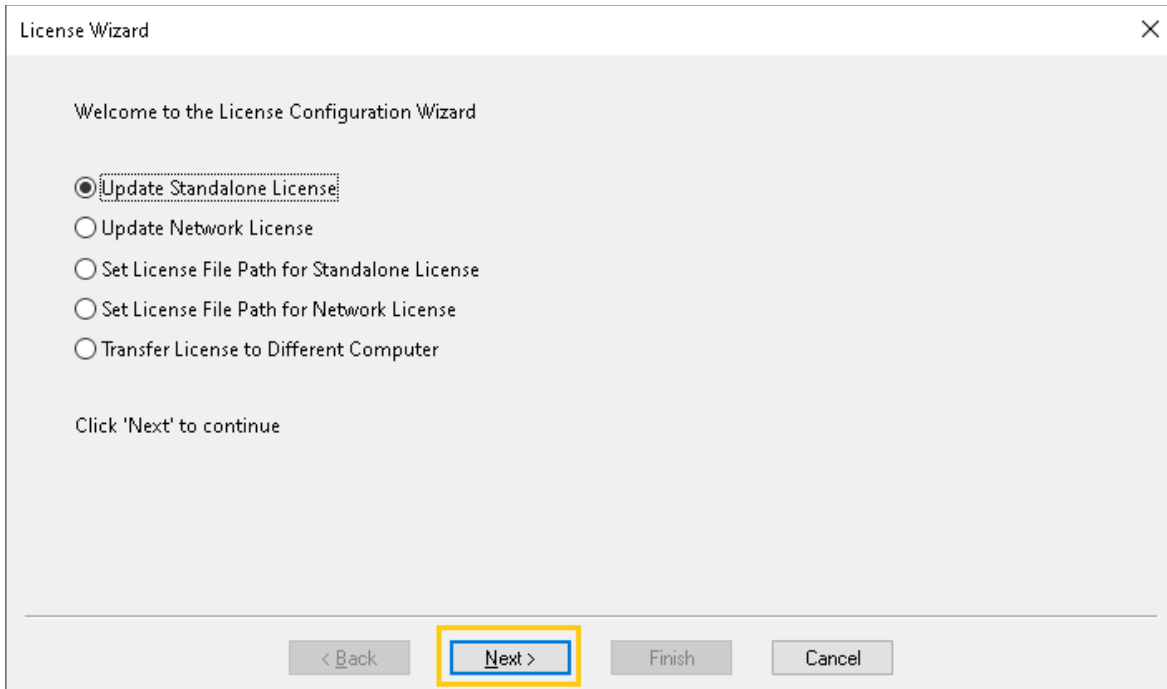


Figure 14. Next button in Update Standalone License process

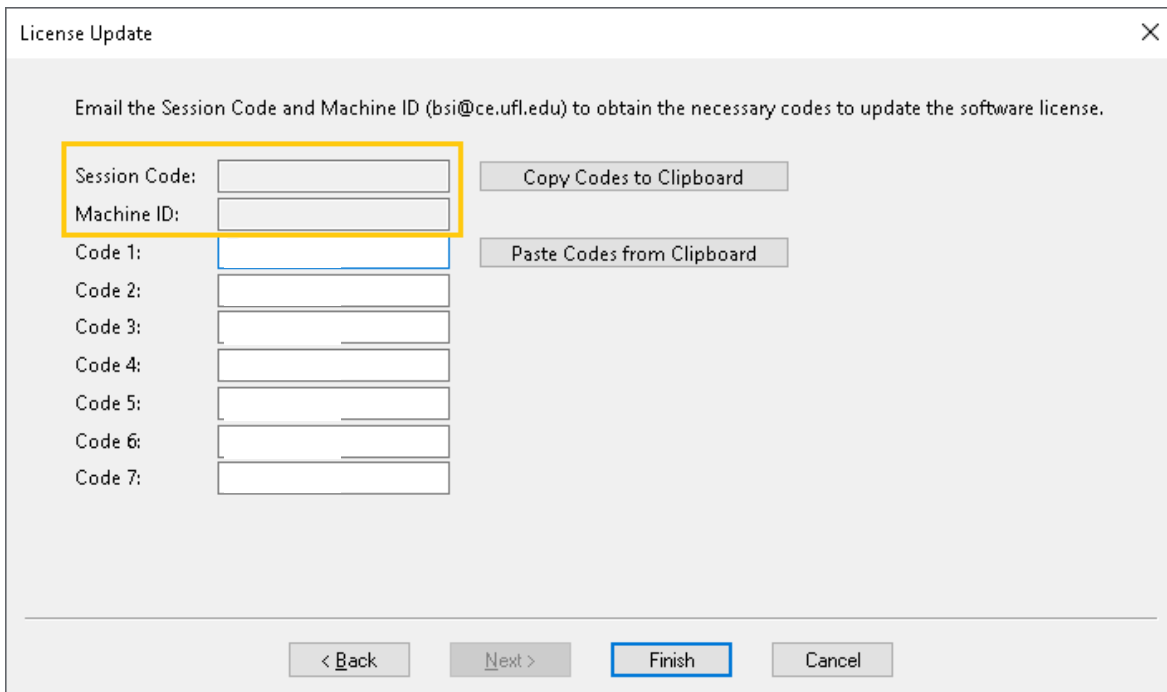


Figure 15. License Update page with Session Code and Machine ID (for standalone license)

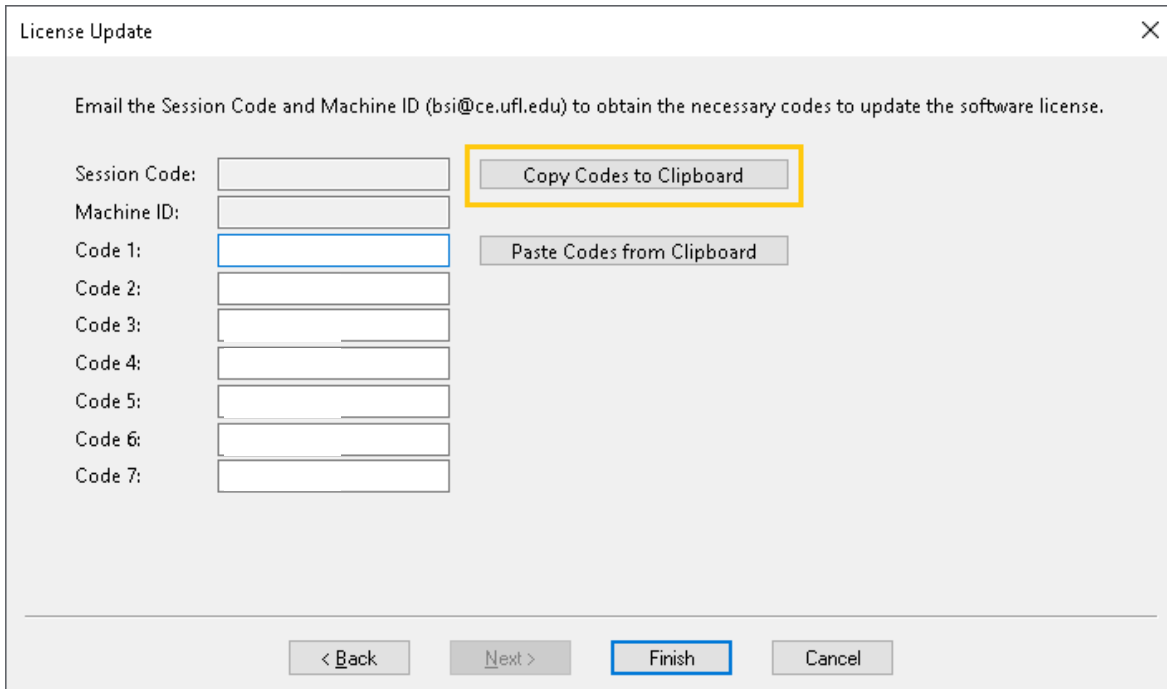


Figure 16. Copy Codes to Clipboard button (for standalone license)

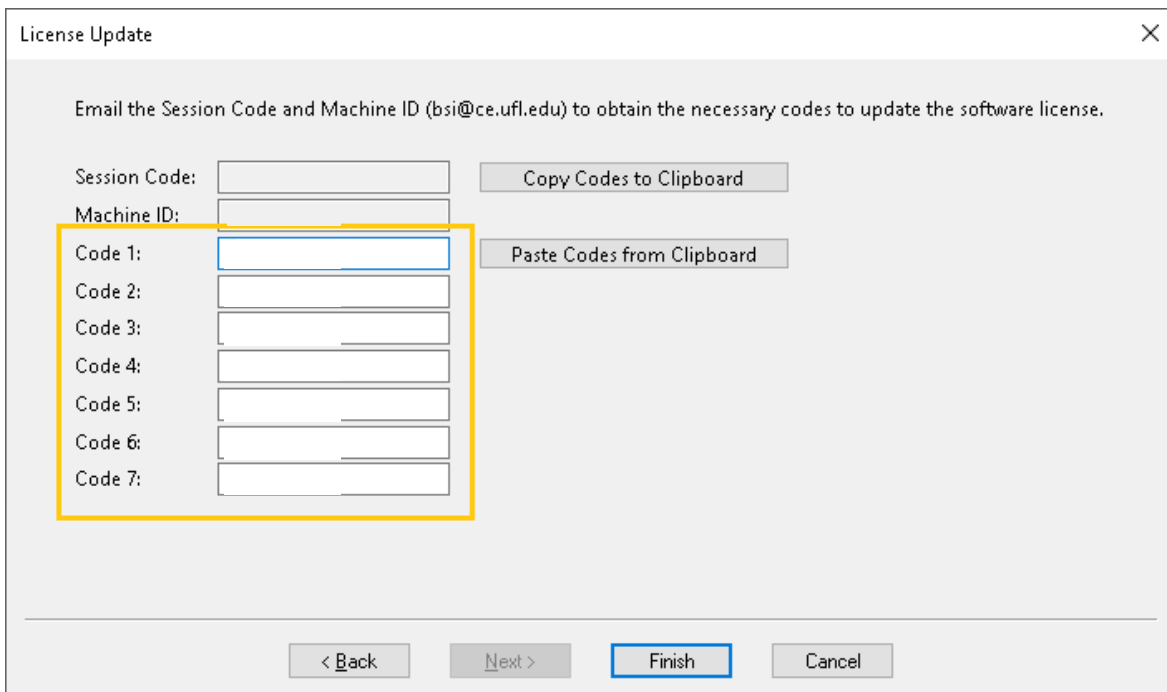


Figure 17. Unlocking codes for Standalone License Update

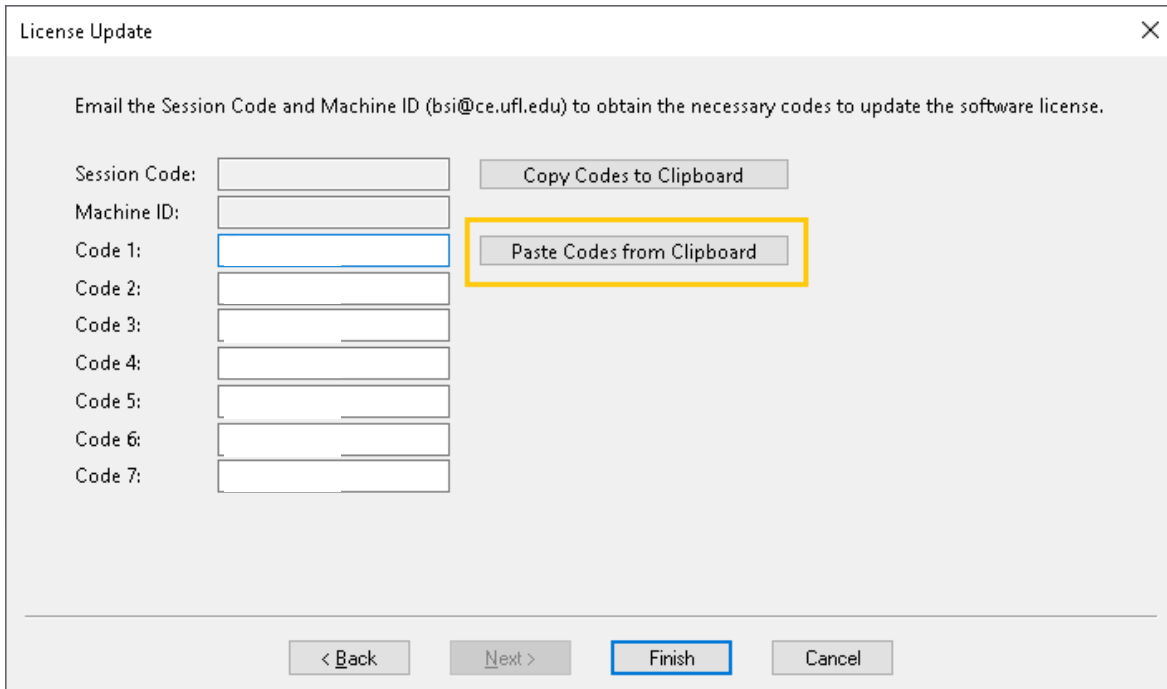


Figure 18. Paste Codes from Clipboard button (for standalone license)

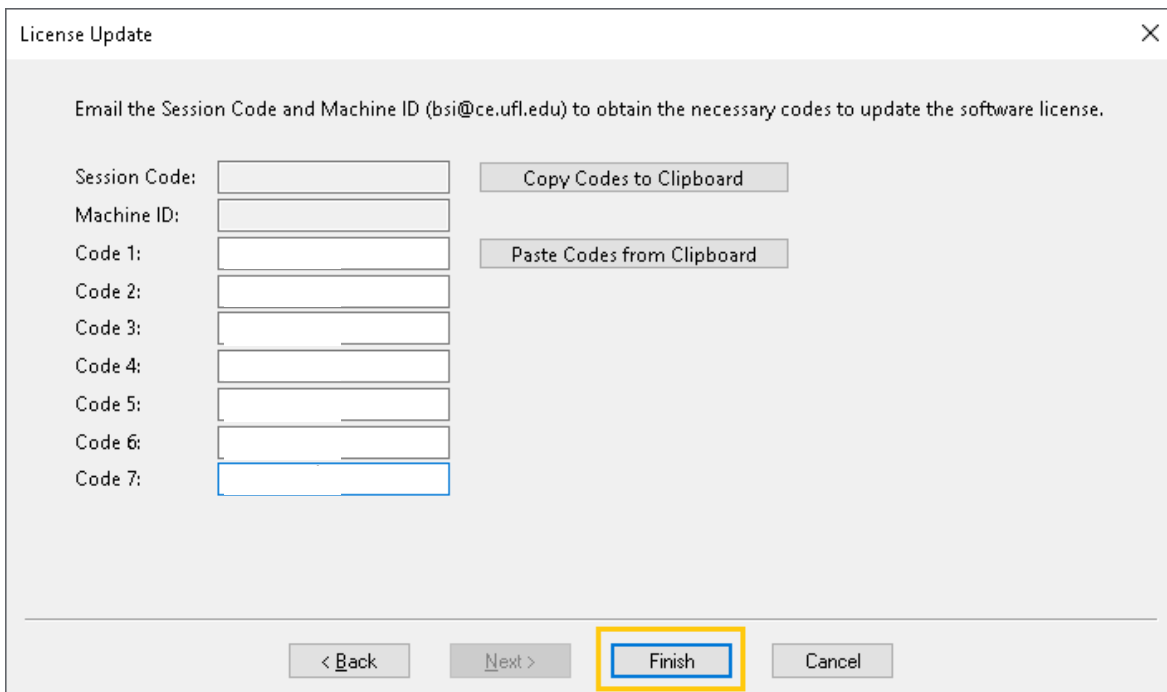


Figure 19. Finish button on License Update page (for standalone license)

2.2.2.3 Configuring a Network License

The Update Network License option is used to update a license file when the license file is hosted on a network server (e.g., serving a Local Area Network). This is known as a Network license configuration. In this type of installation, a number of workstations, each with an installed copy of GeoStat, point to the license file (located on the network server). The Update Network License option is used to put additional time on the license file, for example to extend the license expiration by one year, or to add to or subtract from the number of seats that can be used concurrently on the Network license. To use the Update Network License option, select the Update Network License radio button (Fig. 20) and click the "Next" button (Fig. 21). The License Codes page displays the Session Code and Machine ID (Fig. 22).

At this juncture, contact with BSI must be made to continue the license update. Email the Session Code and Machine ID to bsi@ce.ufl.edu. For convenience and accuracy in copying these codes into an email, the Copy Codes to Clipboard button can be clicked (Fig. 23) to transfer the Session Code and Machine ID to the clipboard.

Upon receiving the codes, BSI will email back the seven required unlocking codes. These seven codes will need to be selected, copied, and then pasted into the seven text boxes on the License Codes page (Fig. 24). Similar to using the Copy Codes to Clipboard button, the Paste Codes from Clipboard button can be used to simultaneously transfer (all seven) codes into the License Wizard.

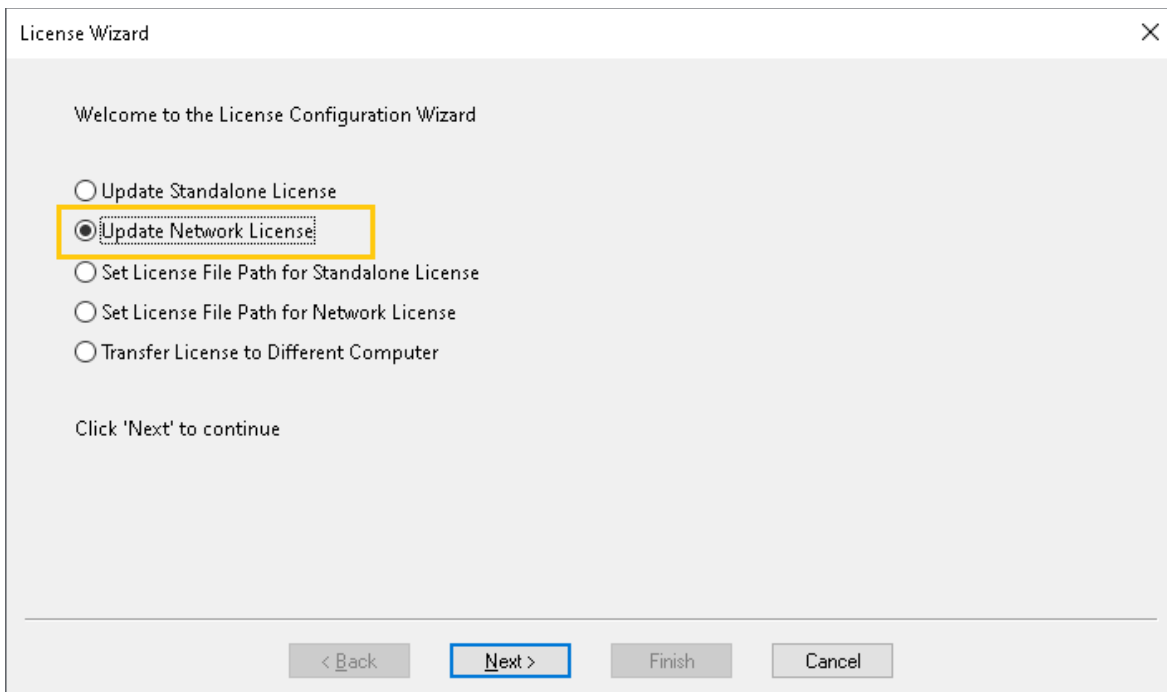


Figure 20. Update Network License radio button

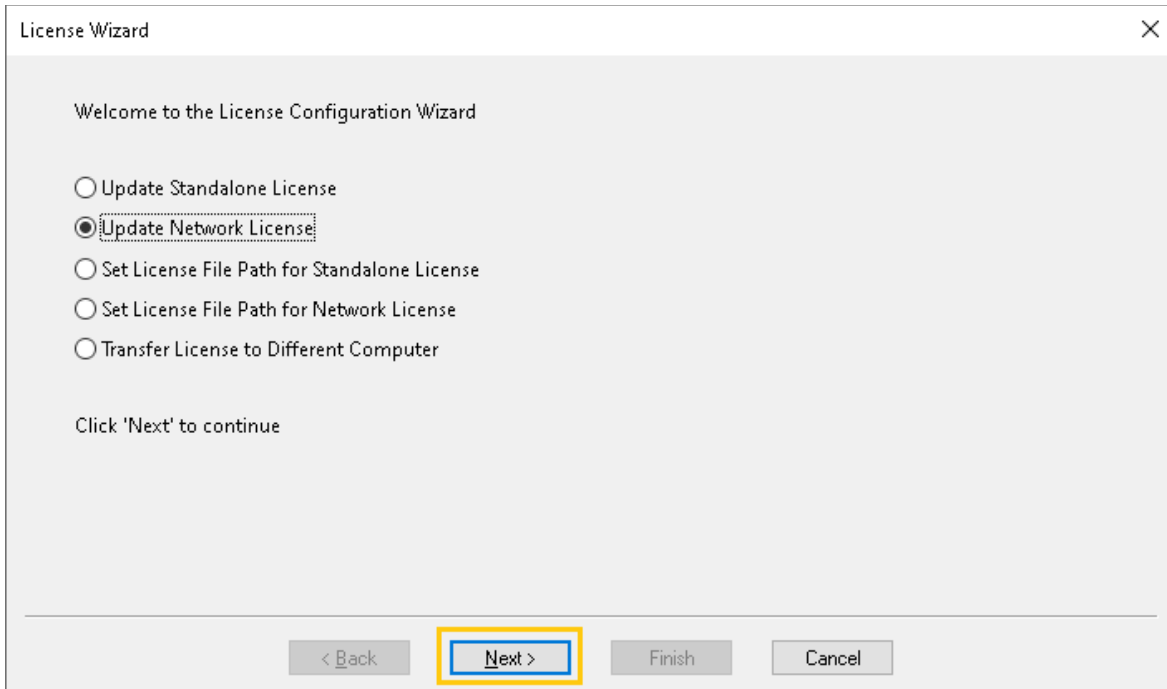


Figure 21. Next button to update a network license

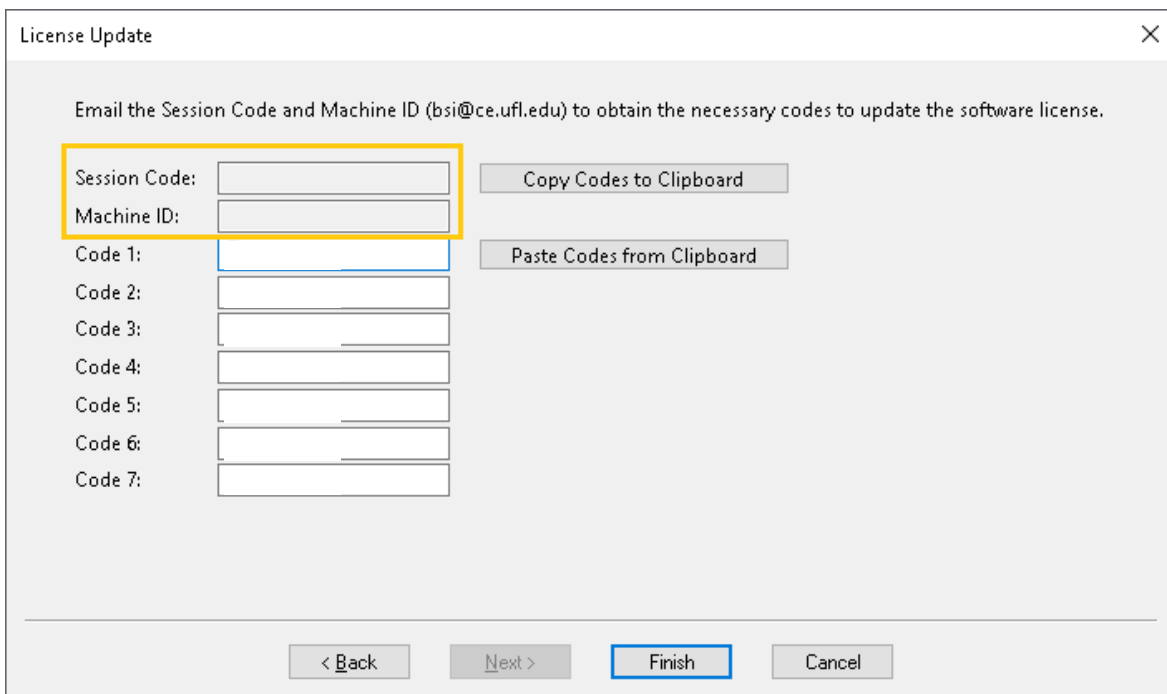


Figure 22. License Update page with Session Code and Machine ID (for network license)

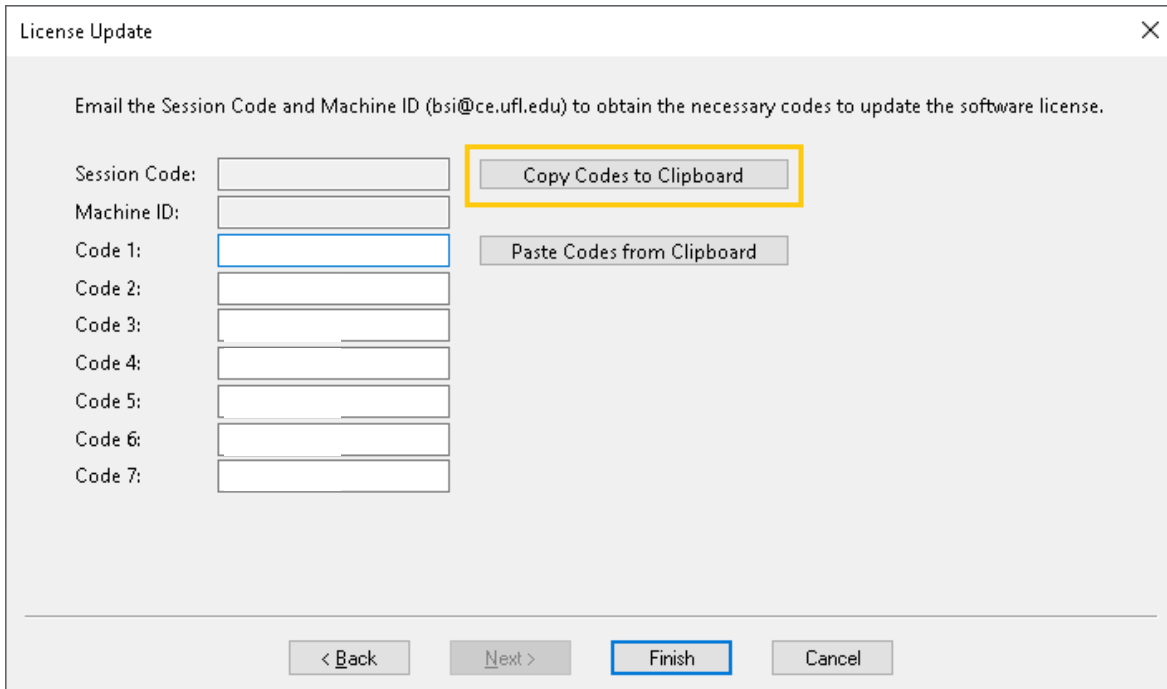


Figure 23. Copy Codes to Clipboard button (for network license)

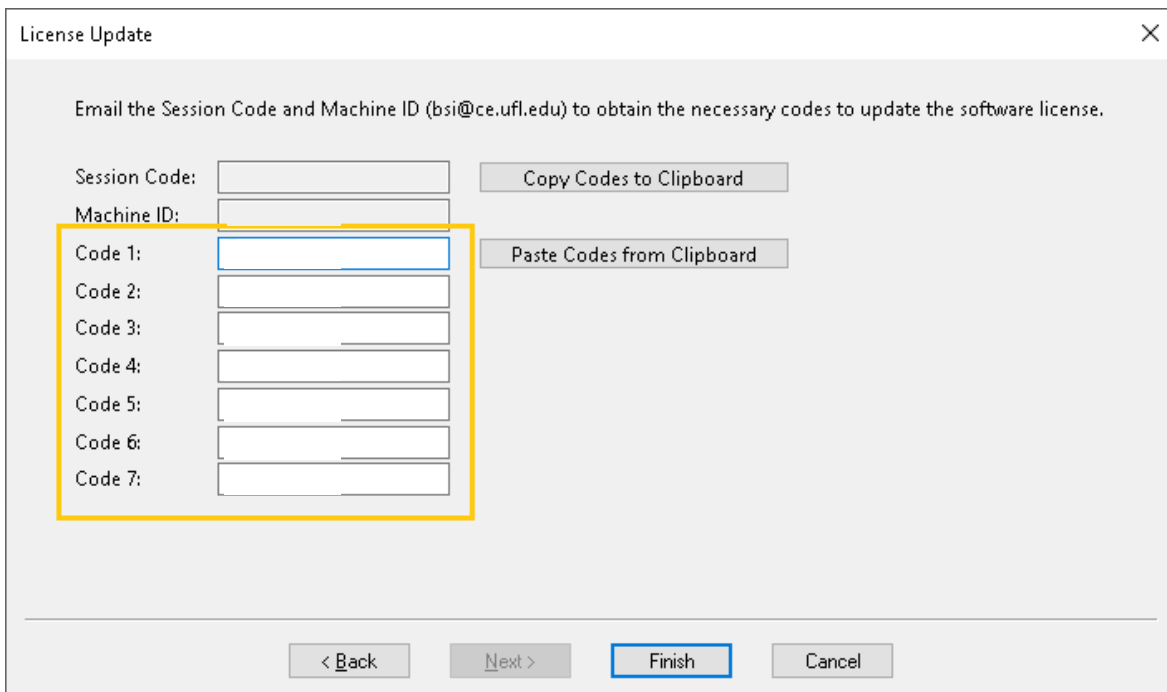


Figure 24. Unlocking codes for Network License Update

Copy the seven unlocking codes from the email (sent from BSI) to the clipboard. Then, paste all seven codes into the License Update page by clicking the Paste Codes from Clipboard

button (Fig. 25). After the codes are copied into the License Codes page, click the “Finish” button to complete the license update (Fig. 26).

The screenshot shows a dialog box titled "License Update" with a close button (X) in the top right corner. Below the title bar, there is a text instruction: "Email the Session Code and Machine ID (bsi@ce.ufl.edu) to obtain the necessary codes to update the software license." The dialog contains several input fields: "Session Code:", "Machine ID:", "Code 1:", "Code 2:", "Code 3:", "Code 4:", "Code 5:", "Code 6:", and "Code 7:". To the right of the "Session Code" and "Machine ID" fields is a button labeled "Copy Codes to Clipboard". To the right of the "Code 1" field is a button labeled "Paste Codes from Clipboard", which is highlighted with a yellow rectangular box. At the bottom of the dialog, there are four buttons: "< Back", "Next >", "Finish", and "Cancel". The "Finish" button is highlighted with a blue rectangular box.

Figure 25. Paste Codes from Clipboard button (for network license)

The screenshot shows the same "License Update" dialog box as in Figure 25. The "Paste Codes from Clipboard" button is no longer highlighted. Instead, the "Finish" button at the bottom of the dialog is highlighted with a yellow rectangular box. All other elements, including the text instruction, input fields, and other buttons, remain the same as in the previous figure.

Figure 26. Finish button on License Update page (for network license)

Upon clicking the "Finish" button, the GeoStat program will automatically close. Upon reopening the program, the update license file will be used. This license update will affect all workstations pointing to the license file that is hosted on the network server. Thus, this update does not need to be performed once per workstation, but instead only once per network.

2.2.3 Setting a Custom License File Path for a Standalone License

The license file (GeoStat.lfx) by default is positioned in the "Users" public directory at the following location: "C:\Users\Public\Documents\BSI\GeoStat". However, if it is so desired, the license file location can be set to a custom location. The Set License File Path for Standalone License option is used to specify the location of the GeoStat license file on a workstation (Fig. 27).

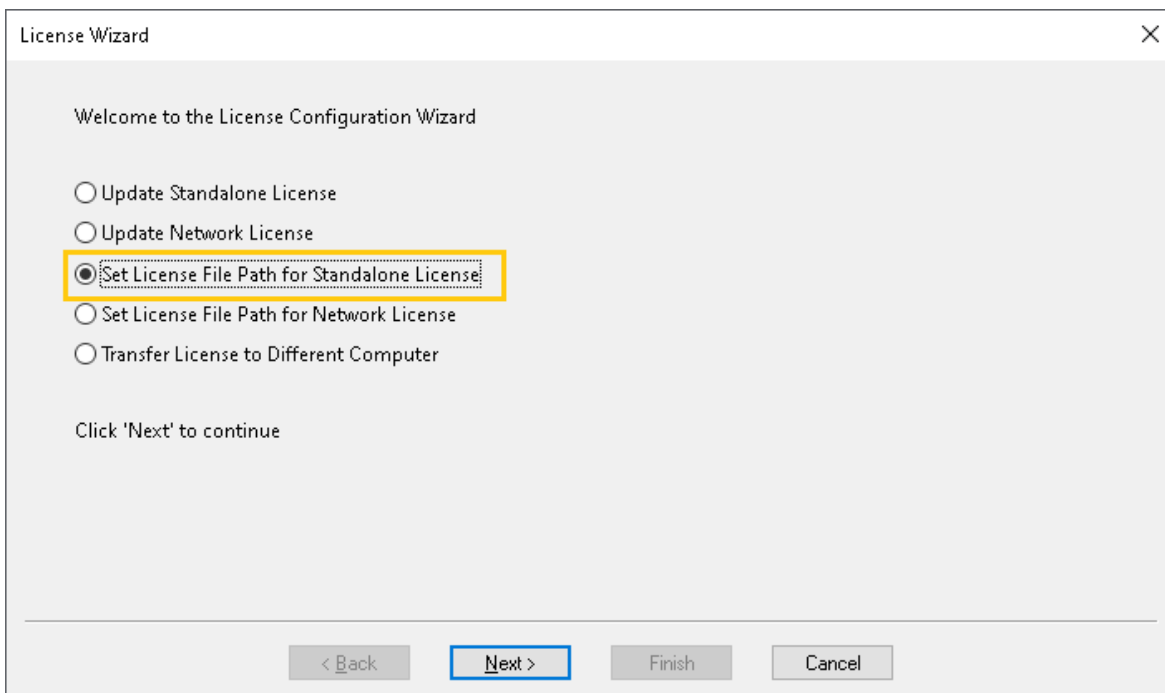


Figure 27. Set License File Path for Standalone License radio button

Though the location of the license file can be changed by using the Set License File Path for Standalone License option, the license file must reside in a folder for which the user has full permissions (read, write, execute). This scope of folder permissions is necessary so that the license file can be manipulated as necessary during operation of the GeoStat software.

To make use of the option for customizing the license file location, select the Set License File Path for Standalone License radio button (as indicated above in Fig. 27). Then, click the "Next" button (Fig. 28). This action will, in turn, launch the "Set License File Path - Standalone" page

(Fig. 29). Then, click the "Browse" button to specify the desired location of the license file (Fig. 30).

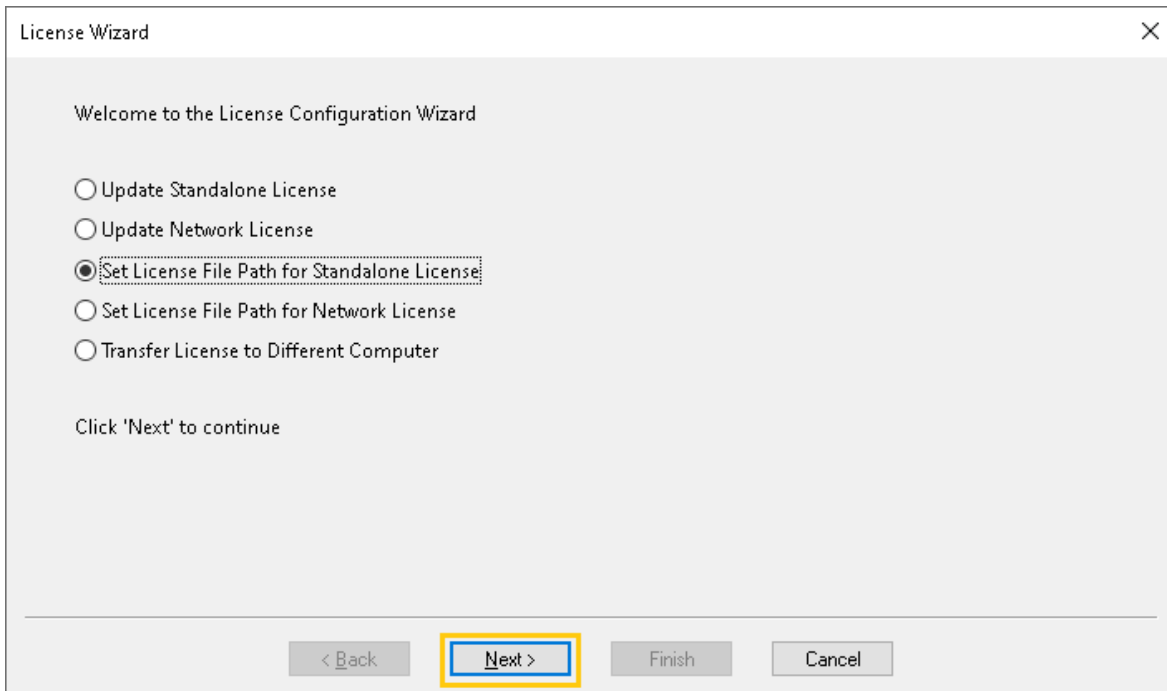


Figure 28. Next button to Set License File Path for Standalone License

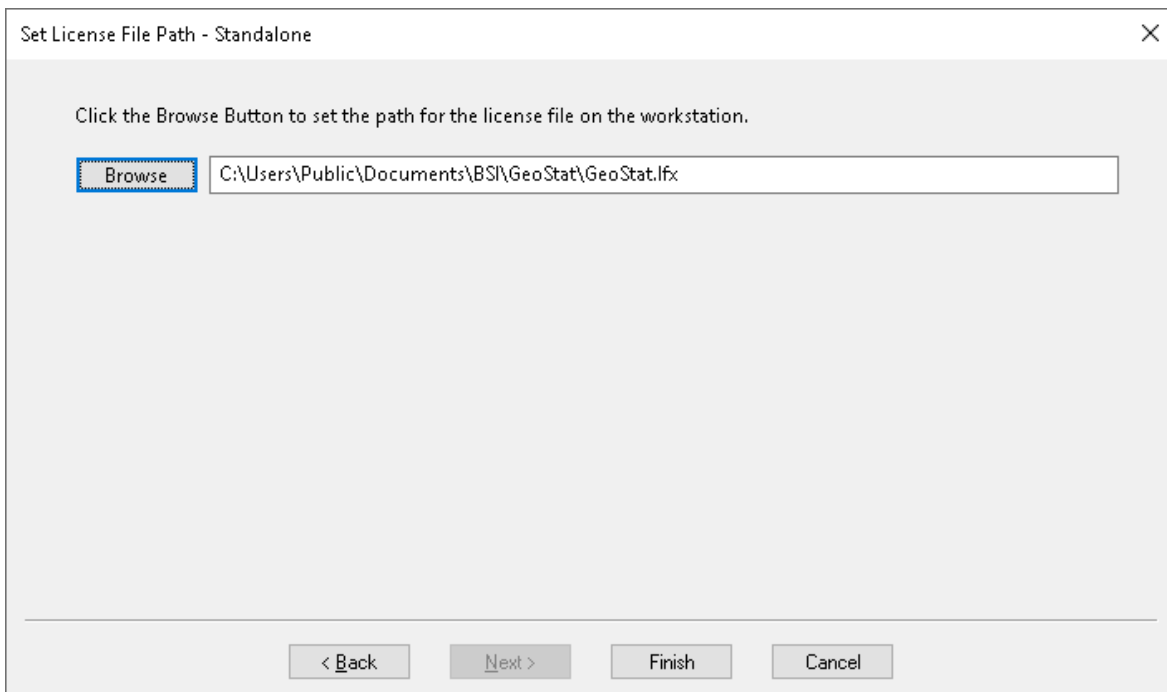


Figure 29. Set License File Path - Standalone page

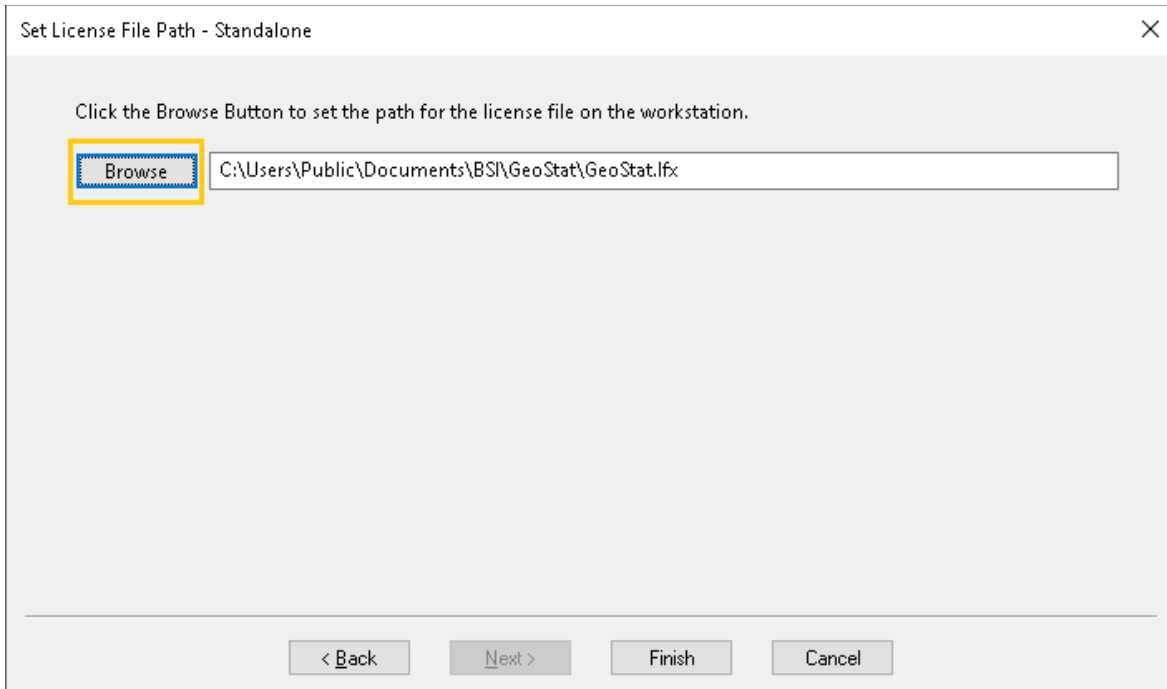


Figure 30. Browse button on Set License File Path - Standalone page

The path to the license file must include, and end with, the name of the license file itself (GeoStat.lfx). As an example of the full (filename included) path: "C:\PathToLicenseFile\GeoStat.lfx". After the path has been specified, click the "Finish" button. The GeoStat program will automatically close. Upon reopening the program, the updated license file path will be used.

2.2.4 Setting the License File Path for a Network License

The Set License File Path for Network License option is used to specify the location of the GeoStat license file on a network server serving a Local Area Network. The license file (GeoStat.lfx) by default is positioned on the local machine, not on a network server. In particular, the default location is in the "Users" public directory with the following full path: "C:\Users\Public\Documents\BSI\GeoStat".

When changing the default path to a desired location on a network server, please note that the license file must reside in a folder for which the user has full permissions (read, write, edit). In this way, the license file can be manipulated as necessary during execution of the GeoStat program. To use this option, select the Set License File Path for Network License radio button (Fig. 31). Then click the "Next" button (Fig. 32). This action launches the "Set License File Path - Network" page (Fig. 33). Then, click the "Browse" button to specify the desired location of the license file.

The specified path must end with the name of the license file (GeoStat.lfx), for example: "\\serverName\BSI\GeoStat\GeoStat.lfx". Note also that adherence to the universal naming convention (UNC) is required in specifying the server name (Fig. 34).

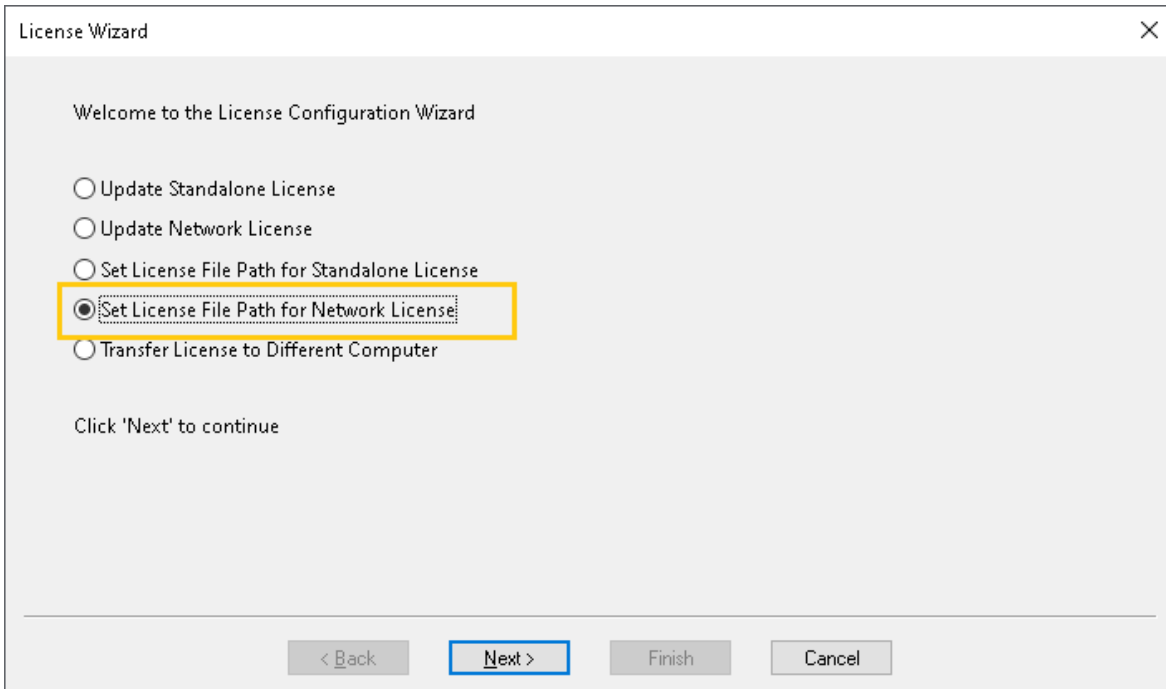


Figure 31. Set License File Path for Network License radio button

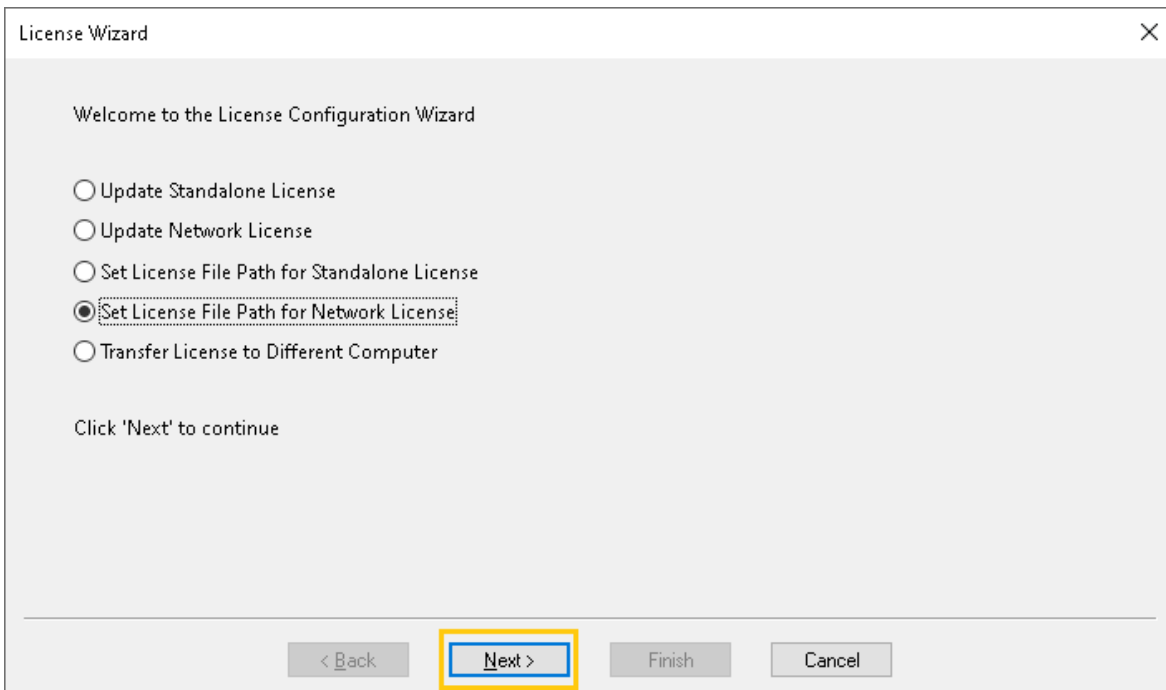


Figure 32. Next button to Set License File Path for Network License

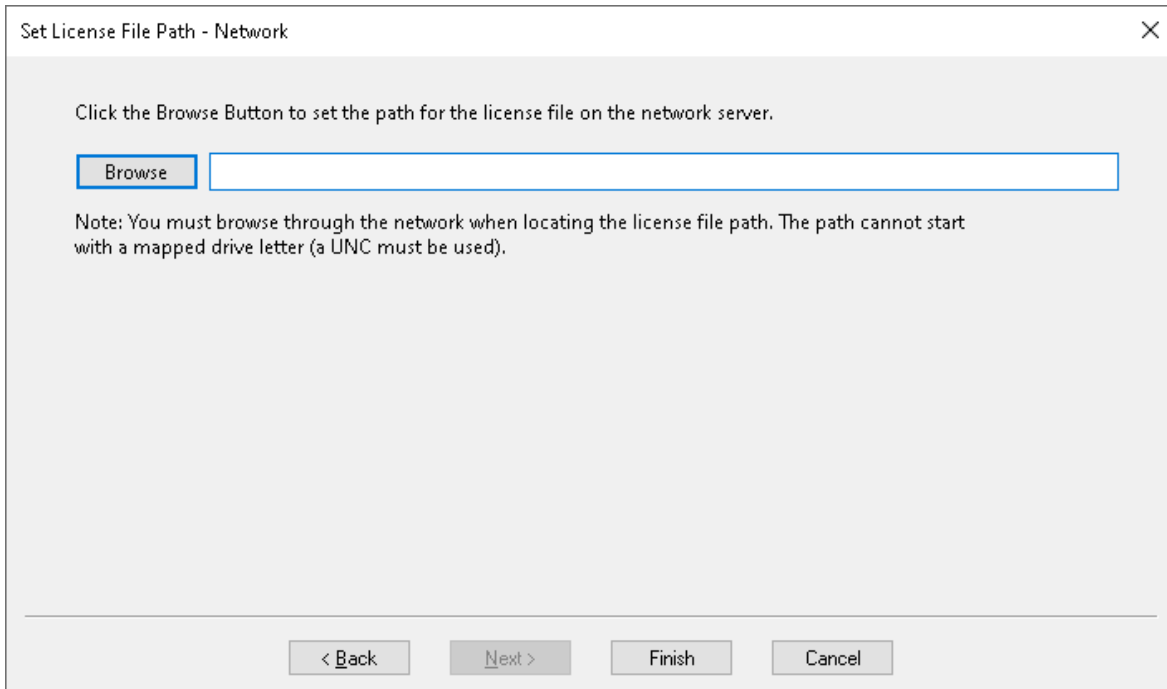


Figure 33. Set License File Path - Network page

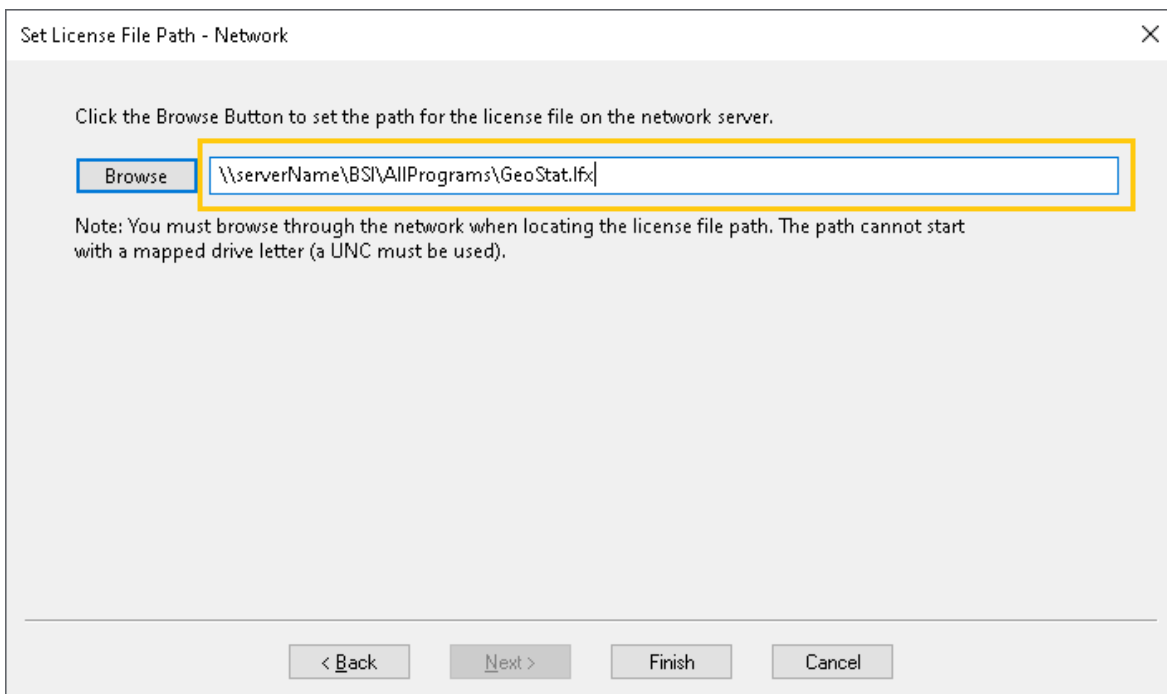


Figure 34. Example of License File path text box using UNC for server name

After the path has been specified, click the "Finish" button (Fig. 35). The GeoStat program will automatically close. Upon reopening the program, the updated license file path will be used.

Using the Set License File Path for Network License option sets the network path to the license file for the workstation from which this type of license action was performed. So as to use the license file's new position for all workstations on the LAN, each workstation on the network must repeat this process of using the "Set License File Path – Network" option from the GeoStat license wizard (recall Fig. 31).

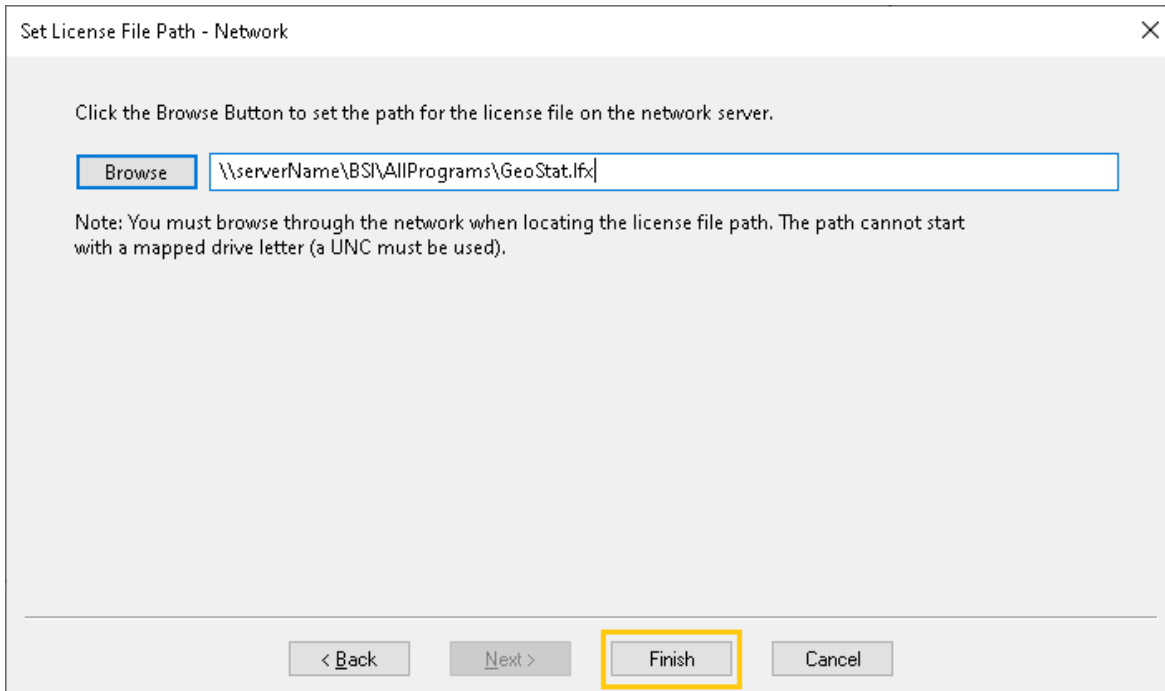


Figure 35. Finish button on Set License File Path - Network page

2.2.5 Transfer a License to a Different Computer

The Transfer License to Different Computer option (Fig. 36) is used to facilitate changing the system on which the GeoStat software is used. License transfers can be performed to change which workstation or which network server hosts the license file. To use this option, select the Transfer License to Different Computer radio button (Fig. 36), and then click the "Next" button (Fig. 37). The License Transfer page will then appear (Fig. 38).

Next, check the "Check to remove the license from the computer" checkbox (Fig. 39). This action will cause the Verification Code for Session page to display (Fig. 40). At this juncture, contact with BSI must be made to continue with the license transfer. Email the Verification Code for Session to bsi@ce.ufl.edu.

BSI will respond with an approval for the license transfer. Then click the "Finish" button (Fig. 41). The GeoStat program will automatically close. Upon reopening the program (from the same workstation in a Standalone license configuration, or any workstation using a network license that has been transferred), program access will not be granted by design. To once

again achieve program access, BSI will need to be contacted to perform a license update on the machine to which the licensing is to transfer.

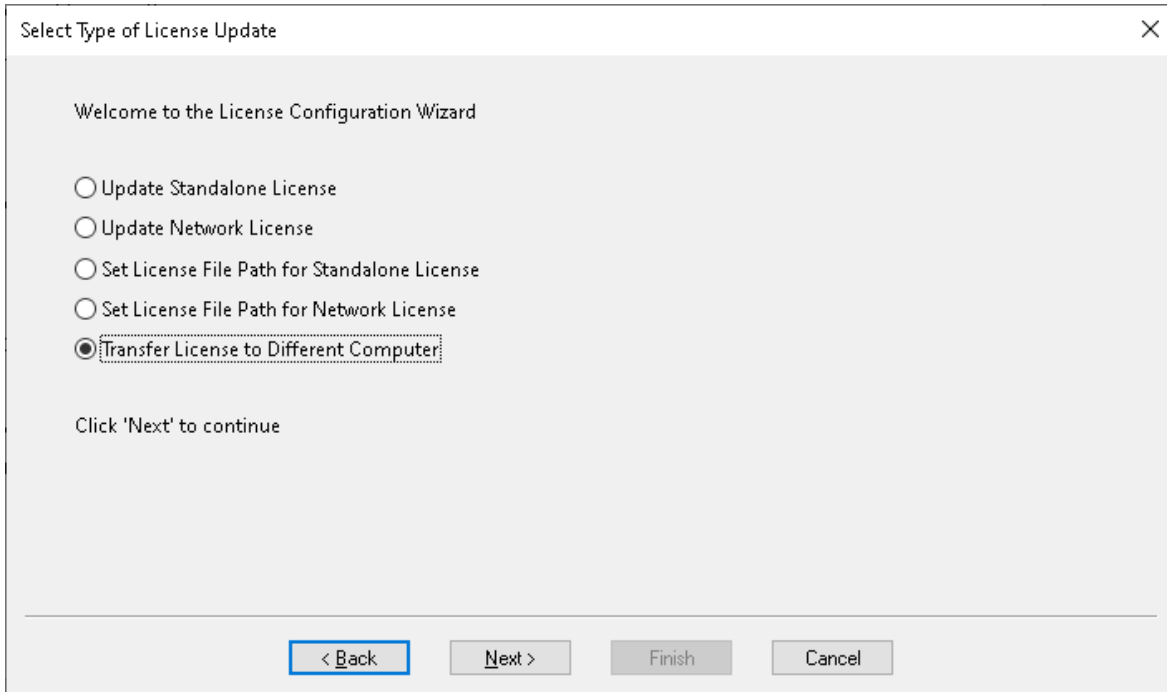


Figure 36. Transfer License to Different Computer radio button

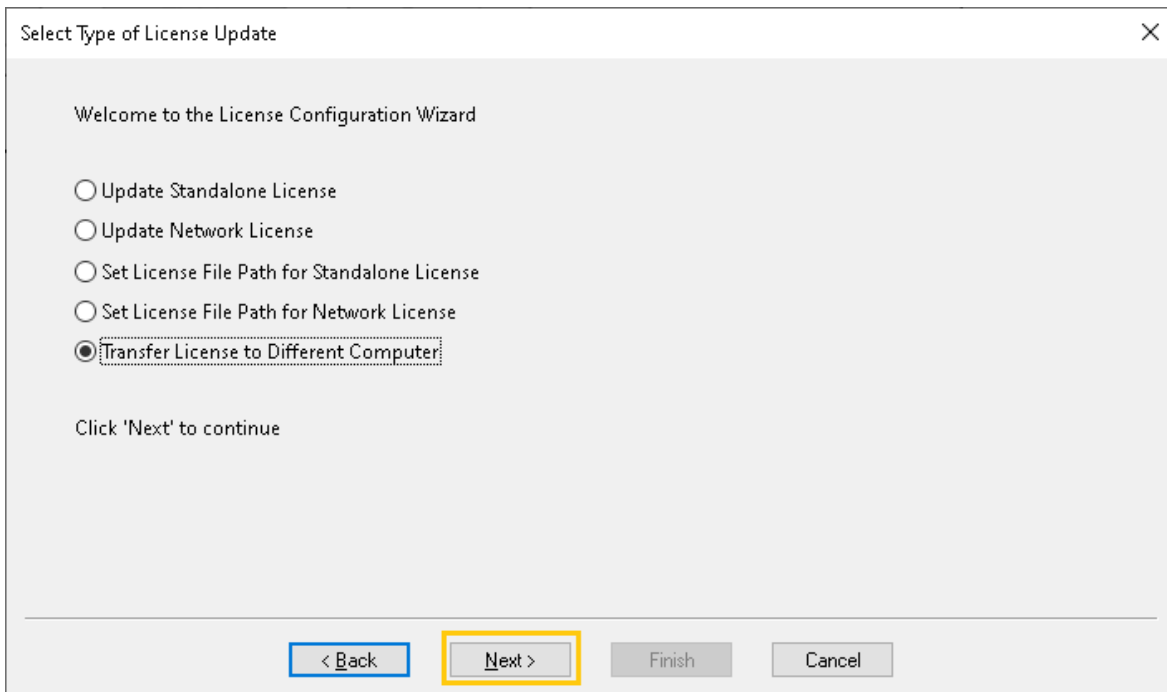


Figure 37. Next button to transfer the license to a different computer

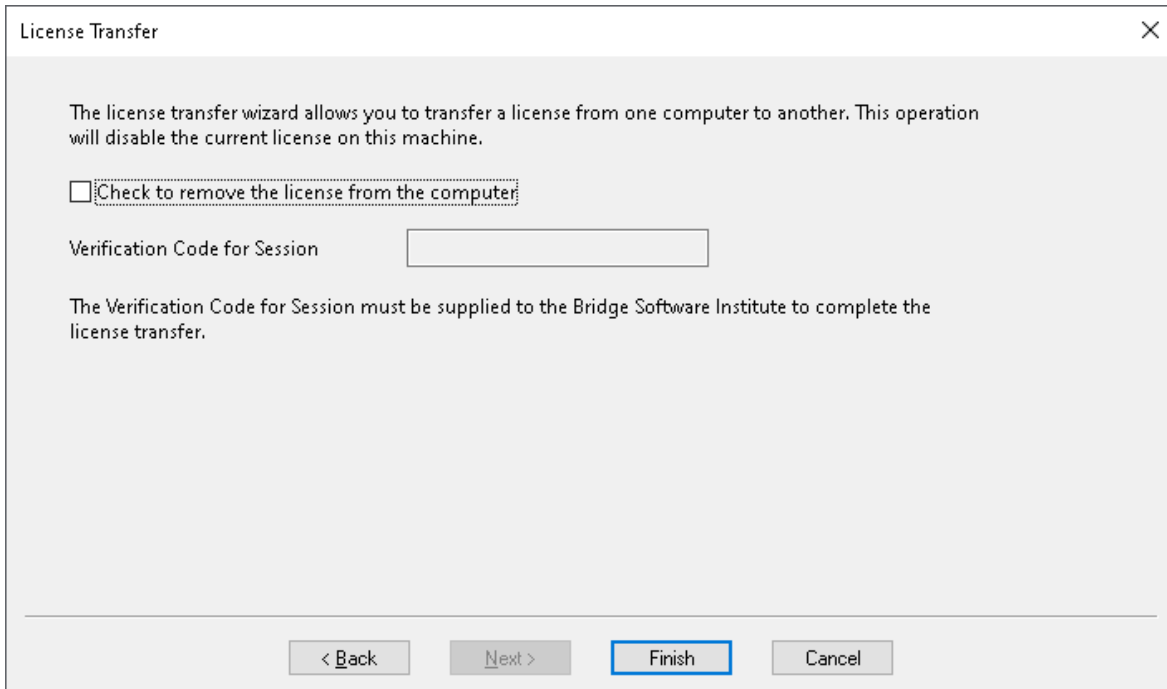


Figure 38. Transfer License to Different Computer page

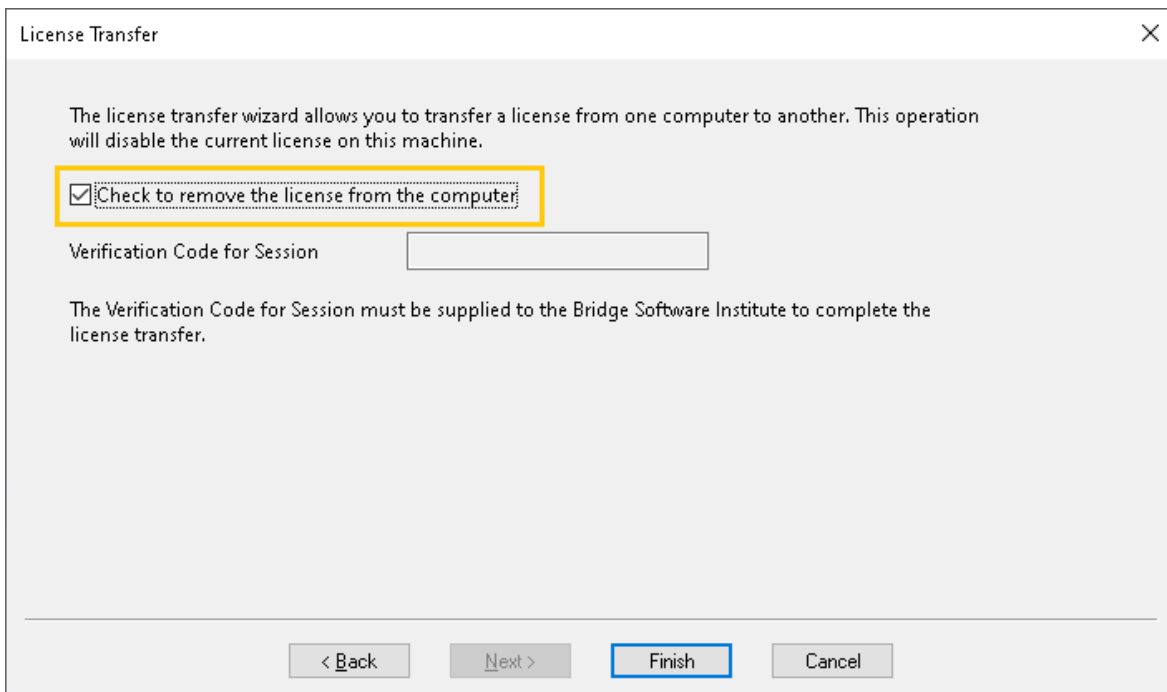


Figure 39. Check to remove the license from the computer checkbox

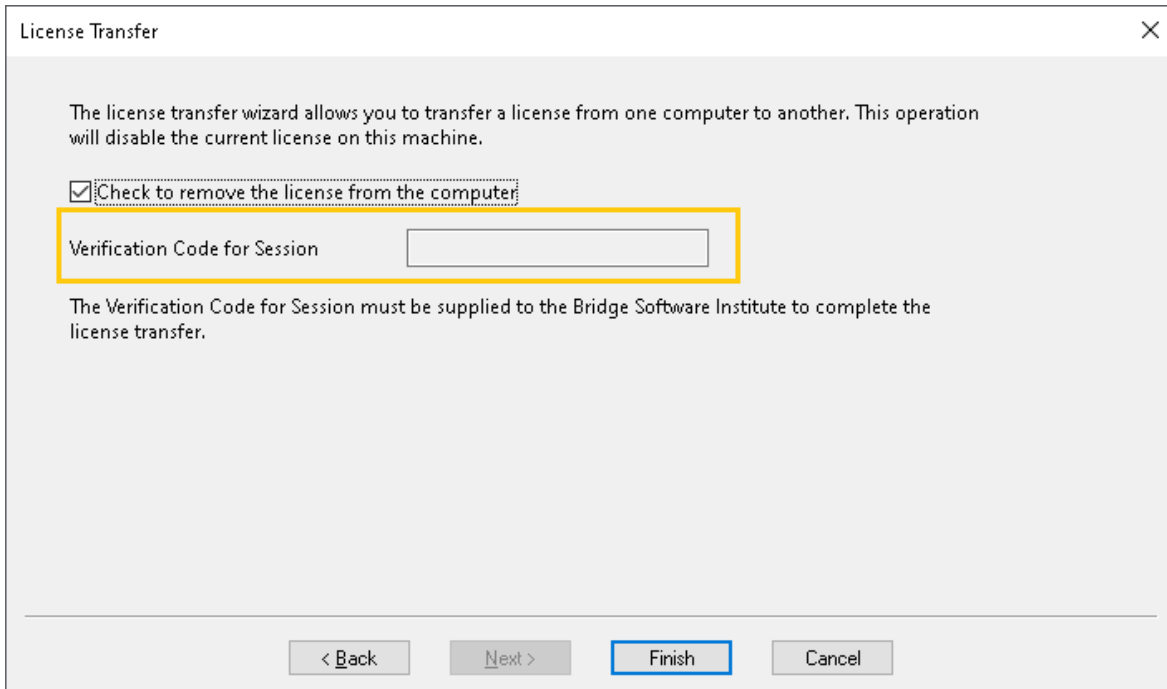


Figure 40. Verification Code for Session on License Transfer page

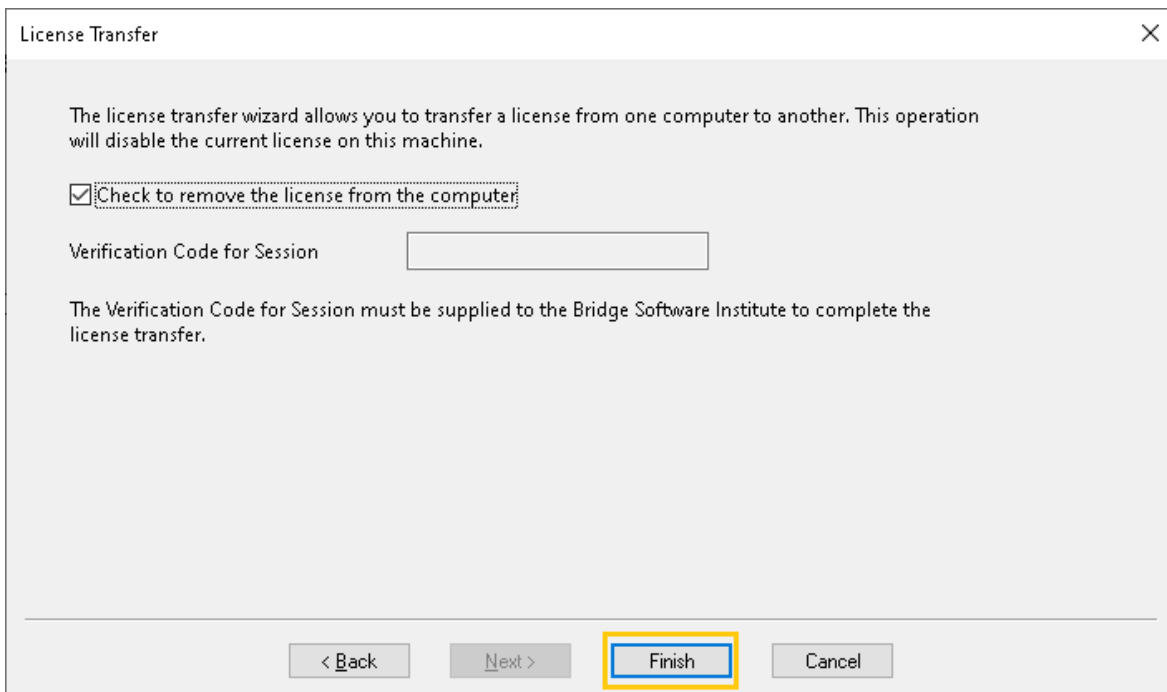


Figure 41. Finish Button on License Transfer page

CHAPTER 3 INPUT FILE FORMAT

3.1 Overview

Regarding GeoStat input file formatting, two overarching categories of data are recognized: (1) Parameters necessary to define the of-interest deep foundation member configuration and conditions (pile or shaft; cross-section and length; soil or rock zones; soil or rock layering; spatial correlation structure; and, empirical method for calculating resistance); and, (2) Geotechnical investigation data acquired for a given site. Documentation pertaining to these two data categories is provided in Sec. 3.2 and Sec. 3.3, respectively.

Given the considerable amount of data typically associated with geotechnical investigations of bridge sites (e.g., blow counts, unit weights, coring data) and, further, the additional inputs required to define the foundation member configuration and conditions, Microsoft® Excel is utilized for housing the contents of GeoStat input files. The standardized input file format is in the form of a non-programmed Excel worksheet, which signifies that no Visual Basic for Applications (VBA) or embedded formulas are present across the entire input deck. This approach allows for convenient tabulation of (potentially) large data sets, but also (due to being “non-programmed”) ensures that uniformity is upheld in practice, with respect to the standard input file format. In addition, the input file format adopted here adheres to a 1:1 mapping between a given tab within the GeoStat UI (see Ch. 4) and a dedicated Excel worksheet tab in the input file itself. Purely illustrative sets of input data are utilized throughout Ch. 3 solely to aid in documentation of the standard input formatting.

3.2 Input Format for Data Pertaining to Member Configuration and Conditions

Documented in Sec. 3.2 is the input file formatting for those parameters that are necessary to define the of-interest deep foundation member configuration and conditions (including member type and section, layering, zones, geostatistics parameters, and method error parameters). Documentation of input file formatting is subdivided into the corresponding UI tab (where UI controls found on each tab are detailed in Ch. 4).

3.2.1 Project Information Tab

A template of the Excel input file format pertaining to the “Project Information” tab is shown in Fig. 42, where illustrative input values are supplied. Note that this Excel worksheet tab must be named “1. Project Information”. In the event that the model file input data are being supplied directly from within Excel (as opposed to from within the UI), data contained within the “1. Project Information” worksheet tab must be populated prior to loading the input file in GeoStat.

There are three distinct regions of tab-specific input data in Fig. 42, and the Excel input data contained within each region of the worksheet tab are subdivided into: (1) Program Data; (2) Project Data; and, (3) Geotechnical Investigation Site Data Locations. Listings of the template input file content within the “1. Project Information” worksheet tab, and how the various inputs are organized, are presented in Sec. 3.2.1.1 through Sec. 3.2.1.4.

	A	B	C	D	E	F
1	This tab must be populated with data prior to loading GeoStat.					
2						
3	Program Data	Input Options	Units	Value		
4	Version			1.1.2		
5	Time			11:32am		
6	Date			9/26/2022		
7	Random Seed			1		
8						
9	Project Item	Input Options	Units	Value		
10	Project Number					
11	Project Name					
12	Engineer					
13	Unit System	[English SI]	ft m	English		
14	Foundation Type	[Drilled Driven]		Drilled		
15	Maximum Phi Factor			0.6		
16						
17	Method Options	Input Options	Units	Value		
18	Driven Piles	[SPT CPT]				
19	CPT Method	[UF LCPC Schmertmann]				
20	Drilled Shafts in Limestone	[McVay side friction MWD]		McVay side friction		
21	Specific Energy Threshold		psi kPa	2000.0		
22	Specific Energy Max		psi kPa	30000.0		
23						
24	Boring Name	Easting	Northing	Ground Surface Elevation	Zone	Include
25						[1 0]
26	1	39.6957	29.6872	0	0	1
27	2	23.5101	41.7242	0	0	1
28	3	10.8588	1.8625	0	0	1
29	4	23.3061	25.0954	0	0	1
30	5	20.2283	34.0703	0	0	1
31	6	46.3901	12.6739	0	0	1
32	7	34.8451	40.3033	0	0	1
33	8	11.4852	17.5605	0	0	1
34	9	35.5553	9.4145	0	0	1
35	10	44.8395	44.2006	0	0	1

Figure 42. “1. Project Information” worksheet tab with illustrative data set (only the first 10 out of 50 total boring locations are displayed)

3.2.1.1 Program Data

Occupying cells A3 through D7 of the “1. Project Information” worksheet tab (Fig. 42) is the Program Data input. As listed in Table 1, the “Program Data” inputs consist of general information about the program version and a fundamental program setting. Namely, the program version is housed here, along with the time and date of the most recent file save operation. In addition, the program setting (the random seed) is included among this input group, where the random seed dictates the sequence of pseudo-random numbers that are generated as part of Geo-statistical calculations. Reproducibility of program results is ensured by including a record of the random seed value among the file input set. Note that input values only need to be supplied within the “Value” column for this subset of input data.

Table 1. "Program Data" input from within the "1. Project Information" worksheet tab

Program Data	Input Options	Units	Value
Version			
Time			
Date			
Random Seed			1

3.2.1.2 Project Data

Cells A9 through D15 of the "1. Project Information" worksheet tab (Fig. 42) are reserved for the "Project Data" input. This subset of input data, listed in Table 2, allows for retention of records such as the project number, project name, and the engineer developing the GeoStat model. Note that, again, input values only need to be supplied within the "Value" column for this subset of input data. Also included among the inputs here are the "Unit System", "Foundation Type", and "Maximum Phi Factor". For two of these latter three inputs, valid input is constrained to those options given within the "Input Options" column. For example, the input supplied under the "Value" column for "Unit System" must be one of "English" or "SI". Likewise, either "Drilled" (for drilled shaft) or "Driven" (for driven pile) must be specified for the "Foundation Type". The "Maximum Phi Factor" (i.e., the maximum value of LRFD resistance factor to use in computing factored resistance) is shown for illustration as being equal to 0.6, but can be input at any value between 0.0 and 1.0.

Table 2. "Project Data" input from within the "1. Project Information" worksheet tab

Project Item	Input Options	Units	Value
Project Number			
Project Name			
Engineer			
Unit System	[English SI]	ft m	English
Foundation Type	[Drilled Driven]		Drilled
Maximum Phi Factor			0.6

3.2.1.3 Method Options

Cells A17 through D22 of the "1. Project Information" worksheet tab (Fig. 42) are reserved for the "Method Options" input. This subset of input data (Table 3) houses input related to the method being used for analysis. For driven pile foundations, either "SPT" or "CPT" can be specified in the "Driven Piles" data row. If "CPT" is specified, then one of the "UF", "LCPC", or "Schmertmann" methods of analysis should also be input. When modeling drilled shafts and limestone is present, then either the "McVay side friction" or Measuring While Drilling, "MWD", approach should be specified in the "Drilled Shafts in Limestone" data row. If the

“MWD” approach is selected, then a value should be supplied for the “Specific Energy Threshold”, where the default value is 2000 psi. In addition, a value of “Specific Energy Max” should be supplied, where the default value is 30,000 psi. For all “Method Options” inputs, values only need to be supplied within the “Value” column.

Table 3. “Method Options” input from within the “1. Project Information” worksheet tab

Method Options	Input Options	Units	Value
Driven Piles	[SPT CPT]		
CPT Method	[UF LCPC Schmertmann]		
Drilled Shafts in Limestone	[McVay side friction MWD]		McVay side friction
Specific Energy Threshold		psi kPa	2000.0
Specific Energy Max		psi kPa	30000.0

3.2.1.4 Geotechnical Investigation Site Data Locations

Beginning in row 24 of the “1. Project Information” worksheet tab (Fig. 42) is GeoStat input on basic information of locations at which geotechnical investigation data have been gathered throughout the site. For each boring (and/or coring) to be housed within the GeoStat input file, one row of data should be populated within this region of the “1. Project Information” worksheet tab; additionally, one Excel worksheet tab must be created for each populated data row. As illustration, 10 out of 50 boring locations are listed in Table 4, and therefore, one additional worksheet tab should be included (per boring) in the Excel input file, where the additional worksheet tabs are named “1”, “2”, “3”, ... , “50”. Data stored within the rows of Table 4 include the Boring Name, Northing, Easting, and Ground Surface Elevation, where units of “ft” or “m” should be used in a consistent manner.

Table 4. “Geotechnical Investigation Site Data Locations” input from within the “1. Project Information” worksheet tab (10 of 50 total boring locations are displayed)

Boring Name	Easting	Northing	Ground Surface Elevation	Zone	Include
					[1 0]
	ft m	ft m	ft m		
1	39.6957	29.6872	0	0	1
2	23.5101	41.7242	0	0	1
3	10.8588	1.8625	0	0	1
4	23.3061	25.0954	0	0	1
5	20.2283	34.0703	0	0	1
6	46.3901	12.6739	0	0	1
7	34.8451	40.3033	0	0	1
8	11.4852	17.5605	0	0	1
9	35.5553	9.4145	0	0	1
10	44.8395	44.2006	0	0	1

The "Zone" data column in Table 4 pertains to assignments of borings as belonging to geological zones. Values of "0" indicate that no zone has been assigned; values greater than "0" signify association of a geological zone with the boring. Also, in the rightmost column is an option ("1" or "0") to "Include" the boring in the specific GeoStat analysis; entering "1" means that the boring will be included and entering "0" means that the boring will not be included in the GeoStat analysis. This option is provided so that all of the geotechnical investigation data for a site can be housed within a single Excel file. In addition, this option allows the engineer to make use of all the data for the site when calculating axial resistance for a pile or shaft located within a specific zone within the site. For instance, the engineer may wish to separate the site into multiple zones (e.g., land versus navigable waterway) with separate layering, correlation, and LRFD resistance assessment.

3.2.2 Profile Tab

A template of the Excel input file format pertaining to the "Profile" tab is shown in Fig. 43, where illustrative input values are supplied. Note that this Excel worksheet tab must be named "2. Profile". Also, as indicated in cell A1 of the template worksheet tab, data may be input directly from within the Excel worksheet or through the GeoStat UI.

	A	B	C	D
1	Tabs 2. through 7. can be populated here or from within GeoStat.			
2				
3	Profile Variable	Input Options	Units	Value
4	Hammer Correction Factor			1
5				
6	Layer	Soil Type	Top Elevation	Bottom Elevation
7		[1 2 3 4]		
8			ft m	ft m
9	1	1	0	-105

a)

	E	F	G	H	I
1					
2					
3					
4					
5					
6	Mean Unit Weight	Coefficient of Variation	kb (Tip Coeff.)	Fs (Side Coeff.)	Include
7					[1 0]
8	pcf kN/m ³				
9	110	0.7	0		1

b)

Figure 43. Excel input file "2. Profile" worksheet tab: a) Columns A through D; b) Columns E through I

The Excel input data contained within each region of the worksheet tab are subdivided into: (1) Hammer Correction Factor; and, (2) Layering. While input pertaining to "Hammer Correction Factor" always occupies the same range of cells in the worksheet tab, the number of rows making up the "Layering" data is model-specific. Listings of the template input file

content within the "2. Profile" worksheet tab, and how the various inputs are organized, are presented in Sec. 3.2.2.1 through 3.2.2.2.

3.2.2.1 Hammer Correction Factor

Contained within cells A3 through D4 of the "2. Profile" worksheet tab (Fig. 43) is input pertaining to the "Hammer Correction Factor". This subset of input data is listed in Table 5 and contains the adjustment to soil-profile layer data (e.g., SPT values) due to automatic versus safety hammers. The correction factor is unitless and is input within the "Value" column. When a value other than 1.0 is supplied for the "Hammer Correction Factor", then values of geotechnical investigation site data such as SPT-N values will be adjusted by the correction factor as statistical processes are carried out.

Table 5. "Hammer Correction Factor" input from within the "2. Profile" worksheet tab

Profile Variable	Input Options	Units	Value
Hammer correction factor			1

3.2.2.2 Layering

Beginning in row 6 of the "2. Profile" worksheet tab (Fig. 43) is GeoStat soil layer data. One row of data should be populated (generally, through use of the GeoStat UI) for each layer. Included in each row (Table 6) is the "Layer" number, along with "Top Elevation" and "Bottom Elevation" (in units of either ft or m). Also input for each row is the "Soil Type", where an integer value between 1 and 5 must be supplied. The range of permissible input values corresponds to the mapping of soil types within the axial capacity software package, referred to as FB-Deep: 1 = Plastic clay; 2 = Clay and silty sand; 3 = Clean sand; 4 = Limestone, very shelly sand; and, 5 = Void.

Table 6. "Layering" input from within the "2. Profile" worksheet tab (Columns A through F)

Layer	Soil Type	Top Elevation	Bottom Elevation	Mean Unit Weight	Coefficient of Variation
	[1 2 3 4 5]				
		ft m	ft m	pcf kN/m ³	
1	1	0	-105	110	0.7

Columns E and F of the "Layering" input (Fig. 43) pertain to the layer "Mean Unit Weight" and corresponding "Coefficient of Variation", where the former parameter is in units of either pcf or kN/m³. Note that input of the mean, and COV values of unit weight (Table 6) are only required if the "Foundation Type" is input as "Drilled" on the "1. Project Information" worksheet tab (recall Table 2). Stated alternatively, the "Mean Unit Weight" and "Coefficient of Variation" input parameters are not required for analysis of driven piles in GeoStat.

Additional layer-specific inputs are provide in columns G through I (Table 7). For analyses making use of "CPT" and the "UF" method, input per layer of a tip coefficient ("kb (Tip Coeff.)") and a side coefficient ("Fs (Side Coeff.)") can be supplied. If no values are supplied within a given layer, then default values will be utilized during analysis, where the listings of default side and tip coefficients for CPT analysis with use of the UF method are given in the FB-Deep Help Manual. In column I is an option ("1" or "0") to "Include" the layer in the specific GeoStat analysis; entering "1" means that the layer will be included and entering "0" means that the layer will not be included in either the GeoStat analysis for determining spatial correlation structures, or in the model analysis files (with FB-Deep formatting) for calculating axial capacities.

Table 7. "Layering" input from within the "2. Profile" worksheet tab (Columns G through I)

kb (Tip Coeff.)	Fs (Side Coeff.)	Include
		[1 0]
		1

3.2.3 Geostatistics Tab

A template of the Excel input file format pertaining to the "Geostatistics" tab in GeoStat is shown in Fig. 44 (columns A through D), Fig. 45 (columns E through L), and Fig. 46 (columns M through T), along with illustrative input values. Note that this Excel worksheet tab must be named "3. Geostatistics". Also, as indicated in cell A1 of the template worksheet tab, data contained within the "3. Geostatistics" worksheet tab can be directly input into the worksheet, or the data can be populated from within the GeoStat UI. Generally, input data for this worksheet tab should be populated through use of the GeoStat UI. Input data contained within the Excel worksheet tab are subdivided into: (1) Layer Detrending; (2) Horizontal Variograms; and, (3) Vertical Variograms. Template input file content within the "3. Geostatistics" worksheet tab, and how the various inputs are organized, are presented in Sec. 3.2.3.1 through Sec. 3.2.3.3.

	A	B	C	D
1	Tabs 2. through 7. can be populated here or from within GeoStat.			
2				
3	Layer	Detrend	Detrend Polynomial Degree	Variogram
4		[Yes No]	[1 2]	[Spherical Exponential]
5				
6	1	No		0 Exponential

Figure 44. Excel input file "3. Geostatistics" worksheet tab, columns A through D

	E	F	G	H	I	J	K	L
1								
2								
3	Horizontal Lag	Number of Horizontal Lags	Horizontal Tolerance	Horizontal Bandwidth	Horizontal Range	Horizontal Nugget	Horizontal Sill	Horizontal Worst Case
4								[Yes No]
5	ft m		ft m	ft m	ft m			
6	1	20	0.5	0	10	0		1 No

Figure 45. Excel input file "3. Geostatistics" worksheet tab, columns E through L

	M	N	O	P	Q	R	S	T
1								
2								
3	Vertical Lag	Number of Vertical Lags	Vertical Tolerance	Vertical Bandwidth	Vertical Range	Vertical Nugget	Vertical Sill	Vertical Worst Case
4								[Yes No]
5	ft m		ft m	ft m	ft m			
6	1	20	0.5	0	5	0		1 No

Figure 46. Excel input file "3. Geostatistics" worksheet tab, columns M through T

3.2.3.1 Layer Detrending

Input data pertaining to detrending of soil layer properties begins in row 3, and occupies columns A through D, of the "3. Geostatistics" worksheet tab (Fig. 44). Consistent with layer data from the "2. Profile" worksheet tab (recall Fig. 43), one row of data should be populated (Fig. 44) for each defined layer. Note that, generally, this subset of input data is populated through use of the GeoStat UI. Included in each row (Table 8) is the "Layer" number and an indicator ("Yes" or "No") of whether or not detrending is to be performed on the layer data. For any layers that are to be detrended, an integer value (1 or 2) of the polynomial degree to which detrending should be carried out must also be input. Otherwise, the corresponding cell within the "Detrend Polynomial Degree" column can remain blank. Input data located within column D, "Variogram", dictates the form of the mathematical fit to the variograms generated for each layer, which consist of "Spherical" and "Exponential".

Table 8. "Layer Detrending" input from within the "3. Geostatistics" worksheet tab

Layer	Detrend	Detrend Polynomial Degree	Variogram
	[Yes No]	[1 2]	[Spherical Exponential]
1	No		Exponential

3.2.3.2 Horizontal Variograms

Columns E through L of the "3. Geostatistics" worksheet tab (Fig. 45) are reserved for input of "Horizontal Variograms" data (one row per layer). See Ch. 4 and the program Technical Manual for definitions and additional details regarding these parameters. Note that this subset of input data is generally populated through use of the GeoStat UI, rather than from

within the Excel worksheet. Included in each row (as listed in Table 9) is the “Horizontal Lag” distance (ft, m); “Number of Horizontal Lags”; “Horizontal Tolerance” (ft, m); and, “Horizontal Bandwidth” (ft, m). Additional inputs include (Table 10): “Horizontal Range”; “Horizontal Nugget”; “Horizontal Sill”; and, an indicator of whether or not (“Yes” or “No) the “Horizontal Worst Case” is to be considered for use when an acceptable horizontal variogram cannot be formed.

Table 9. “Horizontal Variograms” input from within the “3. Geostatistics” worksheet tab

Horizontal Lag	Number of Horizontal Lags	Horizontal Tolerance	Horizontal Bandwidth
ft m		ft m	ft m
1	20	0.5	0

Table 10. Continued “Horizontal Variograms” input from within the “3. Geostatistics” tab

Horizontal Range	Horizontal Nugget	Horizontal Sill	Horizontal Worst Case
			[Yes No]
10	0	1	No

3.2.3.3 Vertical Variograms

Columns M through T of the “3. Geostatistics” worksheet tab (Fig. 46) are reserved for input of “Vertical Variograms” data. See Ch. 4 and the program Technical Manual for additional details regarding these parameters. Note that one row of data is populated per soil layer. As with all other input data on the “3. Geostatistics” worksheet tab, the “Vertical Variograms” input parameters are intended to be populated through use of the GeoStat UI, rather than from within the Excel worksheet. For each layer (i.e., for each row), inputs listed in Table 11 must be supplied, including: “Vertical Lag” distance (ft, m); “Number of Vertical Lags”; “Vertical Tolerance” (ft, m); and, “Vertical Bandwidth” (ft, m). Additional inputs (Table 12) include: “Vertical Range”; “Vertical Nugget”; “Vertical Sill”; and, an indicator of whether or not (“Yes” or “No) the “Vertical Worst Case” is to be considered for use when an acceptable vertical variogram cannot be formed.

Table 11. “Vertical Variograms” input from within the “3. Geostatistics” worksheet tab

Vertical Lag	Number of Vertical Lags	Vertical Tolerance	Vertical Bandwidth
ft m		ft m	ft m
1	20	0.5	0

Table 12. Continued “Vertical Variograms” input from within the “3. Geostatistics” tab

Vertical Range	Vertical Nugget	Vertical Sill	Vertical Worst Case
			[Yes No]
5	0	1	No

3.2.4 Simulation Tab

A template of the Excel input file format pertaining to the “Simulation” tab in GeoStat is shown in Fig. 47, along with illustrative input values. Note that this Excel worksheet tab must be named “4. Simulation”. As noted in cell A1 of the template worksheet tab, data contained within the “4. Simulation” worksheet tab may be input directly from within the Excel environment, or via the GeoStat UI. However, it is generally intended that this collection of parameters would be input from within the GeoStat UI.

The various inputs are organized into several data subsets in the “4. Simulation” worksheet tab: (1) Pile Geometry; (2) Shaft Geometry; (3) Shaft/Pile Length; (4) Shaft/Pile Material; (5) Soil; and, (6) Simulation. Listings of the template input file content within the “4. Simulation” worksheet tab, and how the various inputs are organized, are presented in Sec. 3.2.4.1 through 3.2.4.6. For all inputs contained within the “4. Simulation” worksheet tab, input values need only be supplied within column D, which is labeled as the “Value” column (Fig. 47).

3.2.4.1 Pile Geometry

Contained within cells A3 through D8 of the “4. Simulation” worksheet tab (Fig. 47) are inputs pertaining to “Pile Geometry”. This subset of input data is listed in Table 13 and contains the “Width” (ft, m), “Section Type” (“Square” or “Round” or “Cylinder” or “Pipe” or “H-Section”), “Depth”, “Thickness”, and “Pile End Condition” of the pile. If the pile “Section” is input as “Round” or “Square”, then the pile diameter should be input for “Width”. If the pile “Section” is input as “Cylinder” or “Pipe”, then the pile diameter should be input for “Width”, the wall thickness input for “Thickness”, and the pile end condition input for “Pile End Condition” (0 signifies open, 1 signifies closed). If the pile “Section” is input as “H-Section”, then the pile width should be input for “Width” and the pile depth should be input for “Depth”.

Input data is only required in cells A3 through D8 if the “Foundation Type” parameter is input as “Driven” (i.e., driven pile) on the “1. Project Information” worksheet tab (Fig. 42). Recalling the “1. Project Information” worksheet tab (Fig. 42), and the illustrative data set, the “Foundation Type” is input as “Driven” (i.e., driven pile). Consequently, input pertaining to “Pile Geometry” is required in this instance.

	A	B	C	D
1	Tabs 2. through 7. can be populated here or from within GeoStat.			
2				
3	Pile Geometry	Input Options	Units	Value
4	Width		in mm	0
5	Section	[Square Round Cylinder Pipe H-Section]		Square
6	Depth		in mm	0
7	Thickness		in mm	0
8	Pile End Condition	[0 1]		0
9				
10	Shaft Geometry	Input Options	Units	Value
11	Diameter		in mm	48
12	Casing Length		ft m	0
13	Bell Length		ft m	0
14	Bell Diameter		in mm	0
15				
16	Shaft/Pile Length	Input Options	Units	Value
17	Minimum Length		ft m	52
18	Maximum Length		ft m	80
19	Length Increment		ft m	1
20				
21	Shaft/Pile Material	Input Options	Units	Value
22	Unit Weight		pcf kN/m ³	150
23	Elastic Modulus		ksi MPa	4000
24	Slump		in mm	6
25	Limiting Settlement		%	3
26				
27	Soil	Input Options	Units	Value
28	Water Elevation		ft m	0
29	Reserved	[Yes No]		
30				
31	Simulation Settings	Input Options	Units	Value
32	Number of Simulations			1500
33	Conditional	[Yes No]		No
34	Nearest Boring			B4
35	Northing		ft m	24
36	Easting		ft m	9.37
37	Layer Separation	[1 2 5]		5
38	Unit Weight		pcf kN/m ³	0
39	SPT-N		blows/ft blows/300mm	0
40	Cu		tsf kPa	0

Figure 47. Excel input file "4. Simulation" worksheet tab

Table 13. "Pile Geometry" input from within the "4. Simulation" worksheet tab

Pile Geometry	Input Options	Units	Value
Width		in mm	24
Section	[Square Round Cylinder Pipe H-Section]		Square
Depth		in mm	0
Thickness		in mm	0
Pile End Condition	[0 1]		0

3.2.4.2 Shaft Geometry

Contained within cells A10 through D14 of the "4. Simulation" worksheet tab (Fig. 47) are inputs specific to "Shaft Geometry". This input data (Table 14) includes shaft "Diameter" (ft, m); "Casing Length" (ft, m); "Bell Length" (ft, m); and, "Bell Diameter" (ft, m). Note that if attributes such as casing or bell are not present, then the corresponding entries in the worksheet tab can be supplied as "0" or left blank. For the illustrative data set, a driven pile is modeled, and so, no input is required for "Shaft Geometry".

Table 14. "Shaft Geometry" input from within the "4. Simulation" worksheet tab

Shaft Geometry	Input Options	Units	Value
Diameter		in mm	48
Casing Length		ft m	0
Bell Length		ft m	0
Bell Diameter		in mm	0

3.2.4.3 Shaft/Pile Length

Contained within cells A16 through D19 of the "4. Simulation" worksheet tab (Fig. 47) are inputs specific to "Shaft/Pile Length". The length-related input data (Table 15) includes "Minimum Length" (ft, m); "Maximum Length" (ft, m); and, "Length Increment" (ft, m). The latter input parameter, "Length Increment" allows for several trial embedment lengths to be analyzed between the "Minimum Length" considered and "Maximum Length" considered. "Shaft/Pile Length" data must be input regardless of the foundation type being modeled.

Table 15. "Shaft/Pile Length" input from within the "4. Simulation" worksheet tab

Shaft/Pile Length	Input Options	Units	Value
Minimum Length		ft m	52
Maximum Length		ft m	80
Length Increment		ft m	1

3.2.4.4 Shaft/Pile Material

Contained within cells A21 through D25 of the "4. Simulation" worksheet tab (Fig. 47) are inputs specific to "Shaft/Pile Material". The corresponding inputs (Table 16) include "Elastic Modulus" (ksi, kPa); "Slump" (in, mm); "Limiting Settlement" (%); and, "Unit Weight" (pcf, kN/m³). While input values must always be supplied for "Unit Weight", the "Slump" and "Elastic Modulus" parameters must only be supplied when modeling drilled shafts (and can remain blank otherwise). Further, regarding the "Limiting Settlement" input, which is

technically a limiting parameter concerning member-level response to loading, will be defaulted during analysis of drilled shafts to 5% if input as “0” or left blank.

Table 16. “Shaft/Pile Material” input from within the “4. Simulation” worksheet tab

Shaft/Pile Material	Input Options	Units	Value
Unit Weight		pcf kN/m ³	150
Elastic Modulus		ksi MPa	4000
Slump		in mm	6
Limiting Settlement		%	3

3.2.4.5 Soil

Contained within cells A27 through D29 of the “4. Simulation” worksheet tab (Fig. 47) are general inputs concerning the “Soil” at the location in which the pile (or shaft) is being installed. The corresponding input (Table 17) is “Water Elevation” (ft, m).

Table 17. “Soil” input from within the “4. Simulation” worksheet tab

Soil	Input Options	Units	Value
Water Elevation		ft m	0
Reserved			

3.2.4.6 Simulation Settings

Contained within cells A31 through D40 of the “4. Simulation” worksheet tab (Fig. 47) are “Simulation Settings” inputs, which are also listed in Table 18. The integer-valued input “Number of Simulations” dictates the number of realizations to generate (i.e., number of unique FB-Deep models to create) for computing descriptive statistics (e.g., mean, variance) of the pile (or shaft) soil resistance. The sample size (number of realizations) can be “Conditional” (if input as “Yes”) upon the nearest boring, or unconditional (if “No” is input). If “Yes” is input for the “Conditional” option, then a value must also be supplied for the “Nearest Boring”. Note that the input under the “Value” column for the “Nearest Boring” must exactly match one of the input values beneath the “Boring Name” column from the “1. Project Information” worksheet tab (recall Fig. 42). For instances when the “Conditional” option is set to “Yes”, then the “Northing” (ft, m) and “Easting” (ft, m) of the foundation must also be supplied. Otherwise, if the “Conditional” option is input as “No”, then the “Nearest Boring”, “Northing”, and “Easting” values may be left blank.

In the event that a layered soil profile is modeled, then there may be layers of the same soil type positioned directly atop (or below) one another. To ensure treatment of the two layers as separate entities, a fictitious (thin) soil layer (i.e., a “Layer Separation”) can be inserted between the two real layers. As listed in Table 18, the “Layer Separation” can be specified in the convention of soil types established in the axial capacity software, FB-Deep, where 1 signifies

plastic clay; 2 signifies clay and silty sand; and, 5 signifies a void. The default value for this input parameter, if left blank, is 5 (void). If "Layer Separation" is input as 1 (plastic clay), then a value of undrained shear strength, "Cu" (tsf, kPa), must also be supplied. Similarly, if "Layer Separation" is input as 2 (clay and silty sand), then an uncorrected blow count value, "SPT-N" (blows/ft, blows/300 mm), must additionally be provided.

Table 18. "Simulation Settings" input from within the "4. Simulation" worksheet tab

Simulation Settings		Units	Value
Number of Simulations			1500
Conditional	[Yes No]		No
Nearest Boring			
Northing		ft m	
Easting		ft m	
Layer Separation	[1 2 5]		5
Unit Weight		pcf kN/m ³	0
SPT-N		blows/ft blows/300 mm	0
Cu		tsf kPa	0

3.2.5 Spatial Variability Tab

A template of the Excel input file format pertaining to the "Spatial Variability" tab is shown in Fig. 48, along with illustrative input values. Note that this Excel worksheet tab must be named "5. Spatial Variability". Also, as indicated in cell A1 of the template worksheet tab, data contained within the "5. Spatial Variability" worksheet tab can be directly input into the worksheet, or the data can be populated from within the GeoStat UI. Generally, input data for this worksheet tab should be populated through use of the GeoStat UI. Template input file content within the "5. Spatial Variability" worksheet tab, and how the various inputs are organized, are presented in Sec. 3.2.5.1.

	A	B	C
1	Tabs 2. through 7. can be populated here or from within GeoStat.		
2			
3	Display Side Data	Display Tip Data	Display Total Data
4	[Yes No]	[Yes No]	[Yes No]
5			
6	Yes	Yes	Yes

Figure 48. Excel input file "5. Spatial Variability" worksheet tab

3.2.5.1 Plot Display Settings

Contained within cells A3 through C6 of the "5. Spatial Variability" worksheet tab (Fig. 48) are plot settings for display of computed axial capacity data, which in turn, reflect spatial

variability phenomena associated with the foundation being analyzed. The plot settings (Table 19) include “Display Side Data”, “Display Tip Data”, and “Display Total Data”, where input options consist of “Yes” or “No” for each plot setting. The three plot settings, respectively, signify whether or not to display the progressions of side resistance, tip resistance, and total resistance as a function of embedment length.

Table 19. “Plot Display Settings” input from within the “5. Spatial Variability” worksheet tab

Display Side Data	Display Tip Data	Display Total Data
[Yes No]	[Yes No]	[Yes No]
Yes	Yes	Yes

3.2.6 Method Error Tab

A template of the Excel input file format pertaining to the “Method Error” tab is shown in Fig. 49, along with illustrative input values. Note that this Excel worksheet tab must be named “6. Method Error”. Also, as indicated in cell A1 of the template worksheet tab, data contained within the “6. Method Error” worksheet tab can be directly input into the worksheet, or the data can be populated from within the GeoStat UI.

Generally, input data for this worksheet tab should be populated through use of the GeoStat UI. For GeoStat models associated with drilled shafts, three regions of input data are located within the “6. Method Error” worksheet tab. These regions pertain to method error parameter input for: (1) “Drilled Shaft” foundations; (2) considerations for the “Limestone Model” when MWD analysis is not being considered; and (3) “MWD” considerations for portions of drilled shafts that reside within limestone layers. For driven pile foundations, a unique input region can also be found in the “6. Method Error” worksheet tab, and this tab-specific subset of input data is referred to as “Driven Pile” input. Listings of the template input file content within the “6. Method Error” worksheet tab, and how the various inputs are organized, are presented in Sec. 3.2.6.1 through Sec. 3.2.6.5.

	A	B	C	D
1	Tabs 2. through 7. can be populated here or from within GeoStat.			
2				
3	Method Error Options	Input Options	Value	
4	Driven Pile	[Default Custom]	Default	
5	Drilled Shaft	[Default Custom]	Default	
6	Limestone Model	[Default Custom]	Default	
7	MWD	[Default Custom]	Default	
8				
9	Driven Pile SPT	Intercept	Slope	Coefficient of Variation
10				
11				
12	SPT	0	0	0
13				
14	Driven Pile CPT	Mean		Coefficient of Variation
15				
16				
17	CPT	0		0
18				
19	Drilled Shaft	Exponent for Exponential	Exponent for Power	Coefficient of Variation
20				
21				
22	Clay	0.66	0.98	0.68
23	Sand	0.66	0.98	0.68
24				
25	Limestone Model	Intercept	Slope	Method Error
26				
27				
28	McVay	0.898	0.9	4.519
29	O'Neill	0	0	0
30				
31	MWD	Intercept	Slope	Method Error
32				
33				
34	Limestone	0	0	0

Figure 49. Excel input file "6. Method Error" worksheet tab.

3.2.6.1 Method Error Options

Contained within cells A3 through C7 of the "6. Method Error" worksheet tab (Fig. 49) are inputs specific to "Method Error Options". The input data (Table 20) pertains to the use of default or custom values for the method errors associated with "Driven Pile" foundations, "Drilled Shaft" Foundations, and layers relevant to one of either the "Limestone Model" or "MWD". To use the default method error parameters in GeoStat, the input in column C must be "Default". To use custom method error parameters, the input in column C must be "Custom" and the desired parameters entered into the relevant method error section, as described in the remainder of Sec. 3.2.6.

Table 20. "Method Error Options" input from within the "6. Method Error" worksheet tab

Method Error Options	Input Options	Value
Driven Pile	[Default Custom]	Default
Drilled Shaft	[Default Custom]	Default
Limestone Model	[Default Custom]	Default

3.2.6.2 Driven Pile

Contained within cells A9 through D12 of the "6. Method Error" worksheet tab (Fig. 49) is method error input data specific to driven pile foundations for SPT analysis. As presented in McVay et al. 2012, method error parameters operate based on values input in "SPT" data row, and include an "Intercept", "Slope", and "Coefficient of Variation". Input values may be left blank or input as zero if the foundation type being considered is not that of driven piles (as listed in Table 21). However, if a driven pile foundation is being considered and SPT analysis is being conducted, then these values can be set to default values from within the GeoStat UI.

Table 21. "Driven Pile SPT" input from within the "6. Method Error" worksheet tab

Driven Pile SPT	Intercept	Slope	Coefficient of Variation
SPT	0	0	0

Contained within cells A14 through D17 of the "6. Method Error" worksheet tab (Fig. 49) is method error input data specific to driven pile foundations for CPT analysis. Here, method error parameters operate on values input in the "CPT" data row, and include "Mean" and "Coefficient of Variation". Input values may be left blank or input as zero if the foundation type being considered is not that of driven piles with use of CPT analysis (as listed in Table 22). However, if a driven pile foundation is being considered and CPT analysis is being conducted, then these values can be set to default values from within the GeoStat UI.

Table 22. "Driven Pile CPT" input from within the "6. Method Error" worksheet tab

Driven Pile CPT	Mean		Coefficient of Variation
CPT	0		0

3.2.6.3 Drilled Shaft

Contained within cells A19 through D23 of the "6. Method Error" worksheet tab (Fig. 49) is method error input data specific to portions of drilled shaft foundations that reside in sand or clay layers. As presented in McVay et al. 2012, method error parameters operate on one (or both) of "Clay" layer data and/or "Sand" layer data. Inputs include an "Exponent for Exponential", "Exponent for Power", and "Coefficient of Variation". If a given soil type is not present among the layering being considered for a drilled shaft foundation, then the corresponding row-specific input values may be left blank or input as zero. For example, as

listed in Table 23, if “Sand” layers are defined, but no “Clay” layers are defined, then zero-valued entries can be supplied in the corresponding data row, while non-zero values should be supplied for the method error parameters associated with computed resistances within the “Sand” layers. Note that, for driven pile foundations, this subset of input data (both for “Clay” and “Sand”) can be input as zero-valued or can remain blank.

Table 23. “Drilled Shaft” input from within the “6. Method Error” worksheet tab

Drilled Shaft	Exponent for Exponential	Exponent for Power	Coefficient of Variation
Clay	0.66	0.98	0.68
Sand	0.66	0.98	0.68

3.2.6.4 Limestone Model

Contained within cells A25 through D29 of the “6. Method Error” worksheet tab (Fig. 49) is method error input data for when MWD analysis is not being performed and when one or more layers of “Limestone” are defined in the soil layer profile of the GeoStat model. As presented in McVay et al. 2012, method error parameters make use of the “McVay” approach for side resistance and the “O’Neill” approach for end resistance. Inputs for these two approaches include “Intercept”, “Slope”, and “Method Error” values. If no limestone layers are defined for the foundation soil layering, then all values within this data subset may be left blank or input as zero. The template input, populated with illustrative data, is listed in Table 24, where (just for illustration) values are taken directly from Ch. 3 of McVay et al. (2012).

Table 24. “Limestone” input from within the “6. Method Error” worksheet tab

Limestone Model	Intercept	Slope	Method Error
McVay	0.898	0.9	4.519
O’Neill	0	0	0

3.2.6.5 MWD

Contained within cells A31 through D34 of the “6. Method Error” worksheet tab (Fig. 49) is method error input data for when “MWD” analysis is being conducted and when one or more layers of limestone are defined in the soil layer profile of the GeoStat model. For MWD analysis, method error parameters associated with limestone layers make use of “Intercept”, “Slope”, and “Method Error” values. If no limestone layers are defined for the foundation soil

layering (or if MWD analysis is not being performed), then all values within this data subset may be left blank or input as zero.

Table 25. "Limestone" input from within the "6. Method Error" worksheet tab

MWD	Intercept	Slope	Method Error
Limestone	0	0	0

3.2.7 LRFD- ϕ Tab

A template of the Excel input file format pertaining to the "LRFD- ϕ " tab is shown in Fig. 50, along with illustrative input values. Note that this Excel worksheet tab must be named "7. LRFD-phi" (where "phi" is spelled out instead of presented as a symbol). Also, as indicated in cell A1 of the template worksheet tab, data contained within the "7. LRFD-phi" worksheet tab can be directly input into the worksheet, or the data can be populated from within the GeoStat UI. Generally, input data for this worksheet tab should be populated through use of the GeoStat UI. Template input file content within the "7. LRFD-phi" worksheet tab, and how the various inputs are organized, are presented in Sec. 3.2.7.1.

	A	B	C	D	E
1	Tabs 2. through 7. can be populated here or from within GeoStat.				
2					
3	Plot Type				
4	[Mean CV Phi PhiRn]				
5					
6	PhiRn				

Figure 50. Excel input file "7. LRFD-phi" worksheet tab

3.2.7.1 Plot Type

Contained within cells A3 through A6 of the "7. LRFD-phi" worksheet tab (Fig. 50) is the input that dictates the type of design resistance versus elevation plot to display within the respective tab of the GeoStat UI. Namely, the "Plot Type" can be selected from among the "Mean", "COV" (coefficient of variation), "Phi" (resistance factor), or "PhiRn" (product of the resistance factor and nominal resistance). The template input, populated with illustrative data, is listed in Table 26.

Table 26. "Plot Type" input from within the "7. LRFD-phi" worksheet tab

Plot Type			
[Mean	COV	Phi	PhiRn]
			PhiRn

3.3 Input Format for Geotechnical Investigation Site Data

The GeoStat software makes use of geotechnical investigation site data to aid in: (1) Estimation of the profile of soil layering at a location of interest for a pile or shaft within the site; (2) Quantitative characterization of spatial variability (i.e., formation of spatial correlation structures); and, (3) Realization of many (e.g., thousands) of possible soil-pile (or soil-shaft) configurations for analysis in axial capacity calculation software. Presented in Sec. 3.3 is the input format for data acquired through geotechnical investigation of distinct locations across a given site.

3.3.1 Overview

Soil boring (and/or coring) parameters intended for use in estimating soil layer divisions are identified in Sec. 3.3.4, while those parameters dedicated to formation of spatial correlation structures are identified in Sec. 3.3.5. Boring data inputs (depth, soil type) common to both items are discussed in Sec. 3.3.2 and Sec. 3.3.3. Two illustrative input sets, each for a distinct location within a bridge site, are utilized to illustrate the input format for geotechnical investigation site data (Fig. 51 through Fig. 53).

Recall that, in the GeoStat input file, the worksheet tab "1. Project Information" (Fig. 42) requires input of all boring (and/or coring) locations associated with a given site. Further, one unique worksheet tab is required within the GeoStat input file for each boring location, where the name of the worksheet tab must match a respective boring name specified in the "1. Project Information" worksheet tab (recall Table 2). In the following, geotechnical investigation site data associated with borings "1" (the name of which is listed among the example input in Table 2) and "2" are used to illustrate the input format for GeoStat input files. Note that in these examples, SPT datasets and rock core-run datasets are utilized. However, still other forms of geotechnical site data can be employed (e.g., cone resistance associated with CPT, specific energy associated with MWD). As emphasis, a complete GeoStat input file requires one unique worksheet tab for each boring location across the site. The geotechnical site data can be input directly from within the UI (see Ch. 4), or designated cells can be input from within Excel prior to opening the model file within GeoStat.

For a given boring (e.g., "1"), the site-acquired data is input in a manner that is consistent with the tabulated input format of the axial capacity calculation software, FB-Deep. This approach is adopted to provide convenience in making use of the geotechnical site data (measured

field data) in either software package (GeoStat, FB-Deep). Accordingly, data distributed across the worksheet tab consist of depth, soil type, and measured (or estimated) soil properties.

Depth (column A) and soil type (column B) inputs are discussed in Sec. 3.3.2 and Sec. 3.3.3, respectively, and must be supplied for each data row within the worksheet tab. Worksheet columns C through G (Fig. 51, Table 27 and Fig. 54, Table 30) pertain to soils, while data in columns H through K (Fig. 52, Table 28 and Fig. 55, Table 31) and columns L through O (Fig. 53, Table 29 and Fig. 56, Table 32) pertain to rock (data within these columns are discussed in Sec. 3.3.4 and Sec. 3.3.5).

	A	B	C	D	E	F	G
1	This tab must be populated with data prior to loading GeoStat.						
2							
3	Depth	Soil Type	N. Blows	qt (CPT)	fs (CPT)	Unit Weight	Cu
4		[1 2 3 4 5]					
5	ft m		blows/ft blows/300mm	tsf MPa	tsf kPa	pcf kN/m ³	tsf kPa
6	0		4	0			
7	2.5		4	0			
8	5		4	13			
9	7.5		4	14			
10	10		4	19			
11	12.5		4	16			
12	15		4	19			
13	17.5		4	7			
14	20		4	8			
15	22.5		4	0			
16	25		4	0			
17	27.5		4	0			
18	30		4	10			
19	32.5		4	11			
20	35		4	15			
21	37.5		4	28			
22	40		4	34			
23	42.5		4	22			
24	45		4	25			
25	47.5		4	24			
26	50		4	24			
27	52.5		4	50			
28	55		4	50			
29	57.5		4	50			
30	60		4	50			
31	62.5		4	50			
32	65		4	50			
33	67.5		4	50			
34	70		4	50			
35	72.5		4	50			

Figure 51. Example input file worksheet tab for boring "1", columns A through G (the first 30 out of 100 data rows are displayed)

Note that only those soil (or rock) parameter values that are available need to be input, while cells associated with unavailable (or not applicable) data should remain blank (unpopulated). For brevity, four selected data rows (i.e., four distinct depths) are excerpted in Tables 27-29 and Tables 30-32, and are focused upon in the following sections. In the actual GeoStat input file, one data row should be populated for each depth throughout the boring (as depicted in Fig. 51-53 and Fig. 54-56).

	H	I	J	K
1				
2				
3	e	qu	qt	qb
4				
5	psi kPa	tsf kPa	tsf kPa	tsf kPa
6				
7				
8				
9				
10				
11				
12				
13				
14				
15				
16				
17				
18				
19				
20				
21				
22				
23				
24				
25				
26				
27				
28				
29				
30				
31				
32				
33				
34				
35				

Figure 52. Example input file worksheet tab for boring "1", columns H through K (the first 30 out of 100 data rows are displayed)

	L	M	N	O
1				
2				
3	Em	RQD	Socket Roughness	Rock Recovery
4		[0.0 to 1.0]	[0 1]	[0.0 to 1.0]
5	ksi MPa			
6				
7				
8				
9				
10				
11				
12				
13				
14				
15				
16				
17				
18				
19				
20				
21				
22				
23				
24				
25				
26				
27				
28				
29				
30				
31				
32				
33				
34				
35				

Figure 53. Example input file worksheet tab for boring "1", columns L through O (the first 30 out of 100 data rows are displayed)

	A	B	C	D	E	F	G
1	This tab must be populated with data prior to loading GeoStat.						
2							
3	Depth	Soil Type	N. Blows	qt (CPT)	fs (CPT)	Unit Weight	Cu
4		[1 2 3 4 5]					
5	ft m		blows/ft blows/300mm	tsf MPa	tsf kPa	pcf kN/m^3	tsf kPa
6	0		4				
7	1		4				
8	2		4				
9	3		4				
10	4		4				
11	5		4				
12	6		4				
13	7		4				
14	8		4				
15	9		4				
16	10		4				
17	11		4				
18	12		4				
19	13		4				
20	14		4				
21	15		4				
22	16		4				
23	17		4				
24	18		4				
25	19		4				
26	20		4				
27	21		4				
28	22		4				
29	23		4				
30	24		4				
31	25		4				
32	26		4				
33	27		4				
34	28		4				
35	29		4				

Figure 54. Example input file worksheet tab for boring "2", columns A through G (the first 30 out of 100 data rows are displayed)

	H	I	J	K
1				
2				
3	e	qu	qt	qb
4				
5	psi kPa	tsf kPa	tsf kPa	tsf kPa
6				
7				
8			0.26	
9		1.71		
10		1.73		
11		1.96		
12			0.29	
13		2.21		
14			0.04	
15		2.41		
16		1.93		
17		1.98		
18			0.09	
19			0.1	
20			0.3	
21		1.72		
22		2.21		
23		2.36		
24		2.36		
25			0.21	
26			0.25	
27		1.96		
28		2.19		
29		2.19		
30		2.39		
31			0.11	
32		2.34		
33			0.29	
34		2.24		
35		1.64		

Figure 55. Example input file worksheet tab for boring "2", columns H through K (the first 30 out of 100 data rows are displayed)

	L	M	N	O
1				
2				
3	Em	RQD	Socket Roughness	Rock Recovery
4		[0.0 to 1.0]	[0 1]	[0.0 to 1.0]
5	ksi MPa			
6				
7				
8				
9		0.57		0.99
10				
11				
12				
13		0.1		0.53
14				
15		0.71		0.98
16				
17				
18		0.43		0.67
19				
20				
21				
22				
23				
24				
25				
26				
27		0.17		0.23
28				
29				
30				
31		0.1		0.18
32				
33		0.74		0.99
34				
35				

Figure 56. Example input file worksheet tab for boring "2", columns L through O (only the first 30 out of 100 data rows are displayed)

Table 27. Soil properties within the example boring "1" worksheet tab, columns A through G

Depth	Soil Type	N. Blows		qt (CPT)	fs (CPT)	Unit Weight	Cu
	[1 ... 5]						
ft m		blows/ft blows/30 cm		tsf MPa	tsf kPa	pcf kN/m ³	tsf kPa
0	4	0					
2.5	4	0					
5	4	13					
7.5	4	14					

Table 28. Soil properties within the example boring "1" worksheet tab, columns H through K

e	qu	qt	qb
psi kPa	tsf kPa	tsf kPa	tsf kPa

Table 29. Soil properties within the example boring "1" worksheet tab, columns L through O

Em	RQD	Socket Roughness	Rock Recovery
	[0.0 to 1.0]	[0 1]	[0.0 to 1.0]
ksi kPa			

Table 30. Soil properties within the example boring "2" worksheet tab, columns A through G

Depth	Soil Type	N. Blows	qt (CPT)	fs (CPT)	Unit Weight	Cu
	[1 ... 5]					
ft m		blows/ft blows/30 cm	tsf MPa	tsf kPa	pcf kN/m³	tsf kPa
0	4					
1	4					
2	4					
3	4					

Table 31. Soil properties within the example boring "2" worksheet tab, columns H through K

e	qu	qt	qb
psi kPa	tsf kPa	tsf kPa	tsf kPa
			0.26
	1.71		

Table 32. Soil properties within the example boring "2" worksheet tab, columns L through O

Em	RQD	Socket Roughness	Rock Recovery
	[0.0 to 1.0]	[0 1]	[0.0 to 1.0]
ksi kPa			
	0.57		0.99

3.3.2 Depth

The first (leftmost, or column A) parameter encountered within the "1" and "2" worksheet tabs (Tab 1: Fig. 51 and Table 27; Tab 2: Fig. 54 and Table 30) is that of "Depth" (ft, m). The "Depth" magnitude should be taken relative to the "Ground Surface Elevation" parameter input in the "1. Project Information" worksheet tab (recall Table 2). For example, for "1" the "Ground Surface Elevation" is input as 0 ft. Therefore, a depth of 0 ft corresponds to an elevation of 0 ft. As noted above, one data row in the worksheet tab should correspond to one measurement point within the boring. In addition, cells within column A cannot be left blank (from the topmost depth to the bottommost depth).

3.3.3 Soil Type

The second (from left, or column B) parameter encountered within the "1" and "2" worksheet tabs (Tab 1: Fig. 51 and Table 27; Tab 2: Fig. 54 and Table 30) is that of "Soil Type", which can be input as an integer value ranging from 1 through 5. As indicated previously, GeoStat adheres to the soil-type mapping established in FB-Deep, where for data input in column B: 1 = Plastic clay; 2 = Clay and silty sand; 3 = Clean sand; 4 = Limestone, very shelly sand; and, 5 = Void. As with the "Depth" input data, each populated data row within column B of the worksheet tab must contain an input value of soil type (i.e., one input value of soil type must be provided at each input depth).

3.3.4 Properties for Determining Layer Divisions

The remaining columns in the "1" and "2" worksheet tabs (columns C through L) can be used to estimate soil layer divisions for a candidate pile or shaft location within the site. Plots of soil properties versus elevation and a table of soil profile divisions are located within the GeoStat "Profile" tab (see Ch. 4). Specifically, soil properties (versus elevation) available for plotting include (Table 27, Table 30): SPT-N blow count, "N.Blows" (blows/ft, blows/300 mm); "Unit Weight" (pcf, kN/m³); and, undrained shear strength, "Cu" (tsf, kPa). In addition, for CPT analysis, values of cone resistance, "qt (CPT)" (tsf, MPa), and sleeve friction, "fs (CPT)" (tsf, kPa), can be plotted.

While input values for data such as blow count ("N. Blows") and "Unit Weight" can pertain to the various soil types considered, certain other parameters are only applicable to specific soil types. For example, values of undrained shear strength are typically only applicable to plastic clays ("Soil Type" 1) and clay and silty sand ("Soil Type" 2).

Specific to those layer depths associated with rock ("Soil Type" 4), soil properties that can be plotted for layer determination include (Table 28, Table 29 and Table 31, Table 32): specific energy, "e" (psi, kPa), in association with MWD; unconfined compressive strength, "q_u" (tsf, kPa); tensile strength, "q_t" (tsf, kPa); unit end bearing resistance, "q_b" (tsf, kPa); mass modulus, "E_m" (ksi, MPa); rock quality designation, "RQD" (0.0 to 1.0); "Socket Roughness" (0 for smooth or 1 for rough); and, "Rock Recovery" (0.0 to 1.0). Note that, for data within columns C through O, only those data available should be input, while other cells within columns C through O should remain blank.

3.3.5 Properties for Determining Spatial Variability

Among the soil property inputs distributed among columns C through O, SPT blow counts "N. Blows" (column C, Table 27 and Table 30) are utilized for all soil types in forming soil spatial correlation structures. When CPT data are available, cone resistance ("q_t (CPT)") can be utilized instead of SPT blow counts. Note that, from within a single model file, all available data for the site can be viewed in the form of scatterplots. However, only one of SPT or CPT data can be carried out forward into analysis for determining spatial variability.

For data rows that are associated with rock ("Soil Type" 4), input values of specific energy "e" or unconfined compressive strength "q_u" (Table 28 and Table 31) can be employed in forming spatial variability structures at the candidate pile (or shaft) location. If MWD analysis is being carried out, then values of specific energy ("e") are utilized. Otherwise, values of unconfined compressive strength ("q_u") are utilized. Only populated cells within these columns are carried forward into the statistical calculations, while blank cells are ignored. In other words, only available SPT, CPT (cone resistance), specific energy, or q_u data should be input within the respective data rows, while other cells within these columns should remain blank.

CHAPTER 4

USER INTERFACE CONTROLS

4.1 Overview

The GeoStat UI takes into account a set (or subset) of site geotechnical data (borings/corings) and guides engineers through calculation of pile/shaft axial capacities, with direct consideration of both spatial-variability analysis and method error estimation. Further, for a given pile or shaft member and soil or rock layering, GeoStat generates through-depth profiles of factored axial resistance and the uncertainty of each computed resistance within the profiles.

In particular, the GeoStat UI is organized into seven tabs, which guides engineers through the process of: (1) selecting a foundation type and identifying a set or subset of borings/corings of interest throughout a given site; (2) defining a representative soil or rock layering given the set (or subset) of borings/corings; (3) selecting Geo-statistical parameters and establishing spatial correlation structures for each layer; (4) simulating numerous realizations of through-depth soil strength parameters and determining the associated axial resistances; (5) viewing through-depth profiles of spatially varying resistance; (6) adjusting axial resistance calculations using appropriate method error correlations; and, (7) viewing profile plots of descriptive statistics based on the simulations conducted (e.g., mean, variance, COV, LRFD resistance ϕ factors), as well as factored axial resistance.

The focus of Ch. 4 is to document all controls that are accessible from within the GeoStat UI. Given in Sec. 4.2 are all program file menu and toolbar items. Additionally, UI tabs (and the associated controls) corresponding to each of the seven items listed above are discussed in Sec. 4.3 through Sec. 4.9, respectively.

4.2 File Menu and Toolbar

The GeoStat UI, along with an illustrative set of site data, is shown in Fig. 57. The File Menu and Toolbar controls (highlighted in Fig. 57) are always visible and accessible from within the GeoStat UI, regardless of which of the seven program tabs are being accessed. File main menu items include File, Control, and Help, and are discussed in Sec. 4.2.1 through Sec. 4.2.3. Further, the File Menu controls allow engineers to open, save, and close a project file; modify program settings, modify project settings; access the program manuals, and update the software license. Program toolbar buttons include actions such as New, Open, Save, and Save As, and are discussed in Sec. 4.2.5.

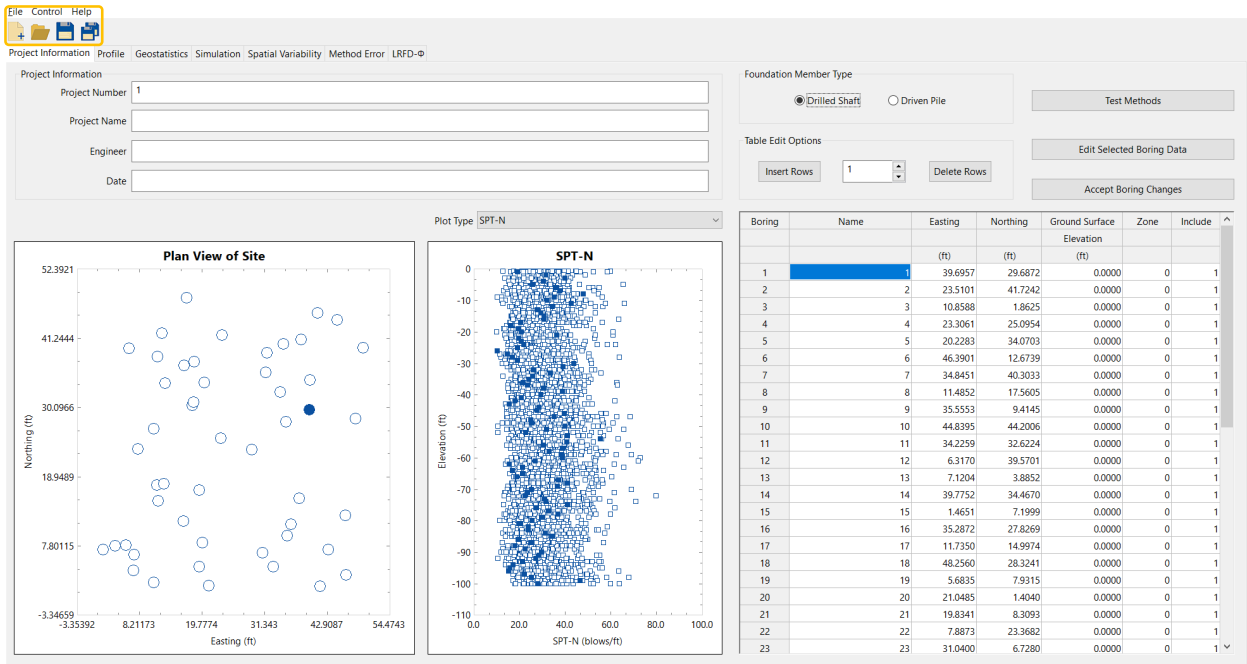


Figure 57. File menu and toolbar controls

4.2.1 File

The File dropdown menu component of the File Menu section of the GeoStat UI (shown in Fig. 58)—and moving from the top of the list downwards—allows for the engineer to create a new GeoStat model; open an existing model file (with Excel format); open an example file (driven pile or drilled shaft foundation); close the current model file; save the current model file to its current directory; save the current model file to a new directory, or, exit GeoStat.

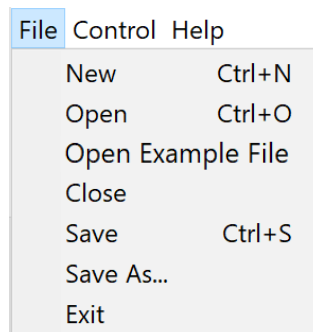


Figure 58. File dropdown menu

4.2.2 Control

The Control dropdown menu component of the File Menu section of the GeoStat UI is shown in Fig. 59. The associated menu options allow for engineers to view and edit high-level program and project (i.e., model-specific) settings.

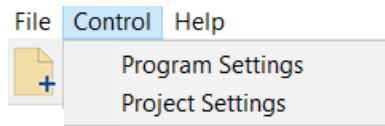


Figure 59. Control dropdown menu

The Program Settings (Fig. 60) dialog allows for selection of whether or not scaling intelligence is used for sizing and positioning of controls throughout the UI (by means of checking the Apply Scaling Intelligence checkbox). Also, the option whether or not to display a message box when the simulation output does not correspond to the current model file. In addition, a custom file path can be specified for use in analyzing all analysis model files that are generated from within GeoStat. Analysis files are always generated in accordance with input format requirements of the axial capacity software, FB-Deep. Also, note that the name of the executable must be included in the path (e.g., "FB-Deep.exe").

Analysis Options are also available from within the Program Settings dialog (Fig. 60). In particular, the option to always (or never) perform individual-layer processing upon changing the selected layer from within the Geostatistics tab can be specified. Additionally, the formulation for computing LRFD resistance (ϕ) factors can be selected. The default formulation is that of Styler (2006); however, that of National Highway Cooperative Research Program (NCHRP) report 507 (Paikowsky, 2004) can also be chosen.

The Project Settings (Fig. 61) dialog allows for specification of the Random Seed and Units convention (English or SI) used by GeoStat. The random seed dictates the sequence of pseudo-random numbers that are generated as part of Geo-statistical calculations. Reproducibility of program results is ensured by including a record of the random seed value among the file input set. In addition, the Max. Resistance Factor Value (i.e., the maximum LRFD resistance, or ϕ , factor) can be input from the Project Settings dialog. This input parameter establishes an upper limit for scaling nominal resistance values when computing factored resistance values. If no value is specified, then the Max. Resistance Factor Value is defaulted to 0.6.

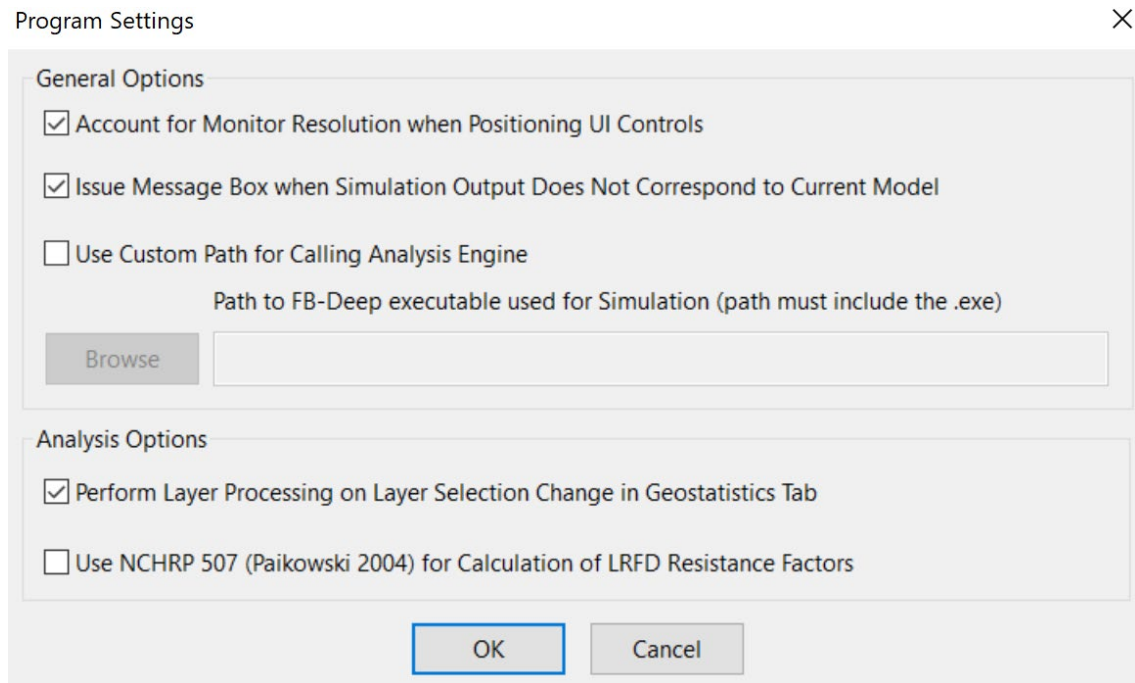


Figure 60. Program Settings dialog

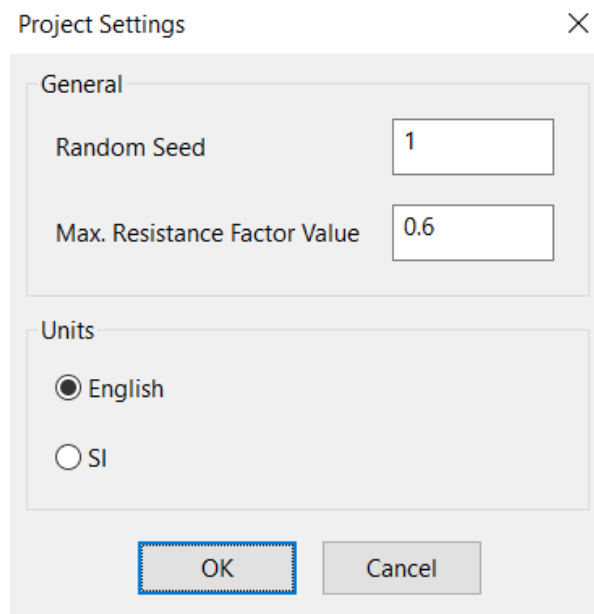


Figure 61. Project Settings dialog

4.2.3 Help

The Help dropdown menu component of the File Menu section of the GeoStat UI is shown in Fig. 62. Moving from the top of the list downwards, available options within the Help menu

item include: access the Help Manual, access the Technical Manual, update the software license (see Ch. 2), and display an About GeoStat dialog.

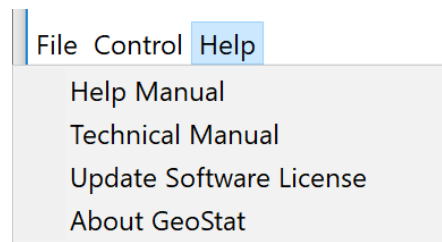


Figure 62. Help dropdown menu

4.2.4 Toolbar Buttons

Four toolbar buttons are available from within the GeoStat UI (Fig. 63). Moving from left to right, the buttons allow for the engineer to create a New model, Open an existing input file, save the currently loaded GeoStat input file, and perform a Save As operation on the currently loaded input file.



Figure 63. Toolbar buttons

4.3 Project Information Tab

Shown in Fig. 64 is the first of seven program tabs, referred to as the Project Information tab. This portion of the GeoStat UI allows for the positions of any subset (or all) borings/corings across the site to be plotted in plan view. Also, a scatterplot of through-depth measurements is provided for available soil parameters of interest. In addition, boring or coring locations can be created and/or deleted and the data within individual borings/corings modified. There are six distinct regions (or frames) of user input data in this tab: (1) Project Information; (2) Foundation Member Type; (3) Table Edit Options; (4) Test Methods dialog; (5) Edit Selected Boring Data; and, (6) Geotechnical Investigation Site Data Locations. Each of the frames are highlighted in Fig. 64. There are also two distinct plot regions in this tab: (7) Plan View of Site and (8) Plot of Soil Properties vs. Elevation (as highlighted in Fig. 64). All input control and plot regions are discussed in the remainder of Sec. 4.3.

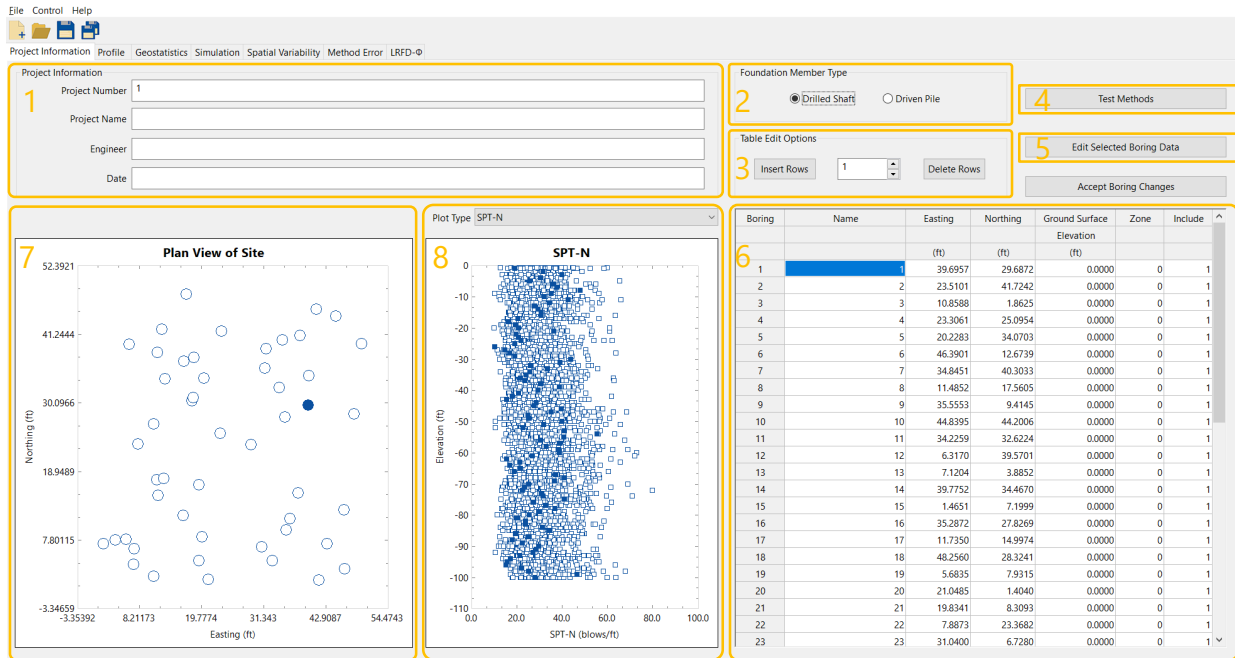


Figure 64. Project Information tab

4.3.1 Project Information Frame

Shown in Fig. 65 is the Project Information frame, where the Project Number, Project Name, Engineer, and Date may be specified. Upon saving the file, the Date field is automatically populated with the current date.

Project Information

Project Number

Project Name

Engineer

Date

Figure 65. Project Information frame

4.3.2 Foundation Member Type Frame

Shown in Fig. 66 is the Foundation Member Type frame, where the engineer can specify the type of foundation member being considered (Drilled Shaft or Driven Pile).

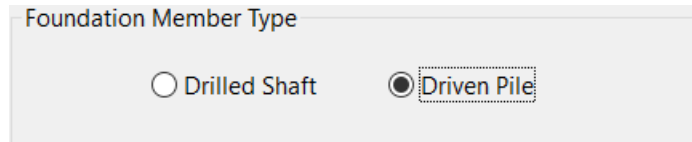


Figure 66. Foundation Member Type frame

4.3.3 Table Edit Options Frame

Shown in Fig. 67 is the table edit options frame, where the user may create and/or delete boring or coring locations. For the creation of one or more boring or coring locations, said number of locations can be specified, and the Insert Rows button can then be clicked. Upon clicking the Insert Rows button, the UI issues a warning (and takes no other action) if the number of rows to be inserted is less than 1. For the deletion of one or more boring or coring locations, said number of locations can be specified, and the Delete Rows button can then be clicked. Upon clicking the Delete Rows button, the UI issues a warning (and takes no other action) if the number of rows to be deleted is less than 1.

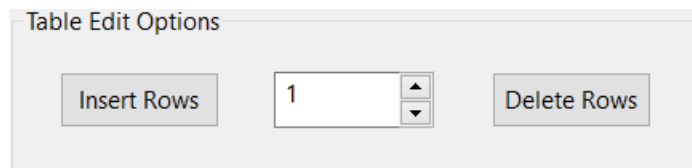


Figure 67. Table Edit Options frame

4.3.4 Test Methods Dialog

To allow for engineers to select the site measurement of interest for use in Geo-statistical analysis of piles, and separately, drilled shafts, the "Test Methods" dialog can be utilized. This dialog is located in the upper right region of the Project Information tab. As shown in Fig. 68, the dialog contains two collections of radio buttons.

The topmost radio buttons, located with the "Driven Pile Method" region allow for one of the "SPT" or "CPT" approaches to be selected. If the "SPT" radio button is selected, then subsequently accessed tabs in the GeoStat make use of SPT-N blow count data, as needed, for processes such as variogram generation and stochastic simulation. Alternatively, if the "CPT" radio button is selected from within the "Driven Pile Method" region, then CPT measurements are made use of for such processes. When making use of CPT data for analysis, the empirical method must also be selected. With respect to the UI controls, the empirical method is selected from within the "CPT Method" region of the dialog (Fig. 68). Available empirical methods are "UF", "LCPC", and "Schmertmann", where the "UF" method is designated as the default selection, upon selecting the "CPT" radio button. Note that those controls located within the "CPT Method" region are enabled only when the "CPT" radio button is selected.

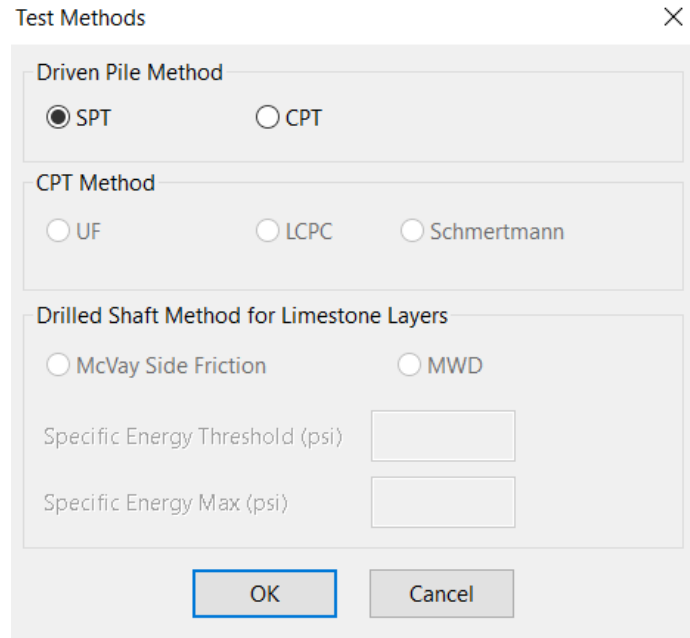


Figure 68. Test Methods Dialog

If the “Test Methods” dialog is entered when the “Foundation Member Type” is selected as “Drilled Shaft” (as selected from the Project Information tab), then the controls specific to driven piles will be disabled. Instead, controls within the frame “Drilled Shaft Method for Limestone Layers” will be enabled, including two radio buttons: “McVay Side Friction” and “MWD”. If the “McVay Side Friction” radio button is selected, then subsequently accessed tabs in the GeoStat make use of measured values of core-run data (i.e., measurements of unconfined compressive strength, q_u) as the primary variable for generating variograms and producing realizations of limestone parameter values (along with use of the formulation from McVay et al. 1992). Stated alternatively, if the “McVay Side Friction” radio button is selected, then MWD data are not utilized for any purpose other than (if data are available) viewing profiles of measurements versus elevation.

If the “MWD” radio button is selected, then calculated values of unconfined compressive strength (as determined from measured values of specific energy) are utilized, along with the formulation from Rodgers et al. (2018), during subsequent activities such as variogram generation and stochastic simulation pertaining to limestone layers. Furthermore, when the “MWD” radio button is selected, a value can be entered for the “Specific Energy Threshold”, where the default value is 2000 psi. Likewise, a value can be entered for the “Specific Energy Max”. Note that the program will not permit a value less than zero to be entered for either of the MWD-related inputs. See the Technical Manual for additional details pertaining to the “Specific Energy Threshold” and “Specific Energy Max” values.

4.3.5 Edit Selected Boring Data Dialog

Shown in Fig. 69 is the Boring Data dialog, which is accessed by clicking the Edit Selected Boring Data button from the Project Information tab (recall Fig. 64). This dialog permits bulk input of boring or coring data (e.g., from Excel). Upon clicking the OK button within the Boring Data dialog, the program checks that the depth values (highlighted in Fig. 69) are input in increasing order. GeoStat adopts the integer mapping to soil types, consistent with the convention implemented in the axial capacity calculation software FB-Deep. Accordingly, if integer values other than 1 through 5 are input beneath the Soil Type column for any row in the Boring Data dialog table, then (upon clicking OK), the program issues a warning and recommends input of revised values. For any row of data input in the Boring Data dialog, the required inputs are Depth and Soil Type (with permitted integer values between 1 and 5). Inputs for all other columns are optional.

Boring Data - 1

Table Edit Options

Insert Rows Delete Rows

Number	Elevation	Depth	Soil Type	N. Blows	qt (CPT)	fs (CPT)	Unit Weight	Cu	e	qu	qt	qb	Em	RQD	Socket Roughness	Recovery
	(ft)	(ft)	[1 2 3 4]	(blows/ft)	(tsf)	(tsf)	(pcf)	(tsf)	(psi)	(tsf)	(tsf)	(tsf)	(ksi)	[0.0 to 1.0]	[0 1]	[0.0 to 1.0]
1	0.0000	0.0000	3	18												
2	-1.0000	1.0000	3	19												
3	-2.0000	2.0000	3	32												
4	-3.0000	3.0000	3	40												
5	-4.0000	4.0000	3	31												
6	-5.0000	5.0000	3	26												
7	-6.0000	6.0000	3	36												
8	-7.0000	7.0000	3	38												
9	-8.0000	8.0000	3	48												
10	-9.0000	9.0000	3	35												
11	-10.0000	10.0000	3	32												
12	-11.0000	11.0000	3	43												
13	-12.0000	12.0000	3	34												
14	-13.0000	13.0000	3	28												
15	-14.0000	14.0000	3	29												
16	-15.0000	15.0000	3	31												
17	-16.0000	16.0000	3	31												
18	-17.0000	17.0000	3	21												
19	-18.0000	18.0000	3	16												

Notes

1. Input all available data for the boring within the table above.
2. For any depths where a given soil property is not available, then leave the corresponding cell blank.
3. Soil Types: 1 = Plastic Clay | 2 = Clay and Silty Sand | 3 = Clean Sand | 4 = Limestone and Very Shelly Sand.

OK Cancel

Figure 69. Boring Data dialog for a driven pile with illustrative data

Shown in Fig. 70 is the Boring Data dialog associated with a purely illustrative data set for modeling of a drilled shaft with use of core-run data. Note the presence of data in columns "qu", "qt", "RQD", and "Rock Recovery". With regard to pairing together parameters such as qu and qt with RQD and Rock Recovery, two optional input methods are available: values of (for

example) q_u and RQD can either be input at the same elevation, or alternatively, at unique elevations. If values of (again, for example) q_u and RQD are input at the same elevation, then these two values will be paired together during analysis. However, for any q_u (or q_t) values that do not contain RQD (and/or Rock Recovery) values at the same elevation, then the RQD (and/or Rock Recovery) values are selected from the general set of values defined across all currently enabled boring locations.

Boring Data - 2

Table Edit Options

Insert Rows 1 Delete Rows

Number	Elevation	Depth	Soil Type	N. Blows	qt (CPT)	fs (CPT)	Unit Weight	Cu	e	q_u	q_t	q_b	Em	RQD	Socket Roughness	Recovery
	(ft)	(ft)	[1 2 3 4]	(blows/ft)	(tsf)	(tsf)	(pcf)	(tsf)	(psi)	(tsf)	(tsf)	(tsf)	(ksi)	[0.0 to 1.0]	[0 1]	[0.0 to 1.0]
1	0.0000	0.0000	4													
2	-1.0000	1.0000	4													
3	-2.0000	2.0000	4								0.2600					
4	-3.0000	3.0000	4							1.7100				0.5700		0.9900
5	-4.0000	4.0000	4							1.7300						
6	-5.0000	5.0000	4							1.9600						
7	-6.0000	6.0000	4								0.2900					
8	-7.0000	7.0000	4							2.2100				0.1000		0.5300
9	-8.0000	8.0000	4								0.0400					
10	-9.0000	9.0000	4							2.4100				0.7100		0.9800
11	-10.0000	10.0000	4							1.9300						
12	-11.0000	11.0000	4							1.9800						
13	-12.0000	12.0000	4								0.0900			0.4300		0.6700
14	-13.0000	13.0000	4								0.1000					
15	-14.0000	14.0000	4								0.3000					
16	-15.0000	15.0000	4							1.7200						
17	-16.0000	16.0000	4							2.2100						
18	-17.0000	17.0000	4							2.3600						
19	-18.0000	18.0000	4							2.3600						

Notes

1. Input all available data for the boring within the table above.
2. For any depths where a given soil property is not available, then leave the corresponding cell blank.
3. Soil Types: 1 = Plastic Clay | 2 = Clay and Silty Sand | 3 = Clean Sand | 4 = Limestone and Very Shelly Sand.

OK Cancel

Figure 70. Boring Data dialog with illustrative data for a drilled shaft

4.3.6 Table Of Geotechnical Investigation Site Data Locations

Shown in Fig. 71 is the table of Geotechnical Investigation Site Data Locations. For each boring or coring present in current input data file this table displays its name, easting, northing, and ground surface elevation. Any of these values may be changed by selecting the appropriate cell, deleting the old value, and entering the new value.

The second column from the right houses the assignment of Zones to borings (values of 0 indicate no zone assignment). For any two or more active borings assigned a zone number greater than zero, a corresponding zonal circle is drawn around said borings in the plan view plots of the site. Note also that the rightmost column of the boring or coring location table (highlighted in Fig. 71) houses the Include column. Here, a value of 1 signifies that the boring

or coring location is to be included in the analysis (i.e., included in the data structures built up and operated upon in subsequent program tabs). A value of 0 indicates that the boring or coring location is to be excluded from the analysis. For boring locations that have been excluded from analysis, no associated plot points will be displayed. To protect against program crashes, any other values input in these locations are interpreted as 0 (exclude), and a value of 0 is saved for these entries upon the next file save event.

Boring	Name	Easting	Northing	Ground Surface	Zone	Include
				Elevation		
		(ft)	(ft)	(ft)		
1	1	39.6957	29.6872	0.0000	0	1
2	2	23.5101	41.7242	0.0000	0	1
3	3	10.8588	1.8625	0.0000	0	1
4	4	23.3061	25.0954	0.0000	0	1
5	5	20.2283	34.0703	0.0000	0	1
6	6	46.3901	12.6739	0.0000	0	1
7	7	34.8451	40.3033	0.0000	0	1
8	8	11.4852	17.5605	0.0000	0	1
9	9	35.5553	9.4145	0.0000	0	1
10	10	44.8395	44.2006	0.0000	0	1
11	11	34.2259	32.6224	0.0000	0	1
12	12	6.3170	39.5701	0.0000	0	1
13	13	7.1204	3.8852	0.0000	0	1
14	14	39.7752	34.4670	0.0000	0	1
15	15	1.4651	7.1999	0.0000	0	1
16	16	35.2872	27.8269	0.0000	0	1
17	17	11.7350	14.9974	0.0000	0	1
18	18	48.2560	28.3241	0.0000	0	1
19	19	5.6835	7.9315	0.0000	0	1
20	20	21.0485	1.4040	0.0000	0	1

Figure 71. Table of geotechnical investigation site data locations

4.3.7 Plan View of Site

Shown in Fig. 72 is the plan view of the site containing the positions of all borings/corings included in the current analysis. The borings/coring plotted as a solid blue circle signifies the borings/coring that is currently selected within the table of Geotechnical Investigation Site Data Locations (recall Fig. 71).

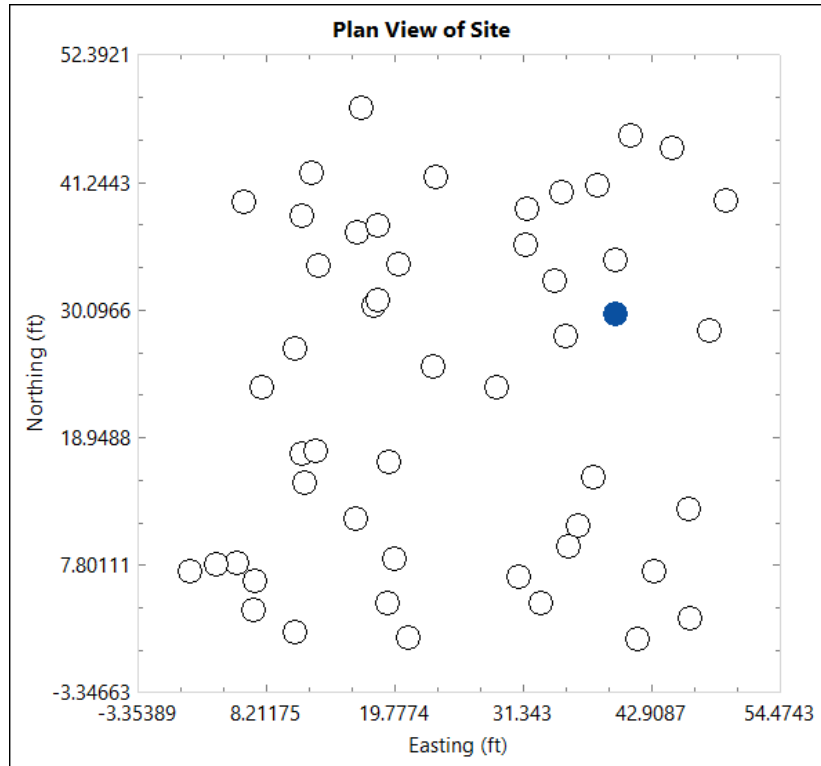


Figure 72. Plan view of site boring or coring locations

4.3.8 Soil Properties vs. Elevation

Shown in Fig. 73 is a plot of elevation vs. SPT-N for each data point across all borings/corings included for the current analysis. The data points rendered in solid blue represent those data points corresponding to the boring(s)/coring(s) currently selected within the table of Geotechnical Investigation Site Data Locations (recall Fig. 71).

Shown in Fig. 74 is a plot of elevation vs. q_u for an illustrative data file, where these values are of particular use when using core-run data to model drilled shafts embedded in limestone/very shelly sand. Shown in Fig. 75 are the options available for the soil property that is to be plotted against elevation. To view the plot of a different soil property vs. elevation, select the desired soil property from the dropdown menu to the right of the Plot Type label. If values for the selected type of data are present (or available) from among the included boring locations in the model file, then the plot will display all available data points.

From among the available types of plot data, the following variables are intended to be associated (as much as possible) with measured values: SPT blow counts (SPT-N); CPT cone resistance (q_t (CPT)); CPT sleeve friction (f_s (CPT)); Unit Weight; undrained shear strength (C_u), specific energy (e), unconfined compressive strength (q_u); tensile strength (q_t); unit end bearing resistance (q_b); mass modulus (E_m); rock quality designation (RQD); and Rock Recovery. All other plot variables are interpreted, or calculated, from measured data.

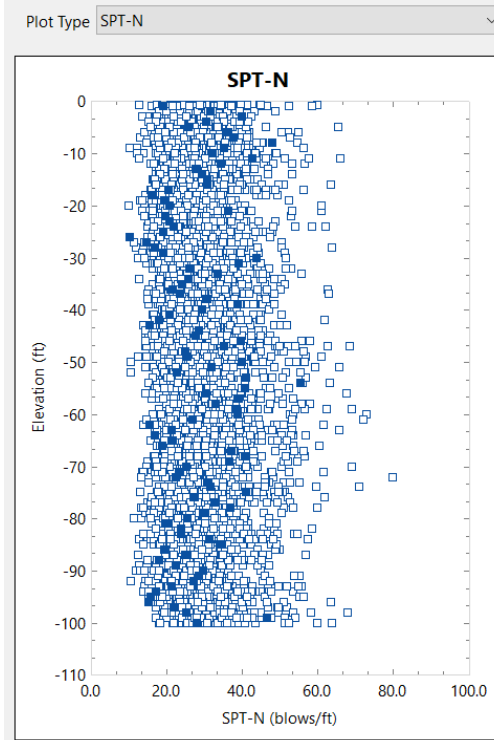


Figure 73. Plot of elevation vs. SPT-N

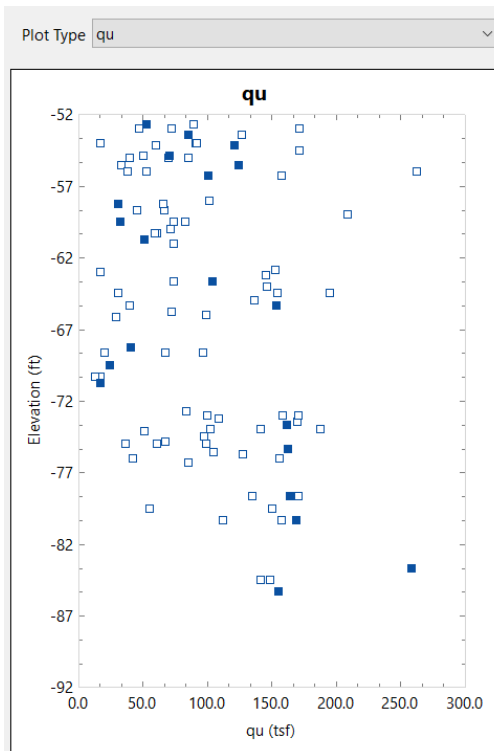


Figure 74. Plot of elevation vs. q_u

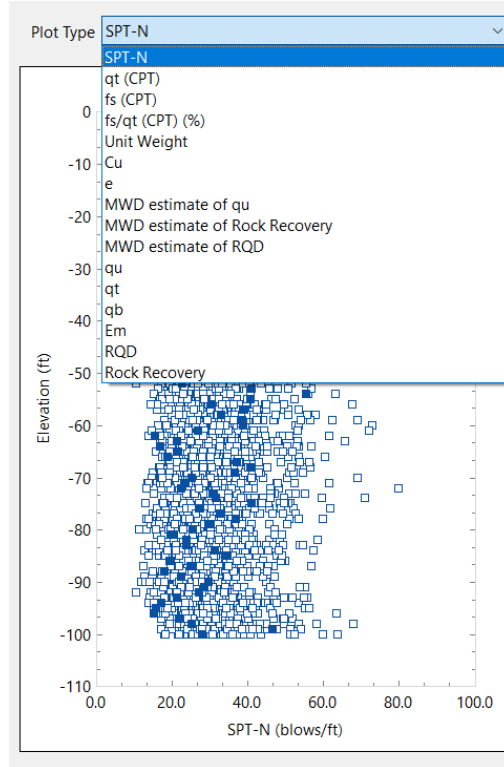


Figure 75. Menu of soil parameters that can be plotted against elevation

4.4 Profile Tab

The second (from left) tab encountered when navigating the GeoStat UI is the “Profile” tab (Fig. 76). Given a collection of included borings/corings (as decided upon from within the Project Information tab), the Profile tab facilitates estimation of representative soil or rock layers for a given location of interest.

There are three distinct regions (frames) of user input data in this tab: (1) Table Edit Options; (2) Correction Factor for Automatic Hammer; and, (3) Layer Profile table (as highlighted in Fig. 76). There is also a distinct region of plots in the left portion of the Profile tab (highlighted in Fig. 76 as region 4), which consists of two independent plots of soil properties vs. elevation and associated plot customization controls. All input frames and plot regions are discussed in the remainder of Sec. 4.4.

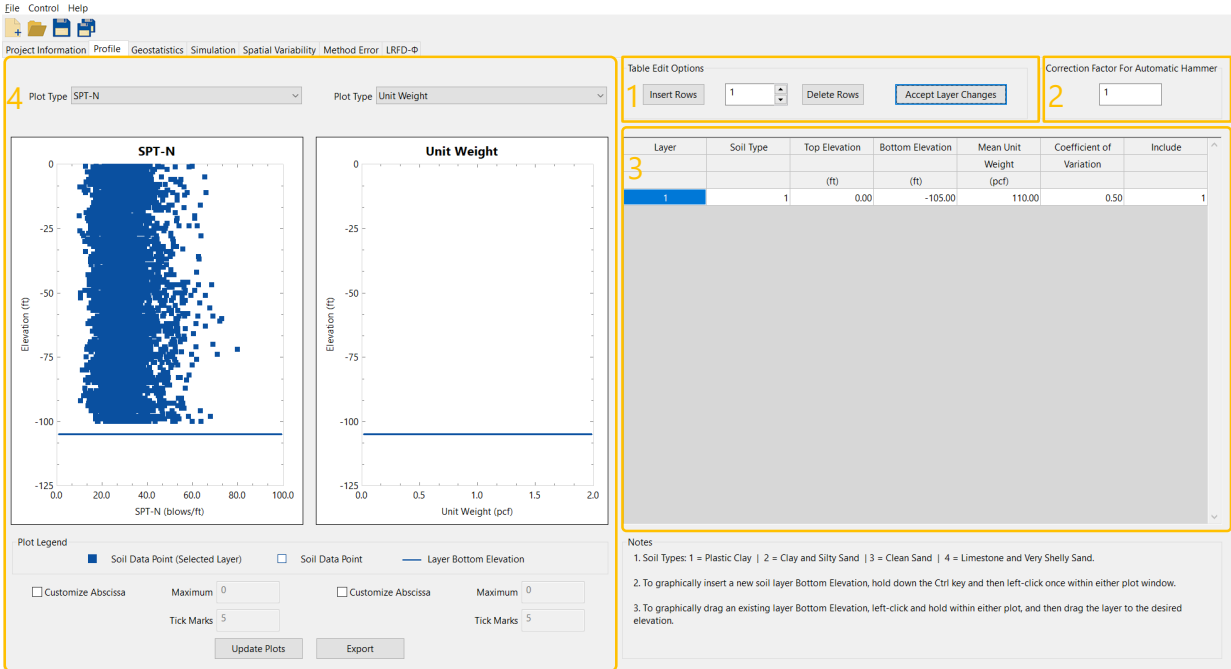


Figure 76. Profile tab

4.4.1 Table Edit Options Frame

Shown in Fig. 77 is the Table Edit Options frame, where the user may create and/or delete layers. For the creation of one or more layers, said number of layers can be specified, and the Insert Rows button can then be clicked. Upon clicking the Insert Rows button, the UI issues a warning (and takes no other action) if the number of rows to be inserted is less than 1. For the deletion of one or more layers, said number of layers can be specified, and the Delete Rows button can then be clicked. Upon clicking the Delete Rows button, the UI issues a warning (and takes no other action) if the number of rows to be deleted is less than 1.

Upon clicking the Accept Layer Changes button, the program checks that all Top Elevation (and separately, Bottom Elevation) values are in decreasing order. For intermediate layers, the program ensures that the Top Elevation (of each intermediate layer) matches the Bottom Elevation of the layer above. Similarly, the program checks that the Bottom Elevation of each intermediate layer matches the Top Elevation of the layer below.

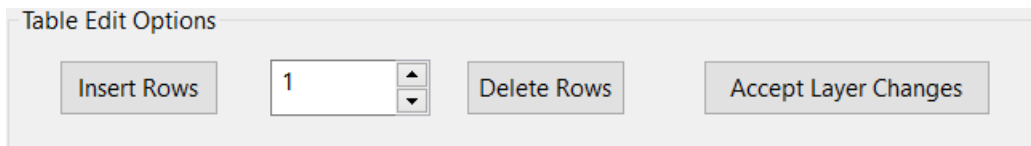


Figure 77. Table Edit Options frame for defining soil or rock layers

4.4.2 Correction Factor for Automatic Hammer Frame

Shown in Fig. 78 is the Correction Factor for Automatic Hammer frame, where the user inputs the adjustment to soil-profile layer data (e.g., SPT values) due to automatic versus safety hammers. The correction factor is unitless and is modified by entering a new value into the text box and pressing the "Update" button. When a value other than 1.0 is supplied for the "Hammer Correction Factor", then values of geotechnical investigation site data such as SPT-N values are adjusted by the correction factor as statistical processes are carried out.

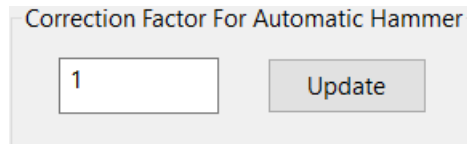


Figure 78. Correction Factor for Automatic Hammer frame

4.4.3 Layer Profile Table

Shown in Fig. 79 are examples of the Layer Profile table, which contains the layering that is to be used during simulation. In addition, top and bottom elevations of soil layers can be input from within the Layer Profile table, as shown in Fig. 79. If integer values other than 1 through 4 are input beneath the Soil Type column, then the program will issue a warning message. Note that: (1) if a driven pile foundation is being considered with use of CPT data, and the UF method is being utilized, then custom values of tip coefficients (k_b) and side coefficients (F_s) can be input per layer; and, (2) if a drilled shaft foundation is being considered, then the Mean Unit Weight and Coefficient of Variation must also be specified.

The rightmost column of the Layer Profile table houses the Include column. Here, a value of 1 signifies that the layer is to be included in the analysis. A value of 0 indicates that layer is to be excluded from the analysis. To protect against program crashes, any other values input in these locations are interpreted as 0 (exclude), and a value of 0 is saved for these entries upon the next file save event. After finalizing any changes made within the layering table, clicking the Accept Layer Changes button (Fig. 77, right) will cause the program to perform several checks which ensure that the input layers are valid (the checks are detailed in Sec. 4.4.1).

Layer	Soil Type	Top Elevation	Bottom Elevation	Include
		(ft)	(ft)	
1	1	0.00	-105.00	1

a)

Layer	Soil Type	Top Elevation	Bottom Elevation	kb (Tip Coeff.)	Fs (Side Coeff.)	Include
		(ft)	(ft)			
1	3	0.00	-46.32	0.42	110.00	1

b)

Layer	Soil Type	Top Elevation	Bottom Elevation	Mean Unit Weight	Coefficient of Variation	Include
		(ft)	(ft)	(pcf)		
1	1	0.00	-105.00	110.00	0.70	1

b)

Figure 79. Layer Profile Table: a) Driven pile foundations with analysis of SPT data; Driven pile foundations with analysis of CPT data and the UF method; b) Drilled shaft foundations

4.4.4 Elevation vs. Soil Parameter Plots

Shown in Fig. 80 is a plot of elevation vs. SPT-N (left side of Fig. 80) and a plot of elevation vs. unit weight (right side of Fig. 80) for each data point within the borings/corings included in the current analysis. The data points highlighted blue represent the data points located within the currently selected layer(s) in the layer profile table (recall Fig. 79). The horizontal lines present in the plots indicate the divisions between distinct layers, as specified in the layer profile table. In addition, moving any of these horizontal lines by dragging them with the cursor will change the layering of the analyses to reflect the new positions of the layer divisions. Changes made to layering within these plots will be reflected in the layer profile table (Fig. 79). In addition, the plot bounds can be customized. Namely, checking the Custom Abscissa box allows for the abscissa axis to be redrawn using the values input for Max and number of Tick Marks.

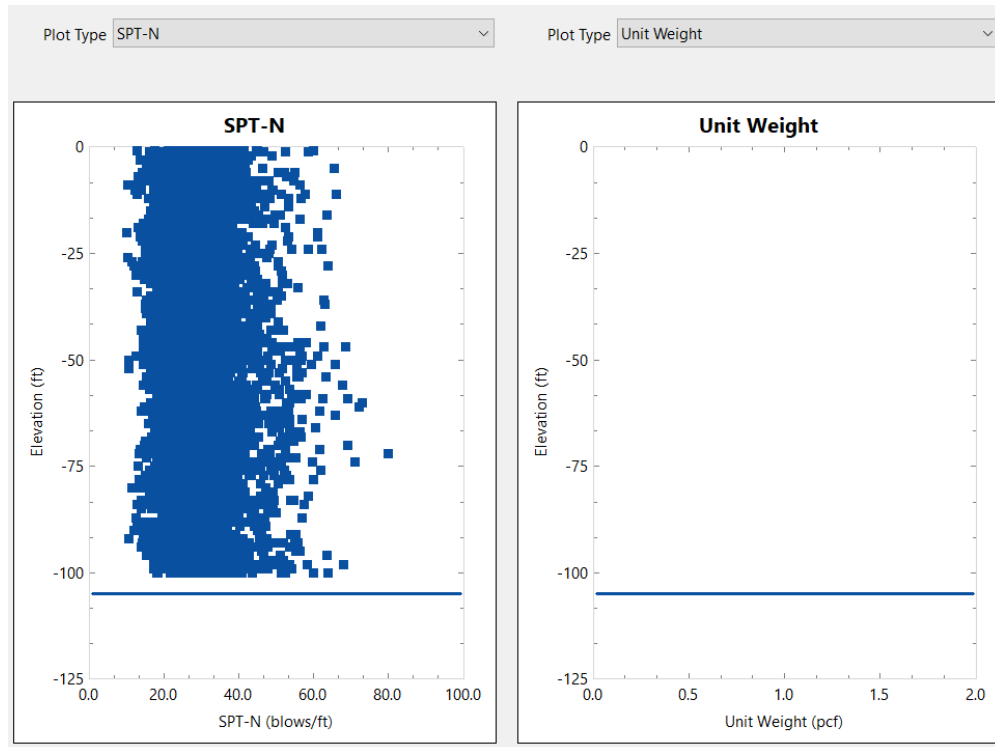


Figure 80. Plots of elevation vs. SPT-N (left) and elevation vs. Unit Weight (right)

Shown in Fig. 81 is a plot of elevation vs. Rock Recovery (left side of Fig. 81) and a plot of elevation vs. q_u (right side of Fig. 81) for an illustrative data file associated with a drilled shaft analysis that makes use of core-run data. Shown in Fig. 82 are the different options available for the soil property that is to be plotted against elevation for the plot on the left side of Fig. 80 and Fig. 81. To view the plot of a different soil property vs. elevation, select the desired soil property from the dropdown menu to the right of the label Plot Type. Changing the plot type in this manner can be performed independently for the plot on the left side and the plot on the right side of Fig. 80 and Fig. 81, respectively. See the discussion in Sec. 4.3 for options regarding how q_u (and/or q_t) values are paired with RQD (and/or Rock Recovery).

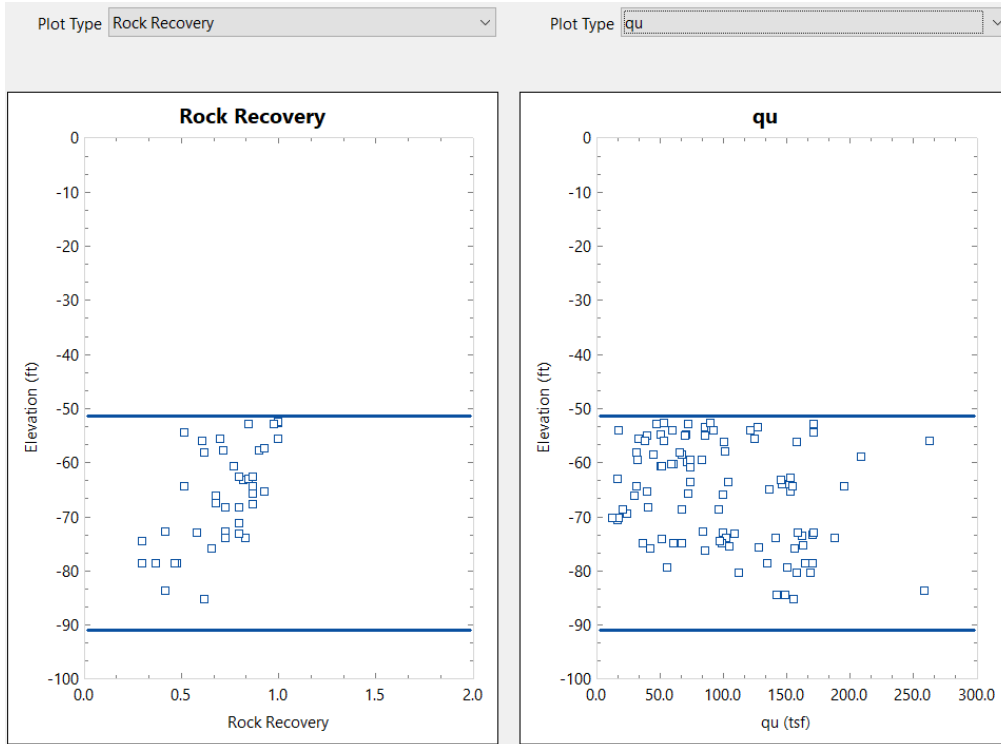


Figure 81. Plots of elevation vs. Rock Recovery and elevation vs. q_u

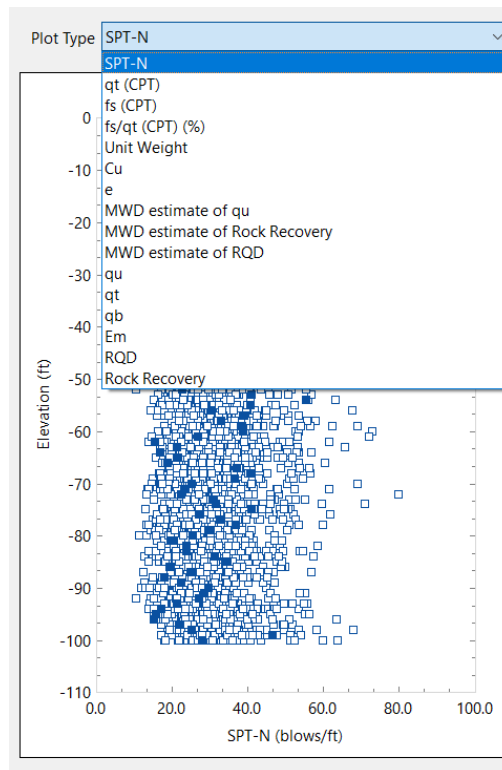


Figure 82. Menu of soil parameters that can be plotted against elevation

4.5 Geostatistics Tab

Spatial correlation structures are determined for included soil or rock layers (based on layering defined in the Profile tab) using controls distributed throughout the Geostatistics tab (Fig. 83). There are several distinct regions of user input data in this tab, including: (1) Layer Selection and Generate Variogram Points; (2) Process Layer and Process Layers; and, (3) Layer Variograms table (as highlighted in Fig. 83). There are also distinct regions of output in this tab: (4) Variogram Point Data; (5) Elevation vs. soil parameter plot; (6) Histogram plot; (7) Horizontal Variogram plot; (8) Vertical Variogram plot; and (9) Export options (also highlighted in Fig. 83). The various regions of the Geostatistics tab are discussed in the remainder of Sec. 4.5.

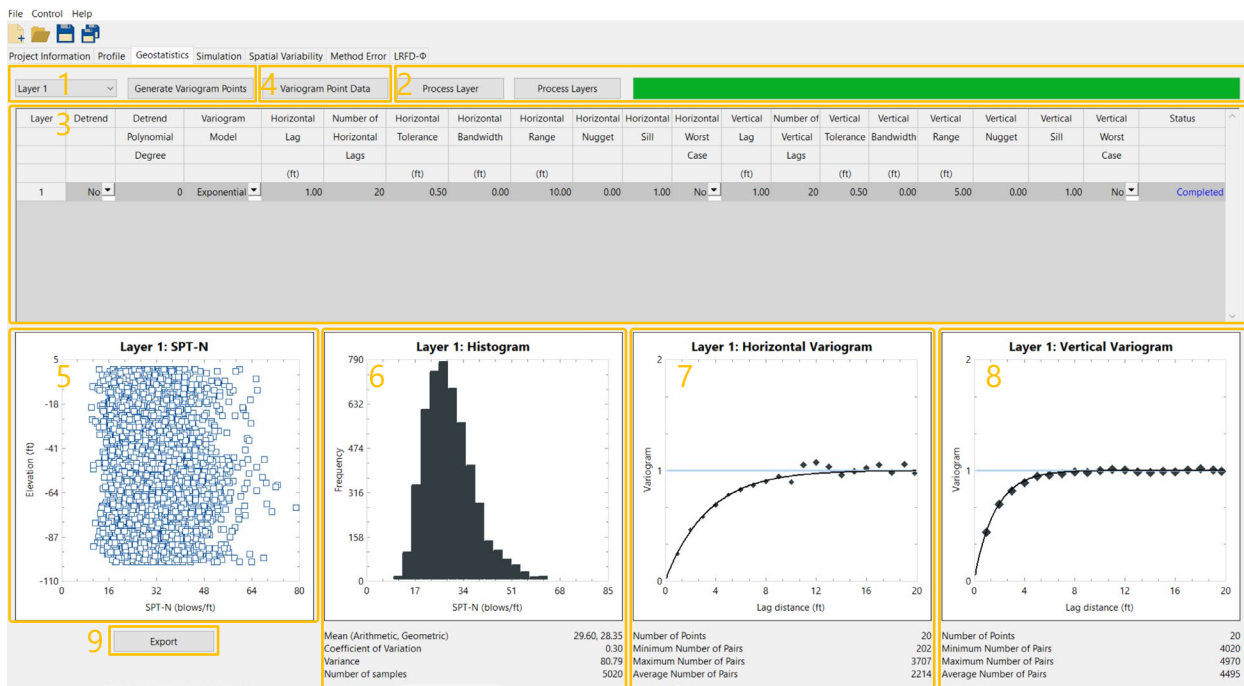


Figure 83. Geostatistics tab

4.5.1 Layer Selection and Generate Variogram Controls

Located in the upper-left portion of the Geostatistics tab are the Layer Selection and Generate Variogram controls (Fig. 84). Soil-spatial parameters are computed for the layer selected in the dropdown menu present on the left side of this frame by pressing the Generate Variogram button. Upon clicking the Generate Variogram button, the program issues a warning message (and indicate the specific issue) in the event that variogram points cannot be generated for a given layer. When valid data are input and variograms can be formed, the two bottom-right plots of Fig. 83 (horizontal and vertical variograms, respectively) are populated with plot points.

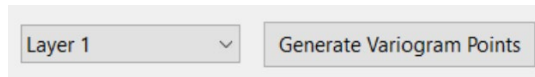


Figure 84. Layer Selection and Generate Variogram Points frame

4.5.2 Process Layer(s) Buttons

Located in the upper-middle and upper-right portions of the Geostatistics tab are the Process Layer and Process Layers buttons, as well as an associated progress bar (Fig. 85). Upon clicking either the Process Layer or Process Layers buttons, the program issues a warning message (and indicates the specific issue) in the event that variogram points cannot be generated. If the desire is to generate variogram points and process the currently selected layer, then Process Layer button should be clicked. Otherwise, if the desire is to generate variogram points and process all layers, then the Process Layers button should be clicked. When valid data are input and variograms can be formed, the two bottom-right plots of Fig. 83 (horizontal and vertical variograms, respectively) are populated with plot points. After this operation is complete, the progress bar will become fully green. Note that the Process Layers button only needs to be pressed one time, regardless of the number of layers that are defined (and included) for analysis.



Figure 85. Process Layer(s) buttons and progress bar

4.5.3 Layer Variograms Table

Insets of the Layer Variograms table are presented in Fig. 86 and Fig. 87, with additional context provided in Fig. 88. Two particularly essential parameters for generating variograms are the lag distance (the distance interval at which to search for pairs of data points) and the number of lag intervals. Note that the site data pertaining to each layer (e.g., SPT, q_u) can also be detrended, where this concept is further discussed in the Technical Manual.

Layer	Detrend	Detrend	Variogram	Horizontal	Number of	Horizontal	Horizontal	Horizontal	Horizontal	Horizontal	Horizontal
		Polynomial	Model	Lag	Horizontal	Tolerance	Bandwidth	Range	Nugget	Sill	Worst
		Degree			Lags						Case
				(ft)		(ft)	(ft)				
1	No	0	Exponential	1.00	20	0.50	0.00	10.00	0.00	1.00	No

Figure 86. Layer Variograms table (left portion)

Vertical Lag	Number of Vertical Lags	Vertical Tolerance	Vertical Bandwidth	Vertical Range	Vertical Nugget	Vertical Sill	Vertical Worst Case	Status
(ft)		(ft)	(ft)					
1.00	20	0.50	0.00	5.00	0.00	1.00	No	Completed

Figure 87. Layer Variograms table (right portion)

Geometric parameters given in the Layer Variograms table are used for searching out and identifying pairs of data points, where the geometric search terms are defined in the schematic of Fig. 88. Searches for pairs of data points are divided into discrete distances ranging from the lag distance up to, and including, the product of the lag distance and number of lags.

Both the tolerance and bandwidth terms are used to define the search domain associated with a given, current lag distance. Tolerance is parallel to the search direction while bandwidth is perpendicular to the search direction. The tolerance is generally limited to one half of the respective base lag distance (i.e., one half of the Horizontal Lag, one half of the Vertical Lag).

With respect to each applicable search direction (horizontal, vertical), the search process is repeated for every data point to identify point pairs. Variogram ordinate values are then computed by operating on distances between pairs of data points. Additional details are found in McVay et al. (2012) and provided in the program Technical Manual.

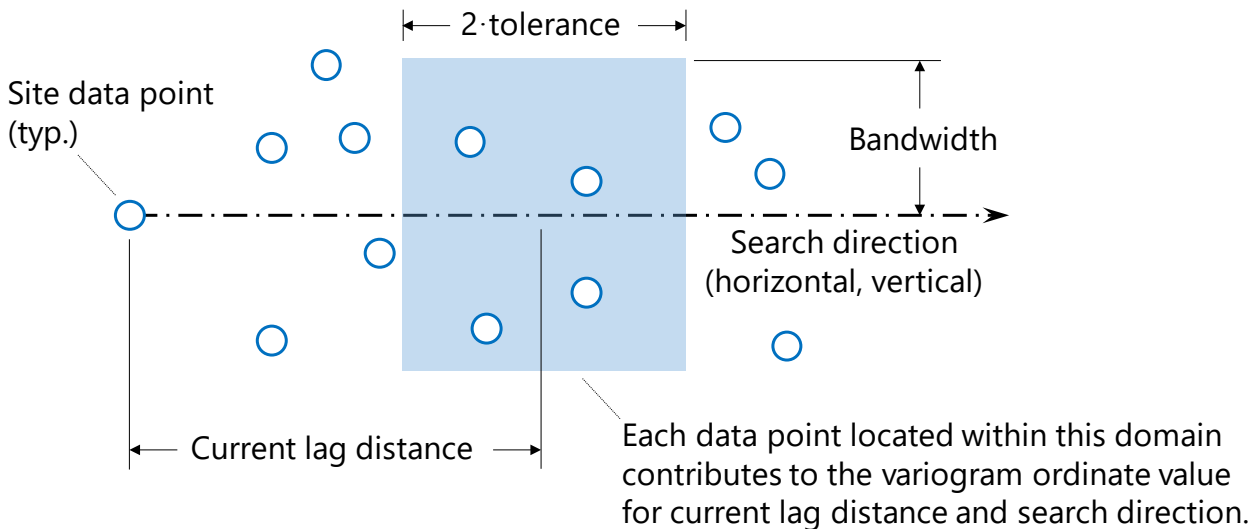


Figure 88. Geometric search terms in Layer Variograms table (adapted from McVay et al. 2012)

If any one of the Horizontal Lag, Number of Horizontal Lags, Vertical Lag, or Number of Vertical Lags are input as non-positive, then the program issues a warning upon any attempts at generating variogram data for the offending layer(s). After successful generation of variograms the Status column in the Layer Variograms table (Fig. 87) indicates that layer processing has "Completed".

4.5.4 Variogram Point Data Dialog

Located in the upper-left portion of the Geostatistics tab is the Variogram Point Data button, which when clicked, causes the Variogram Data dialog to appear. Upon clicking the Variogram Point Data button, the Variogram Point Data dialog appears (Fig. 89), which displays the horizontal and vertical variogram data associated with the currently selected layer in the Layer Variograms table. For both the horizontal and vertical variograms, the Variogram Point Data dialog lists computed values of Lag Distance, the Variogram Value at each distance, and the number of pairs found at each lag distance.

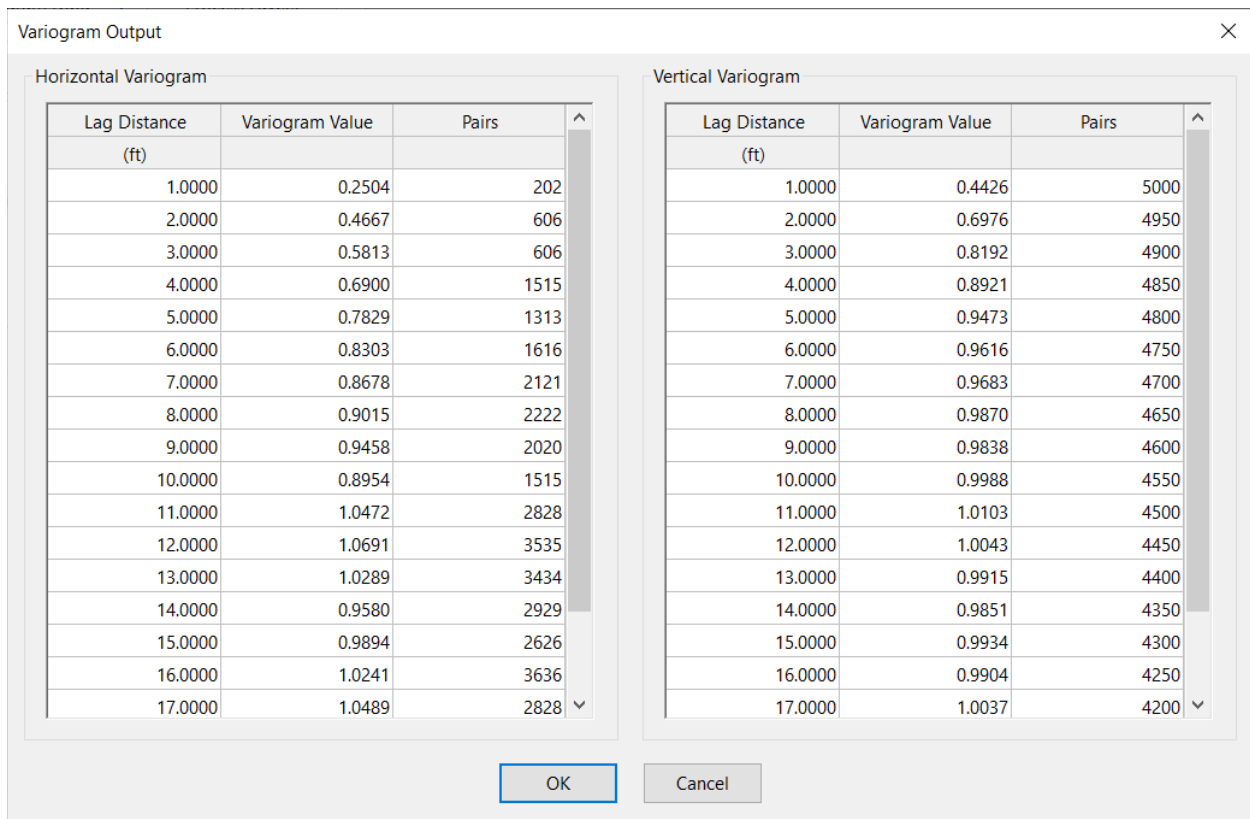


Figure 89. Variogram Point Data dialog

4.5.5 Elevation vs. Soil Properties Plot

Positioned in the lower-left portion of the Geostatistics tab is a scatterplot, which displays profiles of soil data for a selected layer. For driven piles, the relevant type of soil data is that of either SPT-N values, or if analyzing CPT data, cone resistance (q_t (CPT)) values. For drilled shaft foundations being analyzed using core-run data, and when a layer of the type Limestone/Very Shelly Sand is active, then unconfined compression strength (q_u) values are displayed. For analysis with use of MWD data, when layers of type Limestone/Very Shelly Sand are selected, then MWD-based estimates of unconfined compressive strength are displayed (as estimated from specific energy, see the Technical Manual for additional details).

Shown in Fig. 90 is a plot of elevation vs. SPT-N using a purely illustrative set of layer data. In the case of a drilled shaft analysis, the Elevation vs. Soil Properties plot will become a plot of elevation vs. SPT-N for each data point within the borings/corings present in the layer currently selected in the Layer Selection and Generate Variogram frame (recall Fig. 84). Shown in Fig. 91 is such a plot, generated from an input data file intended for use with core-run data and drilled shaft analysis.

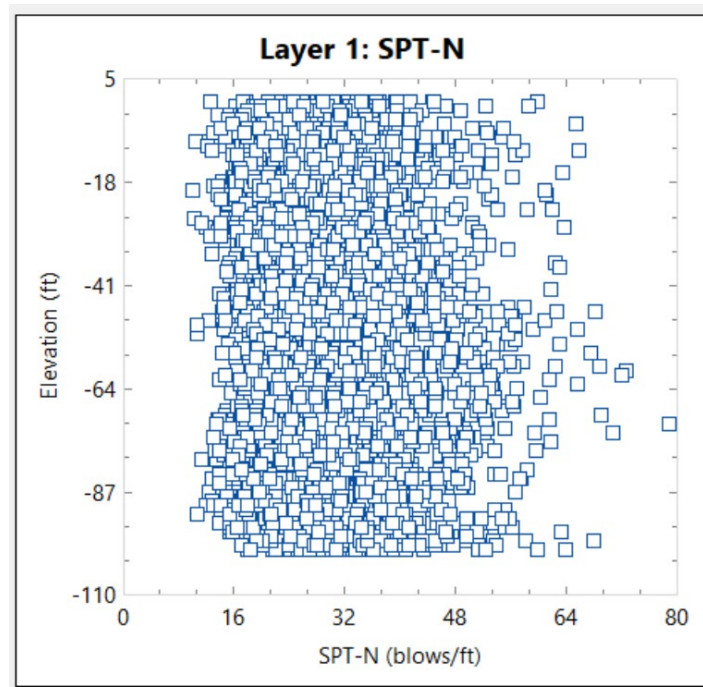


Figure 90. Plot of elevation vs. SPT-N for a selected layer

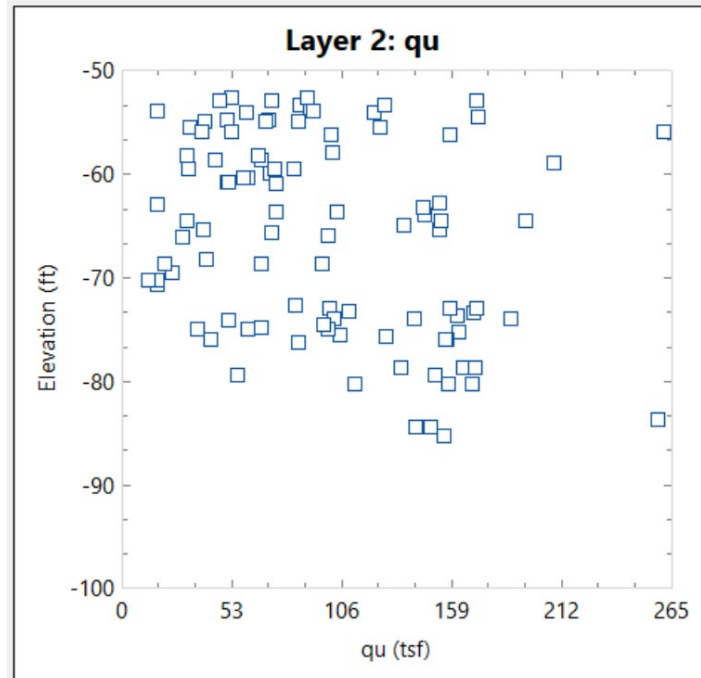


Figure 91. Plot of elevation vs. q_u for a selected layer

4.5.6 Histogram Plot

Shown in Fig. 92 is a histogram of SPT-N (blow count) values, using purely illustrative data, for the borings/corings corresponding to the scatterplot displayed in Fig. 90. Displayed immediately below the histogram are corresponding values of mean (arithmetic, geometric), covariance, variance, and number of samples pertaining to the selected layer.

For instances where CPT data (more specifically, cone resistance, q_t (CPT)) were being utilized within a layer, then the histogram would correspondingly be comprised of q_t (CPT) values. Further, for Limestone/Very Shelly Sand layers associated with core-run data and drilled shafts, the corresponding histograms would correspond to unconfined compressive strength (q_u). Still further, for Limestone/Very Shelly Sand layers associated with MWD data and drilled shaft foundations, then MWD-estimated values of unconfined compressive strength would be used to populate the histogram plots.

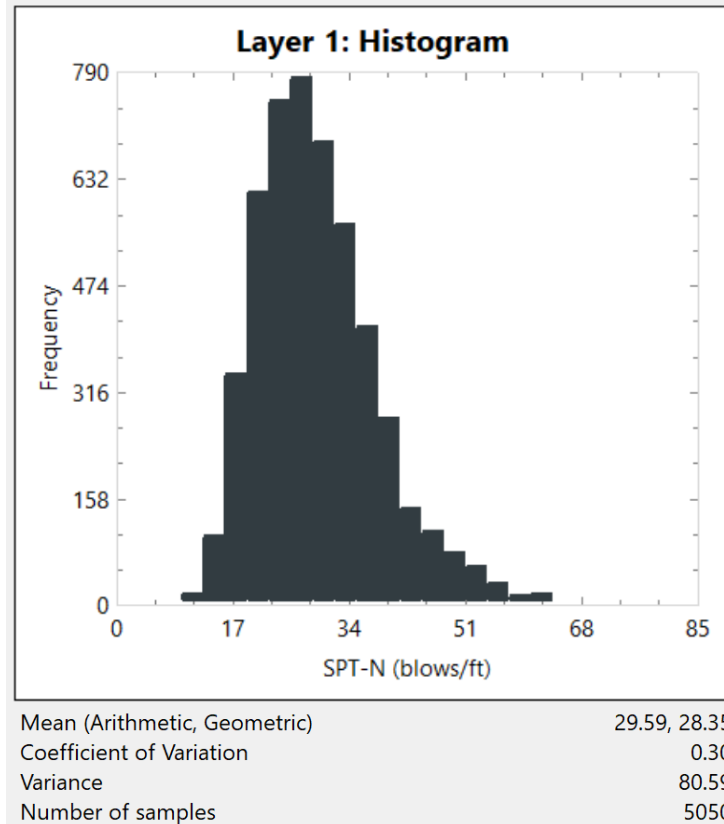


Figure 92. Histogram of SPT-N values

4.5.7 Horizontal Variogram Plot

Shown in Fig. 93 is the horizontal variogram of the layer currently selected in the Layer Selection and Generate Variogram frame (recall Fig. 84). Displayed below the plot are the number of points, minimum number of pairs per point, maximum number of pairs per point, and average number of pairs per point. Dragging the black curve upwards will increase the horizontal sill (and vice versa), and dragging the black curve to the right will increase the horizontal range (and vice versa). These changes are reflected in real-time in the Layers Variogram table (recall Fig. 86).

Three distinct curves are displayed in the horizontal variogram plot. Solid black diamonds indicate the horizontal variogram points obtained from processing the layer-specific data with respect to the horizontal lag distances. Note that the size of each black diamond reflects the number of pairs that are associated with the respective plot point. In addition, the normalized sill of 1.0 is displayed as a constant-valued, soft blue line. Third, the thin black line indicates the current mathematical fit (either exponential or spherical) to the horizontal variogram data points.

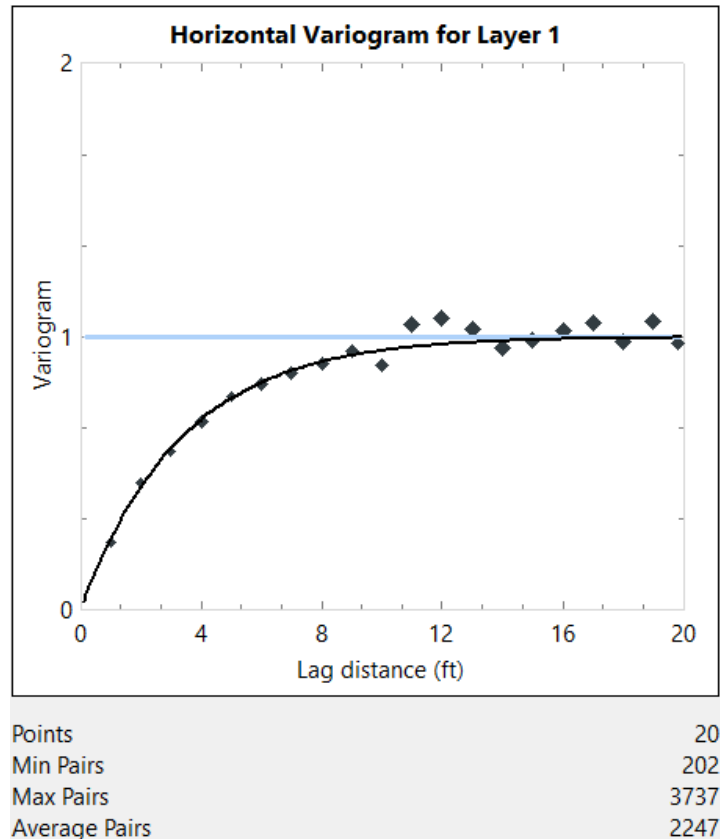


Figure 93. Horizontal variogram for a selected layer

4.5.8 Vertical Variogram Plot

Shown in Fig. 94 is the vertical variogram of the layer currently selected in the Layer Selection and Generate Variogram frame (recall Fig. 84). Displayed below the plot are the number of points, minimum number of pairs per point, maximum number of pairs per point, and average number of pairs per point. Dragging the black curve upwards will increase the vertical sill (and vice versa), and dragging the black curve to the right will increase the vertical range (and vice versa). These changes are reflected in real-time the corresponding row of the Layers Variogram table (recall Fig. 86).

Three distinct curves are displayed in the vertical variogram plot. Solid black diamonds indicate the vertical variogram points obtained from processing the layer-specific data with respect to the vertical lag distances. Note that the size of each black diamond reflects the number of pairs that are associated with the respective plot point. In addition, the normalized sill of 1.0 is displayed as a constant-valued, soft blue line. Third, the thin black line indicates the current mathematical fit (either exponential or spherical) to the vertical variogram data points.

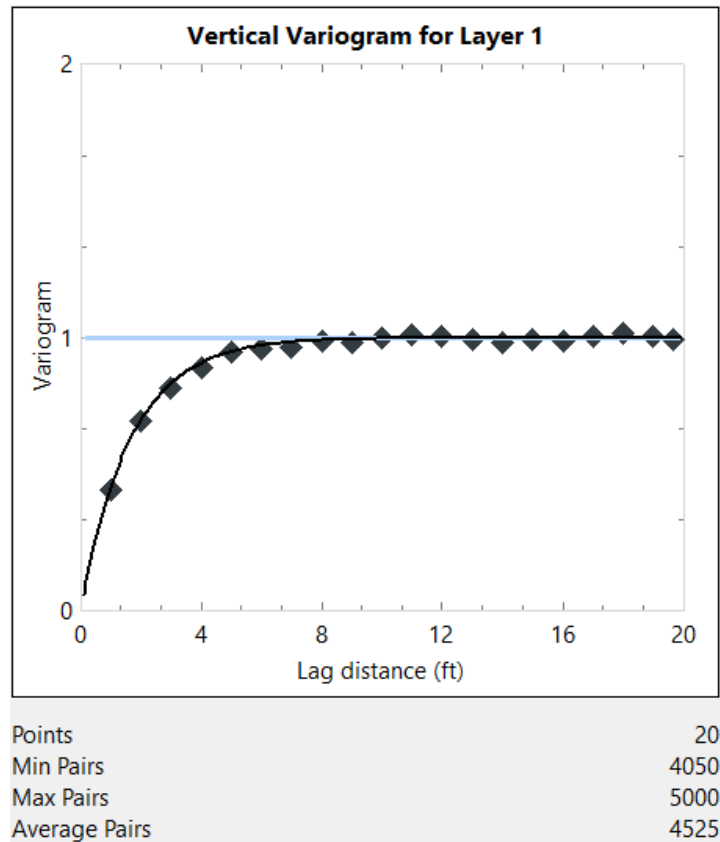


Figure 94. Vertical variogram for a selected layer

4.5.9 Export Layer Data

Clicking the Export button on the Geostatistics tab (Fig. 83, bottom-left) generates and opens an Excel file containing the values used in generating the elevation vs. soil properties scatterplot (e.g., Fig. 90) and histogram plot (e.g., Fig. 92). The Excel workbook tab titled "Scatter" contains the elevation of a given data point in column "A" and the value of the data point in column "B".

For instances where driven piles are being considered in association with analysis of SPT data, or drilled shafts in clayey or sandy soils are considered, then column "B" will display SPT-N values (as displayed for an illustrative data set in Fig. 95). For analysis of driven piles in association with CPT data, then values of cone resistance (q_t (CPT)) will be utilized. For instances where Limestone/Very Shell Sand layers are being considered along with core-run data for analysis of drilled shaft foundations, then column "B" will display q_u values (such as those shown for illustrative purposes in Fig. 96). When drilled shafts are being considered in

conjunction with MWD data, then MWD-based estimates of unconfined compressive strength will be displayed under column "B".

	A	B
1		
2	Elevation	SPT-N
3	(ft m)	(blows/ft blows/300mm)
4	0.0000	29
5	0.0000	35
6	0.0000	31
7	0.0000	21
8	0.0000	25
9	0.0000	45
10	0.0000	26
11	0.0000	35
12	0.0000	30
13	0.0000	25
14	0.0000	34
15	0.0000	26
16	0.0000	33
17	0.0000	31
18	0.0000	24
19	0.0000	27
20	0.0000	28
21	0.0000	33
22	0.0000	29
23	0.0000	32
24	0.0000	27
25	0.0000	24
26	0.0000	18
27	0.0000	40
28	0.0000	45
29	0.0000	42
30	0.0000	39
31	0.0000	22
32	0.0000	25
33	0.0000	25
34	0.0000	29
35	0.0000	37
36	0.0000	41
37	0.0000	29
38	0.0000	23
39	0.0000	23

Figure 95. "Scatter" worksheet tab for an illustrative driven pile data set (the first 35 out of 5050 total data points are displayed)

	A	B
1		
2	Elevation	qu
3	(ft m)	(tsf kPa)
4	0.0000	1.93
5	0.0000	2.33
6	0.0000	2.07
7	0.0000	1.40
8	0.0000	1.67
9	0.0000	3.00
10	0.0000	1.73
11	0.0000	2.33
12	0.0000	2.00
13	0.0000	1.67
14	0.0000	2.27
15	0.0000	1.73
16	0.0000	2.20
17	0.0000	2.07
18	0.0000	1.60
19	0.0000	1.80
20	0.0000	1.87
21	0.0000	2.20
22	0.0000	1.93
23	0.0000	2.13
24	0.0000	1.80
25	0.0000	1.60
26	0.0000	1.20
27	0.0000	2.67
28	0.0000	3.00
29	0.0000	2.80
30	0.0000	2.60
31	0.0000	1.47
32	0.0000	1.67
33	0.0000	1.67
34	0.0000	1.93
35	0.0000	2.47
36	0.0000	2.73
37	0.0000	1.93
38	0.0000	1.53
39	0.0000	1.53

Figure 96. "Scatter" worksheet tab for an illustrative data set involving Limestone/Very Shell Sand layer and core-run data for a drilled shaft foundation (only the first 35 out of 5050 total data points are displayed)

The workbook tab titled "Histogram" contains consecutive, non-overlapping ranges of data in Column "A" and the frequency of data between those interval bounds in column "B". For instances where driven piles are being considered in association with analysis of SPT data, or drilled shafts in clayey or sandy soils are considered, then column "A" will display interval bounds for SPT-N values (as displayed for an illustrative data set in Fig. 97). For analysis of driven piles in association with CPT data, then values of cone resistance (q_t (CPT)) will be

utilized. For instances where Limestone/Very Shell Sand layers are being considered along with core-run data for analysis of drilled shaft foundations, then column "A" will display interval bounds for q_u values (such as those shown for illustrative purposes in Fig. 98). When drilled shafts are being considered in conjunction with MWD data, then intervals associated with MWD-based estimates of unconfined compressive strength will be displayed under column "A".

	A	B
1		
2	SPT-N	Frequency
3	(blows/ft blows/300mm)	
4		2
5		5
6		8
7		11
8		14
9		18
10		21
11		24
12		27
13		30
14		34
15	These values indicate	37
16	histogram bin extents	40
17	(left-open, right-closed)	43
18		46
19		50
20		53
21		56
22		59
23		62
24		65
25		69
26		72
27		75
28		78
		0
		0
		0
		16
		102
		343
		613
		749
		788
		687
		565
		413
		277
		144
		110
		79
		58
		32
		14
		16
		5
		5
		3
		0
		1

Figure 97. "Histogram" worksheet tab for an illustrative driven pile data set (note: the SPT-N blow count values listed indicate the histogram bin extents with a left-open, right closed convention)

	A	B
1		
2	qu	Frequency
3	(tsf kPa)	
4	0.107	0
5	0.320	0
6	0.532	0
7	0.745	16
8	0.958	103
9	1.171	343
10	1.384	616
11	1.597	754
12	1.810	797
13	2.023	693
14	2.236	563
15	2.449	420
16	2.662	277
17	2.875	145
18	3.088	110
19	3.301	79
20	3.514	58
21	3.727	32
22	3.940	14
23	4.153	16
24	4.366	5
25	4.579	5
26	4.792	3
27	5.005	0
28	5.218	1

Figure 98. "Histogram" worksheet tab for a drilled shaft data set (within a Limestone/Very Shelly Sand layer)

4.6 Simulation Tab

Shown in Fig. 99 is the fourth of seven program tabs, the Simulation tab, wherein controls are dedicated to defining the foundation member configuration and conducting statistical simulation. There are eight distinct regions of user input data in this tab: (1) General Geometry frame; (2) Shaft Geometry frame; (3) Pile Geometry frame; (4) Foundation Member Material Properties frame; (5) Soil frame; (6) Layer Separation frame; (7) Simulation frame; and, (8) Run Simulation controls (all highlighted in Fig. 99). There is also one distinct region of display-only (i.e., non-editable) output in this tab: (9) Soil-Spatial Parameters (also highlighted in Fig. 99). The nine regions of the Simulation tab are discussed in the remainder of Sec. 4.6.

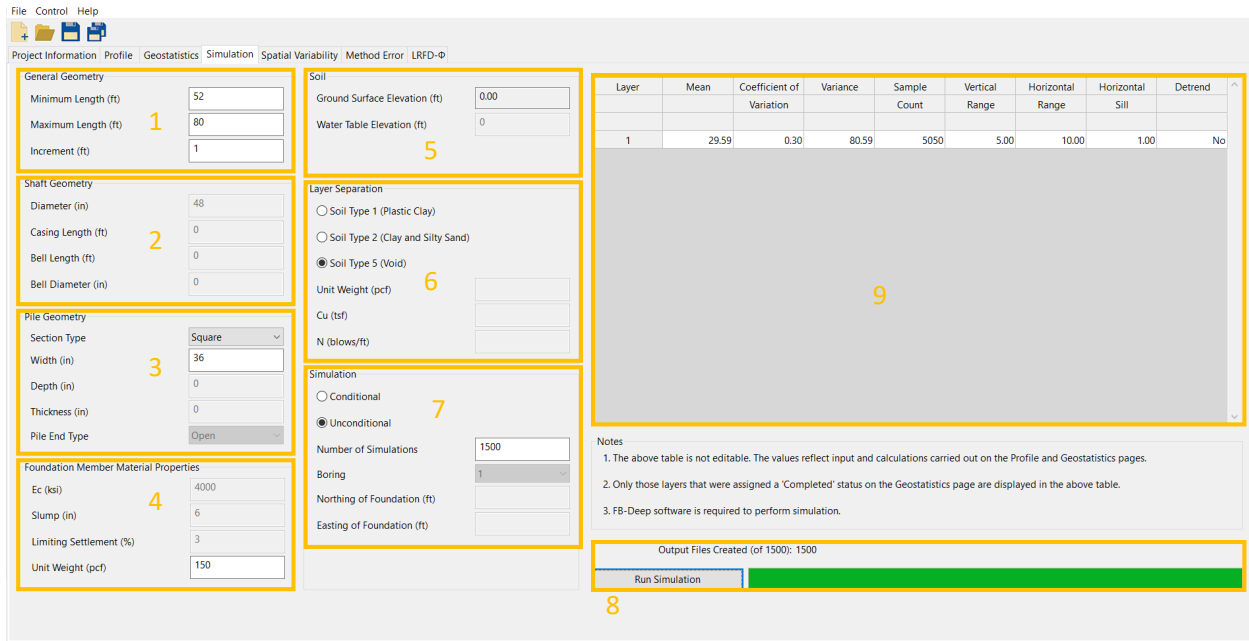


Figure 99. Simulation tab

4.6.1 General Geometry Frame

Located in the upper-left portion of the Simulation tab is the General Geometry frame (an inset is shown in Fig. 100). Within the frame are the controls that dictate the range and increment of embedment lengths to consider during simulation. To protect against formation of improper data in the numerous analysis model files (generated as part of the statistical simulation), only positive values are permitted to be entered. In addition, the program ensures that the range of embedment lengths fall within the soil or rock profile (as defined using controls on the Profile tab, recall Fig. 76). Specific to GeoStat models of pile members, and depending on the soil or rock layering, the program further ensures that adequate soil or rock layering is available given the input value of Maximum Length (e.g., 3.5 pile diameters below and 8.0 pile diameters above for end bearing calculations).

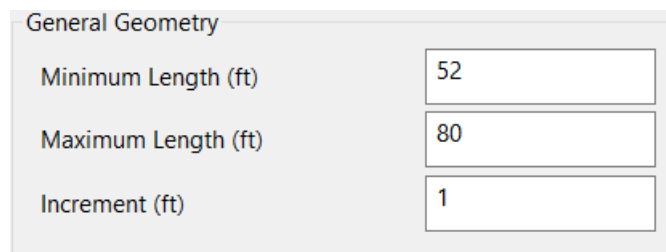
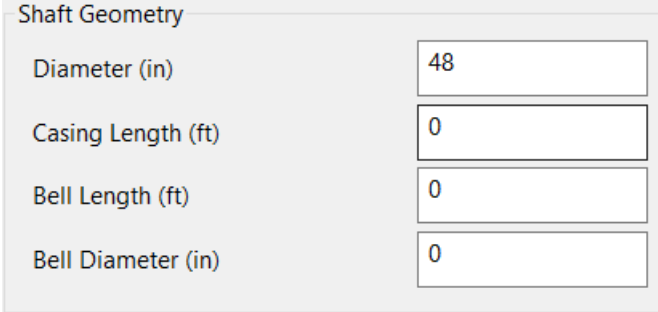


Figure 100. General Geometry frame

4.6.2 Shaft Geometry Frame

For models involving drilled shaft foundations, controls within the Shaft Geometry frame (Fig. 101) are enabled. The program enforces input of only positive-valued entries for Diameter. However, inputs for Casing Length, Bell Length, and Bell Diameter are permitted to be input as equal to or greater than zero.

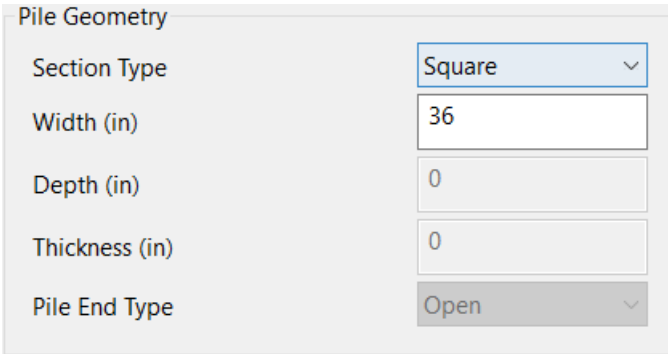


Shaft Geometry	
Diameter (in)	48
Casing Length (ft)	0
Bell Length (ft)	0
Bell Diameter (in)	0

Figure 101. Shaft Geometry frame

4.6.3 Pile Geometry Frame

For modeling of driven piles, certain controls within the Pile Geometry frame (Fig. 102) are enabled. More specifically, depending on the selection of Section Type, only those parameters required to describe the cross-section (for the purposes of soil or rock axial-capacity simulations) become enabled. The section types that can be considered include: Square, Round, Pipe, Cylinder, and H-Section. For square piles, only the Width parameter is required. Regardless of which input parameters are required for a pile cross-section, the program accepts only those that are positive (and otherwise issues a warning). For round piles, only the Width parameter is required (Fig. 103). For a pipe pile, only the Width and Thickness parameters are required (Fig. 104). For a cylindrical pile, only the Width, Thickness, and Pile End Type parameters are required (Fig. 105). For a pile with an H-Section geometry, only the Width and Depth parameters are required (Fig. 106).



Pile Geometry	
Section Type	Square
Width (in)	36
Depth (in)	0
Thickness (in)	0
Pile End Type	Open

Figure 102. Pile Geometry frame for square piles

Pile Geometry	
Section Type	Round
Width (in)	36
Depth (in)	0
Thickness (in)	0
Pile End Type	Open

Figure 103. Pile Geometry frame for round piles

Pile Geometry	
Section Type	Pipe
Width (in)	36
Depth (in)	0
Thickness (in)	0
Pile End Type	Open

Figure 104. Pile Geometry frame for pipe piles

Pile Geometry	
Section Type	Cylinder
Width (in)	36
Depth (in)	0
Thickness (in)	0
Pile End Type	Open

Figure 105. Pile Geometry frame for cylindrical piles

Pile Geometry	
Section Type	H-Section
Width (in)	36
Depth (in)	0
Thickness (in)	0
Pile End Type	Open

Figure 106. Pile Geometry frame for piles with an H-Section Geometry

4.6.4 Foundation Member Material Properties Frame

Material properties of foundation members are specified in the Foundation Member Material Properties frame (Fig. 107 and Fig. 108). Only Unit Weight (Fig. 107) must be supplied when modeling driven piles (the other three controls are disabled for such cases). In contrast, for drilled shaft models (Fig. 108), four parameters are required (modulus of elasticity, E_c ; Slump; Limiting Settlement; and, Unit Weight). Regardless of the foundation member type being modeled, all enabled controls within this frame are checked to prevent input of non-positive values.

Foundation Member Material Properties	
E_c (ksi)	4000
Slump (in)	6
Limiting Settlement (%)	3
Unit Weight (pcf)	150

Figure 107. Foundation Member Material Properties frame for a driven pile

Foundation Member Material Properties	
Ec (ksi)	4000
Slump (in)	6
Limiting Settlement (%)	3
Unit Weight (pcf)	150

Figure 108. Foundation Member Material Properties frame for a drilled shaft

4.6.5 Soil Frame

In order to establish relative positioning of the pile/shaft within the user-defined soil or rock layering, the Ground Surface Elevation must be taken into account. Although this parameter is automatically calculated by the program based on data input on the Profile tab, it is displayed within the Soil frame as a convenience to the engineer (Fig. 109). For drilled shafts, the input box for the Water Table Elevation will be enabled and must also be input.

Soil	
Ground Surface Elevation (ft)	0.00
Water Table Elevation (ft)	0

Figure 109. Soil frame

4.6.6 Layer Separation Frame

Recall that soil or rock layerings are defined from within the UI Profile tab, and can be defined as consisting of any of four soil or rock types (as well as a fifth type corresponding to a void). For generation of analysis model files, the layerings are subdivided into 0.5-ft increments (referred to in this context as sublayers). A subset of the available layer types may be specified for defining those sublayers that fall at the boundaries of layers that are defined on the Profile tab. By default, and as a conservative measure, these “bounding” sublayers (or, layer separators) are designated as Soil Type 5 (Void). If the layer separation consists of a void (Soil Type 5), then the engineer is not required to specify any additional properties. (Fig. 110).

Layer Separation

Soil Type 1 (Plastic Clay)

Soil Type 2 (Clay and Silty Sand)

Soil Type 5 (Void)

Unit Weight (pcf)

Cu (tsf)

N (blows/ft)

Figure 110. Layer Separation frame inputs for Soil Type 5 (Void)

If the layer separation is defined as Soil Type 1 (Plastic Clay), then the engineer must additionally specify representative values of Unit Weight and undrained shear strength, C_u (Fig. 111). If the layer separation is defined as Soil Type 2 (Clay and Silty Sand), then the engineer must specify the Unit Weight and N of the soil (Fig. 112). Note that these latter two selections should be made with caution as use of non-representative parameter values may lead to unconservative predictions of member resistance.

Layer Separation

Soil Type 1 (Plastic Clay)

Soil Type 2 (Clay and Silty Sand)

Soil Type 5 (Void)

Unit Weight (pcf)

Cu (tsf)

N (blows/ft)

Figure 111. Layer Separation frame inputs for Soil Type 1 (Plastic Clay)

Layer Separation

Soil Type 1 (Plastic Clay)
 Soil Type 2 (Clay and Silty Sand)
 Soil Type 5 (Void)

Unit Weight (pcf)

Cu (tsf)

N (blows/ft)

Figure 112. Layer Separation frame inputs for Soil Type 2 (Clay and Silty Sand)

4.6.7 Simulation Frame

Positioned in the lower right portion the Simulation tab is the Simulation frame (Fig. 113). The Simulation frame contains input controls that determine the overall nature of the probabilistic simulation. Namely, either a Conditional (data from nearby borings) or Unconditional (pile/shaft outside of correlation length) simulation can be conducted. In the case of an Unconditional simulation, a value is only needed for Number of Simulations. This parameter dictates the total number of realizations to be generated and then packaged (along with pile/shaft data) into model analysis files, which adhere to FB-Deep input format requirements.

Simulation

Conditional
 Unconditional

Number of Simulations

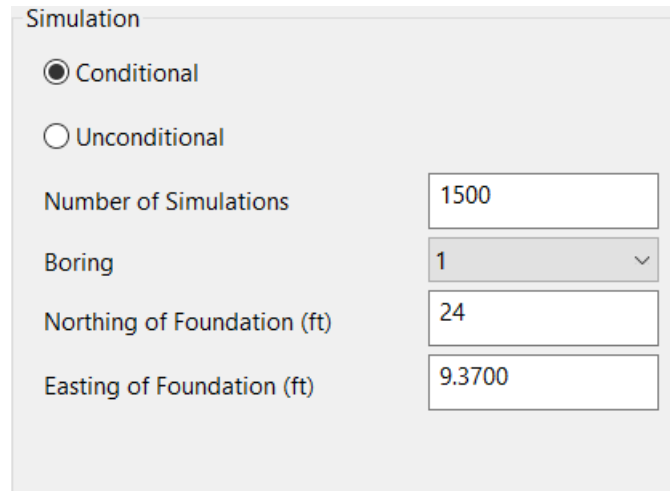
Boring

Northing of Foundation (ft)

Easting of Foundation (ft)

Figure 113. Simulation frame with selection of Unconditional simulation

For Conditional simulations, the Number of Simulations is also required. In addition, the boring nearest to the foundation location being analyzed must be selected from the Boring dropdown menu (Fig. 114). After selecting a boring, the respective positioning values of Northing and Easting will be displayed, and can be further adjusted as appropriate.



The image shows a software interface titled "Simulation". It contains two radio buttons: "Conditional" (which is selected) and "Unconditional". Below these are five input fields: "Number of Simulations" with the value "1500", "Boring" with a dropdown menu showing "1", "Northing of Foundation (ft)" with the value "24", and "Easting of Foundation (ft)" with the value "9.3700".

Figure 114. Simulation frame with selection of Conditional simulation

Faraone (2014) recommended that a minimum of 1000 realizations be considered when conducting stochastic simulation. As reported in McVay et al. (2012), a recommended number of simulations is 2000. For use of GeoStat in design applications, it is recommended that 2000 realizations be considered. See the Technical Manual for additional details.

4.6.8 Run Simulation Button

Positioned in the lower-right portion of the Simulation tab is the Run Simulation button (Fig. 115). Clicking the Run Simulation button prompts GeoStat to first generate the many realizations of soil or rock profiles, taking into account spatial variability phenomena. Next, a folder is created in the same directory as the GeoStat model file and is subsequently populated with model analysis files (one realization corresponds to one input file). Note that the folder name issued is identical to the name of the currently loaded GeoStat model file. Also, the model analysis files satisfy input format requirements required for analysis using the geotechnical axial capacity software, FB-Deep.



Figure 115. Run Simulation button and progress bar

The numerous model analysis files, all stored within the newly created folder, are named using a sequential numbering convention. Therefore, it is useful to save a unique GeoStat input file for each unique instance of carrying out the simulations. Additional details on creation of the model analysis files, and interfacing of the GeoStat UI with analysis executables are provided in Ch. 5.

4.6.9 Soil-spatial Parameters Table

Positioned in the upper right portion the Simulation tab is the Soil-spatial Parameters table (Fig. 116). This table contains soil-spatial parameters for each active layer, given the input selections made from within the Profile tab (Fig. 76) and Geostatistics tab (Fig. 83). Values listed within the table are not editable. Rather, the listings serve as an intermediate summary of layer data, which in turn, can aid in determining whether or not to proceed with simulations (or alternatively, revisit the Profile and/or Geostatistics tabs to adjust the model data).

Layer	Mean	Coefficient of Variation	Variance	Sample Count	Vertical Range	Horizontal Range	Horizontal Sill	Detrend
1	29.59	0.30	80.59	5050	5.00	10.00	1.00	No

Figure 116. Soil-spatial Parameters table

4.7 Spatial Variability Tab

For any complete sets of simulation files, plots of pile/shaft axial resistance can subsequently be viewed from within the Spatial Variability tab (e.g., the illustrative data plotted in Fig. 117). Plots shown on this tab reflect the boring or coring data, soil or rock layering, spatial correlation structures, and foundation member configuration defined on those UI tabs discussed in Sec. 4.1 through Sec. 4.6. There are two distinct regions of user input data in this tab: (1) Import FB-Deep Output button; and, (2) Plot Legend Frame (both highlighted in Fig. 117). Also, five distinct regions of output controls are located within the Spatial Variability tab: (3) Update Plots and Export buttons; (4) Mean Plot; (5) Variance Plot; (6) Coefficient of Variation Plot; and, (7) Phi Plot (as highlighted in Fig. 117). These seven tab regions are discussed in the remainder of Sec. 4.7.

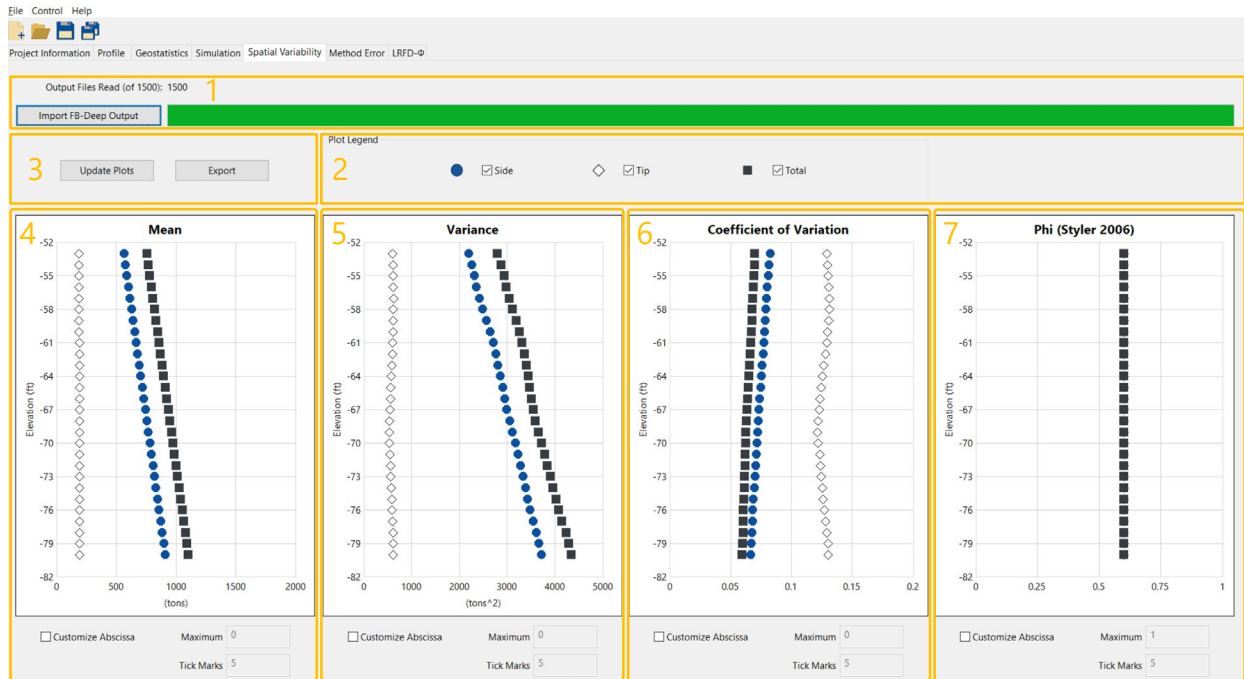


Figure 117. Spatial Variability tab

4.7.1 Import FB-Deep Output Button

Positioned in the upper portion of the Spatial Variability tab is the Import FB-Deep Output button and a paired progress bar (Fig. 118). Pressing the Import FB-Deep Output button opens a menu which allows for the directory containing the model analysis output files of interest to be selected. After the files are imported, the progress bar will become fully green.



Figure 118. Import FB-Deep Output button and progress bar

4.7.2 Plot Legend Frame

The Plot Legend frame allows for the user to select whether or not Side (side friction), Tip (end bearing), and/or Total (total resistance) data points appear on the plots of mean, variance, coefficient of variation, and phi (Fig. 119).

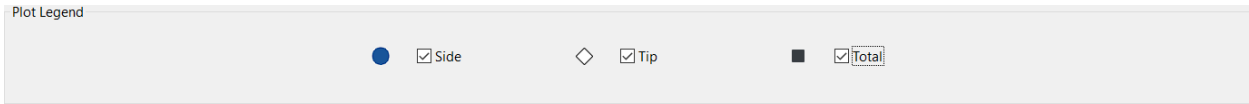


Figure 119. Plot Legend frame

4.7.3 Mean Plot

The Mean plot displays through-depth mean values of one or more of side friction, end bearing, and total resistance. A plot obtained using an illustrative data set is given in Fig. 120. Checking the Custom Abscissa box allows for the abscissa axis to be redrawn using the values input for Max and number of Tick Marks.

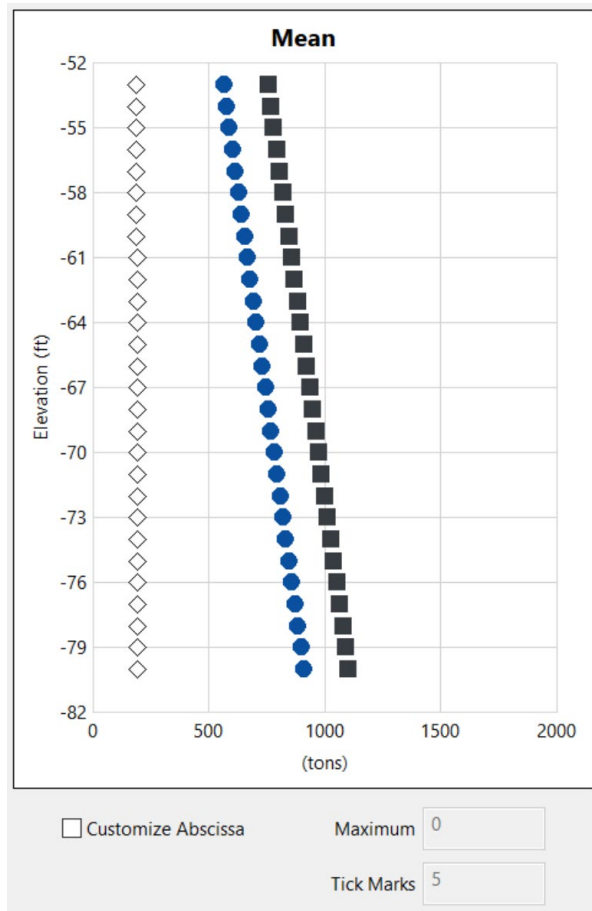


Figure 120. Elevation vs. mean value of axial resistance plot (data for illustration only)

4.7.4 Variance Plot

The Variance plot displays through-depth variances for any (or all) of side friction, end bearing, and total resistance. A plot obtained using an illustrative data set is given in Fig. 121. Checking the Custom Abscissa box allows for the abscissa axis to be redrawn using the values input for Max and number of Tick Marks.

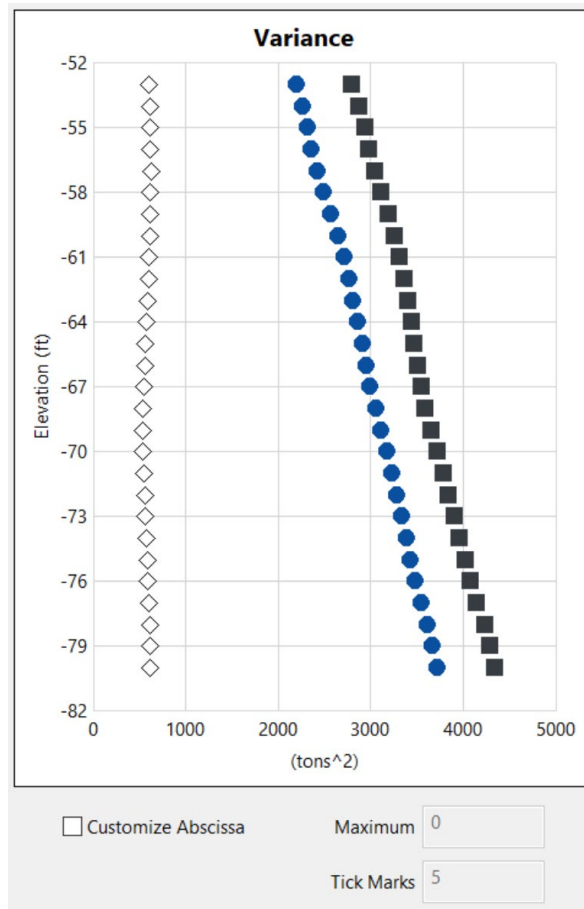


Figure 121. Elevation vs. variance of axial resistance plot (data for illustration only)

4.7.5 Coefficient of Variation Plot

The Coefficient of Variation plot displays through-depth coefficients of variation for side friction, end bearing, and total resistance (or any combination thereof). A plot obtained using an illustrative data set is given in Fig. 122. Checking the Custom Abscissa box allows for the abscissa axis to be redrawn using the values input for Max and number of Tick Marks.

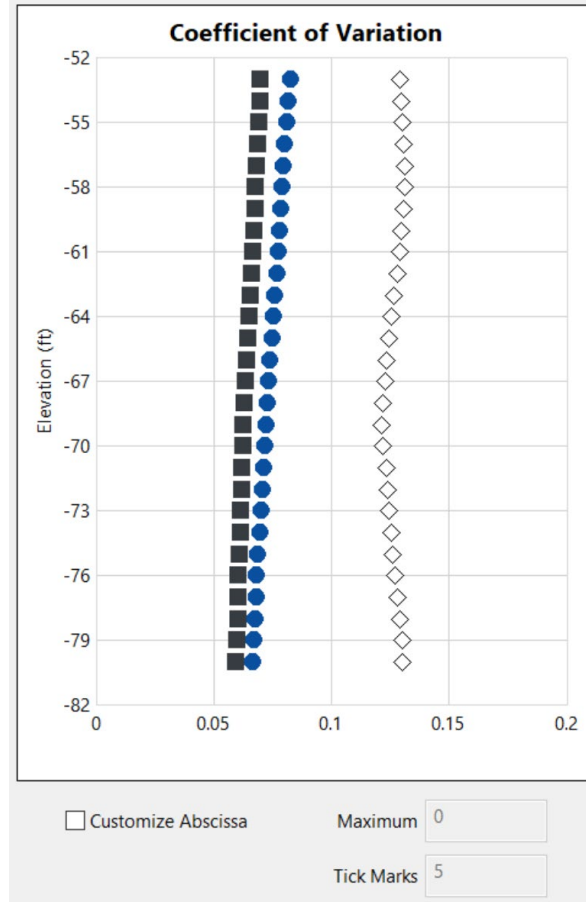


Figure 122. Elevation vs. coefficient of variation of axial resistance plot (data for illustration only)

4.7.6 Phi Plot

The Phi plot displays through-depth mean values of any one (or more) of side friction, end bearing, and total resistance. A plot obtained using an illustrative data set is given in (Fig. 123). Checking the Custom Abscissa box allows for the abscissa axis to be redrawn using the values input for Max and number of Tick Marks.

The resistance (i.e., phi, or ϕ) factors plotted on the Spatial Variability page only take into account the spatial correlation structures associated with the selected site data (and given some layering and set of foundation member parameter values). Calculation and plotting of quantities that incorporate both spatial variability and method error phenomena are documented in Sec. 4.9. Note that: (1) the maximum phi factor can be input from the Project Settings dialog (see Sec. 4.2), where the default value is 0.6; and, (2) either the Styler (2006)

formulation or the NCHRP 507 (Paikowsky, 2004) formulation can be utilized in calculating the phi factor, as specified in the Program Settings dialog (again, see Sec. 4.2).

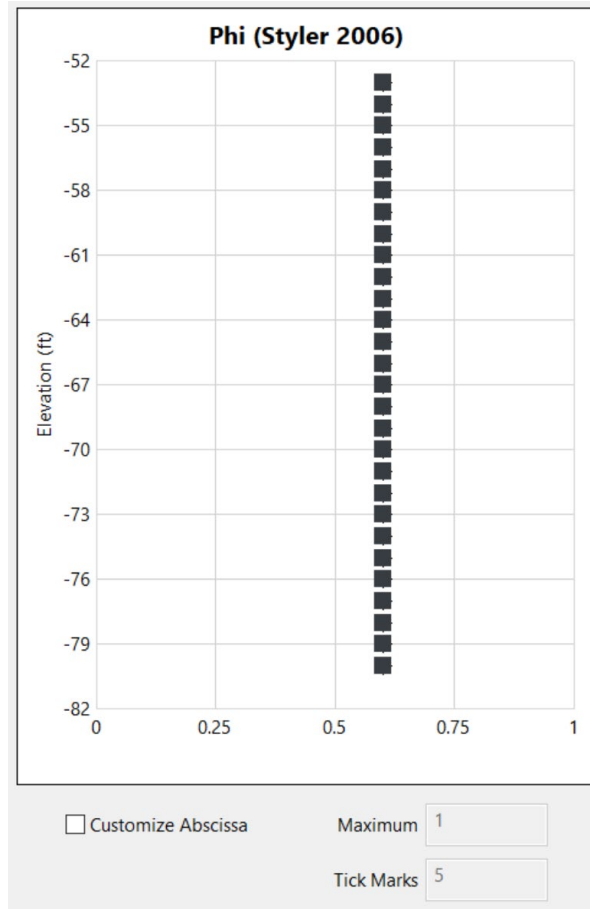


Figure 123. Elevation vs. soil resistance factor (Phi) plot based on soil-spatial variability (data for illustration only)

4.7.7 Update Plots and Export Buttons

The Update Plots button (Fig. 124, left) allows for the engineer to, respectively, update the Mean, Variance, Coefficient of Variation, and Phi plots (recall Fig. 120 to Fig. 123) to account for plot view modifications, such as those that can be made in the Plot Legend frame (Fig. 119). Upon pressing the Update Plots button, all plots in the Spatial Variability tab are redrawn.



Figure 124. Update Plots and Export buttons

Data presented in all plots of the Spatial Variability page can be exported to an Excel file by pressing the Export button (Fig. 124, right). The generated Excel file is exported to the same folder as the model analysis files. Further, the Excel file is populated with four worksheet tabs: "Mean", "Variance", "Coefficient of Variation", and "Phi".

The "Mean" Excel tab contains elevation in column "A", mean side resistance in column "B", mean tip resistance in column "C", and mean total resistance in column "D". Listings obtained using an illustrative data set are given in Fig. 125.

	A	B	C	D
1				
2	Elevation	Side	Tip	Total
3	ft m	(tons kN)	(tons kN)	(tons kN)
4	-52.0000	554.0733	190.1300	744.2033
5	-53.0000	566.8003	190.2786	757.0790
6	-54.0000	579.6560	190.2957	769.9516
7	-55.0000	592.5221	190.2945	782.8167
8	-56.0000	605.2871	190.1586	795.4457
9	-57.0000	618.1313	190.0757	808.2070
10	-58.0000	630.9244	190.1014	821.0258
11	-59.0000	643.7043	190.1421	833.8464
12	-60.0000	656.5729	190.3199	846.8928
13	-61.0000	669.4454	190.5091	859.9545
14	-62.0000	682.2894	190.6043	872.8937
15	-63.0000	695.0795	190.7115	885.7910
16	-64.0000	707.9502	190.8050	898.7551
17	-65.0000	720.8610	190.9958	911.8568
18	-66.0000	733.6712	191.0568	924.7280
19	-67.0000	746.5586	191.0161	937.5747
20	-68.0000	759.4454	190.9856	950.4311
21	-69.0000	772.2748	190.7808	963.0556
22	-70.0000	785.0906	190.6868	975.7773
23	-71.0000	797.7915	190.7550	988.5465
24	-72.0000	810.4674	190.8349	1001.3022
25	-73.0000	823.1625	191.0907	1014.2532
26	-74.0000	835.8369	191.3629	1027.1999
27	-75.0000	848.7531	191.6669	1040.4200
28	-76.0000	861.7286	191.8546	1053.5832
29	-77.0000	874.7603	191.8361	1066.5964
30	-78.0000	887.8631	191.8026	1079.6657
31	-79.0000	900.8702	191.6126	1092.4828
32	-80.0000	913.8405	191.2949	1105.1354

Figure 125. "Mean" Excel tab (data for illustration only)

The "Variance" Excel tab contains elevation in column "A", variance in side resistance in column "B", variance in tip resistance in column "C", and variance in total resistance in column "D". Example listings, obtained using illustrative data, are provided in Fig. 126.

	A	B	C	D
1				
2	Elevation	Side	Tip	Total
3	ft m	(tons^2 kN^2)	(tons^2 kN^2)	(tons^2 kN^2)
4	-52.0000	2140.7353	599.7713	2740.5065
5	-53.0000	2197.0875	604.2177	2801.3052
6	-54.0000	2262.5301	610.3790	2872.9091
7	-55.0000	2321.1250	615.3941	2936.5191
8	-56.0000	2366.4827	617.7802	2984.2629
9	-57.0000	2424.7625	621.8633	3046.6258
10	-58.0000	2495.7989	620.5669	3116.3658
11	-59.0000	2572.1240	618.4384	3190.5624
12	-60.0000	2645.6379	609.9169	3255.5548
13	-61.0000	2712.1377	603.5036	3315.6413
14	-62.0000	2767.9163	598.1102	3366.0265
15	-63.0000	2816.5781	583.8816	3400.4597
16	-64.0000	2867.1185	573.0939	3440.2123
17	-65.0000	2911.7742	563.1510	3474.9252
18	-66.0000	2957.1547	555.9710	3513.1257
19	-67.0000	3002.3070	549.1110	3551.4180
20	-68.0000	3055.6698	539.4362	3595.1060
21	-69.0000	3121.1280	535.0549	3656.1830
22	-70.0000	3182.4386	538.5275	3720.9662
23	-71.0000	3234.8764	552.6834	3787.5598
24	-72.0000	3288.9370	557.8947	3846.8317
25	-73.0000	3342.9073	563.5676	3906.4749
26	-74.0000	3390.8313	574.7151	3965.5464
27	-75.0000	3438.4331	582.8696	4021.3027
28	-76.0000	3487.8566	594.5820	4082.4385
29	-77.0000	3546.0550	604.7011	4150.7561
30	-78.0000	3619.3238	614.1448	4233.4687
31	-79.0000	3672.5805	620.6526	4293.2331
32	-80.0000	3728.1602	617.3163	4345.4765

Figure 126. "Variance" Excel tab (data for illustration only)

The "Coefficient of Variation" tab contains elevation in column "A", coefficient of variation for side resistance in column "B", coefficient of variation for tip resistance in column "C", and coefficient of variation for total resistance in column "D". Example data are listed (for illustration) in Fig. 127.

	A	B	C	D
1				
2	Elevation	Side	Tip	Total
3	ft m			
4	-52.0000	0.0835	0.1288	0.0703
5	-53.0000	0.0827	0.1292	0.0699
6	-54.0000	0.0821	0.1298	0.0696
7	-55.0000	0.0813	0.1304	0.0692
8	-56.0000	0.0804	0.1307	0.0687
9	-57.0000	0.0797	0.1312	0.0683
10	-58.0000	0.0792	0.1310	0.0680
11	-59.0000	0.0788	0.1308	0.0677
12	-60.0000	0.0783	0.1298	0.0674
13	-61.0000	0.0778	0.1290	0.0670
14	-62.0000	0.0771	0.1283	0.0665
15	-63.0000	0.0764	0.1267	0.0658
16	-64.0000	0.0756	0.1255	0.0653
17	-65.0000	0.0749	0.1242	0.0646
18	-66.0000	0.0741	0.1234	0.0641
19	-67.0000	0.0734	0.1227	0.0636
20	-68.0000	0.0728	0.1216	0.0631
21	-69.0000	0.0723	0.1212	0.0628
22	-70.0000	0.0719	0.1217	0.0625
23	-71.0000	0.0713	0.1232	0.0623
24	-72.0000	0.0708	0.1238	0.0619
25	-73.0000	0.0702	0.1242	0.0616
26	-74.0000	0.0697	0.1253	0.0613
27	-75.0000	0.0691	0.1260	0.0610
28	-76.0000	0.0685	0.1271	0.0606
29	-77.0000	0.0681	0.1282	0.0604
30	-78.0000	0.0678	0.1292	0.0603
31	-79.0000	0.0673	0.1300	0.0600
32	-80.0000	0.0668	0.1299	0.0596

Figure 127. "Coefficient of Variation" Excel tab (data for illustration only)

The "Phi" tab contains listings of elevation in column "A", phi for side resistance in column "B", phi for tip resistance in column "C", and phi for total resistance in column "D". The worksheet layout and illustrative data are depicted in Fig. 128.

	A	B	C	D
1				
2	Elevation	Side	Tip	Total
3	ft m			
4	-52.0000	0.6000	0.6000	0.6000
5	-53.0000	0.6000	0.6000	0.6000
6	-54.0000	0.6000	0.6000	0.6000
7	-55.0000	0.6000	0.6000	0.6000
8	-56.0000	0.6000	0.6000	0.6000
9	-57.0000	0.6000	0.6000	0.6000
10	-58.0000	0.6000	0.6000	0.6000
11	-59.0000	0.6000	0.6000	0.6000
12	-60.0000	0.6000	0.6000	0.6000
13	-61.0000	0.6000	0.6000	0.6000
14	-62.0000	0.6000	0.6000	0.6000
15	-63.0000	0.6000	0.6000	0.6000
16	-64.0000	0.6000	0.6000	0.6000
17	-65.0000	0.6000	0.6000	0.6000
18	-66.0000	0.6000	0.6000	0.6000
19	-67.0000	0.6000	0.6000	0.6000
20	-68.0000	0.6000	0.6000	0.6000
21	-69.0000	0.6000	0.6000	0.6000
22	-70.0000	0.6000	0.6000	0.6000
23	-71.0000	0.6000	0.6000	0.6000
24	-72.0000	0.6000	0.6000	0.6000
25	-73.0000	0.6000	0.6000	0.6000
26	-74.0000	0.6000	0.6000	0.6000
27	-75.0000	0.6000	0.6000	0.6000
28	-76.0000	0.6000	0.6000	0.6000
29	-77.0000	0.6000	0.6000	0.6000
30	-78.0000	0.6000	0.6000	0.6000
31	-79.0000	0.6000	0.6000	0.6000
32	-80.0000	0.6000	0.6000	0.6000

Figure 128. "Phi" Excel tab (data for illustration only)

4.8 Method Error Tab

Shown in Fig. 129 is the Method Error tab, which allows for either default or custom adjustments (e.g., those based on load test data) to be made on the simulation results. In turn, these adjustments (intercept, slope, and dispersion) provide a means of accounting for the uncertainty associated with use of various empirical methods for calculating axial resistance.

There are four distinct regions of user input data in this tab: (1) Driven Pile frame; (2) Drilled Shaft frame; (3) Limestone frame; and, (5) Process Method Error button (all highlighted in Fig. 129). The five regions of the Method Error tab are discussed in the remainder of Sec. 4.8.

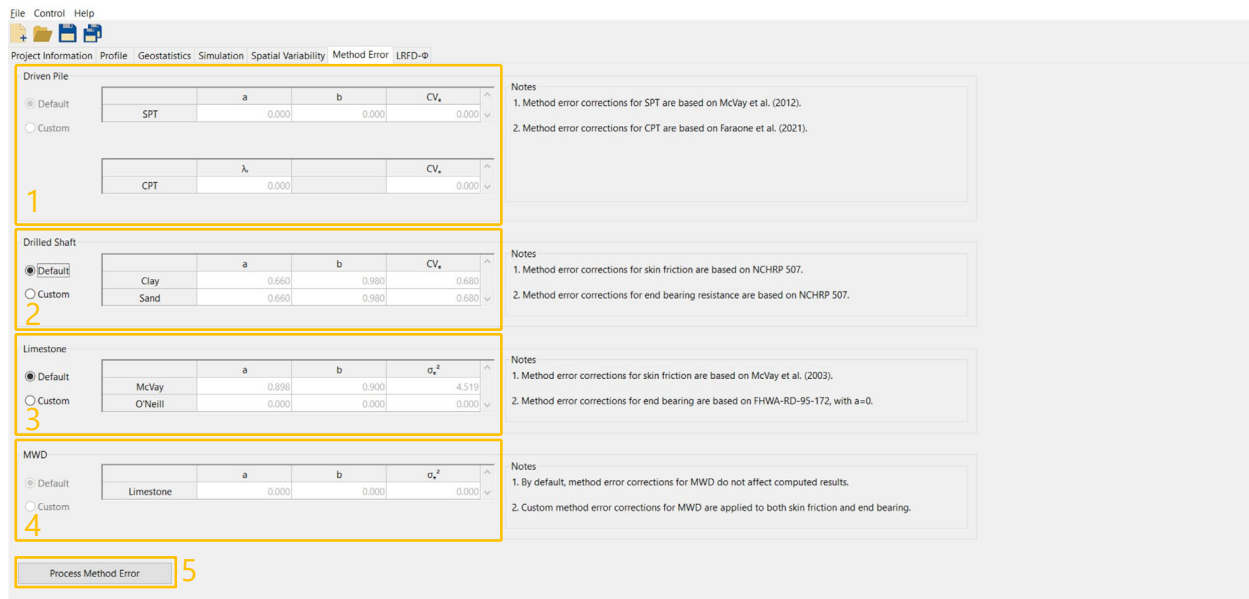


Figure 129. Method Error tab

4.8.1 Driven Pile Frame

Contained within the Driven Pile frame (Fig. 130) is method error input data specific to driven pile foundations. As presented in McVay et al. (2012), and implemented in GeoStat, method error parameters for driven piles with use of SPT data sets operate on “SPT” values. The form of the method error adjustments for driven piles includes an intercept (a), slope (b), and coefficient of variation (CV_e). If CPT data are utilized for analysis, then the method error calculations are based on the approach given in Faraone et al. (2021) and the “CPT” method error parameters: mean error (λ_r), coefficient of variation (CV_e).

Regardless of the use of SPT or CPT approaches, either default or custom values (i.e., corrections derived from load-tests) for the method error parameters may be entered by selecting “Custom” and then entering the desired values. If the Default radio button is selected, then the parameters table will be disabled, signifying that no additional input is required. Further, input controls located within the Driven Pile frame are not enabled if the foundation type being considered is not that of driven pile.

Driven Pile

Default

	a	b	CV _e
SPT	0.000	0.000	0.000

Custom

	λ_r		CV _e
CPT	0.000		0.000

Figure 130. Driven Pile frame

4.8.2 Drilled Shaft Frame

Contained within the Drilled Shaft frame (Fig. 131) is method error input data specific to drilled shaft foundations embedded in Clay or Sand layers. Accordingly, method error parameters, as identified in McVay et al. (2012), operate on one (or both) of "Clay" layer data and/or "Sand" layer data. Inputs include an "Exponent for Exponential" (a), "Exponent for Power" (b), and "Coefficient of Variation" (CV_e). Note that "CV_e" is used here instead of "COV" to distinguish that this instance of coefficient of variation is specific to method error calculations. If the foundation type being considered is a drilled shaft, then default or custom values (i.e., from load-test data) for the method error parameters may be entered by selecting "Custom" and then entering the desired values (no values are required to be input otherwise). Controls located within the Drilled Shaft frame are not enabled if the foundation type being considered is not that of drilled shaft.

Drilled Shaft

Default

	a	b	CV _e
Clay	0.660	0.980	0.680
Sand	0.660	0.980	0.680

Custom

Figure 131. Drilled Shaft frame

4.8.3 Limestone Frame

Contained within the Limestone frame (Fig. 132) is method error input data for when one or more layers of "Limestone" are defined in the soil layer profile of the GeoStat model, and a drilled shaft foundation is being considered along with analysis of core-run data. The GeoStat

software adopts a method error approach based on that documented in McVay et al. (2012) for limestone layers of drilled shaft foundations. More specifically, parameters make use of the “McVay” approach for side resistance and the “O’Neill” approach for end resistance. As an exception, the O’Neill term for “a” is defaulted to zero. The default value of zero is used here to prevent potentially unconservative adjustments to computed capacities when tip resistance does not significantly contribute to total resistance.

Limestone				
<input checked="" type="radio"/> Default <input type="radio"/> Custom				
	a	b	σ_e^2	
McVay	0.898	0.900	4.519	^
O'Neill	0.000	0.000	0.000	v

Figure 132. Limestone frame

Inputs for these two approaches include intercept (“a”), slope (“b”), and method error (“ σ_e^2 ”) values. If no limestone layers are defined for the foundation soil layering, then all values within this data subset may be left blank or input as zero. If there are limestone layers defined for the foundation soil layering (and the foundation type being considered is that of drilled shaft), then custom values for the method error parameters may be entered by selecting “Custom” and then entering the desired values. In this context, custom values are often based on load tests.

4.8.4 MWD Frame

Contained within the MWD frame (Fig. 133) is method error input data for when one or more layers of “Limestone” are defined in the soil layer profile of the GeoStat model, and a drilled shaft foundation is being considered along with analysis of MWD data. Inputs for this approach includes intercept (“a”), slope (“b”), and method error (“ σ_e^2 ”), in association with a linear form of regression (see the Technical Manual for additional details). For method error corrections in limestone layers in association with MWD-related analysis, the default parameters are such that method error corrections have no effect on the computed results. In other words, “a” is defaulted to zero, “b” is defaulted to unity, and “ σ_e^2 ” is defaulted to zero. It is anticipated however that, in practice, site-specific method error parameters (e.g., based on load tests) will typically be applied for these scenarios.

MWD

Default

Custom

	a	b	σ_e^2
Limestone	0.000	0.000	0.000

Figure 133. MWD frame

4.8.5 Process Method Error Button

The Process Method Error button (recall Fig. 129, bottom) is used to accept the applicable inputs present in the Driven Pile frame, Drilled Shaft frame, and the Limestone frame. Note that this button must be clicked prior to navigating onward to the LRFD- ϕ tab.

4.9 LRFD- ϕ Tab

The seventh and final (rightmost) tab in the GeoStat UI (Fig. 134) is the LRFD- ϕ tab, which contains profile plots of mean-valued resistance, coefficients of variation, resistance (ϕ) factors, and factored resistance. Further, plots located within the LRFD- ϕ tab include both the axial resistance quantities associated with spatial variability as well as those of combined spatial variability and method error. If adequate post-processing has not occurred upon reaching this tab, then the UI will issue a warning message in lieu of attempting to generate the summary plots. Examples of inadequacies in post-processing that are detected (when present) include: no results data have been loaded from the Spatial Variability tab; or, the method error has not yet been processed.

There are two distinct regions of user input data in LRFD- ϕ tab: (1) Plot Type dropdown menu (2) Plot Legend frame (both highlighted in Fig. 134). There are also four distinct regions of output in this tab: (3) Update Plots and Export buttons; (4) Side Resistance plot; (5) Tip Resistance plot; and, (6) Total Resistance plot (all highlighted in Fig. 134). The six tab regions are discussed in the remainder of Sec. 4.9.

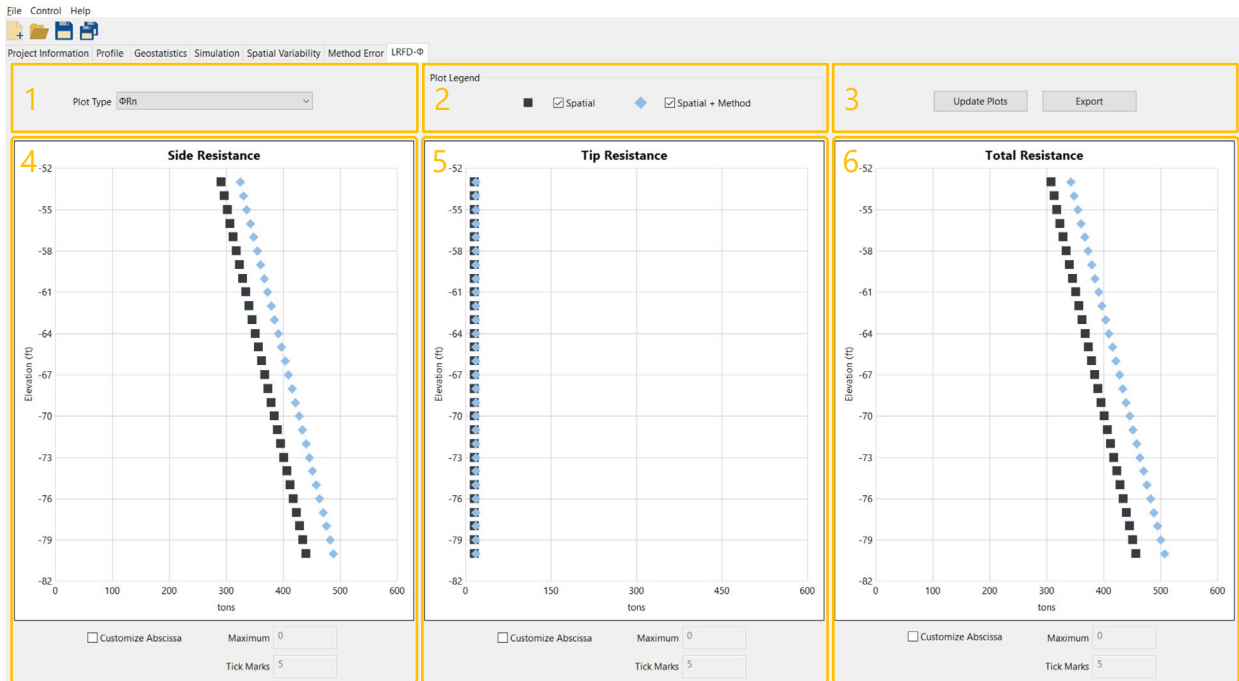


Figure 134. LRFD-φ tab

4.9.1 Plot Type

The Plot Type dropdown menu (Fig. 135) allows for the engineer to select which type of data is to be presented in the Side Resistance plot (see Sec. 4.9.3), the Tip Resistance plot (Sec. 4.9.4), and the Total Resistance plot (Sec. 4.9.5). The options available for plot type are Mean, Coefficient of Variation, Estimated ϕ , and ϕR_n . Note that the formulation used in calculating the LRFD resistance (ϕ) factor is indicated in the pulldown menu listing (e.g., Styler 2006).

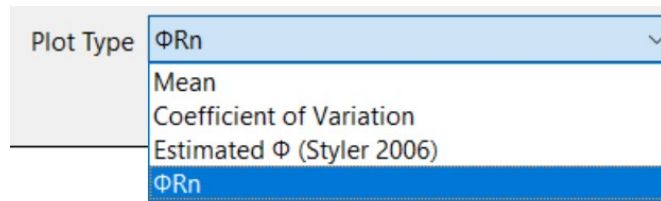


Figure 135. Plot Type dropdown menu

4.9.2 Plot Legend Frame

The Plot Legend frame (Fig. 136) allows for the engineer to select any combination of the Spatial and/or Spatial + Method curves for display in the side, tip, and total resistance plots.



Figure 136. Plot Legend frame

4.9.3 Side Resistance Plot

The Side Resistance plot (Fig. 137) displays the mean, variance, coefficient of variation, or Phi for side resistance. The plots are generated with respect to elevation, and may include only spatial variability and/or combined spatial variability and method error. The curves displayed in the Side Resistance plot vary depending on which settings are chosen in the Plot Type dropdown menu (Fig. 135) and the Plot Legend frame (Fig. 136).

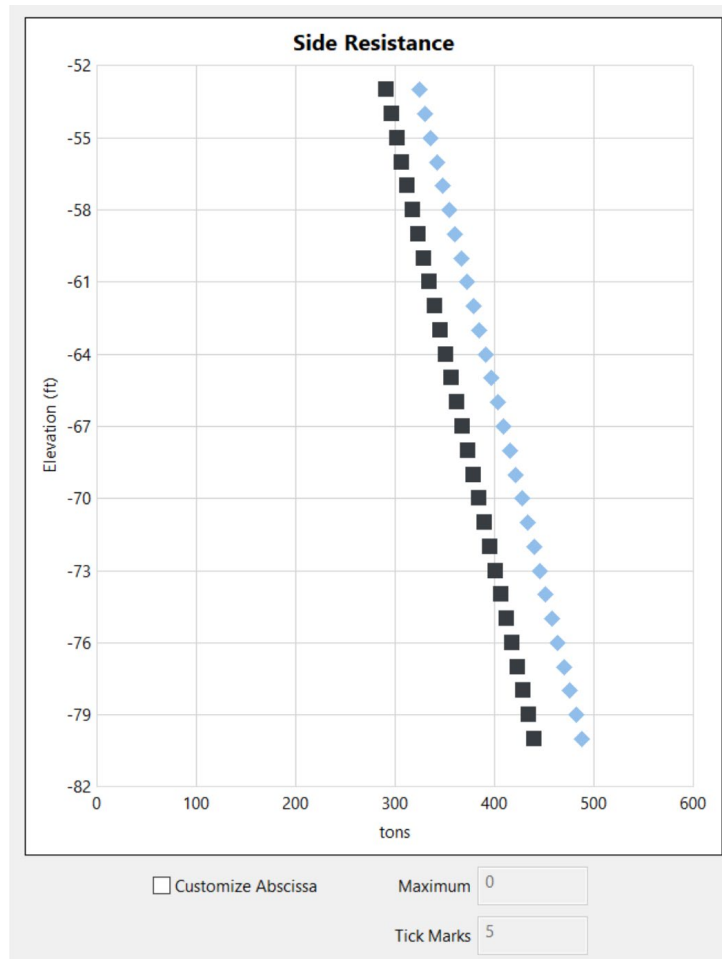


Figure 137. Side Resistance plot (data for illustration only)

Checking the Custom Abscissa box (Fig. 137, bottom-left) allows for the curve(s) to be redrawn along an updated abscissa axis using the values input for Max and number of Tick

Marks. Note that program-generated resistance (ϕ) factors should only be used in conjunction with Owner's guidelines.

4.9.4 Tip Resistance Plot

The Side Resistance plot (Fig. 138) displays the mean, variance, coefficient of variation, or Phi for side resistance. The plots are generated with respect to elevation, and may include only spatial variability and/or combined spatial variability and method error. The curves displayed in the Tip Resistance plot vary depending on which settings are chosen in the Plot Type dropdown menu (Fig. 135) and the Plot Legend frame (Fig. 136).

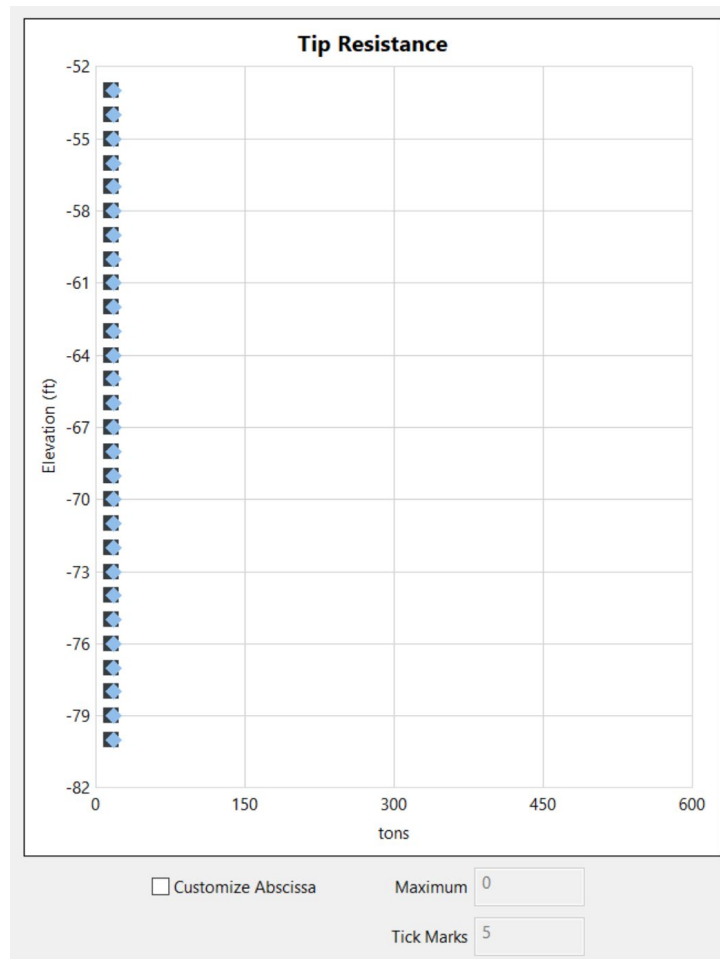


Figure 138. Tip Resistance plot (data for illustration only)

Checking the Custom Abscissa box (Fig. 138, bottom-left) allows for the curve(s) to be redrawn along an updated abscissa axis using the values input for Max and number of Tick Marks. Note that program-generated resistance (ϕ) factors should only be used in conjunction with Owner's guidelines. Also, note that the illustrative plot here indicates relatively low tip resistance. For driven piles and drilled shafts that terminate in sand and clay layers, tip

resistance is determined based on realizations of through-depth profiles of SPT blow counts (or CPT data, depending on the analysis being conducted). For drilled shafts terminating in rock, mass modulus (E_m) influences computed tip resistance. See Ch. 5 and the Technical Manual for additional details.

4.9.5 Total Resistance Plot

The Total Resistance plot (Fig. 139) displays the mean, variance, coefficient of variation, or Phi for total resistance. The plots are generated with respect to elevation, and may include only spatial variability and/or combined spatial variability and method error. Note that the total resistance curves are not produced via simple summation of side and tip resistance curves, but rather, total resistances are determined for each model analysis file analyzed, and only then are total resistance quantities (e.g., mean values vs. elevation) formed.

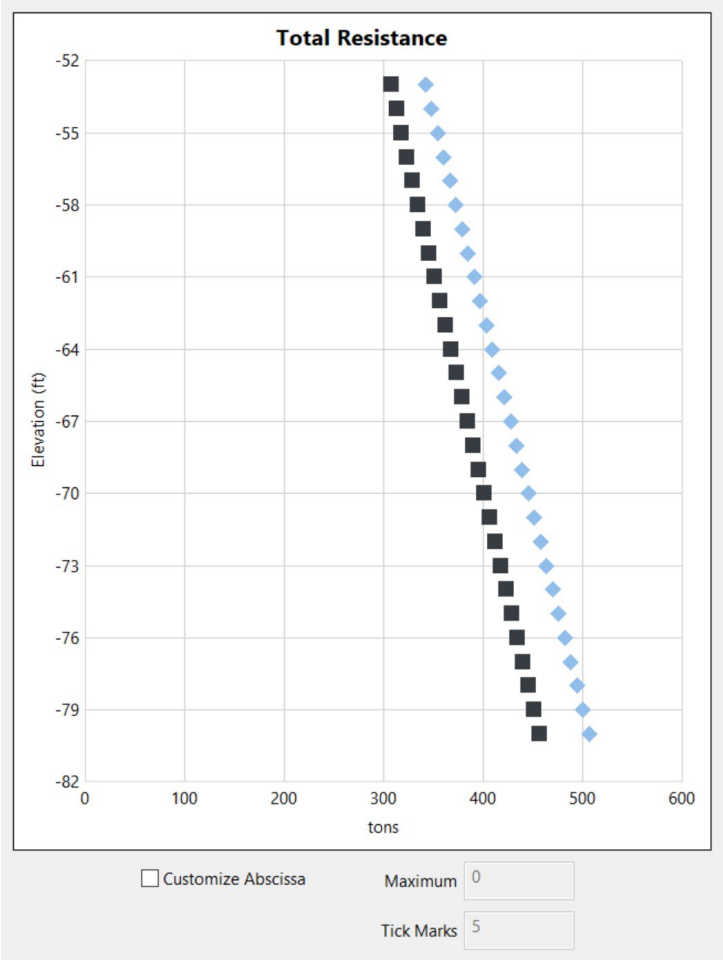


Figure 139. Total Resistance plot (data for illustration only)

The curves displayed in the Tip Resistance plot vary depending on which settings are chosen in the Plot Type dropdown menu (Fig. 135) and the Plot Legend frame (Fig. 136). In addition, checking the Custom Abscissa box (Fig. 139, bottom-left) allows for the curve(s) to be redrawn

along an updated abscissa axis using the values input for Max and number of Tick Marks. Note that program-generated resistance (ϕ) factors should only be used in conjunction with Owner's guidelines.

4.9.6 Update Plots and Export Buttons

The Update Plots button (Fig. 140, left) allows for the engineer to, respectively, update the Side, Tip, and Total resistance plots (recall Fig. 137 to Fig. 139) to account for plot view modifications, such as those that can be made in the Plot Legend frame (Fig. 136). Upon pressing the Update Plots button, all plots in the LRFD- ϕ tab are redrawn.



Figure 140. Update Plots and Export button

Data plotted in the LRFD- ϕ tab can be exported to an Excel file by pressing the Export button (Fig. 140, right). The generated Excel file is exported to the same folder as the model analysis files. Further, four worksheet tabs are contained within the Excel worksheet: "Mean", "Coefficient of Variation", "Phi", and "PhiRn".

The "Mean" Excel tab contains the elevation in column "A"; mean side resistance (spatial only) in column "B"; mean side resistance with both spatial variability and method error in column "C"; mean tip resistance (spatial only) in column "D"; mean tip resistance with both spatial variability and method error in column "E"; mean total resistance (spatial only) in column "F", and, the mean total resistance with both spatial variability and method error in column "G". The Excel tab format, along with a listing of illustrative data, is provided in Fig. 141.

The "Coefficient of Variation" Excel tab contains the elevation in column "A"; coefficient of variation for side resistance (spatial only) in column "B"; coefficient of variation for side resistance with both spatial variability and method error in column "C"; coefficient of variation for tip resistance (spatial only) in column "D"; coefficient of variation for tip resistance with both spatial variability and method error in column "E"; coefficient of variation for total resistance (spatial only) in column "F", and, the coefficient of variation for total resistance with both spatial variability and method error in column "G". The Excel tab format and illustrative data are provided in Fig. 142.

	A	B	C	D	E	F	G
1	Elevation	Side Spatial	Side Spatial + Method	Tip Spatial	Tip Spatial + Method	Total Spatial	Total Spatial + Method
2	ft m	(tons kN)	(tons kN)	(tons kN)	(tons kN)	(tons kN)	(tons kN)
4	-52.0000	476.1754	530.6636	27.6445	31.6973	503.8198	561.1546
5	-53.0000	485.4074	540.8482	27.6456	31.6986	513.0533	571.3351
6	-54.0000	494.5903	550.9767	27.6485	31.7019	522.2390	581.4612
7	-55.0000	503.7759	561.1062	27.6481	31.7015	531.4240	591.5845
8	-56.0000	512.9332	571.2027	27.6460	31.6991	540.5793	601.6735
9	-57.0000	522.1404	581.3524	27.6150	31.6638	549.7552	611.7835
10	-58.0000	531.3882	591.5450	27.5922	31.6380	558.9804	621.9460
11	-59.0000	540.5840	601.6787	27.5895	31.6349	568.1735	632.0715
12	-60.0000	549.7966	611.8290	27.5845	31.6293	577.3813	642.2116
13	-61.0000	558.9881	621.9545	27.5910	31.6366	586.5793	652.3392
14	-62.0000	568.1656	632.0628	27.6103	31.6585	595.7759	662.4639
15	-63.0000	577.3457	642.1724	27.6409	31.6932	604.9866	672.6023
16	-64.0000	586.4965	652.2482	27.6722	31.7288	614.1687	682.7078
17	-65.0000	595.6961	662.3760	27.6798	31.7374	623.3759	692.8394
18	-66.0000	604.8858	672.4914	27.6930	31.7524	632.5786	702.9646
19	-67.0000	614.0805	682.6107	27.7018	31.7624	641.7825	713.0895
20	-68.0000	623.2833	692.7376	27.6859	31.7443	650.9693	723.1942
21	-69.0000	632.5027	702.8810	27.6516	31.7054	660.1543	733.2955
22	-70.0000	641.7584	713.0630	27.6327	31.6840	669.3912	743.4526
23	-71.0000	651.0110	723.2402	27.6107	31.6590	678.6219	753.6013
24	-72.0000	660.2331	733.3823	27.6228	31.6728	687.8560	763.7524
25	-73.0000	669.4570	743.5249	27.6309	31.6819	697.0880	773.8999
26	-74.0000	678.6691	753.6533	27.6323	31.6835	706.3015	784.0257
27	-75.0000	687.8554	763.7518	27.6577	31.7123	715.5130	794.1479
28	-76.0000	697.0105	773.8147	27.6697	31.7260	724.6803	804.2203
29	-77.0000	706.1912	783.9045	27.6806	31.7383	733.8720	814.3182
30	-78.0000	715.3432	793.9613	27.6944	31.7540	743.0376	824.3863
31	-79.0000	724.5614	804.0897	27.6817	31.7396	752.2431	834.4968
32	-80.0000	733.8016	814.2409	27.6651	31.7207	761.4667	844.6260

Figure 141. "Mean" Excel tab (data for illustration only)

	A	B	C	D	E	F	G
1	Elevation	Side Spatial	Side Spatial + Method	Tip Spatial	Tip Spatial + Method	Total Spatial	Total Spatial + Method
2	ft m						
4	-52.0000	0.0435	0.2203	0.1161	0.2413	0.0437	0.2204
5	-53.0000	0.0430	0.2202	0.1152	0.2408	0.0432	0.2204
6	-54.0000	0.0425	0.2201	0.1144	0.2404	0.0427	0.2203
7	-55.0000	0.0421	0.2201	0.1139	0.2402	0.0423	0.2203
8	-56.0000	0.0418	0.2201	0.1140	0.2402	0.0420	0.2202
9	-57.0000	0.0414	0.2200	0.1145	0.2404	0.0417	0.2202
10	-58.0000	0.0411	0.2200	0.1148	0.2406	0.0414	0.2202
11	-59.0000	0.0407	0.2200	0.1148	0.2406	0.0411	0.2201
12	-60.0000	0.0405	0.2199	0.1149	0.2406	0.0408	0.2201
13	-61.0000	0.0402	0.2199	0.1150	0.2407	0.0405	0.2201
14	-62.0000	0.0399	0.2199	0.1148	0.2406	0.0402	0.2201
15	-63.0000	0.0396	0.2199	0.1142	0.2403	0.0399	0.2200
16	-64.0000	0.0394	0.2198	0.1135	0.2400	0.0396	0.2200
17	-65.0000	0.0392	0.2198	0.1134	0.2399	0.0394	0.2200
18	-66.0000	0.0390	0.2198	0.1134	0.2399	0.0392	0.2200
19	-67.0000	0.0387	0.2198	0.1131	0.2397	0.0389	0.2200
20	-68.0000	0.0385	0.2198	0.1126	0.2395	0.0387	0.2199
21	-69.0000	0.0383	0.2198	0.1127	0.2395	0.0384	0.2199
22	-70.0000	0.0379	0.2198	0.1123	0.2393	0.0381	0.2199
23	-71.0000	0.0376	0.2197	0.1118	0.2391	0.0378	0.2199
24	-72.0000	0.0374	0.2197	0.1118	0.2391	0.0376	0.2198
25	-73.0000	0.0372	0.2197	0.1121	0.2393	0.0374	0.2198
26	-74.0000	0.0369	0.2197	0.1126	0.2395	0.0371	0.2198
27	-75.0000	0.0367	0.2197	0.1129	0.2397	0.0369	0.2198
28	-76.0000	0.0365	0.2197	0.1131	0.2397	0.0366	0.2198
29	-77.0000	0.0363	0.2196	0.1131	0.2398	0.0364	0.2198
30	-78.0000	0.0360	0.2196	0.1132	0.2398	0.0361	0.2197
31	-79.0000	0.0358	0.2196	0.1139	0.2402	0.0358	0.2197
32	-80.0000	0.0356	0.2196	0.1141	0.2402	0.0356	0.2197

Figure 142. "Coefficient of Variation" Excel tab (data for illustration only)

The "Phi" Excel tab contains the elevation in column "A"; phi (ϕ) for side resistance (spatial only) in column "B"; phi (ϕ) for side resistance with both spatial variability and method error in column "C"; phi (ϕ) for tip resistance (spatial only) in column "D"; phi (ϕ) for tip resistance with both spatial variability and method error in column "E"; phi (ϕ) for total resistance (spatial only) in column "F", and, the phi (ϕ) for total resistance with both spatial variability and method error in column "G". Excel tab formatting and illustrative data are provided in Fig. 143.

	A	B	C	D	E	F	G
1	Elevation	Side Spatial	Side Spatial + Method	Tip Spatial	Tip Spatial + Method	Total Spatial	Total Spatial + Method
2	ft m						
3							
4	-52.0000	0.6000	0.6000	0.6000	0.5759	0.6000	0.6000
5	-53.0000	0.6000	0.6000	0.6000	0.5767	0.6000	0.6000
6	-54.0000	0.6000	0.6000	0.6000	0.5773	0.6000	0.6000
7	-55.0000	0.6000	0.6000	0.6000	0.5777	0.6000	0.6000
8	-56.0000	0.6000	0.6000	0.6000	0.5777	0.6000	0.6000
9	-57.0000	0.6000	0.6000	0.6000	0.5773	0.6000	0.6000
10	-58.0000	0.6000	0.6000	0.6000	0.5770	0.6000	0.6000
11	-59.0000	0.6000	0.6000	0.6000	0.5770	0.6000	0.6000
12	-60.0000	0.6000	0.6000	0.6000	0.5770	0.6000	0.6000
13	-61.0000	0.6000	0.6000	0.6000	0.5768	0.6000	0.6000
14	-62.0000	0.6000	0.6000	0.6000	0.5770	0.6000	0.6000
15	-63.0000	0.6000	0.6000	0.6000	0.5775	0.6000	0.6000
16	-64.0000	0.6000	0.6000	0.6000	0.5781	0.6000	0.6000
17	-65.0000	0.6000	0.6000	0.6000	0.5782	0.6000	0.6000
18	-66.0000	0.6000	0.6000	0.6000	0.5782	0.6000	0.6000
19	-67.0000	0.6000	0.6000	0.6000	0.5784	0.6000	0.6000
20	-68.0000	0.6000	0.6000	0.6000	0.5788	0.6000	0.6000
21	-69.0000	0.6000	0.6000	0.6000	0.5788	0.6000	0.6000
22	-70.0000	0.6000	0.6000	0.6000	0.5791	0.6000	0.6000
23	-71.0000	0.6000	0.6000	0.6000	0.5795	0.6000	0.6000
24	-72.0000	0.6000	0.6000	0.6000	0.5795	0.6000	0.6000
25	-73.0000	0.6000	0.6000	0.6000	0.5792	0.6000	0.6000
26	-74.0000	0.6000	0.6000	0.6000	0.5788	0.6000	0.6000
27	-75.0000	0.6000	0.6000	0.6000	0.5786	0.6000	0.6000
28	-76.0000	0.6000	0.6000	0.6000	0.5784	0.6000	0.6000
29	-77.0000	0.6000	0.6000	0.6000	0.5784	0.6000	0.6000
30	-78.0000	0.6000	0.6000	0.6000	0.5783	0.6000	0.6000
31	-79.0000	0.6000	0.6000	0.6000	0.5778	0.6000	0.6000
32	-80.0000	0.6000	0.6000	0.6000	0.5776	0.6000	0.6000

Figure 143. "Phi" Excel tab (data for illustration only)

The "PhiRn" (i.e., the product of mean resistance and resistance factor, ϕ) Excel tab contains the elevation in column "A"; factored resistance for side resistance (spatial only) in column "B"; factored resistance for side resistance with both spatial variability and method error in column "C"; factored resistance for tip resistance (spatial only) in column "D"; factored resistance for tip resistance with both spatial variability and method error in column "E"; factored resistance for total resistance (spatial only) in column "F", and, the factored resistance for total resistance with both spatial variability and method error in column "G". Excel tab formatting and illustrative data are provided in Fig. 144.

	A	B	C	D	E	F	G
1	Elevation	Side Spatial	Side Spatial + Method	Tip Spatial	Tip Spatial + Method	Total Spatial	Total Spatial + Method
2	ft m	(tons kN)	(tons kN)	(tons kN)	(tons kN)	(tons kN)	(tons kN)
3							
4	-52.0000	285.7052	318.3982	16.5867	18.2542	302.2919	336.6928
5	-53.0000	291.2444	324.5089	16.5874	18.2801	307.8320	342.8011
6	-54.0000	296.7542	330.5860	16.5891	18.3028	313.3434	348.8767
7	-55.0000	302.2655	336.6637	16.5889	18.3152	318.8544	354.9507
8	-56.0000	307.7599	342.7216	16.5876	18.3111	324.3476	361.0041
9	-57.0000	313.2842	348.8114	16.5690	18.2789	329.8531	367.0701
10	-58.0000	318.8329	354.9270	16.5553	18.2545	335.3882	373.1676
11	-59.0000	324.3504	361.0072	16.5537	18.2520	340.9041	379.2429
12	-60.0000	329.8779	367.0974	16.5507	18.2485	346.4288	385.3269
13	-61.0000	335.3929	373.1727	16.5546	18.2488	351.9476	391.4035
14	-62.0000	340.8993	379.2377	16.5662	18.2676	357.4656	397.4783
15	-63.0000	346.4074	385.3034	16.5845	18.3030	362.9920	403.5614
16	-64.0000	351.8979	391.3489	16.6033	18.3411	368.5012	409.6247
17	-65.0000	357.4177	397.4256	16.6079	18.3502	374.0256	415.7036
18	-66.0000	362.9315	403.4948	16.6158	18.3586	379.5472	421.7787
19	-67.0000	368.4483	409.5664	16.6211	18.3722	385.0695	427.8537
20	-68.0000	373.9700	415.6425	16.6115	18.3746	390.5816	433.9165
21	-69.0000	379.5016	421.7286	16.5910	18.3501	396.0926	439.9773
22	-70.0000	385.0551	427.8378	16.5796	18.3485	401.6347	446.0715
23	-71.0000	390.6066	433.9441	16.5664	18.3460	407.1731	452.1608
24	-72.0000	396.1399	440.0294	16.5737	18.3535	412.7136	458.2515
25	-73.0000	401.6742	446.1150	16.5786	18.3507	418.2528	464.3399
26	-74.0000	407.2015	452.1920	16.5794	18.3383	423.7809	470.4154
27	-75.0000	412.7133	458.2511	16.5946	18.3475	429.3078	476.4887
28	-76.0000	418.2063	464.2888	16.6018	18.3518	434.8082	482.5322
29	-77.0000	423.7147	470.3427	16.6084	18.3573	440.3232	488.5909
30	-78.0000	429.2059	476.3768	16.6167	18.3641	445.8226	494.6318
31	-79.0000	434.7368	482.4538	16.6090	18.3376	451.3458	500.6981
32	-80.0000	440.2810	488.5445	16.5990	18.3217	456.8800	506.7756

Figure 144. "PhiRn" Excel tab (data for illustration only)

CHAPTER 5

GENERATION AND BATCH PROCESSING OF MODEL ANALYSIS FILES

5.1 Overview

Documented in Ch. 5 are those features implemented in the GeoStat software that serve to automate the process of creating analysis model files and perform batch mode computation of the models to determine pile/shaft axial capacities. Those GeoStat UI controls that result in issuance of the system (batch) commands are identified in Sec. 5.2. Documentation is provided in Sec. 5.3 regarding necessary system commands that are issued (automatically) to “silently” perform analyses from within GeoStat. In addition, Ch. 5 documents the manner in which bulk post-processing of the analysis files is automatically carried out by the GeoStat software.

All analysis files created from within the GeoStat UI adhere to the input and output (ASCII) file formats of the pile/shaft axial-capacity calculation software, FB-Deep. Details regarding specific regions of interest within the output files for post-processing of pile analyses are given in Sec. 5.4 and Sec. 5.5. Similarly, documented in Sec. 5.6 are regions of interest in output files for post-processing of shaft analyses.

5.2 Generating Model Analysis Files

Positioned in the lower right portion of the Simulation tab is the Run Simulation button (Fig. 145). Clicking the Run Simulation button prompts GeoStat to first generate the many realizations of soil or rock profiles, taking into account spatial variability phenomena. Next, a folder is created in the same directory as the GeoStat model file and is subsequently populated with model analysis files (one realization corresponds to one file). Note that the folder name issued is identical to the name of the currently loaded GeoStat model file. When combined with file-saving features (such as “Save As”), engineers gain the ability to revisit or edit previously created GeoStat model files and also keep track of which GeoStat model file corresponds to a given collection of model analysis files (and analysis results).

The numerous model analysis files, all stored within the newly created folder, are named using a sequential numbering convention. For example, if 2,000 simulations are to be conducted, then files “1.in” through “2000.in” are created and stored within the dedicated folder for that batch of analyses. Note that if the folder already exists, then any pre-existing files within the folder are deleted prior to population of the model files. Therefore, it is useful to save a unique GeoStat input file for each unique instance of carrying out the simulations.

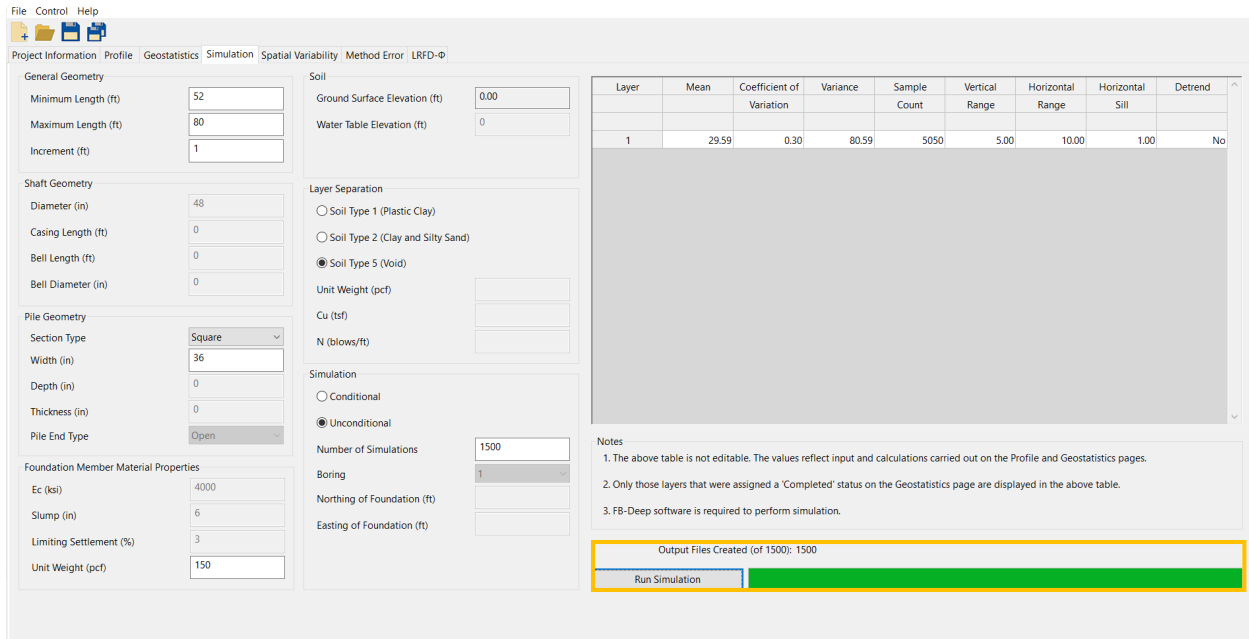


Figure 145. Generation (and analysis) of model analysis files in the Simulation tab

5.3 Running Batch Mode Analysis

As highlighted in Fig. 145, clicking the Run Simulation button performs the action of issuing the “silent” call to carry out batch mode analysis of all newly created analysis files. Clicking the Run Simulation button instructs the GeoStat software to carry out the desired number of realizations, package relevant parameters from each realization into model analysis files (which adhere to the formatting requirements of the FB-Deep software), and then issue the “silent” batch mode analysis command. Approximately 400-500 simulations can be completed per minute for both pile and shaft configurations (including consideration for generating realizations, creating the model analysis files, and running the analyses).

5.3.1 Batch Mode Syntax

By default, a call to “silently” perform batch mode analysis is issued through use of system commands. This “silent” functionality is leveraged in GeoStat to directly perform batch mode analysis (see the Program Settings options detailed in Ch. 1 for alternative approaches). Consequently, GeoStat can effectively employ axial capacity calculation algorithms such as those contained within software packages such as FB-Deep without requiring the engineer to manually open and operate external software packages (including the FB-Deep software).

The syntax of the system command is:

`[executable path] B:1 N:[number of simulations] I:[1.in path]`

where *[executable path]* is the full path to the executable performing the analysis, including the name of the executable file; *[number of simulations]* is the total number of simulations to conduct; *[1.in path]* is the full path to the model file named "1.in" (recall the discussion in Sec. 5.2), including the filename (1.in). The flag characters "B", "N", and "I" are required in all instances for the purpose of distinguishing each component of the command syntax.

5.4 Parsing Output for Driven Piles with Analysis of SPT Datasets

Highlighted in Fig. 146 is the region of interest within analysis output files (created during batch operations) that is specific to analysis of piles in conjunction with SPT datasets. The region of interest is used for the purpose of bulk importing data into the GeoStat UI. All data of interest reside within the output (.out) file region entitled "Driven Pile Capacity". More specifically, the Test Pile Length, Ultimate Side Friction, and Mobilized End Bearing quantities are parsed from the output file. Note that the output file formatting is consistent with that of FB-Deep output for driven pile analysis.

Driven Pile Capacity:
 =====

Section Type: Round
 Pile Width: 48.00 (in)

Test Pile Length (ft)	Pile Width (in)	Ultimate Side Friction (tons)	Mobilized End Bearing (tons)	Estimated Davisson Capacity (tons)	Allowable Pile Capacity (tons)	Ultimate Pile Capacity (tons)
50.00	48.0	553.86	601.35	1155.20	577.60	2357.90
51.00	48.0	560.34	599.81	1160.16	580.08	2359.79
52.00	48.0	566.82	598.39	1165.21	582.60	2362.00
53.00	48.0	573.15	597.95	1171.10	585.55	2367.01
54.00	48.0	579.47	597.54	1177.01	588.51	2372.10
55.00	48.0	585.79	597.11	1182.90	591.45	2377.13

Figure 146. Example excerpt of SPT-based pile analysis output that is read-in from the Spatial Variability tab

5.5 Parsing Output for Driven Piles with Analysis of CPT Datasets

Highlighted in Fig. 147 are two regions of interest within analysis output files, specific to analysis of piles using CPT data. As indicated above, these two regions are used for the purpose of bulk importing of results data into the GeoStat UI. The first region (Fig. 147a) allows for identification of the empirical method employed for pile axial capacity calculations

(e.g., "CPT - UF Method" signifies use of the UF method). Identification of the empirical method at this stage is necessary to maintain a clear division between input (model editing) and output (results processing and viewing) subdomains within the GeoStat UI. The region within CPT-based analysis output files pertaining to pile axial capacities is identified by searching for column-header strings highlighted in Fig. 147b, particularly "Test", "Skin", and "Nominal". Once this latter region is identified, the "Test Pile Length", "Nominal Skin Friction Resistance", "Nominal Tip Resistance", and "Nominal Resistance" columns are read-in and stored for plotting within the GeoStat UI. The collections of read-in capacities are also utilized as part of total uncertainty calculations. Note that the output file formatting is consistent with that of FB-Deep output for driven pile analysis.

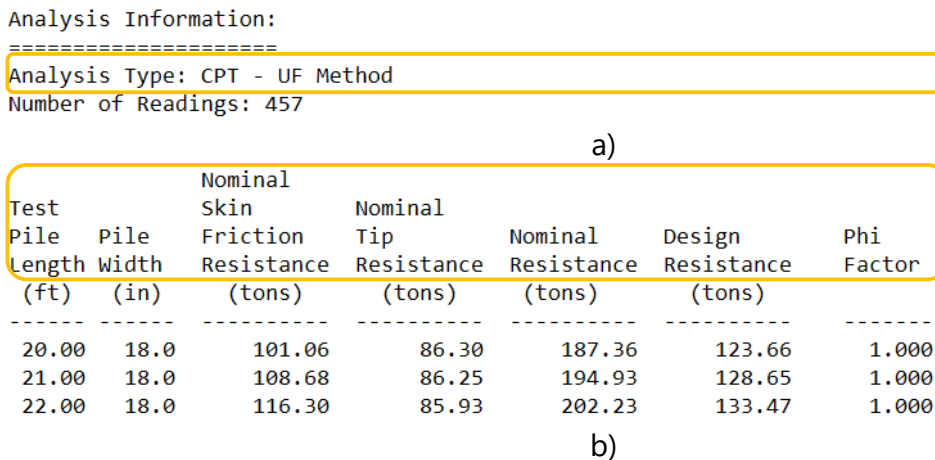


Figure 147. Example excerpt of CPT-based analysis output that is read-in from the Spatial Variability tab: a) Identification of empirical method; b) Identification of output region that reports computed axial capacities

5.6 Parsing Output for Analysis of Drilled Shafts

Depicted in Fig. 148 and Fig. 149 are excerpts from an illustrative output file, which was generated as part of analyzing a shaft foundation member (again, the output file formatting matches that of FB-Deep output files). For the purpose of post-processing data from within GeoStat, shaft geometric properties reported beneath the "SHAFT INFORMATION" header are parsed and retained. Also, both elevation and shaft axial resistance quantities residing beneath the "Skin friction capacity" sub-header are parsed as part of the data importation (including the tabulated columns of Top Elev., Ult. Skin Friction, and integer mapping values of FB-Deep soil types). Further, the ultimate skin friction in the bearing layer is included among the imported data.

SHAFT INFORMATION (Shaft ID = 1)

```

=====
Diameter      = 48.00(in)
Base Diameter = 48.00(in)
Length        = 50.00(ft)
Tip elevation = 32.00(ft)
Case length   = 22.20(ft)
Bell length   = 0.00(ft)
=====
    
```

Skin friction capacity

 Strength reduction factor for skin-friction = 1.00

Layer ID	Top Elev. (ft)	Thick. (ft)	Ult Skin Friction (Tons)	Soil Type
1	82.00	0.50	0.00	5- Cavity layer
2	81.50	12.50	0.00	2- Clay and silty sand
3	69.00	0.50	0.00	5- Cavity layer
4	68.50	6.50	0.00	2- Clay and silty sand
5	62.00	0.50	0.00	5- Cavity layer
6	61.50	6.50	106.77	2- Clay and silty sand
7	55.00	0.50	0.00	5- Cavity layer
8	54.50	4.50	96.33	1- Plastic Clay
9	50.00	0.50	0.00	5- Cavity layer
10	49.50	14.50	258.15	2- Clay and silty sand
11	35.00	0.50	0.00	5- Cavity layer
12	34.50	26.00		4- Lime Stone/Very shelly sand <--- Bearing layer

(* IN LAYERS ABOVE BEARING LAYER)

```

Ultimate skin friction in layers above bearing layer = 461.25(tons)
Ultimate skin friction in bearing layer              = 178.63(tons)
Total Skin Friction                                 = 639.87(tons)
    
```

Figure 148. Example excerpt of shaft analysis output that is read-in from the Spatial Variability tab

While the aforementioned elevation and resistance quantities pertain primarily to skin friction resistance, a second region of interest located among the analysis output is scanned and parsed for the purpose of building up estimates of end bearing resistance. In particular, settlement data found beneath the "Settlement curve" sub-header are focused upon. Recall that one of the GeoStat input parameters associated with modeling of shafts is the Limiting Settlement (%). As part of the data importation from within GeoStat, the end bearing reaction (i.e., Q_b) corresponding to the input value of Limiting Settlement is parsed and retained. Note that linear interpolation is carried out during importation in the event that the input value of Limiting Settlement (from GeoStat) does not exactly match any value found among the reported R(%) values in the model analysis output files.

```

Settlement curve:
-----
**** Capacity is NOT modified by the strength reduction factors ****
---

User-Defined Settlement = 3.00%
Shaft capacity at user-defined settlement = 492.89(tons)

```

R(%)	Settl.(in)	Qs(tons)	Qb(tons)	Qt(tons)
0.1	0.048	231.65	4.08	235.73
0.2	0.096	344.15	6.50	350.65
0.4	0.192	421.65	10.34	431.99
0.6	0.288	458.53	13.57	472.10
0.8	0.384	473.89	16.45	490.34
1.0	0.480	468.49	19.10	487.60
1.5	0.720	453.53	25.06	478.60
2.0	0.960	436.84	30.39	467.23
2.5	1.200	445.48	35.29	480.77
3.0	1.440	453.02	39.88	492.89
4.0	1.920	465.51	48.36	513.87
5.0	2.400	475.45	56.15	531.61
6.0	2.880	483.55	63.45	547.00
7.0	3.360	490.28	70.35	560.63
8.0	3.840	495.95	76.94	572.89

Figure 149. Example excerpt of shaft settlement output that is read-in from the Spatial Variability tab

5.6.1 Distinguishing Between Analysis of Core-run Versus MWD Datasets

Special text indicators are also included within output files pertaining to drilled shafts (when limestone layers are present) to facilitate distinctions between use of core-run datasets versus MWD datasets. For example, highlighted in Fig. 150 is a region of interest within analysis output files, specific to analysis of drilled shafts when limestone layers are present. That is, the highlighted region allows for identification of the empirical method employed for shaft axial capacity calculations in limestone layers (the region indicates MWD-based analysis in Fig. 150). More specifically, the string “__TEST_METHOD_LIMESTONE_MWD” is printed within the “Job name:” field of each analysis output file. Otherwise, if “McVay Side Friction” was selected from within the “Test Methods” dialog, then “__TEST_METHOD_LIMESTONE_MCVAYSIDEFRICTION” is printed in this portion of each analysis output file, indicating use of the methodology from McVay et al. (1992).

General Information:

=====

Input file:

Project number:

Job name: ___TEST_METHOD_LIMESTONE_MWD

Engineer:

Units: English

Figure 150. Example excerpt of shaft settlement output that is read-in from the Spatial Variability tab in association with analysis of MWD datasets

CHAPTER 6 REFERENCES

- Faraone, M. A. (2014). *Geo-statistical Analysis for Reliability Based Design of Foundations*, Dissertation, University of Florida, Gainesville, FL.
- Faraone, M. A., Klammlar, H., McVay, M., Davidson, M., Herrera, R., Horhota, D. (2021). "Design Methodology for site-specific resistance factors based on foundation location and size", *Computers and Geotechnics*, 138:104328.
- FB-Deep [Computer software]. Bridge Software Institute (BSI), University of Florida, Gainesville, FL.
- McVay, M., Klammlar, H., Faraone, M. A., Krishmarao, D., Jenneisch, C. (2012). *Development of Variable LRFD ϕ Factors for Deep Foundation Design Due to Site Variability*, FDOT Research Report BDK75 977-23, Tallahassee, FL.
- Paikowsky, S. (2004). Load and Resistance Factor Design (LRFD) for Deep Foundations. *NCHRP Report 507*, National Cooperative Highway Research Program (NCHRP), Washington, D.C.
- Rodgers, M., McVay, M. C., Ferraro, C., Horhota, D. (2018b). "Measuring Rock Strength While Drilling Shafts Socketed in Florida Limestone", *ASCE Journal of Geotechnical and Geoenvironmental Engineering*, 144(3).
- Styler, M. (2006). *Development and Implementation of the DIGGS Format to Perform LRFD Resistance Factor Calibration of Driven Concrete Piles in Florida*. Master's thesis, University of Florida, Gainesville, FL.

APPENDIX B

GEOSTAT TECHNICAL MANUAL

Presented below is the Technical Manual for the GeoStat software, which is included as a standalone document, and is accessible from within the GeoStat UI. The Technical Manual integrates work carried out during project Task 1 through Task 4. The manual reviews relevant geotechnical engineering concepts associated with use of the GeoStat software. In addition, illustrative examples and technical guidance are provided regarding selection of modeling parameters when developing site and foundation model components within GeoStat. Furthermore, underlying engineering calculations that are carried out when using the GeoStat software are reviewed.



GeoStat



Technical Manual

DISCLAIMER

No warranty, expressed or implied, is made by the Florida Department of Transportation or the University of Florida as to the accuracy and functioning of any programs or the results they produce, nor shall the fact of distribution constitute any such warranty, and no responsibility is assumed by the Florida Department of Transportation or the University of Florida in any connection therewith.

TABLE OF CONTENTS

DISCLAIMER	i
1. INTRODUCTION	1
1.1 Introduction	1
1.2 Background	1
1.3 Technical Manual Scope.....	2
2. SPATIAL VARIABILITY ANALYSIS	4
2.1 Overview.....	4
2.2 Illustrative Set of Geotechnical Site Data	4
2.3 Site Descriptive Statistics	5
2.4 Spatial Correlation	10
2.5 Variograms	12
2.6 Stochastic Simulation	24
2.7 Realization of Layer Data	35
2.8 Resistance Factor (ϕ)	52
3. METHOD ERROR ANALYSIS	54
3.1 Overview.....	54
3.2 Regression Analysis.....	54
3.3 Driven Piles (SPT)	56
3.4 Driven Piles (CPT).....	57
3.5 Drilled Shafts in Sand	60
3.6 Drilled Shafts in Clay.....	61
3.7 Drilled Shafts in Limestone (Core-run Data).....	62
3.8 Drilled Shafts in Limestone (MWD)	66
3.9 Custom Characterization of Method Error	67
3.10 Total Uncertainty	69
4. MODELING OF EXAMPLE SITE A	75
4.1 Overview.....	75
4.2 Cataloging Site Data.....	75
4.3 Initial Definition of Soil or Rock Layering	82
4.4 Initial Selection of Geo-statistical Parameter Values	88
4.5 Alternative Definition of Soil or Rock Layering.....	99
4.6 Alternative Selection of Geo-statistical Parameter Values	100
4.7 Cursory Examination of the Site A Data for Identifying Zones	107
4.8 Performing Stochastic Simulation	109
4.9 Viewing Spatial Variability Results.....	113

4.10 Incorporating Method Error	117
4.11 Viewing Final Results.....	119
5. MODELING OF EXAMPLE SITE B.....	126
5.1 Overview.....	126
5.2 Cataloging Site Data.....	127
5.3 Initial Definition of Soil or Rock Layering	134
5.4 Initial Selection of Geo-statistical Parameter Values	140
5.5 Identifying Geological Zones.....	147
5.6 Characterizing Site Data for Zone 1.....	148
5.7 Characterizing Site Data for Zone 2.....	154
5.8 Observations Regarding Zonal Issues.....	159
5.9 Performing Stochastic Simulation	162
5.10 Viewing Spatial Variability Results	165
5.11 Incorporating Method Error	171
5.12 Viewing Final Results.....	173
6. REFERENCES.....	178

CHAPTER 1 INTRODUCTION

1.1 Introduction

Spatial variability is exhibited among collections of soil and rock properties that are measured across a given bridge site, which casts some level of uncertainty upon properties at locations between those same measurements. Also, when soil (or rock) properties are utilized in estimating design resistances of deep foundation members via empirical methods, an additional component of uncertainty is introduced. Therefore, two sources of uncertainty that factor into estimations of foundation-member soil resistance are spatial variability and method error.

Determination of axial capacities for deep foundation members, absent considerations for these two forms of uncertainty, can lead to either unconservative or overly conservative bridge foundation layouts. In contrast, incorporation of geostatistics into design calculations facilitates characterization of both forms of uncertainty, particularly when estimating axial capacities of deep foundation members such as piles and drilled shafts.

The GeoStat software contains Geo-statistical analysis features and guides engineers through processes such as: (1) identification of geological zones across a given site; (2) selection of representative layers for a foundation location of interest; (3) characterization of spatial variability intrinsic to available site data; (4) assessment of pile/shaft axial resistance (and variability of the assessment), along with incorporation of both spatial variability and method error phenomena; and, (5) estimation of site-specific Load and Resistance Factor Design, LRFD, resistance (ϕ) factors. Furthermore, the GeoStat software is intended for use in: (1) characterization of whether or not adequate site data have been collected; (2) bringing about increased uniformity of design methodologies in practice; and, (3) improved economy of bridge foundation designs. Consequently, the GeoStat software is a suitable tool for design scenarios where determination of deep foundation member resistance (and characterization of resistance uncertainty) is of interest.

1.2 Background

Development of Geo-statistical techniques and synthesis of relevant load-test data for establishing method error estimations was previously carried out as part of Florida Department of Transportation (FDOT) research (documented in McVay et al. 2009; Klammlar et al. 2010). Subsequently, the advantages of directly accounting for spatial variability and method error phenomena were investigated in Faraone (2014). In the aforementioned studies, focus was given to determining axial capacities of pile and drilled shaft members. Also, focus was given to finding the means to estimate site-specific resistance (ϕ) factors, for comparison

to those prescribed in design provisions such as the AASHTO LRFD bridge design specifications (AASHTO 2020) and the FDOT Structures Design Guidelines (FDOT 2022).

In addition to the above, FDOT-funded research was carried out by McVay et al. (2012) to synthesize Geo-statistical techniques, identify correlations for use in method error calculations, and create prototype software for conducting Geo-statistical analysis. The prototype software was configured to operate on collections of geotechnical site data and produce statistical estimates of pile (or shaft) axial capacity along candidate embedment depths. In addition, the software permitted delineation of the influence of spatial variability and method error (as well as the combined influence) on through-depth resistance calculations. Building upon these past research efforts, including software prototyping and Faraone et al. (2021), has led to the development of the GeoStat software.

Deployment of analysis and design tools that aid in characterizing uncertainty and the soil or rock strata at a given location within a bridge site can bring about benefits with respect to both safety and economy of bridge designs (Rivers, 2018). Accordingly, by accounting for the influences that spatial variability and method error have on estimates of foundation member resistances, several aspects of foundation design can be improved upon through use of GeoStat. Namely, these include: determination of representative soil or rock layering at a location of interest; identification of spatial zones (when present) throughout the site; and, assessment of whether or not additional site data need to be collected. In current practice, deep foundation member design typically entails simplified treatments of (or wholly ignoring) phenomena such as soil or rock layering, spatial zones, and spatial variability among sets of measured soil or rock strength data.

Foundation design data generated in this manner overcome significant simplifications typical of current practice, where phenomena such as rock layering, area zones (i.e., spatial variability) are either ignored or indirectly accounted for via significantly more conservative (and more costly) configurations. By incorporating the GeoStat software into bridge design processes, quantitative indicators of scope and sufficiency can be produced for budgeting, and conducting, geotechnical investigations. Also, the ability to quantify variability in foundation resistance quantities (e.g., the effect of pile/shaft lengths on LRFD resistance factors, ϕ), in turn, allows practicing engineers to achieve more optimized and cost-effective foundation designs.

1.3 Technical Manual Scope

Program documentation for the GeoStat software is divided into two components: (1) a Help Manual; and, (2) a Technical Manual. The present report, the GeoStat Technical Manual, is a standalone document, which details engineering calculations originally developed and/or synthesized in McVay et al. (2012); Faraone (2014); and, Faraone et al. (2021). In addition, presented in the Technical Manual are representative (but anonymized) sets of data obtained

from geotechnical investigations of Florida bridge sites. The site data are utilized to provide guidance and recommendations for establishing GeoStat model files and interpreting results.

The Technical Manual provides engineers with a centralized resource to aid in understanding of the underlying algorithms that are utilized during site analysis, realizations of soil or rock layerings, calculations of pile/shaft axial resistances, and calculations of the associated uncertainty. These underlying algorithms are illustrated via two unique case-studies, where data are selected to be representative relative to what would be measured across Florida bridge sites. In addition, for each site, technical guidance is provided concerning characterization of relevant parameters that describe spatial variability of soil or rock resistance from within GeoStat.

Organization of remaining chapters of the GeoStat Technical Manual is as follows:

- Provided in Chapter 2 is a review of statistical and spatial variability concepts that hold relevance with respect to the analysis and simulation algorithms implemented in the GeoStat software. Emphasis is placed on a graphical technique for characterizing spatial variability (referred to as the variogram).
- In Chapter 3, details are provided concerning the various method error formulations available for use.
- Presented in Chapter 4 is a modeling guide, which makes use of data collected from a Florida bridge site, referred to as Example Site A. The guide walks engineers through pertinent technical concepts associated with usage of the GeoStat software.
- In Chapter 5, data from a second site, Example Site B, is made use of to provide an additional instance of an illustrative modeling guide.

CHAPTER 2 SPATIAL VARIABILITY ANALYSIS

2.1 Overview

The GeoStat software is intended for use in guiding engineers through the processes of characterizing the spatial variability associated with geotechnical site data, quantifying foundation member axial resistance, and quantifying the total uncertainty of axial resistance quantities. To make a clear distinction on terminology, variability can be thought of as a non-homogenous subsurface profile that could result from either manmade or natural processes, such as soil or rock layering and/or the presence of zones. In contrast, uncertainty is related to the engineer's limited knowledge of how rock strength varies within the volume of interest. One of the more challenging tasks for geotechnical engineers is the assessment of variability and uncertainty between points of exploration (e.g., standard penetration test, SPT-N, boring).

The focus of Ch. 2 is on those statistical concepts and analytical techniques that are implemented in GeoStat for characterizing spatial variability phenomena and the associated uncertainty in geotechnical engineering applications. Introduced in Sec. 2.2 is an illustrative data set, which is included solely to facilitate elucidation of the requisite statistical concepts. Documented in Sec. 2.3 is the manner by which descriptive statistics are calculated using geotechnical site data. The concept of spatial correlation is introduced and reviewed in Sec. 2.4. Further, both the concepts and graphical techniques that are applied when forming spatial correlation structures of site data, via variograms, are reviewed in Sec. 2.5.

Subsequent to formation of spatial correlation structures, stochastic simulation—or, in this context, statistical interpolation—can be utilized to form point estimates of pile/shaft axial resistance. Technical aspects of the associated simulation processes, as implemented in the GeoStat software, are discussed in Sec. 2.6. Listings of the types of layers available for modeling in GeoStat, along with the associated soil or rock parameters (and empirical relationships) are documented in Sec. 2.7. Presented in Sec. 2.8 is the mathematical form in which uncertainty is summarily expressed for a given estimate of foundation axial resistance (via the resistance factor, ϕ).

2.2 Illustrative Set of Geotechnical Site Data

To illustrate concepts associated with determining both descriptive statistics and Geo-statistical quantities, an illustrative data set is drawn upon. Plotted in plan-view in Fig. 1 are 40 locations from an idealized site, where locations are expressed as pairs of eastings and northings. In this context, each location is associated with a through-depth profile of boring (or coring) data, with corresponding subsets of site measurements (e.g., SPT-N; unconfined compression strength, q_u). Although illustrative in nature, the locations and accompanying profiles of measurements fall into clusters so as to mimic distributions of boring locations that

would be selected for geotechnical investigation prior to bridge construction (e.g., within or near the footprints of substructures along the bridge).

In the following, illustrative site data associated with these 40 locations, and in particular, ensembles of SPT-N blow count values accumulated across various elevation ranges, are utilized to conceptually convey various statistical phenomena. Note that, although SPT-N blow counts are utilized for illustrative purposes in the next several subsections, the statistical constructs discussed below can generally be formed for any set of measurements taken across a bridge site (e.g., q_u).

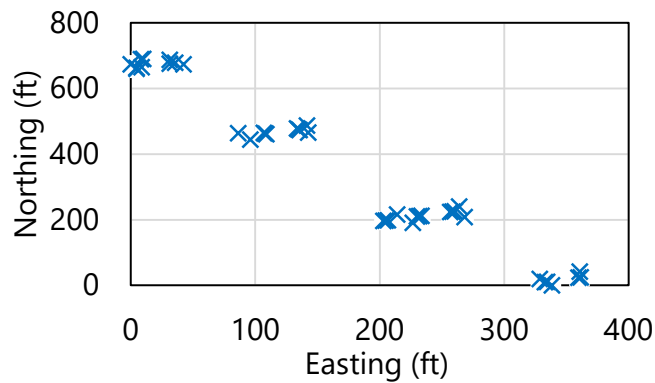


Figure 1. Plan view of illustrative set of 40 boring (and coring) locations

2.3 Site Descriptive Statistics

Descriptive statistics relevant to analysis of geotechnical site data (including histogram, mean, and variance quantities) are discussed throughout Sec. 2.3. See Sec. 2.4 for extension of the descriptive statistics concepts, as pertaining to spatial correlation. In addition, descriptive statistics discussed immediately below are further utilized in Sec. 2.5, where technical documentation is provided concerning the vital graphical concept of variograms.

2.3.1 Histograms

Recalling the 40 illustrative boring (and coring) locations from Fig. 1, consider a scenario where all SPT-N values measured throughout the site are cataloged with respect to elevation. One manner of graphically representing these values is that of the scatterplot, which allows for initial insights to be made regarding the presence of spatial relationships among the data set. For example, an illustrative scatterplot of 88 SPT-N values attributed to an idealized soil layer is provided in Fig. 2. The values fall within elevations ranging between 10 ft and -10 ft.

The SPT-N values (Fig. 2) exhibit appreciable variation (i.e., dispersion, scatter, spread) at a given elevation. Further, a trend is qualitatively observable, where blow count values tend to increase with decreasing elevation (increasing depth). While the scatterplot is extremely useful for gaining insights into spatial phenomena for collections of soil resistance measurements,

data presented in this form do not readily reveal aspects of the ensemble that are related to frequency (i.e., relative likelihood of occurrence).

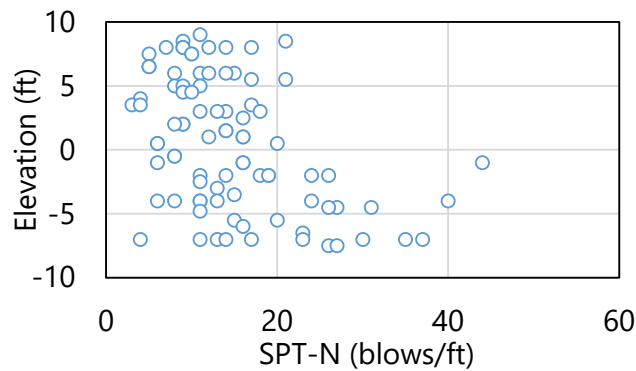


Figure 2. Scatterplot of illustrative set of 88 SPT-N blow counts (elevation range: 10 ft to -10 ft)

As an alternative graphical formation, consider a histogram of the same set of 88 SPT-N blow count values (Fig. 3). The histogram provides a visual representation of the distribution of the data with respect to frequency. The histogram is formed by first calculating a number of intervals (bins, or ranges of SPT-N values). As implemented in the GeoStat software, the following equation is used to calculate the number of bins:

$$n_{bins} = \sqrt{n} \tag{1}$$

where n_{bins} is the integer number of bins and n is the number of points (measurements) in the data set.

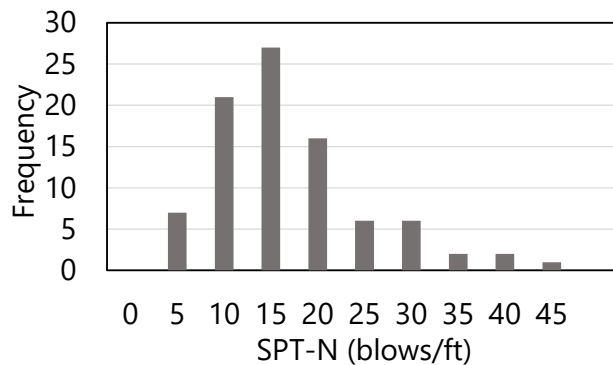


Figure 3. Histogram of illustrative set of 88 SPT-N blow counts (elevation range: 10 ft to -10 ft)

At least two bins—and no more than 25 bins—are permitted when forming histograms in GeoStat. Additionally, the “left-open, right closed” convention is adopted for assigning measured values (q) to bins. This convention signifies adoption of the following two criteria

for assigning a measured value (q) to a bin. Namely, the value must be: (1) equal to or greater than a bin left extent; and, (2) less than right extent of the same bin. As an exception, the rightmost (maximum-value) bin is always “left-open, right-open”.

The maximum bin value (bin_{max}), which lies at the center of the rightmost interval is then determined by:

$$bin_{max} = \max(\{q\}) \quad (2)$$

where $\max()$ denotes the operation of finding the maximum value of an array, and $\{q\}$ is the set of measured values (e.g., SPT-N).

For the 88 SPT-N values, evaluations of Eqn. 1 and Eqn. 2, respectively, give 9 bins and a bin_{max} (center of rightmost interval) value of 45 blows/ft. As the next step in forming the histogram, each of the 88 measured values are then assigned a bin. The cumulative number of values that fall within each bin interval comprise the histogram plotted in Fig. 3.

When data are plotted in histogram form, it is apparent that the distribution of the SPT-N blow count values tend to fall within the range of approximately 10 to 20 blows/ft. In addition, the distribution of the data is such that a skew exists, with a relatively steep reduction in frequency for blow counts less than approximately 10 blows/ft, and a relatively more gradual reduction in frequency for blow counts exceeding approximately 20 blows/ft.

2.3.2 Mean, Median, Standard Deviation, and Variance

From examination of the scatterplot (Fig. 2) and histogram (Fig. 3) of the 88 illustrative SPT-N values (10 ft to -10 ft), it is evident that scatterplots aid in making initial observations regarding spatial characteristics of the data, while histograms aid in assessing data frequency (or how often the data, proportionally, fall within a given range of values). However, scalar-valued descriptive statistics also prove complementary to the above plots for assessing spatial variability, likelihood of occurrence (frequency), and uncertainty of geotechnical site data.

2.3.2.1 Mean and Median

For example, the (arithmetic) mean of the data gives an indicator of expected value, and is expressed as:

$$\mu = \frac{1}{n} \sum q_i \quad (3)$$

where μ is the mean; and is determined by summing the values of each of q_i measurements (1 through n), and then dividing that summation by the total number of measurements (n). The summation over i is from 1 to n , and the geometric mean is the product of the q_i measurements taken to the n^{th} root. While both arithmetic and geometric means are made use of in GeoStat, the former is used to compute resistance (ϕ) factors, while the latter serves to aid in qualitatively characterizing the skew present in distributions of layer-specific data.

In contrast to the mean is the median, which separates the bottom and top halves of the data set. While the mean of the 88 SPT-N blow count values is 15 blows/ft, the median is 13 blows/ft. The median is identified by: (1) sorting the 88 values in increasing order; and, (2) selecting the 44th value from the sorted list.

Recalling the presence of skew in the histogram of Fig. 3, roughly speaking, this is comparable to stating that the mean does not equal the median. This phenomenon is one (among others) that distinguishes idealized histogram shapes. As further illustration, consider two idealized distributions that are germane to geotechnical applications: normal and lognormal distributions (Fig. 4). The normal distribution plotted in Fig. 4a exhibits symmetry (i.e., the mean and median are equal), whereas the distribution in Fig. 4b exhibits right-skew.

These two types of distributions (normal, lognormal) are made frequent use of throughout the present report. For example, the positive and negative residual errors associated with data sets may, in some instances, be characterized as normally distributed. Physical measurements such as unconfined compression strength, q_u , are always positive and tend to exhibit right-skew distributions (characterized as log-normally distributed).

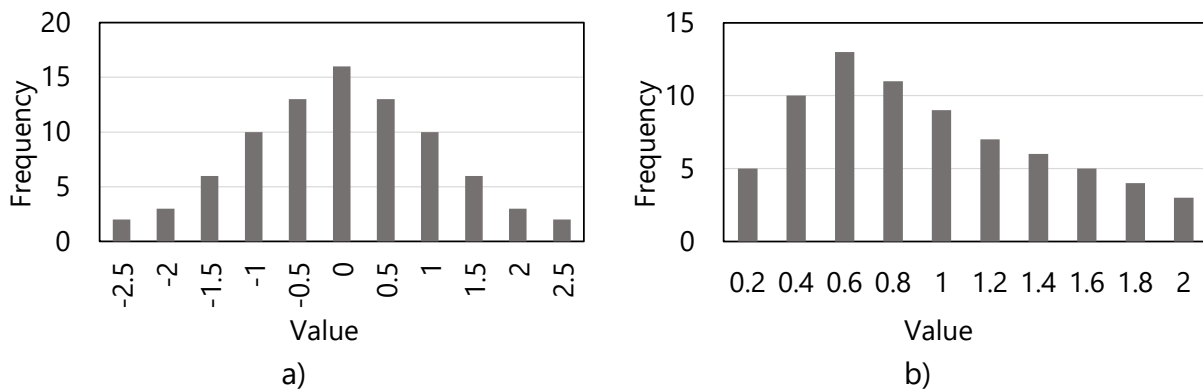


Figure 4. Idealized distribution shapes: a) normal; b) lognormal

2.3.2.2 Standard Deviation and Variance

While descriptive statistics such as the mean (μ) provide point-estimate summary values for the data set, the spread or dispersion of the data set is often quantified using standard deviation, σ (where i is summed from 1 to n):

$$\sigma = \left(\frac{1}{n-1} \sum (q_i - \mu)^2\right)^{0.5} \quad (4)$$

The standard deviation is, roughly, an average of the sum of the differences between each measured value (q_i) and the mean (μ). Another common quantitative representation for the dispersion of the data is that of the variance, which is simply the square of the standard deviation, or σ^2 . Both quantities provide absolute indicators of how far the data extends away from the mean.

2.3.2.3 Coefficient of Variation

A descriptive statistic that provides a relative indication of how much dispersion is present in the data is that of the coefficient of variation, COV:

$$\text{COV} = \frac{\sigma}{\mu} \quad (5)$$

where, for example, a COV value of 1.0 indicates that the magnitude of the data spread is comparable to the magnitude of the mean. The COV for a set of site data has the largest influence on LRFD resistance factors, ϕ , for piles/shafts (and therefore pile/shaft design side friction and end bearing). The larger the COV value, the lower the LRFD- ϕ (or, again, pile/shaft design side friction and end bearing). Scenarios that may lead to relatively high COV values (e.g., values greater than unity) include: (1) too few samples; (2) presence of outlier data (exacerbated by squaring of difference terms in Eqn. 4); and, (3) not breaking up the site into layers or zones—where each constituent data set possesses unique mean and standard deviation (and tends to produce relatively, smaller values of COV). Alternatively stated, the COV value associated with a collection of site data (or that of candidate zones from within a site) is critical to differentiating and identifying layers and zones

For the illustrative set of 88 SPT-N blow count values, the descriptive statistics are listed in Table 1. The mean (μ) is qualitatively reinforced by referring back to the histogram (Fig. 3). In addition, the coefficient of variation (COV) is 0.6, which indicates that the data dispersion is substantial relative to (i.e., 60% as large as) the magnitude of the mean.

Table 1. Descriptive statistics for illustrative set of 88 SPT-N blow counts (elevation range: 10 ft to -10 ft)

Descriptive statistic	Value	Units
Mean (μ)	15.0	blows/ft
Median	13	blows/ft
Standard deviation (σ)	8.3	blows/ft
Variance (σ^2)	68.8	blows ² /ft ²
Coefficient of variation (COV)	0.6	N/A

2.4 Spatial Correlation

As demonstrated above, initial inferences regarding variability and distributions of geotechnical site data are afforded by examination of scatterplots, histograms, and descriptive statistics. However, more explicit statistical assessments are available for characterization of spatial variability phenomena. Introduced in Sec. 2.4 is the concept of spatial correlation and the covariance function, where the latter is used to assess the variability of a mean (e.g., pile/shaft capacities). As an extension of this concept, subsequently introduced in Sec. 2.5 is the key graphical construct for assessing spatial variability from within GeoStat, which is that of the variogram.

2.4.1 Conceptual Illustration

Spatial correlation is a quantitative indication of the strength of the relationship between two physical measurements. One approach to assessing spatial correlation is to plot value pairs for a series of physical distances (McVay et al. 2012). As illustration, three scatterplots of subsets of the 88 SPT-N blow counts at three different prescribed distances are presented in Fig. 5. Also note, even though the illustrative subsets of data are obtained by examining vertical distances between physical measurements, the discussion below also generally applies with respect to horizontal distance.

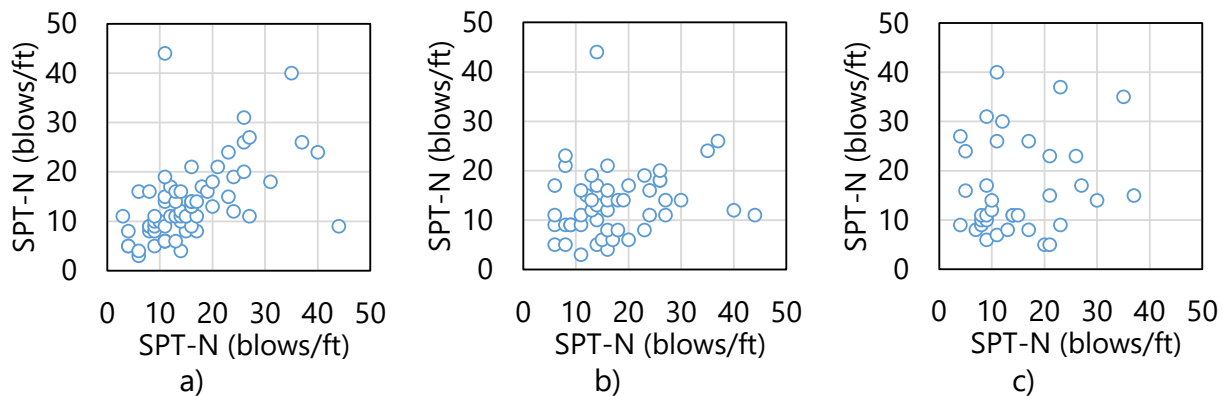


Figure 5. Pairs of illustrative SPT-N blow counts that are separated by a specified vertical distance (elevation range: 10 ft to -10 ft): a) 2.5 ft, 68 pairs; b) 5 ft, 50 pairs; c) 12.5 ft, 41 pairs

Among the 88 measurements, there are 68 pairs of data points that lie approximately 2.5 ft apart. That is, the paired values are positioned at vertical distances of approximately 2.5 ft (typical SPT spacing) with respect to one another (Fig. 5a). At an offset distance (or lag distance, h) of 5 ft, 50 pairs are identified (Fig. 5b). As shown in Fig. 5c, 41 pairs are identified at a lag distance (h) of 12.5 ft. When pairs are formed in this manner, a given point (q_i) is assigned as a member of a pair for every instance where another point (q_j) satisfies the lag distance criterion.

Of particular note when visually scanning from Fig. 5a to Fig. 5c is that the discernibility of correlation (i.e., similar magnitudes) between each paired value steadily degrades with increasing physical distance (lag, h) between points. A clear trend is qualitatively observed (i.e., 45° line) in Fig. 5a ($h = 2.5$ ft), where increasing values of SPT-N blow counts at one location correspond to (correlate with) increasing values of the respective paired values of SPT-N blow counts at distance, h . In contrast, in Fig. 5c ($h = 12.5$ ft) the pairs of points more qualitatively resemble “white noise”, or an illustrative data subset with near-zero correlation.

2.4.2 Covariance

Within the context of geostatistics, the covariance is typically used when quantifying the strength of correlation between pairs of points that satisfy a given lag distance (h). More specifically, covariance is expressed as a function of lag distance (and only accepts points that are physically separated in accordance with lag distance, h):

$$C(h) = \frac{1}{n_{pairs}} \sum (q_i - \mu)^2 \cdot (q_j - \mu)^2 \quad (6)$$

where $C(h)$ is the covariance of the subset of points that are paired; n_{pairs} is the number of pairs; and a double summation is carried out on i, j from 1 to n_{pairs} . When pairs of data are perfectly correlated (i.e., $q_i = q_j$), then the covariance converges to the variance (σ^2) of the data subset (q). When point pairs are not correlated, covariance is 0. In the context of analyzing geotechnical site data—and because correlation tends to decrease with increasing lag distance (h)—the covariance function, $C(h)$ likewise tends to decrease with increasing lag distance (McVay et al. 2012).

2.4.3 Correlation Coefficient

As an additional means of quantifying correlation, a correlation coefficient can be defined as:

$$R(h) = \frac{C(h)}{\sigma^2} \quad (7)$$

where the correlation coefficient, $R(h)$, expressed in this form is dimensionless and is bounded between 0.0 and 1.0. For correlation coefficient values of 1.0, pairs of values are perfectly correlated. A correlation coefficient of 0.0 indicates that no linear relationship exists between the paired points.

2.5 Variograms

Effective use of variograms is critical to successfully characterizing spatial correlation structures that are present among geotechnical site data. Therefore, the next several subsections (within Sec. 2.5) are devoted to formally defining variograms; reviewing common characteristics of variogram curves (e.g., anisotropy); and, delineation of how variograms are computed when using GeoStat.

2.5.1 Variogram Definition

Semi-variograms (commonly referred to as “variograms”) are highly effective constructs for summarily assessing spatial correlations among sets (or subsets) of geotechnical site data. Variograms can be expressed in the following form:

$$v(h) = \frac{1}{2 \cdot n_{pairs}} \sum (q_i - q_j)^2 \quad (8)$$

where the variogram ordinate, $v(h)$, is a function of lag distance (h); and a double summation is carried out on i, j from 1 to n_{pairs} . The variogram as defined in Eqn. 8 includes direct use of the paired physical measurements (q_i, q_j). Differences between measured values are summed across the number of point pairs (n_{pairs}) identified from a wider set of site data. Alternatively stated, the number of pairs, n_{pairs} , is the total number of pairs of physical measurements that were obtained from the site at a distance approximately equal to lag distance, h . In the case of no trend in the data (e.g., increasing values with depth), then the variogram is:

$$v(h) = \sigma^2 - C(h) \quad (9)$$

Here, the variogram is expressed in a form that simultaneously relates lag distance (h) to both covariance, $C(h)$, and variance (σ^2) of all the paired data. Note that the variance (σ^2) of a set of recorded physical measurements is constant, while the covariance, $C(h)$, is a function (among other variables) of lag distance. Further, recall that covariance (Eqn. 6) tends to *decrease* with increasing lag distance (McVay et al. 2012). Consequently, the variogram function tends to *increase* with increasing lag distance.

For a more visual interpretation of variograms, consider the conceptual schematics shown in Fig. 6. Specifically, as shown in Fig. 6a, the variogram indicates a relatively sharp increase (i.e., a sharp reduction in correlation) at small lag distances. With increasing lag distance (h), the idealized variogram of Fig. 6a exhibits asymptotic behavior. Ultimately, the variogram function converges to an ordinate, which in turn, corresponds to the variance (σ^2) of the full data set (i.e., n_{total} pairs of measurements) and covariance $C(h)$ approaches zero.

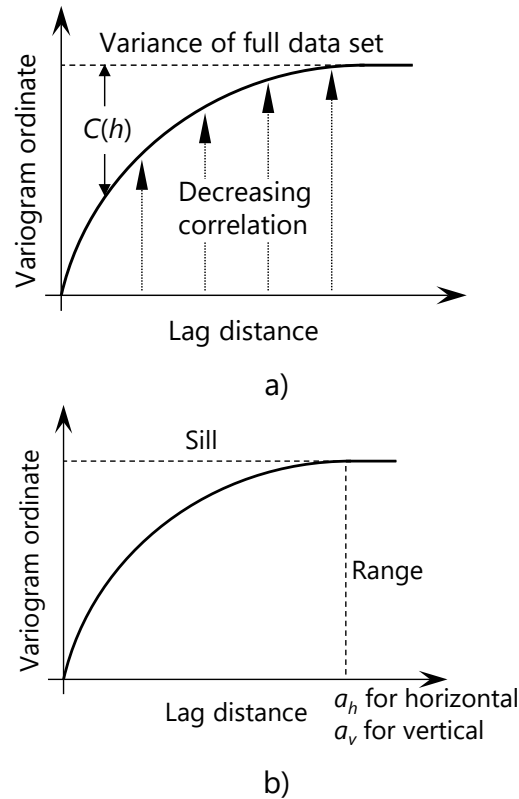


Figure 6. Overview of variograms: a) Conceptual schematic; b) Curve components

Annotations of basic features of variograms are provided in Fig. 6b. The variogram ordinate that corresponds to the variance of the full data set is referred to as the sill. The corresponding lag distance (variogram abscissa value) at which convergence to the sill is attained is referred to as the range (a_h for horizontal, a_v for vertical). Additional features that are commonly present within variograms are discussed in Sec. 2.5.2.

2.5.1.1 Experimental vs Theoretical Variograms

The schematic variogram depictions from Fig. 6 above include continuous, smooth curves to represent the idealized variograms. However, as a distinction, variogram values computed using site data are generally discrete in nature. Discrete collections of variogram points that are directly obtained from sets of physically measured site data are referred to as experimental variograms (Fig. 7a). In contrast, continuous mathematical functions (which are intended for best-fit representations of experimental variogram points) are referred to as theoretical variograms (Fig. 7b). Theoretical variograms, rather than experimental variograms, are used for conducting stochastic simulation to determine deep foundation member axial resistance. Therefore, an important aspect of site modeling within GeoStat is that of ensuring that experimental variograms are appropriately fitted with theoretical variograms.

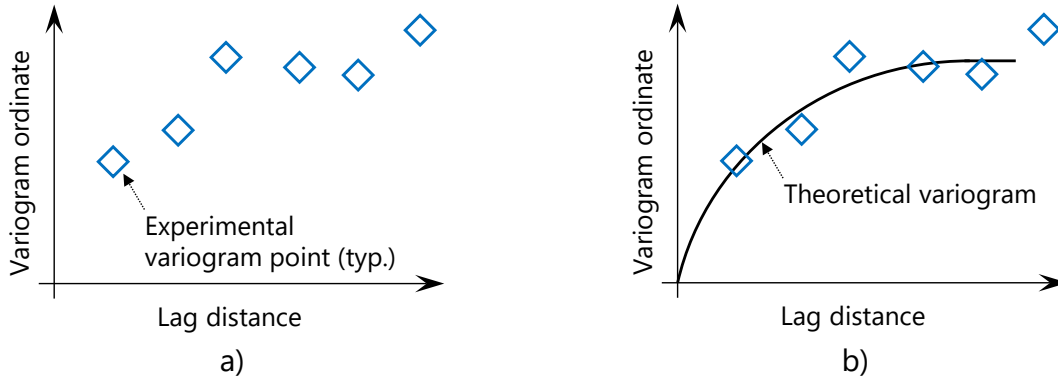


Figure 7. Overview of variograms: a) Experimental variogram; b) Theoretical variogram

Two forms of theoretical functions are available to choose from when modeling spatial correlation structures in GeoStat. A spherical form is expressed as:

$$v_{theoretical}(h) = \sigma^2 \cdot \left(1.5 \frac{h}{a} - 0.5 \left(\frac{h}{a}\right)^3\right); h < a \quad (10)$$

where $v_{theoretical}(h)$ is the ordinate of the theoretical variogram function; and, a is the range (recall Fig. 6b). For h equal to or greater than a , the function ordinate equals σ^2 . The exponential form is expressed as:

$$v_{theoretical}(h) = \sigma^2 \cdot \left(1 - \exp\left(\frac{-3.0|h|}{a}\right)\right) \quad (11)$$

where both of the theoretical expressions typically conform to the overall curve shapes shown in Fig. 7b. When the lag distance (h) approaches the range (a), evaluations of Eqn. 10 and Eqn. 11 approach the variance, σ^2 . The form of the variogram (spherical or exponential) is used to ensure that an estimate (e.g., SPT-N blow count value, q_u) at any location is possible.

2.5.2 Anisotropy

In the context of geotechnical site data, spatial variability phenomena are often direction dependent. More specifically, unique variograms are often necessary to describe spatial correlations in horizontal and vertical directions. For such instances, the soil data is spatially categorized as anisotropic, where several forms of anisotropy are possible.

In rare instances, the same variogram curve may be suitable for describing spatial variability in both the horizontal and vertical directions (isotropic, Fig. 8a). More often, geotechnical site data possess spatial correlation characteristics such that either the range (a), the sill, or both features differ with respect to variogram direction (as shown in the schematics of Fig. 8b through Fig. 8d).

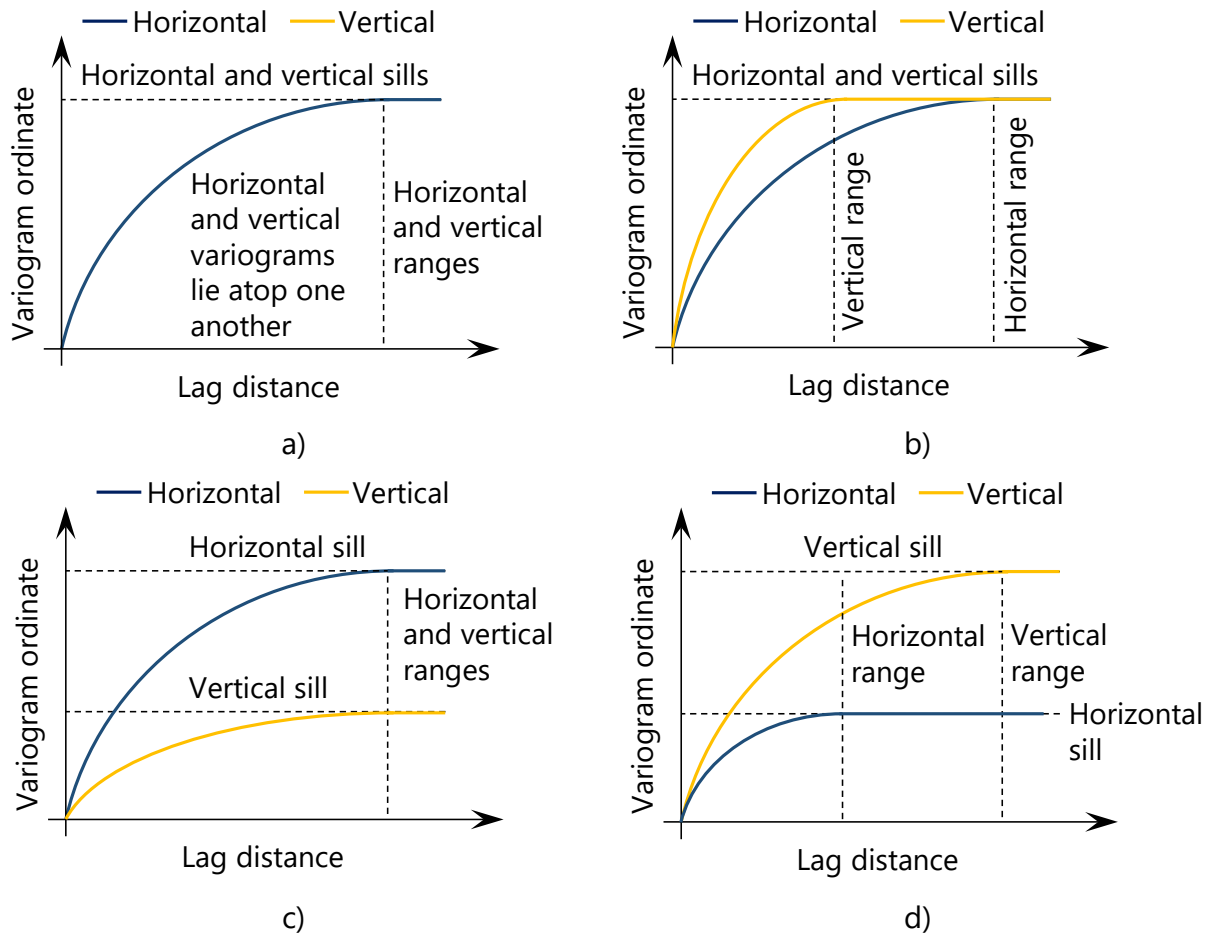


Figure 8. Variogram isotropy and anisotropy: a) Isotropy; b) Geometric anisotropy; c) Zonal anisotropy; d) Geometric and zonal anisotropy (i.e., layering)

When the horizontal and vertical variograms have the same sill, but different range values (a), the condition is referred to as geometric anisotropy (Fig. 8b). The material has a shorter correlation range vertically than horizontally as a result of the soil formation process. Zonal anisotropy (Fig. 8c) signifies that the material has less variability vertically than horizontally, and suggests that the site should be broken into zones to reduce COV (i.e., variability). Combined forms of anisotropy can also occur. As illustration, Fig. 8d shows less variability horizontally than vertically, and is a clear indicator of soil or rock layering.

Of particular note, when data sets exhibit zonal anisotropy (Fig. 8c), then the corresponding variances (σ^2) are also direction dependent. Per McVay et al. (2012), it is very important to identify zonal anisotropy because the overall variance of the data may adversely affect estimation of the data uncertainty when calculating LRFD resistance factors (ϕ). Furthermore, when zonal anisotropy occurs, it may signify that the data set being considered encompasses

multiple geological zones, and requires further division such that one data subset is defined for each zone.

2.5.2.1 Additional Variogram Features

Additional features and phenomena that may appear when constructing variograms are presented in the schematics of Fig. 9. For instances where errors in measurement have occurred, or where only a relatively small number of data pairs are available (McVay et al. 2012), the corresponding variogram (in a given direction) may exhibit the “nugget effect” (Fig. 9a).

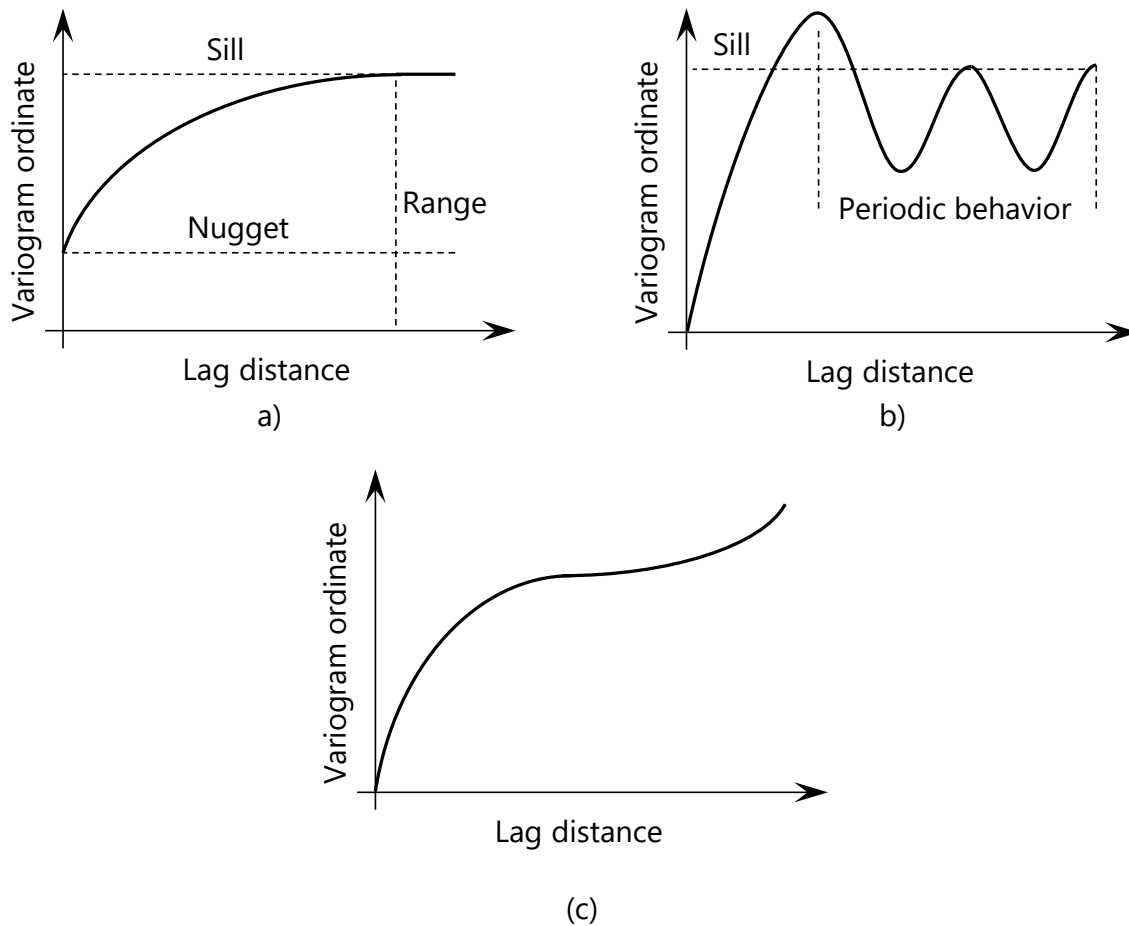


Figure 9. Additional variogram phenomena: a) Nugget effect; b) Cyclic behavior; c) Non-asymptotic behavior

The phenomenon of cyclic behavior is depicted in Fig. 9b. This variogram feature corresponds to use of a data set, that physically, includes spatially periodic bands (i.e., layers) in the facies (Gringarten and Deutsch, 2001). For such instances, particularly for vertical variograms, the data subset may need to be further subdivided (broken up into smaller ranges of elevations). Data which has a trend (e.g., SPT-N or q_u increasing with depth) exhibits non-asymptotic

behavior (Fig. 9c). Therefore, the data violates Eqn. 9 and detrending is necessary (discussed in Sec. 2.5.4).

2.5.3 Variogram Formation

From a computational standpoint, additional considerations are necessary when forming the points of experimental variograms. For example, it is not practical to use only pairs of measurements that exactly satisfy a given lag distance when determining the number of pairs within a data set. Therefore, when forming an experimental variogram in a given direction, a search domain is considered for identifying pairs of measurements (Fig. 10). Searches for pairs of data points are divided into discrete distances ranging from the lag distance (h) up to, and including, the product of the lag distance and number of lags (n_{lags}).

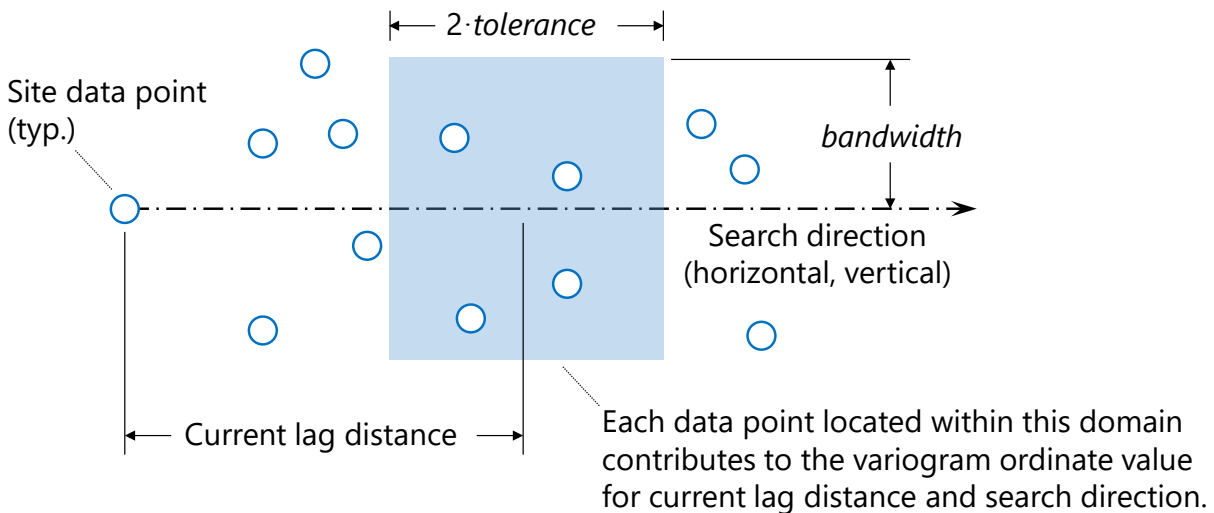


Figure 10. Geometric search terms for forming variograms

Both the tolerance (*tolerance*) and bandwidth (*bandwidth*) terms are used to define the search domain associated with a given, current search distance. Tolerance is parallel to the search direction and bandwidth is perpendicular to the search direction. The tolerance is limited to one half of the respective base lag distance (h). In the case of horizontal searches, bandwidth should be less than or equal to the tolerance, whereas for vertical searches the bandwidth is generally smaller (0 ft to 1 ft) due to prescribed distances between SPT-N profiles and core drilling specimens. Note that for case studies reported in McVay et al. (2012), the recommended bandwidth magnitude was 1 ft (up to 2 ft) for horizontal searches, and 0 ft for vertical searches. Regarding each applicable search direction (horizontal, vertical), the search process is repeated for n data points to identify point pairs (n_{pairs}). Variogram ordinate values are then computed by operating on distances between pairs of data points. The procedures for forming variograms in the horizontal and vertical directions are delineated in Fig. 11 and Fig. 12, respectively.

Horizontal variogram formation

Given $\{Z_{score}\}$, $\{northing\}$, $\{easting\}$, and $\{elevation\}$ for n site data points
 Select h , n_{lags} , *bandwidth*, and *tolerance*
 For $i = 1, n_{lags}$
 ↑ $n_{pairs} = 0$
 ↑ $\epsilon_{Zscore} = 0$
 For $j = 1, n$
 ↑ For $k = 1, n$
 ↑ $\Delta_{north} = \{northing\}_j - \{northing\}_k$
 ↑ $\Delta_{east} = \{easting\}_j - \{easting\}_k$
 ↑ $\Delta_{elev} = \{elevation\}_j - \{elevation\}_k$
 ↑ $\Delta_{horiz} = (\Delta_{north} \cdot \Delta_{north} + \Delta_{east} \cdot \Delta_{east})^{0.5}$
 ↑ If $|\Delta_{elev}| \leq 0.5 \cdot \textit{bandwidth}$
 ↑ If $\Delta_{horiz} \leq h \cdot i + \textit{tolerance}$ & $\Delta_{horiz} \geq h \cdot i - \textit{tolerance}$
 ↑ $\epsilon_{Zscore} = \epsilon_{Zscore} + (Z_{score j} - Z_{score k})^2$
 ↑ $n_{pairs} = n_{pairs} + 1$
 End of loop on k
 End of loop on j
 Determine variogram point:
 Abscissa = $h \cdot i$
 Ordinate = $0.5 \cdot \epsilon_{Zscore} / n_{pairs}$
 Corresponding Pairs = $0.5 \cdot n_{pairs}$
 End of loop on i

Figure 11. Horizontal variogram formation

Vertical variogram formation

Given $\{Z_{score}\}$, $\{northing\}$, $\{easting\}$, and $\{elevation\}$ for n site data points
 Select h , n_{lags} , *bandwidth*, and *tolerance*
 For $i = 1, n_{lags}$
 ↑ $n_{pairs} = 0$
 ↑ $\epsilon_{Zscore} = 0$
 For $j = 1, n$
 ↑ For $k = 1, n$
 ↑ $\Delta_{north} = \{northing\}_j - \{northing\}_k$
 ↑ $\Delta_{east} = \{easting\}_j - \{easting\}_k$
 ↑ $\Delta_{elev} = \{elevation\}_j - \{elevation\}_k$
 ↑ $\Delta_{horiz} = (\Delta_{north} \cdot \Delta_{north} + \Delta_{east} \cdot \Delta_{east})^{0.5}$
 ↑ If $\Delta_{horiz} \leq 0.5 \cdot \textit{bandwidth}$
 ↑ If $|\Delta_{elev}| \leq h \cdot i + \textit{tolerance}$ & $|\Delta_{elev}| \geq h \cdot i - \textit{tolerance}$
 ↑ $\epsilon_{Zscore} = \epsilon_{Zscore} + (Z_{score j} - Z_{score k})^2$
 ↑ $n_{pairs} = n_{pairs} + 1$
 End of loop on k
 End of loop on j
 Determine variogram point:
 Abscissa = $h \cdot i$
 Ordinate = $0.5 \cdot \epsilon_{Zscore} / n_{pairs}$
 Corresponding Pairs = $0.5 \cdot n_{pairs}$
 End of loop on i

Figure 12. Vertical variogram formation

As initial steps in the variogram formation process, data values and corresponding positions for n points are cataloged. The position terms include arrays of northing, $\{northing\}$; easting, $\{easting\}$; and, elevation, $\{elevation\}$. Note that the “raw” measurements of data are not used in variogram formation in GeoStat. Rather, consistent with McVay et al. (2012), a normal distribution standard score (z-score) is assigned to each measurement, relative to the ensemble descriptive statistics of the n data points. The z-scores are cataloged, as $\{Z_{score}\}$, where array entries correspond to those of the positioning arrays. Formation of z-scores for an illustrative data set is given in Sec. 2.5.4.

As the next step in variogram formation, selections are made for lag distance (h), number of lags (n_{lags}), *bandwidth*, and *tolerance*. (recall that the latter two parameters are depicted in Fig. 10 above). Then, for each of n_{lags} , a double loop on the number of data points (n) is iterated upon. For the innermost loop over n data points (the loop on k in both Fig. 11 and Fig. 12), changes in northing (Δ_{north}), easting (Δ_{east}), elevation (Δ_{elev}), and horizontal distance (Δ_{horiz}) are calculated between candidate pairs of data points.

Subsequently, the distance between the two data points being considered is compared to the search domain (recall Fig. 10) for the current search distance. For horizontal variogram searches, horizontal distance (Δ_{horiz}) is associated with *bandwidth*, while elevation (Δ_{elev}) is associated with both the current search distance and *tolerance*. In contrast, for vertical variogram searches, elevation (Δ_{elev}) is associated with *bandwidth*; horizontal distance (Δ_{horiz}) is associated with both the current search distance and *tolerance*.

For each search distance considered, and for pairs of data points that satisfy the search criteria, a squared-difference term (ϵ_{Zscore}) is calculated from the z-scores of the data pairings. The squared-difference term is accumulated each time a pairing is identified. In addition, the pair count (n_{pairs}) is incremented each time a pairing is identified.

After the double loop on n data points is iterated through, the variogram point associated with the current search distance is calculated as shown in the bottom portions of Fig. 11 and Fig. 12. To prevent double-counting of point pairs, the n_{pair} term is divided by 2 at this point in the variogram formation process. After iterating through n_{lags} , the experimental variogram is taken as the catalog of the variogram points.

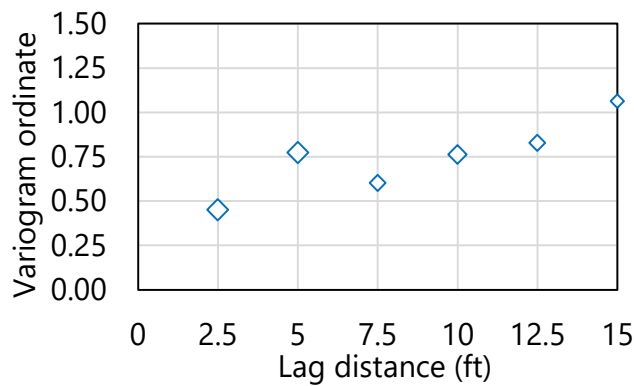
2.5.3.1 Illustrative Example of Variogram Formation

An illustrative example is given in the following of vertical variogram formation. However, the same general concepts apply with respect to formation of horizontal variograms. Recall from Fig. 2 the illustrative data set consisting of ($n = 88$) SPT-N blow counts, over the elevation range 10 ft to -10 ft. Consider (for illustration) selection of a lag distance (h) of 2.5 ft, six lags ($n_{lags} = 6$), and use of recommended values for *bandwidth* (0 ft) and *tolerance* (half of h , 1.25 ft)

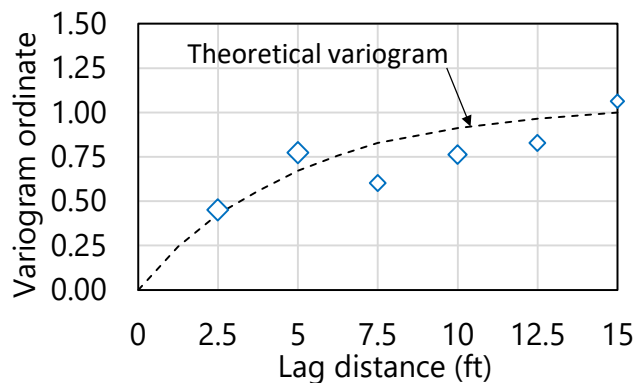
in accordance with McVay et al. (2012). Using the procedure listed above in Fig. 12, vertical variogram abscissa values, ordinates, and pairs (n_{pairs}) of the experimental variogram are produced, as listed in Table 2 and plotted in Fig. 13a.

Table 2. Vertical variogram data for illustrative set of 88 SPT-N blow counts (elevation range: 10 ft to -10 ft)

Abscissa (ft)	Ordinate	Pairs
2.5	0.45	68
5.0	0.77	50
7.5	0.6	27
10.0	0.76	36
12.5	0.83	25
15.0	1.06	12



a)



b)

Figure 13. Vertical variogram for illustrative set of 88 SPT-N blow counts (elevation range: 10 ft to -10 ft): a) Variogram points; b) Variogram points and theoretical fit

GeoStat facilitates interactive graphical selection of theoretical variogram fits, given some experimental variogram (see Ch. 4 of the GeoStat Help Manual for additional details). An overlay of an exponential (theoretical) variogram, with use of Eqn. 11, a range (a) of 15 ft, and

sill of 1.0 is plotted in Fig. 13b. A sill value of 1.0 is selected because the z-scores ($v(h)/\sigma^2$) of the data set are utilized in forming the variogram.

Such use of z-scores, as implemented in GeoStat, is consistent with McVay et al. (2012) and serves to conveniently normalize variogram ordinate values. In this way, a sill value of 1.0 signifies that, for all points separated at a distance equal to or greater than the range (a), the spatial relationship between said data points is no more informative than that of the variance (σ^2) of the n_{pairs} of points that were selected during the pairing process. Stated alternatively (and recalling Eqn. 9), the covariance, $C(h)$, reaches zero at distances equal to or greater than the range (a), and so, only the covariance (σ^2) remains as a non-trivial contributor to the variogram ordinate values.

As an additional observation for this illustrative example, consider the listing of distance-dependent paired values in Table 2, where pair counts range from 12 to 68. It is recommended in McVay et al. (2012) that, ideally, 30 or more pairs should be obtained for each point along the experimental variogram. However, given typical volumes of geotechnical site data, this may not be feasible for all points of experimental variograms. Accordingly, visual emphasis is placed upon those points that are associated with pair counts exceeding 30. More specifically, as implemented in GeoStat and shown in Fig. 13 above, the sizes of plotted experimental variogram points increase in proportion to the number of associated pairs. Therefore, when fitting theoretical variograms to experimental variograms within GeoStat, it is recommended that the theoretical variogram should favor proximity to more prominently drawn (larger) data points rather than smaller data points.

2.5.4 Additional Considerations for Variogram Formation

Discussed immediately below are additional considerations pertaining to variogram formation. First, the concept of data detrending is reviewed, where this operation holds relevance both with respect to variogram formation and stochastic simulation (the latter of which is discussed in Sec. 2.6). In addition, the manner by which normal score (z-score) values are determined and utilized is reviewed. An illustrative data set of SPT-N blow counts is utilized to aid in elucidating the conceptual discussions.

2.5.4.1 Data Detrending

As is discussed in Sec. 2.6, the GeoStat software makes use of stochastic simulation to produce estimates of deep foundation member axial resistance, along with associated characterizations of variability and uncertainty. It is assumed that both the correlation structure and frequency distribution of a given data set (e.g., geotechnical data concentrated within a selected range of elevations, or soil or rock data within a layer) remain approximately constant along the direction of interest (horizontal, vertical). When a data set exhibits these qualities, it is referred to as stationarity. Also, because of the critical role that variograms play

in performing stochastic simulation (discussed later), stationarity is a necessary attribute for data to possess when said data are utilized in forming variograms.

To illustrate the significance (and procedure) of data detrending, recall the illustrative set of 40 borings for an idealized site (Fig. 1). Further, consider an illustrative set of 51 SPT-N blow counts, measured across the elevation range of 30 ft to 10 ft (Fig. 14a). Descriptive statistics for the 51 SPT-N blow counts are listed in Table 3.

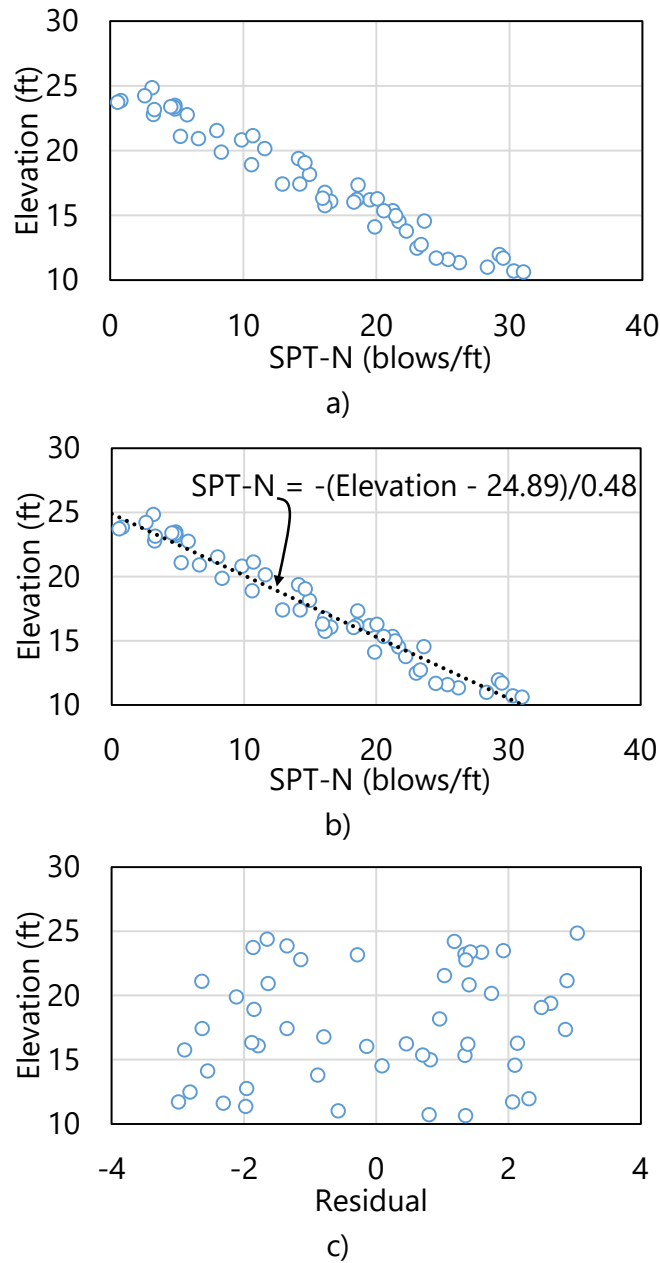


Figure 14. Detrending of illustrative set of 51 SPT-N blow counts (elevation range: 30 ft to 10 ft): a) Scatterplot; b) Scatterplot with inverted trend line; c) Residual

Table 3. Descriptive statistics for illustrative set of 51 SPT-N blow counts (elevation range: 30 ft to 10 ft)

Descriptive statistic	Value	Units
Mean (μ)	14.9	blows/ft
Standard deviation (σ)	8.9	blows/ft
Variance (σ^2)	80.1	blows ² /ft ²
Coefficient of variation (COV)	0.6	N/A

Plotted in Fig. 14b are both the scatterplot points and a linear regression fit. As expressed, the regression curve is inverted such that SPT-N is the dependent variable and elevation is the independent variable. The detrending process is carried out by considering each measured SPT-N value, using the associated elevation to evaluate the inverted regression expression, and then subtracting the inverted function value from the measured SPT-N value. The difference between these two values (inverted expression evaluation and measured value) is referred to as the residual.

Carrying out the detrending process for the 51 SPT-N blow counts produces the scatterplot of residuals shown in Fig. 14c. The qualitative distribution of the residuals resembles that of “white noise” compared to depth (Fig. 14a); however the new residual data may still exhibit correlation between pairs (evident from variogram). However, the collection of residuals (Fig. 14c) approximately uphold stationarity, whereas stationarity is not present among the trend-laden measurements of SPT-N blow counts. Also, the variogram does not reach a constant sill value (recall Fig. 9c). Therefore, the residual data—as opposed to the measured SPT-N values—are used when trends are present among measured values used to form z-scores (discussed immediately below), and subsequently, to form experimental variograms and estimates of properties. The estimates of values for SPT-N (or rock strength, etc.) will have the trend added back prior to pile/shaft capacity estimation. Finally, if trends are not present among the “raw” measurements, then the detrending process is not necessary. The GeoStat software is configured such that any given layer of soil or rock data may or may not be detrended for the purpose of variogram formation, at the discretion of the engineer.

2.5.4.2 Normal Score (Z-Score)

Recall from the step-by-step listings of variogram formation (Fig. 11, Fig. 12) that the z-score transformation (mean of zero, standard deviation of unity) of data points rather than the measured values themselves are used when forming experimental variogram points. As illustrated in previous sections, this approach allows for more consistent interpretations of variograms and adds convenience when selecting theoretical variogram features such as sills. To carry out normal score (z-score) calculation given a data point (q), the following expression is evaluated:

$$Z_{score} = \frac{q - \mu}{\sigma} \quad (12)$$

where the z-score (Z_{score}) is a dimensionless quantity. When detrending is not carried out on a data set, z-scores are computed using the “raw” data (e.g., SPT-N, q_u). However, when detrending is carried out on a data set, z-scores are determined (for the purpose of forming variograms) using residuals rather than the measured data.

As illustration, plotted in Fig. 15 are the z-scores corresponding to the residuals of the 51 SPT-N data points from Fig. 14. Because the mean of the residuals is approximately zero-valued for this illustrative data set, the plots of residuals and the z-scores are proportional to one another.

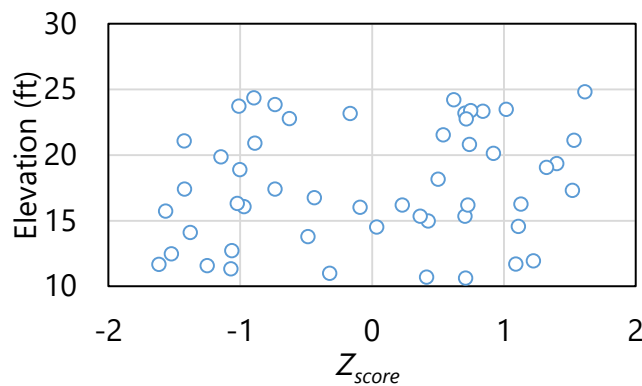


Figure 15. Normal score (Z_{score}) of residuals for illustrative set of 51 SPT-N blow counts (elevation range: 30 ft to 10 ft)

2.6 Stochastic Simulation

Axial resistances of deep foundation members are determined in GeoStat by stochastically simulating realizations (profiles) of geotechnical site data (e.g., SPT-N, q_u); empirically relating geotechnical site data to unit quantities of side and tip resistance (skin friction, f_s ; tip resistance, q_{tip}); and, then integrating the unit quantities. Introduced in Sec. 2.6.1 and Sec. 2.6.2 are the means by which probabilistic simulation can be conducted using GeoStat (unconditional and conditional, respectively). Additional considerations for conducting stochastic simulation (with focus on worst case conditions regarding variability and uncertainty) are documented in Sec. 2.6.3. See Sec. 2.7 for documentation of the empirical relationships used in relating between layer-specific soil or rock parameter values and unit quantities of side and tip resistance.

2.6.1 Unconditional Simulation

Unconditional simulation is analogous to simulation of spatially varying geotechnical properties with complete knowledge of a site (McVay et al. 2012). Further, for unconditional

simulation, the plan-view foundation location is unknown. Stated alternatively, unconditional simulation involves generation of random variable values on a specified geometric grid such that the probability distribution functions (PDFs) and correlation structures of the available points of measured data are (on average) reproduced. Further, results from unconditional simulation represent typical site or zone properties, and the associated LRFD- ϕ value. These aspects of unconditional simulation are in contrast to those of conditional simulation (discussed in Sec. 2.6.2), where realizations of soil or rock profile data are conditioned to specific boring values.

Unconditional simulation is implemented in GeoStat via use of the lower-upper triangular matrix decomposition algorithm (i.e., the *LU* algorithm), and in turn, produces spatially varying vertical profiles of soil or rock parameters that satisfy the variogram of the site (or zone, layers, etc.). The overall unconditional simulation procedure is illustrated in Fig. 16. Major steps include: generation of a geometric grid; generation of covariance matrices (per soil or rock layer); and then, performance of stochastic simulation. In addition, as part of the overall unconditional simulation procedure, vertical variograms (discussed in Sec. 2.5) play an important role, as highlighted in Fig. 16 (upper-right).

As the first major step in the unconditional simulation procedure (Fig. 16, upper-left), a geometric location grid is formed. For a range of candidate embedment lengths (as specified by the engineer), only the corresponding elevations, $\{elevation\}$, are accumulated. In GeoStat, the associated elevations that fall within each soil or rock layer are subdivided into 0.5-ft increments.

As the second major step (Fig. 16, middle-left), covariance matrices, $[C]$, are formed for each soil or rock layer. More specifically, for each of n_{layers} , the corresponding subsets of $\{elevation\}$ values are expanded into matrix form. Here, such expansion denotes that the matrices house columnated differences in vertical position for each location of interest (i.e., each diagonal entry), relative to every other location of interest (i.e., all other column entries). That is, the $\{easting\}$ vector is expanded using the following expression:

$$[\Delta_{elev}] = \{elevation\} \cdot \{1\}^T - (\{elevation\} \cdot \{1\}^T)^T \quad (13)$$

where $[\Delta_{elev}]$ is a matrix of differences in elevation; $\{1\}$ is a vector of unity-valued entries; and, the superscript "T" denotes the transpose operation.

At this stage, the vertical variogram of the current layer holds significance (Fig. 16, upper-right; see Sec. 2.5 regarding formation of variograms). Subsequent to formation of the elevation-difference matrix, all terms are squared and normalized by the square of the range of the theoretical, vertical variogram (a_v):

$$[h_{norm}]_{jk} = ([\Delta_{elev}]_{jk}^2 / a_v^2)^{0.5} \quad (14)$$

where $[h_{norm}]$ is a symmetric matrix of the normalized vertical distance between each location of interest, relative to every other location considered (within the current layer). The subscripts "jk" denote that the total distance is computed on an entry by entry basis. In certain instances, vertical variograms may be formed within a given layer and exhibit features such as the nugget effect (as introduced in Sec. 2.5). For these instances, a normalization scheme analogous to that described above for the vertical range (a_v) is carried out.

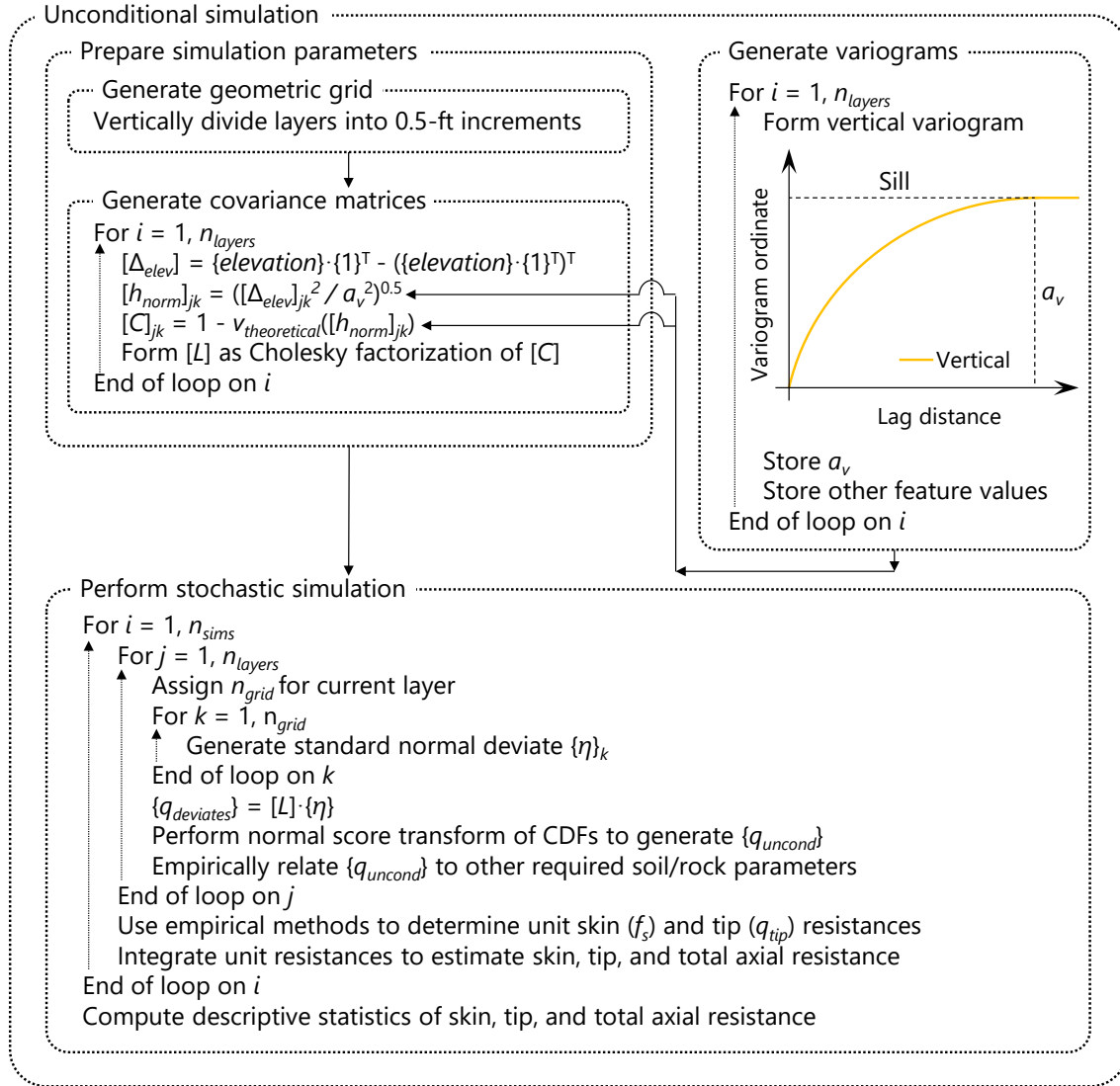


Figure 16. Unconditional simulation procedure

Having formed the matrix of normalized vertical distance for every location of interest within a layer (relative to every other location of interest), the selected form of the theoretical variogram, $v_{theoretical}$, is evaluated (exponential, spherical; as introduced in Sec. 2.5). Recall that,

when forming the entries of $[h_{norm}]$, variogram range values (a_v) are used for normalization. Therefore, evaluations of the theoretical variogram are carried out without direct use of the respective variogram range values. For example, consider a scenario where the exponential form is made use of when forming the theoretical variograms within a given layer. Then solely for the purposes of evaluating the vertical variogram using entries of $[h_{norm}]$ within said layer, the theoretical variogram is modified from that of Eqn. 11 to:

$$v_{theoretical}([h_{norm}]_{jk}) = 1 - \exp(-[h_{norm}]_{jk}) \quad (15)$$

Relative to the variogram definition from Eqn. 9, the variance (σ^2) of all measured data for all locations of interest within the layer is not directly present in Eqn. 15. This is because, as discussed in Sec. 2.5, the variogram formation process in GeoStat involves subjecting measured geotechnical site data to a separate normalization process. As an additional artifact of data normalization, during variogram formation in GeoStat, entries of the covariance matrix, $[C]$, can also be formed without direct use of the data variance:

$$[C]_{jk} = 1 - v_{theoretical}([h_{norm}]_{jk}) \quad (16)$$

The covariance matrix is symmetric and positive definite due to the choice of the $v(h)$ functional form (experimental, spherical). Therefore, Cholesky decomposition is next carried out to obtain the (factorized) lower triangular form of the covariance matrix, $[L]$. As emphasis, formation of the lower triangular matrix is repeated for each layer.

The stochastic simulation is then undertaken (Fig. 16, bottom) for the desired number of soil or rock profiles to be realized (n_{sims}). For each realization, the system layers (n_{layers}) are iterated through. For each layer considered, the number of locations in the geometric grid (n_{grid}) is first assigned, and in turn, iterated through. At this tertiary loop-level, independent values of standard normal deviates are sampled n_{grid} times and stored in vector form $\{\eta\}$. As context, a standard normal deviate is a value sampled from the standard normal distribution (i.e., a unitless normal distribution with mean of 0 and standard deviation of 1). The independently sampled deviate values are then used along with the layer-specific lower-triangular matrix of covariance, $[L]$, to form simulated values of measured properties:

$$\{q_{deviates}\} = [L] \cdot \{\eta\} \quad (17)$$

where $\{q_{deviates}\}$ is the collection of layer-specific, simulated values of soil properties.

The terms in $\{q_{deviates}\}$ are obtained by operating (in part) on normally distributed data (i.e., $\{\eta\}$). However, physically measured data, $\{q\}$, within a given layer may or may not be normally distributed (distribution types such as log-normal are more commonly applicable to strength quantities). Therefore, a normal score transformation is carried out to map from the normally

distributed values making up $\{q_{deviates}\}$ to a distribution that reflects the ensemble of layer-specific physical measurements, $\{q\}$. This procedure is depicted in Fig. 17 for a mapping between normally distributed values of $\{q_{deviates}\}$ and an illustrative set of physical, log-normally distributed data $\{q\}$. Note that the use of a log-normal distribution is utilized here purely as illustration; this transformation procedure applies to other distributions as well.

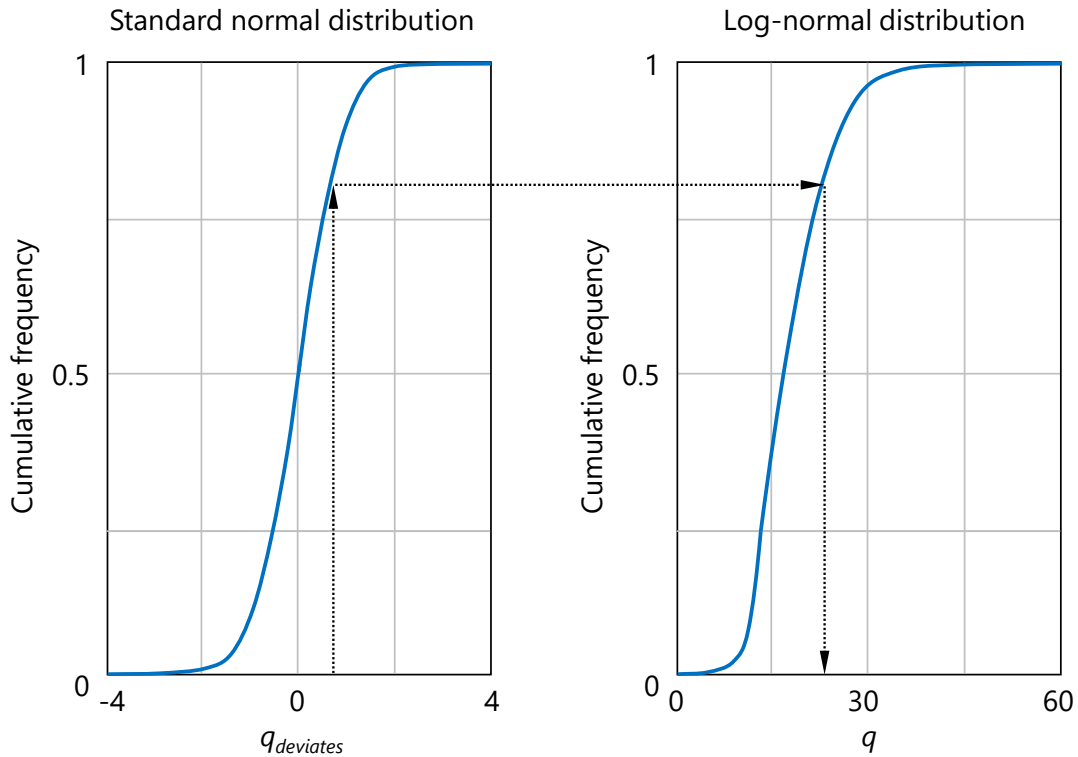


Figure 17. Illustrative normal score transformation (from normal to log-normal) using cumulative distribution functions

The mapping procedure (Fig. 17) involves permuting through each entry of $\{q_{deviates}\}$. For each entry, the associated CDF value of the normally distributed data (Fig. 17, left) is determined. Then, the ordinate axis of the log-normally distributed data is entered at the same cumulative frequency value (Fig. 17, right). The unconditional simulation value is then assigned by honoring the CDF of the physically measured values. The set of values simulated in this manner constitute the unconditionally simulated values $\{q_{uncond}\}$ for the layer currently being considered.

At this step in the unconditional simulation process, the simulated values, $\{q_{uncond}\}$, always correspond to one of: SPT-N blow counts; CPT cone resistance; unconfined compression strength of rock, q_u ; or, unconfined compressive strength as estimated from Measuring While Drilling (MWD) site data. For the purpose of building up required soil or rock parameters within a layer, beyond those of aforementioned parameters, it is necessary to make use of empirical relations. For example, SPT-N and q_u values can be used along with empirical

relationships to estimate the other required soil or rock parameters. Additional details of the required parameters, and associated empirical relationships, are provided in Sec. 2.7.

Continuing with the unconditional simulation procedure (Fig. 16, bottom)—after all layers are iterated through—empirical methods are utilized to relate profiles of soil or rock strength parameters to unit skin friction (f_s) and tip resistance (q_{tip}) quantities. Then, the unit quantities are integrated to form estimates of pile/shaft axial resistance for the current simulation (i.e., pile/shaft configuration and candidate embedment length). The axial capacity calculation software FB-Deep is used for this purpose. See the FB-Deep Help Manual for details regarding empirical determination of unit resistance quantities and integration of these quantities to determine axial, tip, and total resistances of piles/shafts.

The final step of the unconditional simulation procedure (Fig. 16, bottom) is to form descriptive statistics of skin, tip, and total resistances for the pile/shaft section and range of embedment lengths being analyzed. As a result, through-depth profiles of mean-valued resistance are formed. As direct measures of spatial variability, through-depth profiles of variance and coefficient of variation are also quantified. Regarding uncertainty, profiles of LRFD resistance factors (ϕ) are produced as well (see Sec. 2.8 for additional details regarding uncertainty calculations).

2.6.2 Conditional Simulation

Conditional simulation is analogous to conditioning to a specific boring location, where the simulated values of soil or rock strength parameters at said location reproduce corresponding measured values (McVay et al. 2012). As a precursor to conditional simulation, a boring of interest is identified and the plan-view location (easting, northing) is cataloged. This is in contrast to unconditional simulation (discussed in Sec. 2.6.1), where complete site knowledge is assumed, and no plan-view location is specified. Even so, the major steps associated with the conditional simulation procedure (Fig. 18) are similar to those detailed above for unconditional simulation (recall Fig. 16).

In GeoStat, conditional simulation makes use of the *LU* algorithm for producing spatially varying vertical profiles of soil or rock parameters. Major steps include: generation of a geometric grid; generation of covariance matrices (per soil or rock layer); and then, performance of stochastic simulation. In contrast to that of unconditional simulation, both horizontal and vertical variograms play a significant role when conducting conditional simulation. Therefore, conditional simulation should only be conducted if representative variograms can be formed in both the horizontal and vertical directions.

The first major step in the conditional simulation procedure (Fig. 18, upper-left) consists of generating a geometric grid of boring location data. From the plan-view perspective, sets of eastings, $\{easting\}$; and, northings, $\{northing\}$, are accumulated to represent all boring

locations. Then, over a range of candidate embedment lengths (as specified by the engineer), corresponding elevations, $\{elevation\}$, are assembled in the vertical dimension, resulting in n_{grid} geometric location data points. Next, in the GeoStat implementation, the elevation range associated with the current layer is divided into 0.5-ft increments. Note that this subdivision does not affect previously assembled entries of $\{elevation\}$. Rather, the 0.5-ft increments in elevation are used to augment the layer-specific $\{elevation\}$ vector with n_{cond} additional entries. A corresponding number of plan-view position values are used to augment the $\{easting\}$ and $\{northing\}$ vectors. However, the newly added northing and easting values are all set equal to those of the boring selected for conditioning upon.

As the second major step (Fig. 18, middle-left), covariance matrices, $[C]$, are formed for each soil or rock layer. More specifically, for each of n_{layers} , the corresponding subsets of position arrays ($\{easting\}$, $\{northing\}$, and $\{elevation\}$) are expanded into matrix form. This expansion denotes that the matrices house columnated differences in position for each location of interest (i.e., each diagonal entry), relative to every other location of interest (i.e., all other column entries). For example, the $\{easting\}$ array is expanded to form:

$$[\Delta_{east}] = \{easting\} \cdot \{1\}^T - (\{easting\} \cdot \{1\}^T)^T \quad (18)$$

where $[\Delta_{east}]$ is a matrix of differences in easting; $\{1\}$ is a vector of unity-valued entries; and, the superscript "T" denotes the transpose operation. The same manner of expansion is carried out to form the matrix of differences in northing, $[\Delta_{north}]$, and elevation, $[\Delta_{elev}]$, pertaining to the current layer.

At this stage, the horizontal and vertical variograms of the layer hold significance (Fig. 18, upper-right; see Sec. 2.5 regarding formation of variograms). Subsequent to formation of the location-difference matrices, horizontal difference terms (in $[\Delta_{east}]$ and $[\Delta_{north}]$) are normalized by the range of the theoretical, horizontal variogram (a_h). Likewise, vertical difference terms are normalized by the range of the theoretical, vertical variogram (a_v).

Next, the matrices containing the (normalized) location-difference terms are amalgamated into a total difference of distance:

$$[h_{norm}]_{jk} = ([\Delta_{east}]_{jk}^2 + [\Delta_{north}]_{jk}^2 + [\Delta_{elev}]_{jk}^2)^{0.5} \quad (19)$$

where $[h_{norm}]$ is a symmetric matrix of the normalized total distance between each location of interest, relative to every other location considered (within the current layer). The subscripts "jk" denote that the total distance is computed on an entry by entry basis. The normalization scheme discussed here pertains to scenarios where different values are selected for the ranges a_h and a_v . In certain instances, horizontal and vertical variograms may be formed within a given layer and exhibit features such as the nugget effect (as introduced in Sec. 2.5). For these

instances, normalization schemes analogous to that described above for differing range values (a_h , a_v) are carried out.

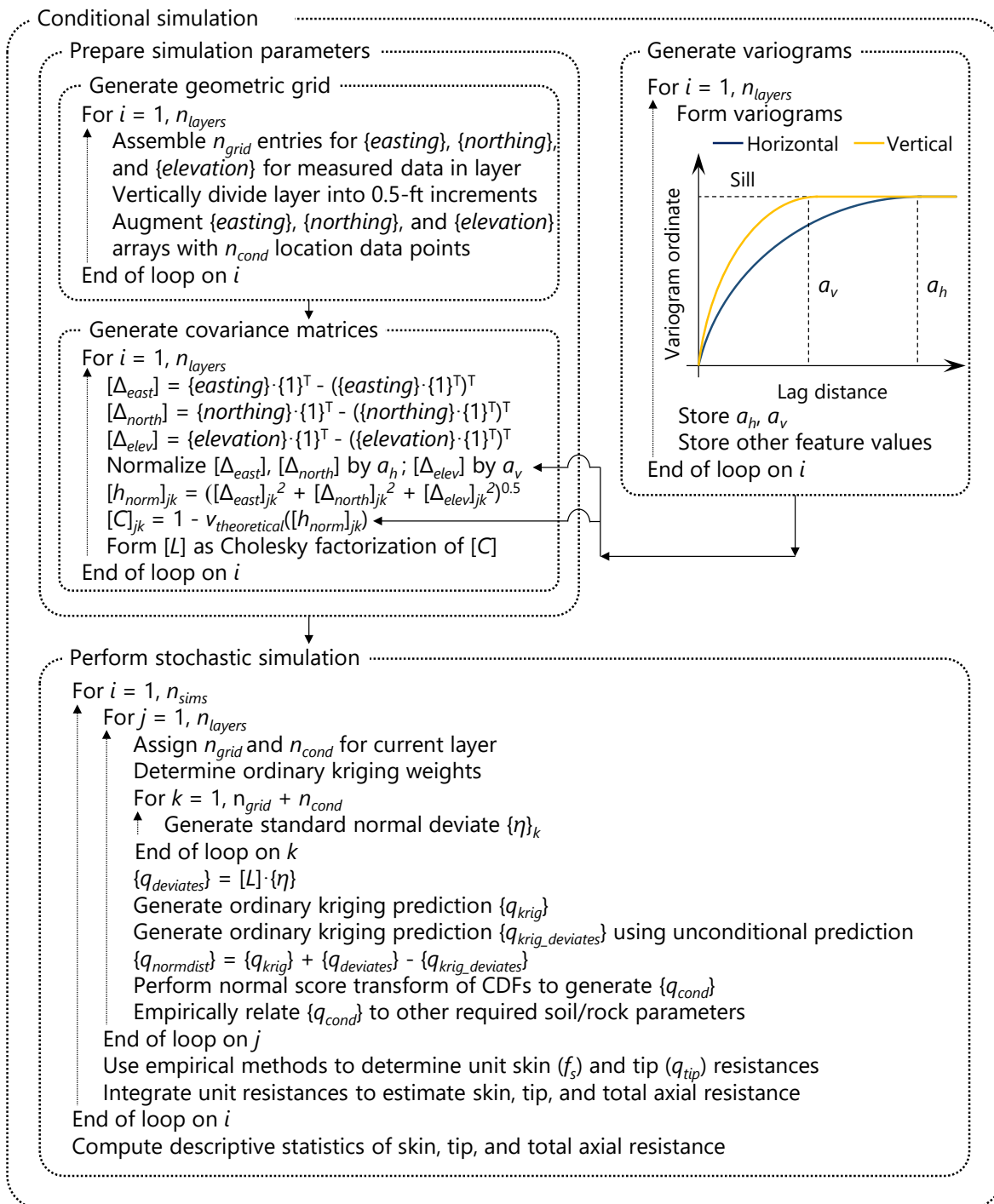


Figure 18. Conditional simulation procedure

Having formed the matrix of normalized total distance for every location of interest within a layer (relative to every other location of interest), the selected form of the theoretical variogram, $v_{theoretical}$, is evaluated (exponential, spherical; as introduced in Sec. 2.5). Recall that, when forming the entries of $[h_{norm}]$, variogram range values (a_h, a_v) are used for normalization. Therefore, evaluations of the theoretical variogram are carried out without direct use of the respective variogram range values. For example, consider a scenario where the spherical form is made use of when forming the theoretical variograms within a given layer. Then solely for the purposes of evaluating entries of $[h_{norm}]$ within said layer, the theoretical variogram is modified from that of Eqn. 10 to:

$$v_{theoretical}([h_{norm}]_{jk}) = (1.5[h_{norm}]_{jk} - 0.5[h_{norm}]_{jk}^3); [h_{norm}]_{jk} < 1 \quad (20)$$

Relative to the variogram definition from Eqn. 10, the variance of all measured data for all locations of interest within the layer (σ^2) is not directly present in Eqn. 20. This is because, as discussed in Sec. 2.5, the variogram formation process in GeoStat involves subjecting measured geotechnical site data to a separate normalization process. As an additional artifact of data normalization during variogram formation in GeoStat, entries of the covariance matrix, $[C]$, can also be formed without direct use of the data variance (σ^2):

$$[C]_{jk} = 1 - v_{theoretical}([h_{norm}]_{jk}) \quad (21)$$

Subsequent to formation of the covariance matrix, which is symmetric and positive definite, Cholesky decomposition is carried out to obtain the (factorized) lower triangular form of the covariance matrix, $[L]$. As emphasis, the lower triangular matrix is uniquely formed for each soil or rock each layer.

The stochastic simulation is then undertaken (Fig. 18, bottom) for the desired number of soil or rock profiles to be realized (n_{sims}). For each realization, the system layers (n_{layers}) are iterated through. For each layer considered, the number of locations in the geometric grid (n_{grid}) and the number of layer-specific locations along the boring being conditioned upon (n_{cond}) are assigned. Ordinary kriging weights are then determined. In GeoStat, the weights are solved in the same manner as that presented in Faraone (2014) and Goovaerts (1997):

$$\sum \omega_j(x_g) \cdot [C]_{ij} + \lambda = [C]_{ig} \quad \forall i = 1, \dots, n_{grid} \quad (22)$$

where ω_j is the ordinary kriging weight; and the summation on j occurs from 1 to n_{cond} . The presence of (x_g) signifies that n_{cond} weights are assigned at each grid location (corresponding to the first n_{grid} entries in $\{eastings\}$, $\{northings\}$, and $\{elevations\}$), and relative to the location of the boring being conditioned upon. The sum of all kriging weights associated with a given location, x_g , must equal unity. Continuing from left to right in Eqn. 22, λ is a Lagrangian operator. On the right-hand side of Eqn. 22, the subscripts "ig" are assigned to the covariance

matrix. The second subscript “ g ” in particular signifies correspondence with the location, x_g . As a more physical interpretation, the kriging weights constitute a relative spatial correlation structure between the 3D locations of the boring being conditioned upon and the 3D locations of all other borings that are pertinent to the layer being considered.

As the next step in conditional simulation, independent values of standard normal deviates are sampled $n_{grid} + n_{cond}$ times and stored in vector form $\{\eta\}$. The independently sampled deviate values are then used along with the layer-specific lower-triangular matrix of covariance, $[L]$, to form simulated values of measured properties:

$$\{q_{deviates}\} = [L] \cdot \{\eta\} \quad (23)$$

where $\{q_{deviates}\}$ is the collection of layer-specific, normally distributed, and unconditionally simulated values of soil properties. The length of $\{q_{deviates}\}$ is equal to the sum of n_{grid} and n_{cond} .

To convert the values associated with unconditional simulation to that of conditional simulation, the previously computed kriging weights are utilized. In particular, as the next step in the conditional simulation process (Fig. 18, bottom), a set of n_{cond} ordinary kriging predictions, $\{q_{krig}\}$, is generated as:

$$\{q_{krig}\}_i = \sum \omega_j^{(i)} \cdot Z_{score}(\{q\}_j) \quad (24)$$

where, relative to Eqn. 22, the kriging weights are expressed such that the superscript, $\langle i \rangle$, signifies the i^{th} column from the kriging weights in matrix form (n_{grid} rows by n_{cond} columns); j is summed from 1 to n_{grid} . Furthermore, recalling Eqn. 12, the term $Z_{score}()$ indicates evaluation of the standard normal score (z-score) for physically measured data points, $\{q\}$, that fall within the current layer.

As an additionally required conversion quantity (unconditional to conditional), a separate set of ordinary kriging predictions are generated, but with use of $\{q_{deviates}\}$:

$$\{q_{krig_{deviates}}\}_i = \sum \omega_j^{(i)} \cdot Z_{score}(\{q_{deviates}\}_j) \quad (25)$$

where j is summed from 1 to n_{grid} .

A set of conditionally simulated soil or rock parameter values are then obtained, where these values are normally distributed. In particular, these values are obtained by combining the n_{cond} entries of $\{q_{krig}\}$, $\{q_{deviates}\}$, and $\{q_{krig_{uncond}}\}$ that are associated with the boring being conditioned upon:

$$\{q_{normdist}\} = \{q_{krig}\} + \{q_{deviates}\} - \{q_{krig_{deviates}}\} \quad (26)$$

where contributing terms are combined in this manner to eliminate the smoothing effect from the ordinary kriging operator, $\{q_{krig}\}_i$; and, to reinstate the spatial variability of the process in the random field (Faraone, 2014).

The terms in $\{q_{normdist}\}$ are obtained by operating (in part) on normally distributed data. However, physically measured data, $\{q\}$, within a given layer may or may not be normally distributed. Therefore, a normal score transformation is carried out to map from the n_{cond} normally distributed values making up $\{q_{normdist}\}$ to a distribution that reflects the ensemble of n_{grid} layer-specific physical measurements, $\{q\}$. Refer to Fig. 17 (as part of the discussion for unconditional simulation) for details of the mapping procedure, which in the present discussion produces conditionally simulated values $\{q_{cond}\}$.

The simulated values, $\{q_{cond}\}$, always correspond to one of: SPT-N blow counts; CPT cone resistance; unconfined compression strength of rock, $q_{u,i}$; or, unconfined compressive strength as estimated from MWD site data. For the purpose of building up required soil or rock parameters within a layer, beyond those of the aforementioned types, it is necessary to make use of empirical relations. For example, SPT-N and q_u values can be used along with empirical relationships to estimate the other required soil or rock parameters. Additional details of the required parameters, and associated empirical relationships, are provided in Sec. 2.7.

After all layers are iterated through in the conditional simulation procedure (Fig. 18, bottom), empirical methods are utilized to relate profiles of soil or rock strength parameters to unit skin friction (f_s) and tip resistance (q_{tip}) quantities. Then, the unit quantities are integrated to form estimates of pile/shaft axial resistance for the current simulation (i.e., pile/shaft configuration and candidate embedment length). The axial capacity calculation software FB-Deep is used for this purpose. See the FB-Deep Help Manual for details regarding empirical determination of unit resistance quantities and integration of these quantities to determine axial, tip, and total resistances of piles/shafts.

The final step of the conditional simulation procedure (Fig. 18, bottom) is to form descriptive statistics of skin, tip, and total resistances for the pile/shaft section and range of embedment lengths being analyzed. As a result, through-depth profiles of mean-valued resistance are formed. As direct measures of spatial variability, through-depth profiles of variance and coefficient of variation are also quantified. Regarding uncertainty, profiles of LRFD resistance factors (ϕ) are produced as well (see Sec. 2.8 for additional details regarding uncertainty calculations).

2.6.3 Special Considerations for Worst Case Conditions

In the case where no acceptable theoretical variogram can be fit to the experimental variogram points (e.g., availability of little, if any, site data), “worst case” conditions can be simulated. In this context, the phrasing “worst case” signifies consideration of: (1) upper bound estimates of spatial variability (e.g., long correlation lengths); and, (2) upper bound estimates of uncertainty which result in lower bound estimates of LRFD resistance factor, ϕ . Consequently, stochastic simulation using worst case conditions tends to require longer piles/shafts to achieve a given magnitude of axial resistance.

The option to conduct unconditional simulation under worst case conditions is available in the GeoStat software, and is implemented consistent with recommendations from McVay et al. (2012) and Faraone (2014). Selection of worst conditions can be made on a layer by layer basis in GeoStat, and with respect to either (or both) the horizontal and vertical directions. Whenever the worst case conditions are applied to the vertical search direction, within a given layer, the range (a_v) is constrained to a large number relative to pile/shaft length (10,000 ft). Regarding the horizontal search direction, if unconditional simulation is being carried out, then horizontal range is constrained to a large number relative to pile/shaft width (again, 10,000 ft). However, when the worst case scenario is assigned for the horizontal search direction within a given layer, and conditional simulation is conducted, then the horizontal range is set to the vertical range ($a_h = a_v$).

2.7 Realization of Layer Data

As part of both the unconditional and conditional simulation procedures (recall Fig. 16 and Fig. 18, respectively), it is necessary for “base” sets of soil or rock parameters to be related to all other required parameters through use of empirical relationships. Recall that the base parameters can be any one of (per layer) SPT-N blow counts, CPT cone resistance, unconfined compression strength (q_u), or unconfined compressive strength as estimated from MWD site data. In the following, all empirical relationships that are made use of during stochastic simulation are delineated. More specifically, listings and discussion are provided concerning: (1) the types of soil or rock layers that can be modeled in GeoStat; (2) the associated (layer-specific) soil or rock parameters required for estimating unit measurements of axial resistance (skin, tip); and, 3) empirical relationships adopted for using “base” values (e.g., SPT-N, q_u) to estimate all other required soil or rock parameters throughout vertically subdivided profiles (in 0.5-ft increments).

Consistent with the axial capacity calculation software, FB-Deep, an integer mapping scheme is adopted in GeoStat in assigning available soil or rock types to a given profile layer. The listing is provided in Table 4. Considerations for each of the available layer types, within the context of performing stochastic simulation using GeoStat, are presented immediately below.

Table 4. Integer mappings for available soil and rock layer types in GeoStat

Soil or rock type	Integer mapping
Plastic clay	1
Clay and silty sand	2
Clean sand	3
Limestone and very shelly sand	4

2.7.1 Use of SPT-N Data in Plastic Clay Layers

Stochastic simulations involving Plastic Clay layers (type 1 from Table 4), along with use of SPT-N blow count values, require the parameters listed in Table 5. The required parameters, as listed, are consistent with that discussed in Sec. 4.2.4.4 of McVay et al. (2012). Namely, for simulations involving driven piles, only values of C_u (undrained shear strength) are required along the vertical dimension of the Plastic Clay layer. For simulations involving drilled shaft foundation members, both γ (unit weight) and C_u (undrained shear strength) are required. During simulation, realizations of SPT-N blow counts are used along with the empirical relationship from (Terzaghi and Peck, 1967) to estimate C_u in units of tsf:

$$C_u = 0.063 \cdot \text{SPT-N} \quad (27)$$

Table 5. Parameters for Plastic Clay layers

Parameter	Piles	Shafts
γ		✓
C_u	✓	✓

Regarding required values for unit weight, γ : mean values and corresponding COVs are directly provided by the engineer as part of the layer definition (see the Help Manual for additional details). Then, for each elevation of interest during the simulation, the input values (mean, COV) are used to form and sample from a lognormal distribution, and in turn, produce statistically independent values for unit weight.

2.7.2 Use of SPT-N Data in Clay and Silty Sand Layers

For Clay and Silty Sand layers (type 2 from Table 4) where SPT-N data are utilized, the required parameters are identical to those of Plastic Clay. Unit weight (γ) and undrained shear strength (C_u) properties are required for drilled shafts, while only C_u (as correlated from SPT-N) is required for simulations involving driven piles. In addition, the correlation from Terzaghi and Peck (1967) is again used when estimating C_u values. Specific to simulations of drilled shaft foundations, values of unit weight (γ) are generated in the same manner as that described above for Plastic Clay layers.

2.7.3 Use of SPT-N Data in Clean Sand Layers

When making use of SPT-N data for realizations of layer data, two parameters are required for embedment depths that correspond to Clean Sand (as listed in Table 6). For driven pile foundations, only SPT-N blow counts are necessary for simulation purposes. When drilled shafts are considered, through-depth values of both the unit weight (γ) and SPT blow count (SPT-N) are required. Vertical profiles of SPT-N blow counts are generated as described previously for unconditional and conditional simulation. Values of unit weight are generated using the same approach as that documented for Plastic Clay layers.

Table 6. Parameters for Clean Sand layers

Parameter	Piles	Shafts
γ		✓
SPT-N	✓	✓

2.7.4 Use of CPT Data for All Soil Layer Types

For Geo-statistical analysis of axial capacities for driven piles, CPT data can be utilized across all soil layer types. Only two types of site measurements are sufficient to conduct Geo-statistical analysis (Table 7): cone resistance ($q_{t,CPT}$), and sleeve friction ($f_{s,CPT}$). Note that CPT-based analysis is not available for drilled shaft members.

Table 7. Parameters for CPT-based analysis across all soil layer types

Parameter	Piles
$q_{t,CPT}$	✓
$f_{s,CPT}$	✓

The process of realizing layer data and performing stochastic simulation (Fig. 19) is initiated by gathering a collection of at least two vertical profiles of CPT cone resistance and sleeve friction measurements. Here, each profile possesses an associated plan-view location (e.g., northing, easting) and each measurement along a vertical profile possesses an associated elevation.

Next, the empirical method to be used during stochastic simulation is selected from that of the Schmertmann (Schmertmann, 1978), UF (Bloomquist et al. 2007), or LCPC methods (Bustamante and Ganeselli, 1982). Subsequently (Fig. 19, center), layers are defined for the collection of CPT data. GeoStat facilitates visual inspection of through-depth profiles for several types of geotechnical site measurements. More specifically, all profiles for a type of measurement are collapsed down to a single plot of a measurement versus elevation (regardless of northing, easting). In this way, indications of the number of layers can potentially be inferred from (for example) sudden changes along the vertical profiles of CPT cone resistance and sleeve friction. Profile plots of the friction ratio may serve as a particularly

effective means of identifying both layer top and bottom elevations as well as soil type. Note that if the UF method (Bloomquist et al. 2007) is selected as the empirical calculation method for CPT analysis, then the side coefficient and tip coefficient must also be given for each layer.

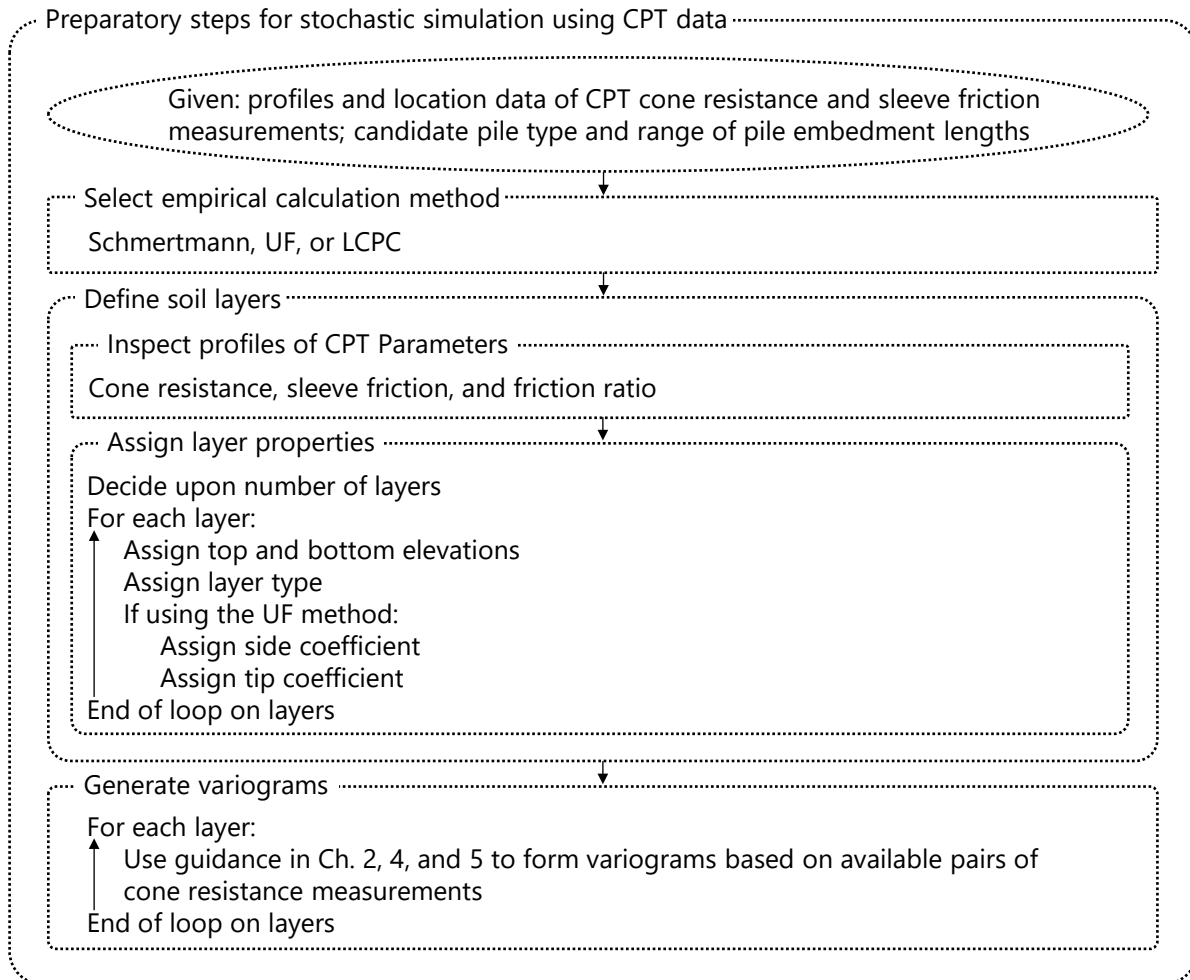


Figure 19. Preparatory steps for performing stochastic simulation of pile axial capacity with use of CPT data

As the final preparatory step preceding stochastic simulation (Fig. 19, bottom), variograms are formed (horizontal, vertical) using available pairs of cone resistance measurements. The GeoStat tool automatically searches for pairs of measurements, per layer, given a specified range of separation (lag) distances and search tolerances. Guidance for selecting variogram lag distance intervals and search tolerance parameters is given in Ch. 2, 4, and 5. Additional key aspects of the layer data realization and CPT-based stochastic simulation procedure are discussed in the remainder of Sec. 2.7.4. Namely, these include: 1) producing through-depth realizations of cone resistance values; 2) co-simulation of sleeve friction values; and, 3) performing axial capacity analysis for each realization.

2.7.4.1 Cone Resistance (q_{t_CPT})

Cone resistance measurements are utilized when forming layer variograms for CPT analysis and serve as the “base” variable for stochastic simulation. The algorithms implemented in GeoStat for the purposes of producing realizations of the “base” variable are robust to the type of geotechnical data being processed. Therefore, the existing algorithm portions of unconditional and conditional simulation—that involve generation of ‘primary’ variable values—are utilized for producing through-depth realizations of cone resistance (q_{t_CPT}) when conducting CPT analysis.

2.7.4.2 Sleeve friction (f_{s_CPT})

Consistent with other forms of analysis available within GeoStat, CPT-based stochastic simulation is conducted such that through-depth values of the “base” variable—cone resistance (q_{t_CPT})—are produced prior to generation of other types of CPT data. Then, other geotechnical parameter values required for axial capacity calculations (e.g., sleeve friction or f_{s_CPT}) are generated via the process of co-simulation. The procedure for simulating values of sleeve friction is presented in Fig. 20.

The co-simulation approach allows for incorporation of the strength of correlation between physically measured values of cone resistance, q_{t_CPT} , and sleeve friction, f_{s_CPT} , on a site-specific (or zone-specific) basis. Two major steps comprise the co-simulation procedure: preparation of simulation parameters (Fig. 20, top); and, performing stochastic simulation to produce counterpart realizations of f_{s_CPT} values (Fig. 20, bottom). The preparatory step begins by iterating through all profiles ($n_{borings}$) of physically measured CPT data to identify pairs of q_{t_CPT} and f_{s_CPT} . Having cataloged the set of physically measured values and the respective elevations within the profile, a nearest-neighbor search is then conducted. Namely, for every value of q_{t_CPT} within $\{q_{t_CPT}\}$, the nearest vertically positioned value of f_{s_CPT} (within $\{f_{s_CPT}\}$) is assigned as a paired value. The resulting profile of paired values of q_{t_CPT} and f_{s_CPT} are then stored, respectively in $\{q_{t_nearest}\}$ and $\{f_{s_nearest}\}$. Note that all profiles of physical measurements contribute to the $\{q_{t_nearest}\}$ and $\{f_{s_nearest}\}$ quantities (i.e., these quantities are site-specific or zone-specific, but not profile specific).

As the next preparatory step in co-simulation of f_{s_CPT} values, data transformations are carried out (Fig. 20, middle). Specifically, for the total number of pairs (n_{pairs}) across all profiles of measured values, the entry-wise natural log is computed for values within $\{q_{t_nearest}\}$ and then stored in $\{q_{t_ln}\}$. Likewise, entry-wise natural log values of $\{f_{s_nearest}\}$ are computed and stored in $\{f_{s_ln}\}$. Next, a regression expression is formed where entries within $\{f_{s_ln}\}$ are designated as the dependent variable:

$$\{f_{s_ln}\} = b \cdot \{q_{t_ln}\} + a \quad (28)$$

where b is the slope of the regression expression and a is the intercept. Note that a correlation coefficient, R , is also produced as part of the regression expression formation.

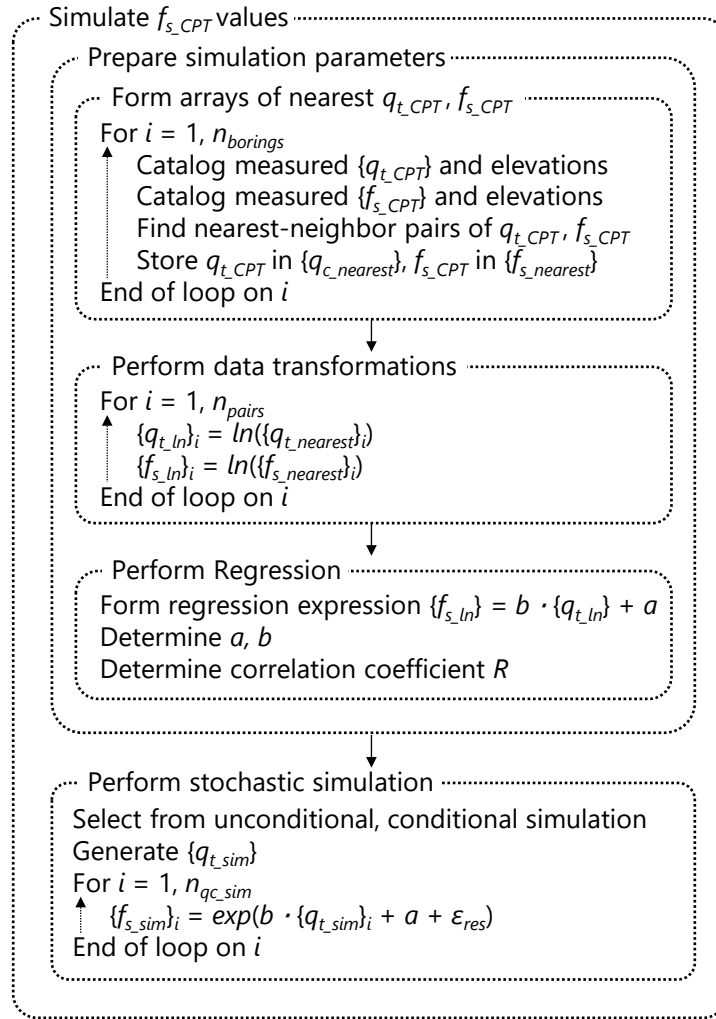


Figure 20. Simulation of sleeve friction, f_{s_CPT}

Stochastic simulation is then carried out using the co-simulated values of sleeve friction (Fig. 20, bottom). Here, a selection is made regarding unconditional or conditional simulation, and the algorithms documented in Ch. 2 are utilized to produce the desired number of simulated profiles of cone resistance, $\{q_{t_sim}\}$. For the number of entries (n_{qt_sim}) comprising a given profile of $\{q_{t_sim}\}$ values, the exponential of the regression expression from Eqn. 28 is utilized:

$$\{f_{s_sim}\}_i = \exp(b \cdot \{q_{t_sim}\}_i + a + \epsilon_{res}) \quad (29)$$

where the i^{th} entry in $\{f_{s_sim}\}$ contains a simulated value of sleeve friction. Note that a residual error term, ϵ_{res} , is introduced when populating entries within $\{f_{s_sim}\}$. For each time Eq. 29 is

evaluated, the residual error (ϵ_{res}) is sampled from a normal distribution with zero-valued mean and variance, σ_{res}^2 , of:

$$\sigma_{res}^2 = \sigma_{f_{s,ln}}^2 \cdot (1 - R^2) \quad (30)$$

where $\sigma_{f_{s,ln}}^2$ is the variance of the entries contained within $\{f_{s,ln}\}$.

2.7.4.3 CPT-based Calculation of Pile Axial Capacity

As the next major step in the overall stochastic simulation procedure, pile axial capacity is calculated throughout a range of desired elevations. That is, one profile at a time is analyzed by relating the associated cone resistance and sleeve friction values to unit resistances and then integrating the unit resistances. The approach adopted herein is to make default use of the axial capacity calculation software FB-Deep to compute CPT-based resistance quantities.

For pile axial capacity analysis with use of CPT data, the FB-Deep software requires as input: the pile type and size; range of candidate embedment lengths; soil layer top and bottom elevations; the empirical calculation method; and, profiles of cone resistance and sleeve friction. Additionally required inputs include the friction ratio ($f_{s,CPT} / q_{t,CPT}$, expressed as a percentage), and specific to use of the UF method (Bloomquist et al. 2007), the layer-specific side friction (F_s) and tip (k_b) coefficients. Guidance on selection of F_s and k_b values per layer is given in the FB-Deep Help Manual, along with default values that are utilized if no custom values are specified. Not that only those pile types indicated in Table 8 may be carried forward into the axial capacity calculations, given a selected empirical method.

Table 8. Applicable pile types for the empirical methods of CPT-based analysis

Empirical method	Square	Round	Cylinder	Pipe	H-section
Schmertmann	✓			✓	
UF	✓	✓			
LCPC	✓	✓	✓	✓	✓

2.7.5 Use of SPT-N Data and Core-run Data in Limestone and Very Shelly Sand Layers

When making use of SPT-N and/or core-run data (e.g., measurements of q_u), layers designated as Limestone and Very Shelly Sand maintain substantially different input parameter requirements depending on the foundation member type (Table 9). When pile foundation members are considered, only values of SPT-N are necessary. The procedures for simulating vertical profiles of SPT-N values are the same as those described previously for unconditional and conditional simulation.

For shaft member portions embedded in Limestone and Very Shelly Sand layers, when core-run data are utilized, the "base" parameter q_u is drawn upon, which is in contrast to the

approach adopted for processing of all other layer types and foundation configurations. The implementation in GeoStat for generating required simulation parameters (for drilled shafts in Limestone and Very Shelly Sand) is consistent with the approach presented in Sec. 4.2.4 of McVay et al. (2012). Accordingly, several types of parameters must be empirically determined prior to computation of unit skin and tip resistance quantities. The required parameters include (Table 9): unit weight (γ), unconfined compression strength (q_u), split tensile strength (q_t), mass modulus (E_m), rock quality designation (RQD), and *recovery*.

Table 9. Parameters for Limestone and Very Shelly Sand layers with use of SPT-N and core-run data

Parameter	Piles	Shafts
γ		✓
SPT-N	✓	
q_u		✓
q_t		✓
E_m		✓
RQD		✓
<i>recovery</i>		✓

Simulated realizations (vertical profiles) of unit weight (γ) are generated in the same manner as that documented above for Plastic Clay layers. In addition, realizations of unconfined compression strength, q_u , are generated using the procedures detailed previously for unconditional (Fig. 16) and conditional (Fig. 18) simulation.

2.7.5.1 Split Tensile Strength (q_t)

The procedure implemented in GeoStat for simulating values of split tensile strength, q_t , is delineated in Fig. 21. Overall, the procedure incorporates site-specific characterization of the strength of correlation that is present between physically measured values of q_t and unconfined compression strength, q_u . Major steps involved in simulating q_t values consist of preparing relevant simulation parameters and then performing stochastic simulation.

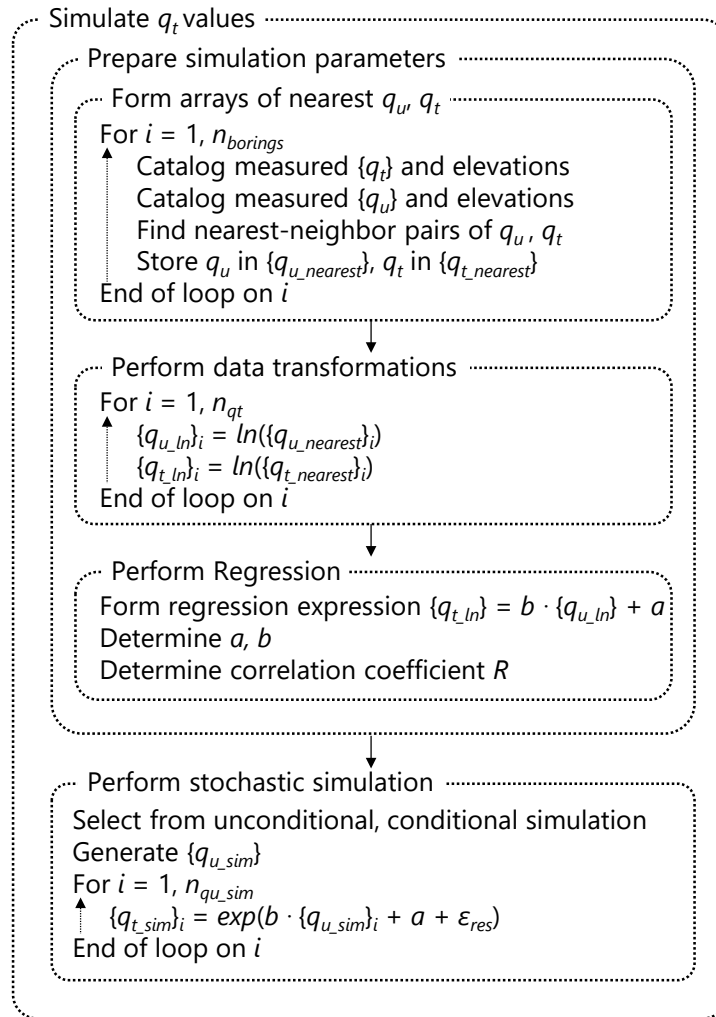


Figure 21. Simulation of split tensile strength, q_t

As the first step in preparing simulation parameters (Fig. 21, top), all borings considered for analysis are iterated through to identify pairs of physically measured q_u and q_t values, which are stored (respectively) in $\{q_{u_nearest}\}$ and $\{q_{t_nearest}\}$. To illustrate the manner by which physical measurements of q_u and q_t are paired together, consider the illustrative core-run data listed in Table 10. Labels listed beneath the Sample column denote the order in which specimen data are reported (1 through 9). Also, the letter “T” signifies that the specimen is used for conducting a split tensile test (to produce q_t). The letter “U” signifies conduction of an unconfined compression strength test to produce q_u .

While core-runs are typically 5 ft in length, the summed length of all recovered specimens within the run do not typically reach 5 ft. Such is the case for the illustrative core-run data of Table 10. Further, the top-to-bottom order of a given set of core-run data may or may not be available. Therefore, it is assumed (in this illustrative scenario) that the specimen data are

ordered from top to bottom of the run (Fig. 22). Based on these assumptions, a nearest-neighbor search is carried out to identify pairs of measured q_u and q_t data.

Table 10. Illustrative laboratory test data for a coring run (adapted from McVay et al. 2012)

Sample	Length (in)	q_t (psi)	q_u (psi)
1T	2.495	150.3842	--
2U	4.376	--	439.014
3T	2.621	128.7227	--
4T	2.492	353.7287	--
5U	3.913	--	454.679
6T	2.473	252.8827	--
7T	2.404	252.7647	--
8T	2.658	281.5633	--
9U	4.811	--	711.509

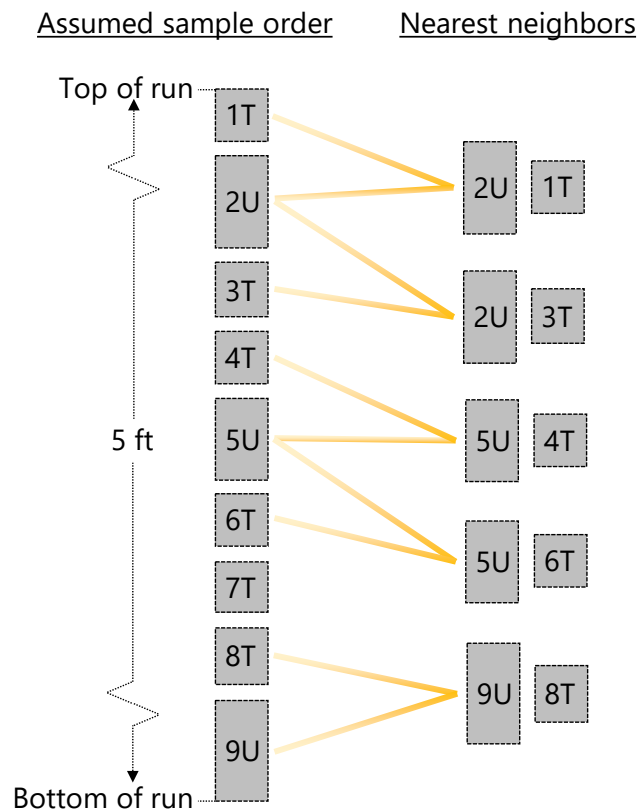


Figure 22. Illustrative core-run specimens with nearest-neighbor pairings for q_u and q_t

Paired values identified as part of a nearest-neighbor search (using the illustrative data set) are depicted in the right portion of Fig. 22. As is the case here, data obtained from an unconfined compression test (q_u) may be identified for use in multiple pairings. For example, specimen 2U is paired with specimen 1T, and independently, specimen 2U is paired with

specimen 3T. For instances where more than two consecutive specimens are used to conduct the same type of testing, then no pairings are identified for the intermediately positioned specimens. For example, specimens 6T, 7T, and 8T are all used for measuring split tensile strength, q_t . Because specimen 7T is bounded (above and below) by two specimens of the same test type, no pair is assigned to the 7T specimen. If it is desired to explicitly pair two measured q_u and q_t values, then the nearest-neighbor search algorithm can be overridden in GeoStat by simply defining said q_u and q_t values at the same elevation (see the Help Manual for details regarding how boring data are input in GeoStat models).

Subsequent to finding nearest neighbors of measured data values across the set of site borings, and forming the $\{q_{u_nearest}\}$ and $\{q_{t_nearest}\}$ quantities, the next step in the overall q_t simulation procedure is carried out (Fig. 21, middle). Namely, each entry in $\{q_{u_nearest}\}$ and $\{q_{t_nearest}\}$ is transformed (using natural log) to produce $\{q_{u_ln}\}$ and $\{q_{t_ln}\}$. Then, regression is carried out upon the transformed data, where entries in $\{q_{t_ln}\}$ are treated as the dependent variable. The form of the regression expression is:

$$\{q_{t_ln}\} = b \cdot \{q_{u_ln}\} + a \quad (31)$$

where, respectively, a and b are the intercept and slope of the regression line fitted to the transformed data. Regression terms for slope (b), intercept (a), and correlation coefficient (R) are retained from this step in the overall procedure, and are made use of during the subsequently conducted stochastic simulation (Fig. 21, bottom).

Having completed preparation of relevant simulation data, either unconditional or conditional simulation is then conducted (recall Fig. 16 and Fig. 18, respectively) to produce a realization of $n_{q_{u_sim}}$ simulated q_u values, $\{q_{u_sim}\}$. Next, for each entry in $\{q_{u_sim}\}$, corresponding values of q_t are computed to populate $\{q_{t_sim}\}$:

$$\{q_{t_sim}\}_i = \exp(b \cdot \{q_{u_sim}\}_i + a + \varepsilon_{res}) \quad (32)$$

where the previously determined components of the regression expression (a , b) are utilized. Additionally, a residual error term, ε_{res} , is introduced. More specifically, for each simulated value of q_t , a corresponding residual term is sampled from a normal distribution with mean of zero and variance, σ_{res}^2 , of:

$$\sigma_{res}^2 = \sigma_{q_{t_ln}}^2 \cdot (1 - R^2) \quad (33)$$

where $\sigma_{q_{t_ln}}^2$ is the variance of the transformed physical measurements of q_t , and the previously determined correlation coefficient (R) is utilized for scaling.

2.7.5.2 Mass Modulus (E_m)

The procedure implemented in GeoStat for simulating values of rock mass modulus, E_m , is delineated in Fig. 23. As implemented, the approach automates site-specific characterization of the strength of correlation that is present between physically measured values of E_m and unconfined compression strength, q_u . Major steps involved in simulating E_m values consist of preparing relevant simulation parameters and then performing stochastic simulation.

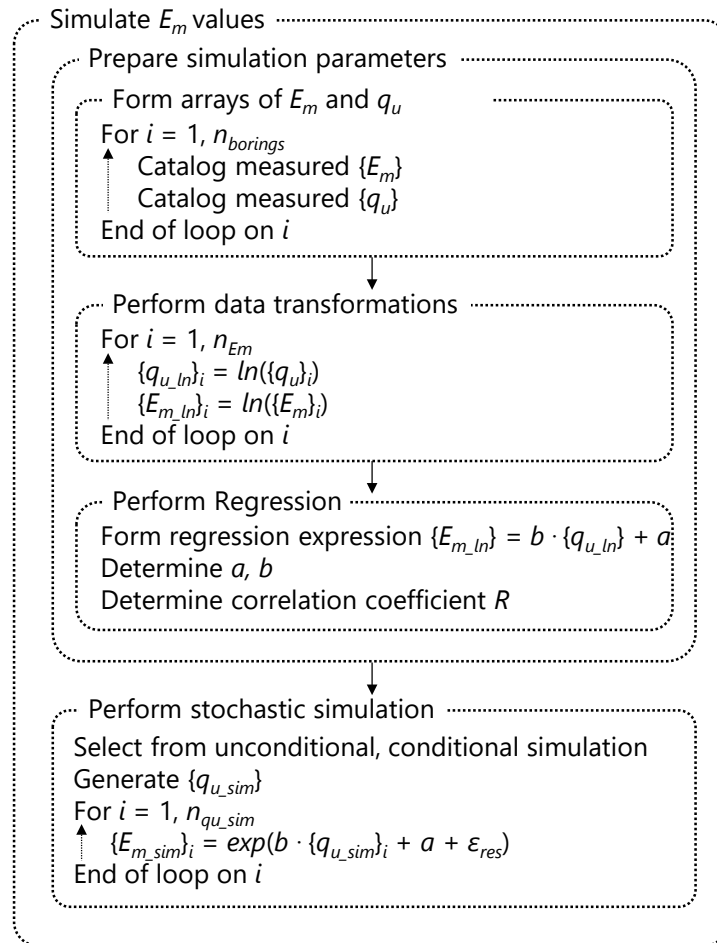


Figure 23. Simulation of mass modulus, E_m

In contrast to simulation of q_t values, pair matching (i.e., nearest-neighbor searching) is not necessary for simulating E_m values. This is because mass modulus is typically determined relative to unconfined compression strength (q_u). Consequently, for all borings considered, measured values of E_m and q_u can be directly cataloged (Fig. 23, top).

Subsequently, each cataloged entry of q_u and E_m is transformed (using natural log) to produce $\{q_{u_ln}\}$ and $\{E_{m_ln}\}$. Then, regression is carried out upon the transformed data (Fig. 23, middle),

where entries in $\{E_{m_ln}\}$ are treated as the dependent variable. The form of the regression expression is:

$$\{E_{m_ln}\} = b \cdot \{q_{u_ln}\} + a \quad (34)$$

where, respectively, a and b are the intercept and slope of the regression line fitted to the transformed E_m and q_u data. The slope (b), intercept (a), and correlation coefficient (R) are retained, and are made use of during stochastic simulation (Fig. 23, bottom).

Either unconditional or conditional simulation is then conducted (recall Fig. 16 and Fig. 18, respectively) to produce a realization of n_{qu_sim} values of unconfined compression strength, $\{q_{u_sim}\}$. Next, for each entry in $\{q_{u_sim}\}$, corresponding values of E_m are computed to populate $\{E_{m_sim}\}$:

$$\{E_{m_sim}\}_i = \exp(b \cdot \{q_{u_sim}\}_i + a + \varepsilon_{res}) \quad (35)$$

where the previously determined components of the regression expression (a , b) are utilized. Additionally, a residual error term, ε_{res} , is introduced, and is sampled from a normal distribution with mean of zero and variance, σ_{res}^2 , of:

$$\sigma_{res}^2 = \sigma_{Em_ln}^2 \cdot (1 - R^2)^2 \quad (36)$$

where $\sigma_{Em_ln}^2$ is the variance of the transformed boring data for E_m , and the previously determined correlation coefficient (R) is utilized for scaling.

2.7.5.3 RQD and Recovery

Regarding Florida limestone, McVay et al. (2012) found no significant correlations between unconfined compression strength (q_u) and RQD (nor q_u and *recovery*). In GeoStat, random selection of the site-wide collection of RQD and *recovery* values is carried out, when such values are required, during simulation. However, if so desired, this process can be overridden in GeoStat by simply defining said RQD and *recovery* values at the same elevation as a given, measured value of q_u .

For example, consider a q_u value and associated elevation, such as would be defined in the Boring Data dialog (see the Help Manual). If an RQD (and/or *recovery*) value is input at that same elevation, then the RQD (and/or *recovery*) value will be associated with the q_u value. Otherwise, when GeoStat carries out the process to pair q_u values and RQD (and/or *recovery*) values, the RQD (and *recovery*) values are selected from the general set of values defined across all currently enabled boring locations.

2.7.6 Use of MWD Data for Analysis of Drilled Shafts in Limestone and Very Shelly Sand Layers

For shaft member portions embedded in Limestone and Very Shelly Sand layers—when MWD data are utilized—site measurements of specific energy (e) are particularly effective for conducting Geo-statistical analysis. That is, several parameters are estimated (directly or indirectly) from specific energy (e) when making use of MWD data for Geo-statistical analysis of drilled shafts within Limestone and Very Shelly Sand layers (Table 11). These parameters include (where it is emphasized that they are estimated, not measured): MWD-based estimates of unconfined compressive strength (q_{u_MWD}); MWD-based estimates of tensile strength (q_{t_MWD}); MWD-based estimates of rock recovery (REC_{MWD}), and MWD-based estimates of RQD (RQD_{MWD}).

The estimation method for each of the parameters is also listed in Table 11, where each parameter is discussed in the remainder of Sec. 2.7.6. Note that, in addition, values of unit weight (γ) and mass modulus (E_m) are required and are generated using the same approach as that documented in Sec. 2.7.5.

Table 11. Parameters estimated as part of MWD-based analysis within Limestone and Very Shelly Sand layers

Parameter	Description	Estimation method
q_{u_MWD}	Unconfined compressive strength	Eqn. 38
q_{t_MWD}	Tensile strength	Eqn. 39
REC_{MWD}	Rock recovery	Fig. 25
RQD_{MWD}	Rock quality designation	Fig. 24

2.7.6.1 MWD-based Estimation of Unconfined Compressive Strength (q_{u_MWD})

An expression of specific energy (e) as related to measurements of unconfined compressive strength (q_u) was proposed in Rodgers et al. (2018b) as:

$$e = 0.0066 \cdot q_u^2 + 13.68 \cdot q_u \quad (37)$$

where units for all variables are in psi. Note that in Eq. 37, measured values of unconfined compressive strength (q_u) serve as the independent variable.

For the MWD-based implementation in GeoStat, a calculated (as opposed to measured) “base” parameter of unconfined compressive strength is drawn upon and is termed as q_{u_MWD} . Here, q_{u_MWD} is calculated (i.e., estimated) from measurements of specific energy, e using an inverted expression of Eq. 37:

$$q_{u_MWD} = \frac{-13.7 + (13.7^2 - 4 \cdot 0.0066 \cdot (-e))^{0.5}}{2 \cdot 0.0066} \quad (38)$$

where units for all variables are in psi. Note that Eqn. 38 is adapted from the SI expression in Rodgers et al. (2018a). Note also, that a maximum value of specific energy is included among the MWD-related inputs available in GeoStat. When evaluating Eqn. 38, values of e are limited to the value of “Specific Energy Max”, as input from within the “Test Methods” dialog.

The “base” parameter, q_{u_MWD} , is utilized for both variogram generation and stochastic simulation. Having established a means of producing values of the “base” variable for MWD analysis (i.e., estimating q_{u_MWD} via Eqn. 38), the algorithms for generating variograms and performing stochastic simulation (discussed earlier in Ch. 2) can be utilized without further modification. In other words, the existing algorithm portions of unconditional and conditional simulation—that involve generation of “base” variable values—are utilized for producing through-depth realizations of q_{u_MWD} when conducting MWD-based stochastic simulation.

2.7.6.2 MWD-based Estimation of Tensile Strength (q_{t_MWD})

When computing axial capacities of drilled shafts in limestone, it is typically necessary to consider additional data types beyond that of unconfined compressive strength. In particular, values of tensile strength are also commonly needed for estimation of unit side shear resistance. Accordingly, as part of producing MWD-based realizations of limestone properties during Geo-statistical simulation in GeoStat, values of tensile strength (q_{t_MWD}) are estimated based on simulated values of q_{u_MWD} . More specifically, the derivation given in McVay and Rodgers (2020) is drawn upon, which makes use of the Florida geomaterials equation:

$$q_{t_MWD} = 0.436 \cdot q_{u_MWD}^{0.825} \quad (39)$$

where units for all variables are in psi. In this way, for every simulated value of q_{u_MWD} that is produced, a corresponding value of q_{t_MWD} is directly calculated using Eqn. 39.

2.7.6.3 MWD-based Estimation of Rock Recovery (REC_{MWD})

The procedure for estimating rock recovery values for use in MWD-based stochastic simulation (REC_{MWD}) is summarized in Fig. 25. First, a given profile of measured values of specific energy (e) versus elevation (z) is divided into n_{int} intervals of 5 ft, starting at the ground surface elevation. A length of 5 ft is adopted to mimic rock coring operations that typically occur over 5-ft intervals (i.e., the typical total length of a core-run). Note that the bottommost interval may be less than 5 ft.

For the i^{th} interval, and in turn, for each measured value of specific energy, e , within the i^{th} interval, a comparison is made with respect to a threshold value. Here, a default specific energy threshold is adopted such that $e_{threshold} = 2,000$ psi. However, note that a custom threshold value may be specified if desired (see the Help Manual for additional details). The

specific energy threshold is used to eliminate any data points that fall below the defined threshold, and thereby, to exclude soil and materials characterized as intermediate geomaterials (IGM) from counting toward the assessment of rock strength. Accordingly, the number of values of specific energy, e , (within the interval) that are equal to or greater than the threshold value, $e_{threshold}$, are accumulated via incrementation of n_{accept} . The MWD-based estimate of the REC_{MWD} value for the interval is then calculated as the number of data points (again, per interval) possessing specific energy values greater than $e_{threshold}$, divided by the total number of data points within the interval (i.e., the ratio of n_{accept} and the pre-excluded data points, n_e). Note that the total number of data points within the interval (n_e) is dependent upon the MWD sampling resolution. Furthermore, note that one unique value of REC_{MWD} is assigned throughout each interval.

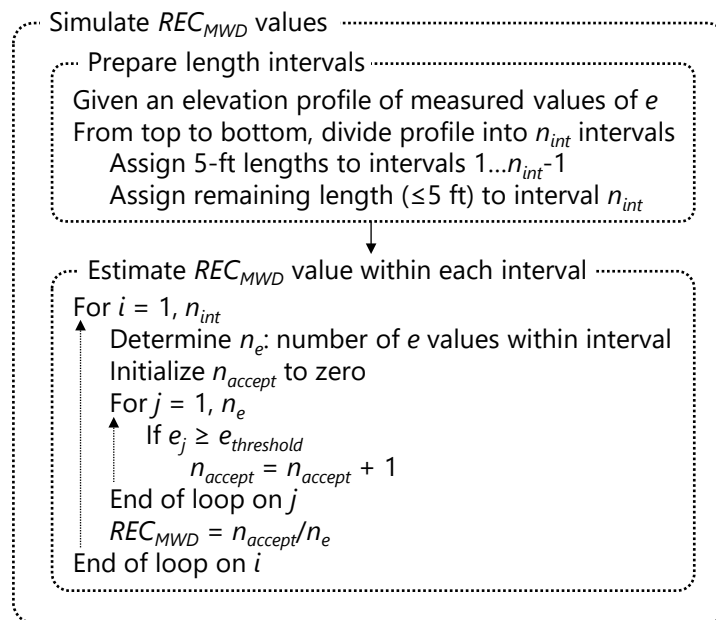


Figure 25. Simulation of MWD-based estimates of rock recovery, REC_{MWD}

During MWD-based stochastic simulation, when the process is carried out to pair simulated q_{u_MWD} values with values of REC_{MWD} , the values are selected from the set of interval-specific values from across all currently enabled boring locations.

2.7.6.4 MWD-based Estimation of RQD (RQD_{MWD})

Estimation of RQD values in association with MWD-based stochastic simulation (RQD_{MWD}) is summarized in Fig. 26. Note that the same overall process as that utilized for (REC_{MWD}) is employed (e.g., one value of RQD_{MWD} is determined per interval). However, for determining values of RQD_{MWD} , differences in elevation (z) associated with consecutive (i.e., sub-interval) data points are summed (L_{sub} in Fig. 26) and checked against the length threshold ($L_{threshold}$) of

4 in. Each consecutive length identified as being equal to or greater than $L_{threshold}$ is then accumulated within L_{RQD_MWD} . After all data points within the interval have been assessed, the accumulation of sub-interval lengths exceeding $L_{threshold}$ (i.e., the accumulated length assigned to L_{RQD_MWD}) is divided by the total length of the interval (L_{int}), thus allowing RQD_{MWD} to be determined within each interval

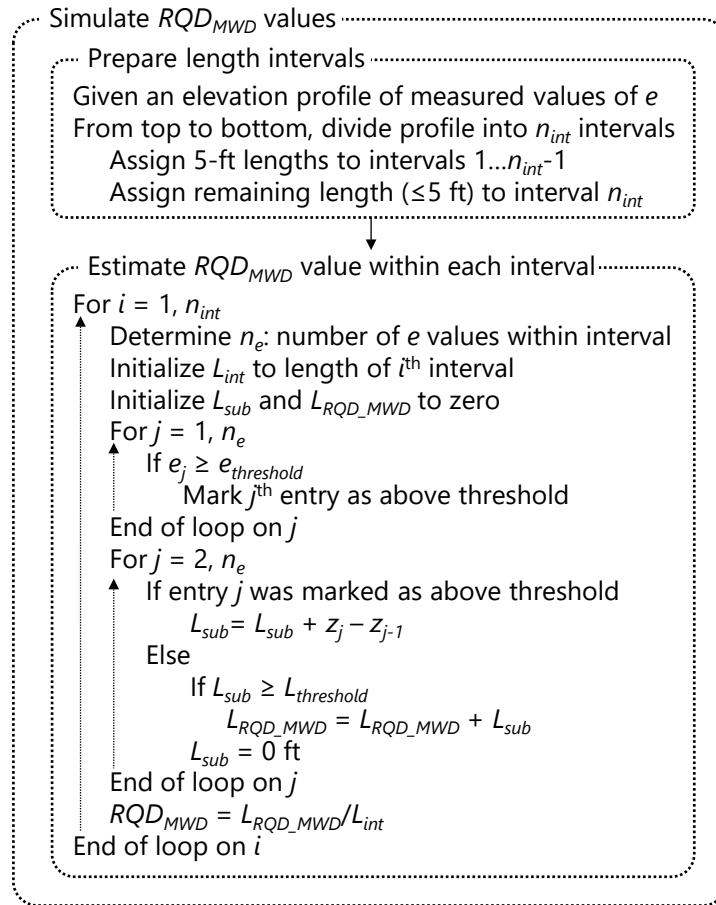


Figure 26. Simulation of MWD-based estimates of rock quality designation, RQD_{MWD}

2.7.6.5 MWD-based Calculation of Unit Side Shear Resistance

As the next major step in the MWD-based stochastic simulation procedure, shaft axial resistance is calculated across a range of candidate embedment lengths. That is, one profile at a time is analyzed by relating the associated limestone parameter values to unit resistances and then integrating the unit resistances. For example, for computing side shear resistance, the expression developed in McVay et al. (1992) is adopted, but with use of MWD-related terms:

$$f_{s_MWD} = 0.5 \cdot (q_{u_MWD} \cdot q_{t_MWD})^{0.5} \quad (40)$$

where $f_{s,MWD}$ is the MWD-based calculation of unit side shear resistance. Note that values of $f_{s,MWD}$ are further scaled by the associated value of REC_{MWD} (which has a domain between 0.0 and 1.0).

2.8 Resistance Factor (ϕ)

The preceding subsections of Ch. 2 document modeling techniques and simulation procedures for characterizing variability (i.e., spatial variability of geotechnical site data). However, the uncertainty associated with a given estimate of pile (or shaft) axial resistance is also critical to foundation design. In LRFD approaches, resistance factors (ϕ) encapsulate both variability and uncertainty phenomena. Further, resistance factors (ϕ) typically range from 0 to 1. The product of computed values of nominal resistance and ϕ produce factored resistance, where the latter quantity is then used for member design. Note that program-generated resistance (ϕ) factors should only be used in conjunction with Owner's guidelines.

2.8.1 Maximum Value

By default, the maximum value for computed resistance factors is limited to 0.6. However, a custom value of the maximum resistance factor can be specified in the Project Settings dialog within the GeoStat UI. Custom values of the maximum are limited to fall between 0.0 and 1.0 (inclusive), whereas all values less than the maximum remain unaffected. See the Help Manual for additional details of how to specify this value within a given GeoStat model.

2.8.2 Default Formulation

The default expression used for resistance factor, ϕ , evaluation in GeoStat is adopted from Styler (2006) and McVay et al. (2012):

$$\phi = \frac{(\gamma_D \cdot \frac{Q_D}{Q_L} + \gamma_L) \cdot \left(\frac{1 + COV_Q^2}{1 + COV_R^2}\right)^{0.5}}{(\lambda_{QD} \cdot \frac{Q_D}{Q_L} + \lambda_{QL}) \cdot \exp(\beta \cdot \ln((1 + COV_R^2) \cdot (1 + COV_Q^2)))^{0.5}} \quad (41)$$

$$COV_Q^2 = \frac{(\lambda_{QD} \cdot \frac{Q_D}{Q_L} \cdot COV_{QD})^2 + (\lambda_{QL} \cdot COV_{QL})^2}{(\lambda_{QD} \cdot \frac{Q_D}{Q_L})^2 + 2 \cdot \frac{Q_D}{Q_L} \cdot \lambda_{QD} \cdot \lambda_{QL} + \lambda_{QL}^2} \quad (42)$$

where COV_R is the coefficient of variation of the nominal resistance (quantified, in part, through spatial variability characterization); COV_Q is the coefficient of variation with respect

to loading as stipulated by Styler (2006). The first-order second-moment (FOSM) LRFD- ϕ , using the Styler (2006) representation of COV_Q , has been shown to be within 3% of the first order reliability method (FORM) LRFD- ϕ (Styler, 2006). All other component terms used in calculating ϕ are listed in Table 12. Values of component terms are taken from McVay et al. (2012).

Table 12. Component terms for default evaluation of LRFD resistance factors, ϕ

Term description	Symbol	Value
Dead load factor	γ_D	1.25
Live load factor	γ_L	1.75
Dead to live load ratio	Q_D/Q_L	2.00
Dead load bias factor	λ_{QD}	1.08
Live load bias factor	λ_{QL}	1.15
Mean resistance bias factor	λ_R	1.0
Dead load coefficient of variation	COV_{QD}	0.128
Live load coefficient of variation	COV_{QL}	0.18
Target reliability index	β	3.0

In Eqn. 41, the term COV_R is contributed to by: (1) spatial variability of site data (quantified as part of stochastic simulation); and, (2) inherent error that arises due to use of empirical methods. Discussion of the latter phenomenon is provided in Ch. 3.

2.8.3 Alternative Formulation

An alternative formulation to that of Styler (2006) can be selected for calculating LRFD resistance factors (ϕ). More specifically, a formulation documented in NCHRP 507 (Paikowsky, 2004) can be utilized:

$$\phi = \frac{\lambda_R(\gamma_D \cdot \frac{Q_D}{Q_L} + \gamma_L) \cdot \left(\frac{1 + COV_{QD}^2 + COV_{QL}^2}{1 + COV_R^2} \right)^{0.5}}{(\lambda_{QD} \cdot \frac{Q_D}{Q_L} + \lambda_{QL}) \cdot \exp(\beta \cdot \ln((1 + COV_R^2) \cdot (1 + COV_{QD}^2 + COV_{QL}^2)))^{0.5}} \quad (43)$$

where all component terms are defined (along with adopted values) in Table 12. As with the default formulation, values of component terms are taken from McVay et al. (2012). Note that selection of the desired formulation is issued from within the Program Settings dialog of the GeoStat UI (see the Help Manual for additional details regarding input specification).

CHAPTER 3 METHOD ERROR ANALYSIS

3.1 Overview

For estimating axial resistances of deep foundation members, total uncertainty of design resistance is comprised of both spatial variability and the uncertainty of “method error”. Method error is defined in McVay et al. (2012) as the total difference between predicted design resistance and the corresponding (physically measured) load-tested resistance. The manner in which method error is utilized when estimating pile (or shaft) axial resistance, as originally developed in McVay et al. (2012), is adopted in the GeoStat implementation. Sources of method error relevant to use of the GeoStat software include: (1) measurement error associated with in-situ testing; (2) intrinsic error in empirical relationships that are used for relating physical measurements to unit resistance quantities; and, (3) intrinsic error in empirical methods used in integrating unit resistance quantities to calculate member-level estimates of pile/shaft axial resistance.

Determination of method error necessitates use of regression concepts. For example, regression analysis of predicted shaft axial resistance versus measured load-test data may be utilized in forming method error relationships for use in design. Accordingly, pertinent concepts of regression analysis are discussed in Sec. 3.2. Sections of Ch. 3 beyond Sec. 3.2 focus on expressions of method error, which are implemented in GeoStat, and further, are specific to foundation member type and the surrounding soil or rock medium. Development of a representative regression curve for axial resistances of driven piles is documented in Sec. 3.3, while considerations for portions of embedded shafts in sand, clay, and rock layers are presented in Sec. 3.4 through Sec. 3.8, respectively. Considerations for incorporating results from custom regression analysis into method error (e.g., from load tests) is discussed in Sec. 3.9. Expressions for quantifying the combined effects of spatial variability and method error of pile/shaft axial resistances (i.e., total uncertainty) are provided in Sec. 3.10. Also indicated in Sec. 3.10 is the significance of total uncertainty with respect to computing LRFD resistance factors (ϕ).

3.2 Regression Analysis

Consider the illustrative schematic of predicted (q_{pred}) and physically measured (q_{meas}) axial resistances plotted in Fig. 27. A linear regression curve passing through the data is also plotted in Fig. 27. All points along the regression curve are described (for this illustration) using intercept, a , and slope, b . While many other regression curve types are possible (e.g., exponential, power functions), the same general concepts as those discussed immediately below remain applicable.

Returning the illustrative data set of Fig. 27, for each plotted point of q_{pred} and $q_{measured}$, the difference between the regression curve ordinate and the physically measured resistance (q_{meas}) is referred to as the error (ϵ) of the regression. To calculate a given value of physically measured resistance (q_{meas}) using the respective prediction (q_{pred}), the regression curve, and regression error (ϵ), the following expression is utilized:

$$q_{meas} = a + b \cdot q_{pred} + \epsilon \quad (44)$$

Due to variations across the set of q_{pred} and q_{meas} values, the regression error (ϵ) varies from point to point. For regression analysis, it is typically desired for the regression expression parameters (a , b) to be selected such that the summation of the squares of errors ($\sum \epsilon^2$) across all pairs of q_{pred} and q_{meas} is minimized.

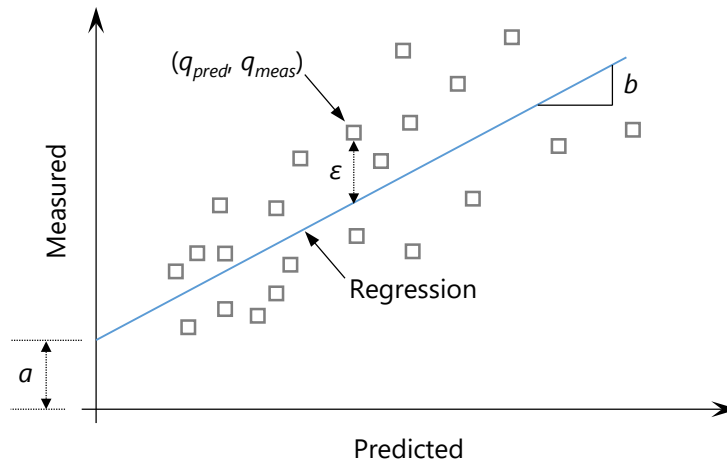


Figure 27. Illustrative scatterplot of measured (q_{meas}) and predicted (q_{pred}) resistances

Recalling the definition of the correlation coefficient (R) from Ch. 2, the slope of the regression curve that satisfies the least-squares error criterion is given as:

$$b = R \cdot \frac{\sigma_{meas}}{\sigma_{pred}} \quad (45)$$

where R is the correlation coefficient between the set of values; σ_{meas} is the standard deviation of all q_{meas} values; and, σ_{pred} is the standard deviation of the corresponding q_{pred} values. Furthermore, the intercept of the regression curve is:

$$a = q_{mean_meas} - b \cdot q_{mean_pred} \quad (46)$$

where q_{mean_meas} is the mean of all q_{meas} values, and q_{mean_pred} is the mean of the corresponding q_{pred} values. The variance of the regression error (σ_{ϵ}^2) can be related to the variance of the measured data (σ_{meas}^2) by:

$$\sigma_{\epsilon}^2 = \sigma_{meas}^2 \cdot (1 - R^2) \quad (47)$$

Documented in the following are regression analyses of collections of measured and predicted axial resistances of deep foundation members, where the concepts, types of quantities, and curve components employed are analogous to those introduced above. Sets of data pertaining to pile and shaft foundation member types, embedded in various media, are analyzed. Additionally, representative regression curves are identified, in relation to method error characterization, for each considered member type and surrounding medium (e.g., clay, sand, limestone).

3.3 Driven Piles (SPT-N)

Plotted in Fig. 28 are pairs of predicted and measured (total) axial resistance pertaining to physically constructed concrete piles, which in turn, are distributed across several bridge sites. The 48 data points (q_{pred}, q_{meas}) were originally gathered from the literature as part of McVay et al. (2012). Also reported in McVay et al. (2012) a representative best-fit regression curve to the 48 predicted and measured (i.e., Davisson) capacity values.

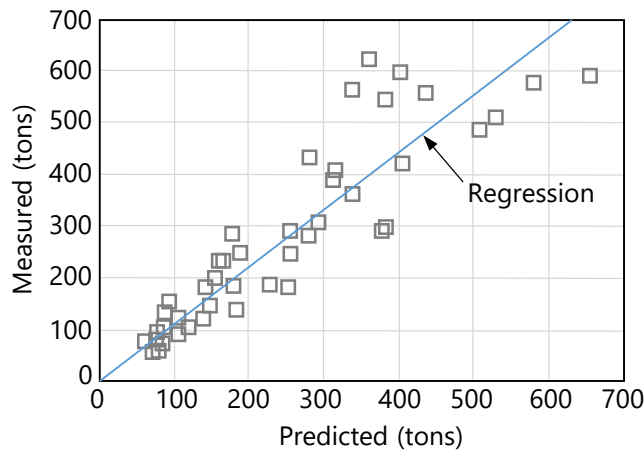


Figure 28. Regression analysis for total axial resistance of concrete piles (McVay et al. 2012)

The form of the regression curve is the product of exponential and power terms. Predicted values of axial resistance (q_{pred}) are taken as the independent variable, and computed values of measured resistance (as opposed to physically measurements of resistance), q_{comp_meas} , are produced:

$$q_{comp_meas} = \exp(a) \cdot q_{pred}^b \quad (48)$$

where recommended values for the regression terms a and b of the ($n = 48$) driven pile data set are listed in Table 13; and q_{comp_meas} is the computed value of resistance obtained from evaluation of the trend line. Also listed in Table 13 is the coefficient of variation of the regression error (COV_ε):

$$COV_\varepsilon = (\exp(\sigma_{\varepsilon \ln}^2) - 1)^{0.5} \quad (49)$$

where COV_ε is a function of the log-transformed variance of the regression error, $\sigma_{\varepsilon \ln}^2$.

Table 13. Regression parameter values for total axial resistance of concrete piles (McVay et al. 2012)

Parameter	Value
a	0.17
b	0.99
COV_ε	0.24
n	48

Together, Eqn. 48, Eqn. 49, and the parameter values listed in Table 13 constitute a representative means of relating between predicted and measured axial resistances of driven piles. See Sec. 3.8 for the means by which selected terms from the representative regression expression are utilized when characterizing total uncertainty.

3.4 Driven Piles (CPT)

To ensure that the default, CPT-based method error approach is implemented in a manner that is representative of Florida bridges, a catalog of measured and CPT-based predictions of Davisson capacities for piles throughout Florida bridge sites is identified and utilized. More specifically, Bloomquist et al. (2007) is drawn upon, encompassing: 21 candidate load-test configurations and more than 10 Florida bridge sites (Table 14). For each configuration, the Davisson capacity associated with the load-test measurement is considered along with respective predictions obtained from use of the Schmertmann, UF, and LCPC (empirical) methods. Note that the predictions were made as part of Bloomquist et al. (2007).

The mean of the ratios (measured divided by predicted, R_{mean_mp}) and corresponding standard deviation (σ_{mp}) associated with each of the Schmertmann, UF, and LCPC methods are listed in Table 15. Respective lower and upper bound thresholds, which are utilized to filter the data, are also given. Applying these filters to the 21 candidate configurations listed in Table 14 results in exclusion of load test 18 for all three empirical methods, and additionally, exclusion of load test 21 when considering the LCPC method (Table 16).

Table 14. Measured versus CPT-based predictions of Davisson capacity for driven piles in Florida (Bloomquist et al. 2007)

Load test	Measured (tons)	Schmertmann (tons)	UF (tons)	LCPC (tons)
1	140	112	152	184
2	165	224	170	264
3	103	217	143	228
4	250	223	266	374
5	266	166	225	273
6	213	205	245	305
7	194	155	192	255
8	283	242	358	434
9	185	275	272	286
10	479	311	375	604
11	479	405	380	545
12	249	174	236	273
13	480	229	303	387
14	250	216	262	337
15	393	283	329	378
16	438	304	411	501
17	425	468	693	792
18	735	187	432	502
19	332	281	221	336
20	250	271	221	317
21	425	310	344	304

Table 15. Descriptive statistics of measured versus predicted pile axial capacity for filter usage

Empirical method	Ratio mean, $R_{mean,mp}$	Ratio standard deviation, σ_{mp}	Filter lower bound, $R_{mean,mp} - 2\sigma_{mp}$	Filter upper bound, $R_{mean,mp} + 2\sigma_{mp}$
Schmertmann	1.32	0.69	0.00	2.71
UF	1.08	0.29	0.50	1.65
LCPC	0.85	0.26	0.33	1.38

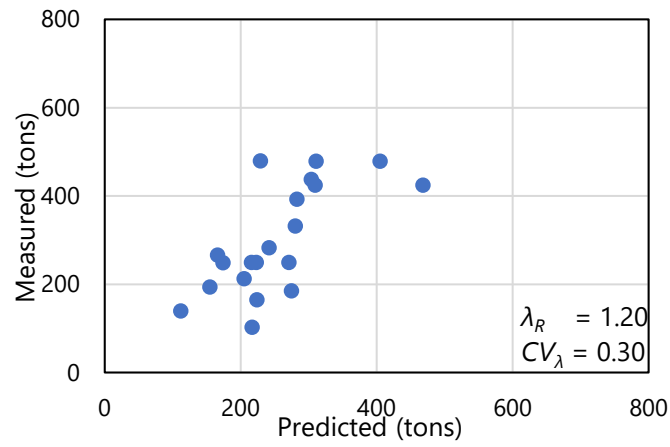
Table 16. Load tests excluded by filter

Empirical method	Load test(s) excluded
Schmertmann	18
UF	18
LCPC	18, 21

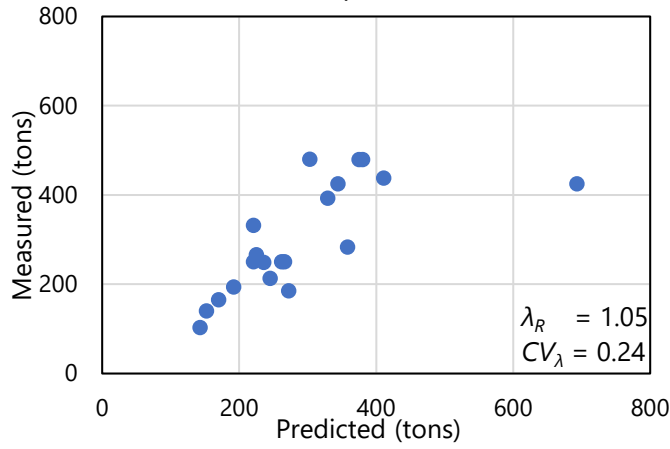
3.4.1 Method Error Parameters

Mean ratios, λ_R and coefficients of variation, COV_{λ} , for use in total uncertainty calculations (discussed later in Ch. 3) are annotated along with scatterplots of (post-filtering) measured versus predicted resistance in Fig. 29. Parameter values are additionally listed in Table 17. For the three CPT-based methods implemented in GeoStat, these parameter values (Table 17) are

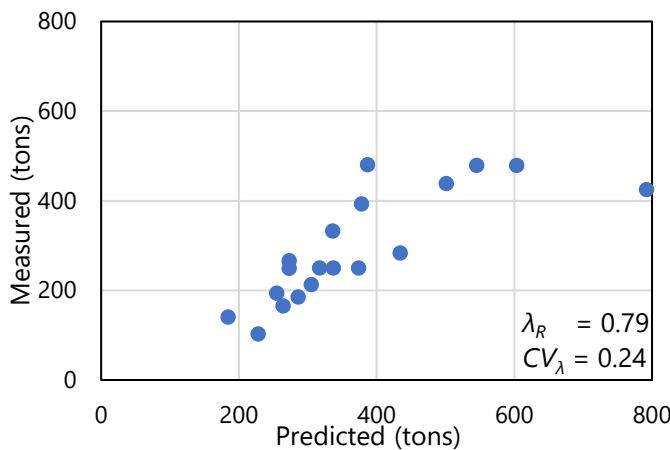
recommended for use when calculating total uncertainty of driven pile axial capacities of Florida bridges, and site-specific load test data are not available.



a)



b)



c)

Figure 29. Scatterplots of (filtered) measured versus CPT-based predictions of pile axial capacity: a) Schmertmann; b) UF; c) LCPC

Table 17. Method error parameters for CPT-based total uncertainty calculations

Empirical method	λ_R	CV_λ
Schmertmann	1.20	0.30
UF	1.05	0.24
LCPC	0.79	0.24

3.5 Drilled Shafts in Sand

Pairs of total predicted and measured axial resistance pertaining to physically constructed drilled shafts in sand are plotted in Fig. 30. The ($n = 31$) data points (q_{pred}, q_{meas}) are directly excerpted from the previously conducted data gathering efforts of McVay et al. (2012). A representative best-fit regression curve to the 31 points, as originally developed in McVay et al. (2012), is:

$$q_{comp_meas} = \exp(a) \cdot q_{pred}^b \quad (50)$$

where the form of the regression expression is defined as the product of exponential and power terms; and q_{comp_meas} is the computed value of resistance obtained from evaluation of the trend line. Recommended values (McVay et al. 2012) for the argument of the exponential function, a , and the exponent, b , are listed in Table 18.

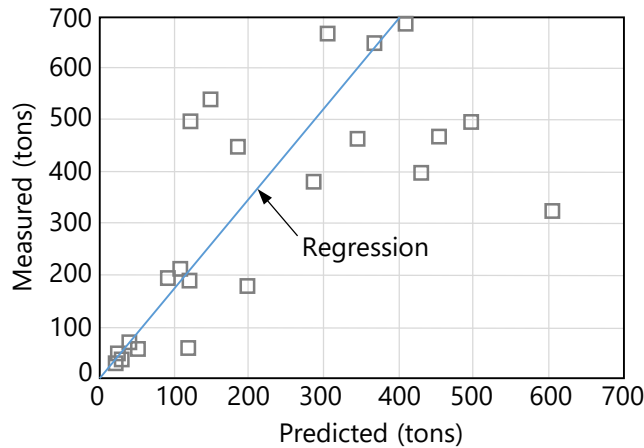


Figure 30. Regression analysis for total axial resistance of drilled shafts in sand (McVay et al. 2012)

Also listed in Table 18 is the coefficient of variation of the regression error (COV_ϵ), which is the same (in form) as that given above for driven piles:

$$COV_\epsilon = (\exp(\sigma_{\epsilon_ln}^2) - 1)^{0.5} \quad (51)$$

where $\sigma_{\varepsilon_{\ln}}^2$ is the log-transformed variance of the regression error for drilled shafts in sand. See Sec. 3.8 for the manner in which terms associated with the representative regression expression for drilled shafts in sand are carried forward into the characterization of total uncertainty.

Table 18. Regression parameter values for total axial resistance of drilled shafts in sand (McVay et al. 2012)

Parameter	Value
a	0.66
b	0.98
COV_{ε}	0.68
n	31

3.6 Drilled Shafts in Clay

Shown in Fig. 31 are ($n = 38$) predicted and measured values of total axial resistance pertaining to physically constructed drilled shafts in clay. The plotted (q_{pred}, q_{meas}) data points are taken directly from McVay et al. (2012). A representative best-fit regression curve to the 38 points, as reported by McVay et al. (2012), is:

$$q_{comp_meas} = \exp(a) \cdot q_{pred}^b \quad (52)$$

where the form of the regression expression is defined as the product of exponential and power terms; and q_{comp_meas} is the computed value of resistance obtained from evaluation of the trend line. McVay et al. (2012) recommended values for regression coefficients, a and b , as listed in Table 19. Also listed therein is COV_{ε} , the coefficient of variation of the regression error. The COV_{ε} term for drilled shafts in clay takes the same form as that given above for driven piles and drilled shafts in sand:

$$COV_{\varepsilon} = (\exp(\sigma_{\varepsilon_{\ln}}^2) - 1)^{0.5} \quad (53)$$

where $\sigma_{\varepsilon_{\ln}}^2$ is the log-transformed variance of the regression error (specific to drilled shafts in clay). Use of the regression analysis results for characterization of total uncertainty, concerning drilled shafts in clay, is discussed in Sec. 3.8.

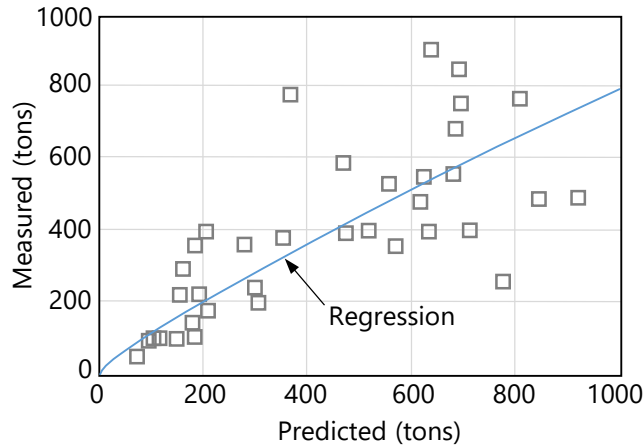


Figure 31. Regression analysis for total axial resistance of drilled shafts in clay (McVay et al. 2012)

Table 19. Regression parameter values for total axial resistance of drilled shafts in clay (McVay et al. 2012)

Parameter	Value
a	0.73
b	0.86
COV_{ε}	0.41
n	38

3.7 Drilled Shafts in Limestone (Core-run Data)

In contrast to the considerations for the combinations of member types and soil types discussed above, relatively more pronounced distinctions are made in regards to method error calculations for drilled shaft portions embedded in limestone layers. More specifically, separate treatments are given for method error arising due to skin friction resistance and end bearing resistance. Considerations for each form of resistance are documented in Sec. 3.6.1 (skin friction) and Sec. 3.6.2 (end bearing).

3.7.1 Skin Friction

Plotted Fig. 32 are predicted and measured values of McVay skin friction resistance pertaining to ($n = 18$) physically constructed drilled shafts embedded in limestone. All plotted (q_{pred} , q_{meas}) data points are taken directly from McVay et al. (2012). Additionally, a representative best-fit regression curve to the 18 points is superimposed on the plot, where the regression analysis was originally conducted in McVay et al. (2012).

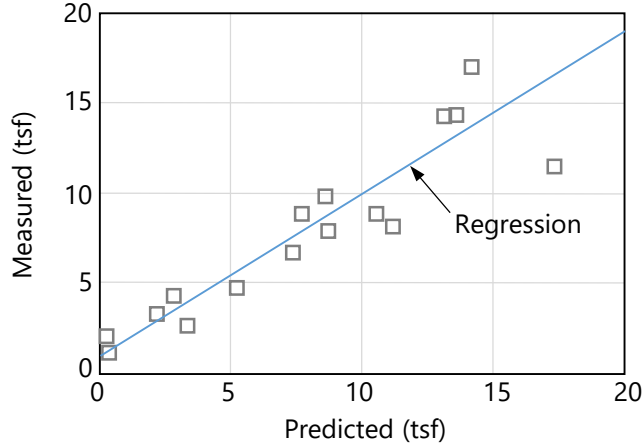


Figure 32. Regression analysis for McVay skin friction of drilled shafts in limestone (McVay et al. 2012)

The regression curve for skin friction (Fig. 32) is linear in form, and is given as:

$$q_{comp_meas} = a + b \cdot q_{pred} \quad (54)$$

where q_{comp_meas} is the computed value of skin friction obtained from evaluation of the trend line. Parameter values for the regression coefficients included in Eqn. 54 (i.e., a , b) are listed in Table 20.

Table 20. Regression parameter values for McVay skin friction of drilled shafts in limestone (McVay et al. 2012)

Parameter	Value
a	0.90
b	0.90
σ_{ϵ}^2	4.52
n	18

Three sequentially evaluated expressions are employed for calculating the method error associated with skin friction resistance (and specific to drilled shafts in limestone). First, the error of the linear regression curve itself is expressed in terms of variance, σ_{reg}^2 :

$$\sigma_{reg}^2 = \frac{n - 1}{n - 2} \cdot \sigma_{q_{meas}}^2 \cdot (1 - R^2) \quad (55)$$

where n is the number of available data points associated with physical measurements (e.g., load test data for skin friction); σ_{meas}^2 is the variance of the collection of q_{meas} values; and, R is the correlation coefficient associated with the pairs of q_{pred} , q_{meas} . Next, the variance of the

error associated with evaluation of the regression expression ($\sigma_{q_{comp_meas}}^2$) is determined using:

$$\sigma_{q_{comp_meas}}^2 = \sigma_{reg}^2 \cdot \left(\frac{1}{n} + \frac{(q_{pred} - q_{mean_pred})^2}{(n-1) \cdot \sigma_{pred}^2} \right) \quad (56)$$

where q_{mean_pred} is the mean of the collection of q_{pred} values; and, σ_{pred}^2 is the variance of the collection of q_{pred} values. The method error attributed to skin friction resistance, for drilled shafts in limestone, is then calculated as:

$$\sigma_{\varepsilon}^2 = \sigma_{q_{comp_meas}}^2 + \sigma_{reg}^2 \quad (57)$$

Note that method error, for these scenarios, is represented using variance rather than COV. Use of the variance attributed to (skin friction) method error in calculation of total uncertainty for drilled shafts in limestone is discussed in Sec. 3.8.

3.7.2 End Bearing

Presented in Fig. 33 are predicted and measured values of O'Neill end bearing resistance for ($n = 11$) physically constructed drilled shafts embedded in limestone. All plotted (q_{pred}, q_{meas}) data points are taken directly from McVay et al. (2012). Also plotted in Fig. 33 is a representative best-fit regression curve to the 11 points. Regression analysis for the 11 points, originally conducted in McVay et al. (2012), is reviewed below.

The regression curve for end bearing (Fig. 33) is linear in form, and is given as:

$$q_{comp_meas} = a + b \cdot q_{pred} \quad (58)$$

where q_{comp_meas} is the computed value of end bearing obtained from evaluation of the trend line. The corresponding parameter values for the regression coefficients a and b are listed in Table 21. Note that the value of a is defaulted to zero rather than 20.5 in GeoStat to prevent potentially unconservative adjustments to resistance when tip resistance is not a significant contributor total resistance.

Three expressions are employed for calculating the method error associated with end bearing resistance (specific to drilled shafts in limestone). First, the error of the linear regression curve itself is expressed in terms of variance, σ_{reg}^2 :

$$\sigma_{reg}^2 = \frac{n-1}{n-2} \cdot \sigma_{q_{meas}}^2 \cdot (1 - R^2) \quad (59)$$

where n is the number of available data points associated with physical measurements (e.g., load test data for end bearing); σ_{meas}^2 is the variance of the collection of q_{meas} values; and, R is the correlation coefficient associated with the pairs of q_{pred} , q_{meas} . Next, the variance of the error associated with evaluation of the regression expression ($\sigma_{q_{comp_meas}}^2$) is determined using:

$$\sigma_{q_{comp_meas}}^2 = \sigma_{reg}^2 \cdot \left(\frac{1}{n} + \frac{(q_{pred} - q_{mean_pred})^2}{(n - 1) \cdot \sigma_{pred}^2} \right) \quad (60)$$

where q_{mean_pred} is the mean of the collection of q_{pred} values; and, σ_{pred}^2 is the variance of the collection of q_{pred} values.

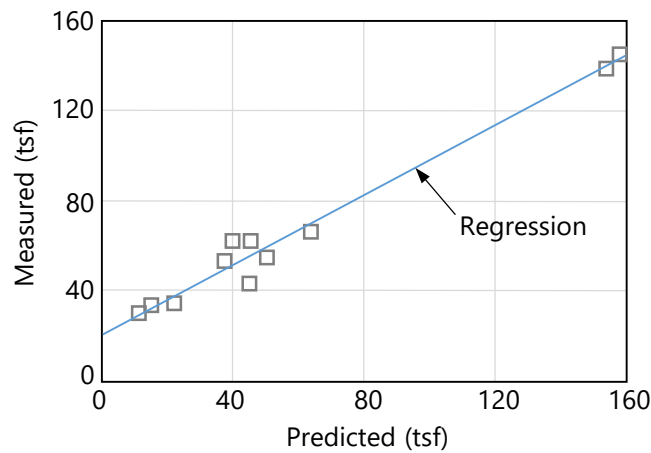


Figure 33. Regression analysis for O'Neill end bearing of drilled shafts in limestone (McVay et al. 2012)

Table 21. Regression parameter values for O'Neill end bearing of drilled shafts in limestone (McVay et al. 2012)

Parameter	Value
a	20.50
b	0.77
σ_{ϵ}^2	48.89
n	11

The method error attributed to end bearing resistance, for drilled shafts in limestone, is then calculated as:

$$\sigma_{\epsilon}^2 = \sigma_{q_{comp_meas}}^2 + \sigma_{reg}^2 \quad (61)$$

As with considerations for skin friction, method error for end bearing resistance of drilled shafts in limestone is represented using variance rather than COV. Use of the variance

attributed to (end bearing) method error in calculation of total uncertainty for drilled shafts in limestone is discussed in Sec. 3.8.

3.8 Drilled Shafts in Limestone (MWD)

Based on field testing and laboratory experiments (McVay and Rodgers, 2020), specific energy has been shown to be an excellent parameter for estimating the side shear resistance of drilled shafts and auger cast piles socketed into limestone. For example, field testing was carried out to measure specific energy and to evaluate nominal side shear for load tested drilled shafts and auger cast piles at multiple Florida bridge sites spread across the state. From the locations tested, a total of 36 data points were collected that directly compared specific energy and mobilized unit side shear. Specific energy was found to correlate with mobilized unit side shear to the extent that the coefficient of determination (R^2) was determined to be 0.99, when the relationships developed by the University of Florida were used. It should be noted that ongoing research is in progress to continue collecting data and update the correlation coefficients.

However, given that the strength of correlation observed between specific energy and unit side shear is near to unity for the available data, an approach is adopted in the GeoStat implementation for MWD such that method error has no effect on the simulation results when the proposed foundation member will have MWD conducted in the footprint at full-scale. This approach is taken because spatial uncertainty and upscaling effects are removed. Even so, the need is anticipated to be able to account for levels of method error specific to a site or zone when MWD will not be conducted in the footprint of the proposed foundation member at full scale. Therefore, the following expression is also made available as part of the implementation to allow for custom (site-specific) method error calculations:

$$q_{comp_meas} = a + b \cdot q_{pred} \quad (62)$$

where q_{comp_meas} is the computed value of resistance that reflects total uncertainty (i.e., takes into account both spatial variability and method error); a (intercept) and b (slope) are regression expression coefficients; and q_{pred} is the predicted value of resistance that incorporates spatial variability.

Adoption of a linear form for the method error expression is consistent with previous implementations of Geo-statistical analysis for drilled shafts in limestone (e.g., McVay et al. 2012; Davidson et al. 2020). Default parameter values are listed in Table 22, where as emphasis, values are selected such that method error has no effect on simulated results ($a = 0$, $b = 1$). Furthermore, the default value of the regression error variance (σ_ϵ^2) is selected as zero. However, values of the regression error variance (σ_ϵ^2) that are non-zero can also be supplied when performing custom method error calculations.

Table 22. Default values of method error parameters for MWD-based total uncertainty calculations

Parameter	Value
a	0.0
b	1.0
σ_{ε}^2	0.0

3.9 Custom Characterization of Method Error

In the event that axial load test data are available for the planned foundation members of a given bridge site, then regression analysis of said data may lead to regression curve parameters different from those presented in Sec. 3.3 through Sec. 3.6. However, for a given member type and surrounding soil or rock layers, the same overall manner of performing regression analysis as that described above can be carried out. That is, if a set of measured and predicted resistances are known for a site, then (for a given foundation member type) the processes documented above can be utilized to conduct customized regression analysis.

Results obtained from "custom" regression analysis can, in turn, be used to model custom (i.e., site-specific) method error in GeoStat. If axial load test data are available for driven piles, then the process described in Sec. 3.3 can be utilized (but with use of the site-specific data). Likewise, processing of site-specific axial load test data for drilled shafts in sand and clay can be carried out using the processes described in Sec. 3.4 and Sec. 3.5, respectively. For portions of drilled shafts in limestone, and for instances where load test measurements can be categorized into skin friction and end bearing, the process documented in Sec. 3.6 can be utilized.

Consider, for example, the procedure for site-specific characterization of method error (Fig. 34) when analyzing driven piles or portions of drilled shafts embedded in sand (and/or clay). As precursors to the method error characterization, a foundation member type (pile, shaft) is selected and n values of q_{meas} are assembled into $\{q_{meas}\}$. The characterization procedure then begins with determination of corresponding sets of predicted values, $\{q_{pred}\}$, (Fig. 34, top). In addition, sets of log-transformed values are generated for measured data, $\{q_{meas_ln}\}$, and predicted data, $\{q_{pred_ln}\}$.

Next, regression parameter values are determined for each of the number of required regression analyses (n_{reg}). For driven piles, n_{reg} is equal to 1 since only a single regression analysis is necessary along the entire pile embedment length. Similarly, for drilled shafts embedded in only sand (or only clay) layers, n_{reg} is also equal to 1. However, for drilled shafts embedded in soil profiles that include both sand and clay layers, generation of two sets of regression analysis parameters are required (one set shaft portions embedded in sand, one set for portions embedded in clay).

For each iteration through the loop on n_{reg} (Fig. 34, middle), the remainder of the current regression analysis is divided into two parts: (1) determination of descriptive statistics; and, (2) determination of regression values. For determination of descriptive statistics, and for iteration i within the loop on n_{reg} , the subsets for each of $\{q_{pred}\}$ and $\{q_{meas}\}$ are first identified. Then, the mean values (q_{mean_pred} , q_{mean_meas}) and standard deviations (σ_{pred} , σ_{meas}) are calculated for the as-identified data subsets. The same identification and calculation steps are carried out with use of the log-transformed data to produce mean (subset) values, ($q_{mean_pred_ln}$ and $q_{mean_meas_ln}$), and standard deviation values, (σ_{pred_ln} and σ_{meas_ln}).

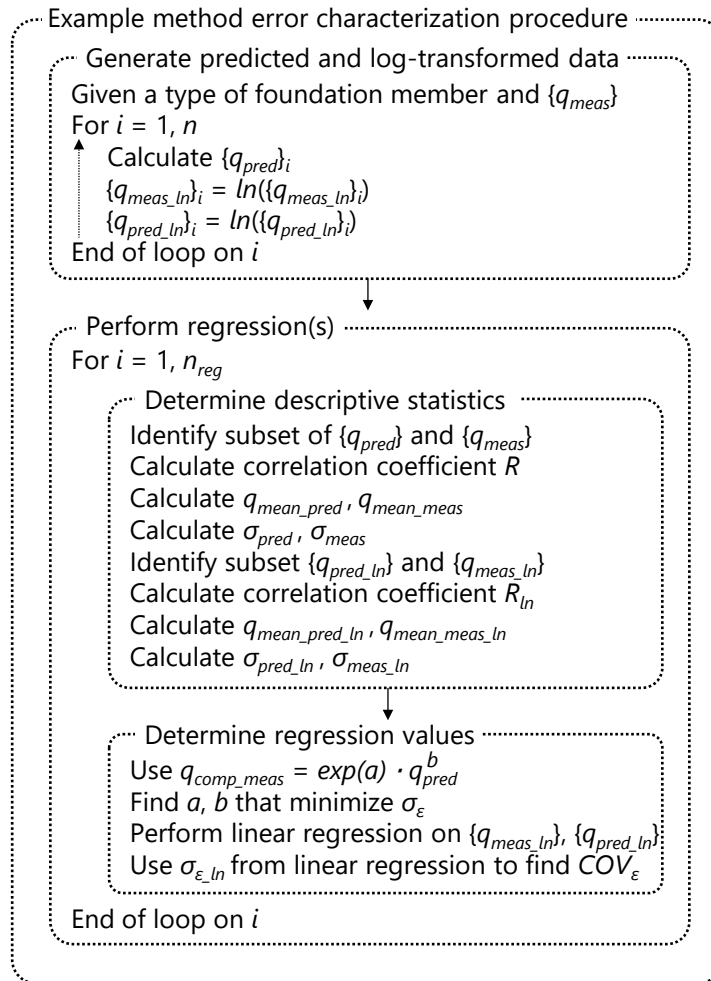


Figure 34. Example method error characterization procedure for driven piles, drilled shafts in sand, and drilled shafts in clay

Next, the associated regression values (a , b) are determined (Fig. 34, bottom) using the same form of regression expression as that given in (for example) Eqn. 48. Also, a separate, linear regression is carried out using the log-transformed data ($\{q_{pred_ln}\}$ and $\{q_{meas_ln}\}$) to find the minimum value of σ_{ϵ_ln} and corresponding regression coefficient, R_{ln} . Then, COV_{ϵ} is calculated

(e.g., as given in Eqn. 49) as a summary representation of the method error for the current iteration through the loop on n_{reg} .

3.10 Total Uncertainty

Recall from Ch. 2 that the LRFD resistance factor (ϕ) represents the total uncertainty attributed to a given resistance quantity. Further, the product of nominal resistance and ϕ gives the (factored) design resistance. As illustration, the default expression for ϕ that is implemented in GeoStat (and adopted from Styler, 2006; McVay et al. 2012) is:

$$\phi = \frac{(\gamma_D \cdot \frac{Q_D}{Q_L} + \gamma_L) \cdot \left(\frac{1 + COV_Q^2}{1 + COV_R^2}\right)^{0.5}}{(\lambda_{QD} \cdot \frac{Q_D}{Q_L} + \lambda_{QL}) \cdot \exp(\beta \cdot \ln((1 + COV_R^2) \cdot (1 + COV_Q^2)))^{0.5}} \quad (63)$$

where all constituent terms are defined as part of documenting Eqn. 41 in Ch. 2. Of particular relevance to method error is the coefficient of variation of member axial resistance, COV_R , which reflects both spatial variability and method error phenomena. Various expressions of COV_R —and terms directly relevant to COV_R —are given immediately below for each foundation member type and soil or rock medium that can be analyzed in GeoStat.

3.10.1 Driven Piles (SPT-N), Drilled Shafts in Sand, and Drilled Shafts in Clay

For driven piles embedded in media consisting of one or more sand, clay, or limestone layers, spatial variability and method error phenomena are combined into COV_R , as presented in Eqn. 64. The expression in Eqn. 64 is also applicable to drilled shaft portions that are embedded in sand or clay layers:

$$COV_R = \frac{(\exp(a)^2 \cdot \sigma_{q_{mean_sim}}^2 + (COV_\varepsilon \cdot q_{mean_sim})^2)^{0.5}}{\exp(a) \cdot \exp(a)^2 q_{mean_sim}^b} \quad (64)$$

where a and b are regression coefficients between measured and predicted values of resistance, with use of the form given in (for example) Eqn. 48; $\sigma_{q_{mean_sim}}^2$ is the variance about the mean of a corresponding set of simulated resistance values (e.g., from unconditional simulation, conditional simulation); and, q_{mean_sim} is the mean value of simulated resistance. Stated another way, the terms q_{mean_sim} and $\sigma_{q_{mean_sim}}^2$ are obtained directly (i.e., without adjustment) from stochastic simulation, and represent contributions to total uncertainty from spatial variability phenomena. Furthermore, the terms a , b , and COV_ε are dependent on foundation member type (and soil type for drilled shafts) and signify method error contributions to total uncertainty.

3.10.2 Driven Piles (CPT)

The approach for incorporating spatial variability and method error into CPT-based Geo-statistical analysis is adopted from Faraone et al. (2021). Key steps of the approach are presented in Fig. 35. As emphasis, this approach is robust to the resistance variable being considered. However, the procedure (as delineated) requires the ratios of measured versus predicted resistance to be lognormally distributed. The overall process begins with collection of load-test data across pertinent sites (Fig. 35, top), including pile properties, soil conditions, and measured resistance (the latter stored in $\{q_{meas}\}$). An empirical method for calculating predictions of axial capacity is then selected (e.g., LCPC, Schmertmann, UF). Next, for each of the number of load tests identified (n_{lt}), the selected empirical method is utilized to calculate respective predictions of axial capacity, stored in $\{q_{pred}\}$. Further, for each load test, the ratio of measured and predicted resistance is determined, $\{R_{mp}\}$.

A filtering step is then undertaken (Fig. 35), which involves calculation of the mean of the ratios of measured versus predicted resistance, R_{mp} . The standard deviation, σ_{mp} , of the entries within $\{R_{mp}\}$ is also determined. A filter is then applied, where any entries in $\{R_{mp}\}$ that lie outside of ± 2 standard deviations (σ_{mp}) from the mean resistance ratio, R_{mp} , are removed. The associated load tests are excluded from further consideration, and n_{lt} is accordingly decremented. In other words, only those load tests that remain after application of the filter are carried further forward into the method error procedure.

Assessment of lognormality is carried out upon the remaining data set (Fig. 35, middle). The assessment begins with selection of an acceptable significance level, p_s , where 5% ($p_s = 0.05$) is typical, and is adopted herein. Then, for each of the (post-filtering) load tests, the $\{R_{mp_ln}\}$ is formed as the entry-wise natural log of $\{R_{mp}\}$. In turn, Lilliefors (1967) statistical test is conducted using $\{R_{mp_ln}\}$ and p_s . Here, because the entries in $\{R_{mp_ln}\}$ have been transformed using the natural log function, the null hypothesis being tested can (effectively) be stated as: the data come from a lognormally distributed population. If the Lilliefors test leads to rejection of the null hypothesis, then the method error procedure is halted and cannot be utilized. Otherwise, if the null hypothesis cannot be rejected, then the method error procedure is applicable and can be continued.

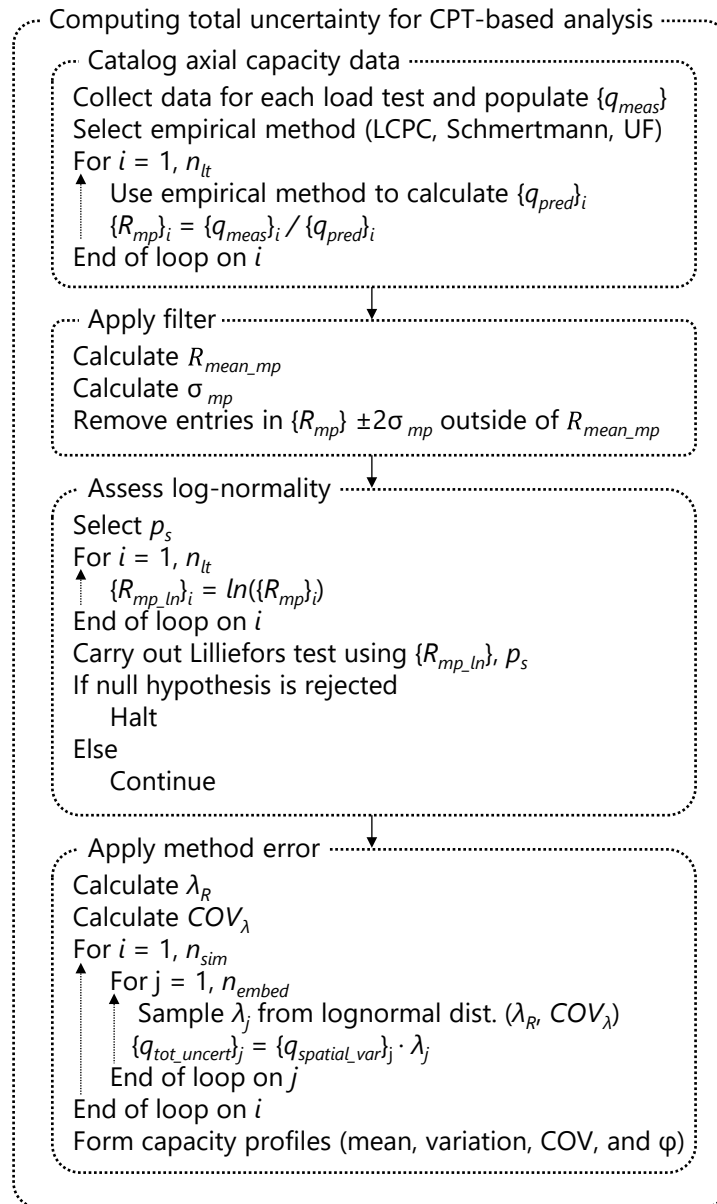


Figure 35. Computing total uncertainty for CPT-based analysis of pile axial capacity

Having collected load test data, formed empirical predictions of axial capacity, applied data filtering, and assessed lognormality, the method error procedure from Faraone et al. (2021) culminates in sampling and applying resistance ratios to resistance quantities obtained from stochastic simulation. In this way, predictions of (for example) axial capacity are produced that reflect both spatial variability and method error phenomena (i.e., total uncertainty). As delineated in Fig. 35, bottom, application of the method error corrections begins with calculation of the mean (again, post-filtering) resistance ratio, λ_R :

$$\lambda_R = \frac{1}{n_{lt}} \sum \lambda_i \quad (65)$$

where λ_i is the ratio of the i^{th} entry in $\{q_{meas}\}$ and, respectively, in $\{q_{pred}\}$ after the filtering step has been completed. Note that i is summed from 1 to n_{lt} . A coefficient of variation, COV_λ , is also calculated with use of Bessel's correction:

$$COV_\lambda = \frac{\left(\frac{1}{n_{lt} - 1} \sum (\lambda_i - \lambda_R)^2\right)^{0.5}}{\lambda_R} \quad (66)$$

Method error is then applied for each of the number of realizations (n_{sim}) produced from stochastic simulation (and which reflect spatial variability phenomena), and in turn, profiles of resistance values, $\{q_{spatial_var}\}$, associated with the number of candidate member embedment lengths considered (n_{embed}). Namely, for the i^{th} profile realization and j^{th} entry of simulated resistance within $\{q_{spatial_var}\}$, a ratio of measured versus predicted resistance, λ_j , is sampled from a lognormal distribution. Note that the lognormal distribution being sampled from satisfies the parameters λ_R and COV_λ . A simulated value of resistance that reflects total uncertainty is then calculated as the product of λ_j and $\{q_{spatial_var}\}_j$, denoted as $\{q_{tot_uncert}\}_j$. Recall that values of λ_R and COV_λ were determined for each of the LCPC, Schmertmann, and UF methods earlier in Ch. 3.

After total uncertainty calculations have been carried out, then COV_R is calculated at elevation intervals in a straightforward manner by drawing (one value of elevation at a time) from the collections of $\{q_{tot_uncert}\}$, across the n_{sim} simulations conducted. Further, profiles of mean capacity can subsequently be formed, along with profiles of variance, coefficient of variation (COV), and LRFD ϕ .

3.10.3 Drilled Shafts in Limestone (Core-Run Data)

For drilled shaft portions that are embedded in limestone layers, total uncertainty is divided into side (skin friction) and tip (end bearing) components.

3.10.3.1 Skin Friction

Specifically, the total uncertainty contributions from spatial variability and method error of skin friction are combined into an expression of COV_R as:

$$COV_R = \frac{(\sigma_{skin}^2)^{0.5}}{A_{skin} \cdot (a_{skin} + b_{skin} \cdot q_{mean_sim_skin})} \quad (67)$$

where $q_{mean_sim_skin}$ is the mean value of simulated (unit) skin resistance along some portion of the shaft length; A_{skin} is the shaft surface area along that same portion; a_{skin} and b_{skin} are associated regression coefficients (corresponding to a and b in Eqn. 54); and, σ_{skin}^2 is a variance term defined as:

$$\sigma_{skin}^2 = A_{skin}^2 \cdot (\sigma_{sim_skin}^2 + \sigma_{\varepsilon_skin}^2) \quad (68)$$

where $\sigma_{sim_skin}^2$ is the variance of the simulated set of unit skin friction resistances; and, $\sigma_{\varepsilon_skin}^2$ is the variance associated with method error and skin friction resistance (corresponding to σ_{ε}^2 in Eqn. 57).

3.10.3.2 End Bearing

An alternative form of COV_R , which describes the total uncertainty contribution from tip resistance, is expressed as:

$$COV_R = \frac{(\sigma_{tip}^2)^{0.5}}{A_{tip} \cdot (a_{tip} + b_{tip} \cdot q_{mean_sim_tip})} \quad (69)$$

where $q_{mean_sim_tip}$ is the mean value of simulated, unit end bearing shaft resistance; A_{tip} is the shaft area available for tip resistance; a_{tip} and b_{tip} are associated regression coefficients (corresponding to a and b in Eqn. 58); and, σ_{tip}^2 is a variance term defined as:

$$\sigma_{tip}^2 = A_{tip}^2 \cdot (\sigma_{sim_tip}^2 + \sigma_{\varepsilon_tip}^2) \quad (70)$$

where $\sigma_{sim_tip}^2$ is the variance of the simulated set of unit end bearing resistances; and, $\sigma_{\varepsilon_tip}^2$ is the variance associated with method error and end bearing resistance (corresponding to σ_{ε}^2 in Eqn. 61).

The total uncertainty contribution for total (combined skin and tip) resistance, expressed as another alternative form of the coefficient of variation, COV_R , is given as:

$$COV_R = \frac{(\sigma_{total}^2)^{0.5}}{A_{skin} \cdot (a_{skin} + b_{skin} \cdot q_{mean_sim_skin}) + (A_{tip} \cdot a_{tip} + b_{tip} \cdot q_{mean_sim_tip})} \quad (71)$$

where σ_{total}^2 is a variance term that includes cross-correlation between skin and tip resistance, and is defined as:

$$\sigma_{total}^2 = \sigma_{skin}^2 + \sigma_{tip}^2 + 2 \cdot R_{skin_tip} \cdot \sigma_{skin} \cdot \sigma_{tip} \quad (72)$$

where R_{skin_tip} is the correlation coefficient between the respective sets of simulated values, q_{sim_skin} and q_{sim_tip} .

3.10.4 Drilled Shafts in Limestone (MWD)

The same approach as that described above in Sec. 3.10.3 is utilized for calculating side and tip contributions to total uncertainty as part of MWD-based Geo-statistical simulation.

CHAPTER 4

MODELING OF EXAMPLE SITE A

4.1 Overview

Presented in Ch. 4 is a detailed walkthrough of geotechnical site modeling and axial resistance simulation for an example bridge site. The data sets discussed herein represent one instance of the types and ranges of geotechnical site data that may be collected when investigating the foundations of a bridge site, but for when only a relatively small set of site data is available. In addition, portions of the overall data set exhibit high levels of variability. Use of the associated site data—within the context of modeling and simulation in GeoStat—is divided into several steps, where such division reflects the left-to-right progression across the seven tabs of the GeoStat user interface (UI). See the Help Manual for detailed descriptions of the GeoStat UI layout.

The site of interest is referred to as Example Site A (or Site A). Cataloging of the available collection of Site A data for modeling within GeoStat is discussed in Sec. 4.2. Initial selection of boundary soil and rock (limestone) layer elevations is discussed in Sec. 4.3. Also documented in Sec. 4.3 are layer-related considerations specific to the type of foundation member being considered (pile, shaft). Initial formation of spatial correlation structures (i.e., variograms) for each defined layer is then discussed in Sec. 4.4.

As will be demonstrated, the relatively limited data set gives way to multiple, possible interpretations concerning layer definitions. A set of alternative layer definitions is presented in Sec. 4.5. Associated Geo-statistical parameters (obtained using the alternative layer definitions) are documented in Sec. 4.6. Zonal issues are not anticipated for the Site A data set (see Ch. 5 for a detailed guide for modeling of zones). Purely for illustration of the concepts and process, a cursory examination of the Site A data set is given in Sec. 4.7 within the context of assessing the presence of zones.

Subsequent to definition of representative layers and characterization of layer-specific correlation structures, the focus of the walkthrough for Site A shifts to stochastic simulation of axial resistance in Sec. 4.8. Interpretation of simulated profiles of axial resistance, which reflect spatial variability phenomena, is provided in Sec. 4.9. Considerations for incorporating method error phenomena into the simulated results are detailed in Sec. 4.10. The combined effects of spatial variability and method error upon computed axial resistance, culminating in profiles of both resistance factors (ϕ) and factored axial resistance, are examined in Sec. 4.11.

4.2 Cataloging Site Data

Shown in Fig. 36 is the first (leftmost) tab encountered within the GeoStat UI, referred to as the Project Information tab. This region of the GeoStat UI facilitates input and organization of

all data obtained from geotechnical investigation of the site. The foundation type is also selected in the Project Information tab (Fig. 36, upper-right).

For Site A, a drilled shaft foundation type is selected. However, throughout Ch. 4, when distinct considerations are required that depend on the selected foundation type (piles, shafts), such distinctions are noted. Otherwise, documentation of parameters selected for site modeling and interpretation of simulation results are generally applicable regardless of the selection for type of foundation member.

4.2.1 Initial Visual Assessment of Site A

For the start of the analysis, all borings for the site should be active. Accordingly, as a starting point, initial characterization of the site data (through the step of forming variograms) is carried out using all available measurements from across the 14 boring locations. Data from 14 unique boring locations are cataloged for Site A, including both SPT-N blow counts and rock-related measurements obtained from numerous core-runs (e.g., unconfined compression strength, q_u). Values of undrained shear strength (C_u) are not available among the site data. However, as discussed in Sec. 2.7, blow count values are simulated and then empirically related to undrained shear strength. The geotechnical investigation of Site A indicates the presence of interspersed bands and layers of clay and limestone across the 14 boring locations. Given the prevalence of limestone throughout Site A, emphasis is initially placed on available measurements of rock strength (as discussed below) when forming components of the GeoStat model.

The plan-view boring locations for Site A are distributed across a footprint, that in turn, extends along several bridges spans (particularly with respect to northing values). A plan view of the 14 boring locations is plotted in the left portion of the Project Information tab, and a corresponding plot of eastings and northings for the boring locations is shown in Fig. 37. As listed in the table on the right portion of the Project Information tab (Fig. 36, right), northing values range from 0 ft to approximately 1500 ft, and easting values range from (approximately) -75 ft to 75 ft. Further, the ground surface elevations across the 14 borings range from 78 ft to 98 ft.

On the Project Information tab (Fig. 36) scatterplot data associated with any currently selected (and active) boring location is highlighted, and can be used to quickly identify borings that contain outlier data or are associated with a unique zone. For each of the 14 boring locations, the respective (boring-specific) geotechnical site data are input in GeoStat using the Boring Data dialog. This dialog is accessible from the upper-right portion of the Project Information tab. For example, site data measured at boring location B-1 (easting of 64 ft; northing of 427 ft) consists of through-depth SPT-N blow count values, and is cataloged as shown in Fig. 38. An additional example is provided in Fig. 39 for boring location B-4 (easting of -24 ft;

northing of 360 ft), which contains a mixture of SPT-N blow count and core-run data (e.g., unconfined compression strength, q_u , split tensile strength, q_t , RQD, *recovery*).

The rightmost plot in the Project Information tab (Fig. 36, middle) facilitates plotting of collections of the desired type of site measurement (e.g., SPT-N, q_u). In addition, data pertaining to any boring location of interest are highlighted (using solid blue plot points), as exemplified for boring location B-1 in Fig. 36.

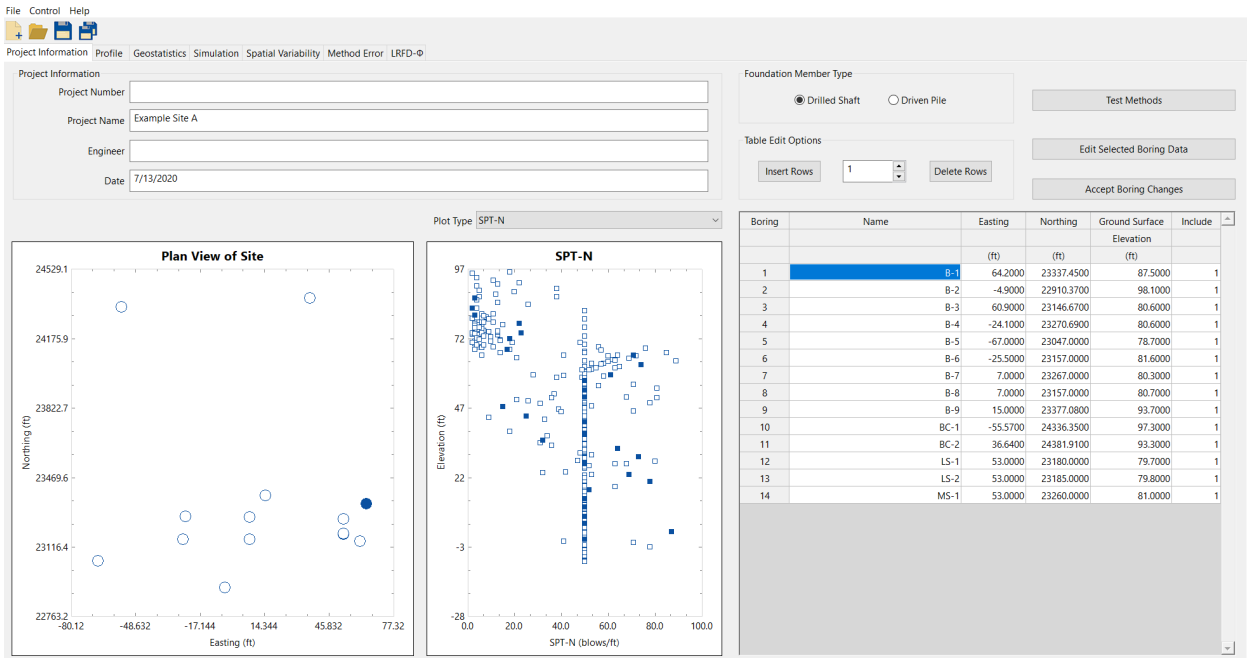


Figure 36. Project Information tab

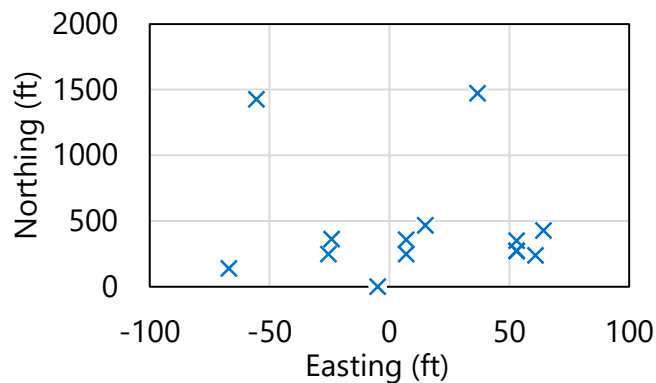


Figure 37. Plan view of 14 boring locations for Site A

Boring Data - B-1

Table Edit Options

Insert Rows 1 Delete Rows

Number	Elevation	Depth	Soil Type	N. Blows	qt (CPT)	fs (CPT)	Unit Weight	Cu	e	qu	qt	qb	Em	RQD	Socket Roughness	Recovery
	(ft)	(ft)	[1 2 3 4]	(blows/ft)	(tsf)	(tsf)	(pcf)	(tsf)	(psi)	(tsf)	(tsf)	(tsf)	(ksi)	[0.0 to 1.0]	[0 1]	[0.0 to 1.0]
1	86.5000	1.0000		2	3											
2	83.0000	4.5000		2	2											
3	80.5000	7.0000		2	3											
4	77.5000	10.0000		2	22											
5	74.0000	13.5000		2	23											
6	72.0000	15.5000		2	18											
7	68.0000	19.5000		2	17											
8	66.0000	21.5000		2	71											
9	62.5000	25.0000		2	74											
10	59.0000	28.5000		2	61											
11	57.0000	30.5000		2	50											
12	53.5000	34.0000		2	50											
13	51.0000	36.5000		2	50											
14	47.5000	40.0000		1	15											
15	44.0000	43.5000		1	25											
16	42.0000	45.5000		1	50											
17	38.0000	49.5000		1	50											
18	35.5000	52.0000		1	32											
19	32.5000	55.0000		1	64											

Notes

- Input all available data for the boring within the table above.
- For any depths where a given soil property is not available, then leave the corresponding cell blank.
- Soil Types: 1 = Plastic Clay | 2 = Clay and Silty Sand | 3 = Clean Sand | 4 = Limestone and Very Shelly Sand.

OK Cancel

Figure 38. Boring Data dialog for boring location B-1

Boring Data - B-4

Table Edit Options

Insert Rows 1 Delete Rows

Number	Elevation	Depth	Soil Type	N. Blows	qt (CPT)	fs (CPT)	Unit Weight	Cu	e	qu	qt	qb	Em	RQD	Socket Roughness	Recovery
	(ft)	(ft)	[1 2 3 4]	(blows/ft)	(tsf)	(tsf)	(pcf)	(tsf)	(psi)	(tsf)	(tsf)	(tsf)	(ksi)	[0.0 to 1.0]	[0 1]	[0.0 to 1.0]
1	79.7000	0.9000		2	8											
2	76.6000	4.0000		2	6											
3	73.4000	7.2000		3	13											
4	70.5000	10.1000		3	19											
5	67.0000	13.6000		3	14											
6	64.3000	16.3000		1	63											
7	61.5000	19.1000		1	63											
8	58.0000	22.6000		1	38											
9	55.5000	25.1000		1	71											
10	53.1833	27.4167		4			103.2000				5.0184			0.5000		0.2200
11	52.3500	28.2500		4			109.3000			60.9264				0.5000		0.2200
12	51.5167	29.0833		4			104.3000				9.3600			0.5000		0.2200
13	50.6833	29.9167		4										0.5000		0.2200
14	49.8500	30.7500		4			102.2000				6.2424			0.5000		0.2200
15	49.0167	31.5833		4			102.1000				6.7896			0.5000		0.2200
16	47.8222	32.7778		4			91.8000				0.6120			1.0000		0.6700
17	47.2667	33.3333		4			95.8000				1.6848			1.0000		0.6700
18	46.7111	33.8889		4			102.8000			23.4792				1.0000		0.6700
19	46.1556	34.4444		4			99.0000			8.6112				1.0000		0.6700

Notes

- Input all available data for the boring within the table above.
- For any depths where a given soil property is not available, then leave the corresponding cell blank.
- Soil Types: 1 = Plastic Clay | 2 = Clay and Silty Sand | 3 = Clean Sand | 4 = Limestone and Very Shelly Sand.

OK Cancel

Figure 39. Boring Data dialog for boring location B-4

Documented in the remainder of Sec. 4.2 are initial characterizations of the various types of measured site data available for Site A. Data are presented in scatterplot form, or as through-depth profiles of measurements accumulated across all 14 boring locations. In this way, initial characterization of trends or groupings among the site data are qualitatively identified, where such identification is necessary (for example) in defining soil or rock layering.

4.2.2 Site Data for Shafts in Limestone

As aforementioned, initial efforts toward characterizing the site emphasize examination of available rock strength data (e.g., q_u), given the frequent occurrence of limestone throughout Site A. Shown in Fig. 40 are measurements of rock strength obtained across the 14 boring locations (and associated core-runs) of Site A. For unconfined compression strength, q_u , 152 measurements are available (Fig. 40a). Also, 191 measurements of split tensile strength, q_t , are available (Fig. 40b).

No immediately apparent q_u - q_t correlations are identified between the scatterplots in Fig. 40. However, while the majority of measured q_u values are less than approximately 10 tsf, relatively higher compression strength values (between approximately 25 tsf and 325 tsf) are concentrated over the approximate elevation range of 45 ft to 30 ft.

Plotted in Fig. 41 are additional measurements pertaining to rock strength, as gathered from across the core-runs of Site A. Concerning rock quality designation (RQD), 338 values are taken from the collection of core-runs (Fig. 41a). Correspondingly, 338 values of *recovery* are included for use in GeoStat modeling of the site (Fig. 41b).

Many interspersed groupings of both RQD and *recovery* values are distributed throughout the scatterplots, and decimal values generally range from (approximately) 0.2 to 1.0. Stated alternatively, despite the relatively large number of measured values available for RQD and *recovery*, no overtly discernible trends or groupings of values are apparent from visual inspection of the scatterplots.

Measured values of unit weight are also examined, but are considered secondary (e.g., for establishment of layering) to measured rock strengths. Depicted in Fig. 42 are measured values of unit weight, γ , available over the elevation range of 67 ft to 9 ft. Relatively weak groupings of values are qualitatively identified over the elevation range of approximately 67 ft to 45 ft, and separately, 45 ft to approximately 9 ft. The 338 measured values of unit weight (γ) vary, approximately, from 90 lb/ft³ to 160 lb/ft³.

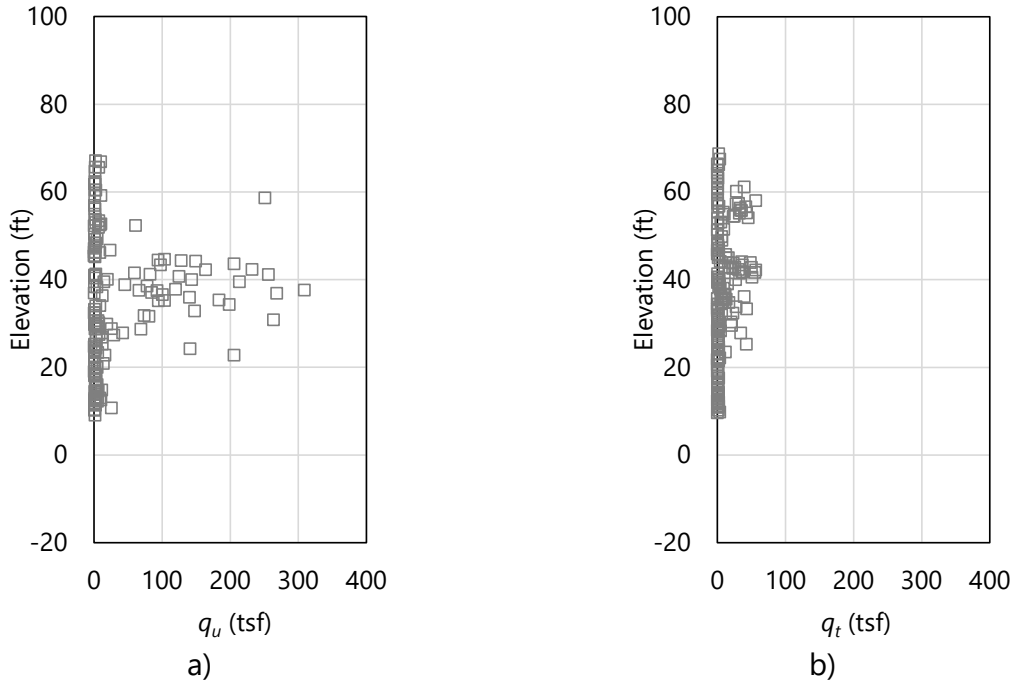


Figure 40. Scatterplots of limestone strength parameters: a) 152 values for unconfined compression strength, q_u , (elevation range: 67 ft to 9 ft); b) 191 values for split tensile strength, q_t , (elevation range: 53 ft to 25 ft)

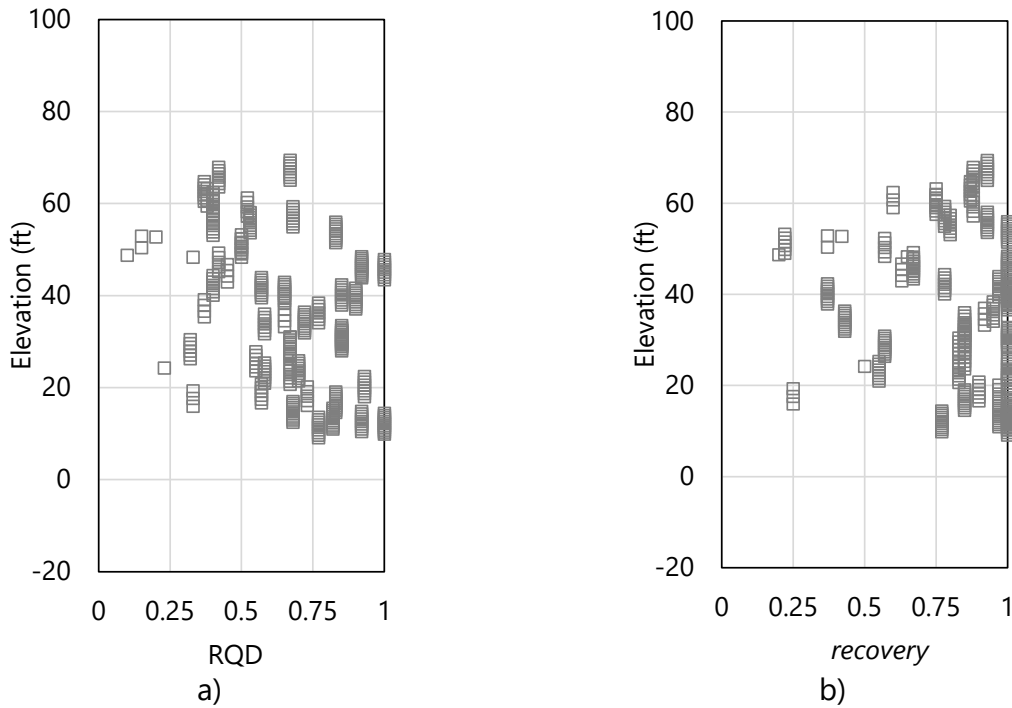


Figure 41. Scatterplots of limestone strength parameters: a) 338 values for RQD (elevation range: 67 ft to 9 ft); b) 338 values for *recovery* (elevation range: 67 ft to 9 ft)

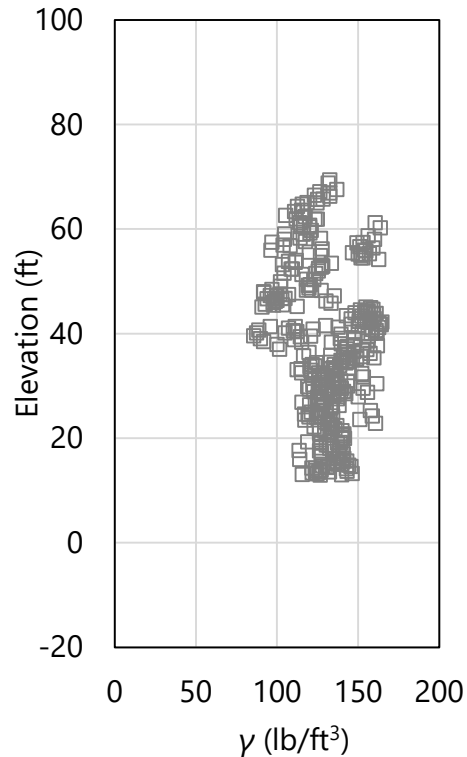


Figure 42. Scatterplot of 338 values of unit weight, γ , (elevation range: 67 ft to 9 ft)

4.2.3 Site Data for Shafts in Clay, Shafts in Sand, and Driven Piles

For portions of drilled shafts and piles embedded in clay and sand, for the example site, SPT-N blow count values are most pertinent in computing axial resistances from within GeoStat. As noted above, values of undrained shear strength (C_u) are not available among the site data, but rather, are estimated via empirical correlation to SPT-N blow count values (see Sec. 2.7 for additional discussion). Plotted in Fig. 43 are 271 SPT-N blow count values, as collected across the 14 boring locations of Site A. Blow count values range from 0 blows/ft to approximately 90 blows/ft. Per the available site data, a relatively high prevalence of blow count values are attributed to refusal-like conditions and thus reported as 50 blows/ft.

A qualitative grouping of SPT-N blow count values is apparent from elevations of 97 ft to approximately 65 ft. An additional grouping is identified from 65 ft to approximately 45 ft, and a third qualitative grouping occurs (approximately) from 45 ft to 20 ft. These visually identified groupings are revisited later as part of defining representative layering for the available Site A data.

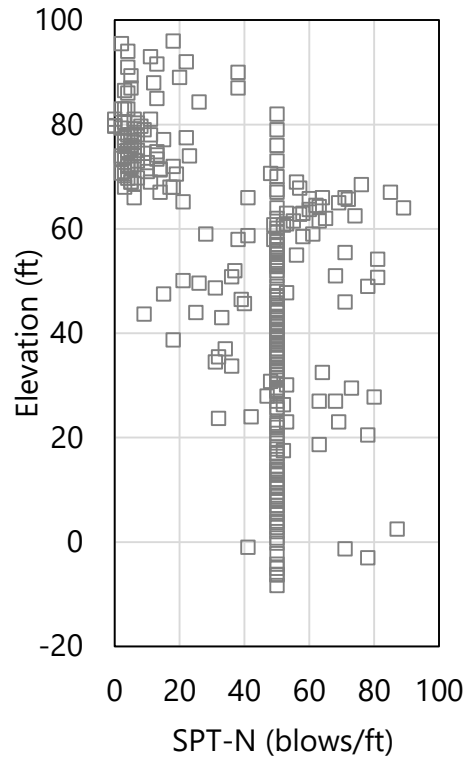


Figure 43. Scatterplot of 271 SPT-N blow counts (elevation range: 96 ft to -10 ft)

4.3 Initial Definition of Soil or Rock Layering

The second of seven tabs (from left to right) in the GeoStat UI is the Profile tab (Fig. 44). Using the controls within this tab, a representative soil or rock layering is defined. Scatterplots of the previously cataloged site data are utilized here (Fig. 44, left and middle) to aid in selection of boundary layer elevations. Layer bottom elevations can be defined through graphical selection within the profile plots. Additionally, all required parameter values for a given layer (e.g., soil or rock type, top elevation, bottom elevation) can be input in the layer data table (Fig. 44, right).

As a first attempt at establishing layer definitions for Site A, consider the soil or rock types and layer elevations given in Table 23. Based on the cataloged site data, with emphasis on rock strengths, four layers are defined and consist of either clay (layer 1) or limestone (layer 2, layer 3, and layer 4). Layer top and bottom elevations span the ranges of elevations identified during the initial review of the site data (documented above). Additional discussion regarding initial selections of the boundary layer elevations is provided in the remainder of Sec. 4.3. Still further considerations are documented in Sec. 4.4, as part of forming the initial (layer-specific) variograms.

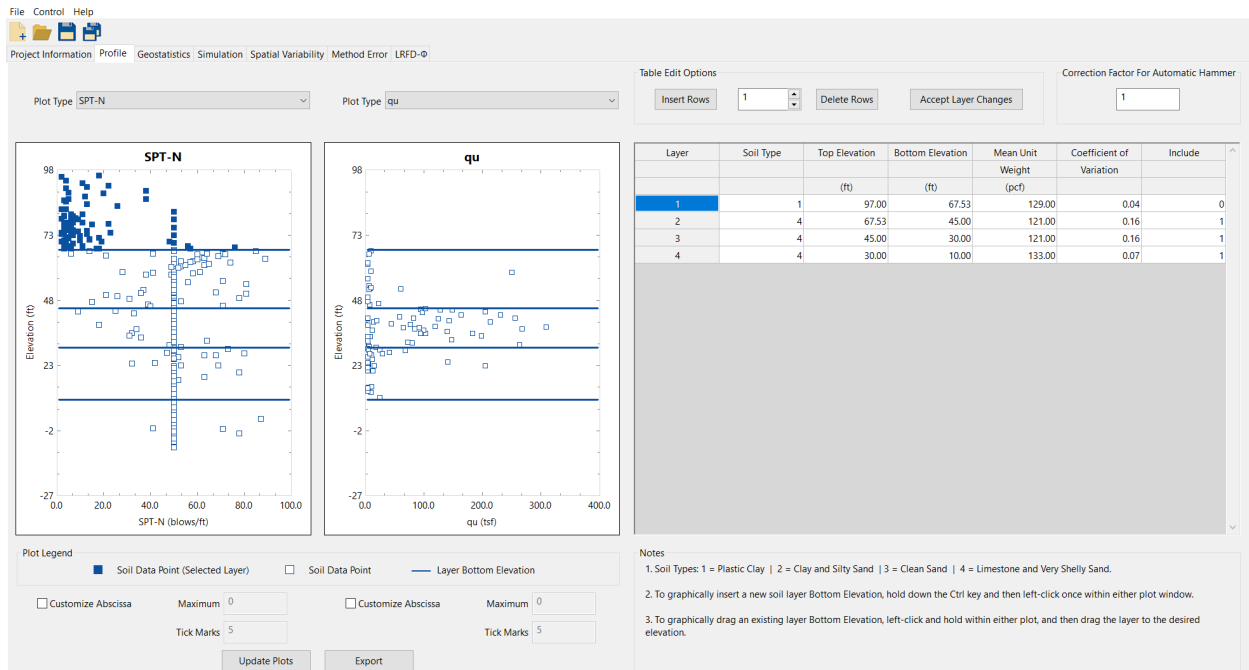


Figure 44. Profile tab

Table 23. Initial selection of layer types and elevation ranges

Layer	Layer type	Top elevation (ft)	Bottom elevation (ft)
1	Clay	97.0	67.5
2	Limestone	65.0	45.0
3	Limestone	45.0	30.0
4	Limestone	30.0	10.0

4.3.1 Initial Selection of Layer Elevations

Selected geotechnical data pertaining to rock strength are made use of for initial definition of the boundary layer elevations. In particular, plotted in Fig. 45 are the layer divisions and ensemble of 152 measurements for unconfined compression strength, q_u . Qualitatively, three through-depth groupings are identified. For example, from approximately 67.5 ft to 45 ft, measured q_u values are generally less than 10 tsf. In accordance with observations made from the review of the full catalog of site data, a concentrated region of relatively higher-magnitude q_u values is designated as a distinct limestone layer. Consequently, layer 2 is defined as a limestone layer from 67.5 ft to 45 ft, and layer 3 (also limestone) is defined as spanning the elevations from 45 ft to 30 ft.

Continued visual inspection of q_u values in Fig. 45 reveals additional groupings of significance for data positioned at elevations below 30 ft. Measurements of q_u , associated with rock strength are generally of low magnitude (i.e., less than 10 tsf). Therefore, layer 4 is defined for

data below 30 ft down to a practical limit for embedment depths (i.e., layer 4 is defined between 30 ft and 10 ft), and is defined as a limestone layer.

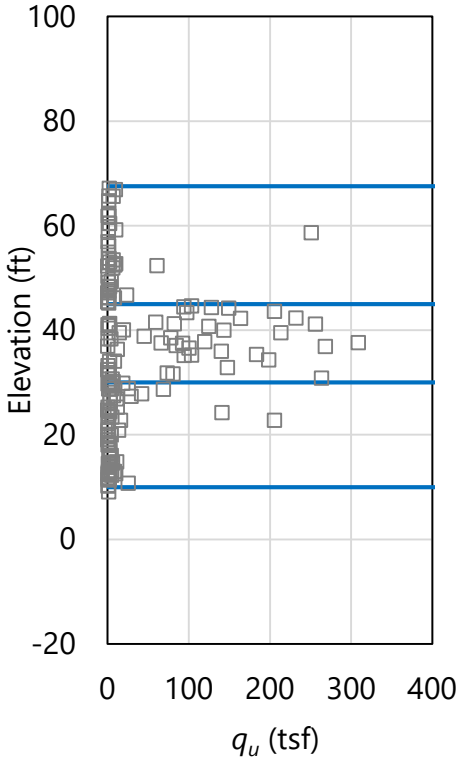


Figure 45. Scatterplot of 152 values for unconfined compression strength, q_u , (elevation range: 67.5 ft to 9 ft) with layer bottom elevations (blue horizontal lines)

The 271 SPT-N blow counts associated with the 14 boring locations of Site A are also examined (secondary to q_u values for this initial examination). A scatterplot of the SPT-N values, along with layer bottom elevations (blue horizontal lines), is presented with respect to elevation in Fig. 46. Consistent with the initial review of the cataloged SPT-N data for Site A, the selected layer divisions are positioned in accordance with qualitative groupings of the SPT-N blow counts. For example, a distinct grouping of blow counts is apparent between 97 ft and 67.5 ft, in comparison to those values cataloged below 67.5 ft. Thus, Layer 1 is defined between 97 ft and 67.5 ft. Similarly, the qualitative grouping of SPT-N blow counts positioned between 67.5 ft and 45 ft (complementary to the above examination of q_u values) further motivates designation of the boundary elevations for layer 3 (45 ft to 30 ft).

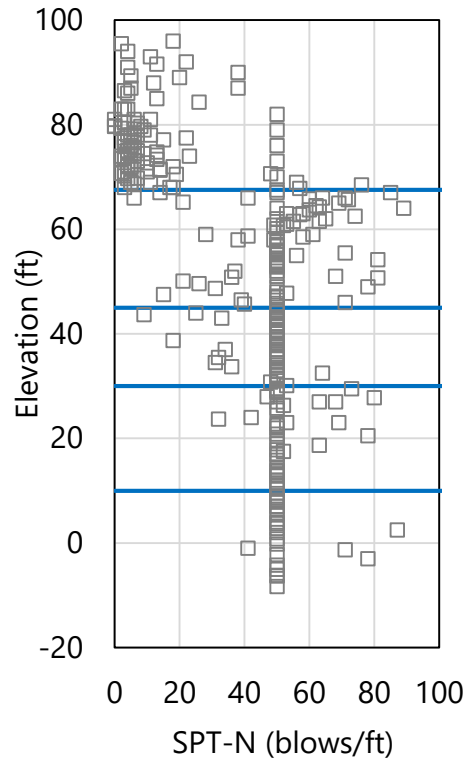


Figure 46. Scatterplot of 271 SPT-N blow counts (elevation range: 96 ft to -10 ft) with layer bottom elevations (blue horizontal lines)

4.3.2 Specifying Unit Weight per Layer when Modeling Drilled Shafts

Axial resistances for both driven piles and drilled shafts can be computed using the GeoStat software. For instances where driven piles are being considered, only the layer types (e.g., clay, sand, limestone) and boundary elevations are required for layer definitions. However, for drilled shafts, descriptive statistics pertaining to unit weight, γ , are additionally required for each defined layer. The descriptive statistics are input in the GeoStat UI (per layer) in the same location as the respective layer top and bottom elevations (recall Fig. 44, right). Required statistics include the mean value of unit weight and the associated COV.

As illustration of how the descriptive statistics are formed when drilled shafts are selected as the foundation type, consider the scatterplot of 338 unit weight (γ) values for Site A (and layer bottom elevations) in Fig. 47. Formation of descriptive statistics for each layer is carried out by: (1) identifying those values of unit weight (γ) that are positioned within the layer; (2) calculating the mean value of the identified γ values; (3) calculating the standard deviation; and, (4) calculating the COV.

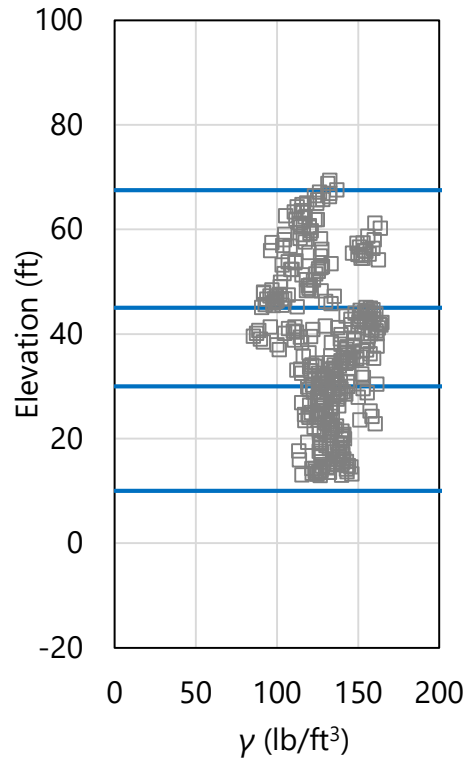


Figure 47. Scatterplot of 338 values of unit weight, γ , (elevation range: 67.5 ft to 9 ft) with layer bottom elevations (blue horizontal lines)

Continuing the illustration, consider the 147 unit weight values (γ) exclusive to layer 4 (Fig. 48). A corresponding histogram of the 147 values is shown in Fig. 49. The distribution of unit weight values, γ , in layer 4 (Fig. 49) qualitatively resembles that of a right-skewed lognormal distribution. Further, the histogram does not exhibit conspicuous features such as bimodal frequency peaks, which if present, would potentially require revisions to the layer elevations defined in Table 23. The mean of the layer 4 unit weight data is calculated as 133 lb/ft³; the standard deviation is calculated as 9.3 lb/ft³; and, the COV is calculated as 0.07. Both the mean and COV values for unit weight, γ , are supplied as part of the layer 4 definition, given that drilled shafts (as opposed to driven piles) are being investigated for Site A.

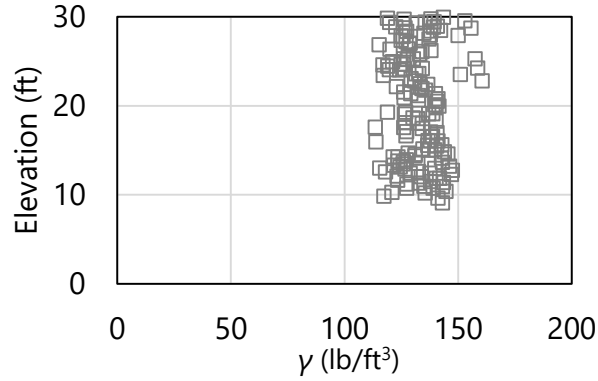


Figure 48. Scatterplot of 147 values of unit weight, γ , (elevation range: 30 ft to 9 ft) within layer 4

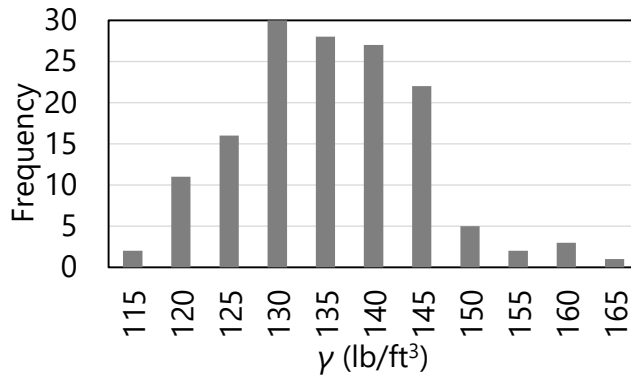


Figure 49. Histogram of 147 values of unit weight, γ , (elevation range: 30 ft to 9 ft) within layer 4

The same procedure as detailed above for layer 4 is carried out for all defined layers of Site A. Respective values of mean unit weight and COV are listed for layer 1 through layer 4 in Table 24. The dispersion of the layer-specific values for unit weight, expressed as COV, range between 0.04 (layer 1) and 0.16 (layer 2). As discussed previously in Ch. 2, these descriptive statistics are utilized when simulating log-normally distributed values of unit weight (γ), as part of stochastic simulation of axial resistance for drilled shaft members.

Table 24. Descriptive statistics for unit weight for each layer

Layer	Mean unit weight (lb/ft ³)	COV
1	129	0.04
2	121	0.16
3	137	0.14
4	133	0.07

4.3.3 Accounting for Steel Casings when Modeling Drilled Shafts

As an additional consideration when modeling axial resistances of drilled shafts, it may be desirable to neglect skin friction resistance near upper portions of the shaft when steel casings are present. As a convenience, for such instances, the option is available to exclude any defined layer from the resistance computation procedures implemented in GeoStat.

For example, if a drilled shaft foundation type is considered for Site A, and a casing is present from the ground surface down to the rock layer (i.e., layer 2), then layer 1 is excluded from axial resistance calculations by setting the Include flag to 0 (as opposed to 1, which signifies inclusion) within the layer data table of the Profile tab (Fig. 44, far right).

4.4 Initial Selection of Geo-statistical Parameter Values

Having defined an initial layering for the Site A geotechnical data, focus of the modeling efforts within GeoStat continues onward to the formation of layer-specific spatial correlation structures (i.e., variograms). Although, as part of the variogram formation for each layer, additional checks are conducted regarding the previously defined layering (as discussed in Sec. 4.4.1).

Variogram formation for each layer is carried out within the Geostatistics tab (Fig. 50) of the GeoStat UI. For any layer that is to be included for simulating axial resistance, various graphical depictions are provided in the bottom region of the Geostatistics tab. From left to right (Fig. 50, bottom), the layer-specific graphical depictions include a scatterplot of the relevant soil or rock parameter, corresponding histogram, horizontal variogram, and vertical variogram.

While the scatterplot and histogram are dictated by the previously cataloged site data and initial layer definitions, the (experimental) variogram points are dependent on selection of variogram parameter values in the table located above the plots (Fig. 50, middle). Documentation of the selection of variogram parameter values for the initial Site A layering is provided later.

However, for drilled shaft portions embedded in limestone layers, values of unconfined compression strength (q_u) are used for computation of variogram points. When forming spatial correlation structures for driven pile foundation members, SPT-N blow count values are utilized in forming variograms. Likewise, for drilled shaft portions embedded in clay layers and drilled shaft portions embedded in sand layers, SPT-N blow count values are again utilized.

For the modeling of Site A, recall that a drilled shaft is selected as the foundation member type. Given the initial (limestone) layer definitions for layer 2, layer 3, and layer 4, variograms

would be formed based on layer-specific ensembles of unconfined compression strength (q_u). Also, because steel casing is assumed to be present down to the rock layer (layer 2), there is no need to form spatial correlation structures for layer 1.

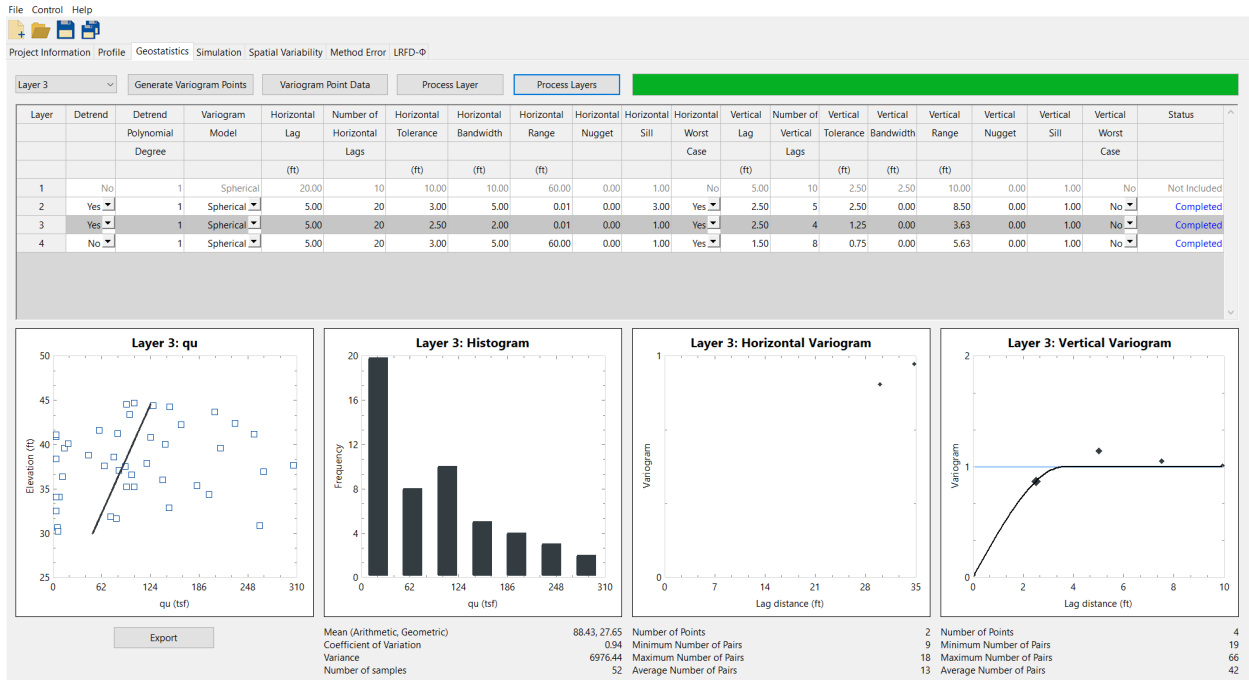


Figure 50. Geostatistics tab

4.4.1 Examining Initial Definition of Layer Data

Prior to selecting variogram parameter values for each layer, both the descriptive statistics and graphical depictions of the layer-specific collections of q_u values are examined. Summary statistics for the relevant types of soil or rock measurements of each layer (q_u , given the initial layer definitions) are listed in Table 25. The sample sizes (i.e., number of measured values) per layer range from 38 to 61 across layers 2 through 4. Values pertaining to layer 1 are not applicable (N/A) because the layer is excluded from the Site A analysis to reflect the presence of a steel casing.

The dispersions associated with layers 2 and 4 are markedly high (COV values are 3.50 for layer 2, 2.63 for layer 4) Such large magnitudes of COV, in part, motivate assessment of the Site A data for alternative layer definitions (as discussed later). The unconfined compression strength value associated with layer 3 also exhibits large variations in an absolute sense (the COV value is 0.94); however, this latter dispersion value is less than (approximately) unity, and so, is less conspicuous.

Concerning examination of graphical depictions of layer-specific data (again, only q_u is applicable here), the scatterplot (e.g., Fig. 50, bottom-left) serves to reveal if trends are present

among the layer data. In the event that a trend is observed among the data attributed to a layer, then detrending is necessary. The detrending process (documented in Ch. 2) is automated in the GeoStat UI. Recalling Fig. 50 (middle-left), if detrending is desired for the data of a given layer, then the respective entry in the Detrend column of the layer data table is set to Yes (as opposed to No). Further, the polynomial degree of the trend is specified. Typically, linear detrending is sufficient for instances when detrending is necessary.

Table 25. Summary statistics for defined layers

Layer	Physical measurement	Sample size	Mean	COV
1	N/A	N/A	N/A	N/A
2	q_u (tsf)	38	11.7	3.50
3	q_u (tsf)	52	88.4	0.94
4	q_u (tsf)	61	12.4	2.63

Regarding the histograms of layer-specific data (e.g., Fig. 50, bottom-center), these plots allow for conspicuous frequency-related features (i.e., bimodal peaks) to be identified. More broadly, in the event that the data distribution for a given layer does not roughly exhibit a lognormal shape, then revisions to the layer definitions (and particularly the layer elevations) may need to be carried out. When conspicuous features are present in a layer-specific histogram, then it may also be necessary to assess the site data for the presence of distinct geological zones. If zones are identified, then modeling of each zone (one subset of boring locations at a time) can lead to more representative layers for a given region within the site, and also, to relatively smaller values of COV for layer-specific data. As a tradeoff though, the number of data points per layer will be reduced as the data set is further subdivided. See Ch. 5 for additional details regarding modeling of zones within sites.

4.4.1.1 Layer 2

A scatterplot of the 38 unconfined compression strength (q_u) values positioned within layer 2 is presented in Fig. 51. All but three values are less than approximately 10 tsf. As part of the present examination it is confirmed that the q_u values are generally contributed to from across all boring locations that contain core-run data. That is, if any one boring location containing core-run data is deactivated, no visual changes are observed within the scatterplot of q_u values. A very weak trend is present in the data that indicates decreases in q_u with increasing depth.

A histogram of the 38 measured q_u values pertaining to layer 2 is presented in Fig. 52. To better reveal the qualitative characteristics of the distribution, the histogram excludes the three q_u values that are greater than approximately 10 tsf. The overall histogram (roughly) resembles that of log-normally distributed data, and possesses a pronounced right skew. Given the absence of conspicuous features (such as bimodal phenomena) in the layer 2

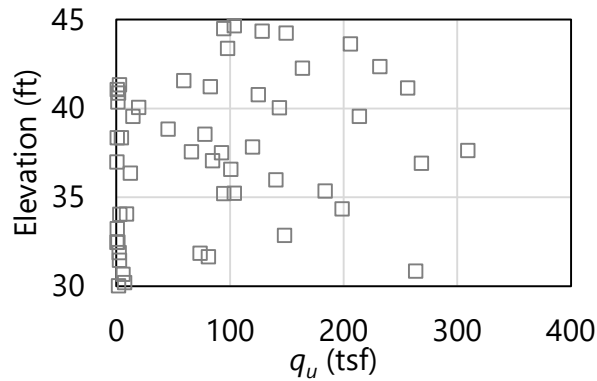


Figure 53. Scatterplot of 52 unconfined compression strength, q_u , values (elevation range: 45 ft to 30 ft) within layer 3

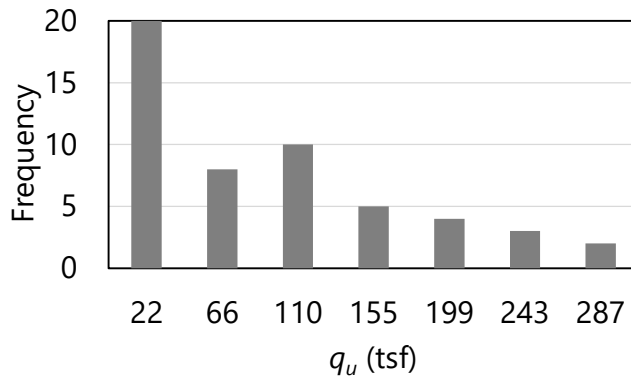


Figure 54. Histogram of 52 unconfined compression strength, q_u , values (elevation range: 45 ft to 30 ft) within layer 3

4.4.1.3 Layer 4

A scatterplot of the 61 unconfined compression strength (q_u) values positioned within layer 4 is presented in Fig. 55. All but 7 values are less than approximately 20 tsf. As with layer 2 and layer 3, it is likewise confirmed for layer 4 that the q_u values are generally contributed to from across all boring locations that contain core-run data. Also, no apparent trend is observed within the layer 4 scatterplot.

A histogram of the 61 measured q_u values pertaining to layer 4 is presented in Fig. 56. To better reveal the qualitative characteristics of the distribution, the histogram excludes the seven q_u values that are greater than approximately 20 tsf. The overall histogram (roughly) resembles that of log-normally distributed data, with a pronounced right skew. Given the absence of conspicuous features (such as bimodal phenomena) in the layer 4 histogram, no revisions are made regarding the initial selection of boundary elevations for layer 4.

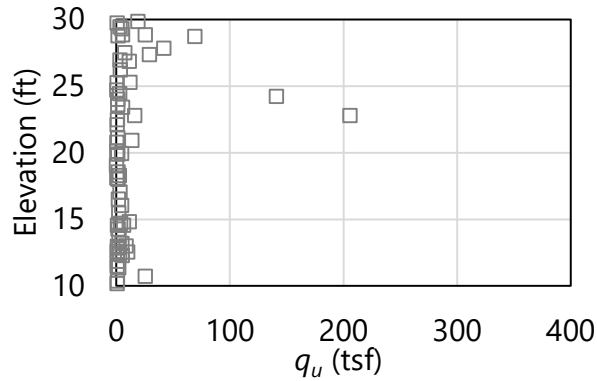


Figure 55. Scatterplot of 61 unconfined compression strength, q_u , values (elevation range: 30 ft to 10 ft) within layer 4

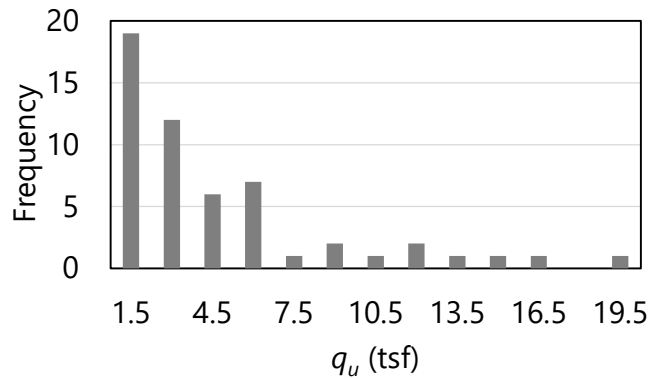


Figure 56. Histogram of 61 unconfined compression strength, q_u , (elevation range: 30 ft to 10 ft) within layer 4

4.4.2 Forming Variograms using Initial Layer Definitions

The above examination reaffirms the initial selections of layer elevations for the geotechnical data of Site A. Despite this reaffirmation, the COV values of q_u for layer 2 and layer 4 (recall Table 25) are conspicuously large and require further consideration, as provided later. As the immediate next step though, the process of forming variograms is undertaken for layer 2 through layer 4.

4.4.2.1 Limitations of the Site A Data Set

Recalling Fig. 37, geotechnical data are available for only 14 boring locations, and those locations are distributed across a plan-view area of approximately 150 ft by 1500 ft. Consequently, the prospect of forming representative spatial correlation structures in the horizontal direction is precluded for Site A. Importantly, this is not to say that the horizontal

variograms are neglected. Rather, worst case conditions (conceptually introduced in Ch. 2) are applicable to the horizontal variograms. More specifically, worst case conditions are applicable to the horizontal variograms because insufficient data are available across the 14 borings of Site A for the purpose of constructing well-formed horizontal variograms. Further recall from Ch. 2 that worst case conditions constitute upper-bound conservatism; worst case conditions are associated with maximally conservative (i.e., highest-valued) variability, lowest-valued resistance factors (ϕ), and ultimately, lowest-valued factored resistances. Use of worst case conditions may lead to designs that are not cost effective due to the associated levels of conservatism.

As detailed in Ch. 2, unconditional (stochastic) simulation for estimating foundation member axial resistance makes use of spatial correlation structures in the vertical direction, as opposed to variograms in the horizontal and vertical directions. Unconditional simulation is elected for Site A to avoid the prospect of generating factored axial resistances under worst case conditions (with respect to the horizontal variograms). Given the small number of relatively distant boring locations (in plan-view) for Site A, focus is given below to formation of vertical variograms. However, the same general concepts apply for instances where sufficient site data are available to construct both horizontal and vertical variograms for a site.

4.4.2.2 Summary of Initial Selections for Variogram Parameter Values

Vertical variogram parameters initially selected for layer 2 through layer 4 of Site A are listed in Table 26. As discussed in Ch. 2, the lag distance, number of lags, tolerance, and bandwidth are all instrumental in forming points of the experimental variogram. Vertical variogram values for range and sill are listed per layer in Table 27, where these values are more strongly related (in GeoStat) to the theoretical variogram (see Ch. 2 for additional details).

Table 26. Layer-specific parameters for vertical variograms

Layer	Lag (ft)	Number of lags	Tolerance (ft)	Bandwidth (ft)
1	N/A	N/A	N/A	N/A
2	2.5	5	1.25	0.0
3	2.5	4	1.25	0.0
4	1.0	8	0.50	0.0

Table 27. Vertical variogram ranges and sills for layers

Layer	Vertical range (ft)	Vertical sill
1	N/A	N/A
2	5.5	1.0
3	3.6	1.0
4	5.6	1.0

As listed above in Table 26, lag distances (i.e., the abscissa spacing between points of the variogram) are selected to range between 1 ft and 5 ft. Selection of these distance values is motivated by characteristic lengths that are relevant to spacings between reported measurements along core-runs. For example, with regards to layer 2, a lag distance of 2.5 ft is on the order of that associated with typical core-run lengths (5 ft).

As detailed for each layer in the content below, use of the above lag distances leads to well-formed vertical variograms for the initial layering of Site A. Regardless, it is recommended that multiple candidates for lag distance be considered prior to finalizing the variogram for a given layer and variogram direction. Furthermore, for each candidate lag distance considered, it is necessary to update the values for tolerance and bandwidth.

Recommendations are given in McVay et al. (2012) for determining values of tolerance and bandwidth, given a candidate value of lag distance. For example, for the selected lag distance of 2.5 ft that is associated with the layer 2 vertical variograms, the tolerance is set to one-half the magnitude of the lag distance (i.e., 1.25 ft) and the bandwidth is set to 0 ft. In particular, setting the bandwidth to 0 ft when constructing vertical variograms is recommended given typical horizontal spacings between boring locations, relative to vertical spacings between data measurements (SPT-N, q_u). Considerations for the number of lags (Table 26); and, values for vertical range and vertical sill (Table 27) are discussed below on an individual layer basis.

4.4.2.3 Layer 2

Vertical variogram points for layer 2 are based upon (vertical) distance-based pairings of measured q_u values. The experimental variogram points for layer 2 are listed in Table 28 and plotted in Fig. 57, and are generated with use of linear data detrending. Also listed in Table 28 are the pairs associated with each variogram point. The data listed in Table 28 are obtained directly from the GeoStat UI by entering the Variogram Data dialog (Fig. 50, top-left).

Table 28. Vertical variogram data for layer 2 (elevation range: 67.5 ft to 45 ft)

Abscissa (ft)	Ordinate	Pairs
2.5	0.87	24
5.0	0.70	22
7.5	1.00	25
10.0	0.88	12
10.0	1.02	15

As discussed in Ch. 2, the number of measured data pairs used in forming an experimental variogram point reflect the strength (or significance) of said point. Further, as is the case for the variogram plots within the GeoStat UI (recall Fig. 50), the experimental variogram point symbols in Fig. 57 are sized (scaled) based on the respective number of pairs used in forming said points. The scaling visually signifies the strength or significance of each variogram point.

A threshold value of approximately 30 (pairs) is recommended in McVay et al. (2012) when judging the significance of an experimental variogram point.

Specific to the vertical variogram for layer 2, pair counts steadily reduce from 24 at a distance of 2.5 ft down to 15 at a distance of 12.5 ft (Table 28). The variogram points roughly indicate convergence toward a sill value of unity, and so, the five generated points along the variogram (i.e., 5 lags) are considered sufficient.

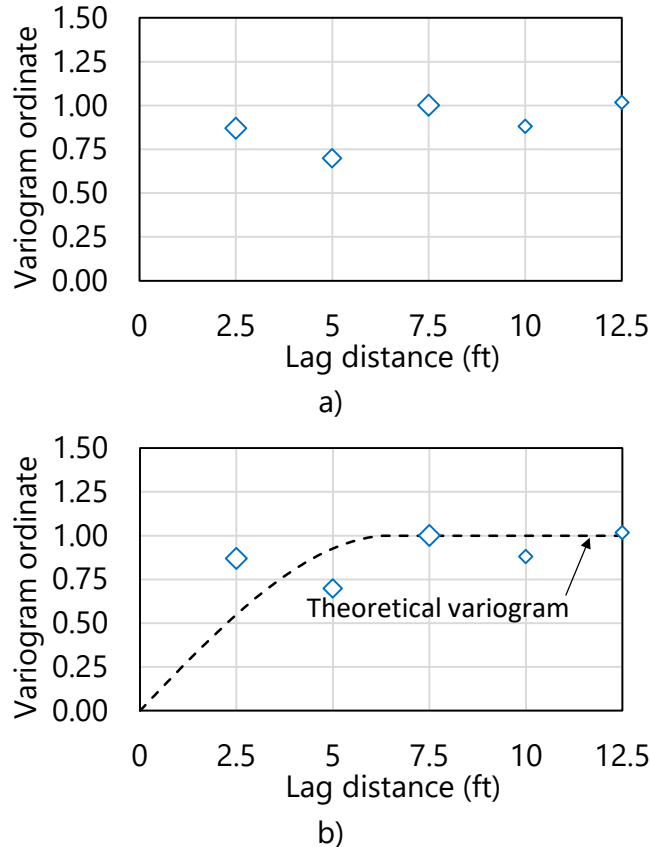


Figure 57. Vertical variogram for layer 2 (elevation range: 67.5 ft to 45 ft): a) Experimental variogram points; b) Experimental variogram points and theoretical (spherical) fit

The experimental variogram points approach the data-wide variance (i.e., a sill value of 1.0) between the second and third variogram points (Fig. 57a). Approximately asymptotic behavior is apparent for increasing vertical distance. As a counterpart, the theoretical variogram selected for layer 2 is displayed in Fig. 57b. The theoretical variogram is graphically fit from within the GeoStat UI by left-clicking and dragging the curve directly within the vertical variogram plot (e.g., Fig. 50, bottom-right). Care is taken to ensure that the theoretical variogram passes through those experimental variogram points possessing the pair counts nearest to 30. As a result, the range and sill values are automatically quantified as 5.5 ft and 1.0, respectively.

4.4.2.4 Layer 3

Vertical variogram points for layer 3 are listed in Table 29 and plotted in Fig. 58. Similar to that of layer 2, initial formation of the (experimental) vertical variogram for layer 3 is based upon identified pairs of unconfined compression strength (q_u). The variogram points are generated (automatically from within GeoStat) using first-order (linear) detrending of the layer data. Also listed in Table 29 are the pairs associated with each layer 3 variogram point.

The pair counts associated with each variogram point steadily reduce from 66 at a distance of 2.5 ft down to 19 at a distance of 10.0 ft. The variogram gives clear convergence toward a sill value of unity, and so, four points along the variogram (i.e., 4 lags) are considered sufficient.

Table 29. Vertical variogram data for layer 3 (elevation range: 45 ft to 30 ft)

Abscissa (ft)	Ordinate	Pairs
2.5	0.87	66
5.0	1.14	50
7.5	1.05	34
10.0	1.01	19

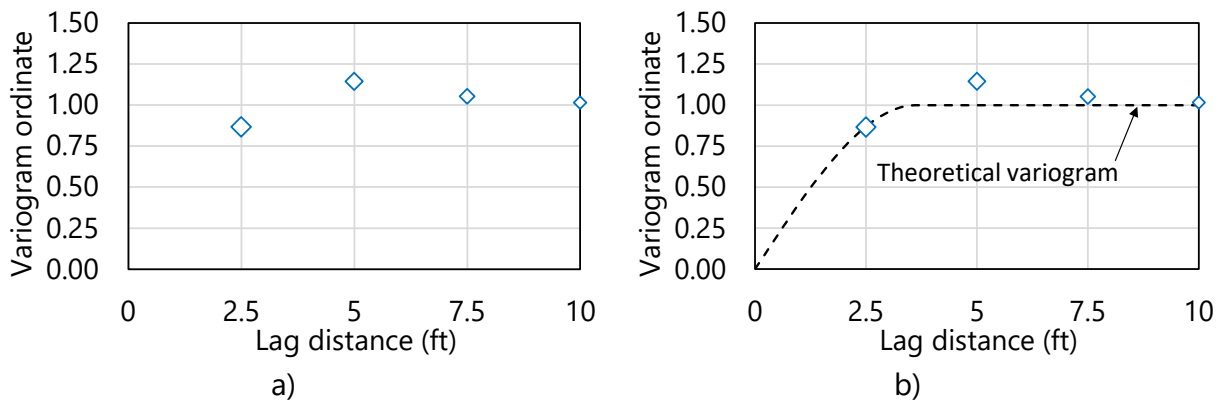


Figure 58. Vertical variogram for layer 3 (elevation range: 45 ft to 30 ft): a) Experimental variogram points; b) Experimental variogram points and theoretical (spherical) fit

The experimental variogram points for layer 3 (Fig. 58a) are fitted with a theoretical variogram (Fig. 58b). Convergence to the sill value (of unity) is judged to occur between the first and second points of the experimental variogram. The range (3.6 ft) and sill (1.0) values are automatically quantified by virtue of employing the graphical selection feature (for characterizing theoretical variograms) implemented in the GeoStat UI.

4.4.2.5 Layer 4

Vertical variogram points for the initial definition of layer 4 are listed in Table 30 and plotted in Fig. 59. Similar to that of layer 2 and layer 3, vertical variogram formation for layer 4 is based upon identified pairs (based on distances between measurements) of q_u values. However, no detrending is included prior to generation of variogram points for layer 4. Also listed in Table 30 are the pair counts associated with each layer 4 (experimental) variogram point.

The pair counts associated with each variogram point consistently reduce from 47 at a distance of 1.5 ft down to 20 at a distance of 12.0 ft. Despite the presence of mild cyclicity, the experimental variogram points clearly trend toward a sill value of unity. As plotted in Fig. 59b, a theoretical (vertical) variogram is generated through use of the graphical fit feature in the GeoStat UI. The corresponding range of the theoretical variogram for layer 4 is defined (graphically) as 5.6 ft.

Table 30. Vertical variogram data layer 4 (elevation range: 30 ft to -10 ft)

Abscissa (ft)	Ordinate	Pairs
1.5	0.40	47
3.0	0.74	42
4.5	0.90	38
6.0	0.80	32
7.5	0.83	29
9.0	1.03	26
10.5	1.02	21
12.5	0.92	20

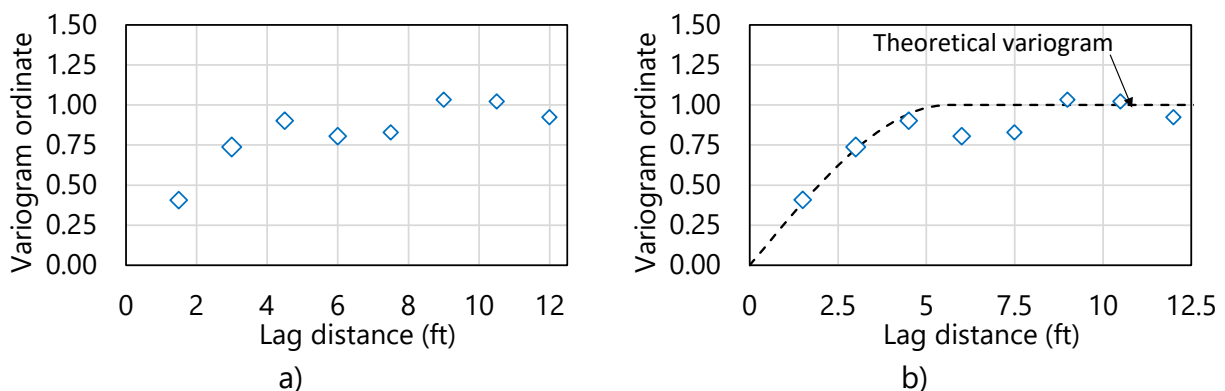


Figure 59. Vertical variogram for layer 4 (elevation range: 30 ft to -10 ft): a) Experimental variogram points; b) Experimental variogram points and theoretical (spherical) fit

4.4.3 Observations Regarding Initial Layer Definitions and Variograms

As noted previously, the volume of available data for Site A is relatively limited, which leads to conspicuously large COV values for the q_u data of layer 2 and layer 4 (recall Table 25). Furthermore, scrutiny of the selected layer elevations (discussed, and reaffirmed, above) does not provide justification for further subdividing the initial selections of layer elevations. In other words, the large COV values for layer 2 (3.49) and layer 4 (2.63) cannot be attributed to the need to further subdivide the layers.

Therefore, with regard to characterization of the relatively limited volume of site data, two options remain at this stage (given that zonal issues are not present): (1) accept the initial layer definitions (soil or rock types; elevations), and the associated (large) magnitudes of COV values for layer 2 and layer 4; or, (2) explore a modification to the layer definitions for layer 2 and layer 4. The latter option is elected and discussed in the following.

4.5 Alternative Definition of Soil or Rock Layering

Recalling that bands and layers of clay are prevalent (along with limestone) among the Site A data, the layer types assigned to layer 2 and layer 4 are modified to clay. Consequently, the relatively more numerous measurements of SPT-N values (as opposed to q_u values) are drawn upon in constructing variograms using the alternative definitions of layer 2 and layer 4.

Scatterplots of the previously cataloged site data are again utilized (recall Fig. 44, left and middle) to aid in selection of boundary layer elevations. Alternative layer definitions formed for Site A are listed in Table 31. Based on the cataloged site data, four layers are defined and consist of either clay (layer 1, layer 2, and layer 4) or limestone (layer 3). Layer top and bottom elevations span the ranges of elevations identified during the initial review of the site data documented above. The only modification (relative to the initial layer definition) is to slightly adjust the bottom of layer 1 to 65 ft. Additional discussion regarding the selections of the boundary layer elevations is provided in the remainder of Sec. 4.5. Still further considerations are documented in Sec. 4.6, as part of forming variograms (based on the alternative layer definitions).

Table 31. Selected layer types and elevation ranges

Layer	Layer type	Top elevation (ft)	Bottom elevation (ft)
1	Clay	97.0	65.0
2	Clay	65.0	45.0
3	Limestone	45.0	30.0
4	Clay	30.0	-10.0

4.5.1 Selecting Alternative Layer Elevations

The 271 SPT-N blow counts associated with the 14 boring locations of Site A, along with layer divisions (blue horizontal lines), are plotted with respect to elevation in Fig. 60. Values of SPT-N blow counts are focused upon because values of undrained shear strength (C_u) are not available for Site A. As an alternative, SPT-N blow counts are examined, simulated, and then empirically related to C_u values (as discussed in Sec. 2.7). Consistent with the initial review of the cataloged SPT-N data for Site A, the selected layer divisions are positioned in accordance with qualitative groupings of the SPT-N blow counts. For example, a distinct grouping of blow counts is apparent between 97 ft and 65 ft, in comparison to those values cataloged below 65 ft. Thus, Layer 1 is defined between 97 ft and 65 ft.

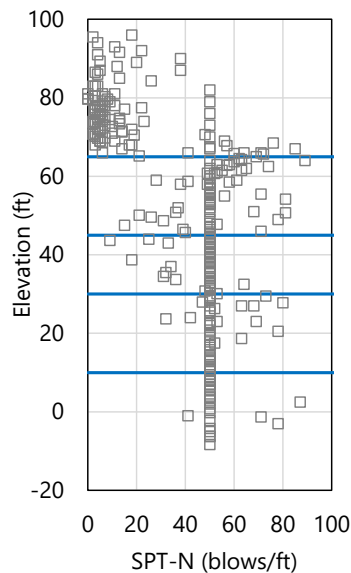


Figure 60. Scatterplot of 271 SPT-N blow counts (elevation range: 96 ft to -10 ft) with layer bottom elevations (blue horizontal lines)

The qualitative grouping of SPT-N blow counts positioned between 65 ft and 45 ft motivates designation of the boundary elevations for layer 2. Regarding layer 3, and because this layer type remains designated as limestone, no modifications are made relative to the initial layer definition (with elevations of 45 ft to 30 ft). The SPT-N blow counts below 30 ft are generally associated with refusal-like conditions. Therefore, layer 4 is defined to bound all data at and below 30 ft (i.e., layer 4 is defined between 30 ft and -10 ft), and is defined as a clay layer (as opposed to limestone). Mean and COV values for unit weight, γ , for all layers are maintained relative to the initial layer definitions (recall Table 24).

4.6 Alternative Selection of Geo-statistical Parameter Values

Having defined an alternative layering for the Site A geotechnical data, focus of the modeling efforts within GeoStat continues onward to the formation of layer-specific spatial correlation

structures (i.e., variograms). As part of the variogram formation for each layer, additional checks are conducted regarding the revisions to the layering definitions (as discussed in Sec. 4.6.1). Also, consistent with the investigation of the initial layer definitions, focus is given to vertical variogram formation. This focus is motivated by the fact that insufficient volumes of Site A data are available for the purpose of constructing horizontal variograms. Importantly, horizontal variograms are not neglected, but rather, are associated with worst case conditions (as introduced in Ch. 2). So as to avoid the potentially extreme conservatism that accompanies use of worst case conditions, unconditional simulation is again elected, and as a result, only the vertical variograms are made use of during simulation.

For the modeling of Site A, recall that a drilled shaft is selected as the foundation member type. Therefore, for layer 2 and layer 4 (of type clay), variograms are formed based on layer-specific ensembles of SPT-N blow count values. Variogram formation for layer 3 is based upon values of unconfined compression strength (q_u). Also, because (for illustration) steel casing is assumed to be present down to the rock layer (layer 3), there remains no need to form spatial correlation structures for layer 1.

4.6.1 Examining Alternative Layer Data

Prior to selecting variogram parameter values for the alternative layer definitions, both the descriptive statistics and graphical depictions of the layer specific collections of SPT-N blow counts (or q_u values) are examined. Summary statistics for the relevant types of soil or rock measurements of each layer (again, for this example site, either SPT-N or q_u) are listed in Table 32. The sample sizes (i.e., number of measured values) per layer range from 52 to 63 across layers 2 through 4. Values pertaining to layer 1 are not applicable (N/A) because the layer is excluded from the Site A analysis to reflect the presence of steel casing.

The dispersions associated with layers 2 and 4 are relatively low (COV values are 0.26 for layer 1, 0.18 for layer 4). The reduction in dispersions partly remedies reservations associated with the initial layer definitions. However, the reduced values of COV in layer 2 and layer 4 (relative to those of the initial layer definitions) are due in some measure to the prevalence of SPT-N blow counts equal to 50, which are distributed throughout each layer. As with the initial layering, the unconfined compression strength values associated with the limestone layer (layer 3, Table 32) exhibit relatively large variations (the COV value is 0.98).

Table 32. Summary statistics for defined layers

Layer	Physical measurement	Sample size	Mean	COV
1	N/A	N/A	N/A	N/A
2	SPT-N (blows/ft)	63	52.4	0.26
3	q_u (tsf)	52	88.4	0.98
4	SPT-N (blows/ft)	63	53.2	0.18

4.6.1.1 Layer 2

A scatterplot of the 63 SPT-N blow counts positioned within layer 2 is presented in Fig. 61. A relatively large portion of the SPT-N blow count data is equal to 50 blows/ft. As part of the present examination, it is confirmed that the blow count data points of 50 blows/ft are generally contributed to from across the 14 boring locations. Also, owing in part to the prevalence of SPT-N blow count measurements recorded at 50 blows/ft, no apparent trend is observed for the layer 2 scatterplot.

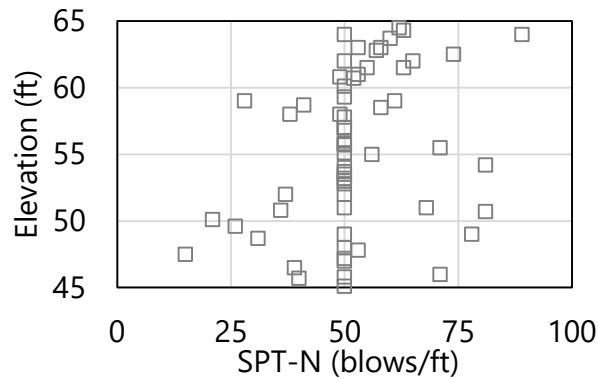


Figure 61. Scatterplot of 63 SPT-N blow count values (elevation range: 65 ft to 45 ft) within layer 2

A histogram of the 63 measured SPT-N blow count values pertaining to layer 2 is presented in Fig. 62. Although a pronounced frequency peak is present for blow count values of 50 blows/ft, the overall histogram (roughly) resembles that of normally or log-normally distributed data. Given the absence of conspicuous features (such as bimodal phenomena) in the layer 2 histogram, no revisions are made regarding the boundary elevations for layer 2 listed in Table 31.

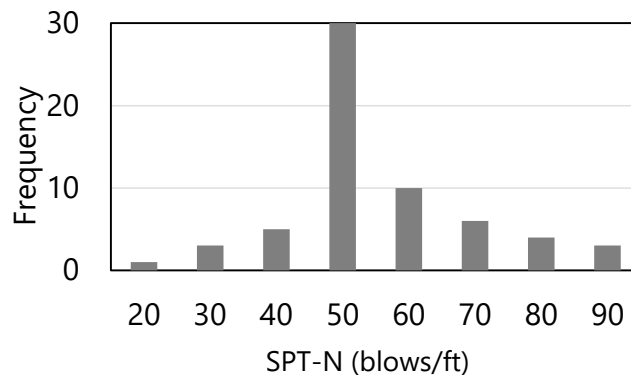


Figure 62. Histogram of 63 SPT-N blow count values (elevation range: 65 ft to 45 ft) within layer 2

4.6.1.2 Layer 3

The layer type (limestone) and elevations (45 ft to 30 ft) initially assigned to layer 3 remain unchanged in the alternative layer definition. Therefore, examination of q_u values positioned within layer 3 is identical to that discussed above in association with the initial layer definition. Stated alternatively, the previous assessment of q_u values within layer 3 still holds, and no modifications are made to layer 3 (relative to the listings of Table 31).

4.6.1.3 Layer 4

A scatterplot of the 63 SPT-N blow counts positioned within layer 4 is presented in Fig. 63. The vast majority of the SPT-N blow count data is equal to 50 blows/ft. As part of the present layer examination, it is confirmed that the blow count data points of 50 blows/ft are generally contributed to from across the 14 boring locations throughout Site A. Also, owing in part to the abundance of SPT-N blow count measurements recorded at 50 blows/ft, no apparent trend is observed for the layer 4 scatterplot.

A histogram of the 63 measured SPT-N blow count values pertaining to layer 4 is presented in Fig. 64. Although a predominant frequency peak is present for blow count values of 50 blows/ft, the overall histogram (roughly) resembles that of log normally distributed data. Given the absence of other conspicuous features in the layer 4 histogram, no revisions are made regarding the boundary elevations for layer 4 (Table 31).

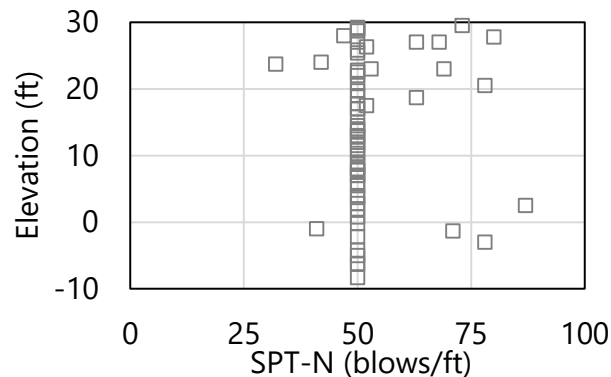


Figure 63. Scatterplot of 63 SPT-N blow count values (elevation range: 30 ft to -10 ft) within layer 4

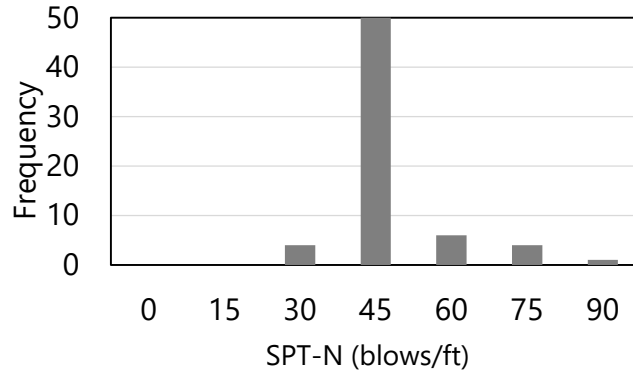


Figure 64. Histogram of 63 SPT-N blow count values (elevation range: 30 ft to -10 ft) within layer 4

4.6.2 Forming Variograms using Alternative Layering

Vertical variogram parameters selected for the alternative definitions of layer 2 through layer 4 of Site A are listed in Table 33. As discussed in Ch. 2, the lag distance, number of lags, tolerance, and bandwidth are all instrumental in forming points of the experimental variogram. Vertical variogram values for range and sill are listed per layer in Table 34, where these values are more strongly related (in GeoStat) to the theoretical variogram (see Ch. 2 for additional details).

Table 33. Layer-specific parameters for vertical variograms

Layer	Lag (ft)	Number of lags	Tolerance (ft)	Bandwidth (ft)
1	N/A	N/A	N/A	N/A
2	2.5	6	1.25	0.0
3	2.5	7	1.25	0.0
4	2.5	8	1.25	0.0

Table 34. Vertical variogram ranges and sills for layers

Layer	Vertical range (ft)	Vertical sill
1	N/A	N/A
2	3.2	1.0
3	4.7	1.0
4	2.3	1.0

As listed above in Table 33, a lag distance of 2.5 ft is selected for the variograms of layer 2 through layer 4. Selection of this distance value is motivated by characteristic lengths that are relevant to spacings between reported SPT measurements. Also, McVay et al. (2012) recommended using lag distances of 2.5 ft when constructing variograms with use of SPT-N blow counts. With regards to layer 3 (which emphasizes q_u values), a lag distance of 2.5 ft is on the order of that associated with typical core-run lengths (5 ft). If core-run data are

positioned over different intervals, then such intervals should be taken into account when selecting a lag distance for modeling of drilled shaft portions in limestone layers.

As detailed for each layer in the content below, use of a uniform lag distance across all layers leads to reasonably well-formed vertical variograms for the Site A modeling. Recommendations given in McVay et al. (2012) are again utilized for determining vertical variogram values of tolerance and bandwidth, given values of lag distance in Table 33. For example, for the selected lag distance of 2.5 ft, the tolerance is set to one-half the magnitude of the lag distance (i.e., 1.25 ft) and the bandwidth is set to 0 ft. Considerations for the number of lags (Table 33); and, values for vertical range and vertical sill (Table 34) are discussed below on an individual layer basis.

4.6.2.1 Layer 2

Vertical variogram points for layer 2 are based upon (vertical) distance-based pairings of measured SPT-N blow count values. The experimental variogram points for layer 2 are listed in Table 35 and plotted in Fig. 65. Also listed in Table 35 are the pairs associated with each variogram point. Pair counts steadily reduce from 51 at a distance of 2.5 ft down to 6 at a distance of 17.5 ft. Beginning at a distance of 12.5 ft, consecutive points of greater distance correspond to pair counts well below the threshold value of 30 pairs. Therefore, 7 points along the variogram (i.e., 7 lags) are considered sufficient for the vertical variogram of layer 2.

While the experimental variogram points approach the data-wide variance (i.e., a sill value of 1.0) at the first variogram point (Fig. 65a), approximately asymptotic behavior is apparent for increasing vertical distance. As a counterpart, the theoretical variogram selected for layer 2 is displayed in Fig. 65b. Care is taken to ensure that the theoretical variogram passes through those experimental variogram points possessing the pair counts greater than 30. As a result, the range and sill values are automatically quantified as 3.2 ft and 1.0, respectively.

Table 35. Vertical variogram data for layer 2 (elevation range: 65 ft to 45 ft)

Abscissa (ft)	Ordinate	Pairs
2.5	0.94	51
5.0	1.00	40
7.5	0.97	22
10.0	1.18	29
12.5	1.11	21
15.0	1.88	14
17.5	0.96	6

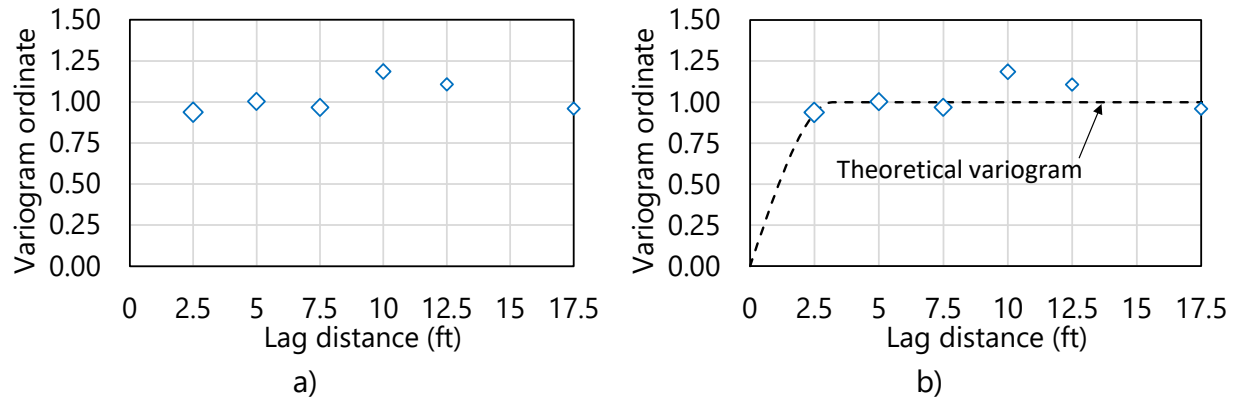


Figure 65. Vertical variogram for layer 2 (elevation range: 65 ft to 45 ft): a) Experimental variogram points; b) Experimental variogram points and theoretical (spherical) fit

4.6.2.2 Layer 3

As aforementioned, the layer type and elevations initially assigned to layer 3 (limestone; 45 ft to 30 ft) remain unchanged in the alternative layer definition. Therefore, the variogram formed for layer 3 is identical to that discussed above in association with the initial layer definition. Stated alternatively, the vertical variogram constructed using q_u values within layer 3 and the initial layer definition still holds.

4.6.2.3 Layer 4

Vertical variogram points for layer 4 are listed in Table 36 and plotted in Fig. 66. Similar to that of the layer 2 definition, vertical variogram formation for layer 4 is based upon identified pairs (based on distances between measurements) of SPT N blow count values. Also listed in Table 36 are the pair counts associated with each layer 4 (experimental) variogram point. The pair counts associated with each variogram point steadily reduce from 46 at a distance of 2.5 ft down to 22 at a distance of 20.0 ft. Beginning at a distance of 17.5 ft, consecutive variogram points of greater distance correspond to pair counts well below the threshold value of 30 pairs. Therefore, 8 points along the variogram (i.e., 8 lags) are considered sufficient for the vertical variogram of layer 4.

The experimental variogram points for layer 4 (Fig. 66a) exhibit slight undulations, but overall asymptotic behavior. With the exception of a single point (7.5 ft, 0.79), experimental variogram points values generally converge to the normalized sill value of 1.0. The theoretical variogram for layer 4 (Fig. 66b) is generated through use of the graphical fit feature in the GeoStat UI. Given the relatively large number of pairs and ordinate associated with the point (2.5 ft, 1.09), the theoretical variogram is constructed to reach a sill of 1.0 at a distance slightly less than 2.5 ft. The corresponding range of the theoretical variogram for layer 4 is defined as 2.3 ft.

Table 36. Vertical variogram data layer 4 (elevation range: 30 ft to -10 ft)

Abcissa (ft)	Ordinate	Pairs
2.5	1.09	46
5.0	1.16	46
7.5	0.79	34
10.0	1.12	38
12.5	1.07	31
15.0	1.12	32
17.5	1.10	23
20.0	0.92	22

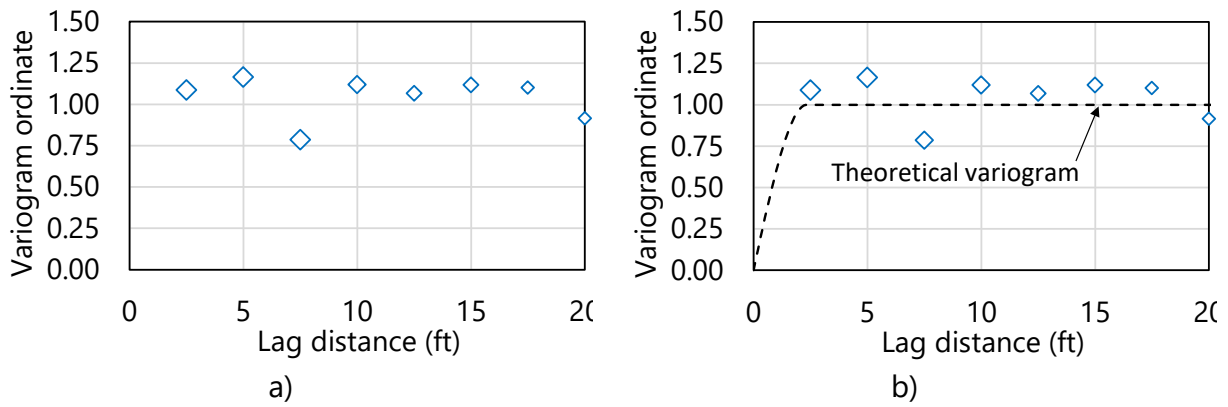


Figure 66. Vertical variogram for layer 4 (elevation range: 30 ft to -10 ft): a) Experimental variogram points; b) Experimental variogram points and theoretical (spherical) fit

4.7 Cursory Examination of the Site A Data for Identifying Zones

Zonal issues are not anticipated in association with modeling of the Site A data (see Ch. 5 for a detailed example of modeling zones). Solely for illustration purposes, prior to moving beyond variogram formation for the alternative layer definitions, a cursory assessment of the available Site A data is carried out to ensure that no distinct geological zones are present. Highlighted in Fig. 67 are two boring locations from within Site A that are relatively far from the remaining 12 boring locations. These two boring locations are excluded from the site modeling and the vertical variograms are reformed using the remaining 12 borings. Note that it is also confirmed that removal of the two borings does not affect the selections for layer elevations (with considerations similar to those documented above). Comparisons between the two sets of variograms are compared in (Table 37, Table 38, Fig. 68, and Fig. 69).

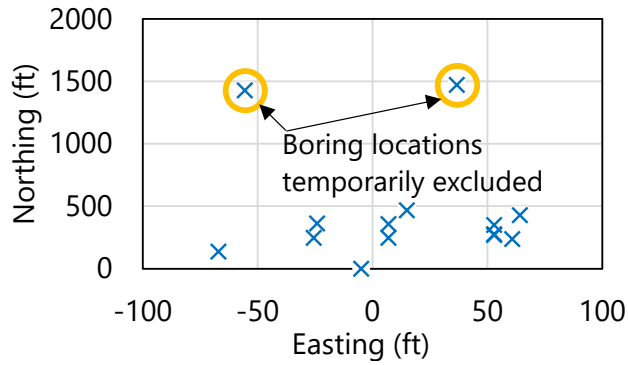


Figure 67. Site A boring locations with indication of temporarily excluded borings

In the comparisons of (experimental) vertical variograms, focus is given to layer 3 and layer 4. This is because resistances from layer 1 and layer 2 are not anticipated to appreciably contribute to the axial resistance of the drilled shaft. More specifically, resistances associated with layer 1 are neglected due to the presence of a steel casing. Resistances attributable to layer 2 are anticipated to be small relative to those attained for embedded shaft portions in the limestone layer (layer 3).

Table 37. Comparison of vertical variogram data for layer 3 when all 14 boring locations are considered versus when two borings are excluded

Abscissa (ft)	Ordinate (all)	Pairs (all)	Ordinate (excluded)	Pairs (excluded)
2.5	0.87	66	0.87	66
5.0	1.14	50	1.14	50
7.5	1.05	34	1.05	34
10.0	1.01	19	1.01	19

Table 38. Comparison of vertical variogram data for layer 4 when all 14 boring locations are considered versus when two borings are excluded

Abscissa (ft)	Ordinate (all)	Pairs (all)	Ordinate (excluded)	Pairs (excluded)
2.5	1.09	46	1.04	44
5.0	1.16	46	1.09	45
7.5	0.79	34	0.75	34
10.0	1.12	38	1.10	38
12.5	1.07	31	1.03	31
15.0	1.12	32	1.07	32
17.5	1.10	23	1.07	23
20.0	0.92	22	0.88	22

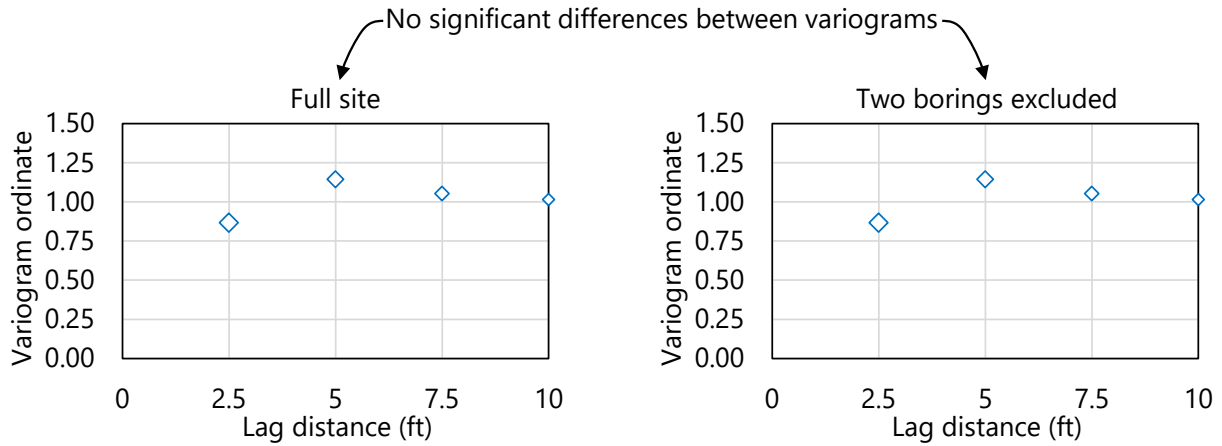


Figure 68. Comparison of experimental vertical variogram points for layer 3 when all boring locations are considered versus when two boring locations are excluded

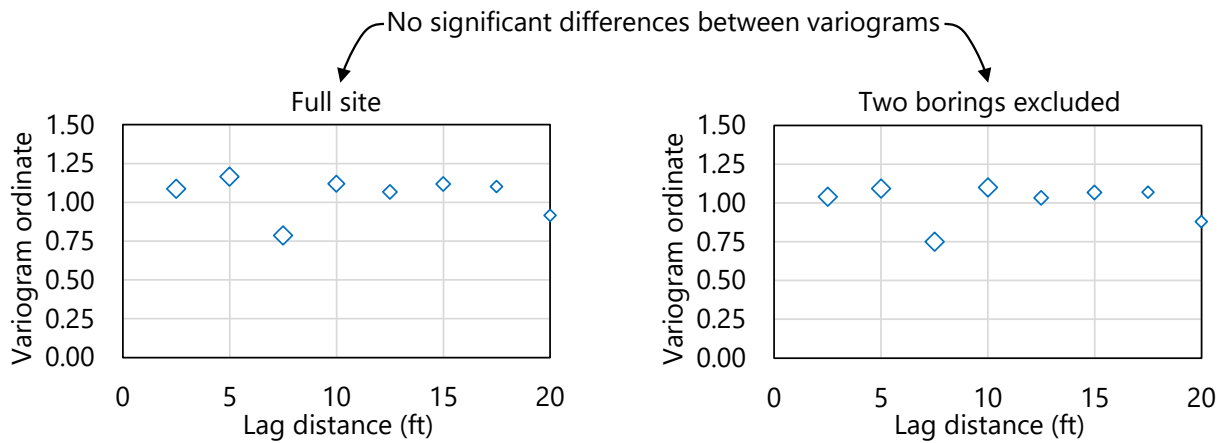


Figure 69. Comparison of experimental vertical variogram points for layer 4 when all boring locations are considered versus when two boring locations are excluded

Exclusion of the two boring locations indicated in Fig. 67 has practically no effect on the vertical variogram of layer 3 (Table 37, Fig. 68). This is because the two excluded borings do not contain any core-run data. The effect that removing the two boring locations has upon the layer 4 variogram (Table 38, Fig. 69) is relatively small.

The variogram ordinate values of layer 4, for a given distance, remain within 6% of one another. Also, the pair counts remain with 5% of one another. While the above assessment is cursory, and solely for illustration, outcomes from the assessment do not indicate zonal issues. In other words, the assessment supports that the 14 boring locations of Site A can be treated

as if the collective geotechnical site data originate from the same, single geological zone. Detailed documentation for modeling of zones within sites is provided in Ch. 5.

4.8 Performing Stochastic Simulation

Using the alternative layering and vertical variograms for the available geotechnical data of Site A, stochastic simulation of axial resistance is carried out in GeoStat as the next major step. Shown in Fig. 70 is the fourth of seven tabs (from left to right) in the GeoStat UI, referred to as the Simulation tab. Discussed below are selections made for relevant foundation member parameters, as well as initial considerations for carrying out simulations.

The screenshot shows the Simulation tab in GeoStat. The interface includes a menu bar (File, Control, Help), a toolbar, and a main workspace. The workspace is divided into several panels:

- General Geometry:** Minimum Length (ft) 40, Maximum Length (ft) 80, Increment (ft) 1.
- Shaft Geometry:** Diameter (in) 48, Casing Length (ft) 32, Bell Length (ft) 0, Bell Diameter (in) 0.
- Pile Geometry:** Section Type: Square, Width (in) 0, Depth (in) 0, Thickness (in) 0, Pile End Type: Open.
- Foundation Member Material Properties:** Ec (ksi) 4000, Slump (in) 6, Limiting Settlement (%) 3, Unit Weight (pcf) 150.
- Soil:** Ground Surface Elevation (ft) 97.00, Water Table Elevation (ft) 75.
- Layer Separation:** Soil Type 1 (Plastic Clay), Soil Type 2 (Clay and Silty Sand), Soil Type 5 (Void) (selected).
- Simulation:** Unconditional (selected), Number of Simulations 2000.
- Simulation Parameters:** Boring B-1, Northing of Foundation (ft), Easting of Foundation (ft).
- Data Table:**

Layer	Mean	Coefficient of Variation	Variance	Sample Count	Vertical Range	Horizontal Range	Horizontal Sill	Detrend
2	12.49	3.49	1894.40	34	9.05	0.01	3.00	No
3	88.43	0.98	7435.37	52	4.70	60.00	1.00	No
4	12.36	2.63	1057.03	61	6.05	60.00	1.00	No
- Simulation Status:** Run Simulation button.

Figure 70. Simulation tab

4.8.1 Selecting the Embedment Range and Interval

For the drilled shaft foundation member being investigated in association with Site A, embedment lengths ranging from 40 ft to 90 ft are considered. Despite the emphasis on modeling of drilled shaft foundations, the following discussion is generally applicable regardless of the type of foundation member being considered. Along these lines, an embedment interval of 1 ft is selected, signifying that axial resistances are to be computed in 1-ft intervals between the 40-ft and 90-ft embedment range. Interval lengths that are small relative to the layer heights are generally recommended for conducting simulations in GeoStat.

Recall that the ground surface elevation is defined as 97 ft (the water table elevation is defined as 75 ft). Candidate shaft configurations for Site A therefore terminate (approximately) at elevations ranging from the center of layer 2 and extending down into layer 4. This range of embedments (40 ft to 90 ft) is considered as it allows for axial resistances to be determined for shafts terminating at a relatively small distance above the limestone layer (Fig. 71), as well as for shaft embedments that extend into and beyond the limestone layer.

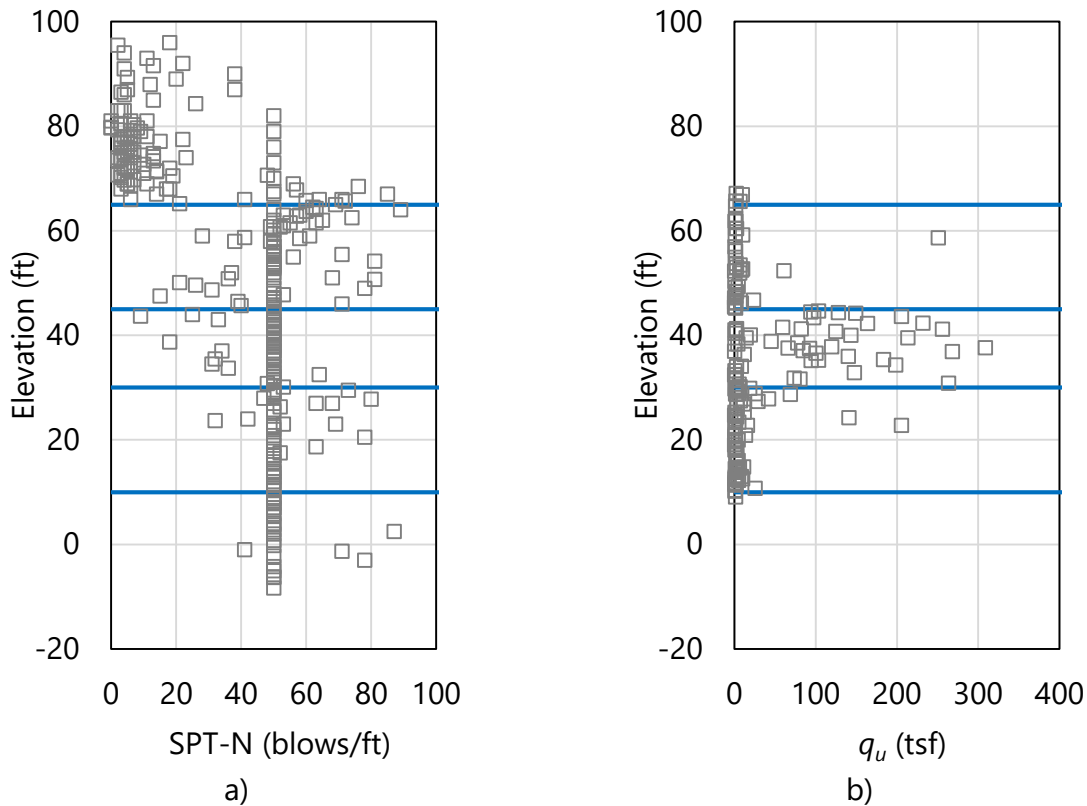


Figure 71. Scatterplots of soil and limestone strength parameters with layer bottom elevations (blue horizontal lines): a) SPT-N blow counts; b) Unconfined compression strength, q_u

4.8.2 Foundation Member Cross-Section

The middle-left portion of the Simulation tab (recall Fig. 70) contains input controls that allow for definition of the foundation member cross-section. Because a drilled shaft is being considered for Site A, only the shaft diameter and casing length are necessary to define the cross-section. These are defined as 48 in. and 32 ft, respectively. For scenarios where a driven pile is selected as the type of foundation member, required inputs for the cross-section geometry vary by the type of pile being considered (e.g., square, cylindrical, h-pile). Additional details for the required input parameters of driven pile cross-sections are detailed in the Help Manual.

4.8.3 Foundation Member Material Properties

GeoStat UI controls positioned in the bottom-left portion of the Simulation tab (recall Fig. 70) pertain to the definition of the foundation member material properties. For driven piles, only the pile unit weight is required. For drilled shafts, unit weight (150 lb/ft³) is also required. Values of shaft elastic modulus, concrete slump, and limiting shaft settlement are additionally required for drilled shafts. These values, respectively, are input as 4000 ksi, 6 in., and 3%, and are necessary for computing shaft end bearing resistance.

4.8.4 Layer Separation

Included among the simulation parameters input on the Simulation tab (Fig. 70, middle) is selection of a soil type for modeling of layer separations. Recall from Fig. 44 that soil or rock layerings are defined from within the Profile tab of the GeoStat UI. Furthermore, layers can be defined as consisting of one of four possible soil or rock types. For generation of analysis model files during stochastic simulation, the “physical” layers are subdivided into 0.5-ft increments (referred to in this context as sublayers).

A subset of the available layer types may be specified for defining those sublayers that fall at the boundaries of layers that are defined on the Profile tab. For use of the GeoStat software in design applications, it is recommended that these sublayers (or, layer separators) be designated as Soil Type 5 (Void). If it is alternatively desired that layer separations not be designated as Soil Type 5 (Void), then additional properties must be specified as delineated (along with additional contextual discussion) in the Help Manual.

4.8.5 Selecting the Simulation Type

As detailed in Ch. 2, either unconditional or conditional (stochastic) simulation can be conducted using GeoStat software. However, as established above, conditional simulation (which requires construction of well-formed horizontal and vertical variograms) is not practical given the available volume of geotechnical data for Site A. When conducting unconditional simulation, only the number of realizations to be generated during simulation must be specified (Fig. 70, bottom-center). Additional considerations for deciding upon the suitable number of realizations for simulation are provided in Sec. 4.9. Input parameters required for conducting conditional simulation are detailed in the Help Manual.

4.9 Viewing Spatial Variability Results

Shown in Fig. 72 is the fifth of seven tabs (left to right) in the GeoStat UI, referred to as the Spatial Variability tab. This tab is intended for use in viewing profiles of computed axial resistance, where the resistance values take into account spatial variability phenomena. Plots of spatial resistance are divided into skin friction (side) resistance, end bearing (tip) resistance, and total resistance. For each type of resistance (skin, tip, total), profile plots of the mean,

variance, COV, and ϕ (reflecting spatial variability only) are provided. In other words, resistance-related quantities plotted on the Spatial Variability tab facilitate visual review of profiles of descriptive statistics obtained from the “raw” simulation results.

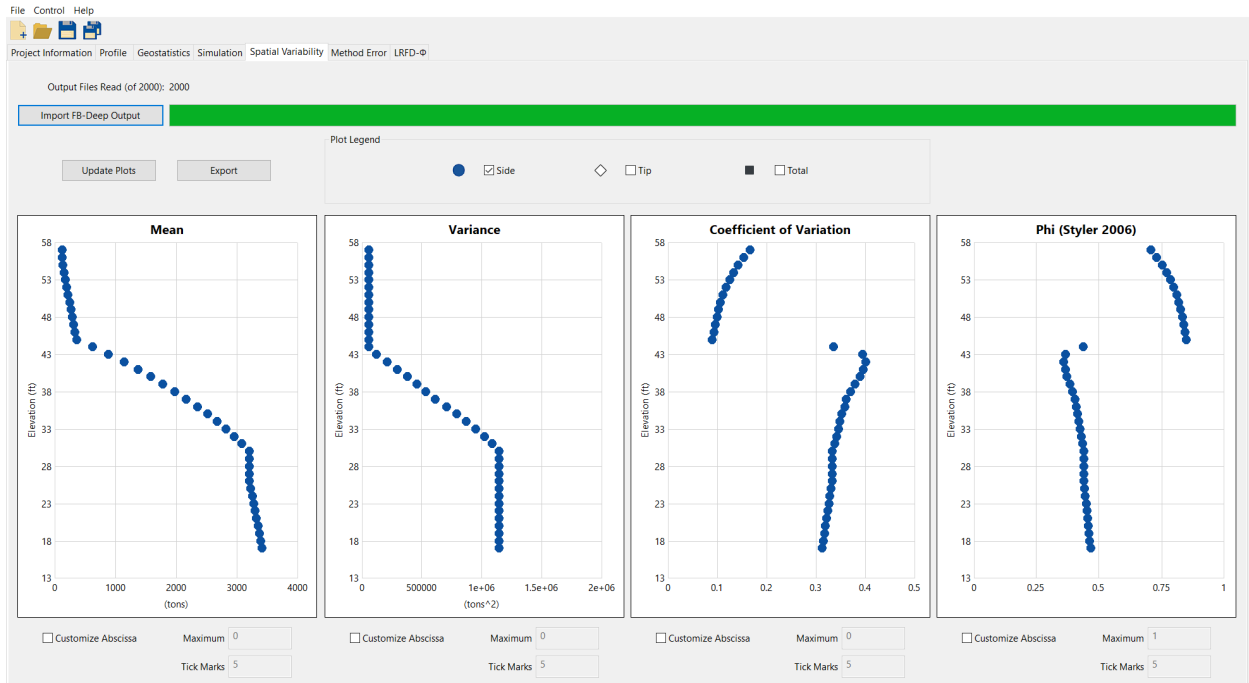


Figure 72. Spatial variability tab

4.9.1 Profiles of Computed Resistance

Profile plots of computed results are presented in Fig. 73 and Fig. 74. Profiles of skin and total resistance quantities—obtained from unconditional simulation with 2000 realizations—are displayed. Also, layer divisions (blue horizontal lines) are superimposed atop the profile plots to distinguish layer 2 from layer 3, and layer 3 from layer 4. The results shown are associated with both the initial (limestone) and the alternative (clay-limestone-clay) layerings developed above.

For the shaft configuration and soil or rock layering considered, skin resistance is clearly the dominant contributor to the mean (Fig. 73a, Fig. 74a) and variance (Fig. 73b, Fig. 74b) quantities for total resistance. Note though that the clay-limestone-clay layering leads to a relatively small proportion of contributions to resistance from end bearing. For the two layerings analyzed, trends in the computed skin and total resistances undergo abrupt shifts as embedment lengths progress into each of layer 2, layer 3, and layer 4.

Relatively substantial increases in resistance (from approximately 500 tons to 3200 tons) occur with respect to shaft embedment depths within the limestone layer (layer 3) of both layerings. Unfactored unit side friction throughout layer 3 is approximately 14 tsf. Only moderate

increases in computed resistance (less than 1000 tons total) occur with respect to depth for embedment depths that terminate within layer 2 and layer 4 (regardless of layer definition). Based on these results, the greatest efficiencies with respect to shaft length may correspond to shaft termination within or below the limestone layer.

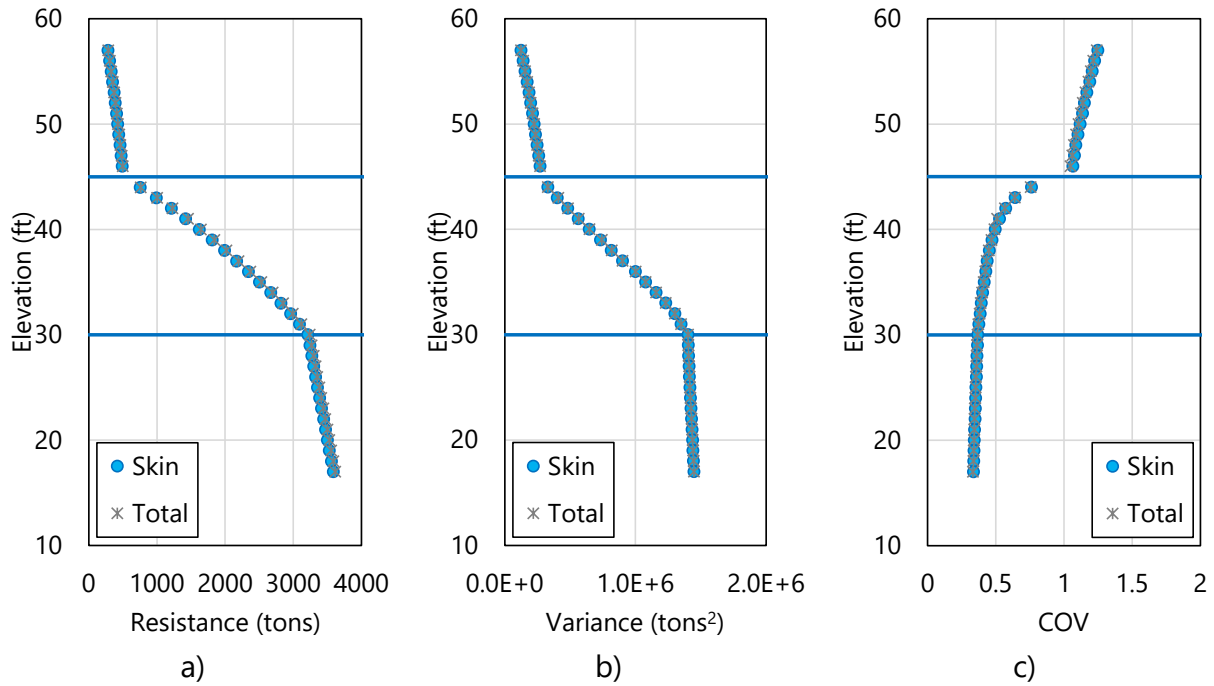


Figure 73. Profile plots obtained from unconditional simulation with limestone layering: a) Mean resistance (spatial variability only); b) Variance; c) COV

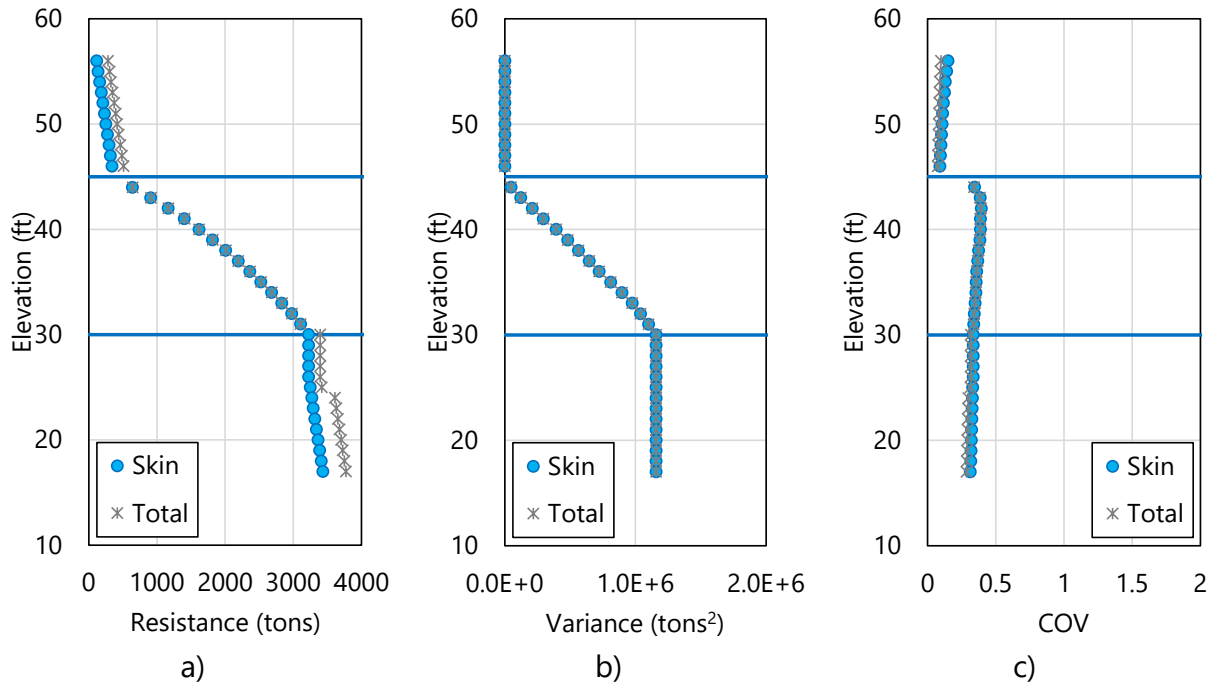


Figure 74. Profile plots obtained from unconditional simulation with clay-limestone-clay layering: a) Mean resistance (spatial variability only); b) Variance; c) COV

Regarding the profile of COV values (Fig. 73c, Fig. 74c), within a given layer, the variability of the computed resistance generally decreases with depth. As an exception for the clay-limestone-clay layering (Fig. 74c), profiles of COV values exhibit localized increases at and near the top portions of the limestone layer. As discussed in Ch. 2 and Ch. 3, smaller COV values associated with estimates of axial resistance correspond to relatively larger values of resistance factors, ϕ . Therefore, both layer interpretations support extending the shaft a considerable distance into or beyond the limestone layer (and further reducing the associated COV) so as to produce relatively more favorable estimates of factored axial resistance.

4.9.1.1 Determining a Suitable Number of Realizations for Simulation

Plotted in Fig. 75 are profiles of total resistance quantities, as obtained from conducting unconditional simulations with 100, 1500, and 2000 realizations, and use of the alternative layering. Visual inspection of the mean total resistance does not reveal appreciable sensitivities with respect to the number of realizations. Critically, though, the variance of the computed resistance Fig. 75b changes substantially when transitioning from 100 realizations to either 1500 or 2000 realizations. In contrast, only slight differences are present with respect to the variance profiles of 1500 and 2000 realizations.

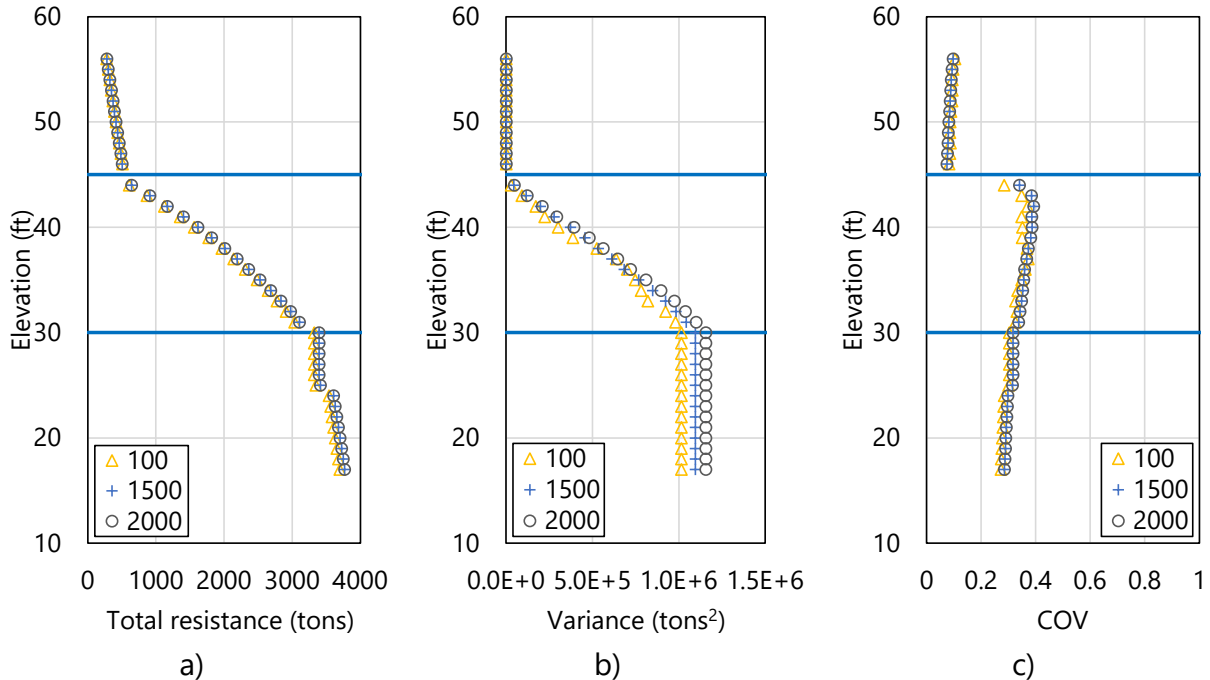


Figure 75. Profile plots obtained from unconditional simulation with 100, 1500, and 2000 realizations: a) Mean total resistance (spatial variability only); b) Variance; c) COV

For all demonstration cases reported in McVay et al. (2012), the associated number of realizations was set to 2000. Further, Faraone (2014) recommended that a minimum of 1000 realizations be considered when conducting stochastic simulation. For use of GeoStat in design applications, it is recommended that 2000 realizations be considered. However, it can always be verified that iterative increases in the number of realizations do not lead to appreciable changes in variance for the computed profiles of resistance.

4.9.2 Resistance Factor (ϕ), Spatial Variability Only

Presented in Fig. 76 are profile plots of resistance factors, ϕ , for skin and total resistance, as obtained from unconditional simulation with 2000 realizations. The plotted profiles only take into account spatial variability, as opposed to the total uncertainty associated with combined spatial variability and method error. As a mirror to the profiles of COV values (recall Fig. 73c, Fig. 74c), the profiles of computed resistance factors, ϕ (spatial variability only), generally increase with respect to depth. Such mirroring includes (for the clay-limestone-clay layering, Fig. 76b) localized increases of ϕ values near the top portions of the limestone in layer 3.

For the limestone layering (Fig. 76a), values of ϕ dramatically increase (from approximately 0.1 to 0.4) in layer 3. For embedments within the limestone layer of the clay-limestone-clay layering (Fig. 76b), values of ϕ range from approximately 0.38 to 0.48 throughout layer 3. For shaft lengths that extend into layer 4, moderate increases in resistance factors occur, reaching values up to 0.44 (Fig. 76a) and 0.53 (Fig. 76b). Given the absence of zones in the Site A data,

influence upon the resistance factors (ϕ) can be attributed, in part, to the relatively high COV values associated with the q_u values of relevant layers (e.g., recall Table 32).

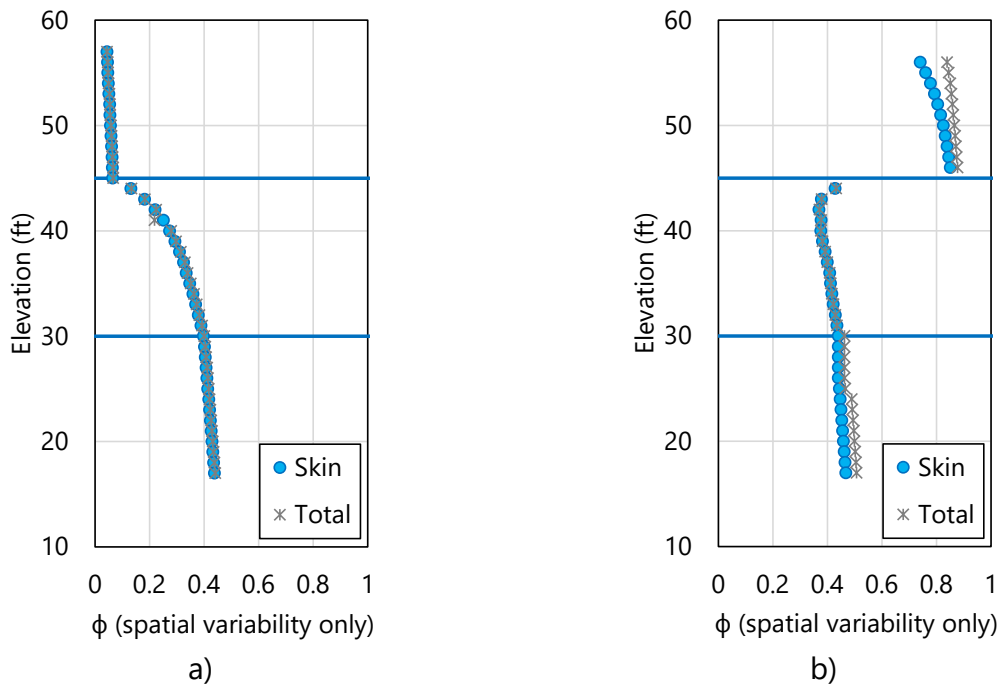


Figure 76. Profile plot of resistance factor, ϕ spatial variability only, obtained from unconditional simulation: a) Limestone layering; b) Clay-limestone-clay layering

Two general strategies are worth emphasizing at this stage for potentially producing relative increases in resistance factors (ϕ). First, if geological zones are present among the site data being characterized, then isolating the zones and repeating the modeling (and simulation) efforts may be of benefit. Second, additional layers may be defined throughout the range of candidate embedment lengths, or the layer definitions may be otherwise modified, to reduce the COV of the measured data per layer.

4.10 Incorporating Method Error

As documented in Ch. 3, two contributors to total uncertainty for estimates of foundation member axial resistance are spatial variability and method error. Method error calculations serve to adjust the “raw” results obtained from stochastic simulation, and in addition, contribute to the calculation of resistance factors (ϕ). In the GeoStat UI, parameters related to method error are specified in the sixth of seven (left to right) program tabs (Fig. 77).

As also detailed in Ch. 3, characterization of method error phenomena in GeoStat is divided into regression expressions for: driven piles, drilled shafts in clay, drilled shafts in sand, McVay skin friction of drilled shafts in limestone, and O’Neill end bearing for drilled shafts in

limestone. Of relevance to the Site A models (initial layering, alternative layering) are portions of drilled shafts in clay and portions of drilled shafts in limestone. Considerations for layer-specific contributions to method error for Site A (including selection of regression parameter values) are discussed immediately below.

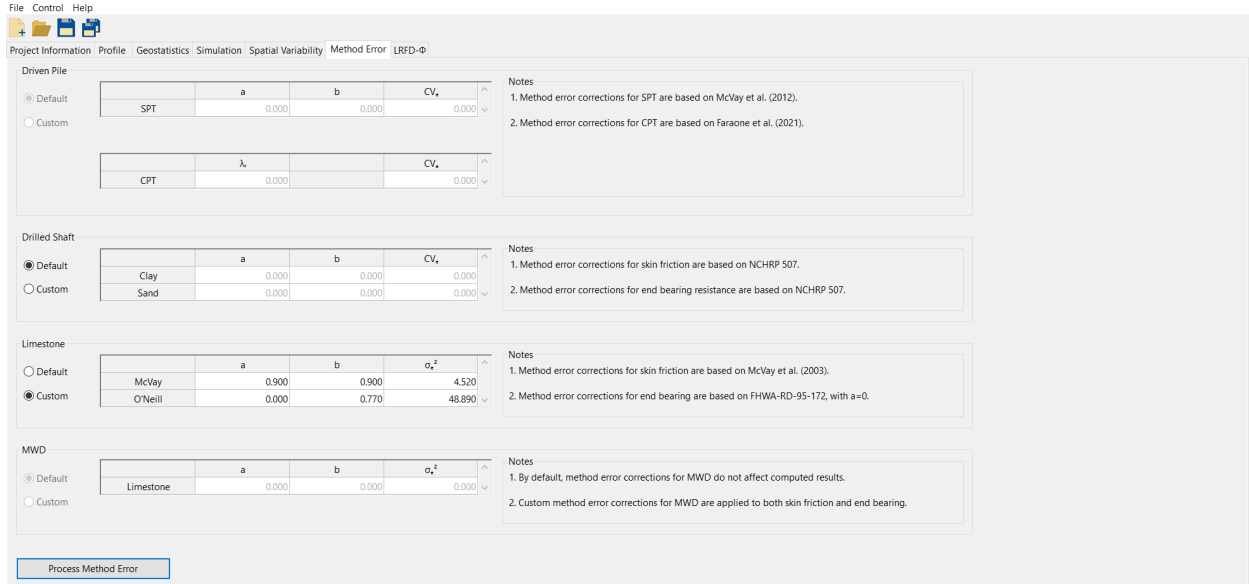


Figure 77. Method Error tab

4.10.1 Shaft Portions in Clay

Regression values pertaining to method error calculations, for portions of the drilled shaft embedded in clay (layer 2, layer 4 of the clay-limestone-clay layering), are listed in Table 39. Lacking numerous instances of load test data for Site A, the listed values correspond to the default regression parameters implemented in GeoStat (and originally recommended in McVay et al. 2012). Additional discussion of how these parameters influence resistance quantities (including ϕ) is provided in Ch. 3.

Table 39. Method error parameter values for shaft portions embedded in clay

Parameter	Value
a	0.73
b	0.86
COV_{ϵ}	0.41

4.10.2 Shaft Portions in Limestone

Regression values pertaining to method error calculations, for portions of the drilled shaft embedded in limestone (applicable to both layer definitions), are listed in Table 40 (skin) and Table 41 (tip). Default regression parameters implemented in GeoStat are utilized for method

error calculations associated with skin friction. For end bearing resistance, all parameters except set to match the default values implemented in GeoStat. Note that the intercept (a) of the regression expression is defined as 0 instead of the value of 20.5 (from O'Neill). This deviation is elected because end bearing does not substantially contribute to the total resistance for the Site A analyses (recall Fig. 73a, Fig. 74a), particularly for shaft embedments that terminate within layer 3.

Table 40. Method error parameter values for skin friction of shaft portions embedded in limestone

Parameter	Value
a	0.90
b	0.90
σ_{ϵ}^2	4.52

Table 41. Method error parameter values for end bearing of the shaft in limestone

Parameter	Value
a	0.00
b	0.77
σ_{ϵ}^2	48.89

4.11 Viewing Final Results

Shown in Fig. 78 is the rightmost (seventh) tab in the GeoStat UI. Profile plots located within this tab facilitate viewing of total resistance quantities that reflect spatial variability phenomena as well as computed results associated with total uncertainty (spatial variability and method error combined). Presented below are profile plots for both the initial (limestone) and alternative (clay-limestone-clay) layer definitions. The types of profile plot data available for viewing include unfactored resistance (e.g., Fig. 79, Fig. 80); corresponding COV values (Fig. 81, Fig. 82); corresponding resistance factors, ϕ , (Fig. 83, Fig. 84); and, factored resistance (Fig. 85, Fig. 86). All plotted results in Fig. 79 through Fig. 86 are associated with unconditional simulation and 2000 realizations.

Trends and phenomena that pertain to the profile plots of mean total resistance, COV, and ϕ values are analogous to those documented above in Sec. 4.9. Of note, however, is that total uncertainty (versus spatial variability alone) tends to more heavily penalize (reduce) computed resistance values. This phenomenon is particularly present in the profile plots of factored resistance for the clay-limestone-clay layering (Fig. 86). Also of note is that the profile of resistance factors (ϕ) varies with respect to depth (Fig. 83, Fig. 84). Computation of profiles of ϕ values is uniquely facilitated through use of GeoStat, and the depth-dependent profiles are more reflective of the site-specific characteristics versus application of a single, prescriptive resistance factor (e.g., a single, prescribed ϕ value).

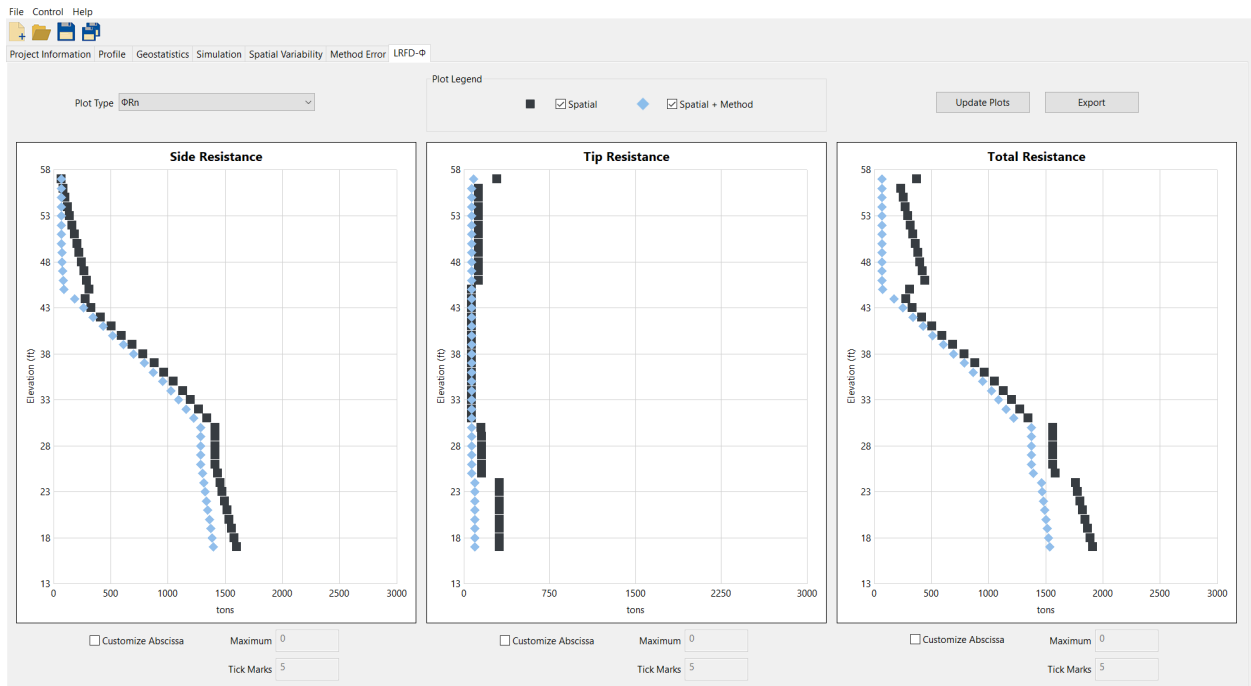


Figure 78. LRFD- ϕ tab for plotting profiles of resistance factors, ϕ , and factored resistances

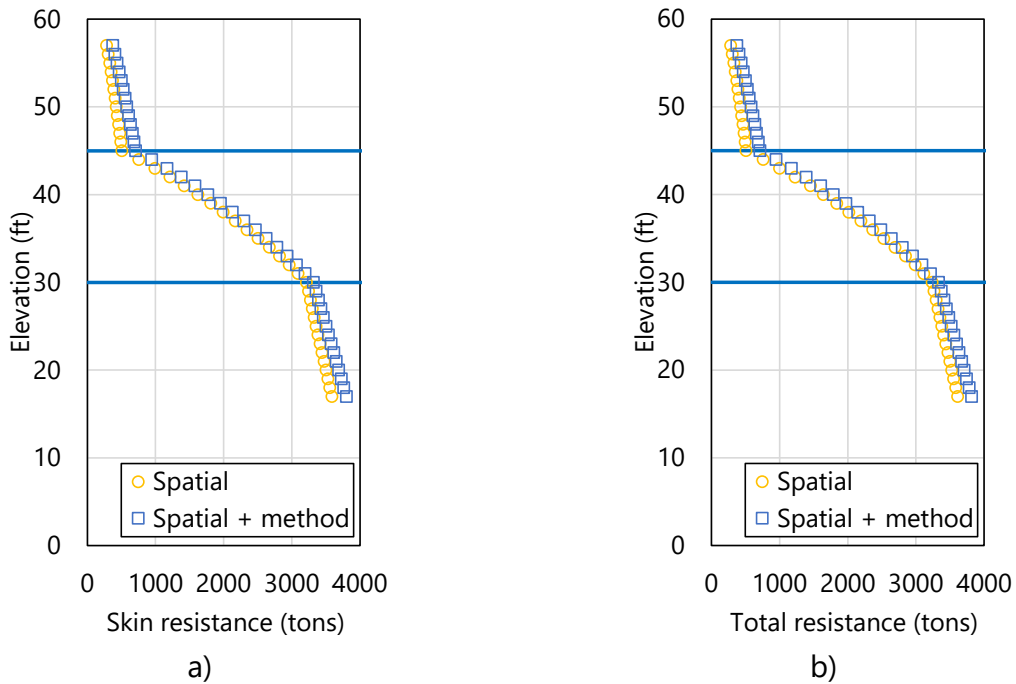


Figure 79. Profile plots of unfactored mean resistance for limestone layering: a) Skin; b) Total

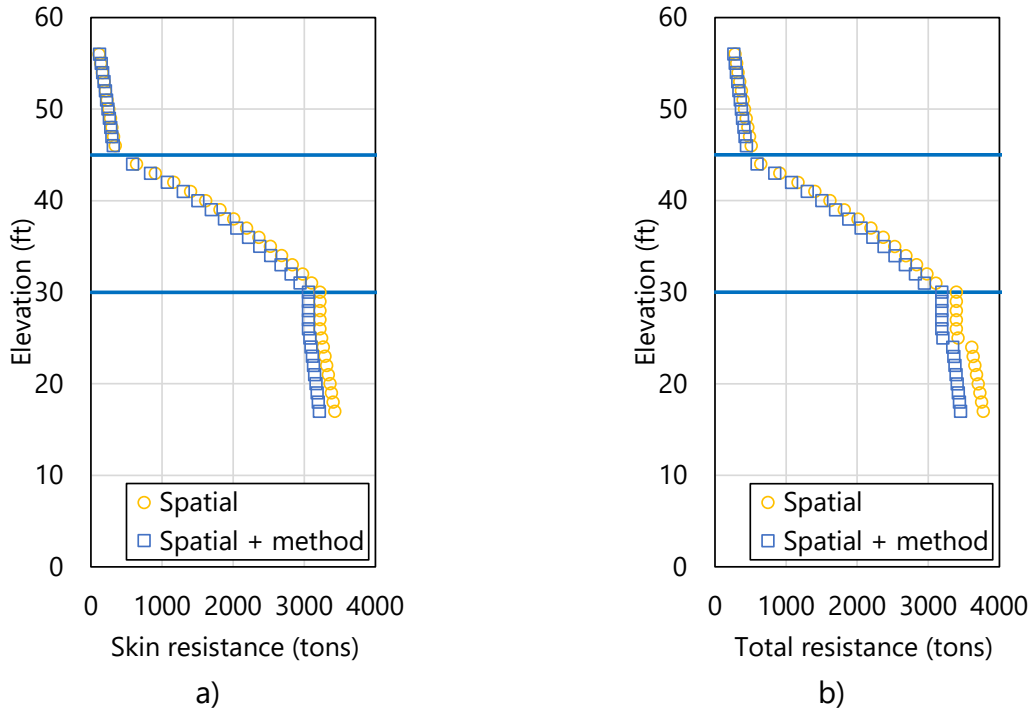


Figure 80. Profile plots of unfactored mean resistance for clay-limestone-clay layering: a) Skin; b) Total

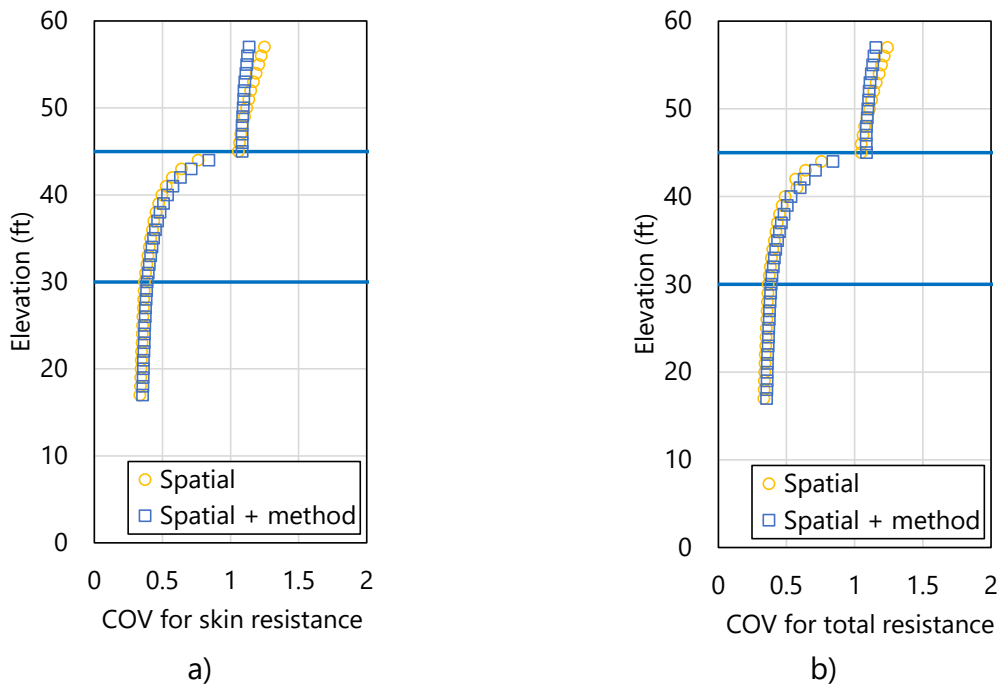


Figure 81. Profile plots of COV for unfactored mean resistance for limestone layering: a) Skin; b) Total

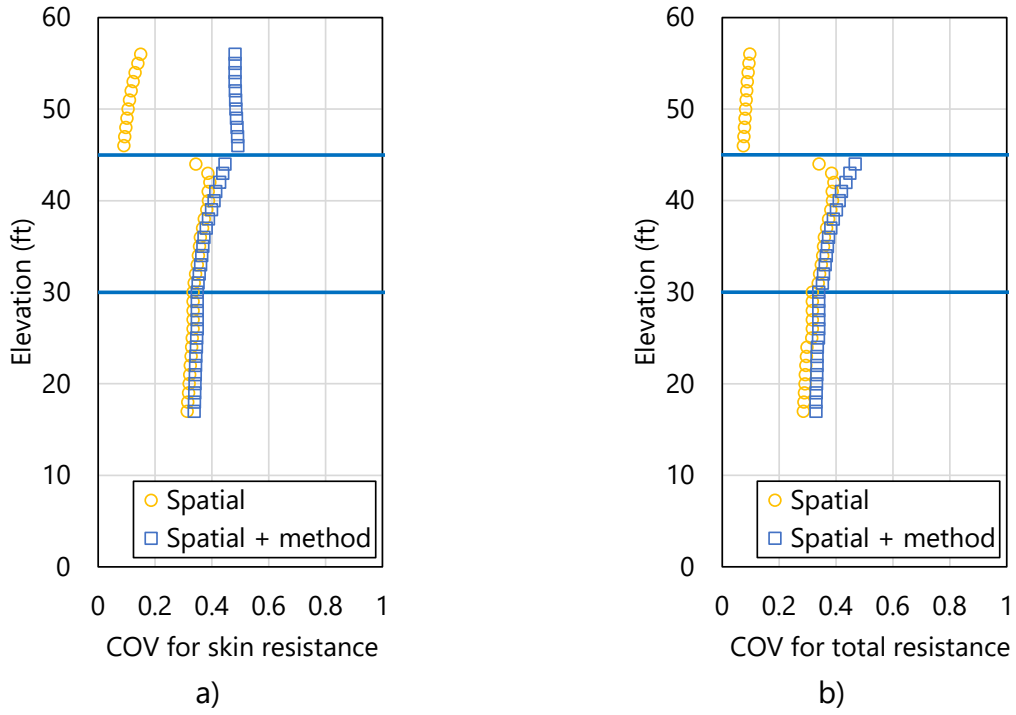


Figure 82. Profile plots of COV for unfactored mean resistance clay-limestone-clay: a) Skin; b) Total

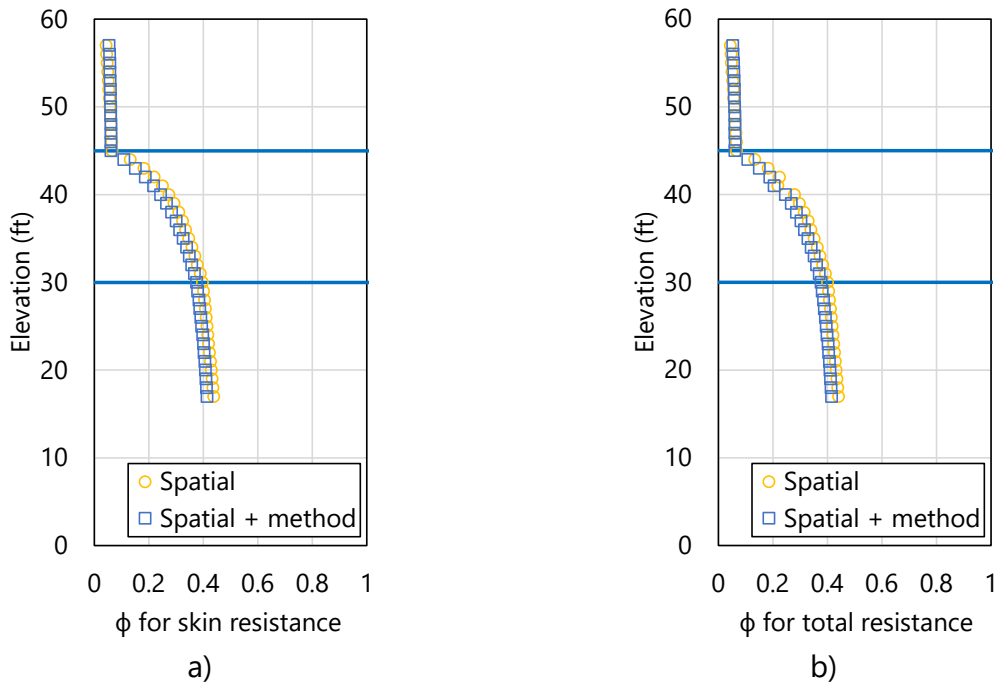


Figure 83. Profile plots of resistance factor, ϕ , for limestone layering: a) Skin; b) Total

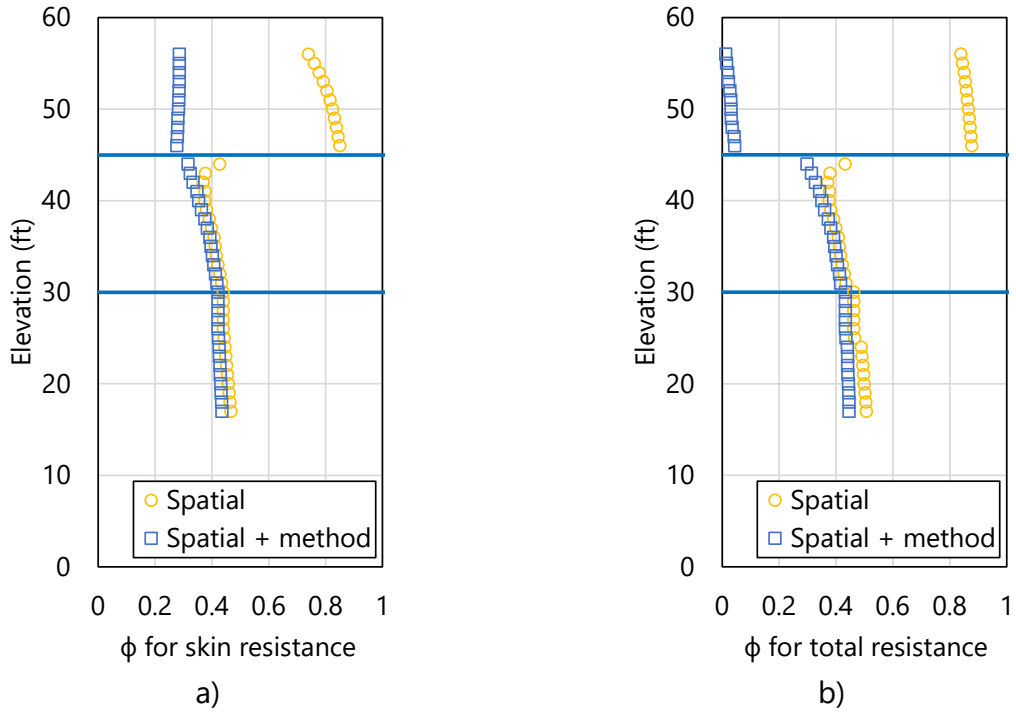


Figure 84. Profile plots of resistance factor, ϕ , for clay-limestone-clay layering: a) Skin; b) Total

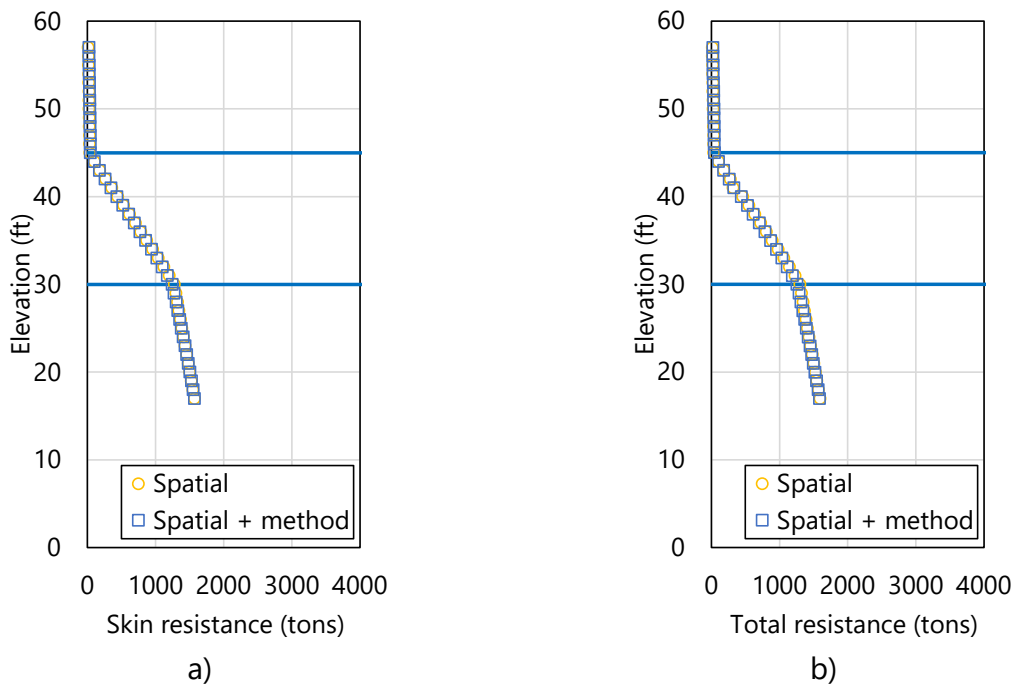


Figure 85. Profile plots of ϕ -factored mean resistance for limestone layering: a) Skin; b) Total

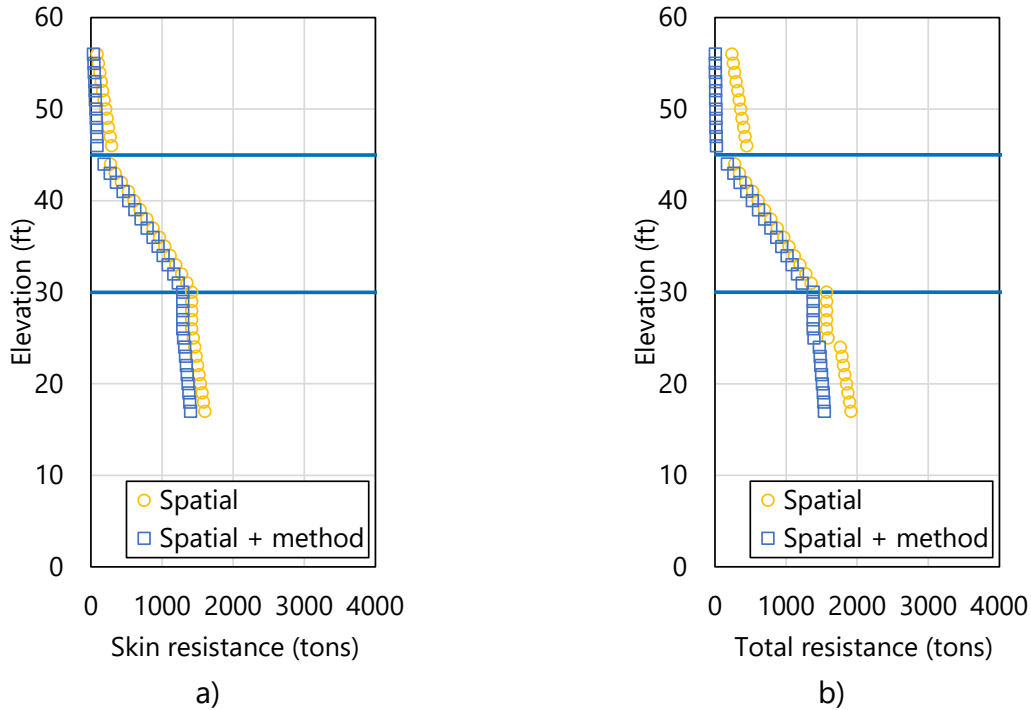


Figure 86. Profile plots of ϕ -factored mean resistance for clay-limestone-clay layering: a) Skin; b) Total

As additional comparisons of the two sets of results, note that initial (limestone) layer definitions produce profiles of unfactored resistance that are of relatively larger magnitude. For example, through the bottom of layer 2, use of the initial layer definitions leads to increased unfactored resistances (by approximately 5% to 10%; Fig. 79 versus Fig. 80), as compared to those obtained from use of the alternative layer definitions (discussed in Sec. 4.5 through Sec. 4.6).

Such differences stem from the use of different empirical expressions for limestone (i.e., McVay side friction) throughout the profile for the initial (limestone) layering, versus the clay portions of the clay-limestone-clay profile for the alternative layering (which make use of the Alpha, α , method). In other words, the clay layers do not contribute as much to unit side resistance as compared to those contributions from the limestone layers. Along these same general lines, different regression expressions are applied when incorporating method error into layer 2 and layer 4 of the clay-limestone-clay profile (versus layer 2 and layer 4 of the limestone profile). This difference, in turn, leads to differences in the profiles when considering spatial-only results versus combined spatial variability and method error phenomena.

Comparing (limestone) Fig. 81 and (clay-limestone-clay) Fig. 82, the COV profile for the limestone layering indicates much more pronounced reductions in COV values within layer 3. As noted above, the profiles of resistance factors (ϕ) mirror the profiles of COV values. The

relative increases in mean resistance (with use of initial layer definitions) are offset by relatively smaller values (approximately 5%) for resistance factors (ϕ). As a result, the factored skin and total resistance profiles are (overall) within approximately 5% of one another (Fig. 85 versus Fig. 86) regardless of the use of the initial or alternative layering definitions (and associated sets of vertical variograms). This suggests that the limestone in layer 3 is a primary driver of axial resistance.

CHAPTER 5

MODELING OF EXAMPLE SITE B

5.1 Overview

Presented in Ch. 5 is a second, detailed walkthrough of geotechnical site modeling and axial resistance simulation for an example bridge site. The data sets discussed in Ch. 5 represent one instance of the ranges and types of geotechnical site data that may be collected when investigating the foundations of a bridge site possessing medium variability. An example site exhibiting high variability is discussed in Ch. 4. In addition, the extent or size of the site of interest in Ch. 5 is large relative to that discussed in Ch. 4. Within the context of modeling and simulation in GeoStat, use of the associated (medium variability, large extent) site data is divided into several steps. Such division reflects the left-to-right progression across the seven tabs of the GeoStat user interface (UI), where the layout of the GeoStat UI is detailed in the program Help Manual.

The site of interest in Ch. 5 is referred to as Example Site B, or, Site B. Cataloging of the available Site B data for modeling within GeoStat is discussed in Sec. 5.2. Initial selection of boundary soil and rock (limestone) layer elevations is discussed in Sec. 5.3. Also documented in Sec. 5.3 are layer-related considerations specific to the type of foundation member being considered (pile, shaft).

Initial formation of spatial correlation structures (i.e., variograms) for each defined layer, and solely for the purpose of identifying geological zones, is then discussed in Sec. 5.4. Observations and considerations related to the identification of geological zones within Site B are discussed in Sec. 5.5. These considerations include assessment of zonal anisotropy and illustration of how zones are defined (modeled) within GeoStat. Two zones are identified among the Site B data set, where detailed walkthroughs of characterizing zone-specific layer definitions and variograms are illustrated in Sec. 5.6 (for zone 1) and Sec. 5.7 (for zone 2). For each of the two illustrations, comparisons are made to respective quantities obtained from the site-wide data set to demonstrate the importance of accounting for geological zones. Summary observations regarding the site-wide, zone 1, and zone 2 data sets (with respect to variograms) are provided in Sec. 5.8.

The focus of the walkthrough for Site B then shifts to stochastic simulation of axial resistance in Sec. 5.9, where one set of simulations is conducted for each of zone 1 and zone 2. Interpretation of simulated profiles of axial resistance, which reflect spatial variability phenomena of the zone-specific data, is provided in Sec. 5.10.

Comparisons are subsequently made between zone-specific simulation results to further emphasize the importance of accounting for distinct geological zones. Considerations for incorporating method error phenomena into the simulated, zone-specific results are detailed

in Sec. 5.11. The combined effects of spatial variability and method error upon computed axial resistance, culminating in profiles of both resistance factors (ϕ) and factored axial resistance, are examined in Sec. 5.12.

5.2 Cataloging Site Data

Shown in Fig. 87 is the first (leftmost) tab encountered within the GeoStat UI, referred to as the Project Information tab. This region of the GeoStat UI facilitates input and organization of all data obtained from geotechnical investigation of the site. The foundation type is also selected in the Project Information tab (Fig. 87, upper-right).

For Site B, a drilled shaft foundation type is selected. See the Example Site A walkthrough (Ch. 4) for documentation of when distinct considerations are required depending on the selected foundation type (piles, shafts). Even so, documentation of parameters selected for site modeling and interpretation of simulation results in Ch. 5 are generally applicable regardless of the selection for type of foundation member.

5.2.1 Initial Visual Assessment of Site B

For the start of the analysis, all borings for the site should be active (included) and zonal issues should be identified from variograms (e.g., recall Fig. 8c) or comparison of properties with depth from boring to boring (i.e., permuting through borings and viewing the scatterplot in Fig. 87). Accordingly, as a starting point, initial characterization of the site data (through the step of forming variograms) is carried out using all available measurements from across the 90 boring locations. Even so, given the large footprint of the site data, the need to divide the site into zones is anticipated.

Data from 90 unique boring locations are cataloged for Site B, including both SPT-N blow counts and rock-related measurements obtained from numerous core-runs (e.g., unconfined compression strength, q_u). The geotechnical investigation of Site B indicates the presence of silty sands at relatively shallow depths. Limestone is commonly encountered at deeper depths, either in the form of relatively thin bands or thick layers across the 90 boring locations. Given the prevalence of limestone throughout Site B, emphasis is initially placed on available measurements of rock strength (as discussed below) when forming components of the GeoStat model.

A plan view of the 90 boring locations is plotted in the left portion of the Project Information tab, and a corresponding plot of eastings and northings for the boring locations is shown in Fig. 88. As listed in the table on the right portion of the Project Information tab (Fig. 87, right), easting values range from 0 ft to approximately 9500 ft, and northing values range from (approximately) 0 ft to 2500 ft. Further, the ground surface elevations across the 90 borings

range from 5 ft to 33 ft. This range of ground surface elevations (nearly 30 ft) is one of several indicators that motivate assessment of the site for division into distinct geological zones.

For each of the 90 boring locations, the respective (boring-specific) geotechnical site data are input in GeoStat using the Boring Data dialog. This dialog is accessible from the upper-right portion of the Project Information tab. For example, site data measured at boring location TS-1 (easting of 799 ft; northing of 339 ft) consists of a mixture of through-depth SPT-N blow count values at shallower depths (as shown in the excerpt of Fig. 89), and core-run data from thick limestone layers at deeper depths. An additional example is provided in Fig. 90 for boring location B-705 (easting of 7197 ft; northing of 403 ft), which contains a mixture of SPT-N blow count and core-run data from core-run data from thin bands of limestone (e.g., unconfined compression strength, q_u ; split tensile strength, q_t , RQD, *recovery*).

The rightmost table column of the Project Information tab allows for any subset of borings (or all borings) to be included or excluded from the site/zone modeling. For instance, in the case of zonal anisotropy, only the borings within the zone of interest would be included (i.e., value set to 1 in far-right table column for two or more borings) for development of summary statistics, variograms, and estimated pile/shaft capacities. The result is then saved in a uniquely named model file, such as Site B – zone 1. Subsequently, other borings would be turned on and prior borings turned off for other zone analyses. On the Project Information tab (Fig. 87) scatterplot data associated with any currently selected (and active) boring location is highlighted, and can be used to quickly identify borings that contain outlier data or are associated with a unique zone.

The rightmost plot in the Project Information tab (Fig. 87, middle) facilitates plotting of collections of the desired type of site measurement (e.g., SPT-N, q_u). In addition, data pertaining to any boring location of interest are highlighted (using solid blue plot points), as exemplified for boring location TS-1 in Fig. 87.

Documented in the remainder of Sec. 5.2 are initial characterizations of the various types of measured site data available for Site B. Data are presented in scatterplot form, or as through-depth profiles of measurements accumulated across all 90 boring locations. In this way, initial characterization of trends or groupings among the site data are facilitated, where such characterization is necessary (for example) to identify zones and define soil or rock layering.

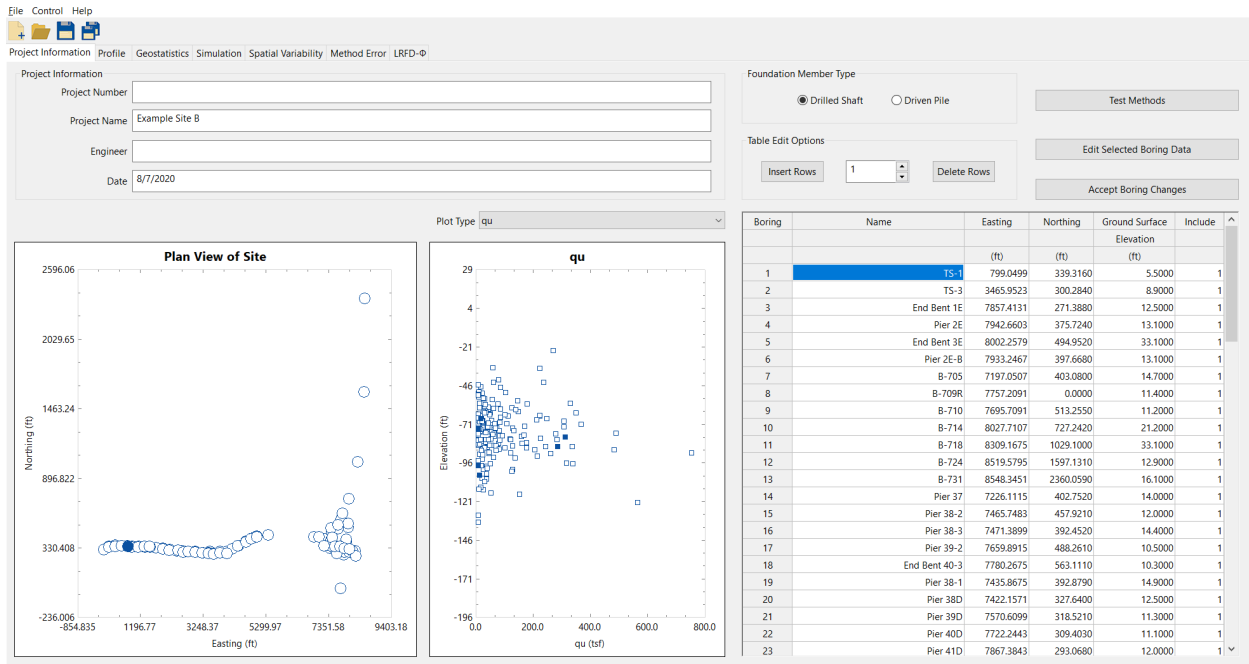


Figure 87. Project Information tab

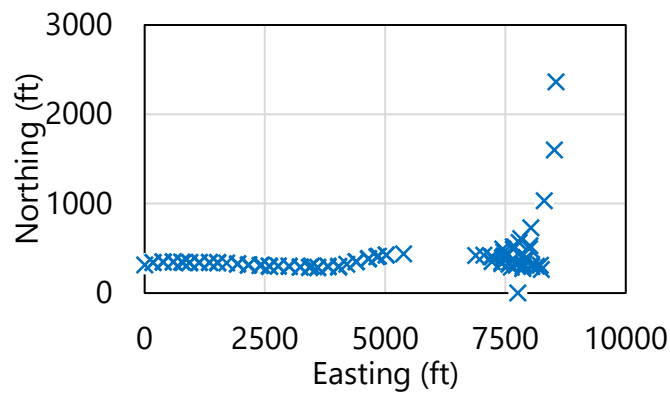


Figure 88. Plan view of 90 boring locations for Site B

Boring Data - TS-1

Table Edit Options

Insert Rows 1 Delete Rows

Number	Elevation	Depth	Soil Type	N. Blows	qt (CPT)	fs (CPT)	Unit Weight	Cu	e	qu	qt	qb	Em	RQD	Socket Roughness	Recovery
	(ft)	(ft)	[1 2 3 4]	(blows/ft)	(tsf)	(tsf)	(pcf)	(tsf)	(psi)	(tsf)	(tsf)	(tsf)	(ksi)	[0.0 to 1.0]	[0 1]	[0.0 to 1.0]
1	0.5000	5.0000		2	13											
2	-1.0000	6.5000		3	13											
3	-2.5000	8.0000		2	13											
4	-7.5000	13.0000		2	14											
5	-9.5000	15.0000		2	19											
6	-12.5000	18.0000		2	16											
7	-14.5000	20.0000		2	19											
8	-16.5000	22.0000		2	7											
9	-18.5000	24.0000		2	8											
10	-20.5000	26.0000		1	0											
11	-24.5000	30.0000		1	0											
12	-26.5000	32.0000		1	0											
13	-29.5000	35.0000		4	10											
14	-31.5000	37.0000		4	11											
15	-33.5000	39.0000		4	15											
16	-35.5000	41.0000		4	28											
17	-37.5000	43.0000		4	34											
18	-39.5000	45.0000		4	22											
19	-41.5000	47.0000		4	25											

Notes

1. Input all available data for the boring within the table above.
2. For any depths where a given soil property is not available, then leave the corresponding cell blank.
3. Soil Types: 1 = Plastic Clay | 2 = Clay and Silty Sand | 3 = Clean Sand | 4 = Limestone and Very Shelly Sand.

OK Cancel

Figure 89. Boring Data dialog for boring location TS-1

Boring Data - B-705

Table Edit Options

Insert Rows 1 Delete Rows

Number	Elevation	Depth	Soil Type	N. Blows	qt (CPT)	fs (CPT)	Unit Weight	Cu	e	qu	qt	qb	Em	RQD	Socket Roughness	Recovery
	(ft)	(ft)	[1 2 3 4]	(blows/ft)	(tsf)	(tsf)	(pcf)	(tsf)	(psi)	(tsf)	(tsf)	(tsf)	(ksi)	[0.0 to 1.0]	[0 1]	[0.0 to 1.0]
1	6.7000	8.0000		2	5											
2	4.7000	10.0000		2	4											
3	-0.3000	15.0000		2	7											
4	-5.3000	20.0000		2	11											
5	-10.3000	25.0000		2	0											
6	-15.3000	30.0000		2	3											
7	-20.3000	35.0000		4	68											
8	-21.8000	36.5000		4			128.3000							0.3200		0.4800
9	-23.3000	38.0000		4						271.3680						
10	-25.3000	40.0000		4							57.2400					
11	-30.3000	45.0000		4	50											
12	-35.3000	50.0000		4	50											
13	-37.3000	52.0000		4	50											
14	-39.3000	54.0000		4	50											
15	-41.3000	56.0000		4	50											
16	-43.3000	58.0000		4	50											
17	-45.3000	60.0000		4	50											
18	-47.3000	62.0000		4	50											
19	-49.3000	64.0000		4	50											

Notes

1. Input all available data for the boring within the table above.
2. For any depths where a given soil property is not available, then leave the corresponding cell blank.
3. Soil Types: 1 = Plastic Clay | 2 = Clay and Silty Sand | 3 = Clean Sand | 4 = Limestone and Very Shelly Sand.

OK Cancel

Figure 90. Boring Data dialog for boring location B-705

5.2.2 Site Data for Shafts in Limestone

As noted previously, initial efforts toward characterizing the site emphasize examination of available rock strength data (e.g., q_u), given the frequent occurrence of limestone bands and layers throughout Site B. Although, initially, the full collection of available site data is examined, considerations are given later to determine whether or not zones are present. Shown in Fig. 91 are measurements of rock strength obtained across the 90 boring locations (and associated core-runs). For unconfined compression strength, q_u , 186 measurements are available (Fig. 91a). Also, 187 measurements of split tensile strength, q_t , are available (Fig. 91b). From a qualitative standpoint, measured values of q_t tend to increase with increasing values of q_u . Additionally, while the majority of measured q_u values are less than approximately 100 tsf, relatively higher compressive strength values (between approximately 100 tsf and 750 tsf) are measured over the approximate elevation range of -40 ft to -135 ft.

Plotted in Fig. 92 are additional measurements pertaining to rock strength, as gathered from across all core-runs of Site B. Concerning rock quality designation (RQD), 364 values are taken from the collection of core-runs (Fig. 92a). Correspondingly, 364 values of *recovery* are included for use in GeoStat modeling of the site (Fig. 92b). Ranges for both the RQD and *recovery* measurements encompass decimal values from approximately 0.05 to 1.0. Despite the relatively large number of measured values available for RQD and *recovery*, no overtly discernible trends or groupings of values are apparent from visual inspection of the scatterplots.

Depicted in Fig. 93 are measured values of unit weight, γ , available over the elevation range of -15 ft to -102 ft. The 23 measured values of unit weight (γ) vary, approximately, from 105 lb/ft³ to 150 lb/ft³. Values of unit weight are considered as secondary to rock strength measurements (q_u , q_t) for activities such as defining layers. Additionally, relatively few measured values of unit weight (23) are available from the Site B data set, and so, visual identification of qualitative trends or groupings is precluded.

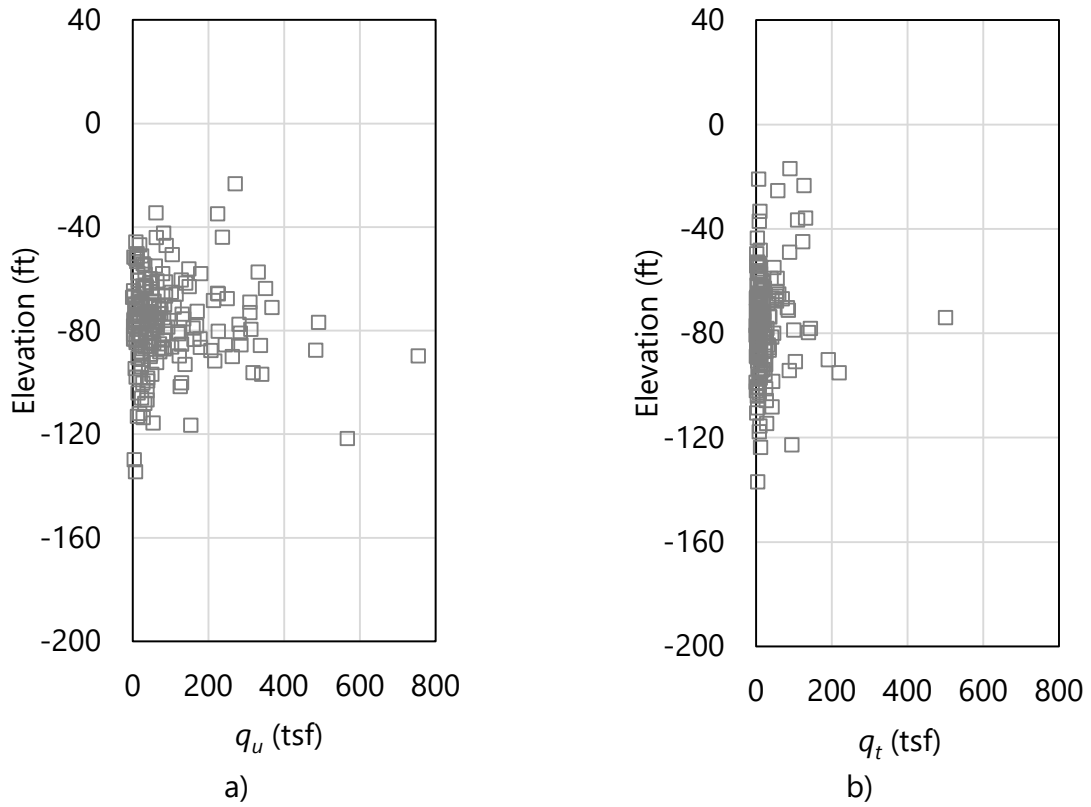


Figure 91. Scatterplots of limestone strength parameters: a) 186 values for unconfined compression strength, q_u , (elevation range: -23 ft to -134 ft); b) 187 values for split tensile strength, q_t , (elevation range: -17 ft to -137 ft)

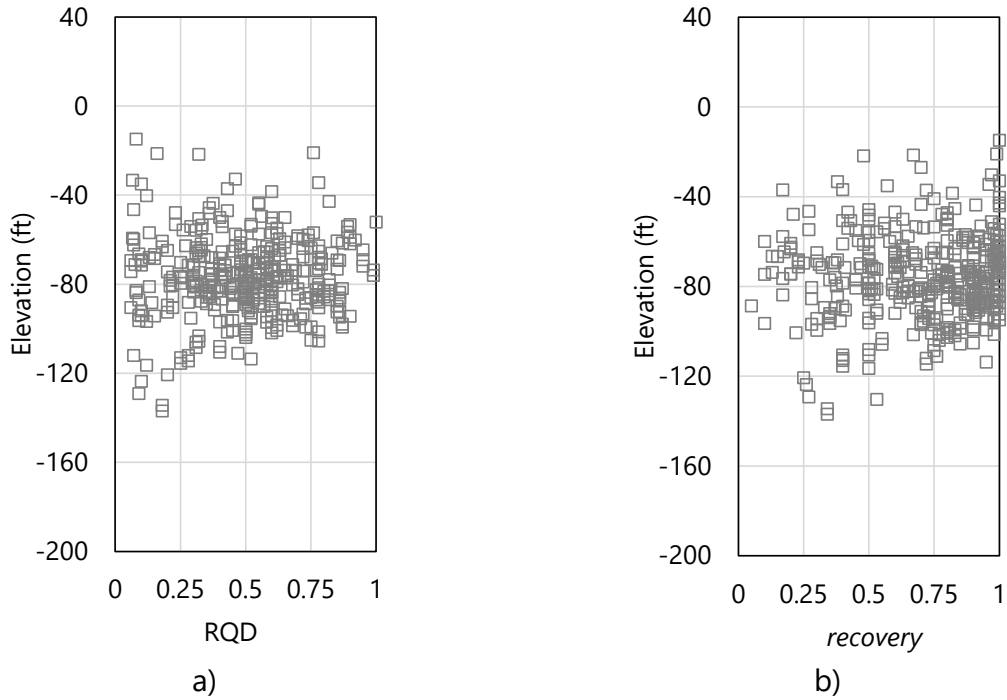


Figure 92. Scatterplots of limestone strength parameters: a) 364 values for RQD (elevation range: -17 ft to -137 ft); b) 364 values for *recovery* (elevation range: -17 ft to -137 ft)

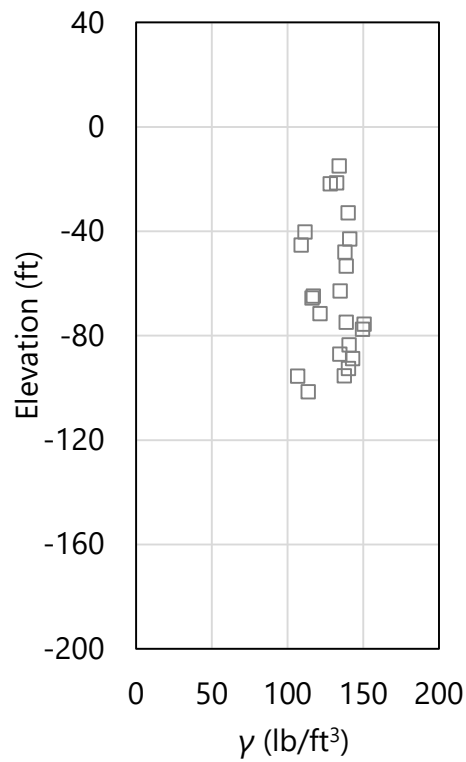


Figure 93. Scatterplot of 23 values of unit weight, γ , (elevation range: -15 ft to -102 ft)

5.2.3 Site Data for Piles, Shafts in Clay, and Shafts in Sand

For portions of drilled shafts and piles embedded in clay and sand, SPT-N blow count values are most pertinent in computing axial resistances from within GeoStat. Plotted in Fig. 94 are 3144 SPT-N blow count values, as collected across the 90 boring locations of Site B. Blow count values range from 0 blows/ft to approximately 95 blows/ft. Per the available site data, a relatively high prevalence of blow count values are attributed to refusal-like conditions and thus reported as 50 blows/ft (e.g., over the elevation range of -10 ft to -160 ft).

A qualitative grouping of SPT-N blow count values is apparent from elevations of 10 ft to approximately -50 ft. For elevations below -50 ft, relatively high levels of dispersion are present among the collection of SPT-N blow counts. These visually identified groupings are revisited later as part of defining representative layering for the available Site B data, and when investigating the presence of zones.

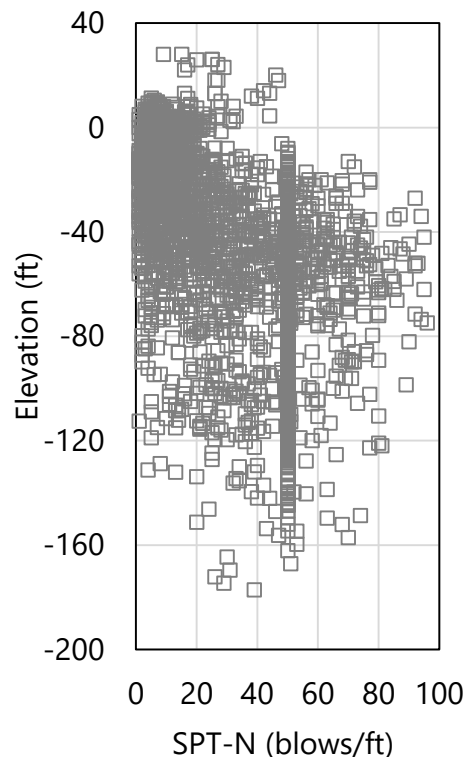


Figure 94. Scatterplot of 3144 SPT-N blow counts (elevation range: 33 ft to -177 ft)

5.3 Initial Definition of Soil or Rock Layering

The second of seven tabs (from left to right) in the GeoStat UI is the Profile tab (Fig. 95). Using the controls within this tab, a representative soil or rock layering is defined. Scatterplots of the previously cataloged site data are utilized here (Fig. 95, left and middle) to aid in selection of boundary layer elevations. Layer bottom elevations can be defined through graphical

selection within the profile plots. Additionally, all required parameter values for a given layer (e.g., soil or rock type, top elevation, bottom elevation) can be input in the layer data table (Fig. 95, right).

As a first attempt at establishing layer definitions for Site B, consider the soil or rock types and layer elevations given in Table 42. Based on the cataloged site data, two layers are defined and consist of either silty sand (layer 1) or limestone (layer 2). Layer top and bottom elevations span the ranges of elevations identified during the initial review of the site data documented above. Additional discussion regarding the selections of the boundary layer elevations is provided in the remainder of Sec. 5.3. Still further considerations are documented in Sec. 5.4, as part of the initial formation of layer-specific variograms.

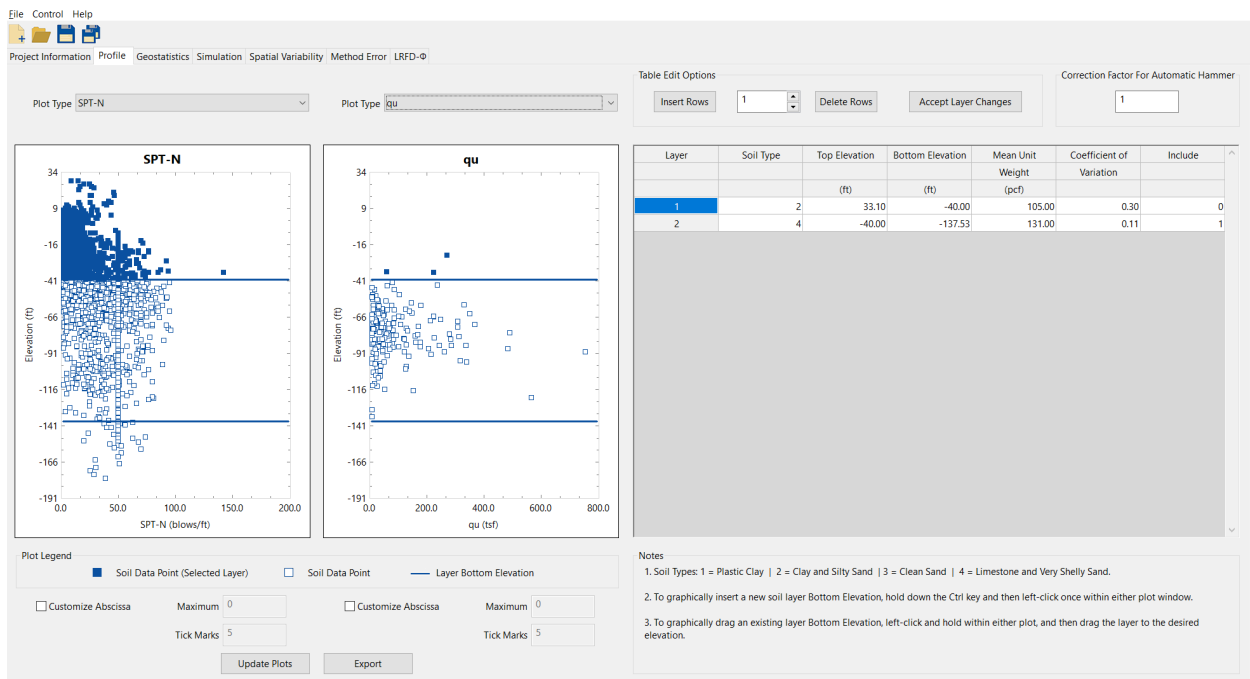


Figure 95. Profile tab

Table 42. Selected layer types and elevation ranges

Layer	Layer type	Top elevation (ft)	Bottom elevation (ft)
1	Silty sand	33.1	-40.0
2	Limestone	-40.0	-137.0

5.3.1 Initial Selection of Layer Elevations

Selected geotechnical data pertaining to rock strength are made use of for initial definition of the boundary layer elevations. Plotted in Fig. 96 are the layer divisions and ensemble of 186 measurements for unconfined compression strength, q_u , and split tensile strength, q_t .

Consistent with the initial review of the cataloged for Site B, the selected layer divisions are positioned in accordance with qualitative groupings identified above. For example, in accordance with observations made from the initial review of the cataloged site data, the concentrated region of relatively higher-magnitude q_u values is designated as a distinct limestone layer, with top elevation of -40 ft. The bottom elevation of layer 2 is defined to encompass the available values of q_u and q_t (i.e., -137 ft in Fig. 96b).

The 3144 SPT-N blow counts associated with the 90 boring locations of Site B, along with layer divisions (blue horizontal lines), are plotted with respect to elevation in Fig. 97. For example, a trend (albeit weak, with pronounced scatter) is discernible among the blow counts between 33 ft and -40 ft, in comparison to the relatively high levels of scatter present for values cataloged below -40 ft. Thus, Layer 1 is defined between 33 ft and -40 ft.

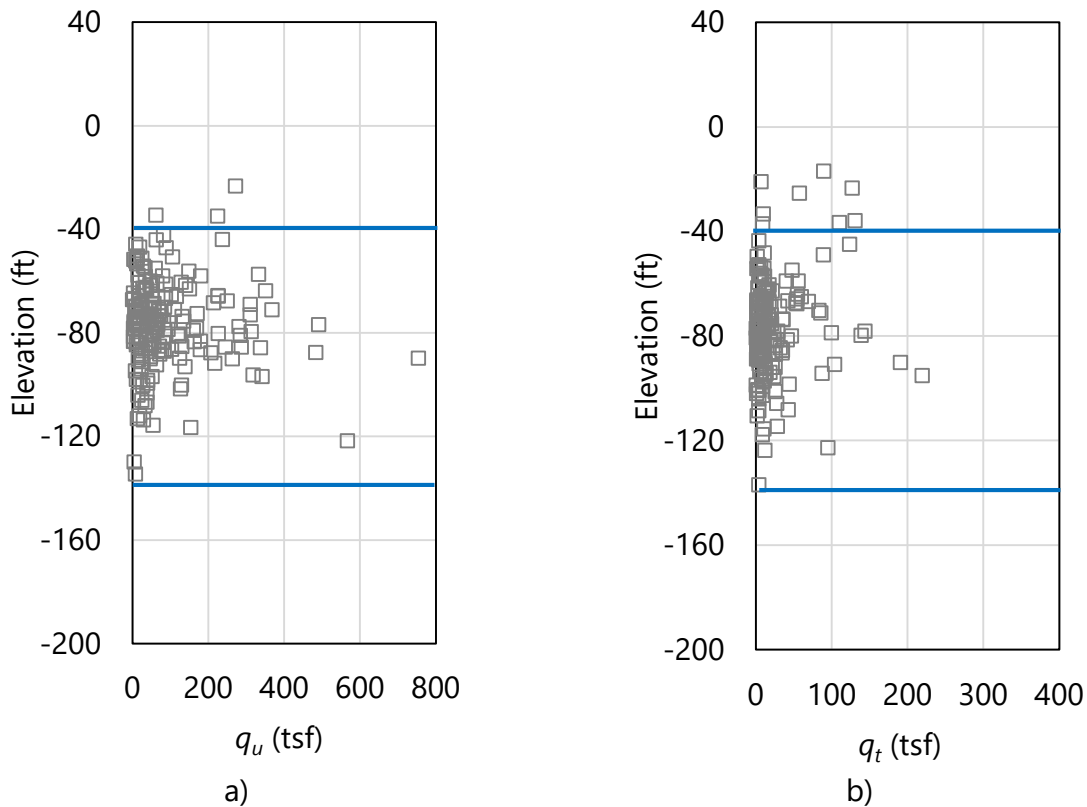


Figure 96. Scatterplot of measured rock strengths with layer bottom elevations (blue horizontal lines): a) 186 values for unconfined compression strength, q_u , (elevation range: -23 ft to -134 ft); b) 187 values for split tensile strength, q_t , (elevation range: -17 ft to -137 ft)

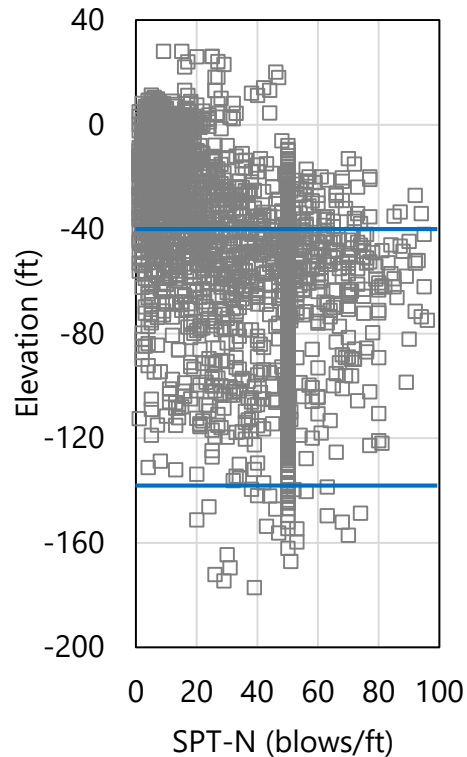


Figure 97. Scatterplot of 3144 SPT-N blow counts (elevation range: 33 ft to -177 ft) with layer bottom elevations (blue horizontal lines)

5.3.2 Specifying Unit Weight per Layer when Modeling Drilled Shafts

For modeling of drilled shafts in GeoStat, descriptive statistics pertaining to unit weight, γ , are required in addition to the boundary elevations of each defined layer. The descriptive statistics are input in the GeoStat UI (per layer) in the same location as the respective layer top and bottom elevations (recall Fig. 95, right). Required statistics include the mean value of unit weight and the associated COV.

As illustration of how the descriptive statistics are formed when drilled shafts are selected as the foundation type, consider the scatterplot of 23 unit weight (γ) values for Site B (and layer divisions) in Fig. 98. Formation of descriptive statistics for each layer is carried out by: (1) identifying those values of unit weight (γ) that are positioned within the layer; (2) calculating the mean value of the identified γ values; (3) calculating the standard deviation; and, (4) calculating the COV.

Continuing the illustration, consider the 17 unit weight values (γ) exclusive to layer 2 (Fig. 99). A corresponding histogram of the 17 values is shown in Fig. 100. Given the relatively few available measurements of unit weight, γ , assessment of the histogram is of limited utility.

Even so, descriptive statistics for the unit weight values positioned in layer 2 are assumed to be somewhat representative for the Site B data. The mean of the layer 2 unit weight data is calculated as 131 lb/ft³; the standard deviation is calculated as 14.4 lb/ft³; and, the COV is calculated as 0.11. Both the mean and COV values for unit weight, γ , are supplied as part of the layer 2 definition.

Of the 23 available values of unit weight, γ , only 6 values fall within the elevation range defined for layer 1. Engineering judgement is therefore exercised to estimate descriptive statistics for layer 1. Given that layer 1 is defined as silty sand, the mean unit weight is defined as 105 lb/ft³, and a relatively high value of COV (relative to layer 2) is assumed as 0.3. The descriptive statistics for layer 1 and layer 2 are listed in Table 43. As discussed previously in Ch. 2, these descriptive statistics are utilized when simulating log-normally distributed values of unit weight (γ), as part of stochastic simulation of axial resistance for drilled shaft members.

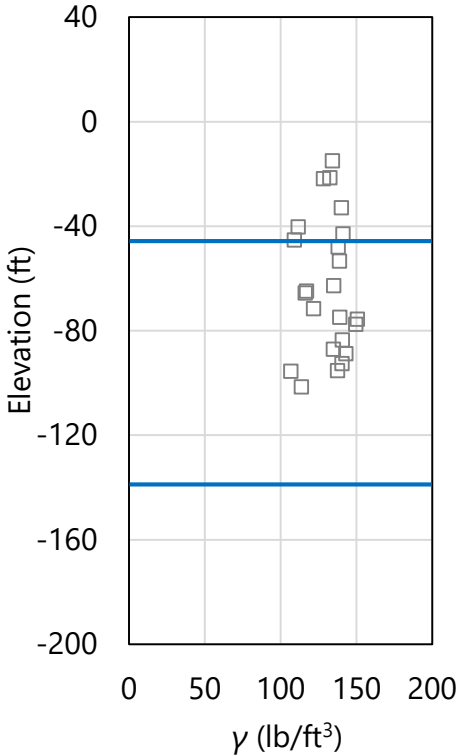


Figure 98. Scatterplot of 23 values of unit weight, γ , (elevation range: -15 ft to -102 ft) with layer bottom elevations (blue horizontal lines)

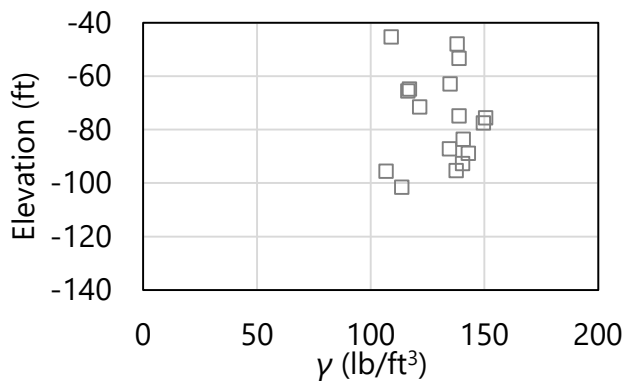


Figure 99. Scatterplot of 17 values of unit weight, γ , (elevation range: -45 ft to -102 ft) within layer 2

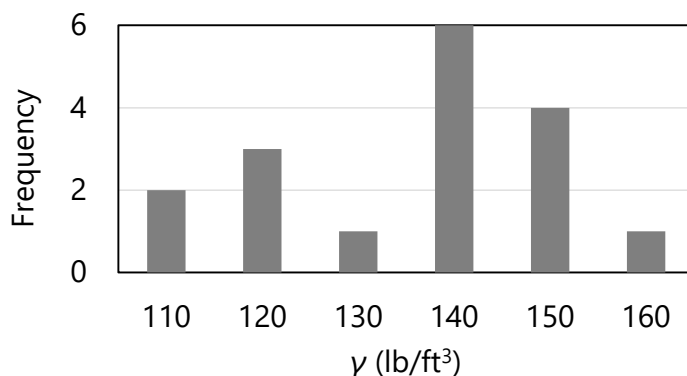


Figure 100. Histogram of 17 values of unit weight, γ , (elevation range: -45 ft to -102 ft) within layer 2

Table 43. Descriptive statistics for unit weight, γ , for each layer

Layer	Mean unit weight (lb/ft ³)	COV
1	105	0.3
2	131	0.11

5.3.3 Accounting for Steel Casings when Modeling Drilled Shafts

As an additional consideration when modeling axial resistances of drilled shafts, it may be desirable to neglect skin friction resistance near upper portions of the shaft when steel casings are present. As a convenience, for such instances, the option is available to exclude any defined layer from the resistance computation procedures implemented in GeoStat.

For example, a drilled shaft foundation type is considered for Site B, and a casing is assumed to be present from the ground surface down to the rock layer (i.e., layer 2). Consequently, layer 1 is excluded from axial resistance calculations by setting the Include flag to 0 (as

opposed to 1, which signifies inclusion) within the layer data table of the Profile tab (Fig. 95, far right).

5.4 Initial Selection of Geo-statistical Parameter Values

Having defined an initial layering for the Site B geotechnical data, focus of the modeling efforts within GeoStat continues onward to the formation of layer-specific spatial correlation structures (i.e., variograms). Recalling the relatively large plan-view area associated with Site B, the need to divide the site data into zones is anticipated, and so, initial formation of variograms (using all Site B data) is carried out to demonstrate such need. As part of the variogram formation for each applicable layer, additional checks are conducted regarding the previously defined layering (as discussed in Sec. 5.4.1). Variogram formation for each layer is carried out within the Geostatistics tab (Fig. 101) of the GeoStat UI.

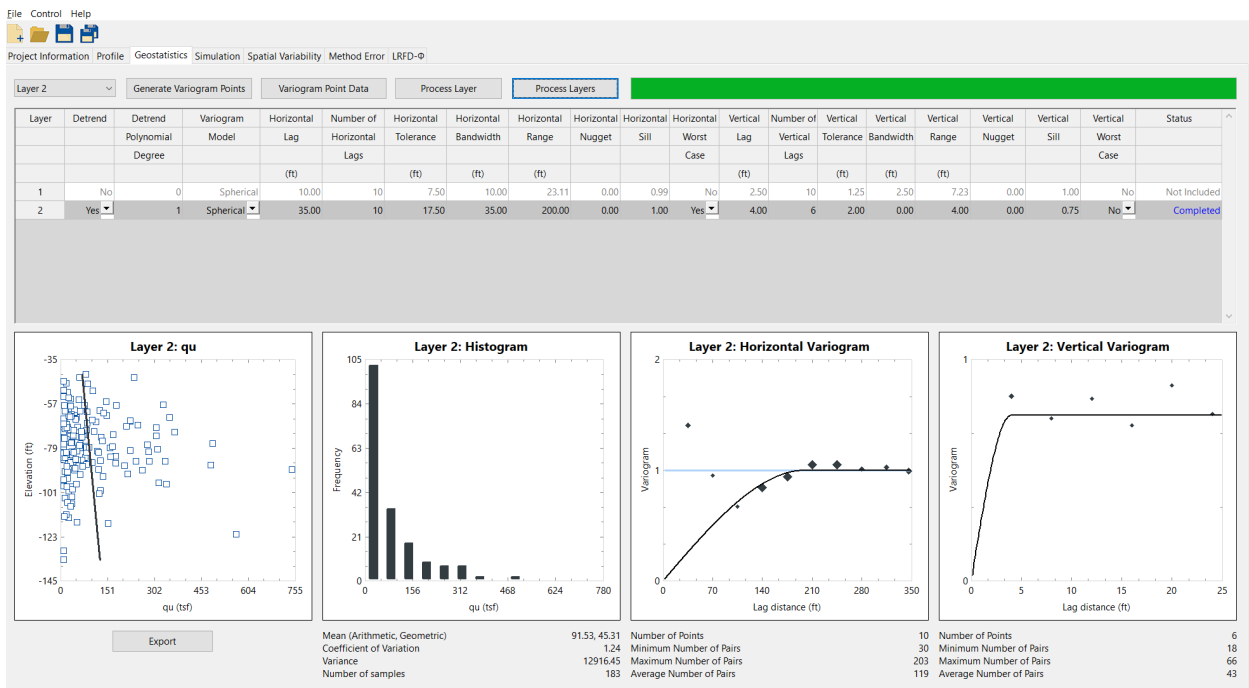


Figure 101. Geostatistics tab

For any layer that is to be included for simulating axial resistance, various graphical depictions are provided in the bottom region of the Geostatistics tab. From left to right (Fig. 101, bottom), the layer-specific graphical depictions include a scatterplot of the relevant soil or rock parameter, corresponding histogram, horizontal variogram, and vertical variogram. While the scatterplot and histogram are dictated by the previously cataloged site data and previously formed layer definitions, the (experimental) variogram points are dependent on selection of variogram parameter values in the table located above the plots (Fig. 101, middle).

When forming spatial correlation structures for drilled shaft portions embedded in sand layers, SPT-N blow count values are utilized. For drilled shaft portions embedded in clay layers, SPT-N blow counts are again utilized, but then empirically related to undrained shear strength (C_u). However, for drilled shaft portions embedded in limestone layers, values of unconfined compression strength (q_u) are used for computation of variogram points. For the modeling of Site B, recall that a drilled shaft is selected as the foundation member type, and that steel casing is present from the ground surface down to the top of layer 2. Therefore, no considerations are necessary in relation to layer 1 (silty sand). Initial formation of variograms for layer 2 (limestone) is based upon values of unconfined compression strength (q_u).

5.4.1 Examining Initial Definition of Layer Data

Prior to selecting variogram parameter values for layer 2, both the descriptive statistics and graphical depictions of the layer-specific collections of q_u values are examined. Summary statistics for the relevant types of soil or rock measurements for layer 1 and layer 2 are listed in Table 44. Values pertaining to layer 1 are not applicable (N/A) because the layer is excluded from the Site B analysis to reflect the presence of a steel casing. The level of dispersion associated with the q_u data of layer 2 is relatively high (COV value is 1.25). Such a relatively large value of COV, in part, motivates assessment of the Site B data for the purpose of identifying distinct geological zones (as discussed in Sec. 5.5).

Table 44. Summary statistics for defined layers

Layer	Physical measurement	Sample size	Mean	COV
1	N/A	N/A	N/A	N/A
2	q_u (tsf)	180	91.5	1.25

Concerning examination of graphical depictions of layer 2 data (q_u), the scatterplot (e.g., Fig. 101, bottom-left) serves to reveal if trends are present among the layer data. In the event that a trend is observed among the data attributed to a layer, then detrending is necessary. The detrending process (documented in Ch. 2) is automated in the GeoStat UI. Recalling Fig. 101 (middle-left), if detrending is desired for the data of a given layer, then the respective entry in the Detrend column of the layer data table is set to Yes (as opposed to No). Further, the polynomial degree of the trend is specified. Typically, linear detrending is sufficient for instances when detrending is necessary.

Regarding the histograms of layer-specific data (e.g., Fig. 101, bottom-center), these plots allow for conspicuous frequency-related features (i.e., bimodal peaks) to be identified. More broadly, in the event that the data distribution for a given layer does not exhibit (roughly) a lognormal shape, then revisions to the layer definitions (and particularly the layer elevations) may need to be carried out. When conspicuous features are present in a layer-specific histogram, then it may be necessary to assess the site data for the presence of distinct

geological zones (as discussed for Site B in Sec. 5.5). If zones are identified, then modeling of each zone (one subset of boring locations at a time) can lead to more representative layers for a given region within the site, and also, relatively smaller values of COV for layer-specific data. Subdivision of the site into zones, though, tends to reduce the number of data points available for modeling of a given layer (and can hinder the formation of variograms). Stated alternatively, a balance is required between subdivision of site data and available data points per layer.

5.4.1.1 Layer 2

A scatterplot of the 183 unconfined compression strength, q_u , values positioned within layer 2 is presented in Fig. 103. Visual examination of the scatterplot (Fig. 103) confirms the relatively high level of dispersion (COV of 1.25) reported in Table 44. Also, owing in part to the level of dispersion among the collected data, only a weak trend (increasing q_u values with increasing depth) is observed from the scatterplot.

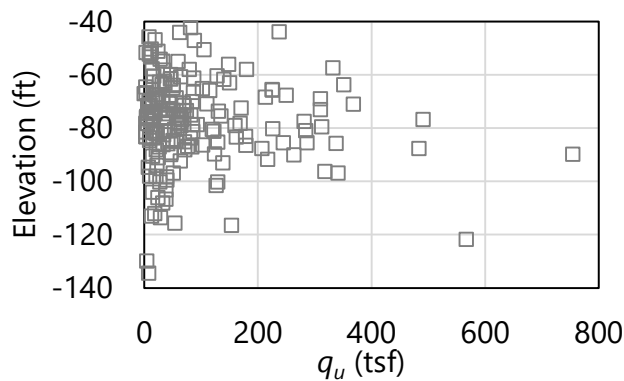


Figure 102. Scatterplot of 183 unconfined compression strength, q_u , values (elevation range: -40 ft to -134 ft) within layer 2

A histogram of the 183 measured q_u values pertaining to layer 2 is presented in Fig. 103. Despite the far-left, pronounced frequency peak for q_u values of approximately 50 tsf, the overall histogram (roughly) resembles that of log-normally distributed data. Furthermore, the right skew of the histogram is markedly elongated and contributes to the associated COV value of 1.25. These observations provide sustained motivation for assessment of distinct geological zones for Site B. However, given the absence of conspicuous features (such as bimodal phenomena) in the layer 2 histogram, no revisions are made regarding the initial selections of boundary elevations for layer 2.

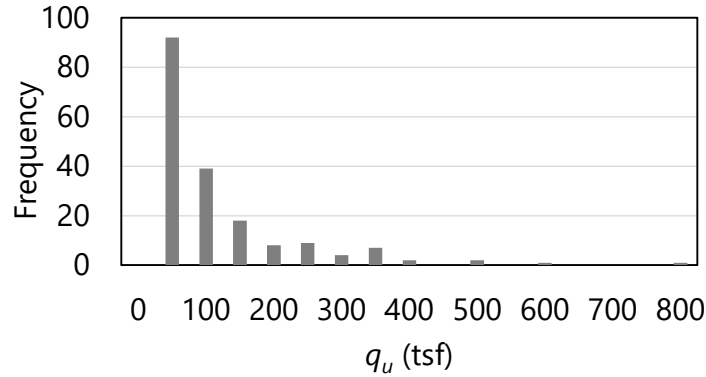


Figure 103. Histogram of 183 unconfined compression strength, q_u , values (elevation range: -40 ft to -134 ft) within layer 2

5.4.2 Forming Variograms using Initial Layer Definitions

The above examination reaffirms the initial selections of layer elevations for the geotechnical data of Site B. The process of forming variograms is next undertaken for layer 2, but solely for the purpose of demonstrating the need to divide the site into zones. Recalling Fig. 88, geotechnical data are available for a relatively large number of boring locations (90). Accordingly, consideration is given to forming initial spatial correlation structures in both the horizontal and vertical directions. Variogram parameters initially selected for layer 2, with consideration of all (90) Site B borings, are listed in Table 45.

Table 45. Layer-specific parameters for variograms with consideration of all Site B borings

Layer	Type	Lag (ft)	Number of lags	Tolerance (ft)	Bandwidth (ft)
1	N/A	N/A	N/A	N/A	N/A
2	Horizontal	35	10	17.5	35.0
2	Vertical	4	6	2.0	0.0

Table 46. Variogram ranges and sills for all Site B borings

Layer	Type	Range (ft)	Sill
1	N/A	N/A	N/A
2	Horizontal	200	1.0
2	Vertical	4.0	0.75

As discussed in Ch. 2, the lag distance, number of lags, tolerance, and bandwidth are all instrumental in forming points of the experimental variogram. Recommendations given in McVay et al. (2012) are utilized in selecting tolerance and bandwidth values listed in Table 45 (detailed for layer 2 below). Variogram values for range and sill are not listed as these values (range, sill) are more strongly related to the theoretical variogram in GeoStat (see Ch. 2 for additional details).

5.4.2.1 Layer 2

As listed above in Table 45, a horizontal lag distance (i.e., the abscissa spacing between points of the horizontal variogram) is selected as 35 ft for the horizontal variogram of layer 2. A relatively large horizontal lag distance (versus vertical lag distance of 4 ft) is selected to reflect the plan-view distances of borings distributed across Site B. The vertical lag distance of 4 ft is selected to be on the order of the distances associated with core-runs (5 ft).

Use of the lag distances specified above lead to qualitatively apparent trends in the respective experimental variograms (presented later). However, it is recommended that multiple candidates for lag distance be considered prior to finalizing the variogram for a given layer and variogram direction. Furthermore, for each candidate lag distance considered, it is necessary to update the values for tolerance and bandwidth.

Recommendations are given in McVay et al. (2012) for determining values of tolerance and bandwidth, given a candidate value of lag distance. Distinctions are made between recommendations for horizontal and vertical variogram parameters. For example, for the selected (vertical) lag distance of 4 ft, the tolerance is set to one-half the magnitude of the lag distance (i.e., 2 ft) and the bandwidth is set to 0 ft. As an additional example, for the horizontal variogram of layer 2, the tolerance (17.5 ft) is again set to one-half of the respective lag distance (35 ft).

Variogram points for layer 2 are calculated, in part, using distance-based pairings of measured q_u values. Linear detrending is applied to the data set (as automated in GeoStat) for the purpose of forming variogram points. The horizontal and vertical (experimental) variogram points for layer 2 are listed in Table 47 and Table 48, respectively. Corresponding plots of the experimental variograms are presented in Fig. 104 (horizontal) and Fig. 105 (vertical). Also listed in Table 47 and Table 48 are the pairs associated with each variogram point. The data listed in Table 47 and Table 48 are obtained directly from the GeoStat UI by entering the Variogram Data dialog (Fig. 101, top-left).

Table 47. Horizontal variogram data for layer 2 (elevation range: -40 ft to -137 ft) with consideration of all Site B borings

Abscissa (ft)	Ordinate	Pairs
35	1.41	66
70	0.96	60
105	0.67	30
140	0.85	157
175	0.94	187
210	1.05	203
245	1.05	174
280	1.01	101
315	1.03	98
350	0.99	122

Table 48. Vertical variogram data for layer 2 (elevation range: -40 ft to -137 ft) with consideration of all Site B borings

Abscissa (ft)	Ordinate	Pairs
4	0.84	66
8	0.74	62
12	0.82	54
16	0.70	32
20	0.88	30
24	0.76	18

As discussed in Ch. 2, the number of measured data pairs used in forming an experimental variogram point reflect the strength (or significance) of said point. Further, as is the case for the variogram plots within the GeoStat UI (recall Fig. 101), the experimental variogram point symbols in Fig. 101 are sized (scaled) based on the respective number of pairs used in forming said points. The scaling visually signifies the strength or significance of each variogram point. A threshold value of approximately 30 (pairs) is recommended in McVay et al. (2012) when judging the significance of an experimental variogram point.

For the layer 2 horizontal variogram of Site B, pair counts well in excess of 30 are generally produced across the variogram points (Table 47), particularly for distances equal to or greater than 140 ft. Points at distances greater than 100 ft conform to asymptotic behavior, with a sill value of unity. A theoretical is fit to the horizontal variogram points, with range of 200 ft and sill of unity. Regarding the vertical variogram for layer 2 (Table 48, Fig. 105), ordinate values considerably less than unity (0.70 to 0.88) occur across all lag distances. For increasing lag distances, the variogram ordinates appear to converge toward an ordinate value of approximately 0.75. Accordingly, a theoretical variogram is fit to the variogram points, with a range of 4 ft and sill of 0.75.

Comparing horizontal (Fig. 104) and vertical (Fig. 105) variogram plots for layer 2 (when considering all 90 boring locations), zonal anisotropy is apparent. Of greatest significance, the sills of the horizontal (1.0) and vertical (0.75) variograms do not converge to the same ordinate value. As detailed in Ch. 2, zonal anisotropy is present when the ordinates of the variograms for a given layer do not converge to the same sill (Fig. 106). Alternatively stated, when data sets exhibit zonal anisotropy, then the corresponding variances are direction dependent. Additionally, it is very likely due to proportionality (i.e., COV, or standard deviation divided by the mean) that if the sill (variance, or, standard deviation squared) is different, then the means will differ by zone and, ultimately, so will the estimated shaft capacities. Still further, if carried forward when zonal anisotropy is present, the overall variance of the data may adversely affect terms that contribute to total uncertainty when calculating LRFD resistance (via the resistance factor, ϕ).

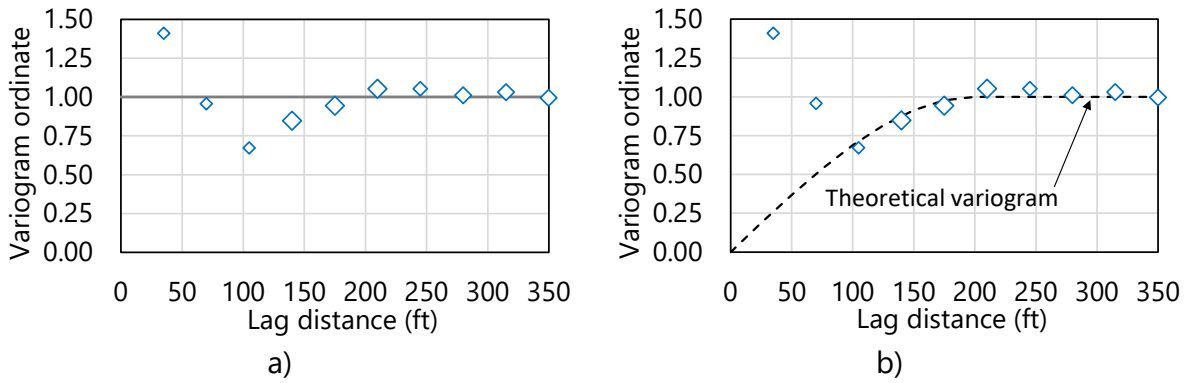


Figure 104. Horizontal variogram for layer 2 (elevation range: -40 ft to -137 ft) with consideration of all Site B boring locations: a) Experimental; b) Experimental with fit

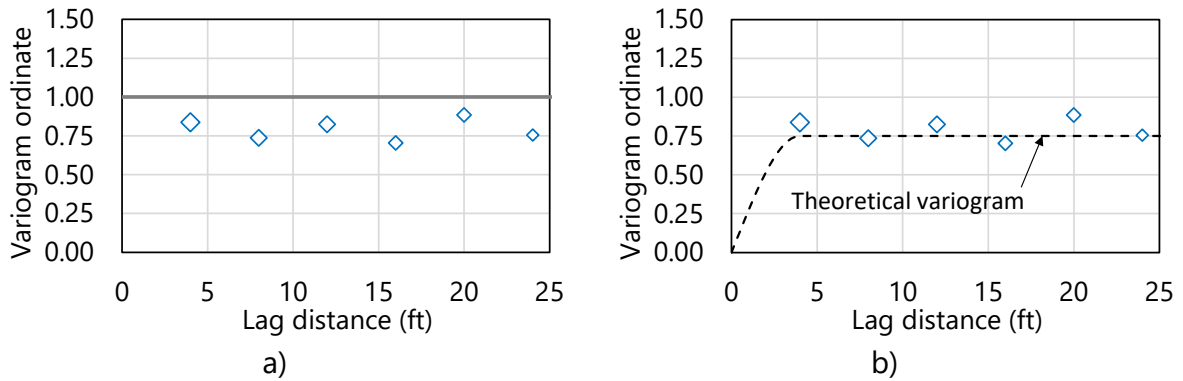


Figure 105. Vertical variogram for layer 2 (elevation range: -40 ft to -137 ft) with consideration of all Site B boring locations: a) Experimental; b) Experimental with fit

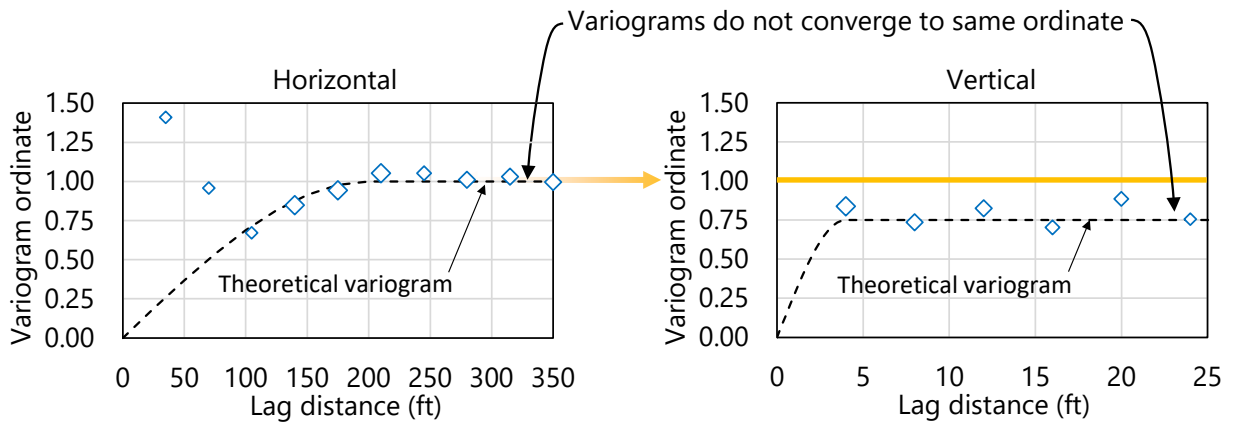


Figure 106. Zonal anisotropy of variograms when all Site B boring locations are considered

Returning to the 90 borings distributed across Site B, differences in the sills of the horizontal and vertical variograms suggest that Site B encompasses multiple geological zones. Therefore, further division of the Site B data, with respect to plan-view positioning, is necessary. As a result, one data subset is defined for each zone (see Sec. 5.6, Sec. 5.7). Summary comparisons of the site-wide and zone-specific data sets are documented in Sec. 5.8.

5.5 Identifying Geological Zones

Three possible means of identifying the need to divide site data into zones are: (1) examination of through-depth scatterplots and histograms of available site data; (2) assessment of the sensitivity to variograms to removal of a subset of boring locations from the variogram formation process; and, (3) identification of variogram phenomena such as zonal anisotropy. Given the presence of zonal anisotropy within the variograms of the Site B data set, further assessment of the available data is carried out to identify distinct geological zones.

Among the 90 borings distributed across Site B, 48 are located along a relatively narrow band of northings (with eastings ranging from 0 ft to approximately 5500 ft). The 48 borings positioned along this "strip" are highlighted in Fig. 107, and are focused upon in the Ch. 5 documentation for modeling of zones. More specifically, to illustrate the process of modeling zone-specific data sets, two distinct zones from within Site B are identified in the following.

Commentary is provided regarding selection of borings that are included in each of the two zones. Also, for each zone, layerings are defined and spatial correlation structures (variograms) are formed. The same general concepts (and overall process) documented below can be applied when investigating and modeling zones in other sites.

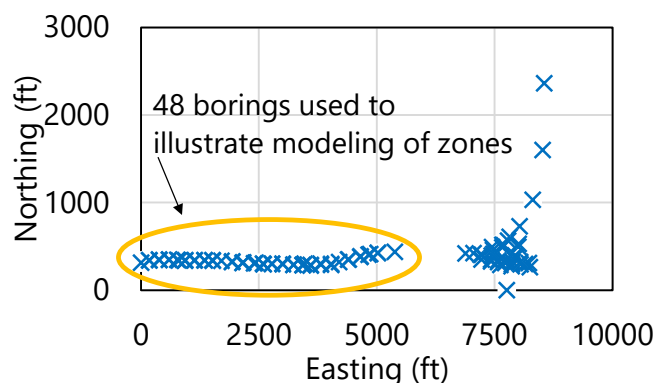


Figure 107. Plan view of Site B boring locations with indication of 48 borings used to illustrate modeling of zones

5.5.1 Recommendation for Model File Handling when Zones are Detected

In general, for each zone identified, it is recommended that a separate GeoStat model be created, where only the boring locations associated with said zone are included for site modeling. A straightforward means for selection of subsets of boring locations is implemented in GeoStat, where data from only those locations are carried forward into site modeling (layer definition and variogram formation) and stochastic simulation processes.

Recalling the Project Information tab (Fig. 87), indication of each boring location that is to be utilized for site modeling and simulation is signified by supplying a value of 1 beneath the Include column (Fig. 87, right). In this way, data from all boring locations across the site can be retained in the zone-specific GeoStat model (if desired). Then, for each identified zone, the associated GeoStat model is configured such that only those boring locations within said zone are assigned a value of 1 beneath the Include column on the Project Information tab.

5.6 Characterizing Site Data for Zone 1

As a practical measure, the "strip" of 48 borings (recall Fig. 107) is divided into two portions, with the leftmost boring locations constituting a candidate zone (referred to as zone 1). This subset of borings is investigated as a candidate, distinct zone by reexamining layering and reforming variograms. Considerations for the remainder of the 48 borings are discussed in Sec. 5.7. As highlighted in Fig. 108, 23 boring locations from within Site B are identified based on visually recognition of clusters of borings in plan-view, followed by practical considerations to divide those clusters into candidate zones. Summarily, the 23 borings making up zone 1 are selected: (1) to illustrate the overall process of modeling zones within a site; and, (2) based on close proximity to one another, or adherence to a plan-view grouping, relative to other boring locations.

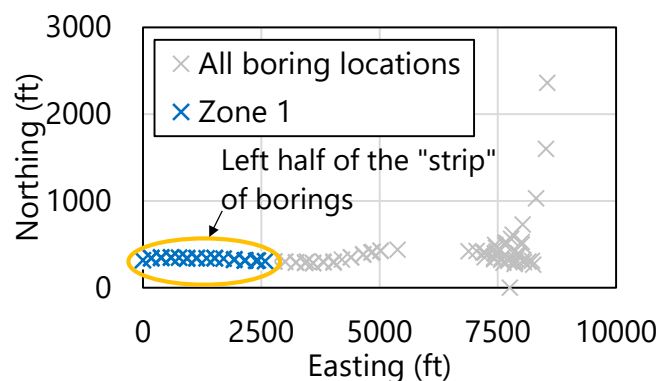


Figure 108. Plan view of Site B boring locations with indication of 23 boring locations that comprise zone 1

In the following, variograms are reformed using the 23 borings selected to comprise zone 1. Subsequently, the variograms pertaining to zone 1 are compared to those previously generated with consideration of all 90 borings from Site B. The effect of isolating the 23 borings, with regard to selecting layer elevations, is also assessed. Detailed comparisons between the site-wide data and zone 1 are presented immediately below. See Sec. 5.8 for summary comparisons between the site-wide and zone-specific data sets.

5.6.1 Defining Soil or Rock Layering for Zone 1

Prior to forming variograms specific to zone 1, the previously defined layering (obtained from examination of all Site B data) is reassessed. The reassessment begins with calculation of the layer summary statistics, but with use of geotechnical site data that are specific to the 23 borings of zone 1. Summary statistics that are obtained when considering all 90 borings of Site B, versus those obtained from the 23 borings making up zone 1, are compared in Table 49.

Table 49. Comparisons of summary statistics for defined layers (all borings versus Zone 1 borings)

Layer	Physical measurement	All			Zone 1		
		Sample size	Mean	COV	Sample size	Mean	COV
1	N/A	N/A	N/A	N/A	N/A	N/A	N/A
2	q_u (tsf)	183	91.5	1.25	48	62	0.80

Recall that a casing is assumed to be present throughout the layer 1 elevation range, and so, no additional considerations are necessary with respect to layer 1. All of the sample size, mean, and COV for layer 2 decrease when transitioning from site-wide analysis to zone 1 analysis. The decrease in COV value corresponds to more favorable (i.e., reduced) estimates of total uncertainty when conducting stochastic simulation. Regardless, further examination of the measured site data within layer 2 is necessary.

5.6.1.1 Layer 2

Scatterplots of the measured q_u values that are positioned within layer 2 (site-wide versus zone 1) are presented in Fig. 109. The q_u values specific to zone 1 begin at an elevation of approximately -50 ft and extend down to approximately 120 ft. Within the range of 100 tsf to 400 tsf, a relatively larger number of measured q_u values are present among the site-wide data (Fig. 109a). Also, the site-wide data set contains many more measured values of q_u that exceed 200 tsf. This difference is reflected in the means (91 tsf versus 62 tsf) and COV values (1.25 versus 0.8). In contrast to the relatively pronounced scatter of the site-wide data, a trend is apparent among the zone 1 data, where q_u values tend to increase with respect to increasing depth (Fig. 109b).

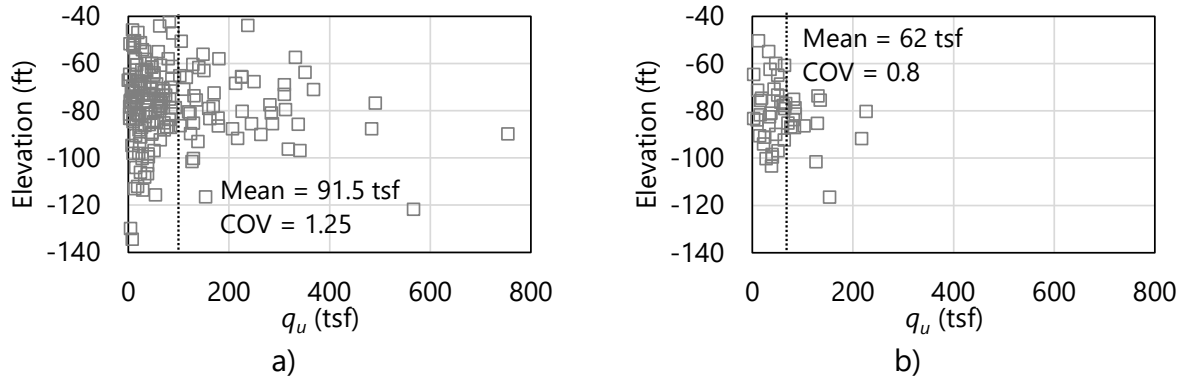


Figure 109. Scatterplots of unconfined compression strength, q_u , values (elevation range: -40 ft to -137 ft) within layer 2: a) All boring locations; b) Zone 1

Histograms of the q_u values pertaining to layer 2, when formed using all 90 borings and when using the 23 borings of zone 1, are presented in Fig. 110. As anticipated, reduced frequency counts are observed for the zone 1 data (Fig. 110b) relative to the site-wide data (Fig. 110a). While the histogram associated with zone 1 (Fig. 110b) qualitatively retains a log-normally distributed shape, the right skew is much less pronounced than that of the histogram for the site-wide data. The less pronounced skew is signified by the relative reduction in both the mean value and COV (recall Table 49).

Based on comparisons of the scatterplots and histograms, two modifications are made to the layer 2 definition: (1) the top and bottom elevations are updated; and, (2) linear detrending is carried out when forming variograms (where the variogram formation is discussed later). The layer 1 definition remains unchanged as a casing is positioned to the top of layer 2. A summary of the revised layer definitions, specific to zone 1, is given in Table 50. Regarding unit weights per layer (as required when modeling drilled shafts in GeoStat), no measurements are available among the zone 1 data set. Consequently, the mean and COV values of unit weight, calculated using the site-wide data set, are utilized (recall Table 43).

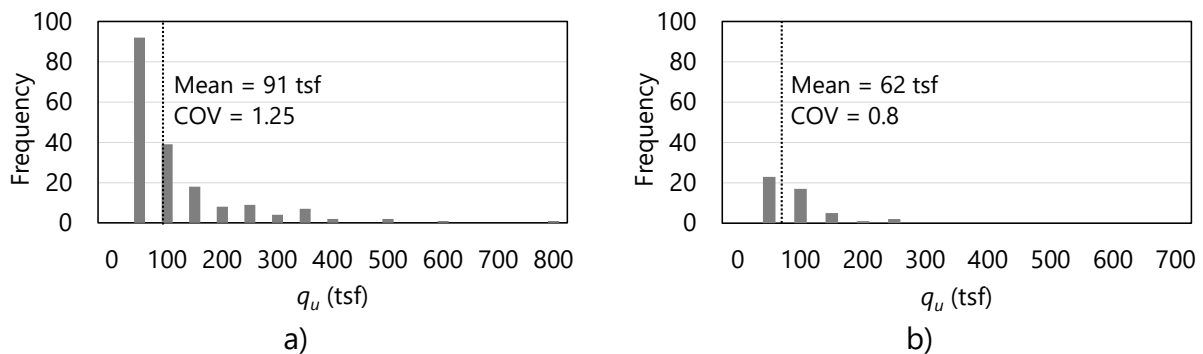


Figure 110. Histograms of unconfined compression strength, q_u , values within layer 2: a) All boring locations; b) Zone 1

Table 50. Selected layer types and elevation ranges for zone 1

Layer	Layer type	Top elevation (ft)	Bottom elevation (ft)
1	Silty sand	3.0	-50.0
2	Limestone	-50.0	-120.0

5.6.2 Selecting Geo-statistical Parameter Values for Zone 1

Having revised the previously defined layer elevations for Site B to reflect the q_u values from the 23 borings of zone 1, the process of forming variograms specific to zone 1 is next undertaken. Recall that a casing is assumed to be present down to the top of layer 2, and so, focus is given to layer 2 in the following discussion. As highlighted in Fig. 108 above, geotechnical data are available for 23 (out of 90) boring locations, and those locations are distributed across a plan-view area of approximately 50 ft by 2500 ft. While the 23 borings constitute a considerable number of locations, no well-formed spatial correlation structures (variograms) are found in the horizontal direction for zone 1. Note that horizontal variograms are not neglected, but rather, worst case conditions (conceptually introduced in Ch. 2) are applicable to the horizontal variograms. More specifically, worst case conditions are assigned to the horizontal variograms only after unsuccessfully iterating upon several trial constructions of the horizontal variograms for zone 1.

As detailed in Ch. 2, unconditional (stochastic) simulation for estimating foundation member axial resistance makes use of spatial correlation structures in the vertical direction, as opposed to variograms in the horizontal and vertical directions. Stated another way, unconditional simulation (discussed later) is elected for zone 1 to avoid the prospect of generating factored axial resistances under worst case conditions (for the horizontal variograms). Therefore, focus is given below to formation of vertical variograms. However, the same general concepts apply for instances where sufficient site data are available to construct both horizontal and vertical variograms for a site.

5.6.2.1 Constructing Variograms for Zone 1

Vertical variogram parameters selected for layer 2, with consideration of the 23 borings making up zone 1, are listed in Table 51 and Table 52. The variogram parameter values are selected in a manner that is, overall, analogous to that detailed previously when considering the site-wide data set (as well as that documented for Example Site A in Ch. 4). The lag distance selected for layer 2 is larger than, but still on the order of, typical lengths for core-run data (5 ft). More broadly, lag distances closer to (or even less than) 5 ft are typical when forming vertical variograms, and should be selected whenever feasible.

Parameter values selected for the vertical variograms of zone 1 (Table 51) differ substantially from respective values selected when considering all 90 borings of Site B (recall Table 45).

Given well-formed vertical variograms for zone 1 (presented below) division of Site B into zones is substantiated by these differences.

Table 51. Layer-specific parameters for vertical variograms of zone 1

Layer	Lag (ft)	Number of lags	Tolerance (ft)	Bandwidth (ft)
1	N/A	N/A	N/A	N/A
2	8	5	4.0	0.0

Table 52. Vertical variogram ranges and sills for zone 1 layers

Layer	Range (ft)	Sill
1	N/A	N/A
2	15.5	1.0

Listings of experimental vertical variogram points for layer 2 are provided in Table 53. Included among the listings are variogram points (and pairs) generated when considering all 90 borings from Site B and when considering the 23 borings from zone 1. Reductions consistently occur in the pair count values when transitioning from the site-wide data to the zone 1 data. This reduction is expected as only 23 boring locations are considered for zone 1, versus the 90 locations that make up the site-wide data. Despite the presence of pair counts below 30 for lag distances approaching 40 ft, the trend in the vertical variogram ordinate values for zone 1 (Table 53) indicate much more clearly distinguishable convergence toward a sill value of 1.

Table 53. Comparison of vertical variogram data for layer 2 when all borings are considered versus when zone 1 borings are considered

Abscissa (ft)	All		Zone 1		
	Ordinate	Pairs	Abscissa (ft)	Ordinate	Pairs
4	0.84	66	8.0	0.77	30
8	0.74	62	16.0	0.96	26
12	0.82	54	24.0	0.95	11
16	0.70	32	32.0	0.89	9
20	0.88	30	40.0	1.03	3
24	0.76	18	--	--	--

Comparative plots of the experimental, vertical variograms (all borings versus zone 1 borings) are presented in Fig. 111. Additionally, the variogram ordinate value of 1.0 is visually emphasized in each plot. Visual comparison of the vertical variogram points (Fig. 111a, Fig. 111b) reveals that the zone 1 variogram converges to unity while the site-wide variogram converges to a value less than unity (0.75). The vertical variogram associated with layer 2 (of zone 1) is generated with linear detrending of the q_u values (recall Fig. 109b), and is replotted in Fig. 112. The act of detrending tends to reduce the COV of the data set. In this case, the

COV (i.e., the standard deviation of the detrended data divided by the mean of the physical measurements) marginally reduces the COV value for layer 2, from 0.80 to 0.78.

The fitted theoretical variogram is of exponential form (as opposed to spherical) as the exponential expression (defined in Ch. 2) better conforms to the experimental variogram points. The range value associated with the theoretical variogram of zone 1 (15.5 ft in Fig. 112) is smaller than the largest abscissa value generated for the experimental variogram (40 ft). This serves to verify that a sufficient number of lag distances are specified as listed in Table 51 above.

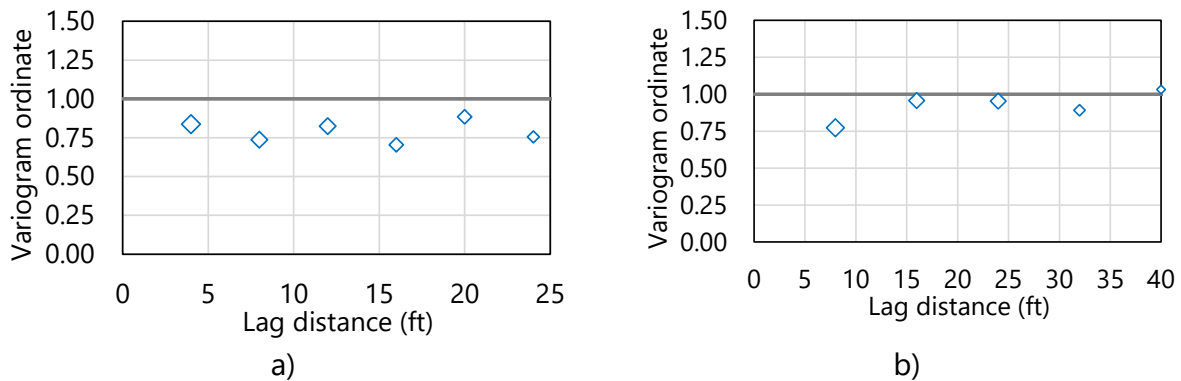


Figure 111. Comparison of vertical variogram points for layer 2: a) All borings; b) Zone 1

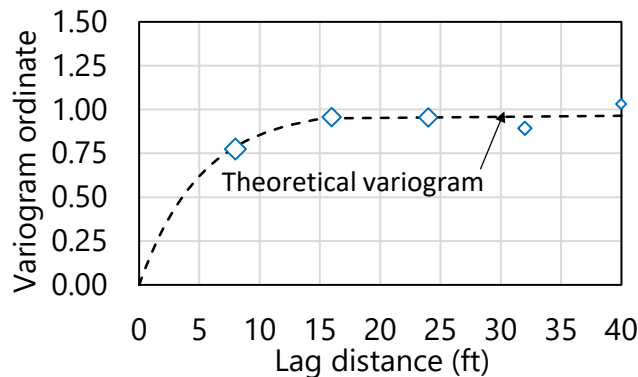


Figure 112. Vertical variogram for layer 2 of zone 1 (elevation range: -50 ft to -120 ft)

Given the well-formed vertical variogram for layer 2 of zone 1, which converges at a sill value of unity, it is reasonable to divide Site B into distinct geological zones. The process of defining and assessing various spatially varying quantities (layers, variograms) for other potential zones within Site B is analogous to that detailed above for zone 1. Discussed immediately below is utilization of similar concepts, relative to those applied above, to investigate an additional zone within Site B. Subsequently, the site-wide and zone-specific variograms are compared

in Sec. 5.8. Further, in Sec. 5.9, data sets for zone 1 and zone 2 are utilized to perform stochastic simulations, and ultimately, compute zone-specific estimates of factored axial resistances for drilled shaft foundations.

5.7 Characterizing Site Data for Zone 2

Recall from Fig. 107 that a “strip” of 48 borings from Site B is divided into two portions, with the 23 leftmost boring locations constituting zone 1. Considerations for the remainder of the 48 borings are discussed throughout Sec. 5.7, where these 25 borings comprise zone 2 (Fig. 113). The 25 borings making up zone 2 are selected: (1) to provide a second illustration of the overall process of modeling zones within a site; and, (2) based on close proximity to one another, or adherence to a plan-view grouping, relative to other boring locations of Site B.

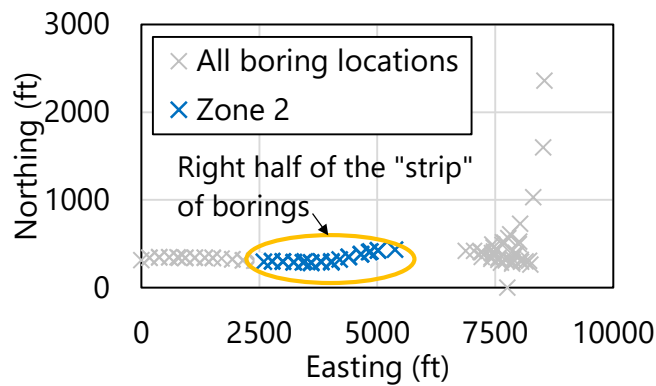


Figure 113. Plan view of Site B boring locations with indication of 25 boring locations that comprise zone 2

In the following, variograms are reformed using the 25 borings selected to comprise zone 2. Subsequently, the variograms pertaining to zone 2 are compared to those previously generated with consideration of all 90 borings across Site B. The effect of isolating the 25 borings, with regard to selecting layer elevations, is also assessed in the following. Here, again, comparisons are made relative to layer definitions associated with the site-wide data. See Sec. 5.8 for comparisons between the site-wide, zone 1, and zone 2 data sets.

5.7.1 Defining Soil or Rock Layering for Zone 2

Prior to forming variograms specific to zone 2, the initial layering definitions produced from examination of all Site B data are reassessed. This reassessment begins with calculation of the layer summary statistics, but with use of geotechnical site data that are specific to the 25 borings of zone 2. Summary statistics that are obtained when considering all 90 borings of Site B, versus those obtained from the 25 borings making up zone 2, are compared in Table 54.

Recall that a casing is assumed to be present throughout the layer 1 elevation range, and so, no additional considerations are necessary with respect to layer 1. All of the sample size, mean, and COV for layer 2 decrease when transitioning from site-wide analysis to zone 2 analysis. The decrease in COV value is not as substantial as that attributed to zone 1 (recall Table 50), and ideally should fall at or below a value of approximately 1.0. Even so, the COV for zone 2 corresponds to more favorable (i.e., reduced) estimates of total uncertainty when conducting stochastic simulation. Especially because the value of COV is greater than 1.0 when considering the zone 2 data set, further examination of the measured site data within layer 2 is necessary.

Table 54. Comparisons of summary statistics for defined layers (all borings versus Zone 2 borings)

Layer	Physical measurement	All			Zone 2		
		Sample size	Mean	COV	Sample size	Mean	COV
1	N/A	N/A	N/A	N/A	N/A	N/A	N/A
2	q_u (tsf)	183	91.5	1.25	46	63	1.15

5.7.1.1 Layer 2

Scatterplots of the measured q_u values that are positioned within layer 2 (site-wide versus zone 2) are presented in Fig. 114. Within zone 2, q_u values begin at an elevation of approximately -45 ft and extend down below -100 ft. Within the range of 100 tsf to 400 tsf, a considerably larger number of measured q_u values are present among the site-wide data (Fig. 114a). Also, the full data set of Site B contains many more measured values of q_u greater than approximately 150 tsf. Consequently, both the mean and COV of the site-wide data (91.5 tsf, 1.25) exceed those of zone 2 (63 tsf, 1.15). In contrast to the relatively pronounced scatter of the site-wide data, a more pronounced trend is apparent among the zone 2 data, indicating an increase (despite still discernible scatter) with respect to increasing depth (Fig. 114b).

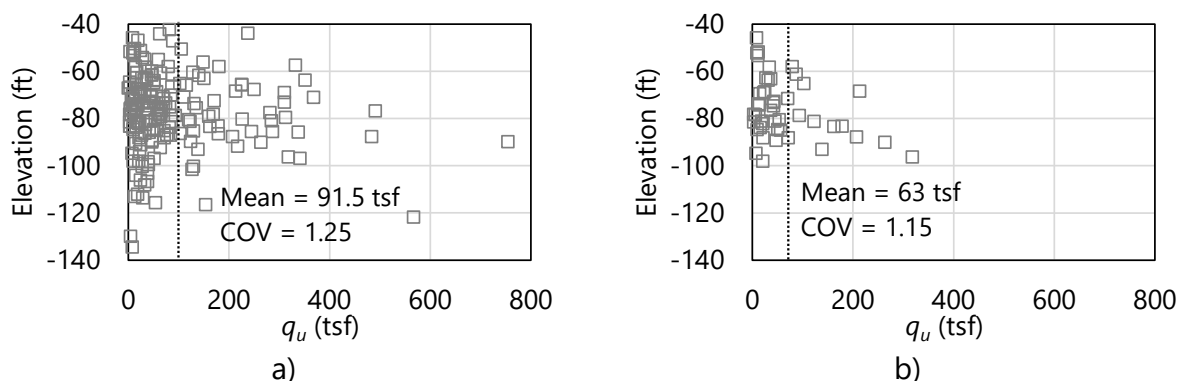


Figure 114. Scatterplots of unconfined compression strength, q_u , values within layer 2: a) All boring locations; b) Zone 2

Histograms of the q_u values pertaining to layer 2, when formed using all 90 borings and when using the 25 borings of zone 2, are presented in Fig. 115. As anticipated, reduced frequency counts are observed for the zone 2 data (Fig. 115b) relative to the site-wide data (Fig. 115a). While the histogram associated with zone 2 (Fig. 115b) qualitatively retains a log-normally distributed shape, the right skew is much less pronounced than that of the histogram for the site-wide data. The less pronounced skew is signified by the relative reduction in both the mean value and COV (recall Table 54).

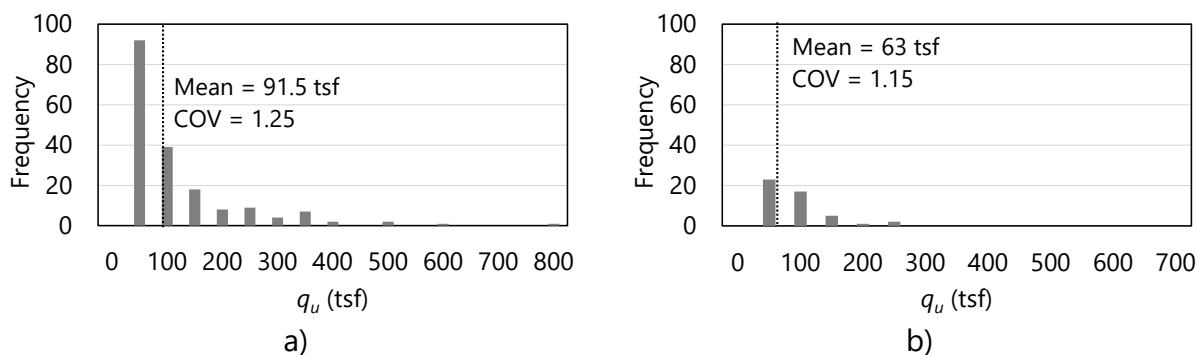


Figure 115. Histograms of unconfined compression strength, q_u , values within layer 2: a) All boring locations; b) Zone 2

Table 55. Selected layer types and elevation ranges for zone 2

Layer	Layer type	Top elevation (ft)	Bottom elevation (ft)
1	Silty sand	9.0	-45.0
2	Limestone	-45.0	-105.0

Based on comparisons of the scatterplots and histograms, two modifications are made to the layer 2 definition: (1) the top and bottom elevations are updated; and, (2) linear detrending is carried out when forming variograms (where the variogram formation is discussed later). The layer 1 definition remains unchanged as a casing is positioned to the top of layer 2. A summary of the revised layer definitions, specific to zone 2, is given in Table 55. Regarding unit weights per layer (as required when modeling drilled shafts in GeoStat), no measurements are available among the zone 2 data set. Consequently, the mean and COV values calculated across the site-wide data set are again utilized for unit weights (recall Table 43).

5.7.2 Selecting Geo-statistical Parameter Values for Zone 2

Having revised the previously defined layer elevations for Site B to reflect the q_u values from the borings of zone 2, the process of forming variograms specific to zone 2 is next undertaken. Recall that a casing is assumed to be present down to the top of layer 2, and so, focus is given to layer 2 in the following discussion. As highlighted in Fig. 113 above, geotechnical data are available for 25 (out of 90) boring locations, and those locations are distributed across a plan-view area of approximately 140 ft by 2700 ft.

Critically, horizontal variograms for zone 2 are not neglected. On the contrary, numerous iterative attempts to construct well-formed horizontal variograms are first undertaken. Having unsuccessfully formed any promising horizontal variograms, and owing to the relatively smaller data set available to zone 2 (relative to the site), worst case conditions are assigned. Furthermore, unconditional simulation (discussed later) is elected for zone 2 to avoid the prospect of generating factored axial resistances under worst case conditions (for the horizontal variograms). Accordingly, focus is given below to formation of well-constructed vertical variograms. Even so, the same general concepts apply for instances where sufficient site data are available to construct both horizontal and vertical variograms for a site.

5.7.2.1 Constructing Variograms for Zone 2

Vertical variogram parameters selected for layer 2, with consideration of the 23 borings making up zone 2, are listed in Table 56 and Table 57. The variogram parameter values are selected in a manner analogous to that detailed previously when considering the zone 1 data set. The lag distance selected for layer 2 (in zone 2) is selected as 2.5 ft, which is on the order of typical lengths for core-run data (5 ft). Selection of this lag distance is typically more desirable than, for example, the relatively large lag distance selected for zone 1 (recall Table 51). The wider set of parameter values selected for the vertical variograms of zone 2 (Table 56) differ substantially from respective values selected when considering all 90 borings of Site B (recall Table 45). Also, the variogram parameters selected for zone 2 differ from those of zone 1 (recall Table 51). Given reasonably well-formed vertical variograms for zone 2 (presented below) division of Site B into zones is further substantiated by such differences.

Table 56. Layer-specific parameters for vertical variograms of zone 2

Layer	Lag (ft)	Number of lags	Tolerance (ft)	Bandwidth (ft)
1	N/A	N/A	N/A	N/A
2	2.5	6	1.25	0.0

Table 57. Vertical variogram ranges and sills for zone 2 layers

Layer	Range (ft)	Sill
1	N/A	N/A
2	5.0	1.0

Listings of experimental vertical variogram points for layer 2 are provided in Table 58. The variogram points for zone 2 are obtained with detrending of the q_u values, where detrending reduces the COV of layer 2 (zone 2) from 1.15 to 1.08. Included among the listings are variogram points (and pairs) generated when considering all 90 borings from Site B and when considering the 25 borings from zone 2. Substantial reductions consistently occur in the pair count values when transitioning from the site-wide data to the zone 2 data. For example, only a single pair is identified at 2.5 ft (this point is effectively neglected). Such reductions are somewhat expected as only 25 borings are considered for zone 2, versus the 90 locations throughout Site B. Despite the presence of pair counts below 30 across all lag distances in zone 2, the trend in the vertical variogram ordinate values for zone 2 (Table 58) indicate convergence toward a sill value equal to unity. As an additional observation, several of the variogram ordinate values exceed unity, which suggests the possible presence of layers in the data set. While insufficient data are available to explore this layering for zone 2, test methods such as MWD may facilitate such refinements for shaft portions in rock.

Table 58. Comparison of vertical variogram data for layer 2 when all borings are considered versus when zone 2 borings are considered

All			Zone 2		
Abscissa (ft)	Ordinate	Pairs	Abscissa (ft)	Ordinate	Pairs
4	0.84	66	2.5	0.13	1
8	0.74	62	5.0	1.19	18
12	0.82	54	7.5	1.23	9
16	0.70	32	10.0	1.04	11
20	0.88	30	12.5	1.10	4
--	--	--	15.0	0.88	9

Comparative plots of the vertical variograms from all of Site B to those of zone 2 are presented in Fig. 116. Additionally, the variogram ordinate value of 1.0 is visually emphasized in each plot. Visual comparison of the vertical variogram points (Fig. 116a, Fig. 116b) reveals that the zone 2 variogram appears to converge toward unity while the site-wide variogram converges to approximately 0.75. The vertical variogram associated with layer 2 (of zone 2) is replotted in Fig. 117, along with the fitted (spherical) theoretical variogram. The range value associated with the theoretical variogram of zone 2 (5.0 ft) is smaller than the largest abscissa value

generated for the experimental variogram (15 ft). This serves to verify that a sufficient number of lag distances are specified as listed in Table 58 above.

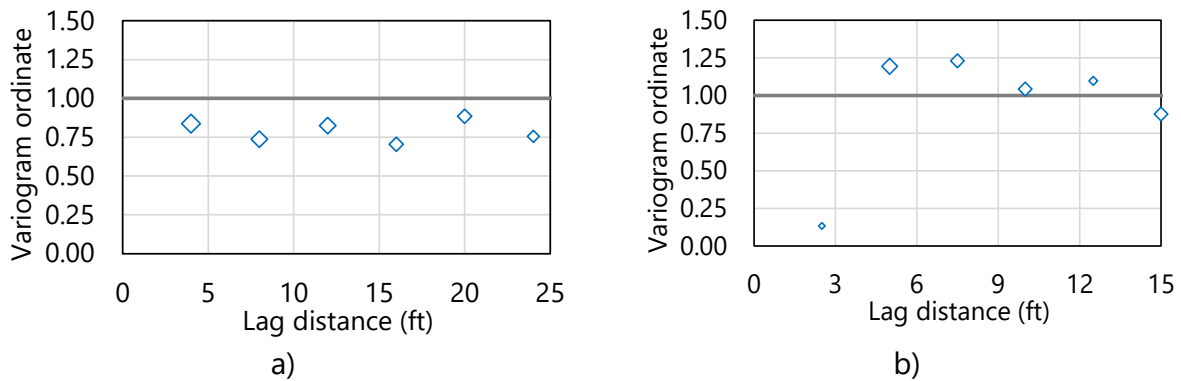


Figure 116. Comparison of vertical variogram points for layer 2: a) All borings; b) Zone 2

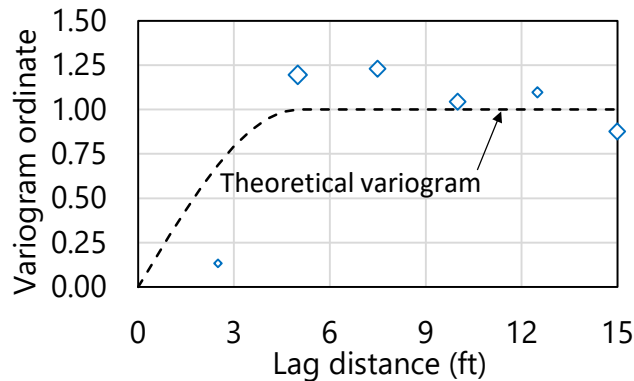


Figure 117. Vertical variogram for layer 2 of zone 2

5.8 Observations Regarding Zonal Issues

Summary comparisons of the site-wide, zone 1, and zone 2 layer data (including variograms) are discussed in the following. These comparisons make clear the need to divide the Site B data set into zones. As demonstrated later in Sec. 5.10, differences in resistance profiles—obtained by performing stochastic simulation for each of zone 1 and zone 2—further substantiate the need to consider the Site B data on a zone by zone basis.

As justification for dividing the site into zones (from the standpoint of layer statistics and spatial correlation structures), consider Fig. 118 through Fig. 120, and Table 59. Presented in Fig. 118 is a scatterplot of the layer 2 data (q_u) when all borings are considered, along with scatterplots of the zone-specific subsets of q_u values. Although qualitative in nature, visual examination of the overlaid scatterplots reveals the presence of more pronounced scatter, across a wider range of values among the site-wide data. Further, it is evident that groupings

of the q_u values local to zone 1 include q_u values of larger magnitude relative to those of zone 2.

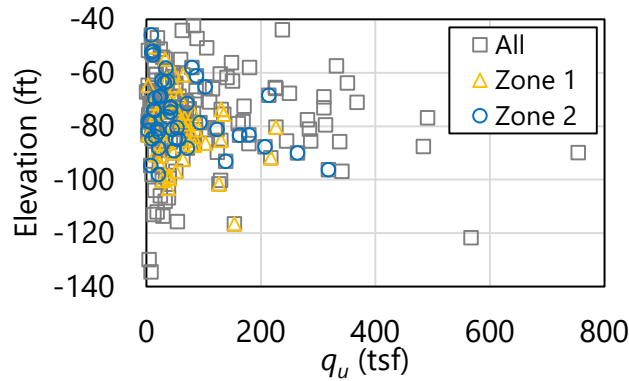


Figure 118. Scatterplots of unconfined compression strength, q_u

Descriptive statistics listed across all borings, zone 1, and zone 2 (Table 59) signify (quantitatively) differences in the three collections of q_u values. For example, the mean of the site-wide values (92 tsf) exceeds those of zone 1 (62 tsf) and zone 2 (63 tsf). Also, while the medians of the site-wide data and zone 1 are equal (50 tsf), that of zone 2 is significantly smaller (37 tsf). Further, consistent with the overlaid scatterplots (Fig. 118), the dispersion attributed to the site-wide data (with variance of 13020 tsf²) is far greater than that of zone 1 (2477 tsf²). In turn, the variance of zone 1 is approximately half of that for zone 2 (5304 tsf²). Relative dispersions (i.e., COV values) are comparable between the site-wide data and zone 2 (both exceed 1), while that of zone 1 is relatively smaller (0.8).

Table 59. Summary statistics for layer 2

Borings	Mean (q_u , tsf)	Median (q_u , tsf)	Variance (tsf ²)	COV
All (90)	92	50	13020	1.25
Zone 1 (23)	62	50	2477	0.80
Zone 2 (25)	63	37	5304	1.15

Such widespread differences in the descriptive statistics correspond to differences in the distributions of q_u values. Presented in Fig. 119 are histograms of the layer 2 data associated with all borings, zone 1, and zone 2. To facilitate visual comparisons, the range of q_u values considered is constrained between 25 tsf and 200 tsf. Ordinates consist of relative frequencies because, expectedly, frequency counts associated with the site-wide data (90 borings) far exceed those of zone 1 (23 borings) and zone 2 (25 borings).

Visual examination of the relative frequencies in Fig. 119 makes apparent that significant fractions of the q_u values within the site-wide data set, as well as those of zone 2, are of magnitudes less than approximately 37.5 tsf. For zone 2, this is the case for nearly half of the

constituent q_u values. In contrast, values are somewhat evenly (but heavily) distributed across a range of values from 0 tsf to approximately 87.5 tsf. Clearly, these three data sets exhibit distinct statistical properties.

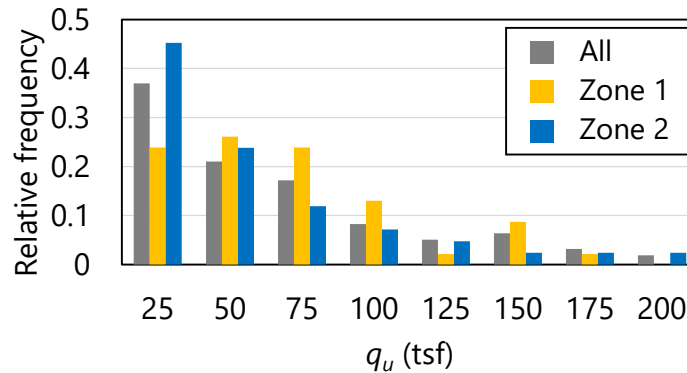


Figure 119. Histograms of unconfined compression strength, q_u , over the range of 25 tsf to 200 tsf

As a culmination of the above discussion, consider the comparative plot of vertical variograms in Fig. 120. Both the experimental variogram points and the theoretical fits are plotted. To facilitate comparisons, the plotted variogram ordinates are not normalized, while the lag distances are normalized (i.e., variogram abscissa values are divided by the maximum abscissa value from the respective set of experimental variogram points). For all variograms, the sill values converge (or should converge) to the variances of the layer data (recall Table 59). As a telling exception, the vertical variogram associated with all borings does not converge to the site-wide variance. This is a strong indicator of zonal issues among the site-wide collection of boring data. Furthermore, the variograms for zone 1 and zone 2 both converge to unique variance values, which are of smaller magnitude than the site-wide variance (as well as that associated with all borings). Therefore, it is concluded that the Site B data set must be divided into zones in order to make representative estimates of axial resistances for deep foundation members.

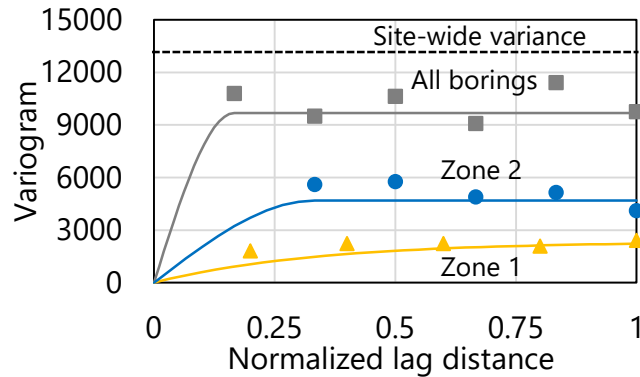


Figure 120. Vertical variograms for layer 2

5.9 Performing Stochastic Simulation

Having established the need to divide Site B into zones, and further, having defined representative layerings and vertical variograms for geotechnical data within zone 1 and zone 2 of Site B, stochastic simulation of axial resistance is carried out in GeoStat as the next major step. In the remainder of Ch. 5 results obtained from stochastic simulation of the zone 1 and zone 2 data sets are documented (and compared). Differences present among the two sets of results clearly demonstrate the need, and value, of dividing sets of site data into zones when appropriate.

Shown in Fig. 121 is the fourth of seven tabs (from left to right) in the GeoStat UI, referred to as the Simulation tab. Data displayed in Fig. 121 corresponds to the zone 1 model. Discussed below are selections made for relevant foundation member parameters specific to zone 1 and zone 2, as well as initial considerations for carrying out the two sets of simulations (again, one set for zone 1 and one set for zone 2).

5.9.1 Selecting Embedment Ranges and Intervals

One drilled shaft foundation member is investigated in association with each of zone 1 and zone 2 from Site B. For the shaft of zone 1, embedment lengths ranging from 55 ft to 110 ft are simulated, where these depths correspond to elevations of -50 ft and -105 ft. For the shaft of zone 2, embedment lengths ranging from 54 ft (elevation of -45 ft) to 114 ft (elevation of -105 ft) are simulated.

Across all shaft lengths considered, an embedment interval of 1 ft is selected. This signifies, for example, that axial resistances in zone 1 are to be computed in 1-ft intervals between the 55-ft and 110-ft embedment range. Interval lengths that are small relative to the layer heights are generally recommended for conducting simulations in GeoStat.

The ground surface elevation is assigned as 5 ft for zone 1 and 9 ft for zone 2. Water table elevations, respectively are assigned as 0 ft and 3 ft for zone 1 and zone 2. Candidate shaft configurations for both zone 1 and zone 2 terminate (approximately) at elevations ranging from the top of layer 2, extending near to the bottom of layer 2 (Fig. 122).

The screenshot displays the 'Simulation' tab of a software application. The interface is organized into several sections:

- General Geometry:** Includes input fields for Minimum Length (ft) set to 55, Maximum Length (ft) set to 110, and Increment (ft) set to 1.
- Soil:** Includes Ground Surface Elevation (ft) set to 5.00 and Water Table Elevation (ft) set to 0.
- Layer Separation:** Features three radio button options: Soil Type 1 (Plastic Clay), Soil Type 2 (Clay and Silty Sand), and Soil Type 5 (Void), with the latter selected.
- Simulation:** Includes radio button options for Conditional and Unconditional, with Unconditional selected. The Number of Simulations is set to 2000.
- Foundation Member Material Properties:** Includes input fields for Ec (ksi) set to 4000, Slump (in) set to 6, Limiting Settlement (%) set to 1, and Unit Weight (pcf) set to 150.
- Simulation Status:** A 'Run Simulation' button is located at the bottom of the interface.

On the right side, a data table is displayed with the following structure:

Layer	Mean	Coefficient of Variation	Variance	Sample Count	Vertical Range	Horizontal Range	Horizontal Sill	Detrend
2	62.02	0.78	2339.05	48	15.54	75.00	1.00	Yes

Below the table, there are two notes:

1. The above table is not editable. The values reflect input and calculations carried out on the Profile and Geostatistics pages.
2. Only those layers that were assigned a 'Completed' status on the Geostatistics page are displayed in the above table.

Figure 121. Simulation tab

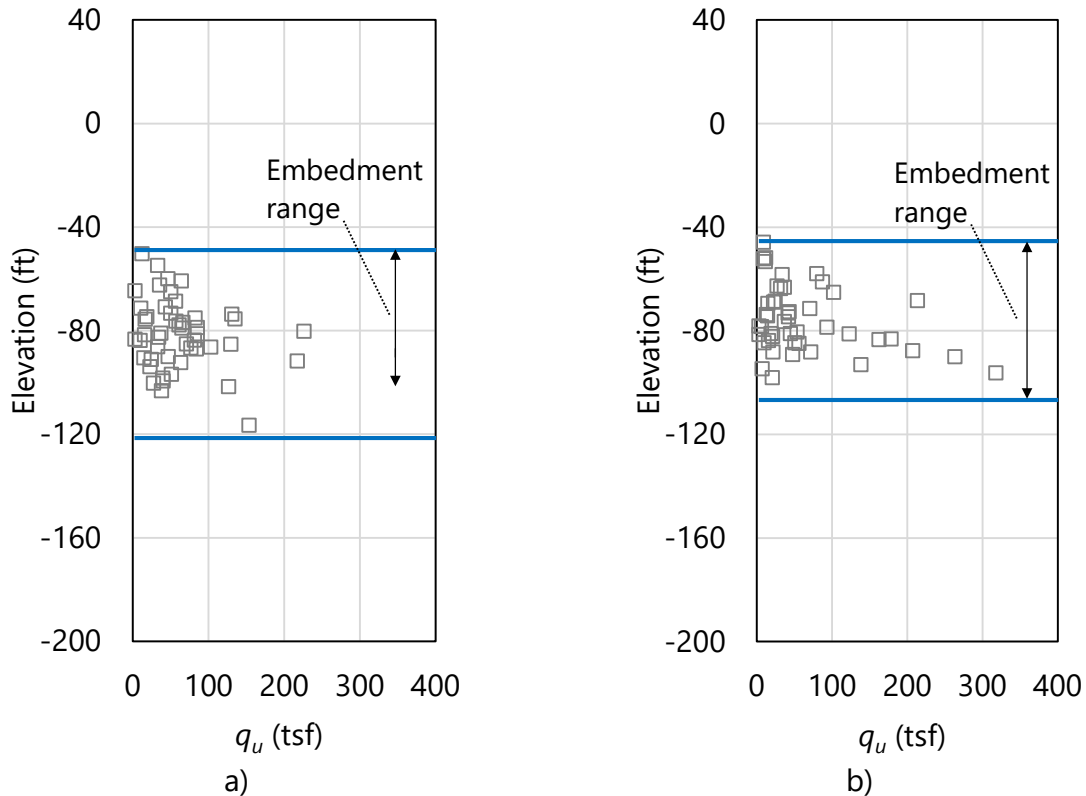


Figure 122. Scatterplots of unconfined compression strength, q_u , with layer divisions (blue horizontal lines): a) Zone 1; b) Zone 2

5.9.2 Foundation Member Cross-Section

The middle-left portion of the Simulation tab (recall Fig. 121) contains input controls that allow for definition of foundation member cross-sections. Because a drilled shaft is being considered for zone 1 and zone 2, only the shaft diameters and casing lengths are necessary to define the cross-section (within the separate model files). Diameters are defined as 41.7 in. for the shafts of zone 1 and zone 2. Casings are also defined in each case, extending down to the top of rock for each zone model. For scenarios where a driven pile is selected as the type of foundation member, required inputs for the cross-section geometry vary by the type of pile being considered (e.g., square, cylindrical, h-pile). Additional details for the required input parameters of driven pile cross-sections are detailed in the Help Manual.

5.9.3 Foundation Member Material Properties

GeoStat UI controls positioned in the bottom-left portion of the Simulation tab (recall Fig. 121) pertain to the definition of the foundation member material properties. For drilled shafts, unit weight (supplied for both zone 1 and zone 2 as 150 lb/ft³) is required. Values of shaft elastic modulus, concrete slump, and limiting shaft settlement are additionally required for drilled shafts. These values, respectively, are input as 4000 ksi, 6 in., and 1% for zone 1;

and, 4000 ksi, 6 in., and 1% for zone 2. Supplying these parameters is only necessary for computing shaft end bearing resistance.

5.9.4 Layer Separation

Included among the simulation parameters input on the Simulation tab (Fig. 121, middle) is selection of a soil type for modeling of layer separations. Recall from Fig. 95 that soil or rock layerings are defined from within the Profile tab of the GeoStat UI. Furthermore, layers can be defined as consisting of one of four possible soil or rock types. For generation of analysis model files during stochastic simulation, the “physical” layers are subdivided into 0.5-ft increments (referred to in this context as sublayers).

A subset of the available layer types may be specified for defining those sublayers that fall at the boundaries of layers that are defined on the Profile tab. For use of the GeoStat software in design applications, it is recommended that these sublayers (or, layer separators) be designated as Soil Type 5 (Void). If it is alternatively desired that layer separations not be designated as Soil Type 5 (Void), then additional properties must be specified as delineated (along with additional contextual discussion) in the Help Manual.

5.9.5 Selecting the Simulation Type

As detailed in Ch. 2, either unconditional or conditional (stochastic) simulation can be conducted using GeoStat software. Unconditional simulation only requires definition of vertical variograms, whereas conditional simulation requires definition of both horizontal and vertical variograms. As discussed previously, unconditional simulation is elected for both the zone 1 and zone 2 models.

When conducting unconditional simulation, only the number of realizations to be generated during simulation must be specified (Fig. 121, bottom-center). For all demonstration cases reported in McVay et al. (2012), the associated number of realizations was set to 2000. Further, Faraone (2014) recommended that a minimum of 1000 realizations be considered when conducting stochastic simulation. For use of GeoStat in design applications, it is recommended that 2000 realizations be considered. However, it can always be verified that further increases in the number of realizations do not lead to appreciable changes in variance for the computed profiles of resistance. Additional considerations for deciding upon the suitable number of realizations for simulation are provided in Ch. 4.

5.10 Viewing Spatial Variability Results

Shown in Fig. 123 is the fifth of seven tabs (left to right) in the GeoStat UI, referred to as the Spatial Variability tab. Results displayed in Fig. 123 correspond to zone 1. This tab is intended for use in viewing profiles of computed axial resistance, where the resistance values take into

account spatial variability phenomena. Plots of spatial resistance are divided into skin friction (side) resistance, end bearing (tip) resistance, and total resistance. For each type of resistance (skin, tip, total), profile plots of the mean, variance, COV, and ϕ (reflecting spatial variability only) are provided.

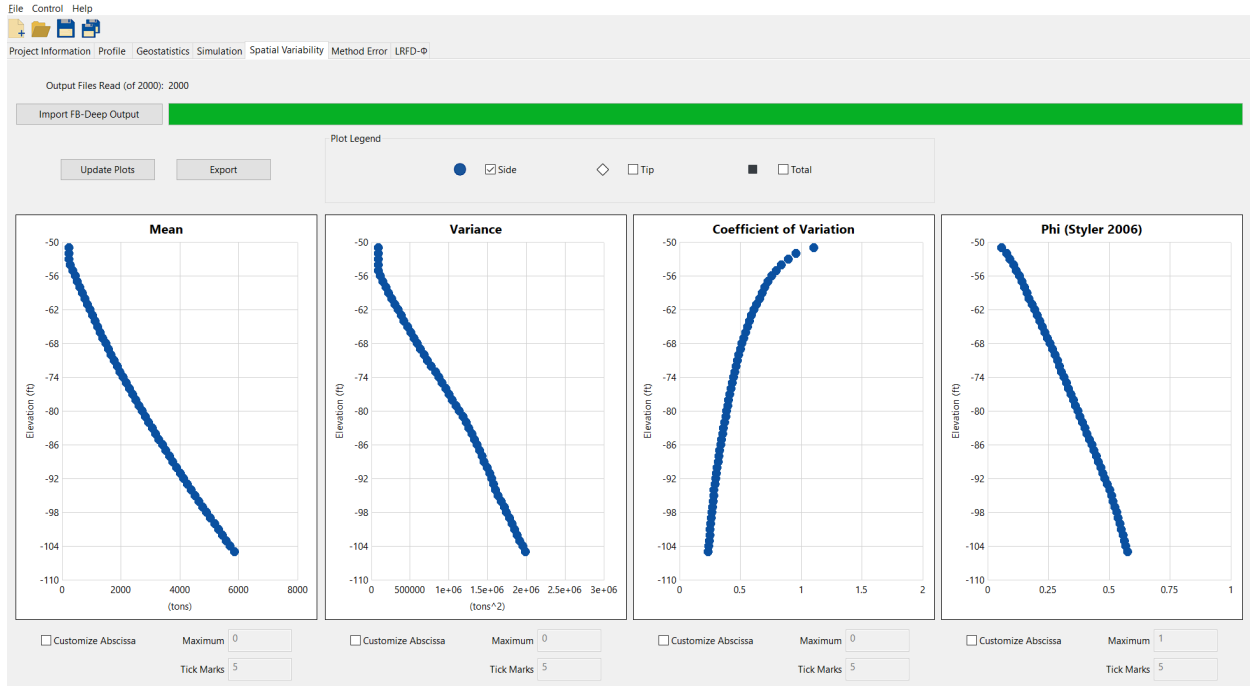


Figure 123. Spatial variability tab

5.10.1 Profiles of Computed Resistance

For both sets of simulation results, physical measurements obtained from test shafts (indicated for each zone in Fig. 124) are available. Also plotted are those borings in closest proximity to the test shaft locations. For zone 1, the constituent borings (Fig. 124a) are roughly positioned to either side of the test shaft location. A similar configuration (with regard to relative positioning) is apparent for the borings comprising zone 2 (Fig. 124b).

Results plots are presented in Fig. 125 for zone 1 and Fig. 126 for zone 2. Namely, profiles of skin and total resistance quantities—obtained from unconditional simulation with 2000 realizations—are displayed. For each shaft configuration and layering considered, skin resistance is clearly the dominant contributor to the mean and variance quantities for total resistance. For the range of zone 1 shaft embeddings, resistance increases (from 0 tons to 5900 tons at -105 ft) roughly in proportion to increasing embedment depth within the limestone layer. The shaft associated with zone 2 also exhibits increasing resistance with increasing depth. However, the maximum resistance reaches a substantially smaller magnitude (4260 tons at -105 ft).

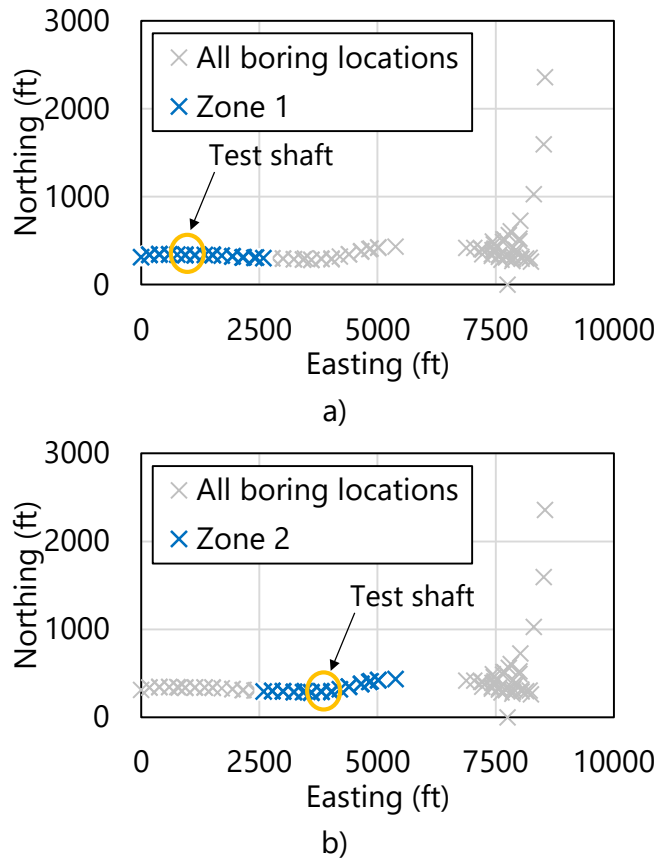


Figure 124. Locations of test shafts in relation to each zone: a) Zone 1; b) Zone 2

Although the shaft for zone 1 possesses the same diameter as that of zone 2 (41.7 in.), it is evident that the limestone in zone 1 allows for relatively greater resistances to be obtained versus that of the limestone in zone 2. Such outcomes would not be discernible without dividing the site into zones, assessing zone-specific spatial variability structures, and then conducting stochastic simulation for each zone.

Regarding computed versus physical measurements, reasonable to favorable comparisons are made between the profiles of computed response and available physical data from the test shaft investigations pertaining to each zone. More specifically, unit side friction quantities are calculated from selected elevation ranges (using the computed profile data), and then compared to corresponding physical data reported among the test shaft results. For zone 1, over the elevation range of -92 ft to -96 ft, the computed profile of side resistance approximately corresponds to 23.5 ksf. The respective value of unit side shear (derived from physical measurements) for the test shaft in zone 1 is 17.5 ksf. As an analogous comparison concerning zone 2, and over the range of -68 ft to -73 ft, the computed results give 12.0 ksf of unit side friction while that of the physical measurements corresponds to 10.4 ksf.

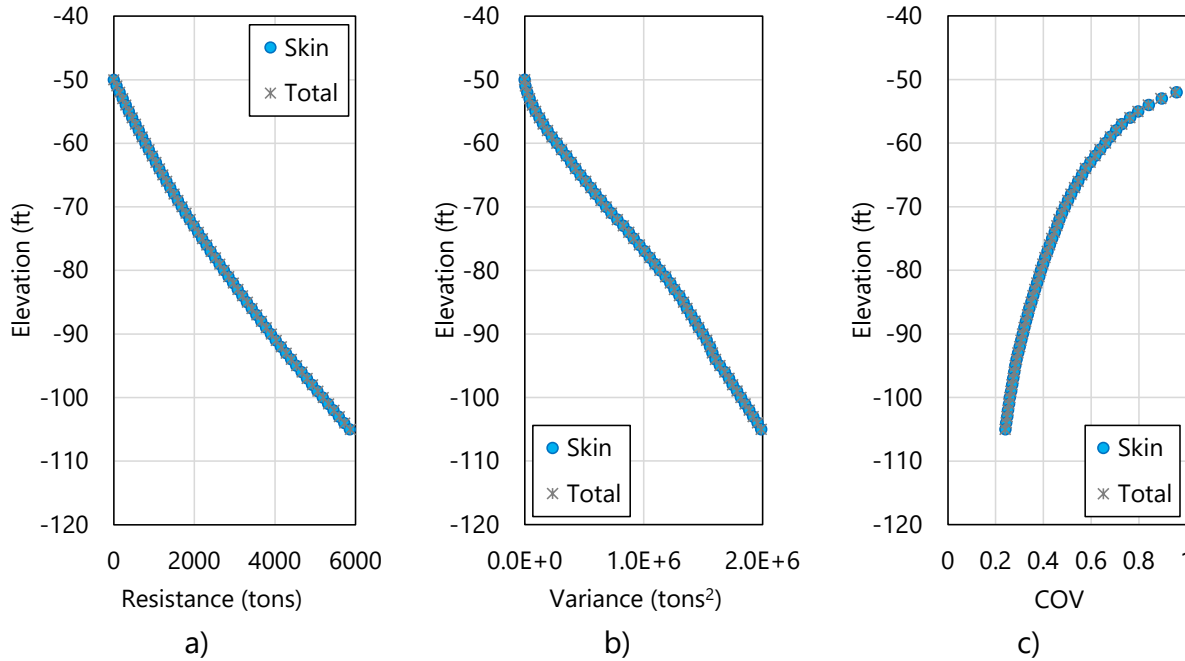


Figure 125. Profile plots obtained from unconditional simulation of zone 1 boring locations with 2000 realizations: a) Mean resistance (spatial variability only); b) Variance; c) COV

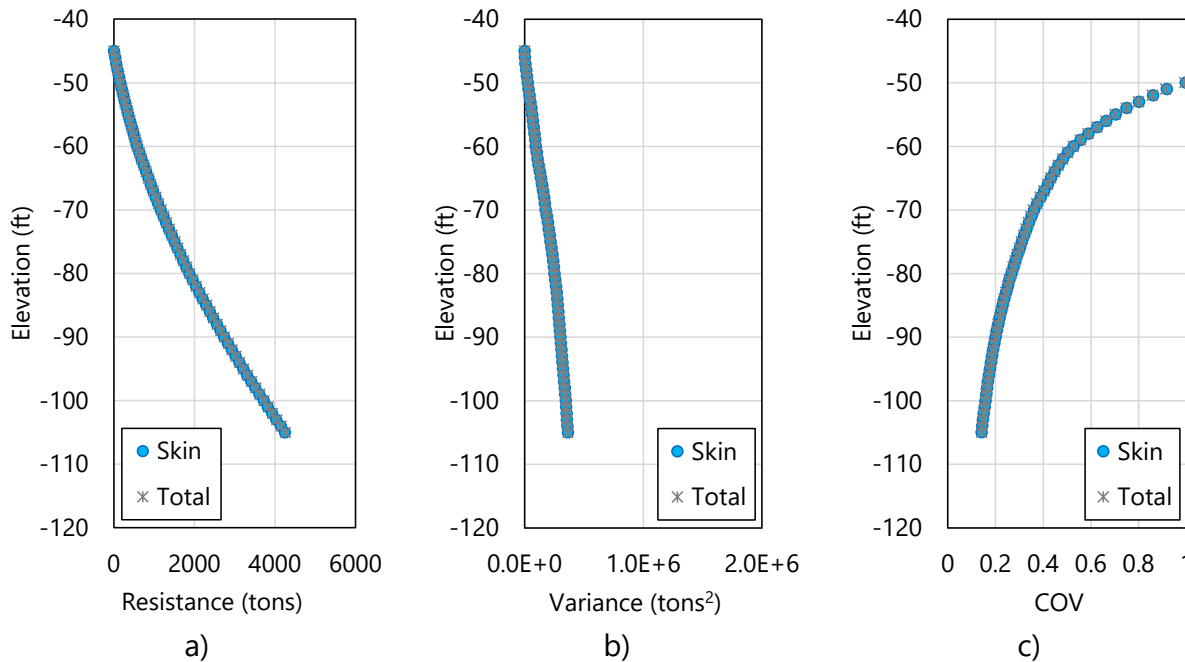


Figure 126. Profile plots obtained from unconditional simulation of zone 2 boring locations with 2000 realizations: a) Mean resistance (spatial variability only); b) Variance; c) COV

Regarding the profiles of variance (Fig. 125b, Fig. 126c), considerably larger magnitudes are computed for zone 1. This is offset though by the relatively larger mean values of resistance computed along the profile of zone 1. Stated another way, for embedment depths corresponding to elevations of approximately -70 ft and below, the COV values associated with each zone are of comparable magnitudes. For the maximum embedments considered, both zones reach COV values of approximately 0.2. As discussed in Ch. 2 and Ch. 3, smaller COV values correspond to relatively larger values of resistance factors, ϕ (and therefore, larger factored resistance values). Therefore, extending the shaft a considerable distance into the limestone layer of each zone (thereby minimizing the associated COVs) may lead to relatively more efficient use of construction materials.

5.10.2 Resistance Factor (ϕ), Spatial Variability Only

Presented in Fig. 127 are profile plots of resistance factors, ϕ , for skin and total resistance, as obtained from unconditional simulation with 2000 realizations. Profile plots are provided for both zone 1 (Fig. 127a) and zone 2 (Fig. 127b). The plotted profiles only take into account spatial variability, as opposed to the total uncertainty associated with combined spatial variability and method error.

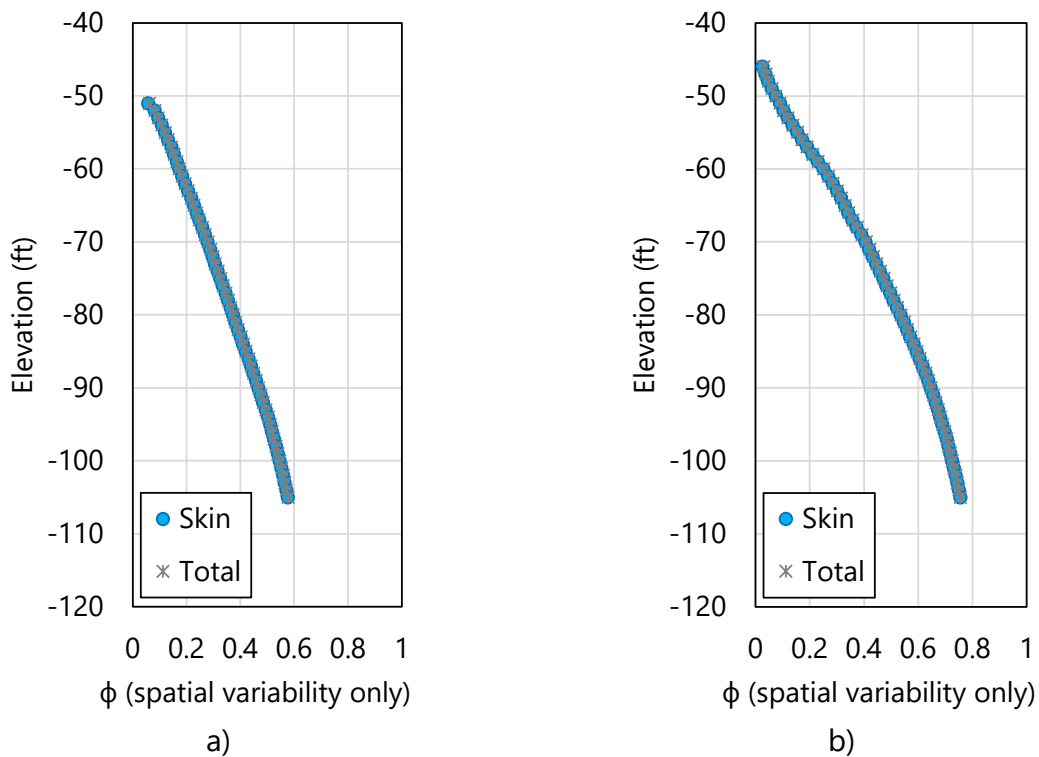


Figure 127. Profile plots of resistance factor, ϕ (spatial variability only), obtained from unconditional simulation with 2000 realizations: a) Zone 1; b) Zone 2

In contrast to the profile of COV values (recall Fig. 125c, Fig. 126c), the profiles of computed resistance factors, ϕ (spatial variability only), generally increase with respect to increasing embedment depth. For zone 1, computed values of resistance factors (ϕ) remain relatively low for embedment depths that fall above elevations of approximately -80 ft (zone 1) or -70 ft (zone 2). For the maximum embedment depth considered, however, the resistance factors (ϕ) for both zone 1 and zone 2 approach a more desirable value of approximately 0.6.

Profiles of resistance factors attributable to spatial variability are contributed to, in part, by two factors: (1) the COV of the layer data; and (2) the range of the variogram. For zone 1, the COV (0.8) is lower than that of zone 2 (greater than 1), but the range assigned to the vertical variogram of zone 1 (15.5 ft) is considerably larger than that of zone 2 (5.0 ft). These two factors offset one another (respectively, in each zone), and as a result, shafts in both zones are able to attain desirable values of resistance factors (ϕ) at maximum embedment depths.

5.10.3 Additional Comparisons of Spatial Variability Results

Accounting for geological zones, isolating the zones, and repeating the variogram modeling efforts is shown to be necessary for the present modeling scenario. Recall (from Table 49) that the COV of the site-wide collection of q_u values in layer 2 is 1.25 while that of q_u values associated with zone 1 is 0.8. The respective COV value for zone 2 is 1.15. The COVs associated with both zone 1 and zone 2 are reduced relative to that of the site-wide data set.

To more fully illustrate the benefit of dividing Site B into zones, consider the two profiles of mean total resistance (spatial variability only) that are plotted in Fig. 128. Here, computed results from zone 1 and zone 2 are plotted together to accentuate comparisons. Clearly, the limestone layer in zone 1 produces greater resistance than that of zone 2.

As one insight into why the two zones produce such different profiles of mean resistance, consider the relative cumulative frequency plots of q_u and q_t in Fig. 129. Recalling Table 49 (for zone 1) and Table 54 (for zone 2), the mean values of q_u for zone 1 (62 tsf) and zone 2 (63 tsf) are of comparable magnitude. However, the distributions of q_u values differ substantially, particularly up to a relative cumulative frequency of 0.75. For example, the median q_u value for zone 1 is 50 tsf, while that of zone 2 is 37 tsf. As detailed in Ch. 2, the distribution of the layer data (e.g., q_u , SPT-N) plays an important role in stochastic simulation (namely, by relating simulated standard normal values to the layer-specific distribution of the physically measured values). Furthermore, the McVay empirical limestone model is used in computing unit side friction ($0.5(q_u q_t)^{0.5}$) for the shafts. Given all of the above, it follows that differences in the distributions of q_u values influence the profiles of (integrated) mean total resistance.

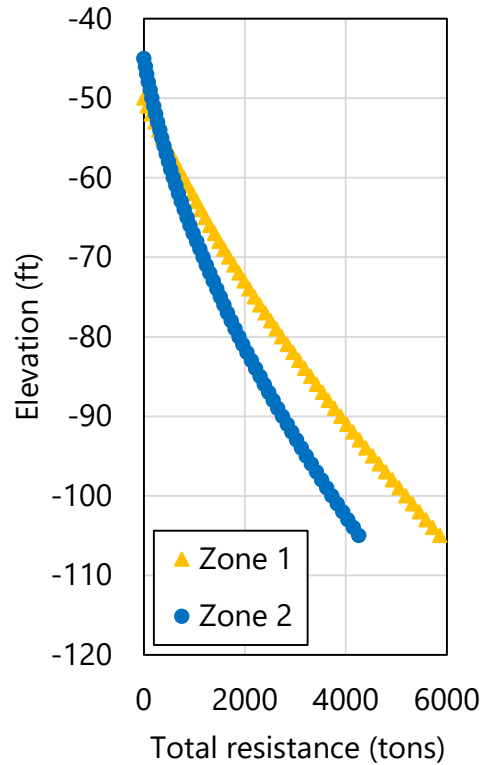


Figure 128. Profile plots of mean resistance (spatial variability only)

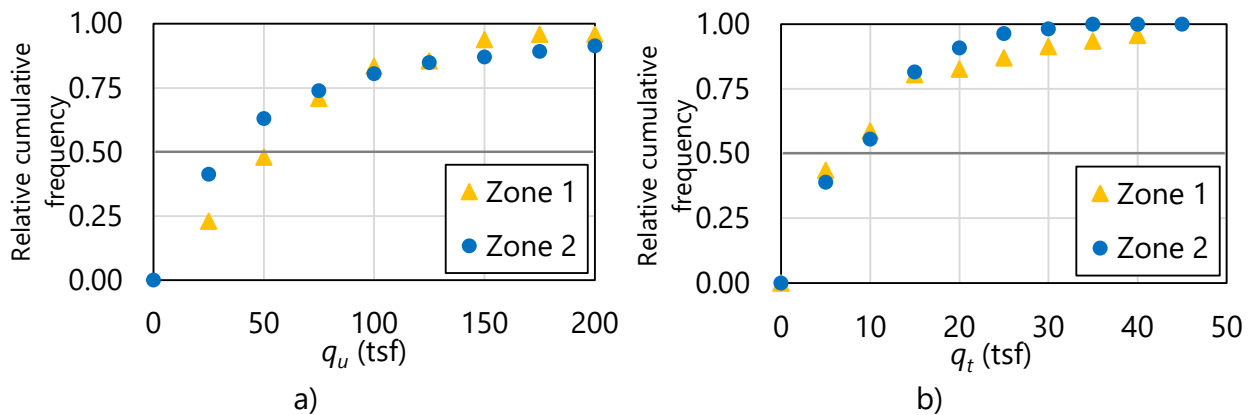


Figure 129. Relative cumulative frequency functions for rock strengths in layer 2: a) q_u ; b) q_t

5.11 Incorporating Method Error

As documented in Ch. 3, two contributors to total uncertainty for estimates of foundation member axial resistance are spatial variability and method error. Method error calculations serve to adjust the "raw" results obtained from stochastic simulation, and in addition, contribute to the calculation of resistance factors (ϕ). In the GeoStat UI, parameters related to method error are specified in the sixth of seven (left to right) program tabs (Fig. 130).

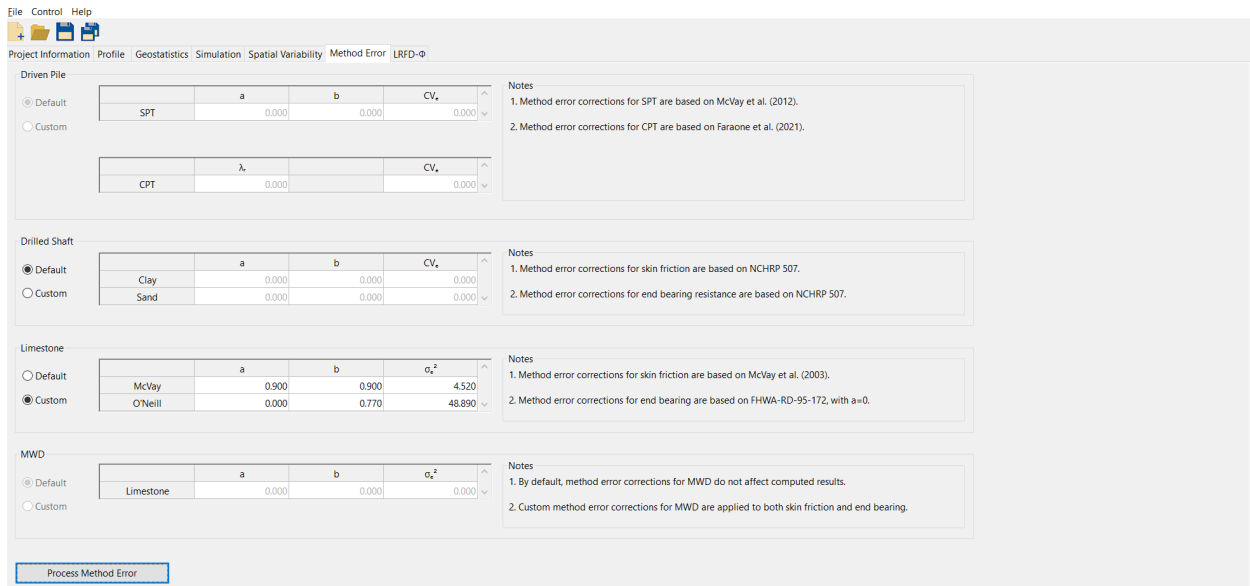


Figure 130. Method Error tab

As also detailed in Ch. 3, characterization of method error phenomena in GeoStat is divided into regression expressions for: driven piles, drilled shafts in clay, drilled shafts in sand, McVay skin friction of drilled shafts in limestone, and O'Neill end bearing for drilled shafts in limestone. Of relevance to both zone and zone 2 are portions of drilled shafts in limestone.

5.11.1 Shaft Portions in Limestone

Regression values pertaining to method error calculations for portions of the drilled shaft embedded in limestone (layer 2) are listed in Table 60 and Table 61. The same regression values are used for both zones. Default regression parameters implemented in GeoStat are utilized for method error calculations associated with skin friction. For end bearing resistance, all parameters are set to match the default values implemented in GeoStat. Of note, the intercept (a) of the regression expression is defined as 0 instead of the value of 20.5 (from O'Neill). This deviation is elected because end bearing only nominally contributes to the total resistance for the Site B analysis (recall Fig. 125, Fig. 126).

Table 60. Method error parameter values for skin friction of shaft portions embedded in limestone

Parameter	Value
a	0.90
b	0.90
σ_e^2	4.52

Table 61. Method error parameter values for end bearing of the shaft in limestone

Parameter	Value
a	0.00
b	0.77
σ_{ϵ}^2	48.89

5.12 Viewing Final Results

Shown in Fig. 131 is the rightmost (seventh) tab in the GeoStat UI. Profile plots located within this tab facilitate viewing of total resistance quantities that reflect spatial variability phenomena as well as computed results associated with total uncertainty (spatial variability and method error combined). The types of profile plot data available for viewing include unfactored resistance (e.g., Fig. 132 for zone 1, Fig. 133 for zone 2); corresponding COV values (Fig. 134, Fig. 135); corresponding resistance factors, ϕ , (Fig. 136, Fig. 137); and, factored resistance (Fig. 138, Fig. 139). All plotted results in Fig. 132 through Fig. 139 are associated with unconditional simulation and 2000 realizations.

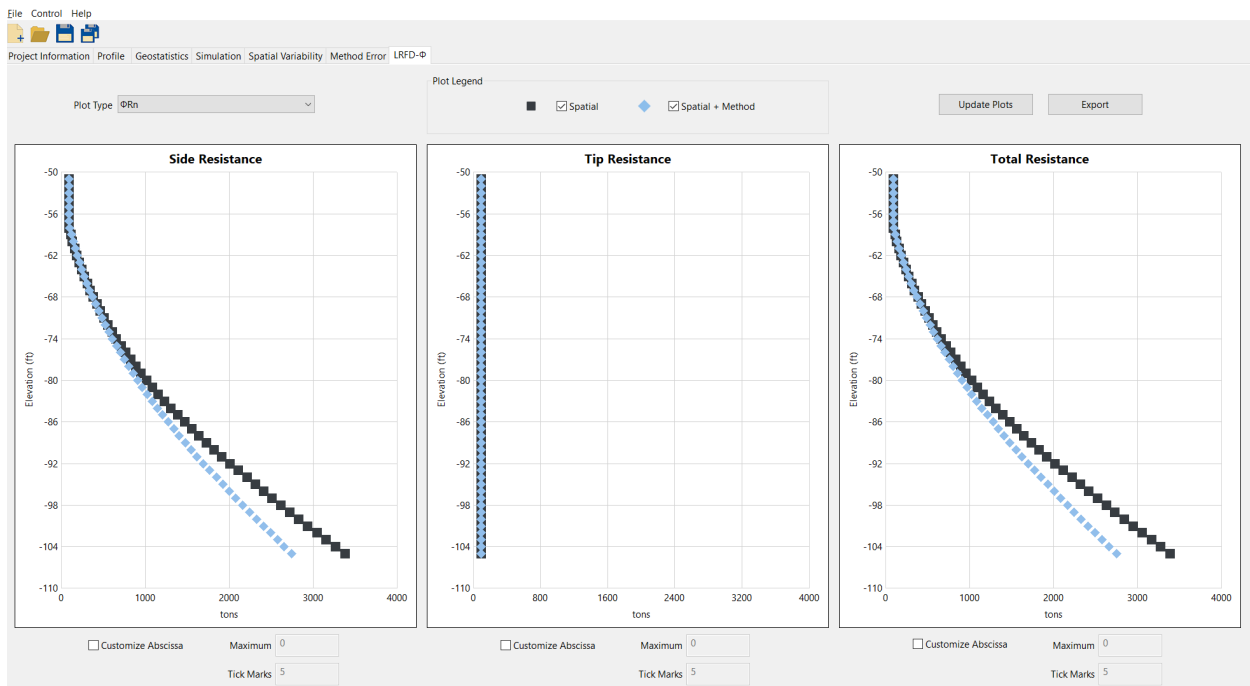


Figure 131. LRFD- ϕ tab for plotting profiles of resistance factors, ϕ , and factored resistances

Trends and phenomena that pertain to the profile plots of mean total resistance, COV, and ϕ values are analogous to those documented above in Sec. 5.10. Of note, however, is that total uncertainty (versus spatial variability alone) tends to more heavily penalize (reduce) computed

resistance values. This phenomenon is present in both the profile plots of unfactored (Fig. 132, Fig. 133) and factored resistance (Fig. 138, Fig. 139).

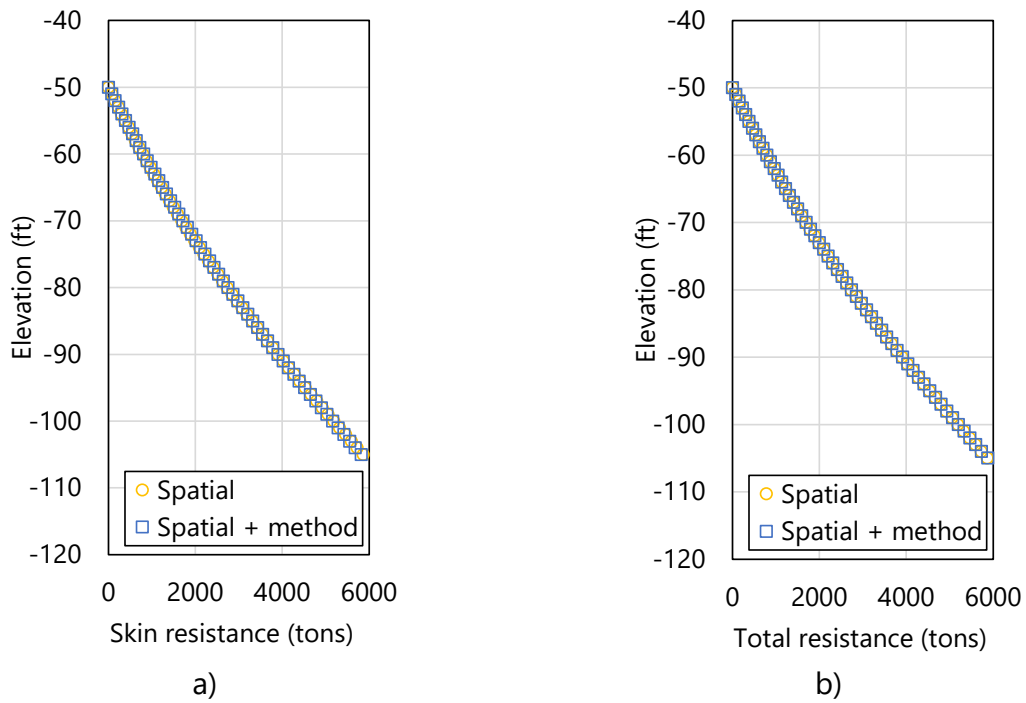


Figure 132. Profile plots of unfactored mean resistance for zone 1: a) Skin; b) Total

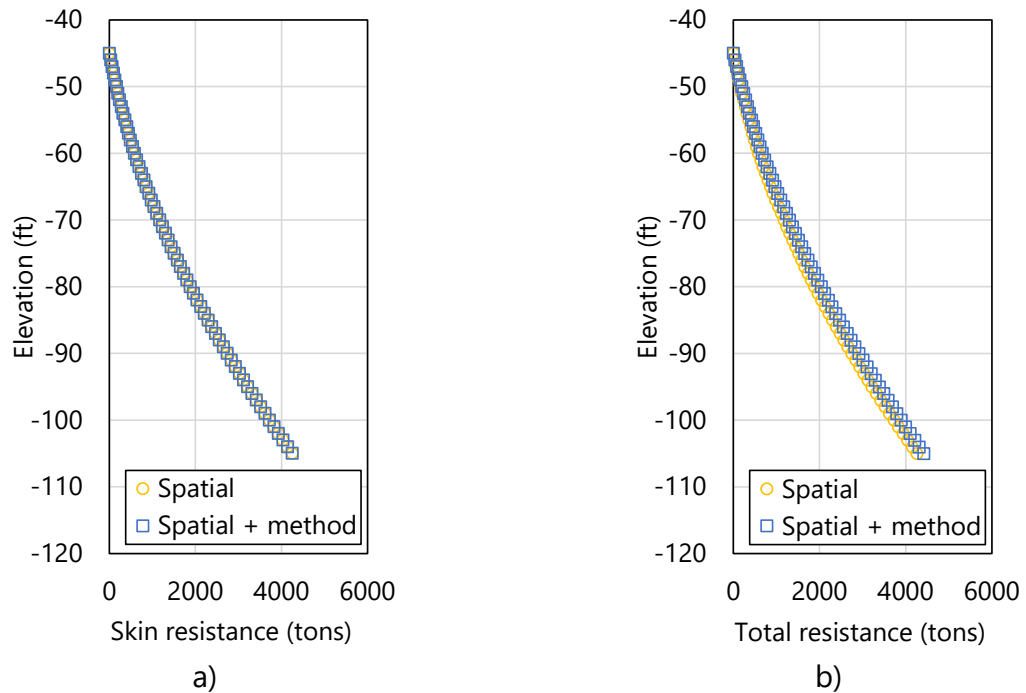
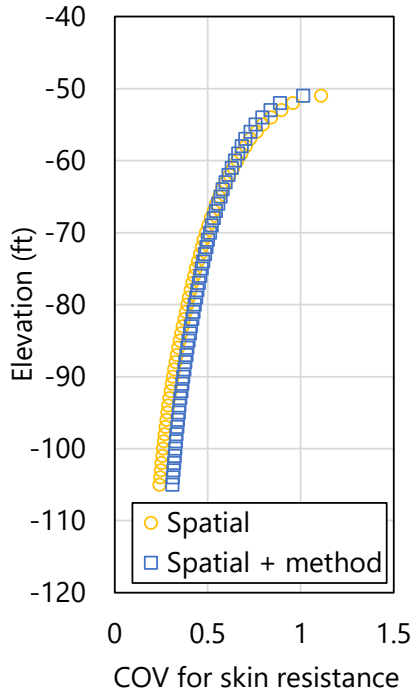
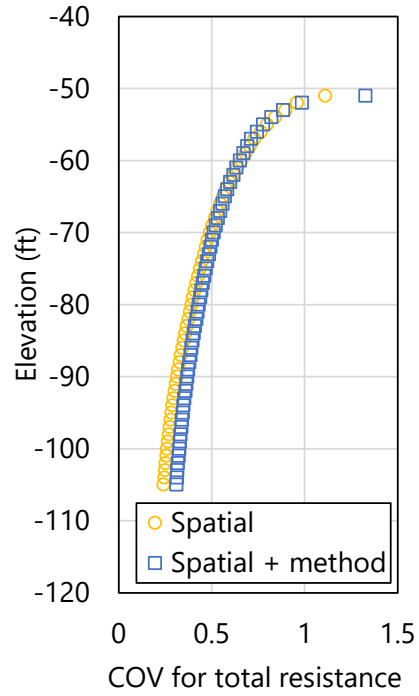


Figure 133. Profile plots of unfactored mean resistance for zone 2: a) Skin; b) Total

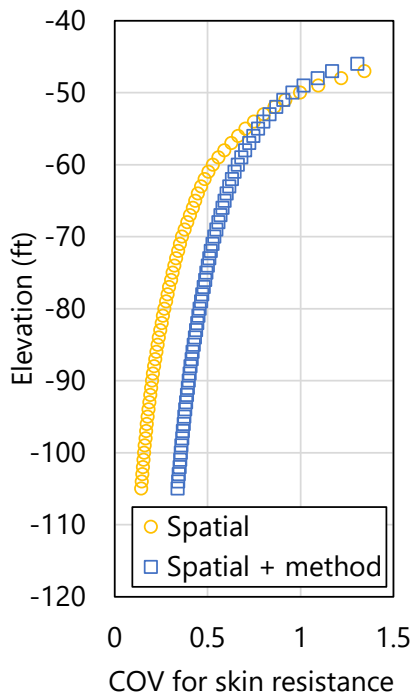


a)

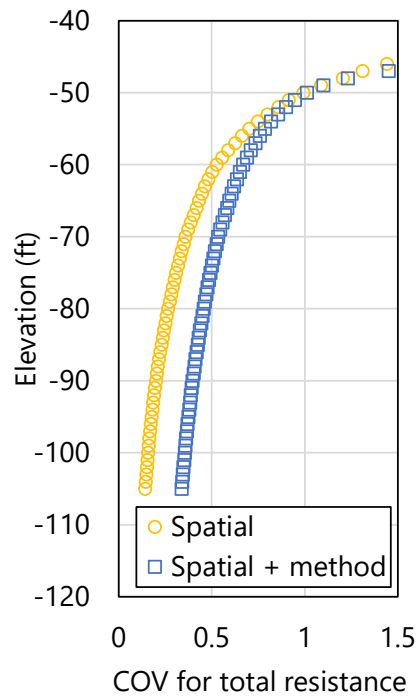


b)

Figure 134. Profile plots of COV for zone 1: a) Skin; b) Total

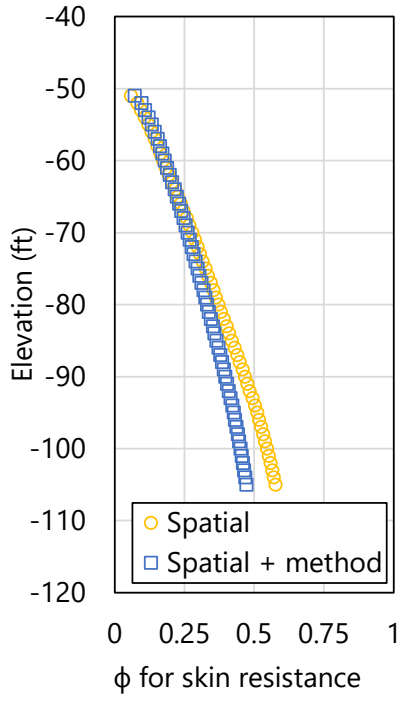


a)

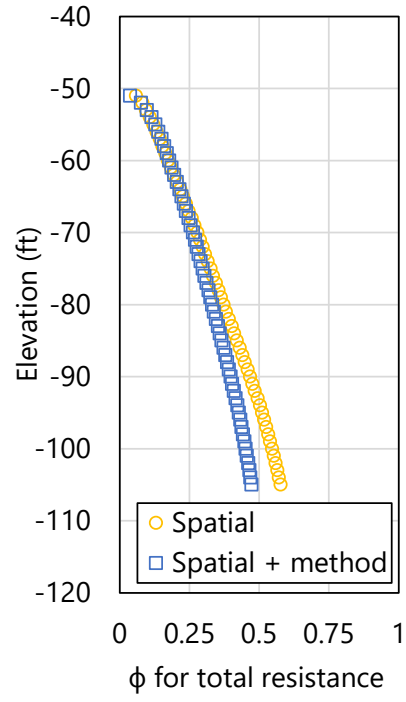


b)

Figure 135. Profile plots of COV for zone 2: a) Skin; b) Total

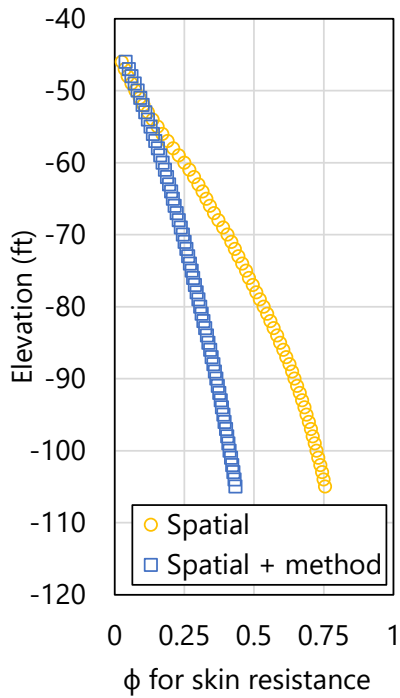


a)

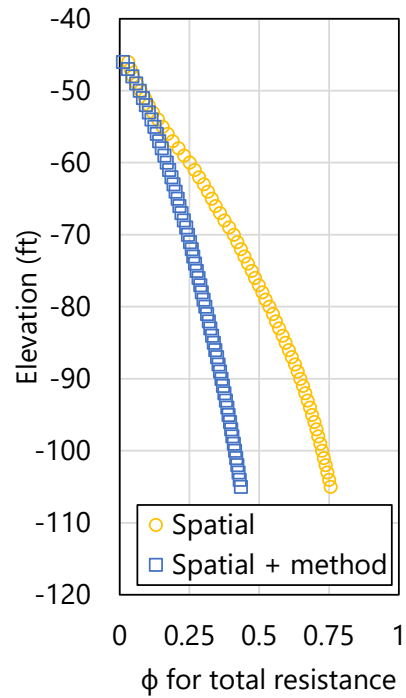


b)

Figure 136. Profile plots of resistance factor, ϕ for zone 1: a) Skin; b) Total

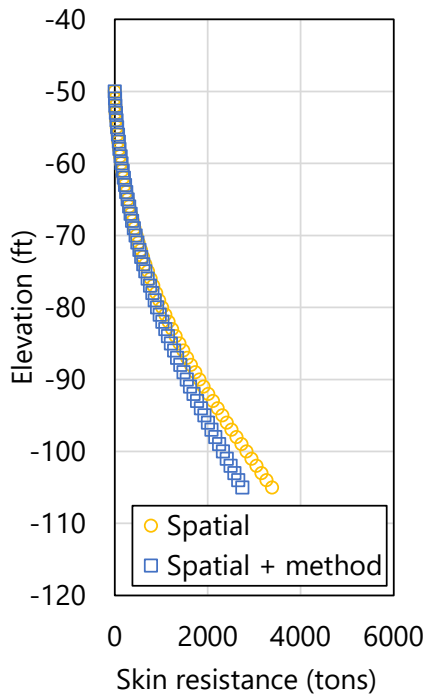


a)

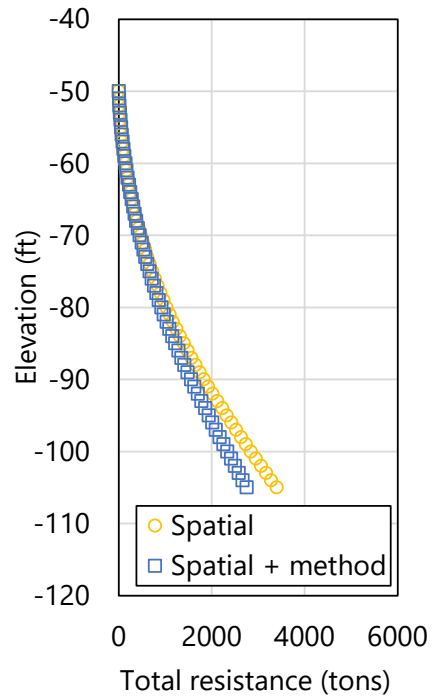


b)

Figure 137. Profile plots of resistance factor, ϕ for zone 2: a) Skin; b) Total

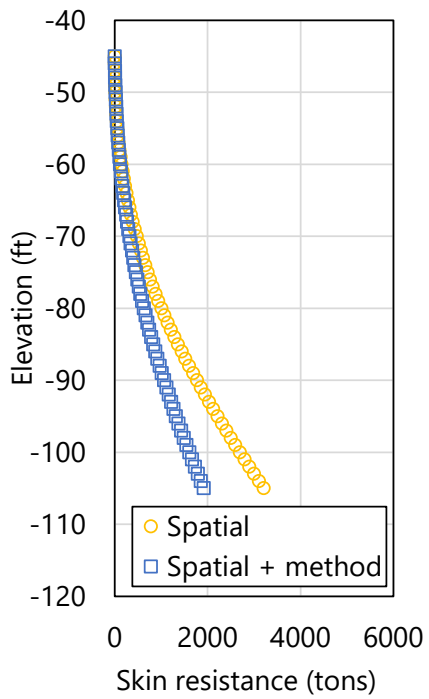


a)

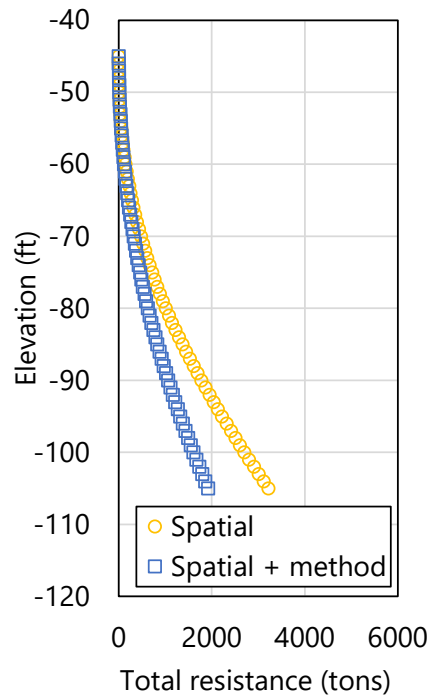


b)

Figure 138. Profile plots of ϕ -factored mean resistance for zone 1: a) Skin; b) Total



a)



b)

Figure 139. Profile plots of ϕ -factored mean resistance for zone 2: a) Skin; b) Total

CHAPTER 6 REFERENCES

- AASHTO. (2020). *LRFD Bridge Design Specifications*, 9th Ed. Washington D.C., Published: Washington D.C.
- Bloomquist, D., McVay, M. C., Hu, Z. (2007). *Updating Florida Department of Transportation's (FDOT) Pile/Shaft Design Procedures Based on CPT & DTP Data*, FDOT Research Report BD545, RPWO # 43, Tallahassee, FL.
- Bustamante, M. and Gianceselli, L. (1982). "Pile bearing capacity predictions by means of static penetrometer CPT." *Proc., 2nd European Symp. On Penetration Testing*, ESOPT-II, Amsterdam, The Netherlands, Vol. 2, 493-500.
- Davidson, M. T., McVay, M. C., Consolazio, G. R., Monari, C. J., Patil, A. P., Faraone, M. A. (2020). *Geo-statistical Deep Foundation Design Software*, FDOT Research Report BDV31-977-108, Tallahassee, FL.
- Schmertmann, J. H. (1978). *Guidelines for Cone Penetration Test. (Performance and Design)*, FHWA-TS-78-209, Washington, D.C
- Faraone, M. A. (2014). *Geo-statistical Analysis for Reliability Based Design of Foundations*, Dissertation, University of Florida, Gainesville, FL.
- Faraone, M. A., Klammlar, H., McVay, M., Davidson, M., Herrera, R., Horhota, D. (2021). "Design Methodology for site-specific resistance factors based on foundation location and size", *Computers and Geotechnics*, 138:104328.
- FDOT. (2022). *Structures Design Guidelines*, Structures Manual, Vol. 1, Tallahassee, FL, Published: Tallahassee, FL.
- Goovaerts, P. (1997). *Geostatistics for Natural Resources Evaluation*. Oxford University Press.
- Gringarten, E., and Deutsch, C. V. (2001). Variogram Interpretation and Modeling, *Mathematical Geology*, 33(4), 507-534.
- Klammlar, H., McVay, M., Horhota, D., and Lai, P. (2010). "Influence of Spatially Variable Side Friction on Single Drilled Shaft Resistance and LRFD Resistance Factors", *ASCE Journal of Geotechnical and Geoenvironmental Engineering*, 136(8), 1114-1123.

- Lilliefors, Hubert W. (1967). On the Kolmogorov-Smirnov Test for Normality with Mean and Variance Unknown, *Journal of the American Statistical Association*. 62 (318): 399-402.
- McVay, M., Klammlar, H., Bloomquist, D., Otero, J., Faraone, M. A. (2009). *Modifications of LRFD Resistance Factors Based on Site Variability*, FDOT Research Report BD-545 RPW76, Tallahassee, FL.
- McVay, M., Klammlar, H., Faraone, M. A., Krishmarao, D., Jenneisch, C. (2012). *Development of Variable LRFD ϕ Factors for Deep Foundation Design Due to Site Variability*, FDOT Research Report BDK75 977-23, Tallahassee, FL.
- McVay, M. C., Rodgers, M. (2020). *Implementation of Measuring While Drilling Shafts in Florida (FLMWDS)*, FDOT Research Report BDV31-977-91, Tallahassee, FL.
- Paikowsky, S. (2004). Load and Resistance Factor Design (LRFD) for Deep Foundations. *NCHRP Report 507*, National Cooperative Highway Research Program (NCHRP), Washington, D.C.
- Rivers, B. (2018). Advanced Geotechnical Methods in Exploration (The A-GaME), *49th Annual Southeastern Transportation Geotechnical Engineering Conference (STGEC)*, Louisville, KY, Oct. 8-11.
- Rodgers, M., McVay, Horhota, D., Hernando, J. (2018a). "Assessment of rock strength from measuring while drilling shafts in Florida limestone", *Canadian Geotechnical Journal*, 55:1154-1167.
- Rodgers, M., McVay, M. C., Ferraro, C., Horhota, D. (2018b). "Measuring Rock Strength While Drilling Shafts Socketed in Florida Limestone", *ASCE Journal of Geotechnical and Geoenvironmental Engineering*, 144(3).
- Schmertmann, J. H. (1978). *Guidelines for Cone Penetration Test. (Performance and Design)*, FHWA-TS-78-209, Washington, D.C.
- Styler, M. (2006). *Development and Implementation of the DIGGS Format to Perform LRFD Resistance Factor Calibration of Driven Concrete Piles in Florida*. Master's thesis, University of Florida, Gainesville, FL
- Terzaghi, K., Peck, R.B. (1967). *Soil Mechanics in Engineering Practice*, 2nd Ed. New York, NY: John Wiley and Sons.